Development of a Comprehensive Method for Modelling Performance of Aircraft Tyres Rolling or Braking on Dry and Precipitation-Contaminated Runways

Prepared for
Transportation Development Centre
of
Transport Canada

by
ESDU International plc

May 2003

Development of a Comprehensive Method for Modelling Performance of Aircraft Tyres Rolling or Braking on Dry and Precipitation-Contaminated Runways

by
K.J. Balkwill
ESDU International plc

May 2003

This report reflects the views of the author and ESDU International plc and not necessarily those of the Transportation Development Centre of Transport Canada or the co-sponsoring organizations.

The Transportation Development Centre and the co-sponsoring agencies do not endorse products or manufacturers. Trade or manufacturers' names appear in this report only because they are essential to its objectives.

Since some of the accepted measures in the industry are imperial, metric measures are not always used in this report.

Un sommaire français se trouve avant la table des matières.

	Transport Canada	Transports Canada			**PUBLICATION DATA FORM**

1. Transport Canada Publication No. TP 14289E	2. Project No. 9454	3. Recipient's Catalogue No.	
4. Title and Subtitle Development of a Comprehensive Method for Modelling Performance of Aircraft Tyres Rolling or Braking on Dry and Precipitation-Contaminated Runways		5. Publication Date May 2003	
		6. Performing Organization Document No. ESDU Memo No. 132	
7. Author(s) K.J. Balkwill		8. Transport Canada File No. 2450-B-14	
9. Performing Organization Name and Address ESDU International plc 27 Corsham Street London N1 6UA United Kingdom		10. PWGSC File No. XSD-8-00628	
		11. PWGSC or Transport Canada Contract No. T8200-8-8513/001/XSD	
12. Sponsoring Agency Name and Address Transportation Development Centre (TDC) 800 René Lévesque Blvd. West Suite 600 Montreal, Quebec H3B 1X9		13. Type of Publication and Period Covered Final	
		14. Project Officer A. Boccanfuso	

15. Supplementary Notes (Funding programs, titles of related publications, etc.)

Co-sponsored by Transport Canada's Civil Aviation Directorate

16. Abstract

An empirical model is defined that describes the decelerating forces acting on aircraft tyres when rolling or braking on surfaces typical of those used for runways and taxiways. The model is valid for uncontaminated surfaces and for those contaminated by water, slush, snow and ice.

In order to calculate decelerating forces, in addition to an approximation to the operating slip ratio for an aircraft's braking system, it is necessary to know values of only eight variables, all of which are used in customary calculations of aircraft performance. In the particular case of winter precipitation, the model includes the statistical variation of the mechanical properties of snows and frictional characteristics for surfaces that are completely covered with ice or compressed snow. All these statistical variations are identified from experiments on aircraft and ground vehicles.

Through the mechanism of a *reference coefficient of friction*, the model can also be used to link the performance of aircraft and ground vehicles. The modelling covers a range of the independent variables sufficient to establish Flight Manual data for any type of aircraft.

17. Key Words Aircraft, braking, contaminant, drag, ground-test machine, ice, landing, runway, slush, snow, take-off, tyre, water	18. Distribution Statement Limited number of copies available from the Transportation Development Centre

19. Security Classification (of this publication) Unclassified	20. Security Classification (of this page) Unclassified	21. Declassification (date) —	22. No. of Pages xlv, 200, apps	23. Price Shipping/Handling

Transports Canada	Transport Canada	**FORMULE DE DONNÉES POUR PUBLICATION**

1. Nº de la publication de Transports Canada	2. Nº de l'étude	3. Nº de catalogue du destinataire
TP 14289E	9454	

4. Titre et sous-titre	5. Date de la publication
Development of a Comprehensive Method for Modelling Performance of Aircraft Tyres Rolling or Braking on Dry and Precipitation-Contaminated Runways	Mai 2003
	6. Nº de document de l'organisme exécutant
	ESDU Memo No. 132

7. Auteur(s)	8. Nº de dossier - Transports Canada
K.J. Balkwill	2450-B-14

9. Nom et adresse de l'organisme exécutant	10. Nº de dossier - TPSGC
ESDU International plc 27 Corsham Street London N1 6UA United Kingdom	XSD-8-00628
	11. Nº de contrat - TPSGC ou Transports Canada
	T8200-8-8513/001/XSD

12. Nom et adresse de l'organisme parrain	13. Genre de publication et période visée
Centre de développement des transports (CDT) 800, boul. René-Lévesque Ouest Bureau 600 Montréal (Québec) H3B 1X9	Final
	14. Agent de projet
	A. Boccanfuso

15. Remarques additionnelles (programmes de financement, titres de publications connexes, etc.)

Coparrainé par la Direction générale de l'aviation civile de Transports Canada

16. Résumé

Le rapport présente un modèle empirique qui décrit les forces de décélération qui agissent sur les pneus d'aéronefs lorsqu'ils roulent ou freinent sur des surfaces comme celles dont sont couramment revêtues les pistes et voies de circulation des aérodromes. Le modèle vaut aussi bien pour des surfaces sèches que pour des surfaces contaminées par de l'eau, de la neige fondante, de la neige et de la glace.

Pour calculer les forces de décélération, outre une approximation du taux de glissement associé au système de freinage d'un aéronef, il faut connaître la valeur de seulement huit variables, qui entrent toutes dans le calcul des performances des aéronefs. Dans le cas particulier des précipitations hivernales, le modèle inclut les variations statistiques liées aux propriétés mécaniques des différents types de neige et à la glissance des surfaces complètement recouvertes de glace ou de neige tassée. Toutes ces variations statistiques sont déterminées à partir d'expériences menées à l'aide d'aéronefs et de véhicules de mesure.

Grâce au mécanisme du *coefficient de frottement de référence*, le modèle peut aussi être utilisé pour décrire des liens entre la performance des aéronefs et celle des véhicules de mesure. La modélisation couvre une plage suffisamment étendue des variables indépendantes pour permettre d'établir les données du manuel de vol de n'importe quel type d'aéronef.

17. Mots clés	18. Diffusion
Aéronef, freinage, contaminant, traînée, appareil de mesure, glace, atterrissage, piste, neige fondante, neige, décollage, pneu, eau	Le Centre de développement des transports dispose d'un nombre limité d'exemplaires.

19. Classification de sécurité (de cette publication)	20. Classification de sécurité (de cette page)	21. Déclassification (date)	22. Nombre de pages	23. Prix
Non classifiée	Non classifiée	—	xiv, 200, ann.	Port et manutention

CDT/TDC 79-005
Rev. 96

Canadä

ACKNOWLEDGEMENTS

EXECUTIVE SUMMARY

Introduction

Research has led to a substantial accumulation of data that leaves no doubt that contamination from precipitation is a major factor in loss of braking friction and hence in incidents and accidents. However, to date, no simple mathematical model has been developed that enables the quantification of these adverse frictional effects from a minimal set of parameters. This report shows how such a model has been developed and can be justified by reference to a wide range of experimental data. The model incorporates data from experiments as diverse as blocks of rubber sliding on glass to a large transport aircraft braking on a runway covered with up to six inches of snow.

The modelling is dependent on knowledge of eight independent variables:

1. Depth of macro-texture
2. Depth of contaminant
3. Density of contaminant
4. Speed
5. Tyre inflation pressure
6. Vertical loading
7. Nominal tyre width
8. Nominal tyre diameter

Of these only the first three are related to the runway and its condition. All the other quantities[1] are part of conventional ground performance calculations. Whilst it is not mentioned in the list, the mode of operation of the aircraft antiskid system is also needed; that is, the range of values of slip ratio over which it operates. This too is normally available or, in the case where the system is not torque-limited, can be inferred from tests on a dry runway.

When a flexible tyre is rolled and braked on a paved surface that is covered with either a fluid or a particulate substance, it is assumed that there are three sources for decelerating force:

1. Rolling resistance due to the absorption of energy in the tyre carcase;
2. Rolling resistance due to moving through or compressing the contaminant;
3. Braking resistance due to the frictional interaction between the tyre compound and the pavement.

Total force resisting motion – ignoring aerodynamic and impingement forces – is taken to be the simple sum of these three components with no cross coupling between the forces. This perception forms the basis of the approach adopted in constructing the various parts of the model described here. Furthermore, in order to preserve both simplicity and consistency, careful attention has been paid to ensuring that the more complex cases contain the less complex as

---

[1]   Tyre inflation pressure is used as an absolute pressure throughout this report. Conventionally, it is quoted as a gauge pressure.

defaults. For example, the case of slipping on a flooded runway defaults to static braking friction logically by setting speed and water depth to zero in the model.

In order to maximise the usefulness of the model, the statistical properties of the model are given. Thus, the uncertainty associated with any prediction made using the model can be readily calculated. Consequently, the effects of such uncertainties can be traced through to the performance of either aircraft or ground vehicles.

Rolling *on* any paved surface

Coefficient of rolling friction on paved runways is shown to correlate with inflation pressure, vertical load and speed. The correlation, which is derived from both single wheel testing and measurements on an aircraft, is acceptable for use as an empirical model. No dependence on the degree of dryness of the surface has been identified.

The uncertainty associated with a value of coefficient of rolling friction calculated from the model is ±0.0012 at the 95% level of probability. This uncertainty is applicable to the range of conditions likely to be encountered in both aircraft operations and research.

Rolling *through* fluid

Decelerating force on a tyre rolling through water is demonstrated to be dependent on seven readily available, independent variables. The combined effect of these seven variables is not simple. A drag coefficient is therefore defined as a function of the ratio of kinetic pressure and tyre inflation pressure ***in absolute measure*** together with tyre geometry and water depth. This drag coefficient is used, together with kinetic pressure and a simple reference area, to calculate drag force. Forces so obtained reflect measured data up to and beyond the observed, characteristic speed for maximum drag, which occurs within the operating range of many tyres.

The effect of slush is verified to be similar to that of water when specific gravity is introduced. However, there is an additional term in the model that accounts for squeezing air from slush and melting the suspended ice.

Random error in calculated drag forces is considered and a simple method is given for calculating the contribution that uncertainty in drag force makes to the statistics of performance estimation.

Rolling *through* snow

A viable mathematical model based on dimensional analysis has been developed to describe the decelerating force acting on an aircraft or a ground vehicle when rolling, unbraked, over a runway contaminated with snow that has been subject only to natural ageing processes. The model is simple in form and accounts for speed, tyre diameter, vertical loading and inflation pressure but depends on knowledge of snow depth and specific gravity. Relevant mechanical

properties – shear strength and shear modulus – are predicted through specific gravity, two exponential equations and a probability distribution.

It is shown that the model is applicable across a wide range of tyre geometries, undercarriage designs and a sufficient range of snow specific gravity.

In modest depths of fresh snow, so that $\sigma < 0.2$ and $d < 2$ in, the model is capable of predicting decelerating force due to rolling to within 2% of aircraft weight at the 95% level of significance. If predictions that are more precise are needed, then specific information on the mechanical properties of the snow is required.

Coefficient of friction for static braking on dry runway

Experimental evidence from a variety of sources is used to develop and justify a simple relationship that describes static coefficient of braking friction for aircraft tyres with an uncertainty that adequately reflects the uncertainties in the measuring process. Given vertical load on the tyre and mean bearing pressure, static coefficient of braking friction for aircraft tyres can be calculated with an uncertainty better than ±0.01 at the 95% level of probability.

For tyres that are typical of those used for specialist ground vehicles, similar relationships are presented but are based on fewer experimental measurements. In these cases, static coefficient of braking friction may also be calculated with an uncertainty better than ±0.01 at the 95% level of probability.

The simple correlation is ideally suited to be the starting point for development of a model that enables the prediction of coefficient of braking friction over the full operational range of aircraft and ground vehicles.

Coefficient of friction for full skid on dry runway

Data from skidding and slipping experiments conducted at NASA Langley are used to substantiate a mathematical description of the effect of speed on coefficient of braking friction in a full skid on dry runways. The formulation is an extension of that used to calculate static coefficient of braking friction.

Although the experimental process led to uncertainties in measured friction coefficient that are larger than those generally expected, use of the correlation as a model results in uncertainties of estimate in the order of ±0.012 at the 95% level of statistical significance.

Coefficient of friction for slipping on dry runway

The mathematical model for coefficient of braking friction in a fully developed skid on a dry runway is extended to include the effects of slip ratio by introducing one additional freedom. This model is shown to be consistent with experiment.

Although the scatter of the experimental data about the model is quite large, it is estimated that the uncertainty in an estimate of coefficient of braking friction from the model is in the order of $U[\mu_{SLIP\,DRY}] = \pm 0.01$ at the 95% level of significance.

In addition, the model can be used to calculate maximum values of coefficient of braking friction. The uncertainty of this calculation is $U[\mu_{MAX\,DRY}] = \pm 0.016$ at the 95% level of significance.

Pressure under tyre running on wet runway

The three-zone model of the area under the footprint of an aircraft tyre rolling or skidding on a wet runway is used as the basis for a scheme to represent the mean pressures over the footprint.

It is shown that, under static conditions, the tyre inflation pressure – in **absolute measure** – is a good approximation to the bearing pressure under load. It is argued that the pressure in the region of dry contact may then be equated to that pressure. The pressure in the most forward of the three zones is shown to be identical to the kinetic pressure. A formula that relates the pressure in the region of viscous contact to kinetic pressure is developed: this formula closely represents a well-established set of measurements made by NASA.

Using the correlations, the uncertainty associated with the calculated mean pressure in any one zone is shown to be ± 5 lbf/in^2 at the 95% level of significance.

Coefficient of friction for full skid on wet runway

The mathematical model used to describe coefficient of braking friction in full skid on a dry runway is extended to incorporate the effects of wet runways. Data from systematic testing on single wheels are used to show that the model is sufficiently robust to predict coefficients of friction for aviation-style tyres skidding under a wide range of conditions.

Surface finishes for which data have been compared range from smooth concrete through fine-textured asphalts to mixed-aggregate asphalts with good drainage. Although the smooth surfaces are not typical of modern runways, the balance between micro- and macro-texture for all the other surfaces is believed to represent constructions used in current aviation practice.

Investigations of the distribution of measured data about the model show that there is significant *between*-test and *within*-test variability for both of the test facilities from which data have been acquired. However, the size of the sample is so large and the data are so extensive in scope that the uncertainty in an estimate of $\mu_{SKID\,WET}$ from the model is ± 0.003 at the 95% level of significance over the full operational range of tyres and runways used in civil aviation.

Coefficient of friction for slipping on wet runway

The mathematical model for coefficient of braking friction in a fully developed skid on a wet runway is amended to include the effects of slip ratio by introducing one additional freedom. This extended model is shown to be consistent with experiment.

Although the scatter of the experimental data about the model is quite large, the comparison with experiment is based on a large sample: it is calculated that the uncertainty in an estimate of coefficient of braking friction from the model is in the order of $U\left[\mu_{SLIP\ WET}\right]_{0.95} = \pm0.006$ at the 95% level of significance.

In addition, the model can be used to calculate maximum values of coefficient of braking friction in the wet. Sufficient measurements of this quantity were observed in the series of experiments used to substantiate the modelling; the uncertainty of such a calculation is in the order of $U\left[\mu_{MAX\ WET}\right]_{0.95} = \pm0.01$ at the 95% level of significance.

Coefficient of friction for braking on ice- and snow-covered runways

The mathematical model developed for braking on dry runways is shown to be capable, with minor modifications, of providing a means of estimating the braking performance of aircraft when operating on runways contaminated with winter precipitation. These modifications are solely to values of reference coefficient of friction.

It is shown that reference coefficient of friction is dependent on ground temperature. However, ground temperature has not been published for many of the experiments considered. As an alternative, three types of "ice" are identified and reference coefficient of friction is shown to be a Normally distributed statistic with a mean value that is determined by type.

In addition, it is shown that the model can be used to calculate the James Braking Index and Runway Condition Reading. It is therefore arguable that the reference coefficient of friction can be used as a general Runway Friction Indicator.

SOMMAIRE

Introduction

Les résultats des recherches menées à ce jour sont formels : la contamination due aux précipitations est un facteur important de la perte de frottement de freinage et, partant, des incidents et accidents d'aviation. Cela étant, personne à ce jour n'a développé de modèle mathématique simple permettant de quantifier cette perte de frottement à partir de quelques paramètres. Le présent rapport montre comment un tel modèle a été élaboré et comment il peut être justifié au moyen d'un large éventail de données expérimentales, issues de diverses expériences allant d'essais de glissement de blocs de caoutchouc sur une plaque de verre à des essais de freinage d'un gros porteur sur une piste recouverte d'une couche de neige pouvant atteindre six pouces d'épaisseur.

L'élaboration du modèle nécessite la détermination de huit variables indépendantes :

1. Épaisseur de la macro-texture
2. Épaisseur de la contamination
3. Densité de la contamination
4. Vitesse
5. Pression de gonflage des pneus
6. Charge verticale
7. Largeur nominale des pneus
8. Diamètre nominal des pneus

Seules les trois premières de ces variables ont trait à la piste et à son état. Toutes les autres[1] entrent dans les calculs classiques des performances des aéronefs au sol. En outre, même si le mode de fonctionnement du système antidérapage de l'aéronef ne figure pas dans la liste des variables, il est essentiel de connaître la plage des valeurs de taux de glissement dans laquelle le système entre en action. Là encore, il est habituellement aisé d'obtenir cette information; au cas contraire, si le système n'est pas à limitation de couple, ces données peuvent être déduites d'essais sur chaussée sèche.

Lorsqu'un pneu souple roule et freine sur une surface revêtue recouverte soit d'un liquide soit de particules solides, on suppose une force de décélération engendrée par trois phénomènes :

1. la résistance au roulage due à l'absorption d'énergie par la carcasse du pneu;
2. la résistance au roulage due au déplacement dans la contamination ou à l'écrasement de la contamination;
3. la résistance au freinage due à l'interaction de frottement entre le pneu et la chaussée.

La force totale qui s'oppose au mouvement – sans compter la force aérodynamique et la traînée due au choc des projections – est considérée comme étant la simple somme de ces trois

---

[1] Dans le rapport, la pression de gonflage des pneus est considérée comme une pression absolue. Il s'agit, par convention, de la pression manométrique.

composantes, sans couplage croisé des forces. Cette façon de voir est à la base de la démarche utilisée pour élaborer les divers éléments du modèle décrit ici. De plus, pour s'assurer que le modèle soit à la fois simple et cohérent, les chercheurs ont fait en sorte que les cas les plus complexes englobent, implicitement, les cas les moins complexes. Par exemple, le cas du glissement sur une piste inondée comprend, par défaut, les cas de frottement de freinage statique, les variables vitesse et profondeur d'eau étant logiquement réglées à zéro dans le modèle.

Pour maximiser l'utilité du modèle, les auteurs en donnent les propriétés statistiques. Ainsi, l'incertitude de toute prévision peut facilement être calculée. Il est donc possible de tenir compte des effets de ces incertitudes dans le calcul des performances des aéronefs ou des véhicules de mesure.

Roulage *sur* une surface revêtue

Une corrélation a été établie entre le coefficient de frottement de roulage sur des pistes revêtues et la pression de gonflage, la charge verticale et la vitesse. Cette corrélation, établie à partir des résultats d'essais d'une roue et des mesures prises sur un aéronef, est acceptable à titre de modèle empirique. Aucun rapport de dépendance avec le degré de sécheresse de la surface n'a été déterminé.

L'incertitude d'une valeur de coefficient de frottement de roulage calculée à l'aide du modèle est de ±0,0012, à un niveau de probabilité de 95 %. Cette incertitude s'applique à tout l'éventail des conditions susceptibles de se présenter aussi bien en situation réelle que lors d'essais.

Roulage *dans* un liquide

La force de décélération agissant sur un pneu qui roule dans l'eau s'est révélée dépendante de sept variables indépendantes, faciles à déterminer. L'effet combiné de ces sept variables est complexe. Un coefficient de traînée est donc défini comme étant une fonction du rapport de la pression cinétique et de la pression de gonflage des pneus (en *mesure absolue*) à la géométrie des pneus et à la profondeur de l'eau. Ce coefficient de traînée, conjugué à d'autres données (la pression cinétique et les caractéristiques d'une aire de référence), sert à calculer la résistance. Les forces ainsi obtenues reflètent les données mesurées jusqu'à la vitesse caractéristique observée pour la traînée maximale (et au-delà), laquelle est comprise dans la plage des vitesses d'exploitation acceptables de nombreux pneus.

L'effet de la neige fondante s'avère similaire à celui de l'eau, lorsque la variable densité relative est incorporée au modèle. Le modèle comprend toutefois un terme additionnel qui rend compte de l'extraction de l'air de la neige fondante et de la fonte de la glace en suspension.

La résistance calculée comprend une erreur aléatoire, et une méthode simple est proposée pour calculer l'effet de l'incertitude de la résistance sur l'estimation des performances des aéronefs.

Roulage *dans* la neige

Une analyse dimensionnelle a mené à l'élaboration d'un modèle mathématique viable de la force de décélération qui agit sur un avion ou sur un véhicule de mesure lorsqu'il roule, sans freiner, sur une piste couverte de neige soumise au seul processus de vieillissement naturel. Ce modèle, de forme simple, tient compte de la vitesse, du diamètre des pneus, de la charge verticale et de la pression de gonflage; on doit toutefois connaître l'épaisseur et la densité relative de la neige. Des propriétés mécaniques pertinentes – résistance au cisaillement et module de compressibilité – sont dérivées de la densité relative, de deux équations exponentielles et d'une distribution de probabilité.

Le modèle se révèle applicable à une large gamme de géométries de pneus et de trains d'atterrissage, et à une plage satisfaisante de densités relatives de la neige.

Dans de faibles épaisseurs de neige fraîche, soit lorsque $\sigma < 0,2$ et $d < 0,2$ po, le modèle peut prévoir une force de décélération due au roulage précise à 2 % du poids de l'aéronef, à un niveau de signification de 95 %. Une plus grande précision exigerait des données plus précises sur les propriétés mécaniques de la neige.

Coefficient de frottement – freinage statique sur piste sèche

Des données expérimentales de diverses sources sont utilisées pour élaborer et justifier une relation simple qui décrit le coefficient statique de frottement de freinage pour des pneus d'aéronefs, avec une incertitude conforme aux incertitudes de la mesure. Compte tenu de la charge verticale sur le pneu et de la pression d'appui moyenne, le coefficient statique de frottement de freinage peut être calculé avec une incertitude inférieure à ±0,01, à un niveau de probabilité de 95 %.

Des relations semblables sont présentées pour les pneus qui équipent couramment les véhicules de mesure, mais celles-ci s'appuient sur des données expérimentales plus limitées. Le coefficient statique de frottement de freinage peut tout de même être calculé avec une incertitude inférieure à ±0,01, à un niveau de probabilité de 95 %.

La corrélation simple est idéale comme point de départ de l'élaboration d'un modèle qui permet de prévoir le coefficient de frottement de freinage dans toute la gamme des conditions d'exploitation d'aéronefs et de véhicules de mesure.

Coefficient de frottement – dérapage complet sur piste sèche

Les données issues d'essais de dérapage et de glissement menés au Langley Research Center de la NASA ont servi à établir un modèle mathématique de l'effet de la vitesse sur le coefficient de frottement de freinage lors d'un dérapage complet sur piste sèche. L'équation est dérivée de celle utilisée pour calculer le coefficient statique de frottement de freinage.

Même si, au terme des expériences, l'incertitude du coefficient de frottement mesuré est supérieure aux valeurs généralement admises, l'utilisation de la corrélation en tant que modèle produit une incertitude de l'ordre de ±0,012, à un niveau de signification de 95 %.

Coefficient de frottement – glissement sur piste sèche

Un degré de liberté a été ajouté au modèle mathématique du coefficient de frottement de freinage en dérapage complet sur piste sèche, de façon qu'il tienne compte des effets du taux de glissement. Ce modèle s'avère représenter adéquatement la situation réelle.

Malgré une dispersion relativement importante des données expérimentales, on estime que l'incertitude d'une estimation du coefficient de frottement de freinage établie à l'aide du modèle est de l'ordre de $^{U}\left[\mu_{SLIPDRY}\right] = \pm 0,01$, à un niveau de signification de 95 %.

De plus, le modèle peut servir à calculer les valeurs maximales du coefficient de frottement de freinage. L'incertitude de ce calcul est de $^{U}\left[\mu_{MAX\ DRY}\right] = \pm 0,016$, à un niveau de signification de 95 %.

Pression d'appui sur le pneu – roulage sur piste mouillée

Le modèle à trois zones de l'aire située sous l'empreinte d'un pneu d'aéronef qui roule ou dérape sur une piste mouillée sert de base à une technique utilisée pour représenter les pressions moyennes qui s'exercent sous l'empreinte.

Il a été démontré que, dans des conditions statiques, la pression de gonflage du pneu – en ***mesure absolue*** – constitue une bonne approximation de la pression d'appui sur le pneu lorsqu'il supporte une charge. Les auteurs estiment que la pression dans la région de contact sec pneu/piste peut être assimilée à cette pression. La pression dans la zone antérieure s'est avérée équivalente à la pression cinétique. Les chercheurs ont élaboré une formule qui décrit la relation entre la pression dans la région de contact visqueux et la pression cinétique : cette formule représente, à peu de choses près, un ensemble bien établi de mesures faites par la NASA.

L'incertitude du calcul de la pression moyenne dans l'une ou l'autre des zones à l'aide des corrélations se situe à ±5 lbf/po^2, à un niveau de signification de 95 %.

Coefficient de frottement – dérapage sur piste mouillée

Le modèle mathématique qui décrit le coefficient de frottement de freinage au dérapage sur piste sèche est élargi pour incorporer les effets de pistes mouillées. Les résultats d'essais systématiques réalisés avec des roues seules servent à démontrer que le modèle est suffisamment robuste pour prévoir les coefficients de frottement pour des pneus d'aéronefs en dérapage dans un large éventail de conditions.

Les revêtements de surface pour lesquels des données ont été comparées vont du béton lisse à des bitumes constitués de granulats mélangés offrant un bon drainage, en passant par des bitumes

à texture fine. Même si les pistes, de nos jours, sont rarement constituées de surfaces lisses, les autres surfaces considérées constituent un échantillon équilibré de micro-textures et de macro-textures qui, croit-on, est représentatif des pistes actuelles.

La comparaison des données observées et du modèle révèle une variabilité significative des résultats, d'un essai à l'autre et lors d'un même essai, dans le cas des deux sites d'essai qui ont fourni les données. Toutefois, la taille de l'échantillon et la portée des données sont tellement vastes que l'incertitude d'une estimation de $\mu_{SKID\ WET}$ est de ±0,003, à un niveau de signification de 95 %, pour toute la gamme des pneus et des pistes utilisés en aviation civile.

Coefficient de frottement – glissement sur piste mouillée

Un degré de liberté a été ajouté au modèle mathématique du coefficient de frottement de freinage en dérapage sur piste mouillée pour tenir compte des effets du taux de glissement. Ce modèle étendu s'est révélé une représentation adéquate de la situation réelle.

Les données expérimentales sont relativement dispersées par rapport au modèle, mais la comparaison s'appuie sur un vaste échantillon. L'incertitude d'une estimation du coefficient de frottement de freinage établie à l'aide du modèle est de l'ordre de $U\left[\mu_{SLIP\ WET}\right]_{0,95} = \pm 0,006$, à un niveau de signification de 95 %.

De plus, le modèle peut servir à calculer les valeurs maximales du coefficient de frottement de freinage sur piste mouillée. Suffisamment de mesures ont été faites de cette valeur au cours de la série d'expériences réalisées pour justifier le modèle; l'incertitude de ce calcul est de l'ordre de $U\left[\mu_{MAX\ WET}\right]_{0,95} = \pm 0,01$, à un niveau de signification de 95 %.

Coefficient de frottement – piste glacée et piste enneigée

Le modèle mathématique élaboré pour le freinage sur piste sèche s'est révélé capable, moyennant de légères modifications, de prévoir la performance en freinage d'aéronefs sur des pistes contaminées par des précipitations hivernales. Ces modifications touchent uniquement les valeurs du coefficient de frottement de référence.

Il a été établi que le coefficient de frottement de référence dépend de la température du sol. Toutefois, dans beaucoup des expériences prises en compte, la température du sol n'a pas été publiée. Pour pallier cette lacune, les chercheurs ont défini trois types de «glace», et le coefficient de frottement de référence se révèle être une statistique obéissant à une distribution normale, dont la valeur moyenne est déterminée pour chaque type.

De plus, le modèle se révèle utile pour calculer le coefficient de freinage James et le code de l'état de la piste (RCR). Il est donc permis de penser que le coefficient de frottement de référence peut être utilisé comme un indicateur général de la glissance de la piste.

TABLE OF CONTENTS

LIST OF FIGURES

LIST OF TABLES

NOTATION

A list of the general notation for the whole document is presented in this part. Many of the symbols are used in their standard sense. However, an attempt has been made to eliminate complexity. To this end, superscripts have been avoided and subscripts have been used in what is hoped is a clear and natural way.

One significant departure from common usage has been adopted. Symbols succeeded by square brackets are used to indicate that the quantity within the brackets is operated upon by the symbol that precedes the bracket. For example, the string $\ln[x]$ is to be interpreted as the natural logarithm of the variable x. Again, the string $P[z < z_0] = 0.95$ is to be interpreted as the probability that $z < z_0$ is 95%.

Symbol	Description	British Units[1]	Metric Units
a	half maximum length of footprint	ft	m
a_0	empirically determined constant		
A	total area of cross-section of inlet stream tubes	ft^2	m^2
A^*	statistic for Anderson-Darling test		
A_F	area of footprint	ft^2	m^2
b	half maximum width of footprint (Section 4)	ft	m
b	characteristic speed (Section 5)	ft/s	m/s
C_D	drag coefficient due to fluid displacement by single tyre		
C_G	decelerating force coefficient for tyre rolling in clay		
C_L	lift coefficient		
C_u	shear strength of medium	lbf/ft^2	N/m^2
$C_{u\,REF}$	reference value of shear strength of snow	lbf/ft^2	N/m^2
C_Z	normal force coefficient for tyre rolling in clay		
d	depth of fluid contaminant or other medium	ft	m
d_0	reference depth fluid contaminant or other medium	ft	m
d_{tex}	depth of macro-texture of runway	ft	m
d_{tex_0}	reference depth of macro-texture of runway	ft	m

---

[1]   Consistent, British, units are used throughout this document. However, the model presented is empirical and some equations contain dimensional constants. Care must therefore be exercised when converting to other systems of units.

Symbol	Description	British Units[1]	Metric Units
D	aerodynamic force parallel with air path (Appendix E)	lbf	N
D	diameter of inflated tyre (Sections 4 and 10)	ft	m
D	wheel diameter (Section 5)	ft	m
E	Young's modulus	lbf/ft^2	N/m^2
$f[\ ]$	empirical function of quantities in [ ] (Section 3)		
g	acceleration due to gravity	ft/s^2	m/s^2
G	horizontal force (Appendix D)	lbf	N
G	rolling resistance force	lbf	N
G_1	fluid drag force on single wheel	lbf	N
G_C	fluid drag force due to compression of medium	lbf	N
G_{ROLL}	rolling resistance	lbf	N
G_S	shear modulus of medium	lbf/ft^2	N/m^2
$G_{S\ REF}$	reference value of shear modulus of snow	lbf/ft^2	N/m^2
G_{SNOW}	decelerating force due to rolling through snow	lbf	N
G_T	decelerating force due to rolling through fluid	lbf	N
k	factor		
k	factor on inlet mass flow ratio (Appendix D)		
L	aerodynamic lift	lbf	N
m	mass	slug	kg
m	parameter in distribution (Appendix E)		
$\dot{m}$	air mass flow per unit time	slug/s	kg/s
m_1, m_2	empirically determined exponents		
M_{300}	engineering stress to produce strain of 300%	lbf/ft^2	N/m^2
n	number of wheels on aircraft landing gear		
n	number of wheels (Appendix D)		
n	parameter in distribution (Appendix E)		
N	speed number		
p	tyre inflation pressure, absolute	lbf/ft^2	N/m^2
p_a	atmospheric pressure	lbf/ft^2	N/m^2
p_b	mean bearing pressure under footprint	lbf/ft^2	N/m^2
p_i	tyre inflation pressure, gauge	lbf/ft^2	N/m^2
P	power	ftlbf/s	Nm/s
$P[\ ]$	probability of event in [ ]		

Symbol	Description	British Units[1]	Metric Units
q	kinetic pressure	lbf/ft^2	N/m^2
q_v	pressure in Zone 3 of footprint (Section 9)	lbf/ft^2	N/m^2
q_v	pressure in zone 2 (Sections 10 and 11)	lbf/ft^2	N/m^2
r	exponent in calculation of C_u G_S		
R	radius of inflated tyre	ft	m
R_{VOID}	void ratio		
s	slip ratio (Sections 7, 8, 11 and 12, and Appendix E)		
s	rut depth (Section 5)	ft	m
s'	transformed slip ratio		
s'_x	$100 \times x$ percentage point of distribution of s'		
S	reference area	ft^2	m^2
S_F	footprint area	ft^2	m^2
S_i	area of Zone i $(i = 1, 2, 3)$ under footprint (Section 10)	ft^2	m^2
t	Time	s	s
$\hat{T}$	transformed ground temperature		
T	temperature	C	F
$U[\ ]_{0.95}$	uncertainty associated with parameter in $[\ ]$		
v	volume (Sections 4 and 5)		
v	translation speed of tyre footprint (Sections 7, 8, 11 and 12)	ft/s	m/s
v_0	volume of slush before contact with tyre	ft^3	m^3
v_c	compressed volume of slush	ft^3	m^3
$\text{var}[\ ]$	variance of quantity in [ ]		
V	ground speed of vehicle (Sections 7, 8, and 12)	ft/s	m/s
V	ground speed (except Sections 7, 8, and 12)	ft/s	m/s
V_C	"critical" ground speed at which fluid drag force is maximum (customary modelling not followed here)	ft/s	m/s
V_E	equivalent airspeed	ft/s	m/s
V_T	true airspeed	ft/s	m/s
w	width of inflated tyre	ft	m
w_{max}	maximum width of inflated tyre in motion	ft	m
W	weight (Section 5)	lbf	N

Symbol	Description	British Units[1]	Metric Units
W	work done in compressing slush	ftlbf	Nm
Z	net vertical load on wheel (Section 5)	lbf	N
z	percentage point of Normal distribution		
Z	normal (to runway) load on wheel	lbf	N
Z	normal (to runway) load on undercarriage (Appendix D)	lbf	N
Z	tyre vertical load (Sections 6, 7, 8, 9, 10, 11 and 12)	lbf	N
Z_M	normal (to runway) load on one main-wheel	lbf	N
Z_N	normal (to runway) load on one nose-wheel	lbf	N
$\beta_1[m,n]$	probability density of beta distribution of the first kind		
$\mathrm{B}[m,n]$	Beta function of m and n		
γ_0	constant in definition of force to compress slush (=0.2)	ft^{-2}	m^{-2}
$\delta[\ ]$	increment of quantity in $[\ ]$		
$\Delta[\ ]$	deviation of measured value of quantity in $[\ ]$ from model		
$\overline{\Delta}$	mean value of $\Delta[\ ]$		
Δ'	standardized value of $\Delta[\ ]$		
$\hat{\Delta}$	transformed value of Δ'		
ε	runway slope	radian	radian
$\mathrm{E}[\ ]$	value of quantity in $[\ ]$ from model		
Γ_G	decelerating force function		
η_0,η_1,η_2	empirical constants for aircraft tyres		
θ	ratio of kinetic pressure and absolute inflation pressure (Section 9)		
θ	variable defined in text (except Section 9)	rad	rad
μ	coefficient of friction (Section 6)		
μ	coefficient of braking friction (Section 6)		
μ_{MAX}	maximum available coefficient of braking friction		
$\mu_{MAX\ DRY}$	maximum available coefficient of braking friction		
$\mu_{MAX\ WET}$	maximum available coefficient of braking friction in wet		
μ_0	coefficient of braking friction at $V=0$		

Symbol	Description	British Units[1]	Metric Units
μ_{REF}	reference coefficient of braking friction		
μ_{REF}	empirically derived reference coefficient of friction (Sections 6, 7, and 8)		
$\mu_{REF\ ICE}$	empirically derived reference coefficient of friction		
μ_{ROLL}	coefficient of rolling friction		
$\mu_{SKID\ DRY}$	coefficient of braking friction in full skid on dry runway (Sections 7, 8, 10 and 11)		
$\mu_{SKID\ DRY}$	coefficient of sliding friction on dry runway		
$\mu_{SKID\ ICE}$	coefficient of braking friction in full skid on icy runway		
$\mu_{SKID\ STATIC}$	coefficient of sliding friction at $V = 0$		
$\mu_{SKID\ STATIC}$	coefficient of braking friction at $V = 0$ (Sections 6 and 7)		
$\mu_{SKID\ WET}$	coefficient of sliding friction on wet runway		
$\mu_{SKID\ WET}$	coefficient of braking friction in full skid on wet runway (Sections 10 and 11)		
$\mu_{SLIP\ DRY}$	coefficient of slipping friction on dry runway		
$\mu_{SLIP\ DRY}$	coefficient of braking friction when slipping on dry runway (Sections 8 and 11)		
$\mu_{SLIP\ ICE}$	coefficient of braking friction when slipping on icy runway		
$\mu_{SLIP\ WET}$	coefficient of slipping friction on wet runway		
$\mu_{SKID\ STATIC}$	coefficient of sliding friction at $V = 0$		
$\mathrm{M}[\ ]$	measured value of quantity in $[\ ]$		
ν	Poisson's ratio		
ρ	density of respective medium	slug/ft^3	kg/m^3
ρ_1	density of slush before contact with tyre	slug/ft^3	kg/m^3
ρ_c	density of slush after compression	slug/ft^3	kg/m^3
$\sigma[\ ]$	standard error of quantity in $[\ ]$		
σ	specific gravity of fluid contaminant		
$\xi_0, \xi_1, \xi_2, \xi_3$	variables used in process of modelling		
$\xi_{01}, \xi_{11}, \xi_{12}, \xi_{21}, \xi_{22}, \xi_{23}$	coefficients in model		
ζ_0	constant in definition of coefficient of rolling friction	lbf$^{1/3}$	N$^{-1/3}$

Symbol	Description	British Units[1]	Metric Units
ζ_1	constant in definition of coefficient of rolling friction	ft^{-1} lbf$^{-1/3}$	m^{-1} N$^{-1/3}$
χ^2	test statistic		
$\varphi, \varphi_0, \varphi_1, \varphi_2$	variables used in process of modelling		
$\varphi_{10}, \varphi_{11}$	constants in model		
φ_β	coefficient in correlation of decelerating force		
φ_δ	coefficient in correlation of decelerating force		
Φ	function of wheel geometry and snow properties		
λ	proportion of vertical load carried by nose undercarriage		
ω	angular velocity of wheel	rad/s	rad/s

Suffices

0	conditions in free stream
1	conditions at plane of inlet
ICE	refers to ice
ICE 1	refers to runway covered with ice or compressed snow
ICE 2	refers to runway covered with loose snow
ICE 3	refers to runway covered in glare ice
M	main wheel/undercarriage
N	nose wheel/undercarriage
SNOW	refers to snow
TOTAL	total for whole aircraft

Numerical values of constants – British and Metric Units

Symbol	British		Metric	
	Value	Unit	Value	Unit
a_0	3.138		3.138	
d_0	3.333×10^{-4}	ft	1.016×10^{-4}	m
d_{tex_0}	1.95×10^{-4}	ft	5.9436×10^{-5}	m
$C_{u\ REF}$	5.6×10^{4}	lbf/ft^2	2.6813×10^{6}	N/m^2
$G_{s\ REF}$	7.305×10^{7}	lbf/ft^2	3.4977×10^{9}	N/m^2
m_1	0.4		0.4	
m_2	2.4		2.4	
γ_0	0.2	ft^{-2}	2.15278	m^{-2}
$E[\mu_{REF\ ICE\ 1}]$	0.36		0.36	
$E[\mu_{REF\ ICE\ 2}]$	0.25		0.25	
ζ_0	0.0062	lbf$^{-1/3}$	3.7699×10^{-3}	N$^{-1/3}$
ζ_1	2.31×10^{-5}	ft^{-1} lbf$^{-1/3}$	4.60824×10^{-5}	m^{-1} N$^{-1/3}$
η_0	0.416	lbf$^{1/3}$	0.6842	N$^{1/3}$
η_1	0.019	lbf$^{1/3}$ft^{-1}	0.1025	N$^{1/3}$m^{-1}
η_{20}	2.5		2.5	
η_{21}	-12		-12	
σ_{ICE}	0.92		0.92	
$\sigma[\mu_{REF\ ICE}]$	0.084		0.084	
φ_{10}	-0.0282		-0.0282	
φ_{11}	3.9		3.9	
φ_{12}	1.9		1.9	
ξ_{01}	13.11		13.11	
ξ_{11}	1.93	ft$^{-3/4}$	4.7049	m$^{-3/4}$
ξ_{12}	0.16		0.16	
ξ_{21}	0.463	ft	0.1411	m
ξ_{22}			0.8	
ξ_{23}	3.75	ft	1.143	m

MATHEMATICAL MODELS

Rolling Resistance Cases

Case	Description and Equation	Section
Rolling *on* any paved runway $s = 0$	Plausible empirical relation describes data from tests on single wheels and on a complete aircraft. $$\mu_{ROLL} = \left(\zeta_0 + \zeta_1 V^2/2g\right)\left(\frac{Z^{1/3}}{p/p_a}\right)$$	3
Decelerating force on single tyre rolling *through* fluid $s = 0$	Systematic tests on single tyres conducted in United States and United Kingdom form the basis of an empirical model. Model matches data from tests done on full-scale aircraft for whole of ground speed range in water and in slush. $$G_1 = G_T + G_C$$ $$G_T = \left(\sigma\rho V^2/2\right)\times\left(d\sqrt{Z/p}\right)C_D$$ $$G_C = \gamma_0 wD\sigma d\sqrt{pZ}\ln[1/\sigma]$$ $$C_D = \xi_0\left(\frac{1+\sin[\theta]}{2}\right)+\xi_1\left(\frac{\cos[\theta]}{2}\right)^4+\xi_2\left(\frac{1-\sin[\theta]}{2}\right)\left(\frac{\cos[\theta]}{2}\right)^2$$ $$\theta = \tan^{-1}[1-q/p]:\xi_0 = \xi_{01}\left(w/D\right)^2:\xi_1 = \xi_{11}D^{3/4}\left(\xi_{12}+d/w\right)\left(D/w\right)$$ $$\xi_2 = \frac{\xi_{21}}{w\left\{\xi_{22}\left(1-\left(\frac{D}{\xi_{23}}\right)^2\right)+\frac{d}{w}\right\}}:\xi_2\geq 0:q=\frac{1}{2}\sigma\rho V^2$$	4

Case	Description and Equation	Section
Decelerating force on single tyre rolling *through* snow $s = 0$	Tests on aircraft and ground vehicles have been used to establish plausible set of mechanical properties for snow. Relationship connecting decelerating force, tyre properties and snow state based on analogy between snow and soft ground. $$G_{SNOW} = \left[\frac{\text{O}[G_{SNOW}]}{\text{E}[G_{SNOW}]}\right] G_S (Z/p)(s_{RUT}/D)^{4/3}\left(1 + \frac{\rho_{SNOW}V^2}{C_u}\right)^{1/4}$$ $$R_{VOID} = 1 - \sigma_{SNOW}/\sigma_{ICE}: \quad s_{RUT}/D = R_{VOID}(d/D)$$ $$C_u = C_{u\,REF}\,e^{-13.82 R_{VOID}^{2.5}}, \; G_S = G_{S\,REF}\,e^{-13.82 R_{VOID}^{1.5}}$$ The parameter $\dfrac{\text{O}[G_{SNOW}]}{\text{E}[G_{SNOW}]}$ is the ratio of observed (O) and expected (E) values of G_{SNOW}. A value of this parameter for a snow-covered runway can be deduced from the above equations if a measured value of G_{SNOW} is available. When no measurement of G_{SNOW} is available, the table below gives percentage points in the distribution of the parameter. Regardless of whether the above equations are used to deduce a value of the parameter, or to predict G_{SNOW}, values of d and σ_{SNOW} are required (measured or assigned). **Percentage points of distribution of ratio of observed (O) and expected values (E) of decelerating force due to rolling through snow** | Probability	$\dfrac{\text{O}[G_{SNOW}]}{\text{E}[G_{SNOW}]}$
---	---
2.5	0.390
5	0.453
10	0.534
50	0.939
55.8	1
90	1.639
95	1.929
97.5	2.235		5

Braking on Dry Runway

Case	Description and Equation	Section
Static braking on dry runway $V = 0$	Equation constructed to accommodate fundamental empirical observations that static friction coefficient is a function of the cube root of load and pressure at interface of rubber compound and hard surface. Full-scale tyre data reconciled with fundamental data by equating bearing pressure to inflation pressure in ***absolute measure***. Equation fits all available measured data. $$\mu_0 = \frac{\mu_{REF}}{\left(1 + \eta_0 \dfrac{p/p_a}{Z^{1/3}}\right)}$$	6
Full skid on dry runway $s = 1$	It is assumed that η_0 in equation for μ_0 represents absorption of strain energy in the footprint. To model effects of speed, it is assumed that kinetic energy affects the friction coefficient in the same way as strain energy. $$\mu_{SKID\ DRY} = \frac{\mu_{REF}}{\left(1 + \left(\eta_0 + \eta_1 \dfrac{V^2}{2g}\right)\dfrac{p/p_a}{Z^{1/3}}\right)}$$	7
Braking on dry runway[1] $0 < s < 1$	Coefficient of braking friction in full skid on dry runway is modified empirically to fit measured data. Slip speed of footprint determines kinetic energy absorbed by tyre. $$\mu_{SLIP\ DRY} = \frac{\mu_{REF}\left(1 - e^{\eta_{21}s}\right)}{\left(1 + \left(\eta_0 + \eta_1 \dfrac{v^2}{2g}\right)\dfrac{p/p_a}{Z^{1/3}}\right)} : v = sV$$	8

In principle, μ_{REF} can be found from any of the relationships in this model or the one for braking on wet runway herein. In practice, the simplest methods are

- Use dry runway test data for μ_0, $\mu_{SKID\ DRY}$ or $\mu_{SLIP\ DRY}$.
- In absence of measured data for aircraft use $\mu_{REF} = 0.909$.

Section 6 of the report gives values of μ_{REF} for some ground-test-machine tyres.

---

[1] Note that values of μ_{max} follow from the equation given here. It is the maximum value of $\mu_{SLIP\ DRY}$ for a given set of values of independent variables.

Braking on Wet Runway

Case	Description and Equation	Section
Pressure under tyre running on wet runway for all values of s	Footprint assumed to conform to "*three-zone*" model. Slip speed of footprint determines kinetic pressure under tyre. Pressure in zone 1 is kinetic pressure. That in zone 2 described by empirical equation that fits data measured **under** rib of tyre on smooth surface. Pressure in zone 3 is inflation pressure in **absolute measure**.	9
	$$v = sV: \ p = p_i + p_a: \ q = \rho v^2/2$$ $$\varphi = \frac{\sin\left[q/p\right]}{\sin\left[q/p\right] + \cos\left[q/p\right]}$$ $$q_v = q + a_0 p \varphi^{m_1} \left(1-\varphi\right)^{m_2}$$	
Full skid on wet runway $s = 1$	Coefficient of braking friction in full skid on dry runway is modified empirically to fit several sets of measurements on single tyres collected at both NASA Langley and the Road Research Laboratory in United Kingdom.	10
	$$\mu_{SKID\ WET} = \frac{\mu_{REF}}{\left(1 + \left(\eta_0 + \eta_1 \frac{V^2}{2g}\right)\frac{p/p_a}{Z^{1/3}}\right)} \frac{\left(1 - \varphi_0\, q/p\right)}{\left(1 + \varphi_1\, q_v/p_a\right)}$$ $$\ln\left[\frac{\left(1 - e^{(-d/d_0)}\right)}{E[\varphi_1]}\right] = \varphi_{12}\left(1 - e^{(-d_{tex}/d_{tex0})}\right)\left(\ln\left[\frac{1}{1 - Z/pwD}\right]\right)^n$$ $$n = \varphi_{10}\left(1 + \varphi_{11} \ln\left[d_{tex}/d_{tex_0}\right]\right)$$	
Braking on wet runway[2] $0 < s < 1$	Coefficient of braking friction in full skid on wet runway is modified empirically to fit measured data collected at Road Research Laboratory and NASA on single tyre.[3] Slip speed of footprint determines kinetic energy absorbed by tyre and kinetic pressure under tyre.	11
	$$\mu_{SLIP\ WET} = \frac{\mu_{REF}\left(1 - e^{\eta_2 s}\right)}{\left(1 + \left(\eta_0 + \eta_1 \frac{v^2}{2g}\right)\frac{p/p_a}{Z^{1/3}}\right)} \frac{\left(1 - \varphi_0\, q/p\right)}{\left(1 + \varphi_1\, q_v/p\right)}$$ $$\eta_2 = \left\{1 + \eta_{20}\left(\frac{q/p_a}{1 + q/p_a}\right)\right\}\left\{\frac{\eta_{21}}{\left(1 + q/p_a\right)}\right\}, \ \varphi_0 = \frac{2/\pi}{\left(1 + d_{tex}/d\right)}$$	

---

[2]   Note that values of μ_{max} follow from the equation given here. It is the maximum value of $\mu_{SLIP\ WET}$ for a given set of values of independent variables.

[3]   Kinetic pressure used in calculating the exponent η_2 is calculated at the axle translation speed. There is no variation in the exponent for a dry runway because the density of the contaminant is zero: thus, kinetic pressure is zero.

Braking on Ice and Snow-Covered Runway

Case	Description and Equation	Section
Static braking on ice- and snow-covered runway $V = 0$	Ice-covered runway assumed to be similar to dry runway. Reference coefficient of friction may be affected by ground temperature. Too little evidence available to establish correlation so reference coefficient of friction on runways covered by ice and compressed snow treated as a **statistical** variable. Reference coefficient of friction can be deduced for any tyre by selecting the type of surface and choosing a percentage point in the appropriate distribution. $$\mu_{0\ ICE} = \frac{\mu_{REF\ ICE}}{\left(1 + \eta_0 \dfrac{p/p_a}{Z^{1/3}}\right)}$$	12
Full skid on ice- and snow-covered runway $s = 1$	As for dry runways, it is assumed that η_0 in the equation for μ_0 represents absorption of strain energy in the footprint. To model effects of speed, it is assumed that kinetic energy affects the friction coefficient in the same way as strain energy. $$\mu_{SKID\ ICE} = \frac{\mu_{REF\ ICE}}{\left(1 + \left(\eta_0 + \eta_1 \dfrac{V^2}{2g}\right)\dfrac{p/p_a}{Z^{1/3}}\right)}$$	12
Braking on ice- and snow-covered runway[4] $0 < s < 1$	Coefficient of braking friction in full skid on icy runway is modified in the same way as for dry runways.[5] Slip speed of footprint determines kinetic energy absorbed by tyre. $$\mu_{SLIP\ ICE} = \frac{\mu_{REF\ ICE}\left(1 - e^{\eta_2 s}\right)}{\left(1 + \left(\eta_0 + \eta_1 \dfrac{v^2}{2g}\right)\dfrac{p/p_a}{Z^{1/3}}\right)}$$	12

In principle, the reference coefficient of friction, $\mu_{REF\ ICE}$, can be deduced from measurements of $\mu_{0\ ICE}$, $\mu_{SKID\ ICE}$ or $\mu_{SLIP\ ICE}$.

Where such measurements are available from an aircraft or ground-test machine, a deduced value of $\mu_{REF\ ICE}$ for any ice surface can be applied for any other tyre on that surface.

---

[4] Note that values of μ_{max} follow from the equation given here. It is the maximum value of $\mu_{SLIP\ ICE}$ for a given set of values of independent variables.

[5] Kinetic pressure used in calculating the exponent η_2 is calculated at the axle translation speed. There is no variation in the exponent for an icy runway because the density of the fluid contaminant is zero: thus, kinetic pressure is zero.

If no measured data are available, values may be deduced from

$$\mu_{REF\ ICE\ i} = \mathrm{E}\left[\mu_{REF\ ICE\ i}\right] + z\sigma\left[\mu_{REF\ ICE}\right] \text{ for } i = 1, 2 \text{ or}$$

$$\mu_{REF\ ICE_i} = 0.25\hat{T}^{1/2}\left(1 - 0.8\hat{T}\right) \text{ for } i = 3,$$

where $i = 1$: loose snow,
           $i = 2$: ice and compressed snow,
           $i = 3$ glare ice and
   $\hat{T} = 1 + T/50$ and T is measured in °C.

1. INTRODUCTION

Extensive research effort has been directed towards collecting information to show that braking friction on paved runways is adversely affected by contamination of all kinds. Over the years, this research has led to a substantial accumulation of data that leaves no doubt that contamination from precipitation is a major factor in loss of braking friction and hence in incidents and accidents. However, to date, no simple mathematical model has been developed that enables the quantification of these adverse frictional effects from a minimal set of parameters.

In response to a short-term requirement, a method was developed to predict the relationship between the braking performance on wet, paved runways for aircraft and that for ground vehicles (see Reference 1). This method is a statistical representation that radically simplifies a complex problem. It does provide, from minimal information, a satisfactory calculation of friction coefficient in the wet for all aircraft and ground vehicles operating on paved runways. It is based on the observation that the coefficient of braking friction in the wet may be represented by a relatively simple factor applied to the (given) coefficient of braking friction in dry conditions. This factor is a function of speed, tyre inflation pressure and depth of macro-texture of the runway surface.

Furthermore, the force ***normal*** to the plane of a yawed wheel behaves in a manner analogous to that generated ***parallel*** to the plane of a braked wheel. Thus, the method of Reference 1 was found to be equally applicable to ground-based machines that make use of yawed wheels to classify the friction characteristics of runways.

However, that method is not amenable to generalisation. Nor is it capable of predicting coefficients of braking friction on uncontaminated paved surfaces or on those contaminated with substances other than water of limited depth. In order to cover this less restricted case, it is essential to develop a mathematical model that is based more on physics and less on statistical observation.

This report shows how the (empirical) model has been developed and can be justified by reference to a wide range of experimental data. The model incorporates data from experiments as diverse as blocks of rubber sliding on glass to a large transport aircraft braking on a runway covered with up to six inches of snow. The structure of this report is designed to reflect the structure of the model.

This introduction gives an outline of the whole model and explains the foundation of the various formulations within the model. The modelling is dependent on knowledge of eight independent variables:

1. Depth of macro-texture
2. Depth of contaminant
3. Density of contaminant
4. Speed
5. Tyre inflation pressure
6. Vertical loading
7. Nominal tyre width
8. Nominal tyre diameter

Of these only 1, 2 and 3 are related to the runway and its condition. All the other quantities[1] are part of conventional ground performance calculations. Whilst it is not mentioned in the list, the mode of operation of the aircraft antiskid system is also needed: that is, the range of values of slip ratio over which it operates. This too is normally available or can be inferred from tests on a dry runway.

Sections 3 to 12 contain the core of the mathematical model. In addition to a statement of the mathematical description, each section contains extensive illustrations of the model in relation to experimental data. Furthermore, a statistical description of the relationship between the modelling equations and experimental data is given for every section. This statistical description is designed so that calculations can be made of the contribution of individual components of force to uncertainty in performance.

---

[1] Tyre inflation pressure is used as an absolute pressure throughout this report. Conventionally, it is quoted as a gauge pressure.

2. DESCRIPTION OF MODEL

2.1 General

When a flexible tyre is rolled and braked on a paved surface that is covered with either a fluid or a particulate substance, it is assumed that there are three sources for decelerating force:

1. Rolling resistance due to the absorption of energy in the tyre carcase;
2. Rolling resistance due to moving through or compressing the contaminant;
3. Braking resistance due to the frictional interaction between the tyre compound and the pavement.

Total force resisting motion – ignoring aerodynamic and impingement forces – is taken to be the simple sum of these three components with no cross coupling between the forces. This perception forms the basis of the approach adopted in constructing the various parts of the model described here. Furthermore, in order to preserve both simplicity and consistency, careful attention has been paid to ensuring that the more complex cases contain the less complex as defaults. For example, the case of slipping on a flooded runway defaults to static braking friction logically by setting speed and water depth to zero in the model.

This method of constructing the mathematical model has some consequences. First, rolling resistance, in as far as it derives from the energy absorbed in the tyre due to flexing in rolling, is dependent on the peripheral speed of the wheel. When the wheel is in a full skid, the peripheral speed is zero and there is no rolling resistance. That is, rolling resistance is perceived to be a function of slip ratio and forward speed. Although no great harm occurs if this is overlooked, it is well that any analysis accounts properly for all components of force.

Again, when rolling freely through such particulate matter as snow, there are two forces in addition to the rolling resistance just considered:

1. A force due to compressing the snow;
2. A force due to displacing the snow from the path of the wheel.

In the modelling described, this distinction is not explicitly recognised. Therefore, strictly, the modelling does not account properly for the case of a full skid in loose snow. It is contended, however, that the ploughing motion implicit in the modelling is a sufficiently large contribution to the total resistive force to offset this objection.

2.2 Section 3: Rolling Resistance on Paved Runways

Conventionally, in performance estimation, rolling resistance has been treated rather as a catchall to enable a balance of forces at, or near to, the unstick point. In general, this has resulted in the use of a constant value for rolling resistance coefficient that is invariant with speed for the whole aircraft. Although such an approach is wrong in principle, in practice it leads to no significant error, particularly because, in a take-off, forces from the power units are at least an order greater than rolling resistance force.

For the work undertaken here, details of the development and source of resistance may be important. Rolling resistance has therefore been treated in as appropriate manner as is possible. A model is provided that enables a precise calculation of coefficient of rolling resistance that is a function of speed, vertical load and inflation pressure. Because rolling resistance coefficient is a result of the energy produced by tyre flexing, no effect arises from the state of wetness of the runway.

2.3   Section 4: Decelerating Forces for Tyre Rolling Through Water or Slush

Treatments of this phenomenon have invariably run into difficulties. These have arisen from the nature of the treatments and the way in which fluid drag is affected by speed. Specifically, at low speeds, fluid drag varies approximately as the square of speed. This has led to the conventional treatment of using a constant value of drag coefficient and kinetic pressure to calculate drag. An area based on fluid depth and width of the intersection of the deflected tyre and fluid surface has been used in such treatments.

However, this approach is complicated and fails to account for the well-known tendency (see Figure 2.1) for drag to reach a maximum within the operational speed range. In order to account for this, the conventional approach has been modified. Drag coefficient has been correlated with kinetic pressure, tyre inflation pressure, tyre geometry and fluid depth. In addition, a reference area based on vertical load and inflation pressure has been used. This has resulted in a model that describes the motion of tyres that are used for ground vehicles and aircraft over the operational speed range.
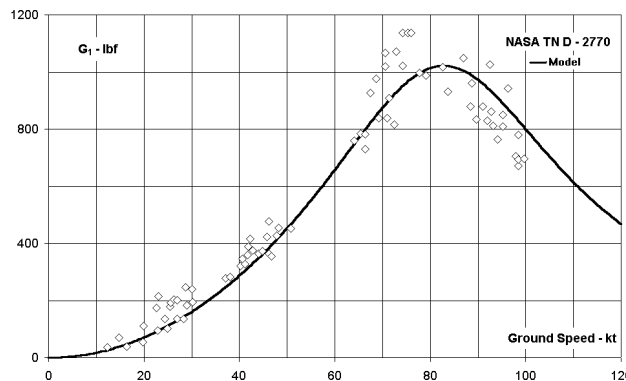
Figure 2.1: Effect of speed on fluid drag

2.4   Section 5: Decelerating Forces for Tyre Rolling Through Snow

The established model used to describe the force that resists the motion of an aircraft tyre when rolling through such a particulate medium as snow is based on the presumption that snow and water are similar substances. This approach leads to the expectation that the decelerating force is directly proportional to snow depth and the square of speed. Figure 2.2 is a typical example of data collected from unbraked rolling tests for an aircraft on a runway contaminated with loose snow.
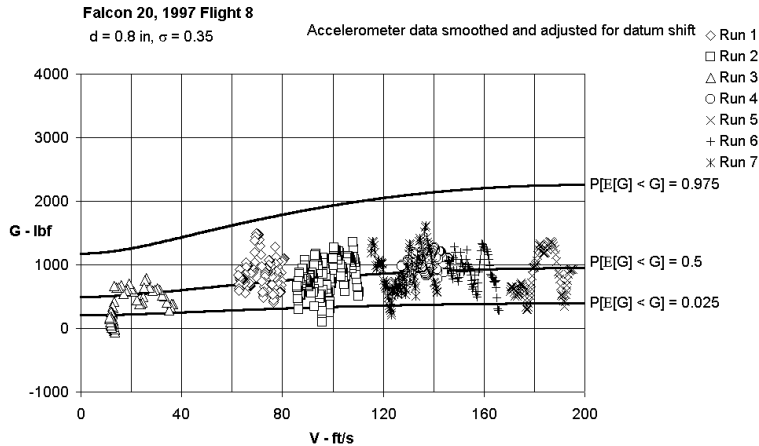
Figure 2.2: Decelerating force for aircraft rolling through snow

The effect of speed on decelerating force is almost negligible. In addition, there is a clear indication that there exists a positive value for decelerating force when speed is close to zero. In order to construct a more plausible model than that conventionally used, an analogy with motion through soft soils has been explored. A major difficulty was immediately encountered. In the modelling inferred from the soft-soil study, it was necessary to include both shear strength and shear modulus of the snow. In all the testing, that was to hand, the condition of the snow was described solely by its specific gravity. Now, snow is thermodynamically unstable and is susceptible to changes in mechanical properties even in the short term, due to the effects of wind and heat exchanges with the environment. Specific gravity is, therefore, by no means the only determiner of mechanical properties. The relevant mechanical properties have therefore been inferred from the testing. Although a strong dependence on specific gravity has been identified, the residuals about the correlation are the subject of a statistical study. Nevertheless, there is adequate evidence to enable a sufficiently precise estimate to be made of the effects of loose snow on decelerating force when rolling and braking.

2.5   Sections 6, 7 and 8: Coefficient of Braking Friction on Dry Runways

All attempts that have been made to formulate prediction methods for tyre-runway friction coefficients have been based on experimental evidence without a firm theoretical framework. Some workers conducted experiments with rubber blocks on smooth surfaces and demonstrated coefficients of braking friction to be dependent on both the normal load and the mean pressure in the interface. These observations have been used here to form the basis of a mathematical model.

It is presumed that there exists a reference coefficient of friction for a specific rubber compound sliding on a typical, dry runway surface. From this, the model builds from the static case – when the friction coefficient derives from the absorption of strain energy in the tyre – to the case of skidding at speed. In this latter case, the friction coefficient is presumed to arise from the absorption of both strain energy and kinetic energy in the footprint. The effect of slip ratio is accommodated using an exponential factor.

5

2.6 Section 9: Pressures Under Footprint of Tyre on Wet Runway

Observations of the pattern of wetting in tyre footprints moving on a variety of surfaces led early investigators to the concept of the "three-zone" model. In this formulation, the most forward zone of the footprint is perceived to be where the impact of the tyre on the surface fluid is sufficient to overcome the inertia of the fluid. Fluid is forced from the path of the tyre either as spray or into the drainage paths provided in the tyre tread or the paved surface. In the second zone, conditions are in transition and a rapid outflow of fluid is prevented by viscous effects. The third zone is predominantly dry and it is assumed that all braking friction is generated in this region. Relative sizes of the three zones depend on many factors that include the following:

- surface texture
- fluid depth, density and viscosity
- tyre construction, tread pattern and inflation pressure
- vertical load
- time for a tread element to pass through the contact area

Pressures in the three zones are modelled here from experimental evidence and are used in predicting coefficients of braking friction on wet and flooded runways.

2.7 Sections 10 and 11: Coefficient of Braking Friction on Wet Runways

In the context of the model presented in this report, wet refers to all conditions where a runway is contaminated by a fluid. This includes slush after account has been taken of the squeezing of the air from the mixture and the melting of the ice under the footprint. Coefficient of braking friction for skidding in the wet is related to that in the dry by means of a factor. This factor depends on the extent and nature of contamination together with runway texture depth and tyre parameters. These include mean pressures under the footprint. The effect of slip ratio is accounted in the same manner as for the case of a dry runway. However, the exponential function includes a variation with speed and density of contaminant. When defaulting from wet to dry, it is necessary to set both the density and depth of contaminant to zero. Table 2.1 shows the range of the parameters covered in the experimental verification of the model.

Table 2.1: Range of variables covered in verifying model of braking friction in the wet

Texture depth (in)	$0.0039 \leq d_{tex} \leq 0.0669$
Water depth (in)	$0.02 \leq d \leq 0.15$
Inflation pressure (psig)	$25 \leq p_i \leq 260$
Speed (kn)	$0 \leq V \leq 100$
Normal Load (lbf)	$2000 \leq V \leq 20000$

2.8 Section 12: Coefficient of Baking Friction on Ice or Snow

It is assumed that there is no difference in principle between the frictional interaction of tyre compounds and ice and that between tyre compounds and wet or dry runways. In this context, compacted snow is treated as a type of ice, whilst the passage of a tyre through loose snow is

assumed to leave a track of loosely compacted snow that behaves like a further type of ice. There are, therefore, three types of "ice" that are distinguished statistically when braking action is considered.

The statistical distinction is made through a reference coefficient of friction. This parameter is described for each type of ice as a normally distributed statistic with a mean value and a standard deviation.

Furthermore, it is shown that the reference coefficient of friction can be deduced from the readings of a James Braking Decelerometer or *vice versa*. Thus, it can be concluded that the reference coefficient of friction is the Friction Index that has been sought for so long.

3. ROLLING RESISTANCE ON PAVED RUNWAYS

In principle, rolling friction coefficient is a minor contributor to the longitudinal force balance for aircraft operations. In a ground-run to un-stick, the contribution of thrust to the longitudinal balance of forces is at least an order of magnitude greater than that of rolling friction. It is therefore often assumed sufficient to use a single value for coefficient of rolling friction, which is invariant with speed, tyre loading and inflation pressure. That value is often assigned solely to achieve a close approximation to measurements of ground-rolling distance at a specified weight. For this reason, the value chosen is often more nearly appropriate to a speed near to that for lift-off at the specified weight: significant details in the time history of acceleration can sometimes be obscured.

Of course, in an operational context, such effects are rarely of importance. However, in the process of research, fine details are often crucial. In particular, an empirical model is to be sought for the coefficient of friction when slipping in deep water. A review of the available data suggests that it is probably appropriate to formulate that model so that the coefficient of rolling friction is accounted. It is for this reason that rolling friction has been studied, a correlation produced and that correlation recommended as part of the empirical model for aircraft tyres operating on paved surfaces.

3.1 Modelling

The majority of testing for rolling resistance has been done on automobile tyres; the workers[2] in this field have recognised that their experimental correlations are probably inapplicable to the specific design of tyres used for aircraft. Data for aircraft tyres operating in dry and damp conditions from Reference 3 and in dry conditions from Reference 4 have been used to produce a relationship that is believed to be generally applicable. The parameters used have not been derived from any coherent dimensional or similarity analysis. The approach is, therefore, empirical but includes suggestions contained in the literature that has been reviewed for the project.

A parametric representation of the data is shown in Figure 3.1. Also shown in that figure is the correlation,

$$\frac{p/p_a}{Z^{1/3}}\mu_{ROLL} = \zeta_0 + \zeta_1 \frac{V^2}{2g} \qquad\qquad 3.1$$

where $p = p_i + p_a$, $\zeta_0 = 0.0062$ lbf$^{-1/3}$ and $\zeta_1 = 2.31 \times 10^{-5}$ lbf$^{-1/3}$ ft^{-1}.

This equation describes the data so that the scatter, expressed in terms of friction coefficient, has a standard error $\sigma[\Delta[\mu_{ROLL}]] = 0.0047$. If the correlation is used to obtain a value (see Reference 5)

---

[2]   Reference 2 contains a compendium of data for automobile tyres. There are some data collected in the 1930s for aircraft style tyres. These can be correlated using the approach adopted here. However, the values of rolling friction are much lower than those collected in References 3 and 4. The information is not considered relevant to "modern" tyres for use on aircraft.

for $\mathrm{E}[\mu_{ROLL}]$ then, because the correlation is based on 61 measurements, the standard error of such a value [4] is $0.0047/\sqrt{61} \approx 0.0006$.

The three sets of data on which the model is based are shown in Figures 3.2 to 3.4. Figure 3.5 is a plot of the distribution of the deviations of the measurements from the model.

3.2   Discussion

An estimate of the precision of measurements is given in none of the sources of data. It is therefore not possible to make an *a priori* estimate of the probable extent of "scatter" about any correlation that may be attempted. In the absence of such an estimate, reliance has to be placed on the plausibility of both the parameters used in the correlation and in the extent of the residual scatter.

The parameters used in the correlation of Equation 3.1 are unexceptional. The ratio of the inflation pressure to the cube root of the load has been suggested by researchers in the field of rubber technology albeit in relation to skidding. The specific kinetic energy developed by the tyre is an obvious parameter to attempt to relate to the heat energy absorbed in the carcase. It is unfortunate that the data sets available are limited in the range of normal (to runway) loading and of inflation pressure. However, the modelling matches the available data and is unlikely to lead to gross errors even when extrapolated to encompass the full range of operational (and research) conditions.

Furthermore, there is no indication that runway dampness has any significant effect on rolling friction. The data for the case that p_i = 90 psig are plotted in Figure 3.3. These measurements for dry and damp conditions could be interpreted to suggest a difference between the two cases. However, a *t*-test reveals that the difference is not significant at the 10% level. Data for inflation pressure so that p_i = 150 psig (see Figure 3.2) show that there is no question of a difference between tests in the dry and damp.

Figure 3.5 shows the quality of the fit. The standard error of the measured rolling-friction coefficient about the correlation is less than one half of one per cent of the tyre normal load. Because the correlation is based on some 60 measurements, any estimate of rolling friction from the correlation, used as a model, may be expected to be precise in a practical sense. The correlation is therefore acceptable as a credible model for coefficient of rolling friction for aircraft tyres under operational and research conditions.
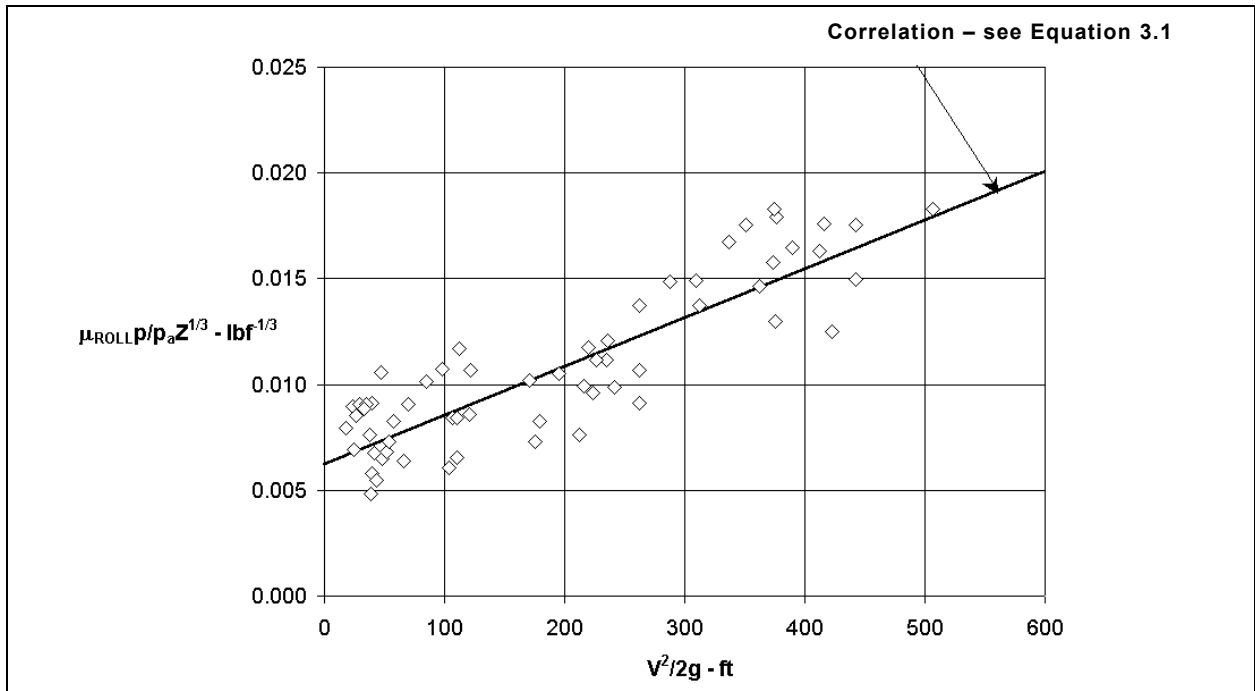
Figure 3.1: Correlation of coefficient of rolling friction with inflation pressure, vertical load and speed
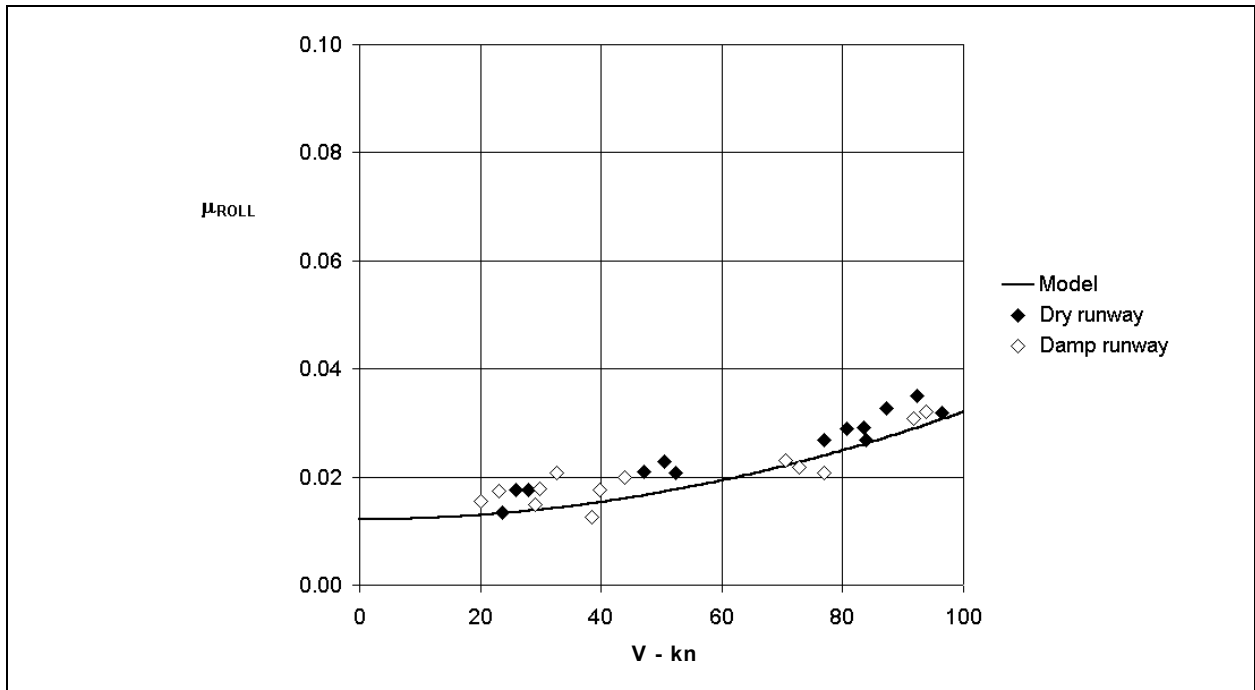
Figure 3.2: Effect of speed on coefficient of rolling friction: p_i = 150 psig, Z = 10500 lbf
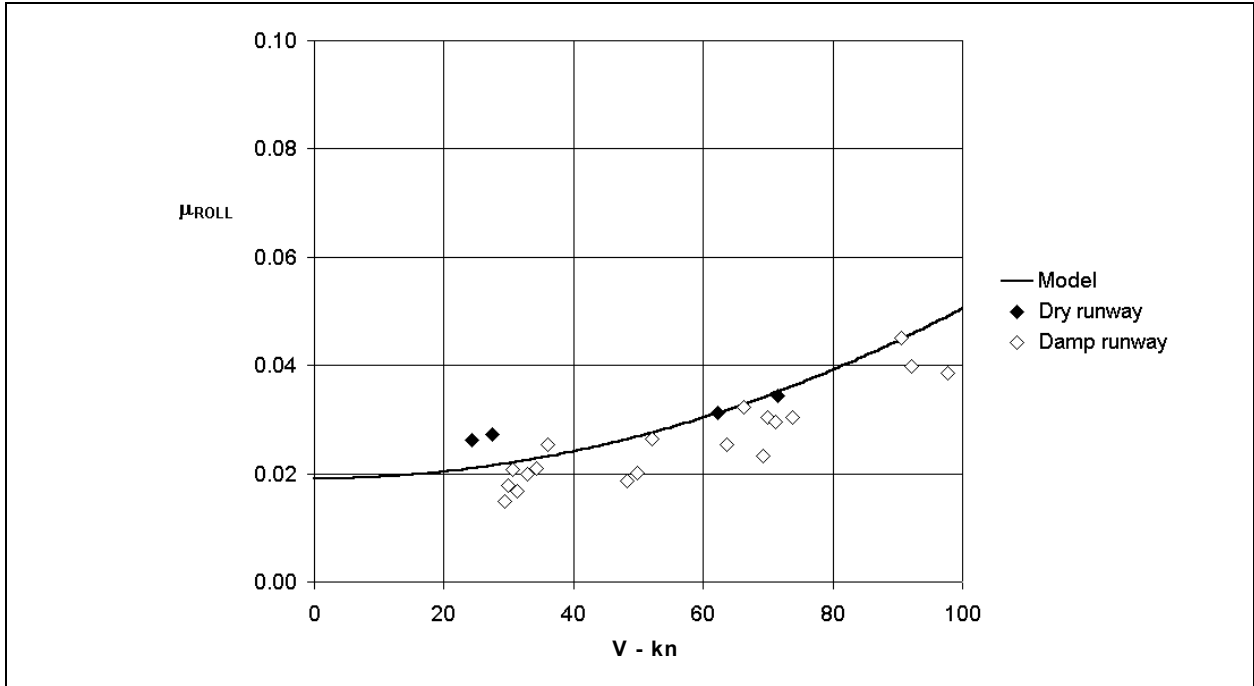
Figure 3.3: Effect of speed on coefficient of rolling friction: $p_i = 90$ **psig,** $Z = 10500$ **lbf**
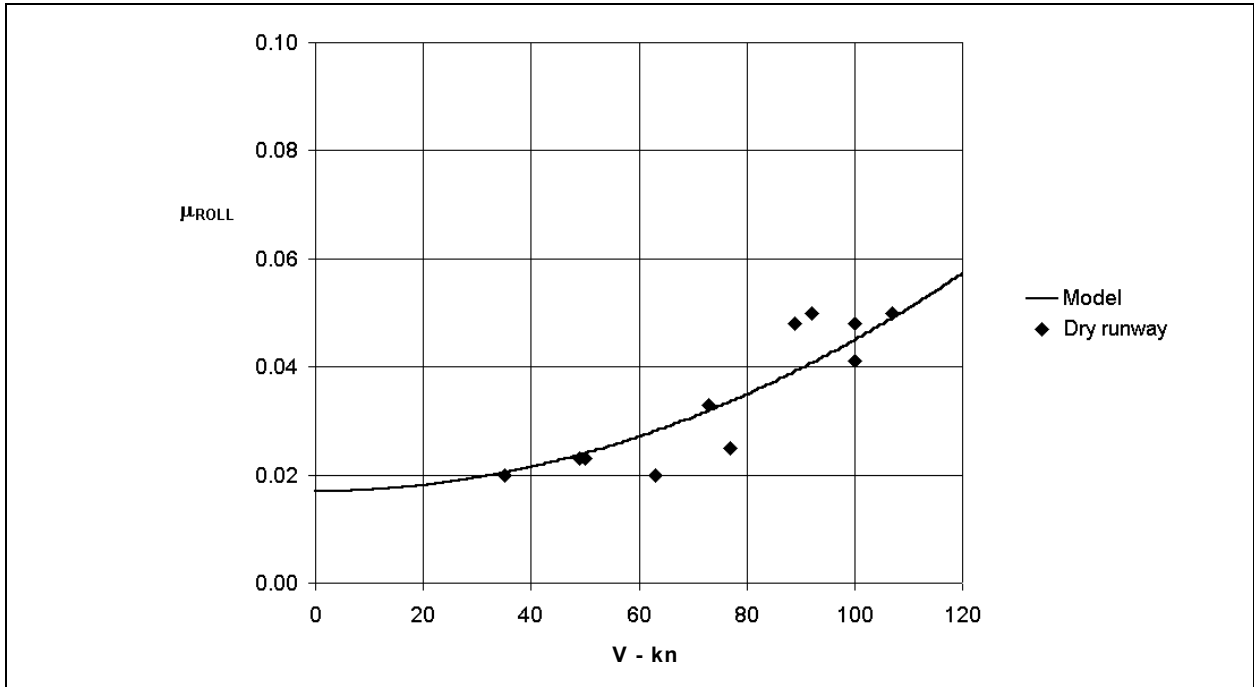
Figure 3.4: Effect of speed on coefficient of rolling friction: $p_i = 110$ **psig,** $Z = 12500$ **lbf**
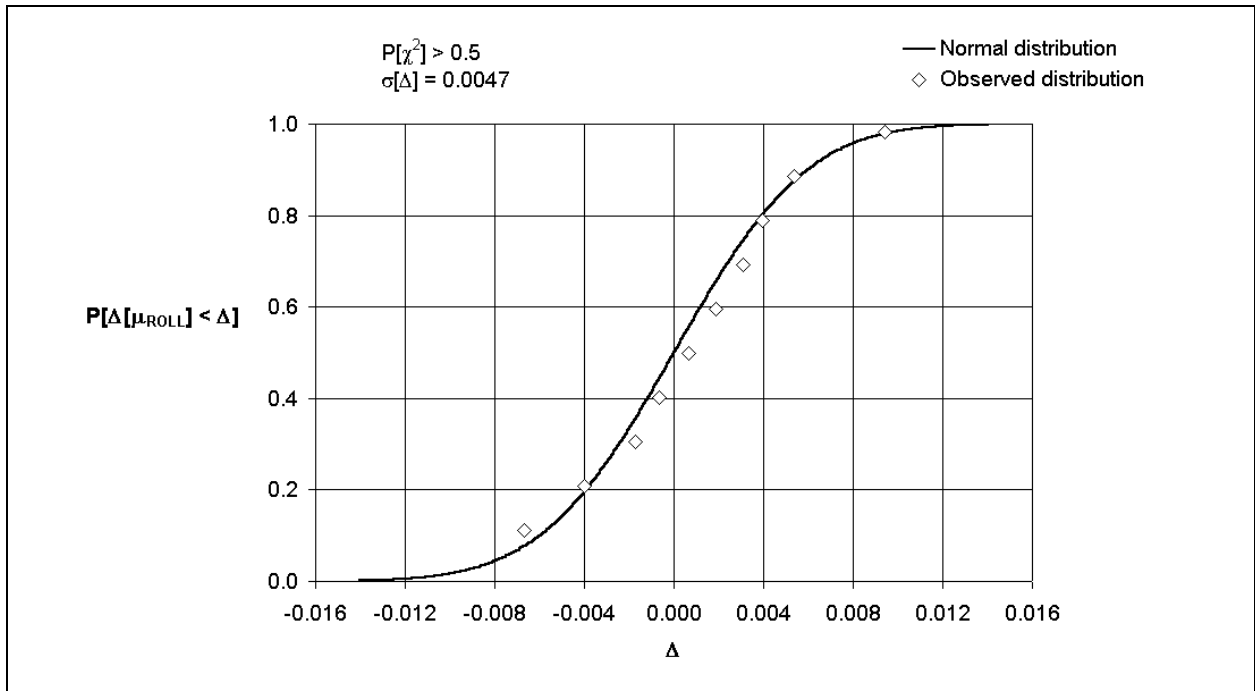
Figure 3.5: Distribution of measured values of coefficient of rolling friction about model

4. DECELERATING FORCES FOR TYRE ROLLING THROUGH WATER OR SLUSH

The motion of a pneumatic tyre, when rolling freely through surface water, is resisted by two significant forces: a frictional force arising from more or less dry contact with the surface and a fluid dynamic force arising from the impact of the tyre on the water. Frictional rolling resistance for aircraft type tyres is treated in Section 3. In this Section, the fluid dynamic (decelerating) force generated by aircraft type tyres is considered.

Experimental evidence can be drawn upon to show that, for a given style of tyre, the fluid dynamic force is affected by at least the following variables.

- Speed
- Depth of contaminant
- Density of contaminant
- Tyre inflation pressure
- Vertical loading
- Tyre width and
- Tyre diameter

Attempts have been made to analyse the problem in terms of a drag coefficient defined on an area determined by the depth of the contaminant and the width of the tyre at its intersection with the surface. These attempts have all been hindered by the tendency, as speed increases, for tyres to rise in the surface contaminant, eventually to lose direct contact with the surface and thus, to aquaplane. The effect of this sequence of events on "drag coefficient" is shown in Figure 4.1. Further difficulties arise in this modelling when consideration is given to the transition from the region where the drag coefficient is almost constant to the regime beyond a characteristic speed where both drag force and drag coefficient diminish.
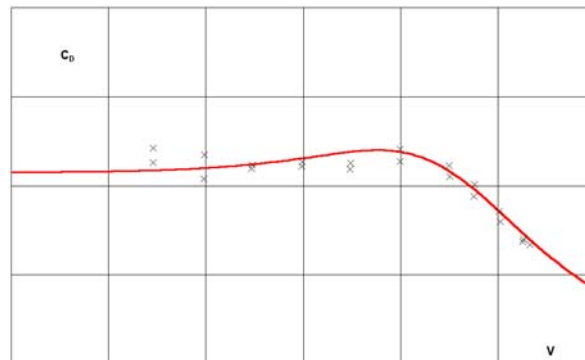
Figure 4.1: Effect of speed on drag coefficient

Efforts to relate phenomena associated with fluid dynamic drag and lift to the conventional aquaplaning speed have also been frustrated by at least two major obstacles. First, the relationship generally used to calculate aquaplaning speed is inappropriate for low inflation pressures; second, depth of contaminant has an effect on the speed at which fluid dynamic drag

reaches a maximum. No account of depth is taken in the conventional formulation for aquaplaning speed.

In summary, there is no simple theory that can be used as a framework for describing the effect of the variables listed above. This is a consequence of the complex interactions between the rigid ground, the elastic tyre and the fluid. In conventional aeronautics, the geometries considered are all more or less rigid and there is generally no constraint on the direction that deflected fluid can assume. Furthermore, although conventional hydrodynamic theory deals successfully with free surfaces, the depth of fluid encountered on runways is so limited, that the conventional assumptions are almost certain to be violated. In the absence of a theoretical framework, the correlation process evolved and presented here for relating fluid dynamic forces to the seven variables listed above, is entirely empirical.

Such standard concepts as drag coefficient have been used – albeit, in this study, the lateral dimension used to define reference area is not that conventionally adopted. Furthermore, the ratio q/p is not usually used in the calculation of drag coefficient. It is, however, a convenient way of relating pressure forces and inertial forces and in that sense is analogous to the square of Mach number as used in conventional aeronautics.

A mathematical model is described that enables the calculation of the decelerating force exerted on a single wheel rolling freely through a fluid medium. The majority of the data used to establish the mathematical model were collected from tests in which the contaminant was water. However, some of the data used were collected from tests in which the contaminant was a mixture of water and crushed ice. The specific gravity of these mixtures covers a range that encompasses the values appropriate to natural slush. It is therefore presumed that the model may be applied to motion through natural slush.

Although the model is purely empirical, it has the merit of simplicity, precision and statistical integrity. In addition, it is based upon data that cover a substantial range of fluid depth, specific gravity, tyre fineness ratio, inflation pressure, vertical loading and speed. However, no attempt has been made to account for forces other than those due to the displacement and compression[3] of fluid. The effect of spray impingement on undercarriages or any other part of an airframe is not addressed. Study of the effects of slip ratio may be possible in the future should data from some other available references be found suitable.

Initially, the mathematical model is defined without comment. Then, a derivation of the effect of compressing slush is outlined. Some of the more important aspects of the model, including the range of applicability, are considered. Finally, the data in the six sources are considered in relation to the mathematical model. This discussion also covers the statistical properties of the correlation, which are read across into the model.

---

[3] In this study, slush is assumed to be a compressible mixture of water, ice and air.

4.1 Model

The following set of equations defines fully the means of calculating drag due to rolling in water or slush. A distinction has to be recognised between ribbed-tread and smooth-tread[4] tyres. However, this distinction is solely in the numerical constants that occur in the equations. In all aspects of the *form* of the model, there is no distinction to be made between ribbed-tread and smooth-tread tyres.

$$G_1 = \frac{1}{2}\sigma\rho d \left(\frac{Z}{p}\right)^{1/2} V^2 C_D + \gamma_0 w D \sigma \left(pZ\right)^{1/2} d \ln\left[\frac{1}{\sigma}\right] \qquad 4.1$$

$$C_D = \xi_0 \left(\frac{1+\sin[\theta]}{2}\right) + \xi_1 \frac{\cos^4[\theta]}{4} + \xi_2 \frac{\cos^2[\theta]}{4}\left(1-\sin[\theta]\right) \qquad 4.2$$

$$\theta = \tan^{-1}\left[\left(1-q/p\right)\right] \qquad 4.3$$

For ribbed-tread tyres, the following relations hold:

$$\xi_0 = \xi_{01}\left(\frac{w}{D}\right)^2 \qquad 4.4$$

$$\xi_1 = \xi_{11}D^{3/4}\left(\xi_{12}+\frac{d}{w}\right)\left(\frac{D}{w}\right) \qquad 4.5$$

$$\xi_2 = \frac{\xi_{21}}{w\left\{\xi_{22}\left(1-\left(\frac{D}{\xi_{23}}\right)^2\right)+\frac{d}{w}\right\}} : \xi_2 \geq 0. \qquad 4.6$$

4.2 Effect of Slush on Drag Due to Fluid Displacement

In the course of the analysis leading to the establishment of a mathematical model, it became clear that specific gravity, by itself, was not sufficient to account for the effect of slush. An effect in addition to that accountable with specific gravity was marginally noticeable at the lower normal loads reported in Reference 9. However, at the larger values of normal load, the effect was so pronounced that the integrity of the set of data could have been doubted. However, the tests had been conducted so that the water and slush information had been collected in the same run; there could, therefore, be no real doubt concerning the integrity of the data. In an attempt to reconcile the data sets, the following was considered.

---

[4] In the current version, smooth tread data have not been fully analysed so the modelling equations are not given.

17

It is generally accepted that slush is a compressible mixture containing, in the main, water, ice and air. Assuming this compressible mixture is "crushed" by the passage of a tyre then, the volume of slush to be compressed in one revolution of the wheel is

$$v_o = \pi D d w_{\text{max}} \qquad\qquad 4.7$$

Work done (per revolution) in compressing the fluid is

$$W = \int_{v_c}^{v_0} p \, dv \qquad\qquad 4.8$$

Assume $pv = \text{constant}$, then

$$W = \text{constant} \times \ln\left[v_0 / v_c\right] \qquad\qquad 4.9$$

Now, mass of fluid is conserved, so that

$$\rho_1 v_0 = \rho_c v_c \qquad\qquad 4.10$$

Thus

$$W = \text{constant} \times \ln\left[\rho_c / \rho_1\right] \qquad\qquad 4.11$$

Let pressure of the slush under the footprint after compression be the inflation pressure *p*, it follows that

$$\text{constant} = \pi D d w_{\text{max}} \, p \, \rho_1 / \rho_c \qquad\qquad 4.12$$

and, therefore

$$W = \pi D d w_{\text{max}} \, p \ln\left[\rho_c / \rho_1\right] \rho_1 / \rho_c \quad \text{per revolution} \qquad\qquad 4.13$$

Power absorbed is work done per unit time and in this case is given by the product of the work done per revolution and the number of revolutions per unit time. That is

$$P = \frac{WV}{\pi D} \qquad\qquad 4.14$$

However, power is also the product of force and speed; thus, the force required to compress the slush is

$$G_C = \frac{W}{\pi D} = \frac{\rho_1}{\rho_c} d w_{\text{max}} \, p \ln\left[\rho_c / \rho_1\right] \qquad\qquad 4.15$$

18

Now, maximum width of the tyre in the compression motion is related to tyre geometry and footprint area. Consider that the footprint is intermediate between a rectangle and an ellipse. The footprint area is given by

$$S = Z/p = kab \qquad\qquad 4.16$$

where a is half maximum footprint length
              b is half maximum footprint width and
              k is a factor so that $\pi \leq k \leq 4$.

Equation 4.16 can be recast in terms of the fineness ratio of the footprint

$$\frac{Z}{p} = kb^2 (a/b) \qquad\qquad 4.17$$

Rearranging

$$b = \frac{1}{k^{1/2}} \left(\frac{b}{a}\right)^{1/2} \left(\frac{Z}{p}\right)^{1/2} \qquad\qquad 4.18$$

Assuming that w_{max} is related to b, then

$$w_{max} = \xi_3 \left(\frac{Z}{p}\right)^{1/2} \qquad\qquad 4.19$$

where the variable ξ_3 is a function of tyre geometry and may be obtained by studying the available experimental data.

If the assumption is made that the final density of the compressed slush is that of water, then the relation for the compression force in Equation 4.15 can be written

$$G_C = \xi_3 \sigma (pZ)^{1/2} d \ln[1/\sigma] \qquad\qquad 4.20$$

This expression can be applied to the experimental data to enable ξ_3 to be derived. A relation has been found which describes the three experiments adequately:

$$\xi_3 = \gamma_0 wD \qquad\qquad 4.21$$

where $\gamma_0 = 0.2$ per ft^2.

When this relationship is used in the correlation process, data measured in slush-like media and data measured in water can be reconciled.

4.3   Basis of Model

The model presented in Equation 4.1 is an empirical representation of the fluid dynamic drag force on a single tyre rolling freely over a surface covered with a shallow layer of liquid or a slush-like medium. It has been based on the series of tests reported in References 3, 8 and 9. In addition, the effect of the slush-like medium has been obtained from the tests reported in References 6 and 9. The wide applicability of the modelling has been further demonstrated by comparison with the data sets reported in References 6 and 7. These latter sets were not used in the construction of the model because water depth, in particular, was not defined precisely.

In the process of modelling, it has been assumed that the fluid dynamic drag force can be fully defined in terms of the seven variables listed at the beginning of this section. The ranges of these variables as used to define, or confirm, the model are as follows in Table 4.1.

Table 4.1: Ranges of variables over which model defined and confirmed

Variable	Range
Speed	$15 < V < 120$ kn
Depth of contaminant	$0.1 < d < 2$ in
Specific gravity of contaminant	$0.5 < \sigma < 1$
Tyre inflation pressure	$20 < p < 350$ psig
Vertical loading	$50 < Z < 10200$ lbf
Inflated tyre width	$2.35 < w < 13.5$ in
Inflated tyre diameter	$8.9 < D < 43$ in

Typically, fluid dynamic drag for a tyre rolling at low speed in a shallow layer of fluid varies approximately with the square of speed. However, as speed increases towards what has been termed a *critical* speed, this drag reaches a maximum. At speeds greater than the critical speed, the drag decreases in a way that depends on the other six variables listed in Table 4.1. In order to model these trends over the full range of the variables covered in the database, it has been found necessary to depart from what has become established practice in this field of study. Thus, instead of defining drag coefficient on a precisely defined area – the product of contaminant depth and the width of the deflected tyre at the surface of the fluid – a more general, ***reference***, area has been used. This area is the product of fluid depth and a reference length calculated by taking the square root of the footprint area.

In Section 9, it is shown that the mean bearing pressure in the footprint area under static conditions, is closely approximated by tyre inflation pressure – expressed in ***absolute measure***. Thus, the (static) area of the footprint is given by

$$S_F = Z/p \qquad\qquad 4.22$$

Therefore, the (convenient) reference length is $(Z/p)^{1/2}$ and the reference area for drag coefficient follows as

$$S = d\left(Z/p\right)^{1/2} \qquad\qquad 4.23$$

Customarily, drag coefficient for a tyre rolling in shallow surface water has been treated as a constant up to the characteristic speed. Figure 4.1 illustrates that this is a reasonable approximation. Various approaches have been adopted for speeds beyond the characteristic speed. In the modelling developed here, drag coefficient is treated as a variable throughout the speed range. Such a treatment would normally rely upon the establishment of a similarity analysis that sought to determine a transformation of geometric and fluid properties that described the variation of drag coefficient over the operational envelope as a set of ***non-dimensional*** relations. This approach has not been fully followed; on the contrary, reliance has been placed on identifying a series of curves based around a transformation of speed. Then, coefficients in the fitted curves have been related to geometric parameters.

Choice of speed related variable was made intuitively. Kinetic pressure is a conventional variable to choose. In addition, tyre inflation pressure (in absolute measure) is taken to be a valid and convenient variable with which to create a non-dimensional kinetic pressure.[5] Now, the ratio q/p has a potential range so that $0 \leq q/p \leq \infty$. When fitting curves involving variables of such a range it is often useful to work in terms of the sine or cosine of the inverse tangent. In this case, the parameter $(1-\sin\theta)/2$, where $\theta = \tan^{-1}(1-q/p)$ has been chosen. Thus, the parameter varies so that $0.146 \leq (1-\sin\theta)/2 \leq 1$ as the ratio q/p varies from 0 to $+\infty$. This artifice has enabled the identification of a relatively simple set of relationships.

4.4   Reliability of Model

In the figures discussed in this sub-section, all the solid lines have been calculated from the modelling described in sub-sections 4.1 and 4.2. Thus, the drawn curves are not "fitted" to the individual sets of data.

Figures 4.2, 4.3 and 4.4 show the effects of water depth, inflation pressure and tyre load on fluid dynamic drag over a range of speed for a small, ribbed tyre in a test rig. The measured data have been adjusted for an approximation to the friction drag between the wheel and the belt. The model describes the data with adequate precision. The characteristics of the variation of drag with speed exhibited in the measured data are well described with the sole exception of the measurements at 20 psig in Figure 4.4, at speeds greater than 70 feet per second. There is no indication in the reference that there is any unique feature in this particular test. Consequently, no explanation other than transducer malfunction is offered here, for the departure of the model from this set of test data. In defence of the model, the behaviour at low speed for this specific case is predicted equally as well as in all other cases.

The data shown in Figure 4.5 is the standard set of information for a full-scale aircraft tyre. Again, the mathematical model describes the trends in the set with a precision that reflects the

---

[5]   In fact, a customary approach to correlation has been to use the ratio V/V_C where V_C has been identified as a function of inflation pressure (in relative measure).

scatter in the measurements. More importantly, these data show that the modelling confirms that there is a consistency between small and large tyres.

Similarly, the effect of tyre pressure on the drag force generated in water by aircraft tyres is evident by comparing Figures 4.5 and 4.6, which show tests at the same water depth and similar vertical loadings. The model faithfully reproduces the observed increase in drag force that arises from a reduction in inflation pressure. The non-linear effect of water depth, which appears in the model from the inverse dependence of ξ_2 on depth, is demonstrated in the data shown for the Canberra aircraft in Figures 4.6 and 4.7. The effect is not great; in fact, it is not at all obvious from Figure 4.2. Given only the data from the small tyre tests, it is easy to see how a linear dependence on depth could be built into an empirical modelling based on constant drag coefficient.

Figures 4.8 and 4.9 contain data that have not been used to construct the model. The reason for not including these data arises from the imprecise definition of water depth in the experiments. However, close inspection of the presentation reveals that the model reflects adequately the trends with water depth. It is satisfying that the effect of tyre pressure is reflected so well in both these data and the model. There is clear evidence in the measurements that a maximum value for drag is reached at the lower of the two pressures tested – 115 psig. No such maximum can be detected at the higher pressure – 350 psig – for the range of ground speed covered in the experiment.

Figures 4.10 to 4.14 show the relative effect of slush over a wide range of the independent variables. As in the case of water, the model reflects the measured trends consistently. Unfortunately, the range of speed covered in the testing is insufficient to demonstrate the existence of the maximum value in drag force when rolling through slush. Thus, there is this one small area of study that needs to be addressed in order to confirm fully the current modelling.

4.5   Statistics of Correlation

Decelerating force is the dependent variable which is the subject of all the experiments considered in formulating the mathematical model. Thus, because each individual experiment is established to consider a specific range of force, the precision with which the forces are measured varies from experiment to experiment. In order to formulate an uncertainty appropriate for the whole range of the current model it is therefore necessary to find a transformed value of force that exhibits a measure of consistency for all the experiments. An understandable choice would be, of course, drag coefficient. However, drag coefficient is notoriously imprecise at very low speeds because it is defined on the inverse of the square of speed. Thus, any uncertainty in force *measurement* is magnified when a force *coefficient* is formed.

Another possible parameter is the drag per unit reference area or *drag pressure*. This quantity is defined as pG_1/Z. The difference in measured drag pressure and that calculated from the model is

$$\Delta\left[pG_1/Z\right] = \mathrm{E}\left[pG_1/Z\right] - \mathrm{M}\left[pG_1/Z\right]\qquad\qquad 4.24$$

The distribution of this parameter is symmetric about zero with a standard error of 1035lbf/ft^2 for the 376 measurements that have been used to establish the model (see Figure 4.15). However, the distribution does not conform to the standard normal distribution. Uncertainty statements for non-normal distributions are not directly usable in conventional methods. To enable a usable statement to be made about the uncertainty of drag pressure (calculated from the model) the distribution of $\Delta\left[p_1 G_1 / Z\right]$ needs to be transformed so that a normal distribution results.

Now, the standardised variable

$$\Delta' = \frac{\left(\Delta - \overline{\Delta}\right)}{\sigma[\Delta]} \qquad\qquad 4.25$$

can be transformed to

$$\hat{\Delta} = 2.88 \frac{(-1)^n \Delta'}{(1+\Delta')} : \; n = 1, \; \Delta' < 0; \; n = 0, \; \Delta' \geq 0. \qquad\qquad 4.26$$

Using a χ^2-test at the 10% level of significance, this variable conforms to the standard Normal distribution. The 2.5% and 97.5% points of the standard Normal distribution are ± 1.96. Thus, when $\hat{\Delta} = 1.96$, $\Delta' = 2.13$ and the uncertainty in drag pressure at the 95% level of confidence is

$$U[\Delta]_{0.95} = \pm 2.13 \times 1035 = \pm 2205 \; \mathrm{lbf}/\mathrm{ft}^2 \qquad\qquad 4.27$$

The correlation is based on 376 measurements; the uncertainty in drag *pressure* derived from the model is therefore $\pm 2205/\sqrt{376} = \pm 114 \; \mathrm{lbf}/\mathrm{ft}^2$ at the 95% level of significance. In order to estimate the uncertainty of a calculated drag *force*, it is necessary only to know the inflation pressure (in absolute measure) and the normal load on the tyre.

Thus,

$$U[G_1]_{0.95} = \pm 114 \times \frac{Z}{p} \; \mathrm{lbf} \qquad\qquad 4.28$$

is a sufficient definition of the uncertainty of a calculated drag force when rolling through a fluid-like medium. This formulation can be used in standard methods for predicting the uncertainty of estimates of the ground performance of aircraft.
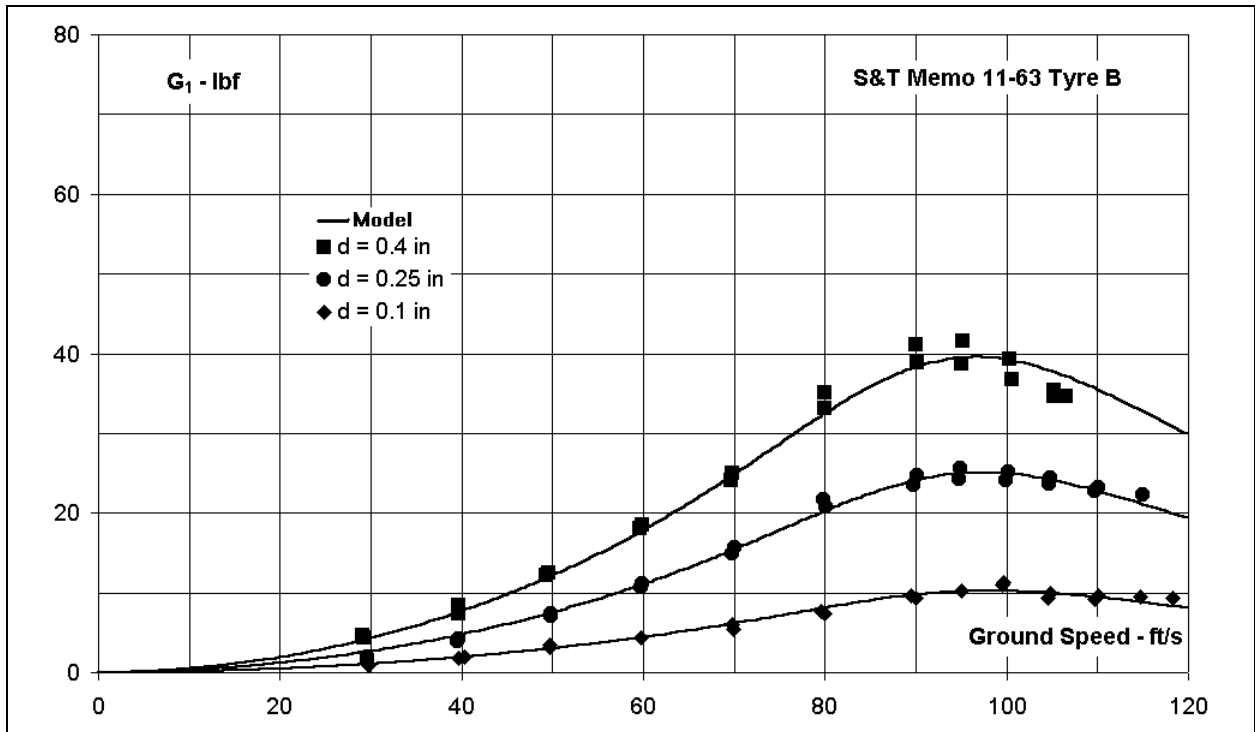
Figure 4.2: Effect of speed on drag force in water – small tyre in test rig:
Z = 200 lbf, p = 30 psig
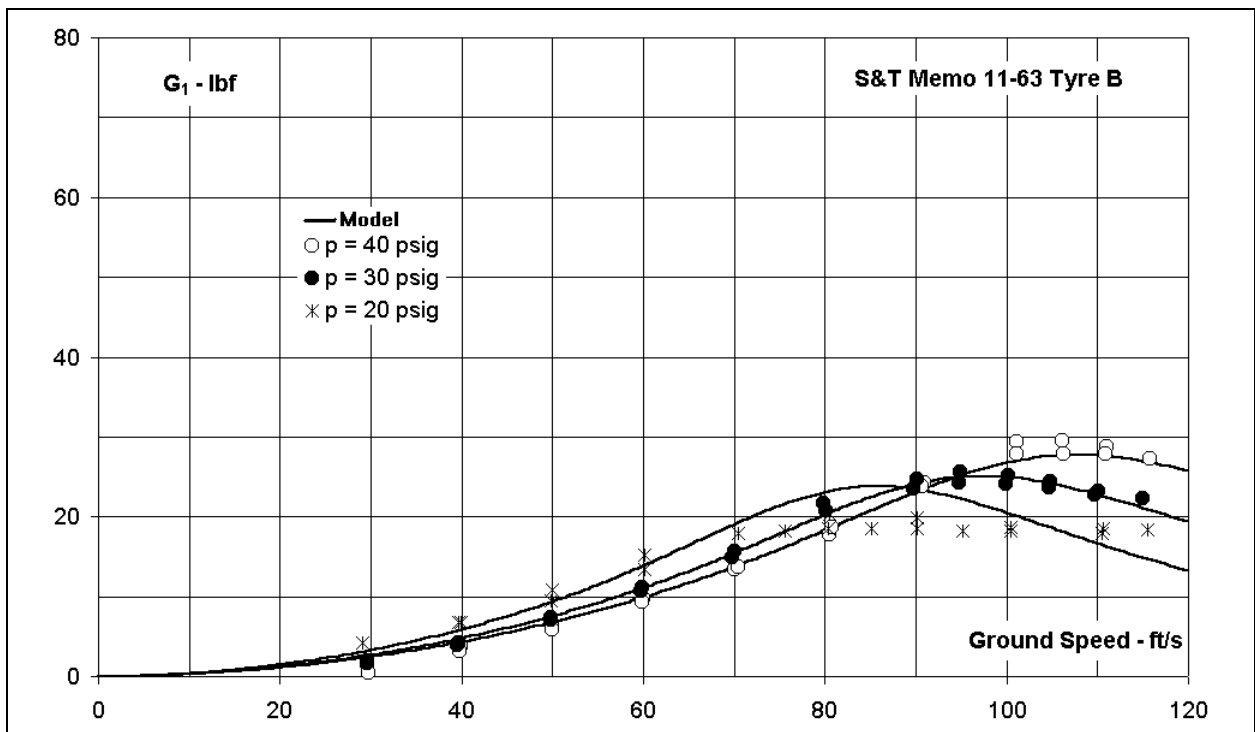
Figure 4.3: Effect of speed on drag force in water – small tyre in test rig:
Z = 200 lbf, d = 0.25 in
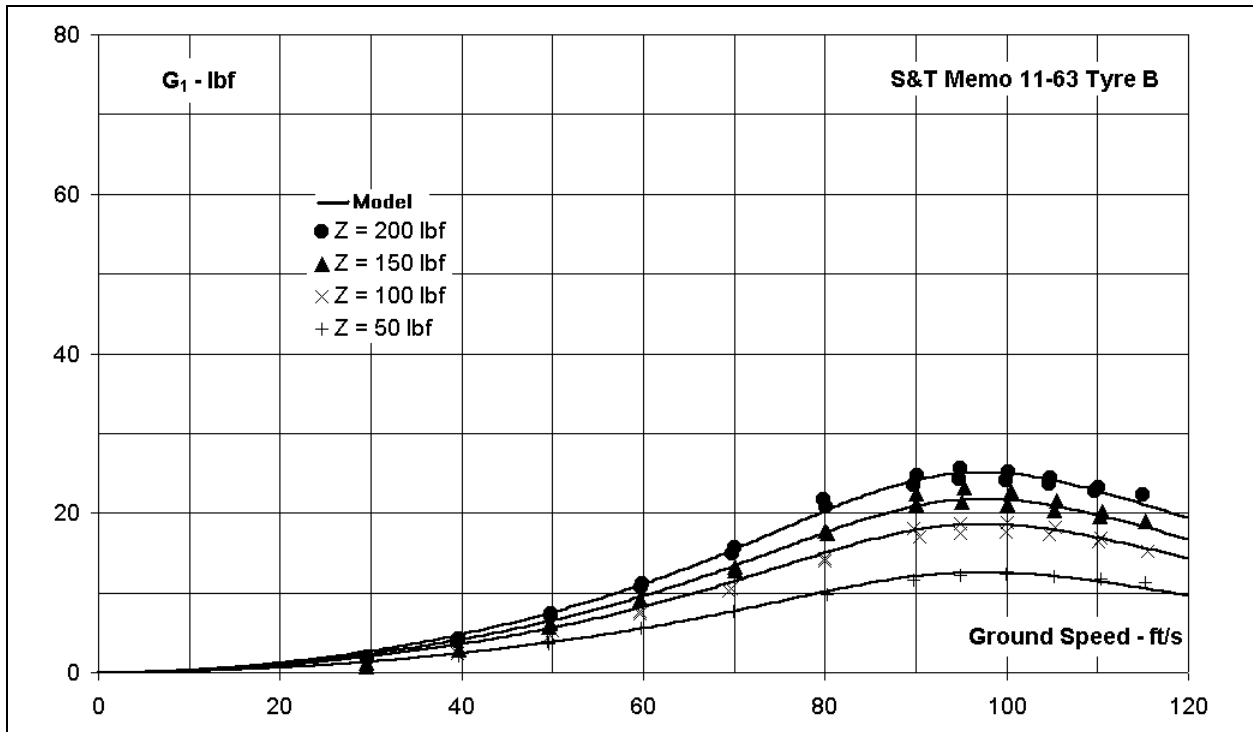
Figure 4.4: Effect of speed on drag force in water – small tyre in test rig:
Z = 200 lbf, d = 0.25 in
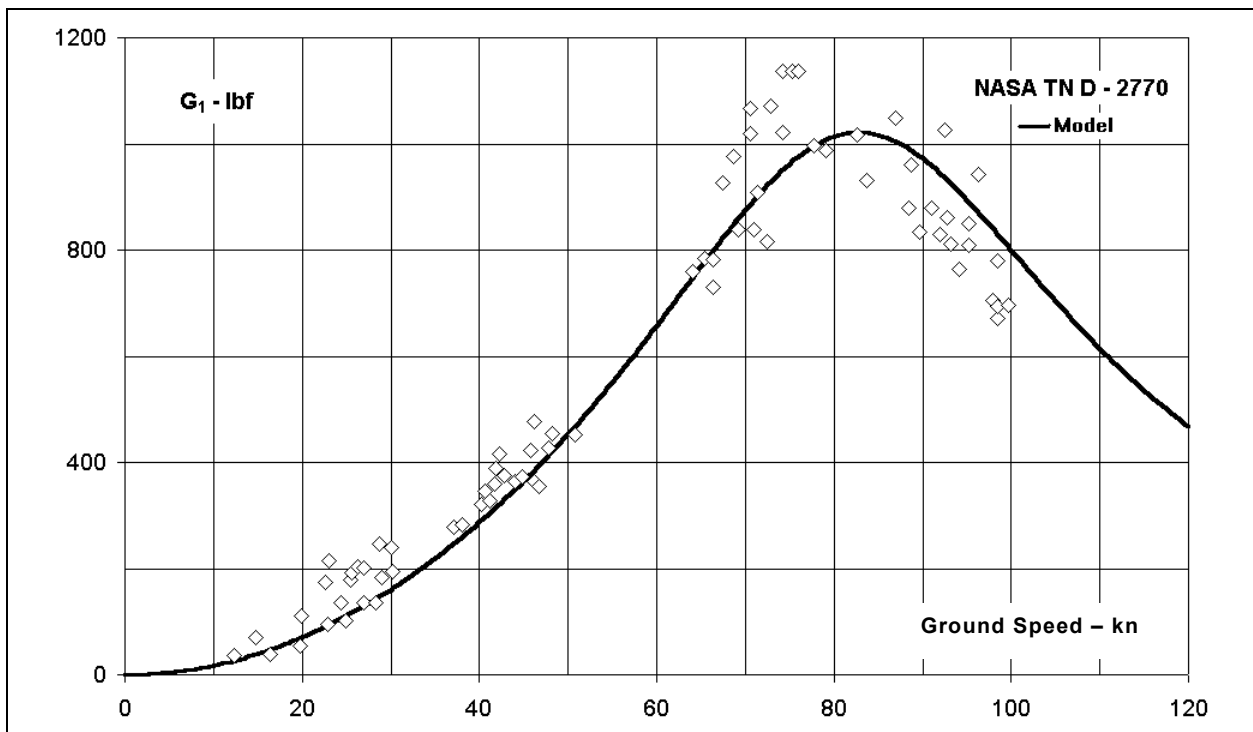
Figure 4.5: Effect of speed on drag force in water – aircraft tyre in NASA test rig:
p = 90 psig, d = 1 in
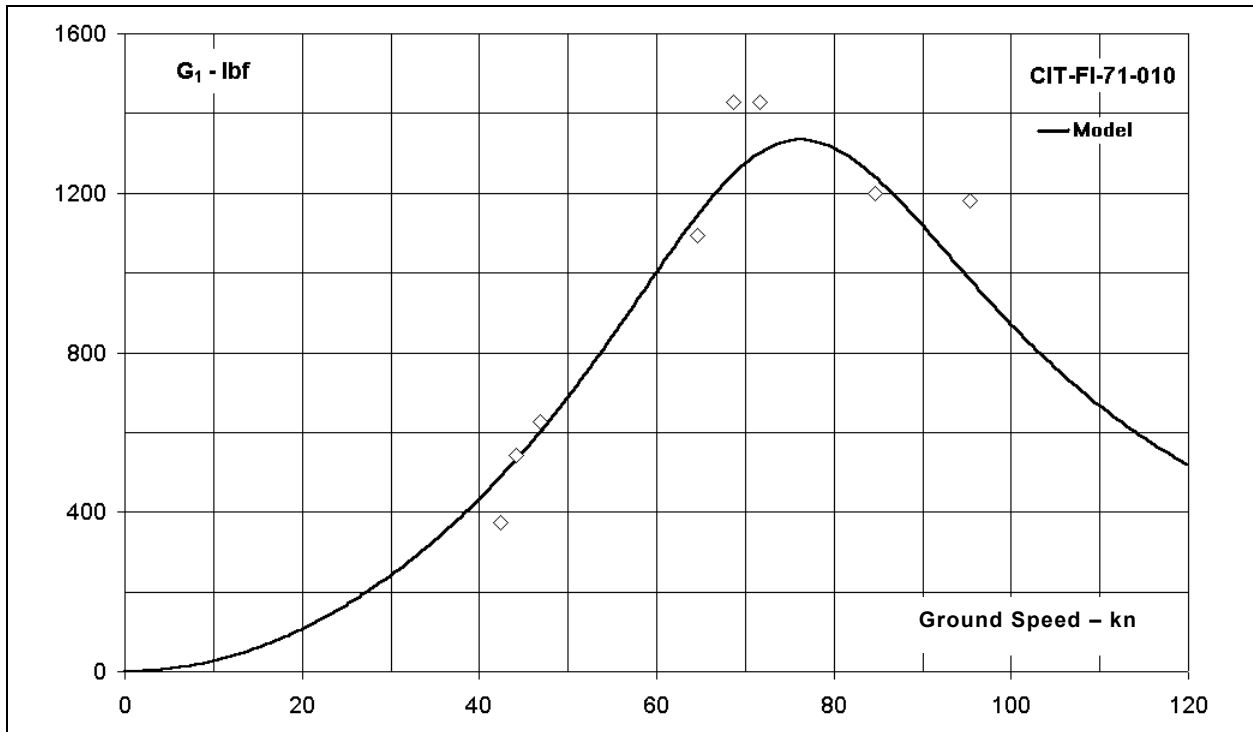
Figure 4.6: Effect of speed on drag force in water – Canberra aircraft:
p = 68 psig, d = 1 in
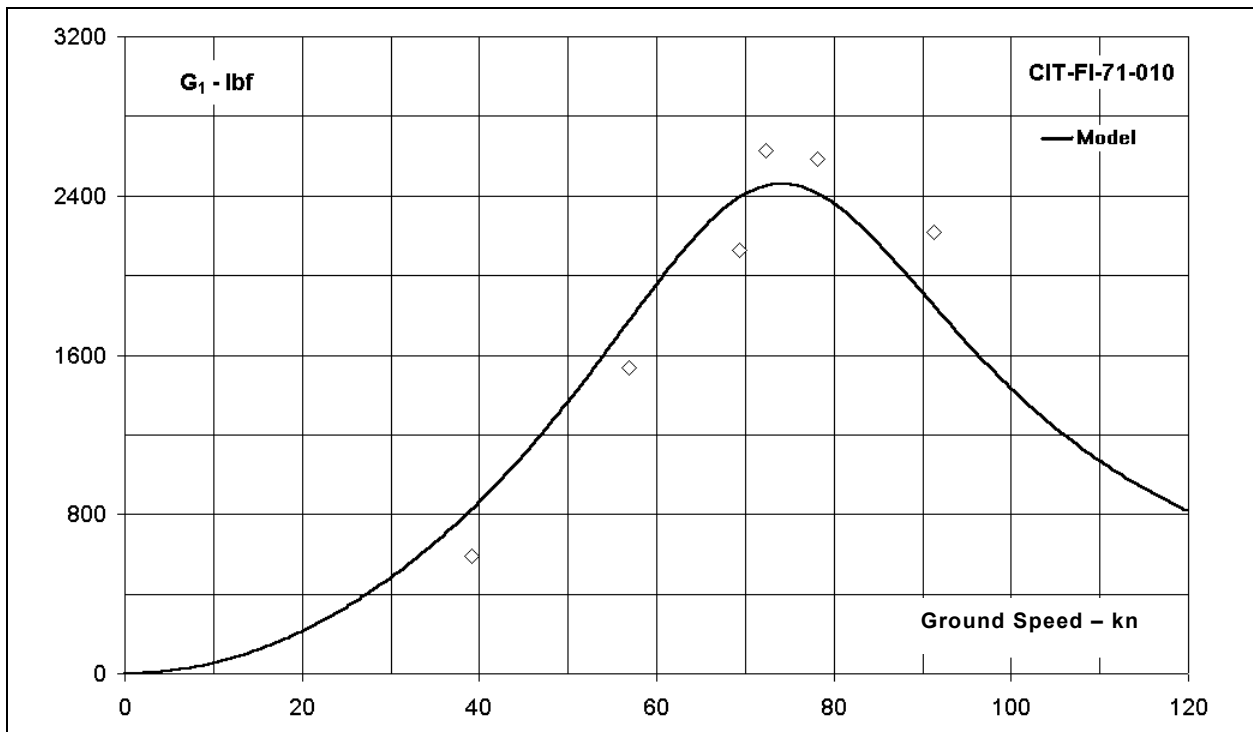
Figure 4.7: Effect of speed on drag force in water – Canberra aircraft:
p = 68 psig, d = 2 in

26
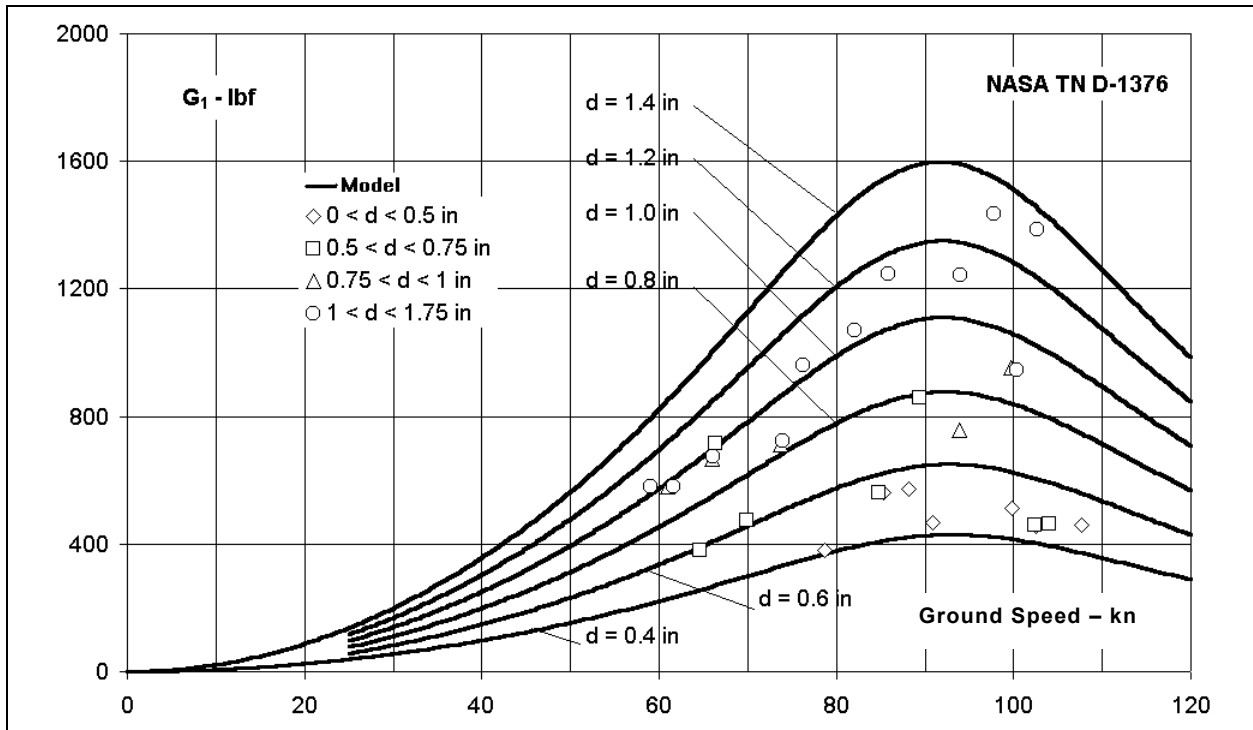
Figure 4.8: Effect of speed and water depth on drag force in water aircraft tyre in NASA test rig: p = 115 psig
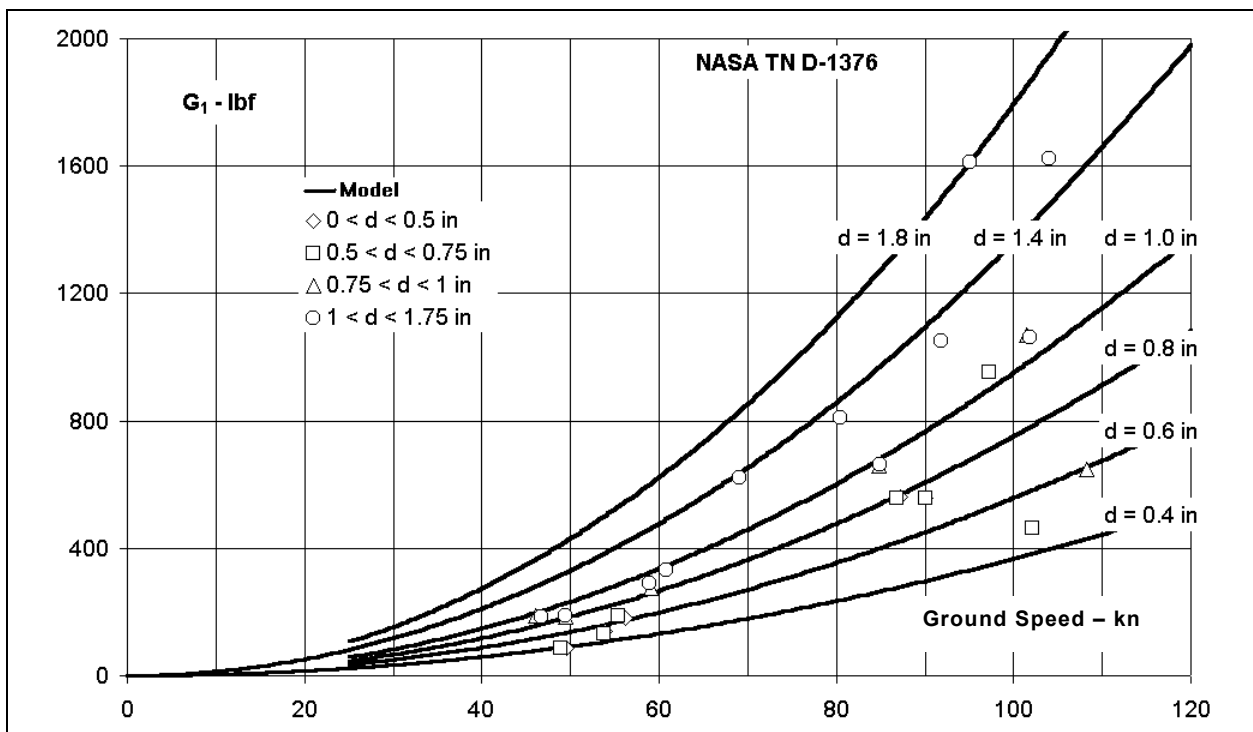
Figure 4.9: Effect of speed and water depth on drag force in water aircraft tyre in NASA test rig: p = 350 psig
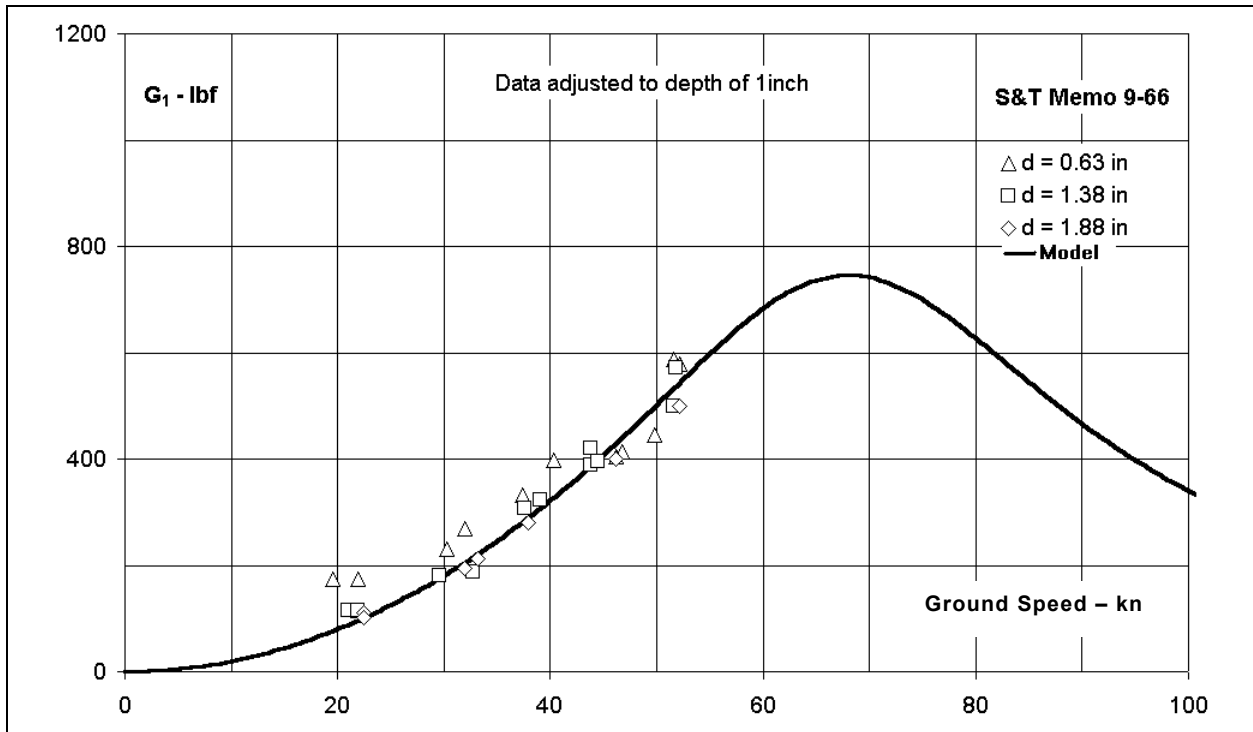
Figure 4.10: Effect of speed on drag force in water aircraft tyre on heavy load test vehicle: p = 55 psig
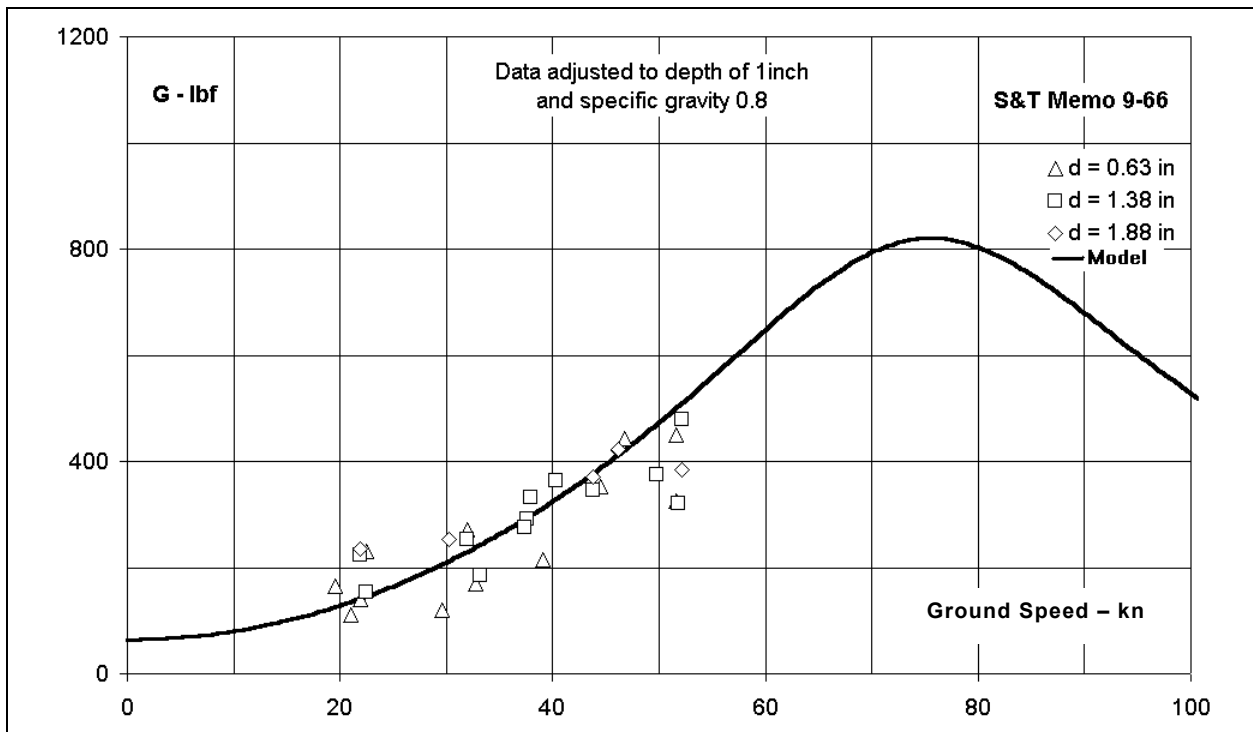
Figure 4.11: Effect of speed on drag force in slush aircraft tyre on heavy load test vehicle: p = 55 psig
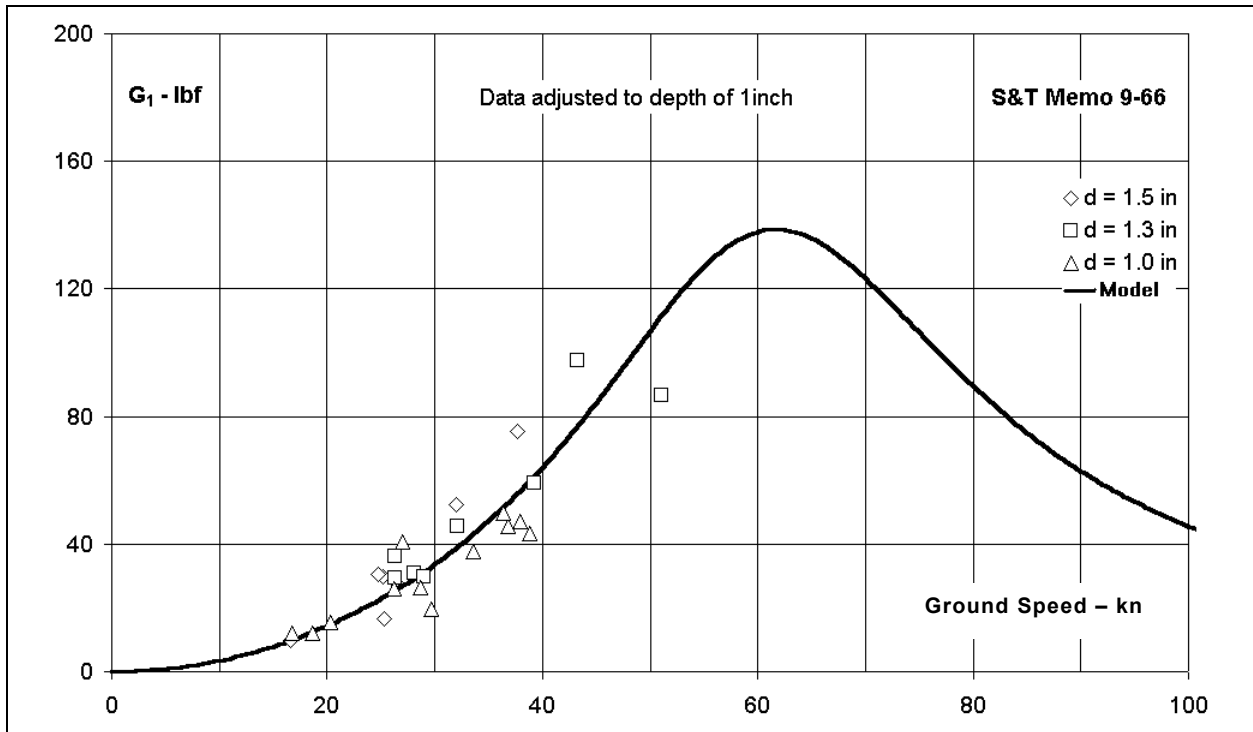
Figure 4.12: Effect of speed on drag force in water small tyre in test rig: p = 40 psig
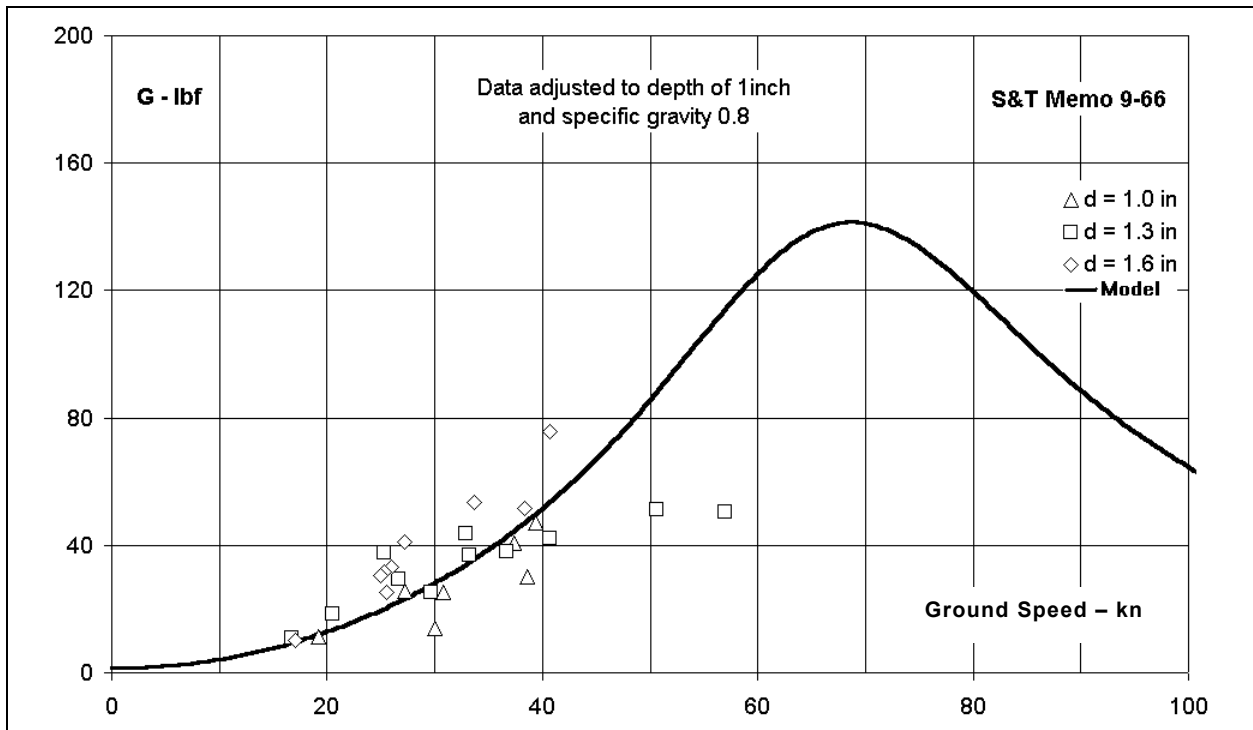
Figure 4.13: Effect of speed on drag force in slush small tyre in test rig: p = 40 psig
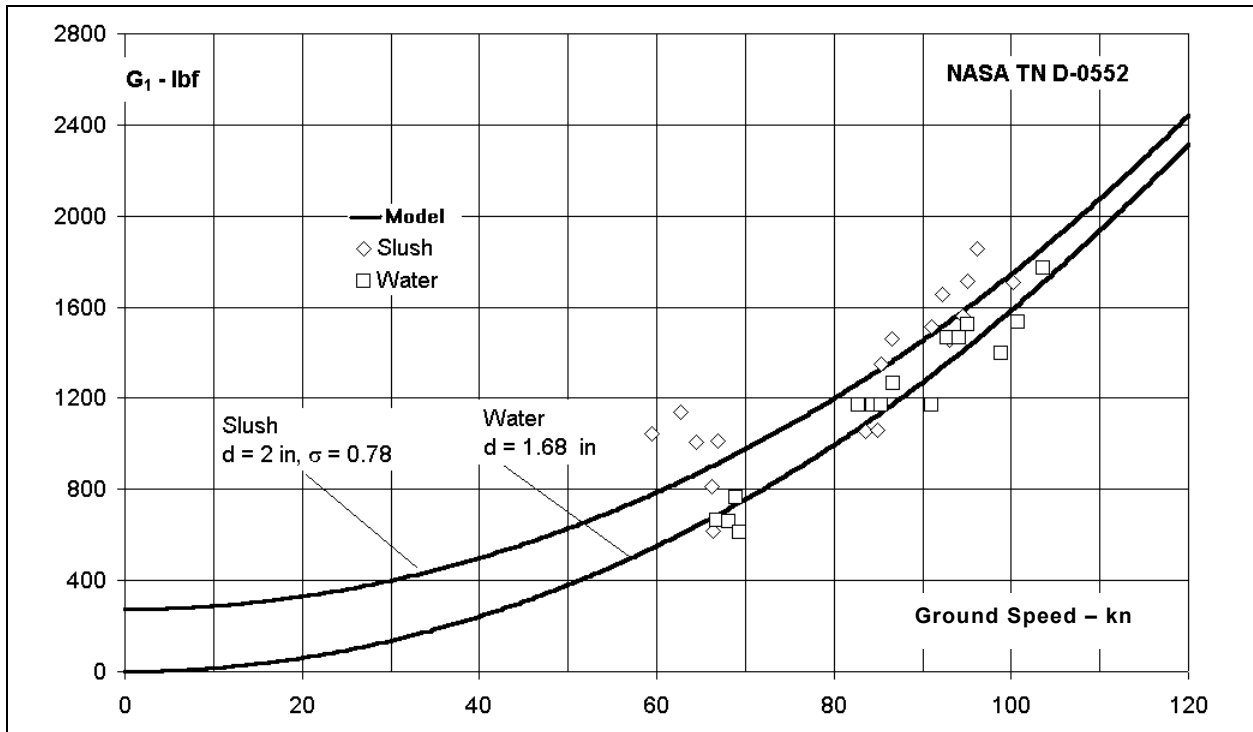
Figure 4.14: Effect of speed and fluid medium on drag force aircraft tyre in NASA test rig: p = 350 psig
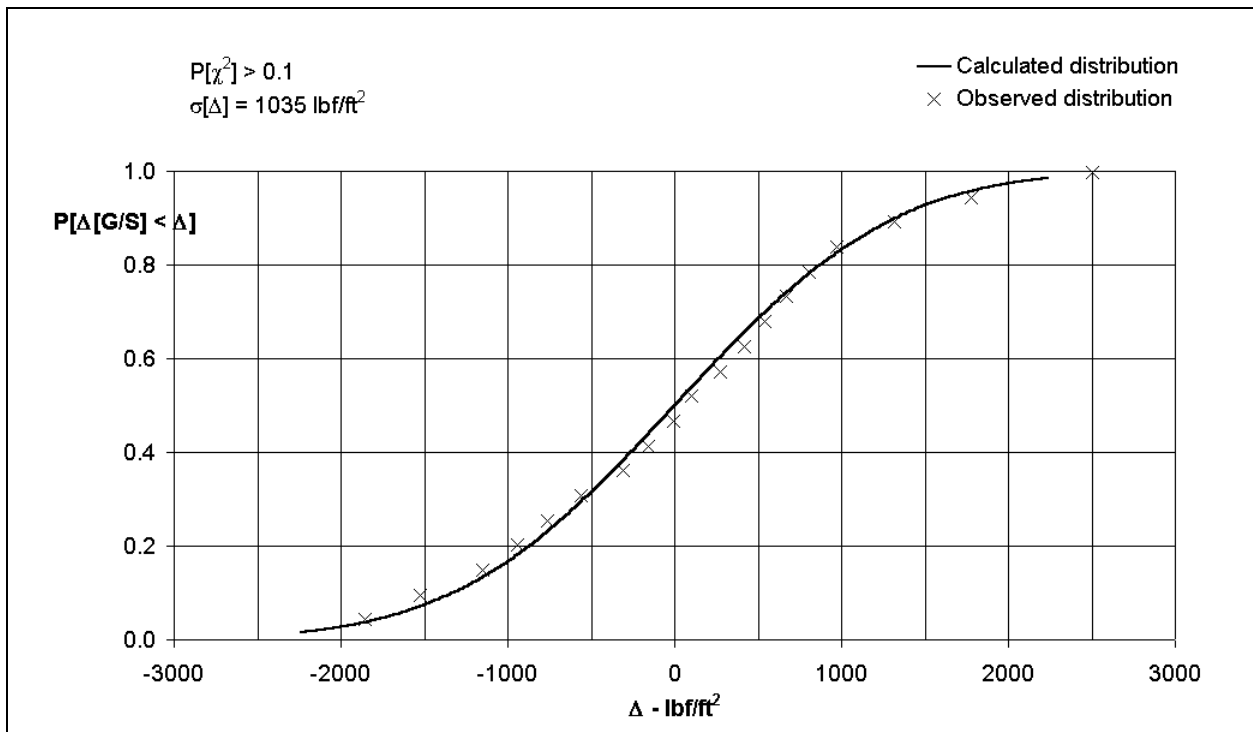
Figure 4.15: Distribution of measured drag pressure about correlation all conditions and tyres

5. DECELERATING FORCES FOR TYRE ROLLING THROUGH SNOW

In this section, an hypothesis is developed that builds on the results of experiments conducted on scale models of aircraft tyres rolling in saturated clays. From this, a mathematical model is constructed that relates relevant mechanical properties of snow to specific gravity. Further, resistive forces due to multi-wheeled vehicles rolling in snow are shown to be related to these mechanical properties, to wheel loading, to geometry and to the depth of the rut created by the passage of wheels through the contaminant.

The problem of snow mobility has been addressed by researchers in independent institutes and within the motor industry. This research has concentrated on traction, braking and directional control – Reference 12 is a typical example – and complex models of the interfaces between tyres, road and media have been developed. A major use to which the results of the research have been put is in the development of tyre treads for automobiles in order to optimise designs for specific uses. In the case of aircraft, tread designs have been optimised on other criteria, so that, for aircraft, the main concerns are rolling and braking using simple tyre treads and standardised carcass constructions. In order to model the total decelerating force in a braked ground run, it is necessary to determine rolling and braking forces separately. For simplicity, it is usually assumed that the decelerating forces generated by braking action can be superimposed on those generated in rolling. Thus, the total decelerating force – excluding aerodynamic and power forces – in a braked ground run for an aircraft is the simple sum of those from rolling and braking.

A further concern in the operation of aircraft is to determine the condition of runways so that operational safety is not compromised. For this purpose, a variety of ground vehicles is used. However, there are at least two drawbacks in the process. First, there is not a generally agreed method for relating the forces measured on a ground-test vehicle and those measured on another such or on an aircraft. Second, there is neither a physically viable mathematical model nor a feasible statistical description that separates and describes the rolling and braking components of decelerating force for either aircraft or ground-test machines.

The conventional model used for calculating the force that resists an *aircraft* tyre when rolling through dry snow on a paved runway is based on the precept that water, slush and dry snow are similar media. This is clearly incorrect physically in that water is an incompressible fluid; slush is a mixture of water, ice and air and is therefore compressible but not compactable,[6] and dry snow is a mixture of ice and air that is compactable.[7]

It is shown in Section 4 that a modification of the conventional approach to modelling the effects of water and slush can be used to predict the variation of rolling resistance with density, depth and speed. A satisfactory match to the data from Reference 9, in particular, was established for water and slush. However, this modified model was not capable of predicting the measured

---

[6] When slush is acted upon by the passage of a vehicle, it is assumed that the mixture **under the footprint** becomes converted to water and no solid matter remains.

[7] When snow is acted upon by the passage of a vehicle, it is assumed that the matter **under the footprint** becomes compacted to ice and the air is forced out.

values of rolling resistance due to snow presented in that reference. The match is closer than that achieved using the conventional approach, in that the modified model allows for a compression term that is independent of speed. In cases for which snow is fresh and dry, this compression term is a close match with measurements at speeds close to zero.

Whilst doubts could be expressed concerning the state of the snow used for the experiments described in Reference 9, other sets of data investigated, notably those in Reference 13, also failed to conform to the conventional model (whether or not the modification was used). The state of the snow used in the experiments described in this last reference was certainly not in doubt.

Figure 5.1 is a typical example of measurements obtained on a complete aircraft in dry snow. At low speeds, the compression term clearly warrants its inclusion. However, the non-conformity between the model and measurements in dry snow becomes well marked at the higher speeds. At 140 ft/s, the calculated value is double the measurement and as speed increases towards that for unstick, the trend is clearly for the match to deteriorate.

In Figure 5.1, the aircraft (Citation II) has a takeoff weight in the order of 12000 lbf. The effect of the over-estimate of resistance due to snow is, therefore, a significant proportion of the available specific excess thrust at unstick. Furthermore, the stopping performance will be over-estimated if use is made of the model based on the assumed physical similarity of snow and slush.
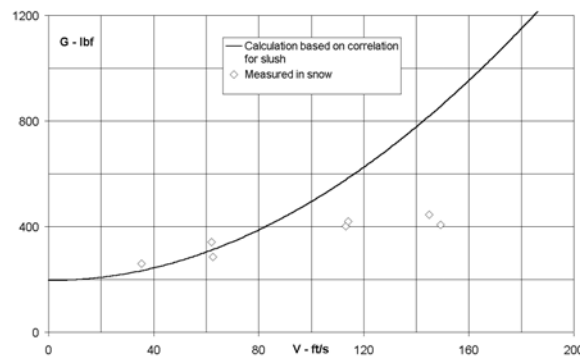
Figure 5.1: Citation II rolling in dry snow

The measured data in Figure 5.1 also reflect the conclusion drawn in References 14, 15 and 16: that there is little or no effect of speed on rolling resistance in snow for the aircraft testing discussed – the Falcon 20. This conclusion is valid for all tests irrespective of whether the snow considered is freshly fallen, naturally aged or has been subjected to repeated mechanical handling. It is therefore plain that a radical change in approach is needed if a simple, yet useful, estimation method is to be successfully developed for aircraft.

A similar situation exists in the case of the ground vehicles that are used to determine runway conditions. As far as can be determined, there is no completely systematic study of *rolling* resistance in snow for any one of the vehicles in use. Reference 17 contains a set of data for a research vehicle travelling at speeds up to ten feet per second. An analysis of these data is given

in sub-section 5.4. That analysis serves to illustrate a possible approach to the problem of relating the rolling performance of a ground vehicle to that of an aircraft.

5.1   Model Development

Conventionally for aircraft operations, snow state has been described solely with respect to its density and depth. This arises because the conventional model, as described above, is based on the erroneous identification of a physical similarity between water, slush and snow. This perception has led to the invalid conclusion that kinetic pressure is the sole determiner of inertial effects.

The study reported in Reference 18 is based on dimensional analysis and establishes that, in saturated clays, inertial effects on rolling resistance are determined, not only by speed and density, but also by shear strength. This is illustrated in Figure 5.2, which shows the effect of speed number N on a non-dimensional group Γ_G that completely describes rolling resistance and rut depth for a scaled model of an aircraft tyre rolling in saturated clay for a range of vertical loads and inflation pressures. The form of the data presented in Figure 5.2 is derived in Appendix A. A consequence of this analysis of the data from Reference 18 is that the depth of the rut created by passage of a wheel is an important element in the problem.
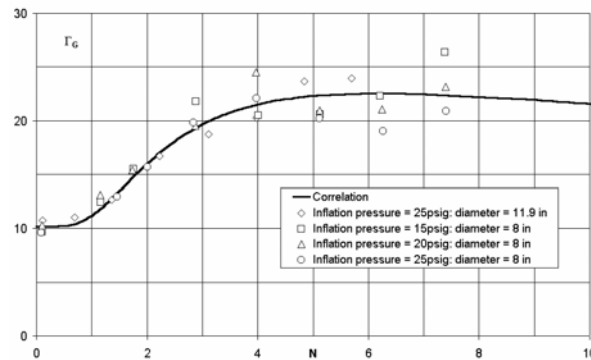
Figure 5.2: Rolling resistance in soft ground

In shallow snow on a paved runway, at *low* loadings, compressive strength determines the extent of rut creation. However, the gross loadings produced by the passage of an aircraft will presumably always result in a compressive failure of snow. Thus, under these circumstances, rut depth may be determined solely by the potential for compaction. This is confirmed below, where experimental evidence is used to show that rut depth (s) is a function only of void ratio (R_{VOID}) and snow depth (d).

The dimensional analysis given in Reference 18 derives a coefficient of resistive force in unbraked rolling that is assumed dependent on shear strength and an arbitrary area. Although this is clearly correct dimensionally, the analysis ignores the strains induced at failure in the medium under stress. Shear modulus, which is the ratio of shear stress at failure (shear strength) to shear strain at failure, is a more appropriate property on which to base a coefficient. Shear strength is, however, an appropriate quantity with which to define a speed number.

In summary, an interpretation of the dimensional analysis contained in Reference 18 leads to the conclusion that "snow" needs to be defined by depth and three mechanical properties: density, shear strength and shear modulus. However, in practice, it is not appropriate to expect aircraft operators to monitor such a range of parameters when considering payload and operational safety. Thus, a set of special relationships is sought that will reduce the need to monitor so many properties. At the same time, these relationships need to be sufficiently conservative and statistically robust so that safety, in particular, is not compromised.

The mathematical model for aircraft state parameters and their interaction with snow properties derives from the dimensional analysis of Reference 18. It is based on test results in *unworked* snow from the Beverley, the Citation II and the Falcon 20; it is confirmed by comparison with results from similar tests using a Boeing 727 and a Boeing 737. In addition, data from the CRREL instrumented vehicle and a Swedish trailer rolling in unworked snow have been analysed in order to provide sufficient evidence to enable a statistical assessment of the modelling of snow properties. Table 5.1 summarises the testing that has been used both to develop the mathematical model and to corroborate its applicability.

Table 5.1: Summary of aircraft and vehicular testing considered

Aircraft or Vehicle	Medium	Reference	Presented in
Beverly	Natural Snow	21	Section 5.3
Boeing 727	Natural Snow	22	Section 5.3
Boeing 737	Natural Snow	22	Section 5.3
Citation II	Natural Snow	13	Section 5.3
Falcon 20 1997	Natural Snow	15	Section 5.3
Falcon 20 1998	Natural Snow	16	Section 5.3
CRREL Instrumented Vehicle (CIV)	Natural Snow	17	Section 5.4
Aircraft Tyre Model	Natural Snow	23	Section 5.4
Aircraft Tyre Model	Saturated Clays	18	Appendix A

4.2 Prediction of Snow Properties

In the comprehensive review, Reference 20, undertaken by the Cold Regions Research and Engineering Laboratory (CRREL), it is observed that, apart from avalanche studies, little or no use has been made of the mechanical properties of snow for general engineering applications. There are reasons for this neglect – not least that snow is thermodynamically unstable and therefore its properties change with time on exposure to mechanical force and heat exchange with the surroundings. Under practical conditions, many different types of snow are encountered. In principle, these are not classifiable using a single quantity although simple classifications have been attempted – one such is given in Reference 12 and is reproduced in Table 5.2. In that case, density (or specific gravity) is used as the reference parameter.

Table 5.2: Classification of snow (from Reference 12)

Type of Snow	Specific Gravity
New	$0.05 < \sigma_{SNOW} < 0.15$
Powder	$0.1 < \sigma_{SNOW} < 0.5$
Compacted	$0.4 < \sigma_{SNOW} < 0.7$
Wet	$0.3 < \sigma_{SNOW} < 0.7$
Ice	0.92

There is considerable overlap between classification and range of specific gravity. At constant specific gravity, there are different classifications that have differing mechanical properties. This, in turn gives rise to a range of forces resisting motion for a given specific gravity. Thus, density of snow is only one of the properties that are important to the generation of forces that resist the motion of a rolling wheel. Such analyses as those in Reference 20 suggest that the microstructure of a snow is of equal importance to density in determining mechanical properties. In principle, this is true. However, airport authorities generally keep runways clear of snow. At most, a runway will be contaminated with snow that is less than a day old. Thus, for aircraft operations on snow-contaminated runways, a limited range of snows can be assumed.[8] In such circumstances, the relevant mechanical properties may be predictable within tolerable statistical limits by using density (or void ratio) as the sole independent variable.

Not all the experiments to determine resistive forces for aircraft moving in snow have been conducted in new snow. Experiments performed in mechanically handled snow are not considered directly relevant in the modelling process for rolling resistance. However, much of the testing in worked snow has included braked runs. Thus, it is necessary to establish rolling resistance so that it is possible to identify the specific contribution that the action of braking makes to decelerating force.

5.2.1   Void ratio

In the modelling process developed here, snow is considered as a powder. When treating powders, the ratio of the space between grains (void) and the total volume of the powder is called the void ratio. Thus, for snow,

$$R_{VOID} = \frac{v_{VOID}}{v_{SNOW}} \tag{5.1}$$

Now, if dry snow is a mixture of ice and air,

$$v_{VOID} = v_{SNOW} - v_{ICE} \tag{5.2}$$

Dividing through by v_{SNOW},

---

[8]   Under some circumstances, runways are contaminated with compressed snow. It is shown in Section 12 of this report that this condition can be treated statistically as a type of ice.

$$R_{VOID} = 1 - \frac{v_{ICE}}{v_{SNOW}}$$ 　　　5.3

Further,

$$v_{SNOW} = \frac{m_{SNOW}}{\rho_{SNOW}}; \text{ and } v_{ICE} = \frac{m_{ICE}}{\rho_{ICE}}.$$ 　　　5.4

Substituting in Equation 5.3,

$$R_{VOID} = 1 - \frac{m_{ICE}}{m_{SNOW}} \frac{\rho_{SNOW}}{\rho_{ICE}}$$ 　　　5.5

However, ignoring the mass of air, the mass of ice present in dry snow is equal to the mass of the snow. Thus, $m_{ICE}/m_{SNOW} = 1$ and, therefore,

$$R_{VOID} = 1 - \frac{\rho_{SNOW}}{\rho_{ICE}}$$ 　　　5.6

This can be written in terms of specific gravity[9] so that

$$R_{VOID} = 1 - \frac{\sigma_{SNOW}}{\sigma_{ICE}}$$ 　　　5.7

For a given type of snow, by using void ratio to correlate snow properties that vary with density, it becomes easier to ensure that the correlated snow properties tend to those of ice. The device has been used in fitting equations to data obtained from analysis of measurements of decelerating forces for aircraft and other vehicles rolling in snow.

5.2.2 Rut depth

A key feature of the suggested modelling scheme is a non-dimensional rut depth s/D – the ratio of rut depth to wheel diameter. In rolling in and over a relatively thin snow cover on a solid runway surface, a heavily loaded wheel may be considered to compress the snow under the footprint to ice. The depth of the rut created by the passage of one wheel over such a snow-covered runway may then be approximated by considering the following:

$$m_{SNOW} = \rho_{SNOW} S d_{SNOW}$$ 　　　5.8

$$m_{ICE} = \rho_{ICE} S \left(d_{SNOW} - \mathrm{E}[s] \right)$$ 　　　5.9

---

[9]　Throughout this report, it is assumed that ice has a specific gravity of 0.92.

36

But

$$m_{ICE} \approx m_{SNOW} \qquad\qquad 5.10$$

Equating Equations 5.9 and 5.10 and re-arranging,

$$E[s] = \left(1 - \frac{\rho_{SNOW}}{\rho_{ICE}}\right) d_{SNOW} \qquad\qquad 5.11$$

Hence, dividing through by wheel diameter, D and substituting from equation 5.6,

$$E\left[\frac{s}{D}\right] = R_{VOID}\frac{d_{SNOW}}{D} \qquad\qquad 5.12$$

Non-dimensional rut depth was identified (raised to the power 4/3) statistically, when soft ground data given in Reference 18 were analysed. That analysis is summarised in Appendix A. No information for rut depths has been published from the aircraft experiments considered here. However, data from Table 3 in Reference 18 (summarised in Table 5.3) can be used to validate a simple relationship. In Figure 5.3, the parameter s/D is plotted against $E[s/D]$. The figure shows that the correlation

$$s/D = E[s/D] \qquad\qquad 5.13$$

is a satisfactory fit to the data, which are normally distributed about the fit (see Figure 5.4) with a standard deviation $\sigma[\Delta[s/D]] = \pm 0.014$. Because there are 44 measurements in the set, a 95% confidence interval for an estimate of non-dimensional rut depth, $E[s/D]$, is ± 0.004 approximately.

The upper bound of the non-dimensional rut depth $(s/D \le 0.4)$ covered in this set of measurements is more than sufficient to include any value likely to be encountered in practical operations involving aircraft and ground vehicles on runways contaminated with snow.

5.2.3 Shear strength

Data for this snow property are presented in Figure B6 of Reference 20 as a hatched plot of shear strength, C_u, against density for *bonded*[10] snow. No measurements are presented: but an approximate temperature range for the original data sets is given so that $-10C < T < -3C$. It is assumed, therefore, that values of shear strength are not greatly affected by temperature in that range.[11] The centre of the scatter band presented is fitted approximately by the equation

---

[10]   The term bonded is not defined in the reference.
[11]   Clearly, as temperature rises towards melting point, shear strength will tend to zero.

$$C_u = C_{u\,ICE}\,e^{-12.8\,R^2_{VOID}} \;\; \text{lbf/ft}^2 \qquad\qquad 5.14$$

It is noted that Reference 20 contains neither a statistical description of the scatter nor any description of the experimental procedures used to obtain the information. The data sets included in the presentation were collected by various investigators at dates ranging from 1939 to 1975.

Table 5.3: Measured data from tests on CIV (Reference 17)

Series	Test	V – ft/s	d - ft	ρ slug/ft^3	s - ft	D – ft	p - psig	G - lbf	Z - lbf
1	1	4.6	0.440	0.31	0.325	2.40	15	78	1558
1	2	4.6	0.509	0.31	0.394	2.40	15	94	1494
1	3	6.0	0.492	0.33	0.410	2.40	15	71	1548
1	4	6.0	0.610	0.33	0.495	2.40	15	125	1529
2	1	4.6	0.535	0.31	0.436	2.46	26	112	1581
2	2	4.6	0.545	0.31	0.446	2.46	26	89	1526
2	3	7.9	0.600	0.33	0.502	2.46	26	104	1600
2	4	7.9	0.627	0.33	0.535	2.46	26	106	1523
3	1	4.8	0.692	0.43	0.561	2.46	26	107	1590
3	2	4.8	0.682	0.43	0.551	2.46	26	140	1453
3	3	8.2	0.650	0.43	0.518	2.46	26	120	1606
3	4	8.2	0.673	0.43	0.551	2.46	26	168	1451
3	5	1.9	0.659	0.43	0.528	2.46	26	106	1510
3	6	1.9	0.673	0.43	0.541	2.46	26	143	1541
3	7	5.0	0.591	0.43	0.476	2.46	26	108	1546
3	8	5.0	0.623	0.43	0.509	2.46	26	156	1498
4	1	4.6	0.696	0.43	0.531	2.40	15	93	1633
4	2	4.6	1.230	0.43	1.066	2.40	15	264	1519
4	3	6.2	0.728	0.43	0.564	2.40	15	118	1640
4	4	6.2	0.673	0.43	0.509	2.40	15	102	1461
4	5	5.0	0.587	0.43	0.423	2.40	15	77	1590
4	6	5.0	0.584	0.43	0.420	2.40	15	84	1513
4	7	4.4	0.666	0.43	0.502	2.40	15	106	1587
4	8	4.4	0.679	0.43	0.515	2.40	15	108	1510
4	9	4.8	0.728	0.43	0.564	2.40	15	117	1527
4	10	4.8	0.709	0.43	0.545	2.40	15	103	1593
4	11	7.5	0.715	0.43	0.551	2.40	15	85	1596
4	12	7.5	0.751	0.43	0.587	2.40	15	114	1535
5	1	5.5	1.171	0.31	1.007	2.46	26	262	1572
5	2	4.3	1.181	0.31	1.017	2.46	26	295	1619
5	3	6.9	1.063	0.31	0.899	2.46	26		1518
5	4	6.9	1.037	0.31	0.873	2.46	26		1530
5	5	6.5	1.102	0.31	0.938	2.46	26		1476
5	6	6.5	1.102	0.31	0.938	2.46	26		1566
7	1	4.6	0.446	0.21	0.315	2.46	26	38	1567
7	2	4.6	0.417	0.21	0.285	2.46	26	41	1553

Table 5.3: Measured data from tests on CIV (Reference 17) (continued)

Series	Test	V – ft/s	d - ft	ρ slug/ft^3	s - ft	D – ft	p - psig	G - lbf	Z - lbf
7	3	8.7	0.548	0.21	0.449	2.46	26	52	1543
7	4	8.7	0.528	0.21	0.397	2.46	26	62	1589
7	5	4.6	0.577	0.21	0.495	2.46	26	48	1520
7	6	4.6	0.515	0.21	0.400	2.46	26	94	1618
9	1	3.8	0.528	0.45	0.427	2.46	26	197	1551
9	2	3.8	0.420	0.45	0.164	2.46	26	117	1618
9	3	5.3	0.610	0.45	0.279	2.46	26	187	1575
9	4	5.3	0.354	0.45	0.295	2.46	26	98	1619

5.2.4 Shear modulus

Although shear modulus is not presented directly in Reference 20, Figure B1 of that reference is a presentation of data for Young's modulus from a variety of sources. Data from one source, the results of a comprehensive study made in the Caucasus Mountains between 1948 and 1962, are presented as a best fit to Young's modulus together with values of Poisson's ratio. In previous work, as implied in Reference 20, snow has been treated as an isotropic material; on this basis shear modulus is related to Young's modulus and Poisson's ratio by

$$G_S = \frac{E}{2(1+\nu)} \qquad\qquad 5.15$$

A mean value for Poisson's ratio for the snows studied is $\nu = 1/3$. Using this value, the curve

$$G_S = G_{S\,ICE}e^{-11.35R_{VOID}} \text{ lbf/ft}^2 \qquad\qquad 5.16$$

is an adequate fit to the data for shear modulus from Reference 20.

5.2.5 Snow properties from aircraft and ground vehicle studies

A process has been adopted which uses the snow properties outlined above to determine approximations to both shear strength and shear modulus. These approximations serve as starting values in iterations to find "best" fits to measurements of decelerating force as these vary with ground speed. Now, for a single wheel rolling in a compactable medium, the analysis of Reference 18, as modified in Appendix A, can be interpreted to enable the formulation of resistive force as

$$G = G_S \Phi f\left[1 + \rho V^2 / C_u\right] \qquad\qquad 5.17$$

where $\Phi = (s/D)^{4/3}(Z/p)$ and the function $f\left[1 + \rho V^2 / C_u\right]$ is to be determined from inspecting the data.

The values of shear strength and shear modulus (from Equations 5.14 and 5.16 respectively) were used to calculate $\left(G/\Phi G_S\right)$ and $\left(1+\rho V^2/C_u\right)$. It was then possible to identify the function as

$$f = \left(1+\rho V^2/C_u\right)^{1/4} \qquad\qquad 5.18$$

Of course, in the case of a multi-wheeled aircraft, the geometric function Φ must be calculated for each effective wheel. A composite value is, therefore,

$$\Phi_T = n_M \left(s/D\right)_M^{4/3} \left(Z/p\right)_M + n_N \left(s/D\right)_N^{4/3} \left(Z/p\right)_N \qquad\qquad 5.19$$

The correlating Equation 5.17 may then be re-written so that

$$G = G_S \Phi_T \left(1+\rho V^2/C_u\right)^{1/4} \qquad\qquad 5.20$$

For each of the 31 sets of data, Equation 5.20 was solved iteratively for values $\mathrm{O}\!\left[G_S\right]$ and $\mathrm{O}\!\left[C_u\right]$ so that the sum of the deviations

$$\Delta[G] = G - \mathrm{O}\!\left[G_S\right]\Phi\left(1+\rho V^2/\mathrm{O}\!\left[C_u\right]\right)^{1/4} \qquad\qquad 5.21$$

was zero and the variance of the sum was near to a minimum.[12] To complete the modelling process, the observed snow properties are correlated with void ratio. Using the standard process of least squares, the correlations were identified to be:

$$\mathrm{E}\!\left[G_S/G_{S\ ICE}\right] = e^{-13.82\,R_{VOID}^{1.5}}$$
$$\mathrm{E}\!\left[C_u/C_{u\ ICE}\right] = e^{-13.82\,R_{VOID}^{2.5}} \qquad\qquad 5.22$$

The scatter of the observations about the correlations is not even approximately Normal. So, in order to estimate the effects of uncertainty in snow properties an approximation to the distributions is needed. In both cases, define

$$\Theta[\ ] = \frac{\mathrm{O}[\ ]}{\mathrm{O}[\ ]+\mathrm{E}[\ ]} \qquad\qquad 5.23$$

If $\mathrm{O}[\ ]\geq 0$ and $\mathrm{E}[\ ]>0$ then $0\leq\Theta[\ ]<1$. It is then possible that $\Theta[\ ]$ is a beta variable of the first kind. In fact, using a χ^2 test, it can be shown that the probability exceeds 0.25 that both $\Theta\!\left[C_u\right]$ and $\Theta\!\left[G_S\right]$ are distributed like $\mathrm{B}\!\left[6,6.5\right]$. See Figures 5.5 to 5.8. Percentage points of the distribution are shown in Table 5.4.

---

[12] This process is closely analogous to a least squares calculation.

Table 5.4: Percentage points of the Beta distribution $B[6, 6.5]$

P	0.025	0.05	0.1	0.5	0.558	0.9	0.95	0.975
Θ	0.222	0.258	0.302	0.479	0.5	0.659	0.706	0.745
$O[\ ]/E[\ ]$	0.285	0.348	0.433	0.919	1	1.933	2.401	2.922
$O[G]/E[G]$	0.390	0.453	0.534	0.939	1	1.639	1.929	2.235

Now, if Equation 5.20 is re-written to define $O[G]$ so that

$$O[G] = O[G_S]\Phi\left(1 + \rho V^2 / O[C_u]\right)^{1/4}$$

5.24

and if Equation 5.24 is re-written to define $E[G]$ so that

$$E[G] = E[G_S]\Phi\left(1 + \rho V^2 / E[C_u]\right)^{1/4}$$

5.25

then, dividing Equation 5.24 by Equation 5.25 and manipulating with Equation 5.23, it can be shown that

$$\frac{O[G]}{E[G]} \approx \left\{\frac{\Theta}{1-\Theta}\right\}^{3/4}$$

5.26

Values of $O[G]$ at selected probability levels can be calculated using the percentage points listed in Table 5.4 with a re-arrangement of Equation 5.26. Thus

$$O[G] = \left\{\frac{\Theta}{1-\Theta}\right\}^{3/4} E[G].$$

5.27

5.3 Aircraft Studies

This sub-section is a review of the results of the testing on the five types of aircraft that have been used both to establish the mathematical model for snow properties and to corroborate it. It has been shown in sub-section 5.2 that shear strength and shear modulus for *unworked* – but not necessarily *fresh* – snow can be related to specific gravity through the void ratio using Equation 5.22. The range of the properties data is such that the correlating functions are exponentials; the spread of the measurements about the correlations is not Normal. From this it follows that standard uncertainty analyses are not valid; hence, a non-standard treatment has been developed to assess the effect of random variations in snow properties (at constant void ratio) on calculations of resistive force.

The only uncertainties in resistive force treated in this sub-section are those due to uncertainties in snow properties. Other such sources of uncertainty as contaminant depth, specific gravity and the design features of individual instrumentation systems are not considered. It is of note that, because the variation of shear strength and shear modulus with void ratio is exponential, the

effect of uncertainty in specific gravity on resistive force is substantial in cases where the depth of snow (and hence resistive force) is significant. In fact, it can be shown that

$$\frac{\partial G}{\partial R_{VOID}} = \frac{4}{3}\frac{G}{R_{VOID}} + \frac{1}{4}\left(\frac{N^2}{1+N^2}\right)G\left\{\frac{5}{2}rR_{VOID}^{3/2} - \frac{R_{VOID}}{1-R_{VOID}}\right\} - \frac{3}{2}rR_{VOID}^{1/2}G \qquad 5.28$$

Equation 5.28 shows that the influence of uncertainty in void ratio on uncertainty in resistive force is directly proportional to the value of resistive force G.

At the beginning of this section, mention was made both of the thermodynamic instability and of the importance to be attached to the microstructure of snow. Both of these phenomena give rise to variability in the relation between the mechanical properties of snow and specific gravity. In general, when comparing measured data to a model, it is necessary to account for uncertainties inherent in the conditions in which the experiment was conducted. For an aircraft rolling in snow, this accounting is even more important than is generally the case. This arises because of the variability in conditions that are an inevitable consequence of the dependence of mechanical properties on microstructure, conditions at the time of snowfall and subsequent weathering – even in the short term. In the experiments from which data have been used to construct a mathematical model, the snow has been described solely with reference to its specific gravity. Hence, the variability in mechanical properties has been accounted statistically.

Referring back to Equation 5.27 and Table 5.4, a 95% confidence interval for an individual experiment can be calculated. The lower bound of one such interval is given by

$$O[G]_{0.025} = 0.39E[G_S]\Phi\left(1+\rho V^2/E[C_u]\right)^{1/4} \qquad 5.29$$

and the upper bound of the interval is given by

$$O[G]_{0.975} = 2.235E[G_S]\Phi\left(1+\rho V^2/E[C_u]\right)^{1/4} \qquad 5.30$$

Figures 5.9 to 5.17 have been prepared to show the way in which aircraft data are described by the model. The first six examples have been used in the construction of the model. However, the last two – the Boeing 727 and 737 – have not been included in the modelling in order to test the predictive capabilities of the method.

5.3.1   Beverley

Two cases are available for this aircraft (see Reference 21). Both were run through naturally aged snow; results are shown in Figures 5.9 and 5.10. Operationally, both sets of conditions would be unlikely to be encountered because of the depth of snow and of the relatively high specific gravity. The high value of specific gravity is a result of weathering over several weeks. Results for both tests are close to the 50% level of probability, which suggests that the structure of these particular snows is close to a "typical" value for the deposition conditions and weathering at an airport. It is therefore assumed that the process of correlating snow properties

from the various experiments has resulted in the identification of a type of snow that is likely to be encountered in this kind of terrain.

A further reason for the relatively high proportion of aircraft weight represented by the measured snow resistance is the low inflation pressure for the tyres. In Equation 5.17, resistance due to snow is directly proportional to the parameter Φ. This parameter, in turn, is inversely proportional to inflation pressure – in absolute measure. For the Beverley, inflation pressure is 48 psig for the main wheels and 57 psig for the nose wheels. These low values contribute to the high levels of resistance to motion through snow.

5.3.2   Citation II

Although the test data for this aircraft (see Reference 14) were collected from an experiment in "fresh, dry" snow, the modelling indicates that the snow is near to the upper bound of the distribution of properties (see Figure 5.11). In the reference, the structure of the snow is not reported. It is therefore not possible to judge whether the statistical approach adopted here is appropriate to this particular case.

In principle, the uncertainties that have been addressed by studying the distribution of snow properties at constant void ratio are at the core of the problem of resistive forces due to aircraft rolling through snow. In the case of the Citation II, under these particular experimental conditions, the uncertainty in force that has been credited to snow properties is not serious in absolute terms.

5.3.3   Falcon 20

For this aircraft,[13] operated by Transport Canada, twenty test runs from four test flights have been analysed. The data, compared with the model are shown in Figures 5.12 to 5.15. The data have been extracted from time histories of acceleration and speed from References 15, 16 and 17. In all cases, ground speed was compared to integrated accelerometer data; where necessary small adjustments – never greater than ±0.01 – were made to the accelerometer readings to ensure a match between measured speed and that from the integrated accelerometer readings. In addition, after the integration check had been done, accelerometer data were smoothed using a simple exponential smoothing algorithm with a damping factor of 0.7. Although the speed traces were quite smooth, the same exponential smoothing was used for speed in order to account for the small phase shift that is introduced in the smoothing process.

In the main, the data in Figures 5.12 to 5.15 show considerable scatter despite the smoothing. This may be due to signal conditioning in the accelerometer circuits or could be due to the location of the transducers. All four of the figures have been plotted to the same scale so that the relative size of the scatter can be judged by eye. It is of note that there is a suggestion in the data that the oscillatory time responses are in fact related to position down the runway at North Bay. However, investigations of these phenomena are beyond the scope of this study.

---

[13]   See Appendices D and E for treatment of the aircraft aerodynamics, propulsion and braking system.

Figure 5.12 illustrates the results from seven runs on a single flight over a range of speed so that $10 < V < 200 \, \text{ft/s}$. The 50% point on the distribution of snow properties adequately represents the data. However, the specific gravity of the snow is much greater than that expected on a runway contaminated with fresh snow. Such a contamination is more likely to be represented by specific gravities like those illustrated in Figures 5.13 and 5.14. The depths of the contamination in those two cases are not great. In fact, it is not possible to identify any significant contaminant drag given the scatter in the measurements presented in Figure 5.13. There is a suggestion that the data in Figure 5.14 may be represented by the upper bound of the 95% confidence interval for snow properties.

Substantial contaminant drag is evident in the test runs shown in Figure 5.15. Again, the specific gravity is probably unrepresentative of new snow. The combination of depth and specific gravity are sufficient to enable an identification of drag. The 50% point in the distribution of snow properties is adequate to describe the data from runs 1, 2 and 3. However, runs 4 and 5 suggest that a slightly greater percentage point may be appropriate. Of course, since there is no indication of how snow properties and specific gravity varied during the flight, the variability may be due to these sources. On the other hand, the effect of rutting over the course of the flight may be more significant at this nominal depth.

5.3.4   Boeing 727 and 737

Data from these two aircraft, which took part in the study reported in Reference 22, have not been used in constructing the mathematical model for the resistive force due to rolling through snow and for snow properties. Data from a test run on each aircraft are plotted in Figures 5.16 and 5.17. The 50% point in the distribution of snow properties describes the data for the Boeing 727 adequately. However, data from a test run on the Boeing 737 are better fitted by a percentage point intermediate between the 50% point and the lower bound of the 95% confidence interval discussed in sub-section 5.2. Both results are encouraging in that, broadly, the tests confirm two effects. First, the similarity between the variation with speed due to motion on soft ground and through snow is confirmed. This similarity is the basis of the modelling process described in sub-sections 5.1 and 5.2. Second, the two sets of data provide evidence that the statistical model of snow properties is applicable for airport terrains.

5.4   Ground Vehicle Studies

Experiments on ground vehicles have been used to augment the available aircraft data. Those reported in Reference 23 were conducted on a single wheel using two different tyres. The first tyre was specifically designed for friction measurements; these results are plotted in Figures 5.18 to 5.22. The tyre was inflated to 24 psig and a vertical load of 1080 lbf was applied. Snow properties that describe the data lie between probability levels of 0.5 and 0.9. However, the maximum force measured amounts to no more than some 8% of the vertical load. There is no indication in the reference as to the likely precision of the measured data.

The second tyre was designed for use on an aircraft. A vertical load of 8720 lbf was applied at two inflation pressures – 60 psig and 80 psig. Data are plotted in Figures 5.23 and 5.24. The plots show the effect of rut depth at the two inflation pressures. Snow properties that describe the data

lie at the 50% level of probability. The effect of inflation pressure is marginal, as would be expected. The maximum measured resistive force due to snow was in the order of 3% of the applied vertical load.

Referring to Figure 5.22, it is of note that, even though the snow properties used to describe the data are at the 80% level of probability, the use of the 50% probable value would have engendered a maximum under-prediction of only 25 lbf – which amounts to approximately 2.5% of the vertical load. Thus, these data confirm that the representation of snow properties is sufficiently precise to describe the motion of tyres rolling through the kinds of fresh, un-weathered snow that are likely to be encountered on exposed runways.

Data from Reference 17 (see Table 5.3) were collected in a series of experiments using an instrumented road vehicle. The experiments were conducted by driving through fresh snow of variable depth at speeds no greater than some 10 ft/s. Drag loads due to snow on only the front wheels have been considered.

Because of the variability in depth, the data for each test series has been presented here as the quotient of force and the ratio of rut depth to wheel diameter (raised to the power 4/3). Data are plotted in Figures 5.25 to 5.31. Snow properties in the probability range of 0.02 to 0.7 have been used to describe the data. In this series of tests snow depths of over a foot were encountered. Thus, drag loads of some 17% of vertical load were measured. However, the method used to predict drag loads is sufficient to account for all the test results within the 95% confidence band proposed in sub-section 5.2.

5.5   Example – Boeing 737

Consider the Boeing 737 as operated by NASA and reported in Reference 22. It is required to estimate the decelerating force in a headwind of 10 kn, due to rolling through two inches of slightly aged snow with specific gravity 0.2 in the landing configuration. In this flap and spoiler configuration, as shown in Table 5.5, at ground attitude, the wing-body generates significant lift coefficient. This has to be accounted because the parameter Φ_{TOTAL} (see Equation 5.19) depends on wheel load.

To estimate rut depth use Equation 5.12, where void ratio is calculated using Equation 5.7. Expected values of the snow properties – shear strength and shear modulus – are calculated using Equation 5.22. The expected value of decelerating force can then be calculated using Equation 5.20. In order to put the values of decelerating force into the same context as friction forces, the expected values calculated so far can be normalised with respect to aircraft weight. These values are shown in Table 5.6 in the column headed $\mathrm{E}[G/W]$.

Estimates of probable values of G/W at probability levels of common interest are also shown in Table 5.6 and are plotted in Figure 5.32. Values are calculated using a rearrangement of Equation 5.26 so that

$$G/W = \left\{ \frac{\Theta}{1-\Theta} \right\}^{3/4} \mathrm{E}\left[G/W\right] \qquad\qquad 5.31$$

where Θ is the relevant percentage point of the distribution $\mathrm{B}\left[6, 6.5\right]$ to which the snow properties have been shown to conform. These percentage points are given in Table 5.4.

Table 5.5: Conditions and aircraft parameters for Boeing 737[14]

Flap	40			$\mathrm{E}\left[C_u\right]$ - lbf/ft^2	31.3			T - K	263
Spoilers	OUT			$\mathrm{E}\left[G_s\right]$ - lbf/ft^2	5108			λ	0.11
C_D	0.285			d - in	2			S_W - ft^2	980
C_L	0.242			σ	0.2				
W - lbf	80 000			R_{VOID}	0.783				
V_H - kn	10			s - in	1.565				
$(p_i)_N$ - psig	135	n_N	2	w_N - in	7.7	D_N - in	24	$(s/D)_N$	0.065
$(p_i)_M$ - psig	155	n_M	4	w_M - in	14	D_M - in	40	$(s/D)_M$	0.039

Inspection of Figure 5.32 shows that the expectation of equivalent friction coefficient for rolling through two inches of slightly aged snow at speeds up to some 180 ft/s at the 50% level is in the order of 0.01. At the upper bound of a 95% confidence interval (the 97.5 percentage point of the distribution), the equivalent friction coefficient is in the region of 0.03. There is, therefore, an uncertainty in equivalent friction coefficient of 0.02 due to uncertainty in snow properties at this specific gravity at the (single-tailed) 97.5% level of significance.

Table 5.6: Calculated parameters for Boeing 737 in snow

V - kn	V_{TAS} - kn	V_{EAS} - kn	$(W-L)$ - lbf	Z_N - lbf	Z_M - lbf	Φ_{TOT}	$\mathrm{E}\left[G\right]$ - lbf	$\mathrm{E}\left[G/W\right]$
0.0	10.0	10.5	79912	4395	17780	0.0494	252.2	0.0032
20.0	30.0	31.4	79208	4356	17624	0.0489	492.8	0.0062
30.0	40.0	41.9	78592	4323	17487	0.0486	593.3	0.0074
40.0	50.0	52.3	77800	4279	17311	0.0481	567.9	0.0084
50.0	60.0	62.8	76833	4226	17095	0.0475	745.1	0.0093
60.0	70.0	73.3	75689	4163	16841	0.0468	803.4	0.0100
70.0	80.0	83.7	74369	4090	16547	0.0459	852.2	0.0107
80.0	90.0	94.2	72873	4008	16214	0.0450	892.4	0.0112
90.0	100.0	104.6	71202	3916	15842	0.0440	924.6	0.0116
100.0	110.0	115.1	69354	3814	15431	0.0428	949.1	0.0119
110.0	120.0	125.6	67330	3703	14981	0.0416	966.3	0.0121
120.0	130.0	136.0	65131	3582	14492	0.0402	976.2	0.0122
$P\left[G < \mathrm{E}\left[G\right]\right]$	0.010	0.025	0.100	0.500	0.900	0.975	0.990	
$(\Theta/1-\Theta)^{3/4}$	0.327	0.390	0.533	0.939	1.639	2.226	2.630	

---

[14] Aircraft data taken from Reference 22.

Table 5.6: Calculated parameters for Boeing 737 in snow (continued)

V - ft/s	G/W	G/W	G/W	G/W	G/W	G/W	G/W	
0	0.0010	0.0012	0.0017	0.0030	0.0052	0.0070	0.0083	
34	0.0020	0.0024	0.0033	0.0058	0.0101	0.0137	0.0162	
51	0.0024	0.0029	0.0040	0.0070	0.0122	0.0165	0.0195	
68	0.0028	0.0033	0.0045	0.0079	0.0138	0.0188	0.0222	
84	0.0030	0.0036	0.0050	0.0087	0.0153	0.0207	0.0245	
101	0.0033	0.0039	0.0054	0.0094	0.0165	0.0224	0.0264	
118	0.0035	0.0042	0.0057	0.0100	0.0175	0.0237	0.0280	
135	0.0037	0.0044	0.0060	0.0105	0.0183	0.0248	0.0293	
152	0.0038	0.0045	0.0062	0.0109	0.0189	0.0257	0.0304	
169	0.0039	0.0046	0.0063	0.0111	0.0194	0.0264	0.0312	
186	0.0040	0.0047	0.0064	0.0113	0.0198	0.0269	0.0318	
203	0.0040	0.0048	0.0065	0.0115	0.0200	0.0272	0.0321	
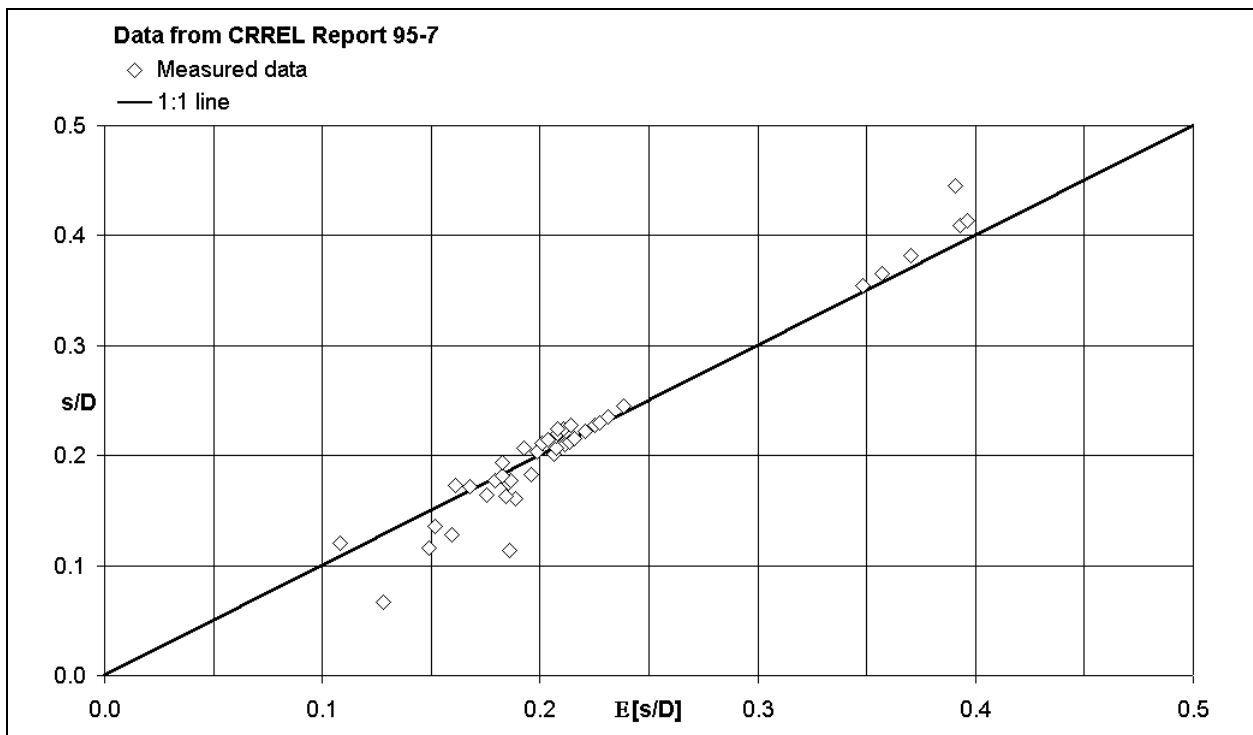
Figure 5.3: Comparison of measured rut depth with calculated value
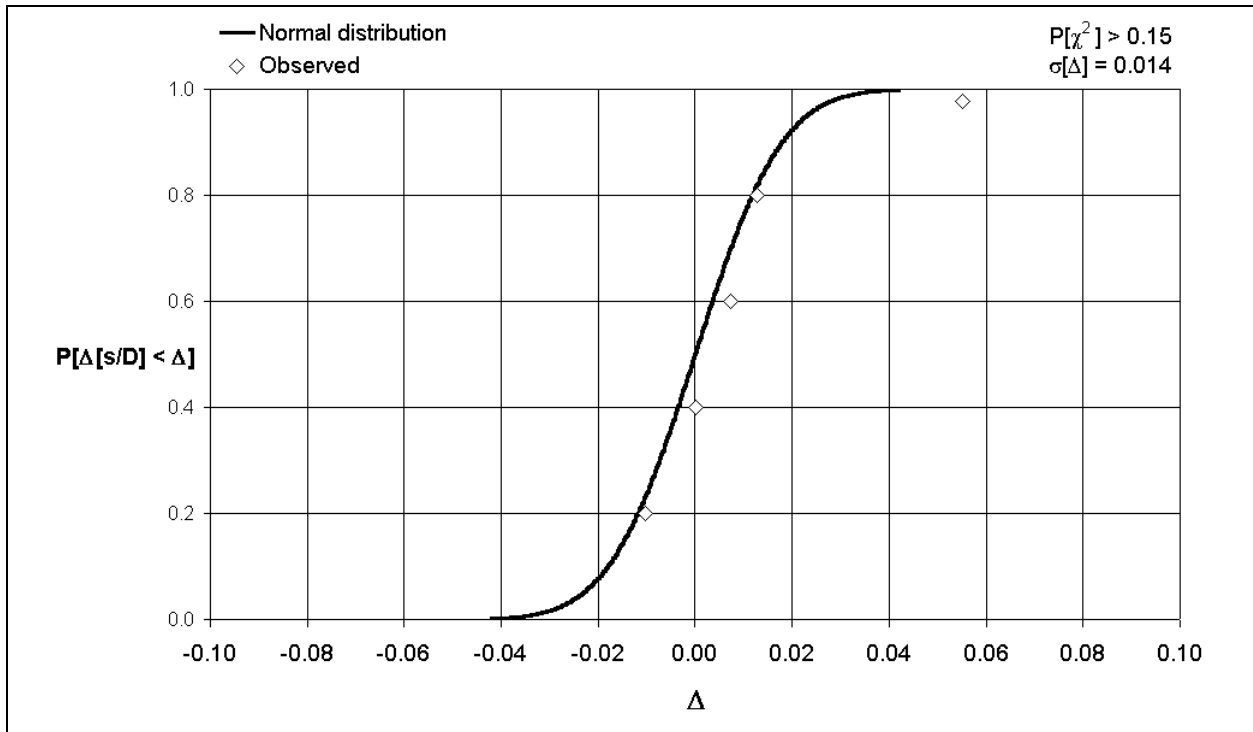
Figure 5.4: Distribution of deviation of measured rut depth from model
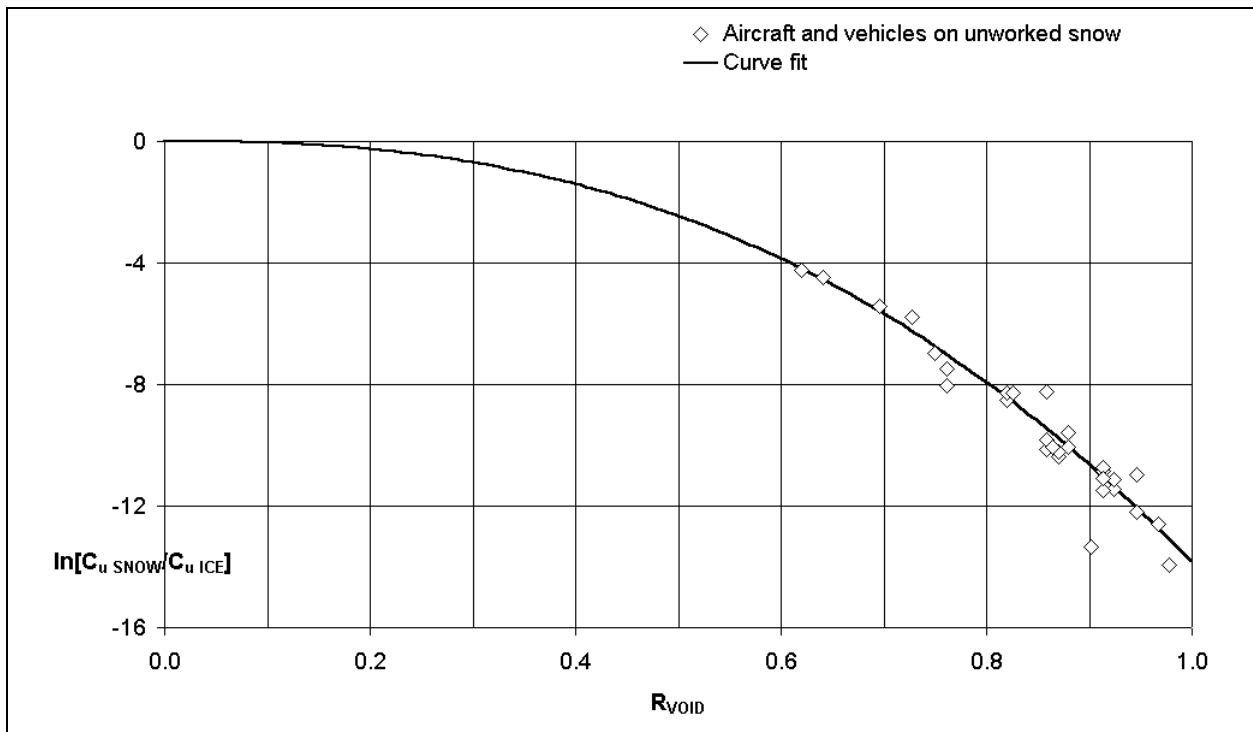
Figure 5.5: Effect of void ratio on shear strength of snow
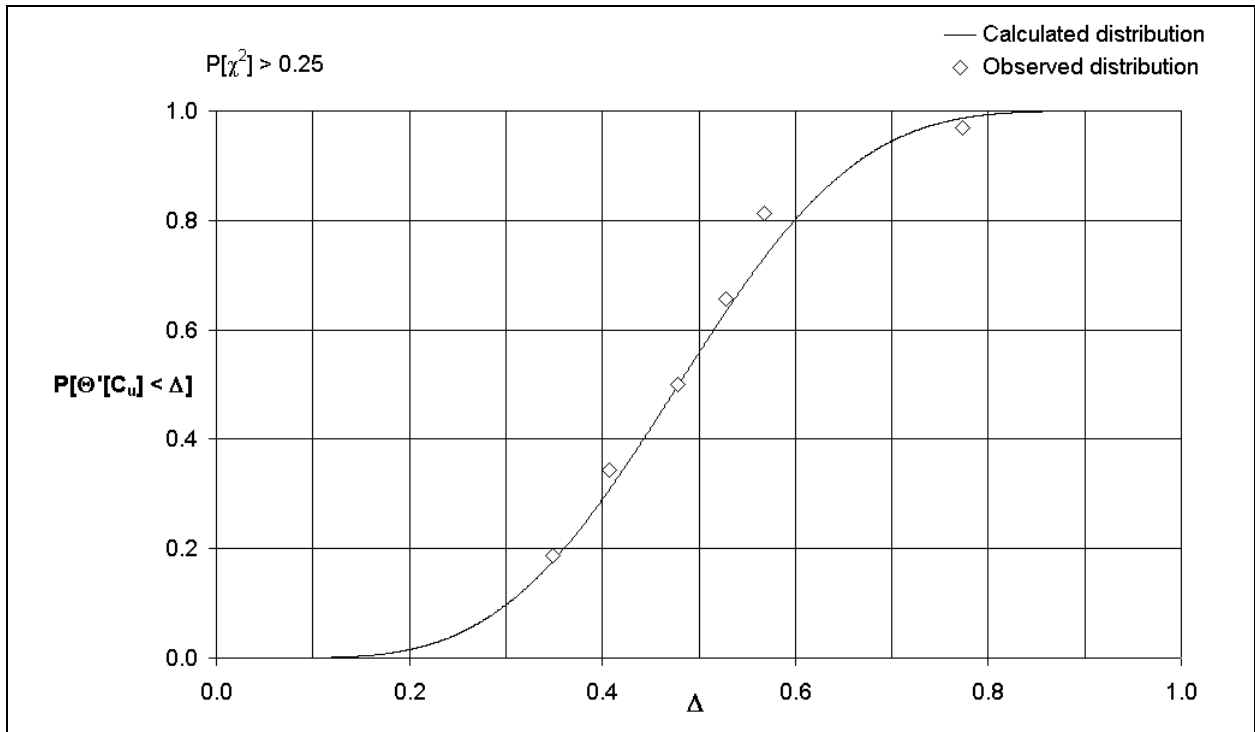
Figure 5.6: Distribution of transformed shear strength about correlation
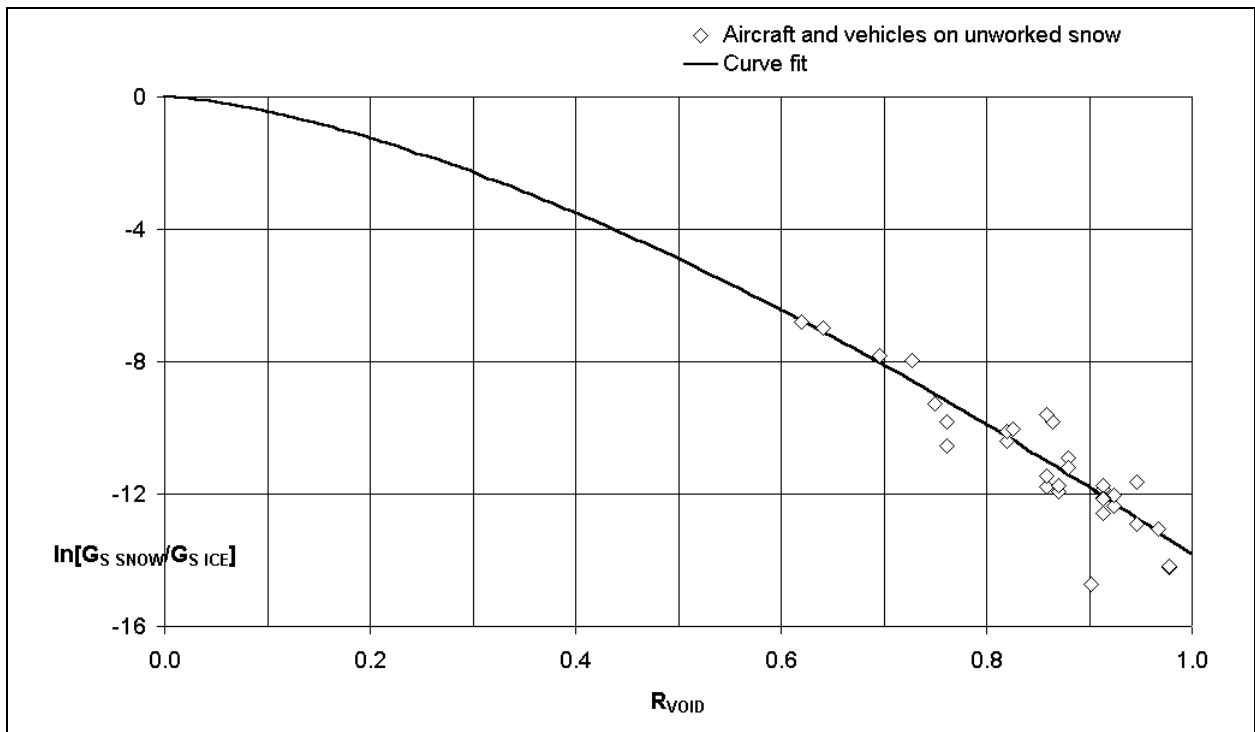
Figure 5.7: Effect of void ratio on shear modulus of snow
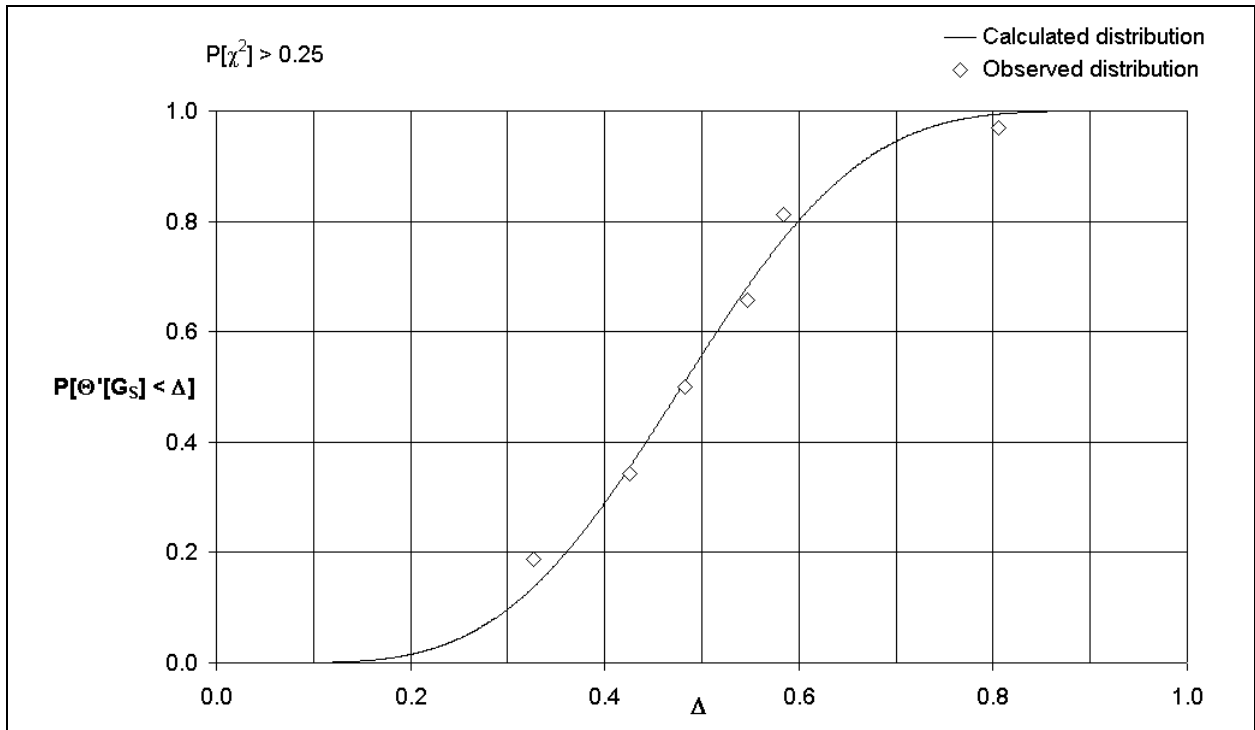
Figure 5.8: Distribution of transformed shear modulus about correlation
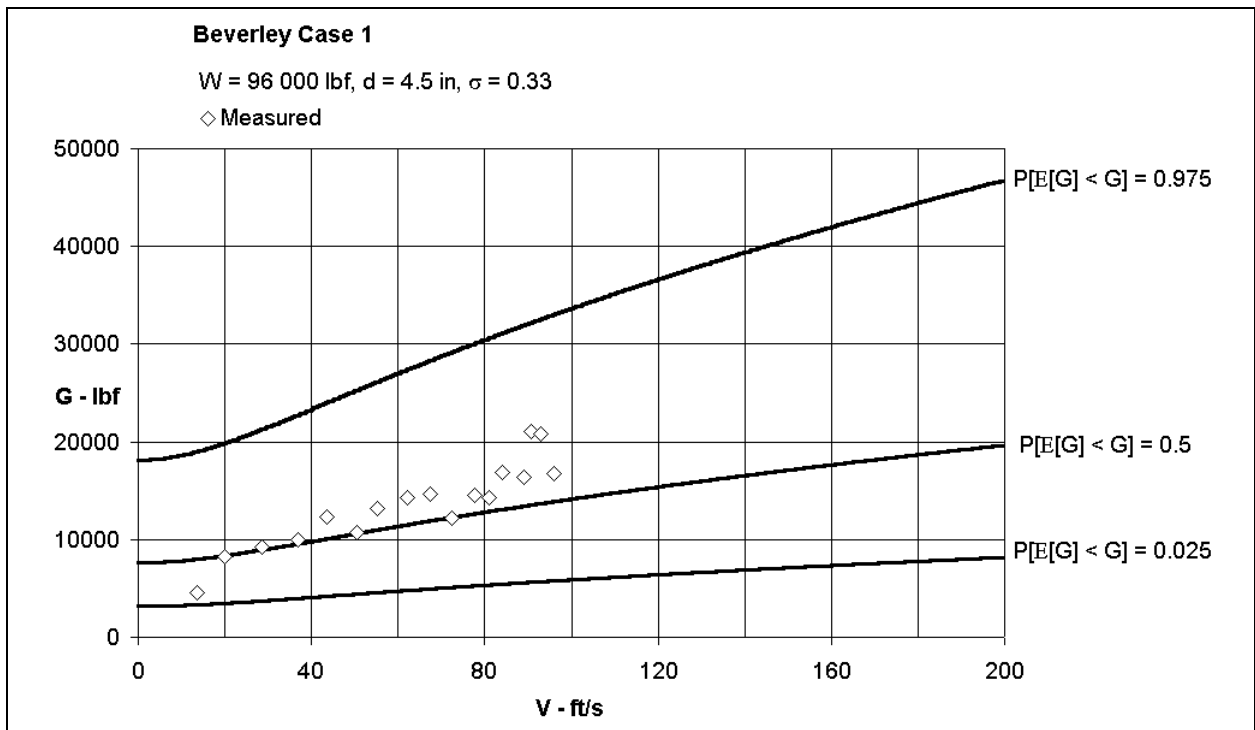
Figure 5.9: Effect of ground speed on resistive force due to aircraft rolling in snow – Beverley Case 1
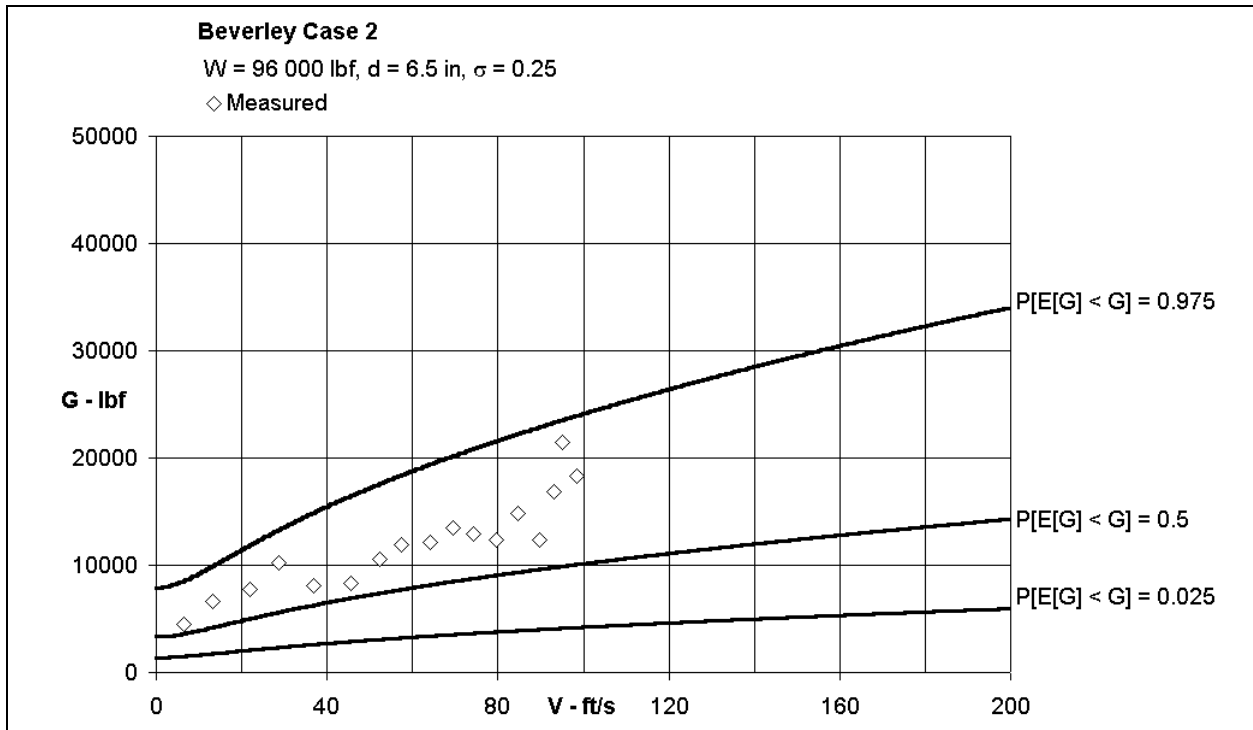
Figure 5.10: Effect of ground speed on resistive force due to aircraft rolling in snow – Beverley Case 2
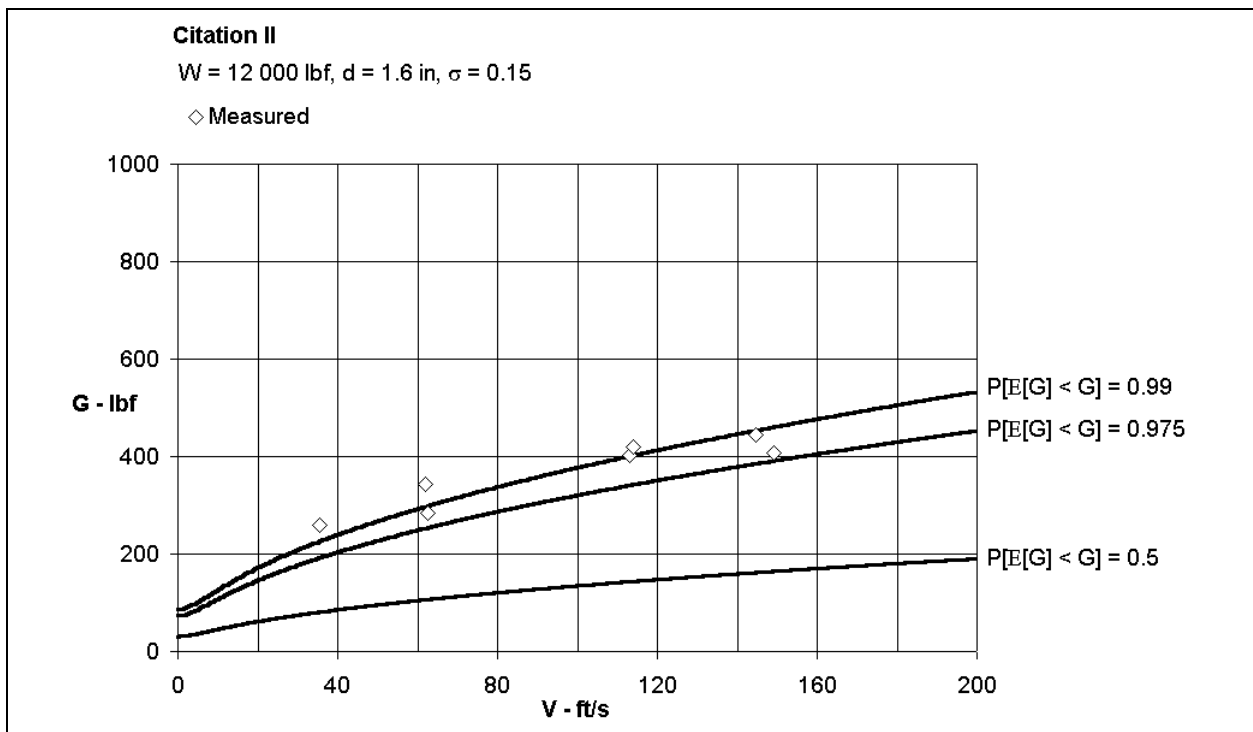
Figure 5.11: Effect of ground speed on resistive force due to aircraft rolling in snow – Citation II
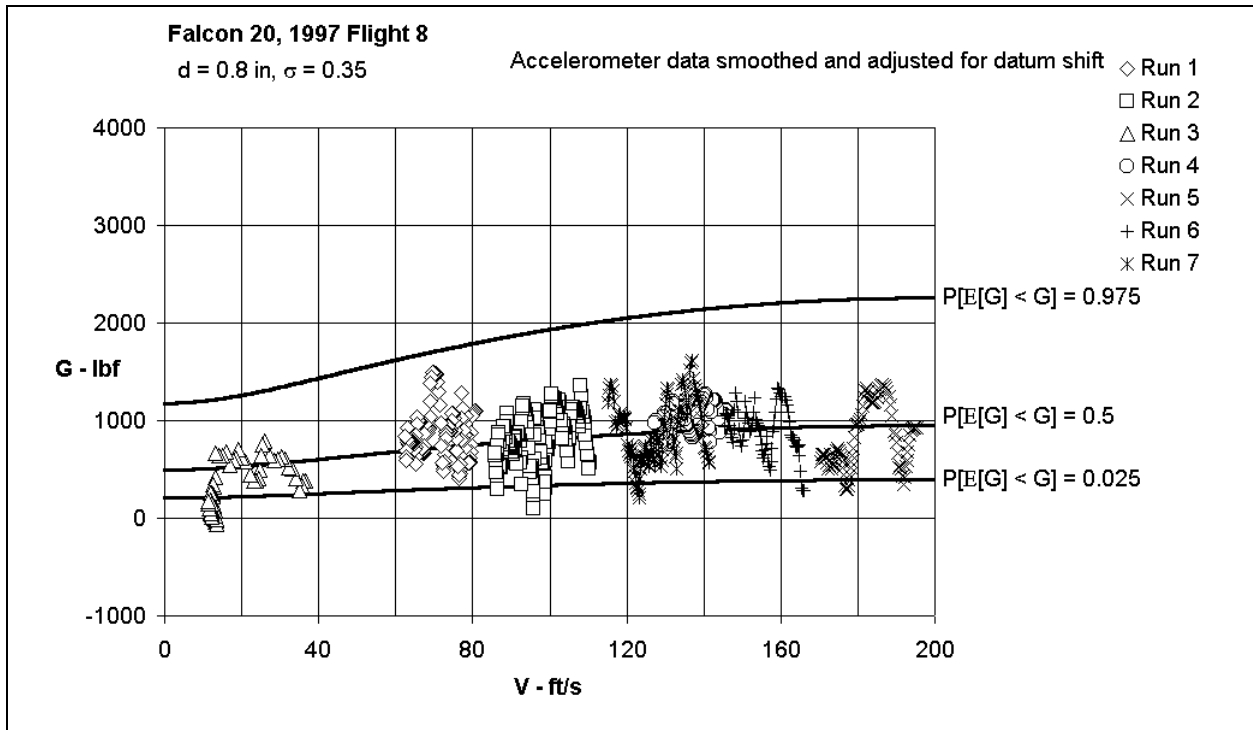
Figure 5.12: Effect of ground speed on resistive force due to aircraft rolling in snow – Falcon 20, 1997
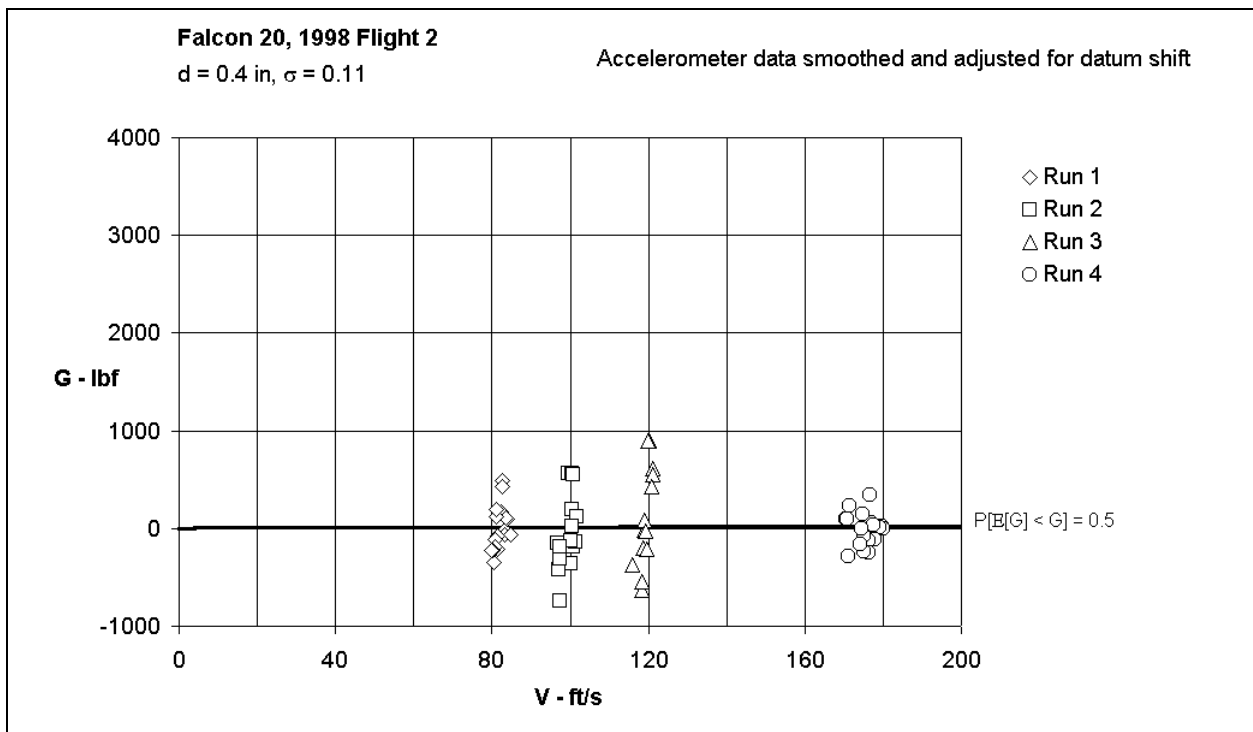
Figure 5.13: Effect of ground speed on resistive force due to aircraft rolling in snow – Flacon 20, 1998 Flight 2
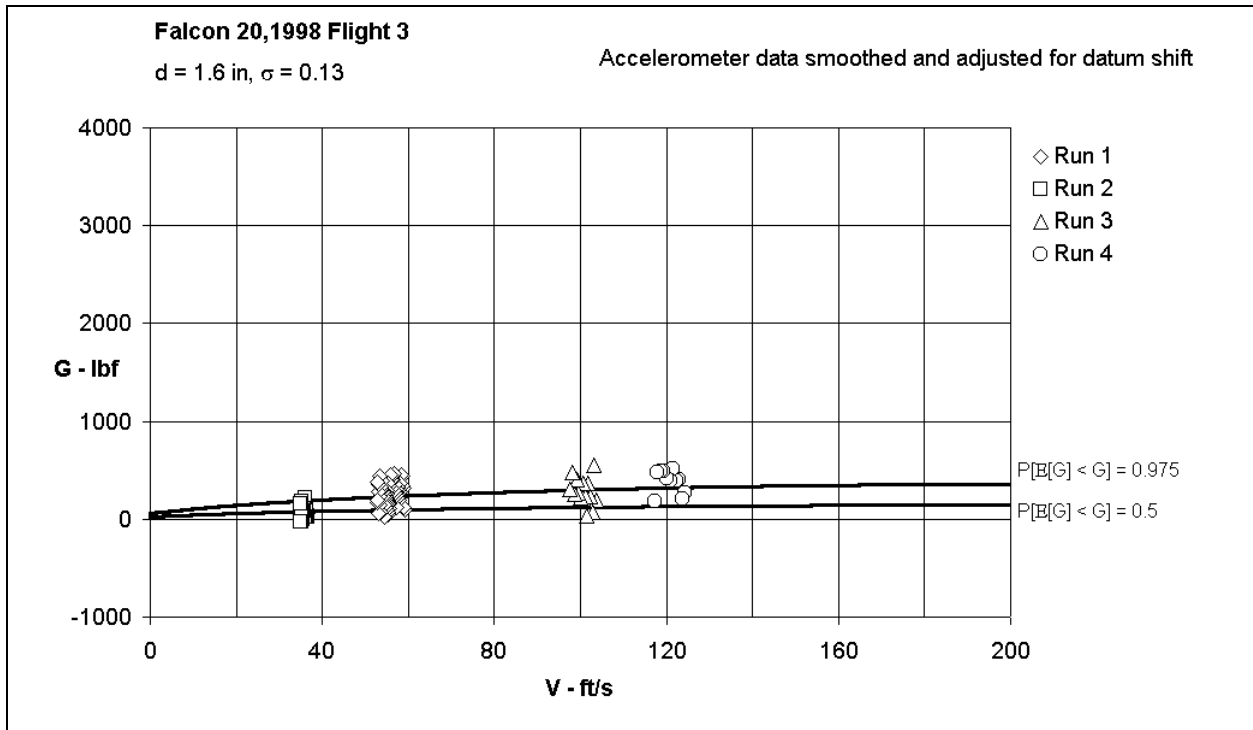
Figure 5.14: Effect of ground speed on resistive force due to aircraft rolling in snow – Falcon 20, 1998 Flight 3
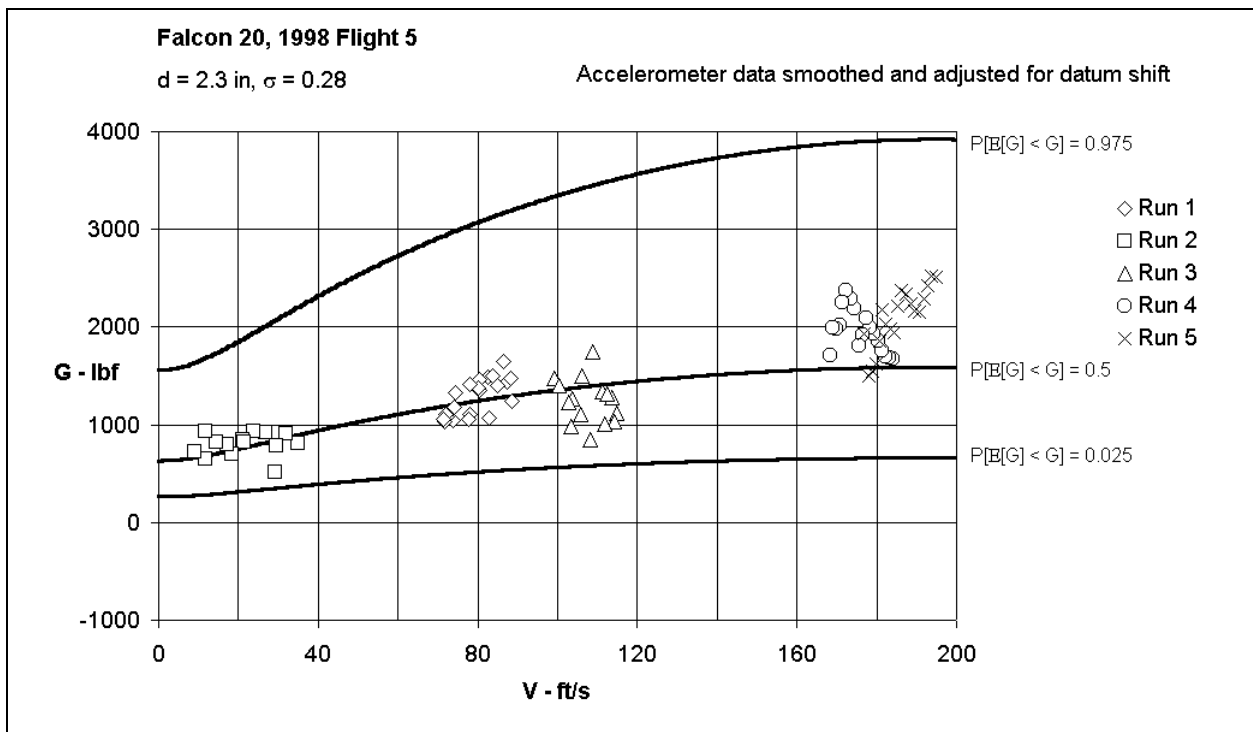
Figure 5.15: Effect of ground speed on resistive force due to aircraft rolling in snow – Falcon 20, 1998 Flight 5
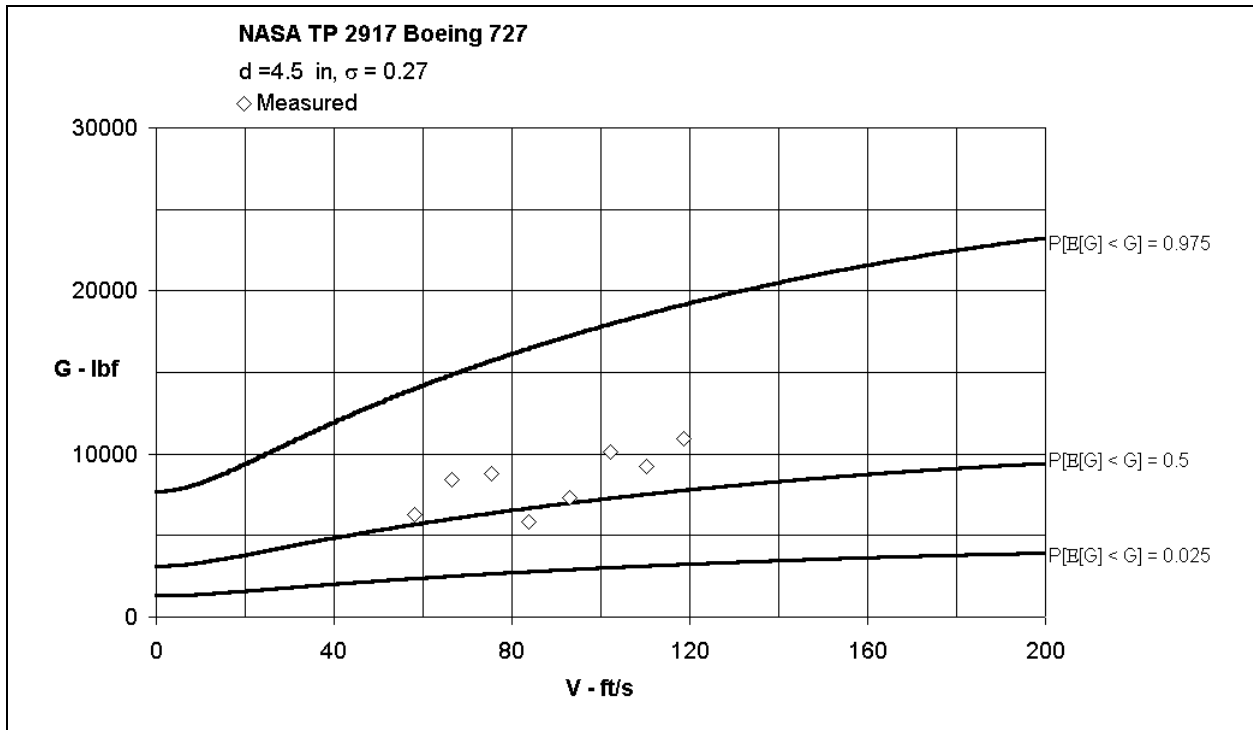
Figure 5.16: Effect of ground speed on resistive force due to aircraft rolling in snow – Boeing 727
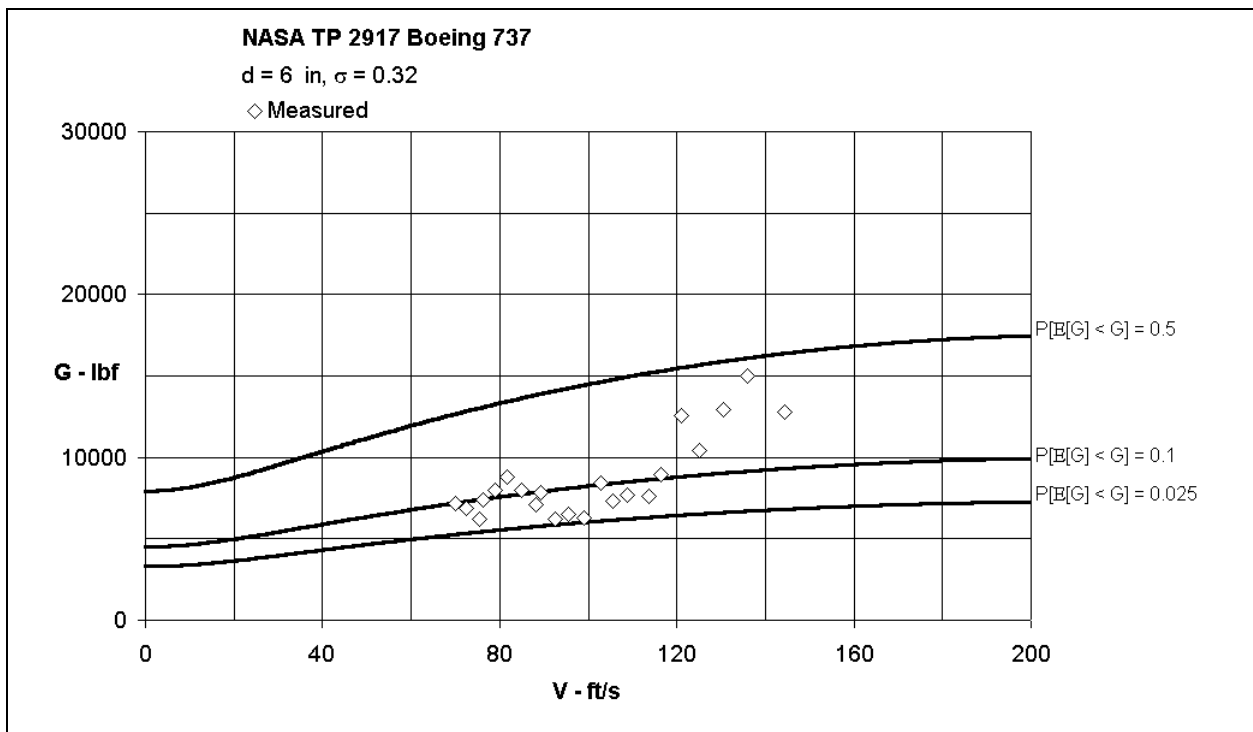
Figure 5.17: Effect of ground speed on resistive force due to aircraft rolling in snow – Boeing 737

54
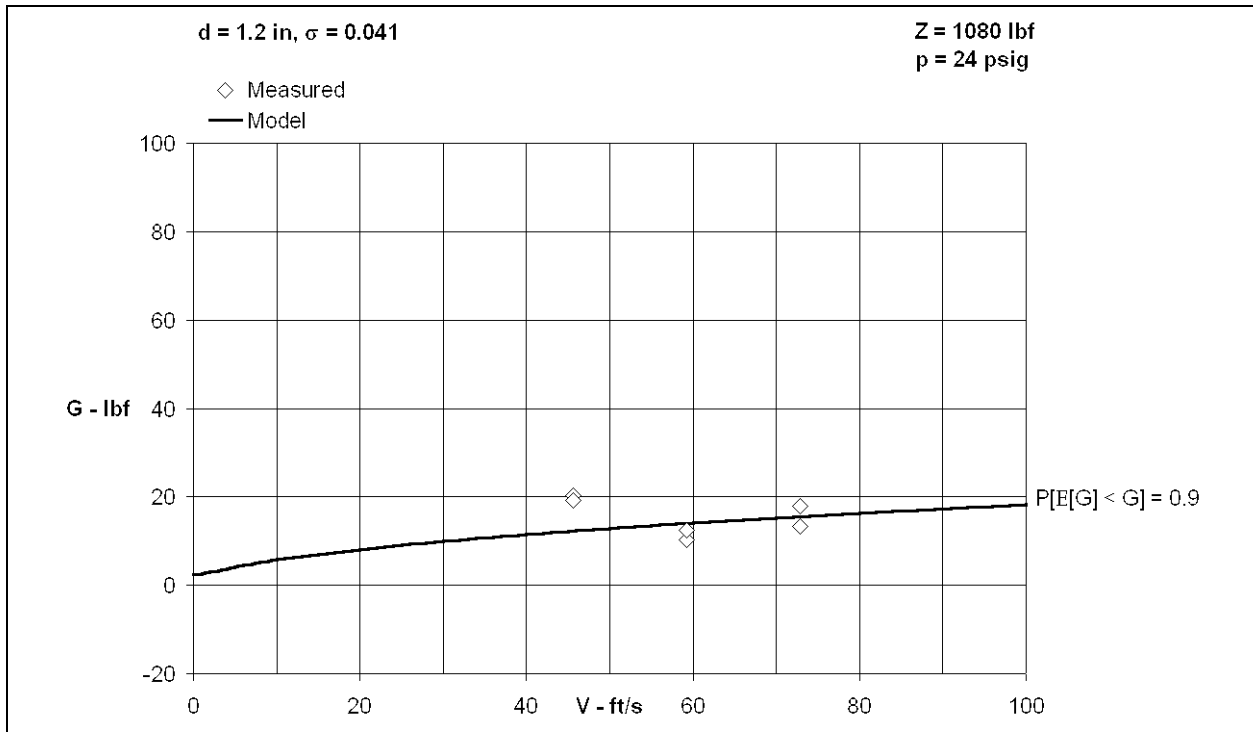
Figure 5.18: Effect of ground speed on resistive force for single tyre rolling in snow
(*d* = 1.2 in, σ = 0.041)
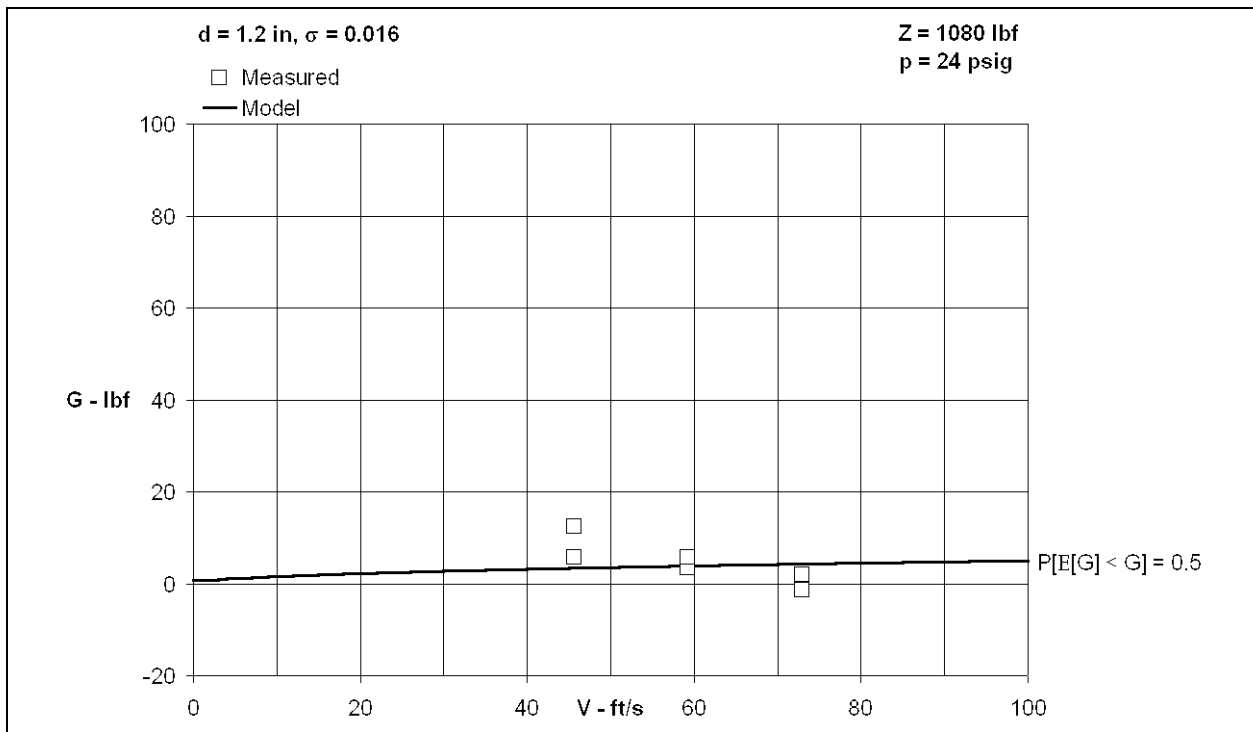
Figure 5.19: Effect of ground speed on resistive force for single tyre rolling in snow
(*d* = 1.2 in, σ = 0.016)
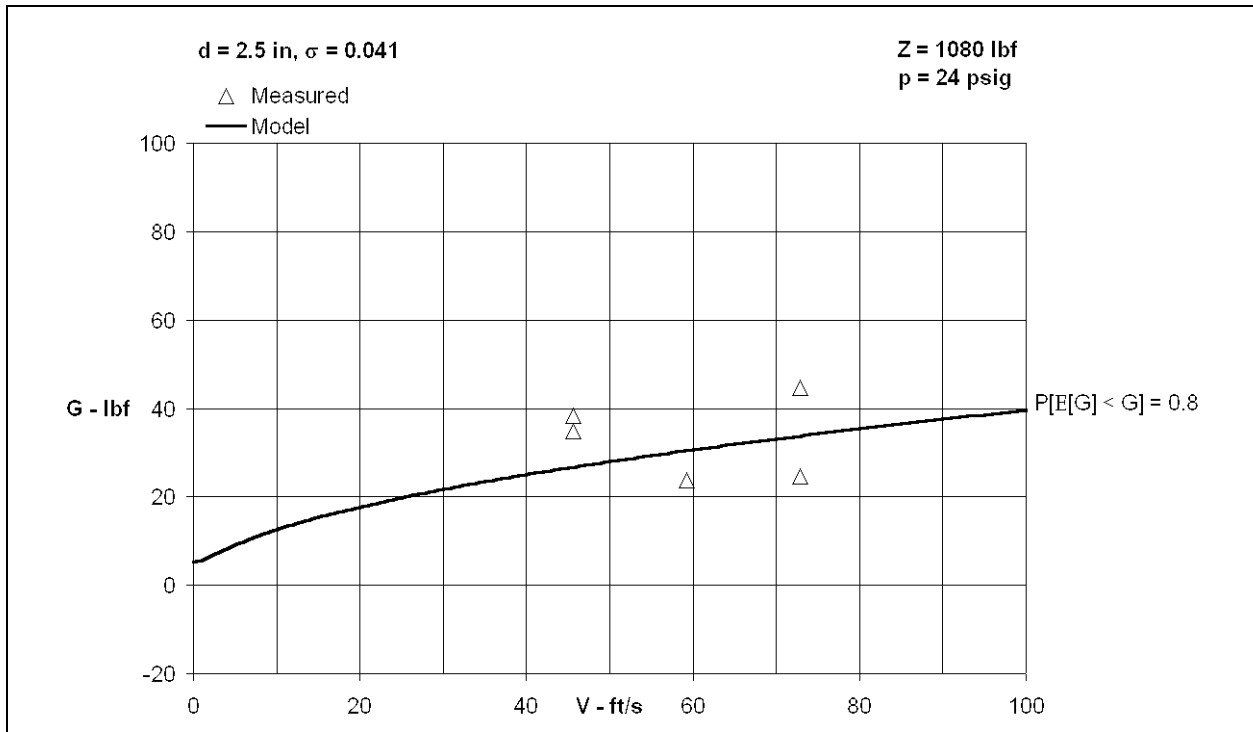
Figure 5.20: Effect of ground speed on resistive force for single tyre rolling in snow
(d = 2.5 in, σ = 0.041)
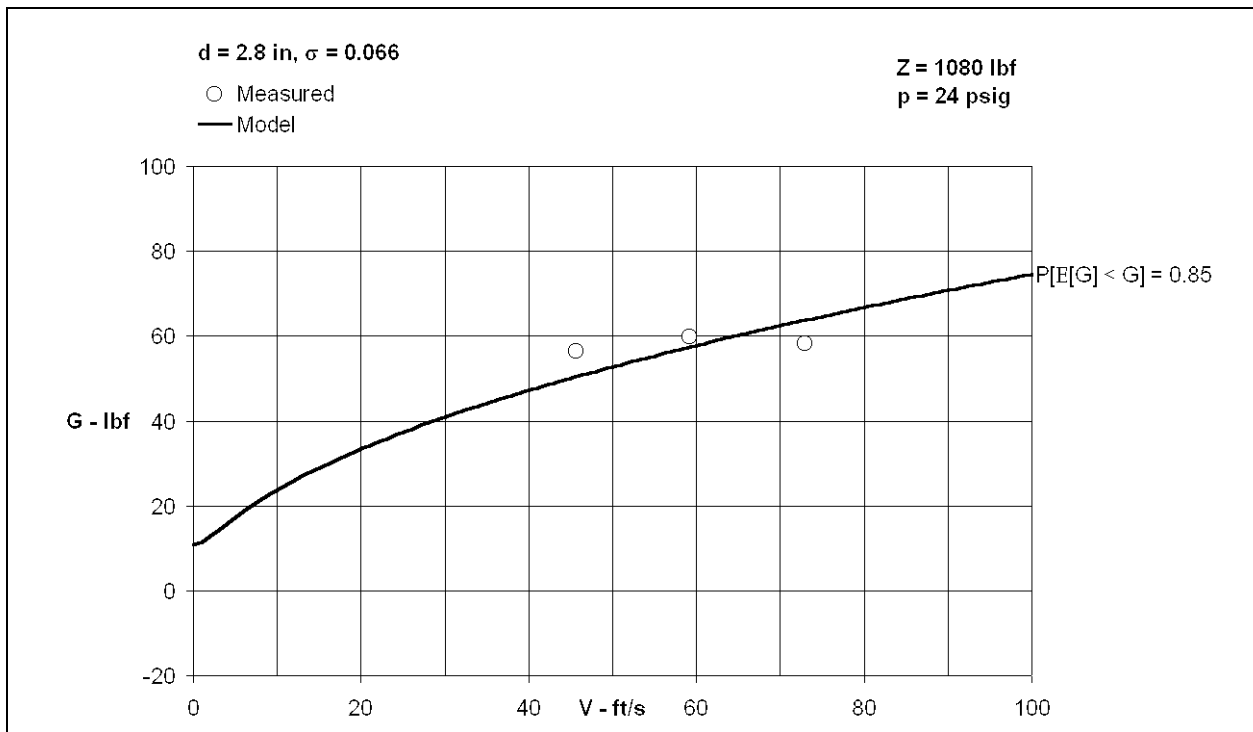
Figure 5.21: Effect of ground speed on resistive force for single tyre rolling in snow
(d = 2.8 in, σ = 0.066)
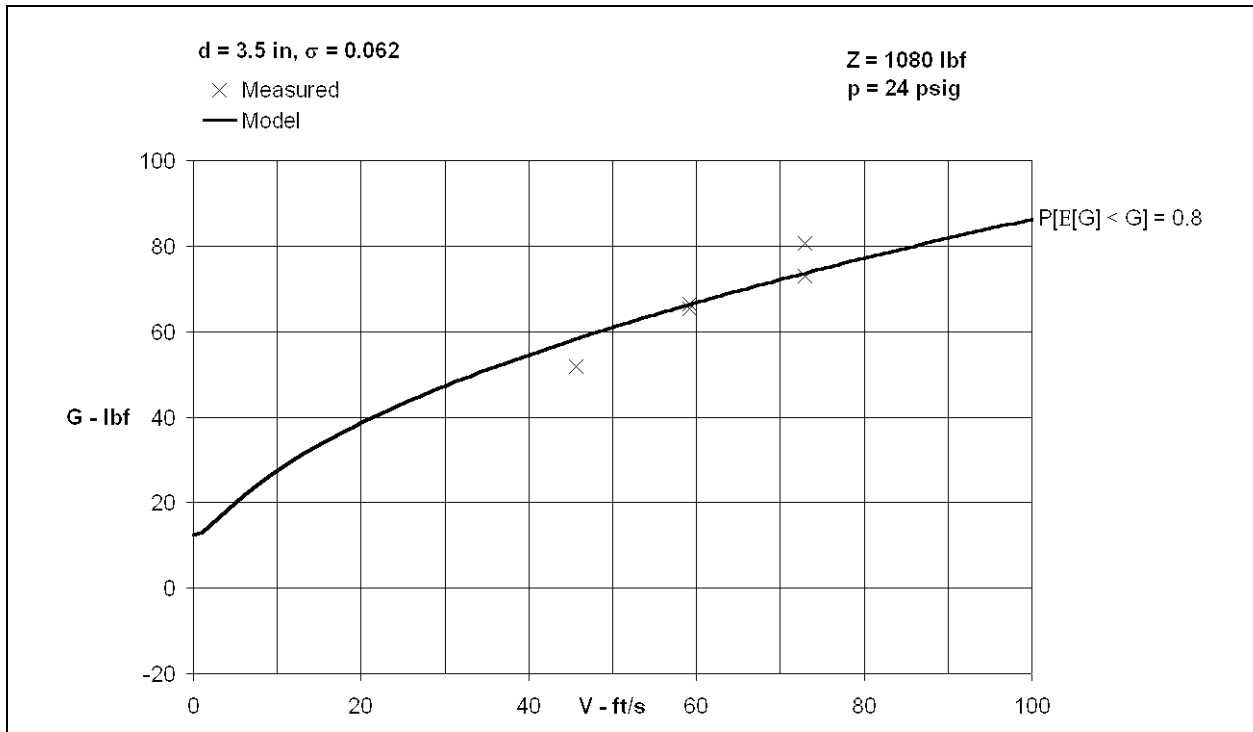
Figure 5.22: Effect of ground speed on resistive force for single tyre rolling in snow
(d = 3.5 in, σ = 0.062)
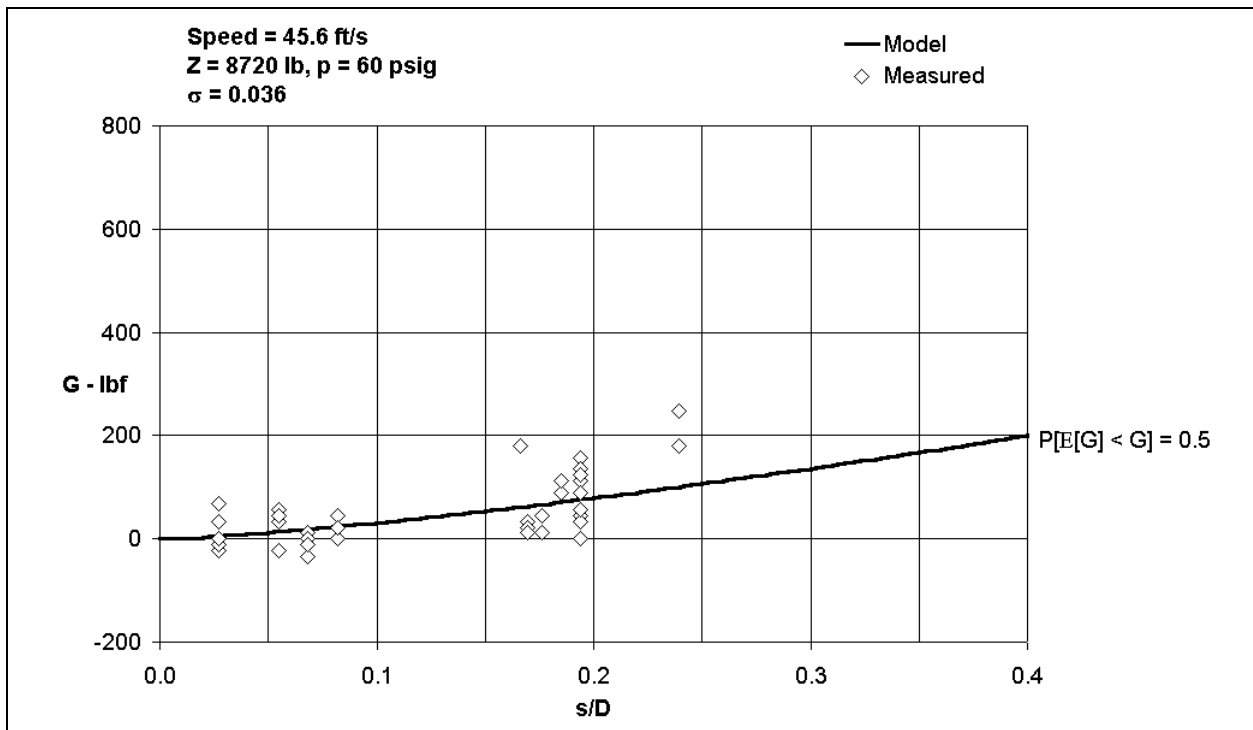
Figure 5.23: Effect of rut depth on resistive force for single tyre rolling in snow
(p = 60 psig, σ = 0.036)

57
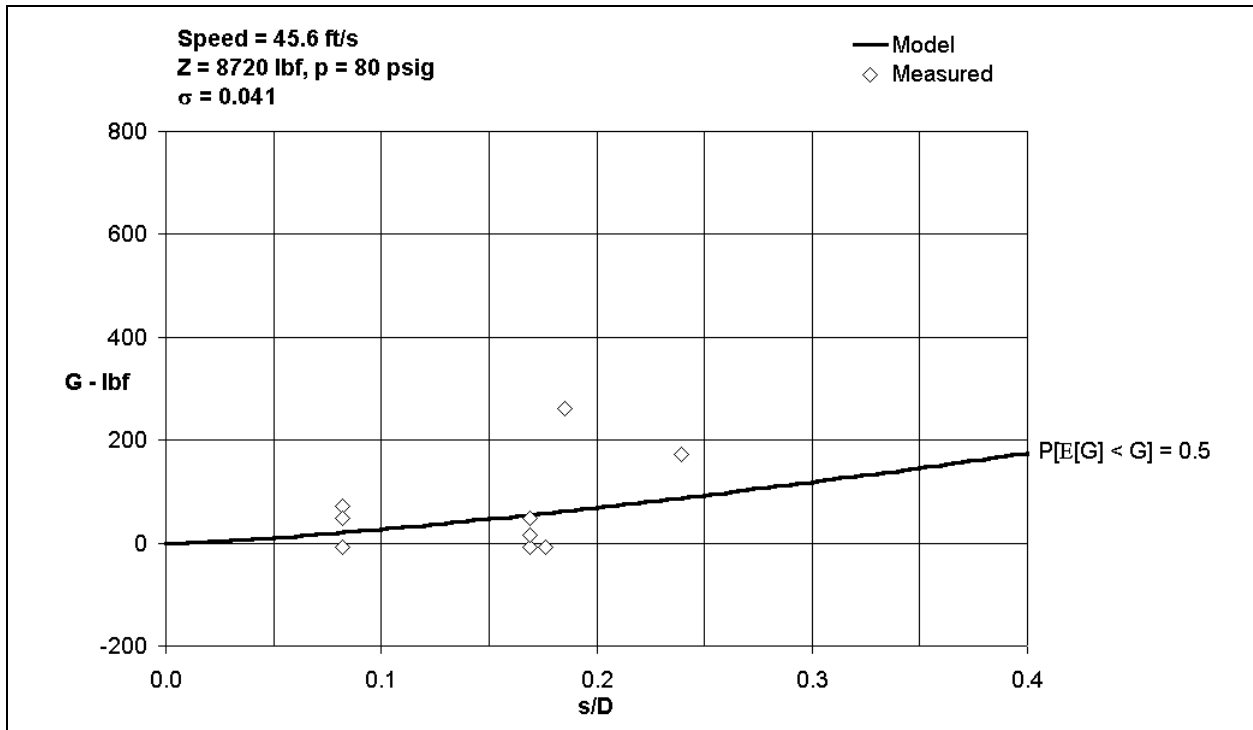
Figure 5.24: Effect of rut depth on resistive force for single tyre rolling in snow
(p = 80 psig, σ = 0.041)
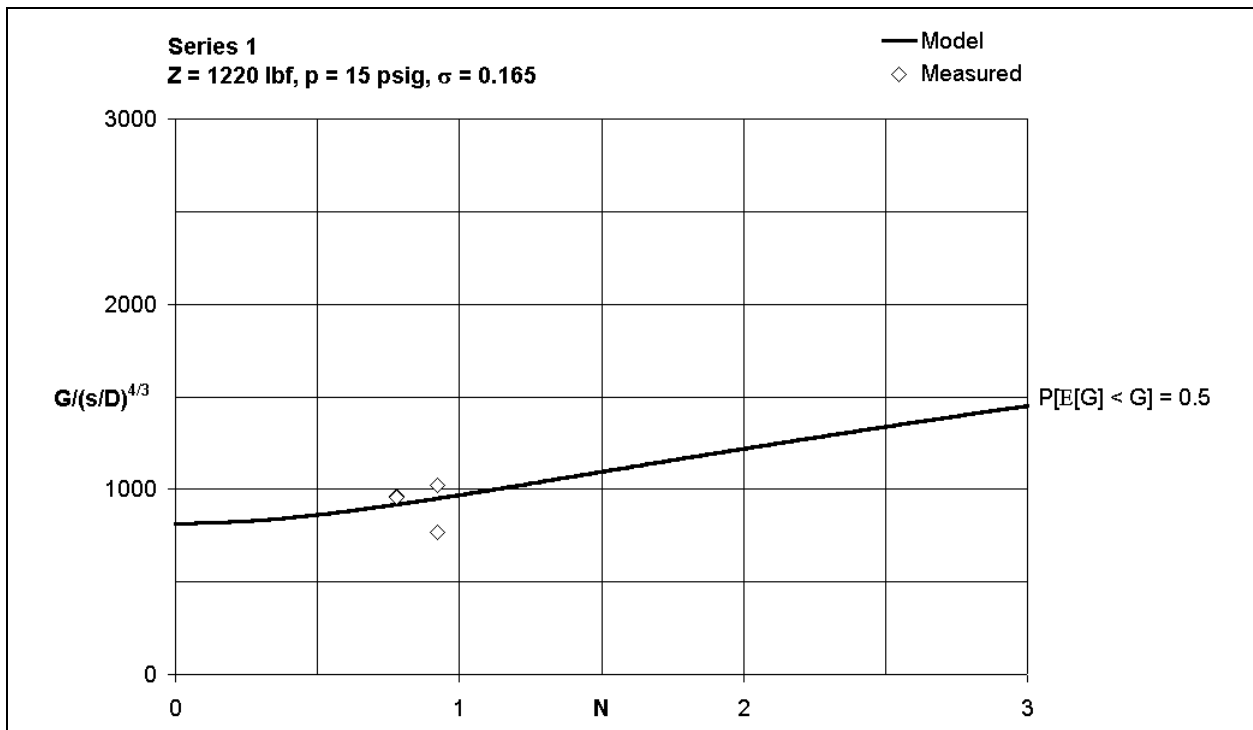
Figure 5.25: Effect of speed number on decelerating force parameter – CRREL vehicle
(Series 1)
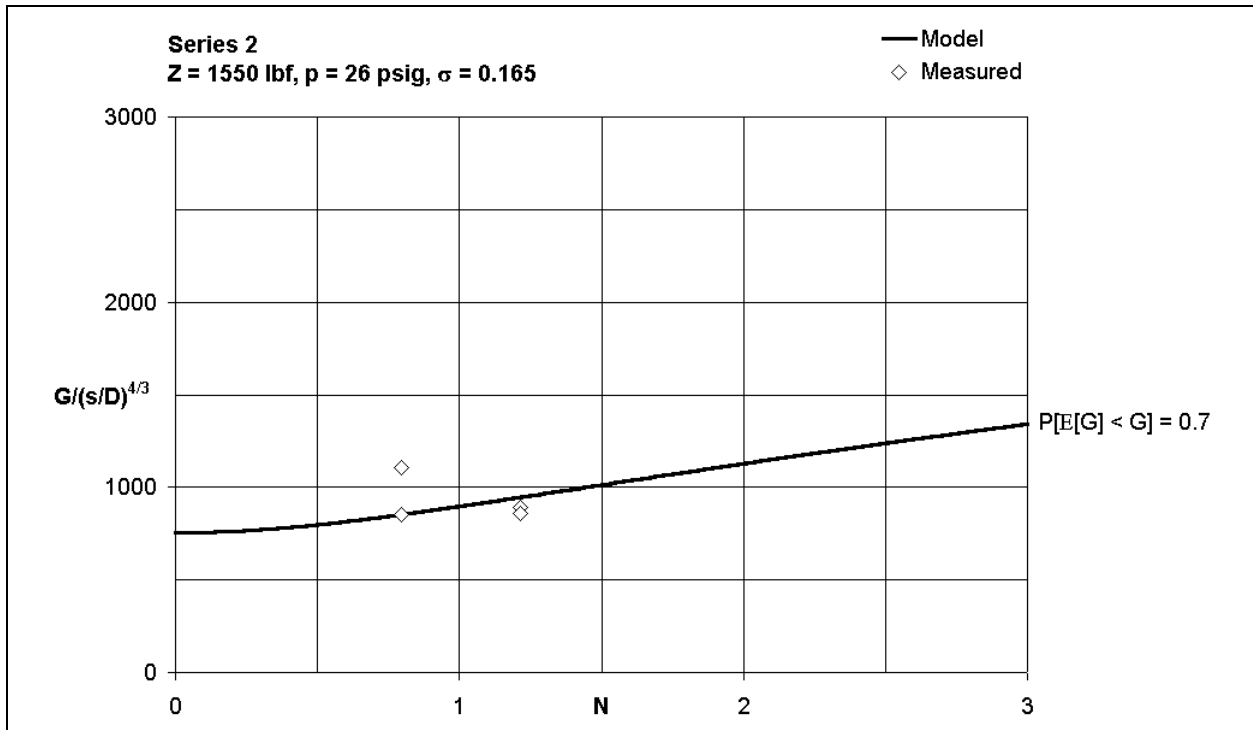
Figure 5.26: Effect of speed number on decelerating force parameter – CRREL vehicle (Series 2)

Figure 5.27: Effect of speed number on decelerating force parameter – CRREL vehicle (Series 3)
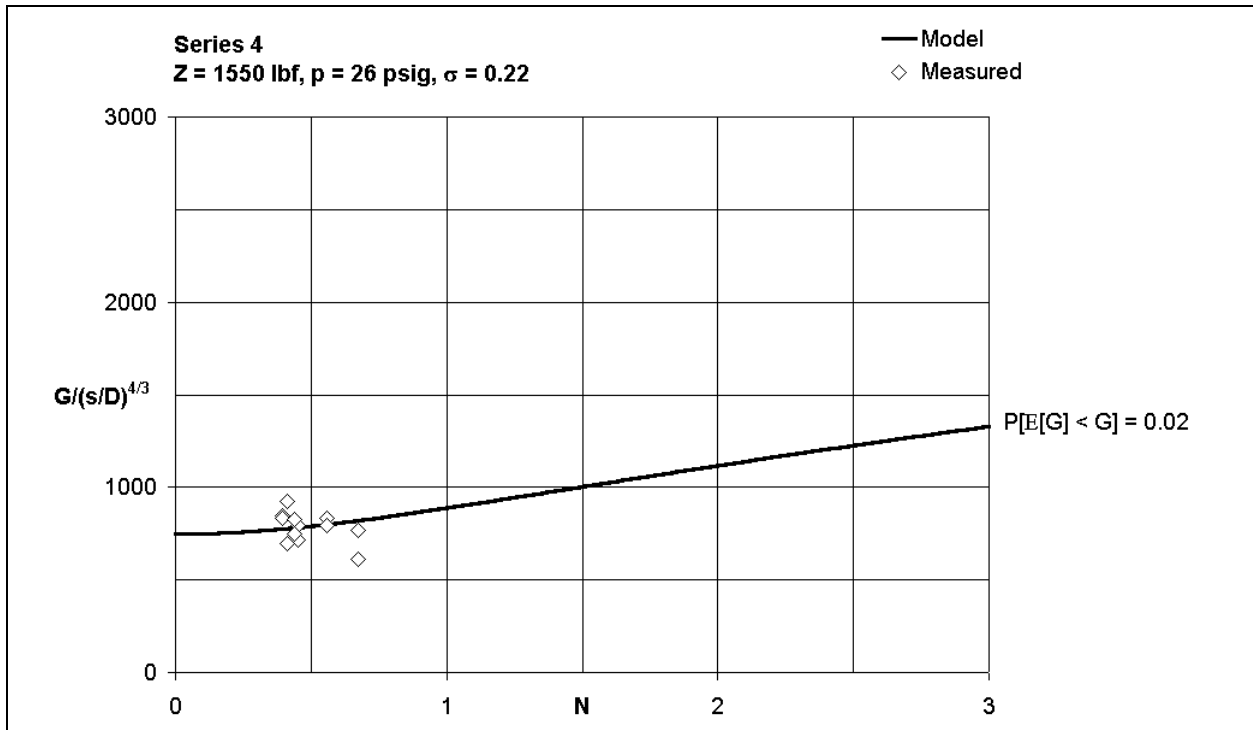
Figure 5.28: Effect of speed number on decelerating force parameter – CRREL vehicle (Series 4)
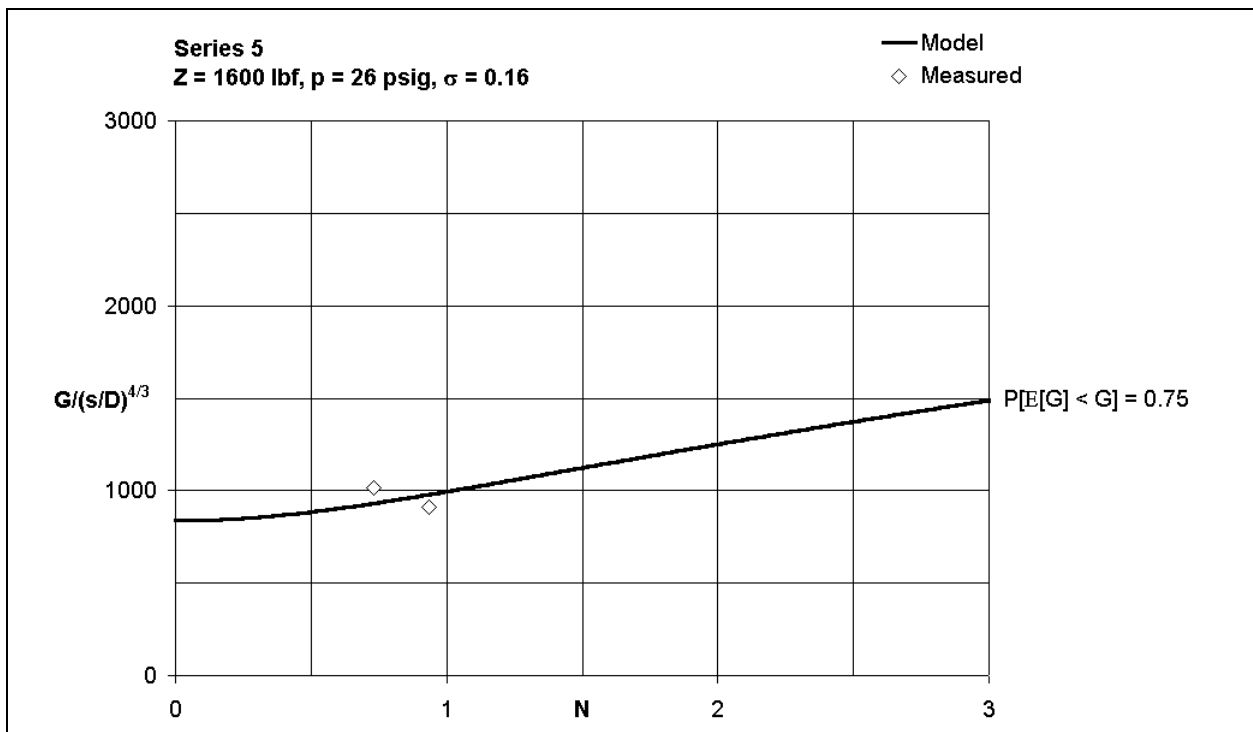
Figure 5.29: Effect of speed number on decelerating force parameter – CRREL vehicle (Series 5)
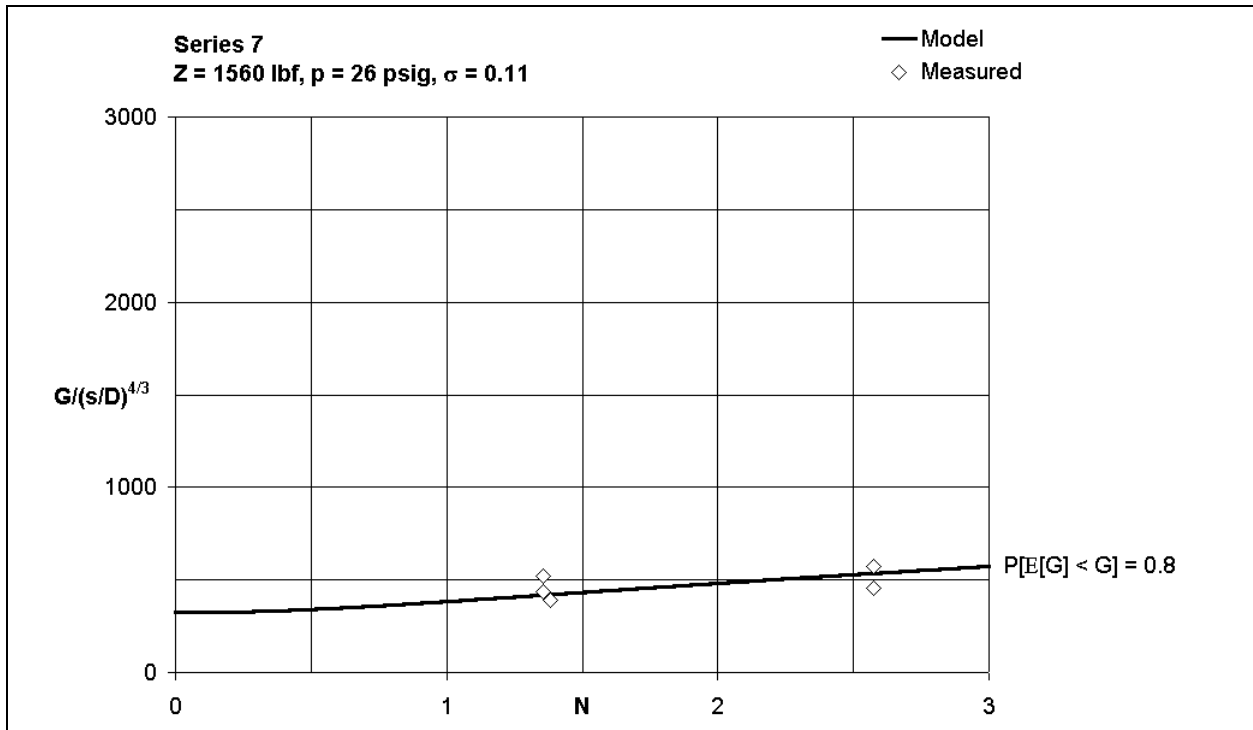
Figure 5.30: Effect of speed number on decelerating force parameter – CRREL vehicle (Series 7)
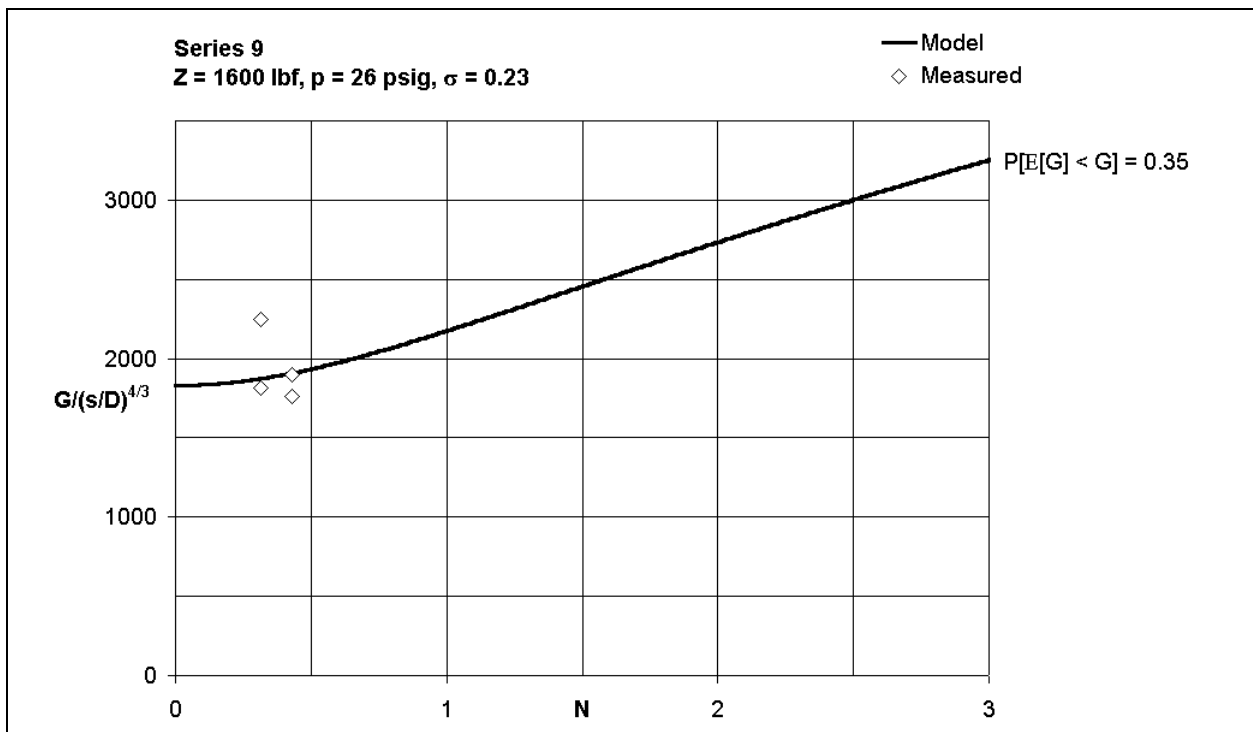
Figure 5.31: Effect of speed number on decelerating force parameter – CRREL vehicle (Series 9)
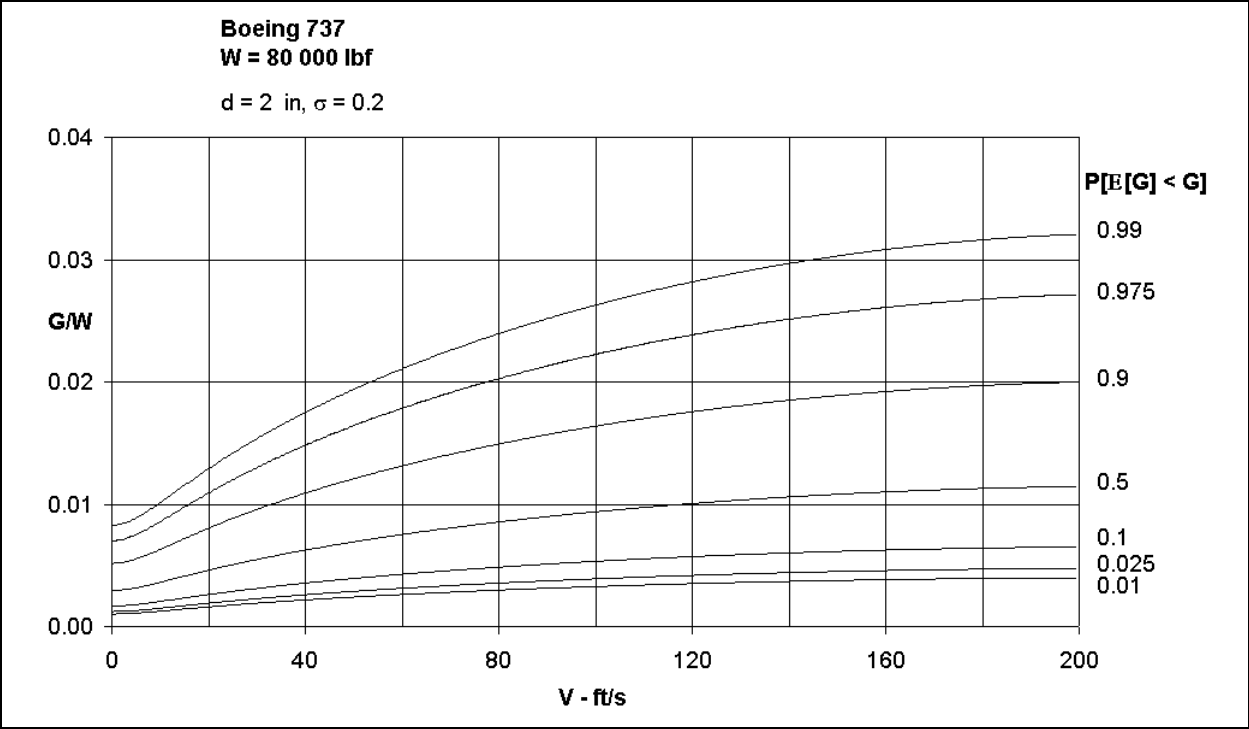
Figure 5.32: Effect of ground speed on normalised decelerating force for the range of probable snow properties

6.   STATIC COEFFICIENT OF BRAKING FRICTION

Prediction of static coefficient of friction between a tyre and a dry runway has invariably been addressed empirically. The approach adopted in this section is similar. However, in addition to tests using standard aircraft tyres, the method developed makes use of early experimental work on rubber hemispheres and blocks reported in Reference 26. These experiments were designed, in part, to test the hypothesis that the relatively large deflections of rubber hemispheres could be predicted, using a relation similar to that developed theoretically, to account for small deflections under load of relatively inflexible materials.

By measuring the effect of vertical load on the diameters of segments of deflected hemispheres made from rubbers of varying hardness, it was argued in Reference 26 that

$$\mu Z^{1/3} = \text{ constant} \qquad\qquad 6.1$$

Furthermore, measurements of friction coefficient between those same rubbers and glass were made.

Surprisingly, the relationships developed in Reference 26 for the effect of bearing pressure and load did not account for the observation of Reference 27 that

$$\mu \propto 1/(a+bp). \qquad\qquad 6.2$$

where a and b are constants for any compound and are to be determined by experiment.

In this section, it is shown that the experimental evidence from Reference 26 *can* be interpreted so that a combination of Equations 6.1 and 6.2 represents the data. A similar relationship is shown to hold for the data in References 28 to 32 from experiments on a range of tyres at speeds near to zero. This correlation is the starting point for the model that has been developed to account for the variation of the coefficient of braking friction on hard-paved runways at all speeds, whether contaminated or not.

6.1   Experiments with Rubber Blocks

The experiments reported in Reference 26 were designed specifically to determine the effect of both bearing pressure and vertical load on the friction coefficient between rubber and a hard (smooth) glass surface. Three different unloaded vulcanizates of natural rubber were tested; the hardness of the rubbers was $13,000 < M_{300} < 103,000$ lbf/ft^2 as conventionally assessed. The effect of load was obtained by compressing hemispheres of the compound and measuring the diameter of the circle of contact. In the experiment, it is shown that the diameter of the circle of contact is directly proportional to the cube root of the load. Because the friction coefficient is, by definition, inversely proportional to the area of contact, it follows that friction coefficient is inversely proportional to the cube root of vertical load as in Equation 6.1.

It was found not possible to obtain a precise measure of the *static* coefficient of friction; therefore, a series of measurements of friction coefficient was made at a speed so that $V < 0.001$ in/s over a range of bearing pressures so that $560 < p < 4700$ - lbf/ft^2 and normal loads so that $2 < Z < 17$ lbf . Results from this part of the experiment are shown in Figure 6.1 where μ is plotted against the empirical function $f[p, Z, M_{300}] = \left(\dfrac{p/p_a}{Z^{1/3} \left(1 + 0.012\, M_{300}/p_a\right)} \right)$.

The correlation shown on the figure is

$$\mu = \frac{3.882}{\left(1 + 2f[p, Z, M_{300}]\right)} \qquad\qquad 6.3$$

The form of the correlating function[15] $f[p, Z, M_{300}]$ is arbitrary in that it is one of the simplest ways that the variables can be combined so that the data collapse onto a single characteristic. Inspection of Figure 6.1 indicates that the function describes the data most satisfactorily at high values of pressure. At low values of pressure, the variation with hardness appears not to be so consistent. A similar effect can be seen in the original analysis of the data. However, wholly plausible reasons were not suggested by the experimenter; the effect may be a consequence of the difficulties in setting up those particular experiments. The format of Equation 6.3 is sufficiently convenient and flexible to lead to a practical method for calculating the braking friction of tyres for aircraft and ground vehicles.

6.2   Experiements with Tyres

All the experimental evidence analysed in this section was collected by NASA over a period of several years and reported in References 28 to 32. In particular, the aircraft style tyres were tested by towing aircraft (with brakes locked) at speeds so low as to be effectively zero.

Friction coefficients have been correlated in this study using the following procedure. Equation 6.3 can be recast for a specific compound and design of tread so that

$$\mu_{SKID\ STATIC} = \frac{\mu_{REF}}{\left(1 + \eta_0 \dfrac{p/p_a}{Z^{1/3}}\right)} \qquad\qquad 6.4$$

where η_0 subsumes elements unknown for the specific compound and tread design.

By taking reciprocals of both sides, Equation 6.4 can be recast,

---

[15]   Note that this function is not dimensionless as written. Thus, when converting from one unit system to another, care must be taken to account for this.

$$\frac{1}{\mu_{SKID\ STATIC}} = \frac{1}{\mu_{REF}} + \left(\frac{\eta_0}{\mu_{REF}}\right)\left(\frac{p/p_a}{Z^{1/3}}\right) \qquad\qquad 6.5$$

Equation 6.5 can be solved using the method of least squares[16] for the whole set of measurements for aircraft tyres which are shown in Figure 6.2. The correlation identified is

$$\mu_{SKID\ STATIC} = \frac{0.909}{\left(1 + 0.416\dfrac{p/p_a}{Z^{1/3}}\right)} \qquad\qquad 6.6$$

Thus, $\mu_{REF} = 0.909$ and $\eta_0 = 0.416$. The distribution of the measured data about the correlation was tested for Normality using a χ^2-test. It was found that $P\left[\chi^2\right] > 0.25$; it may therefore be presumed that the properties of the Normal distribution may be applied. Thus, because the correlation is based on 100 measurements and $\sigma\left[\Delta\left[\mu_{SKID\ STATIC}\right]\right] = 0.045$, the uncertainty $\left(U\left[\mathrm{E}\left[\mu_{SKID\ STATIC}\right]\right]\right)$ of an expected value of static friction coefficient is in the order of ± 0.01 at the 95% level of probability. The accumulative distribution is shown for reference in Figure 6.3.

The experimental data from References 28 to 31 have been correlated by NASA using only the inflation pressure as a variable. This does not lead to substantial error in estimating static coefficient of braking friction under normal operational circumstances. Dependency on vertical load is relatively weak and aircraft tyres are generally operated over a limited range of load for a given inflation pressure. Therefore, for the loads normally used for aircraft operations, large errors do not occur. However, in some of the experiments considered in subsequent parts of this study, the relative range of vertical loads is substantial. Omission of the effect of load, in the static case, would have led to a consequential failure to achieve satisfactory correlations.[17] In the process of correlating the data for tyres from References 28 to 31, it is noted that the reciprocal of measured friction coefficient is Normally correlated with the variable $\dfrac{p/p_a}{Z^{1/3}}$. It is not always the case that re-arranging variables (by taking the reciprocal of the dependent variable and forming the deviation of the resulting reciprocal from the inverted correlation) will result in a set of deviations that is Normally distributed. In this case, however, the distribution of $\Delta\left[\mu_{SKID\ STATIC}\right]$, where

$$\Delta\left[\mu_{SKID\ STATIC}\right] = \mathrm{M}\left[\mu_{SKID\ STATIC}\right] - \mathrm{E}\left[\mu_{SKID\ STATIC}\right] \qquad\qquad 6.7$$

can be shown to be not significantly different from a Normal distribution. It is therefore appropriate to use the properties of the Normal distribution to calculate confidence limits for a calculation of static coefficient of friction for aircraft tyres from the correlation of Equation 6.6.

---

[16] See Reference 5 for details of this method and for all other statistical techniques used.
[17] This is especially true for analysis of skidding data in the wet.

Measurements of μ for the ASTM E524 and E249 tyres were made over a limited range of the parameter $\dfrac{p/p_a}{Z^{1/3}}$ as shown in Figure 6.2. It is therefore not possible to identify both μ_{REF} and η_0 for those tyres. As an approximation, it is assumed that the value of $\eta_0 \left(=0.416\right)$ that is applicable for the aircraft tyres can be used for these ASTM tyres. Using this value, the relation

$$\mu_{SKID\ STATIC} = \frac{1.374}{\left(1+0.416\dfrac{p/p_a}{Z^{1/3}}\right)} \qquad 6.8$$

describes the data for the E524 tyre and

$$\mu_{SKID\ STATIC} = \frac{1.223}{\left(1+0.416\dfrac{p/p_a}{Z^{1/3}}\right)} \qquad 6.9$$

describes the data for the E249 tyre.

Now, the data for both these tyres were collected using the same experimental process. The distribution of the measurements about the correlations of Equations 6.8 and 6.9 may therefore be combined. Because the sample contains only 17 measurements, the Anderson-Darling test, rather than a χ^2-test, was used to show that the distribution of these deviations was Normal with standard deviation $\sigma\left[\Delta\left[\mu_{SKID\ STATIC}\right]\right]=0.0224$. The uncertainty associated with an expected value of static friction coefficient $\left(E\left[\mu_{SKID\ STATIC}\right]\right)$ calculated from this correlation is, therefore, in the order of ±0.01 at the 95% level of probability for the ASTM tyres. For reference, the accumulative distribution is shown in Figure 6.4.

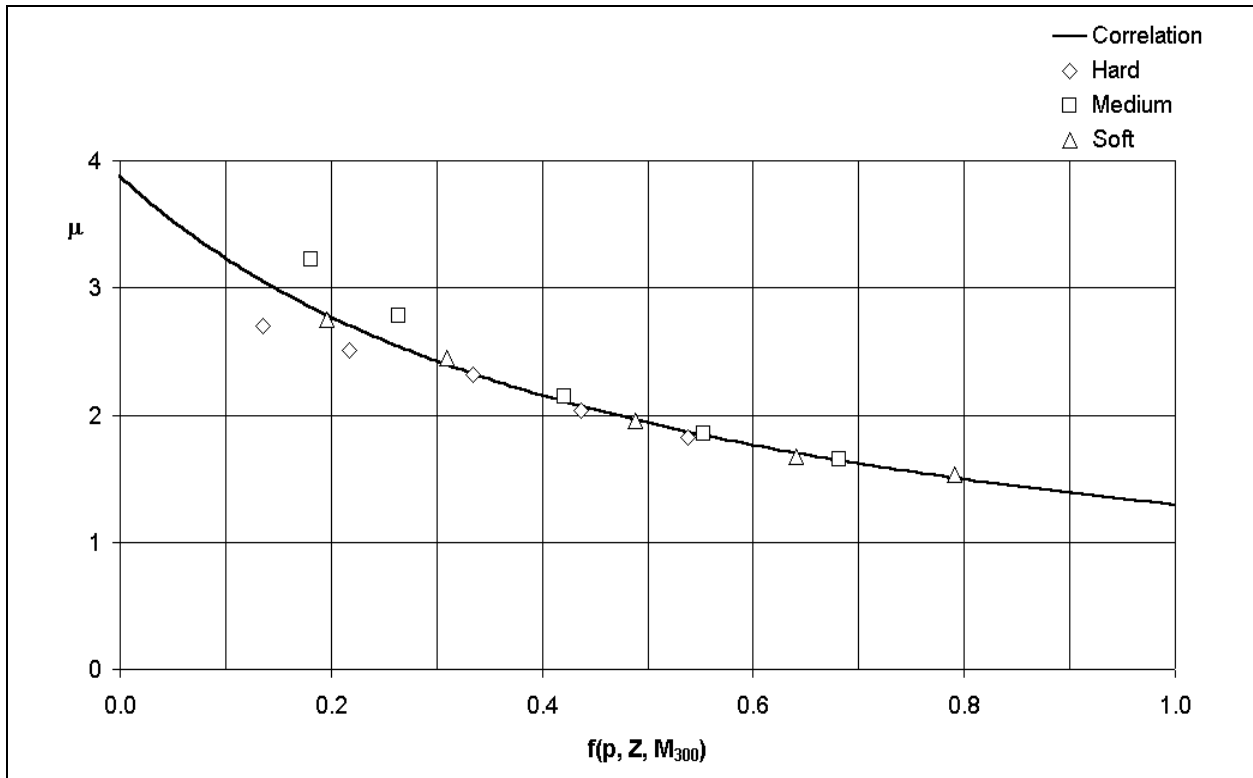**Figure 6.1: Effect of bearing pressure, normal force and hardness on static friction coefficient for three vulcanizates of natural rubber**
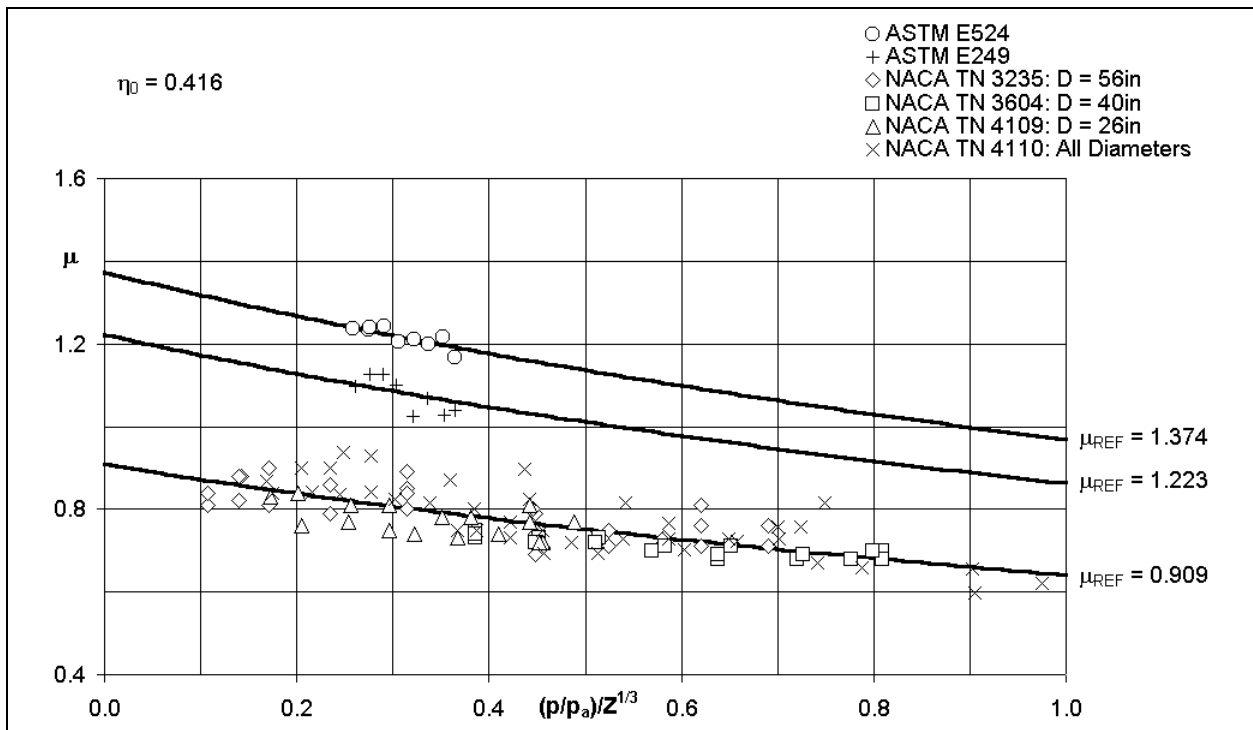
Figure 6.2: Effect of bearing pressure and normal force on static friction coefficient for three types of tyre
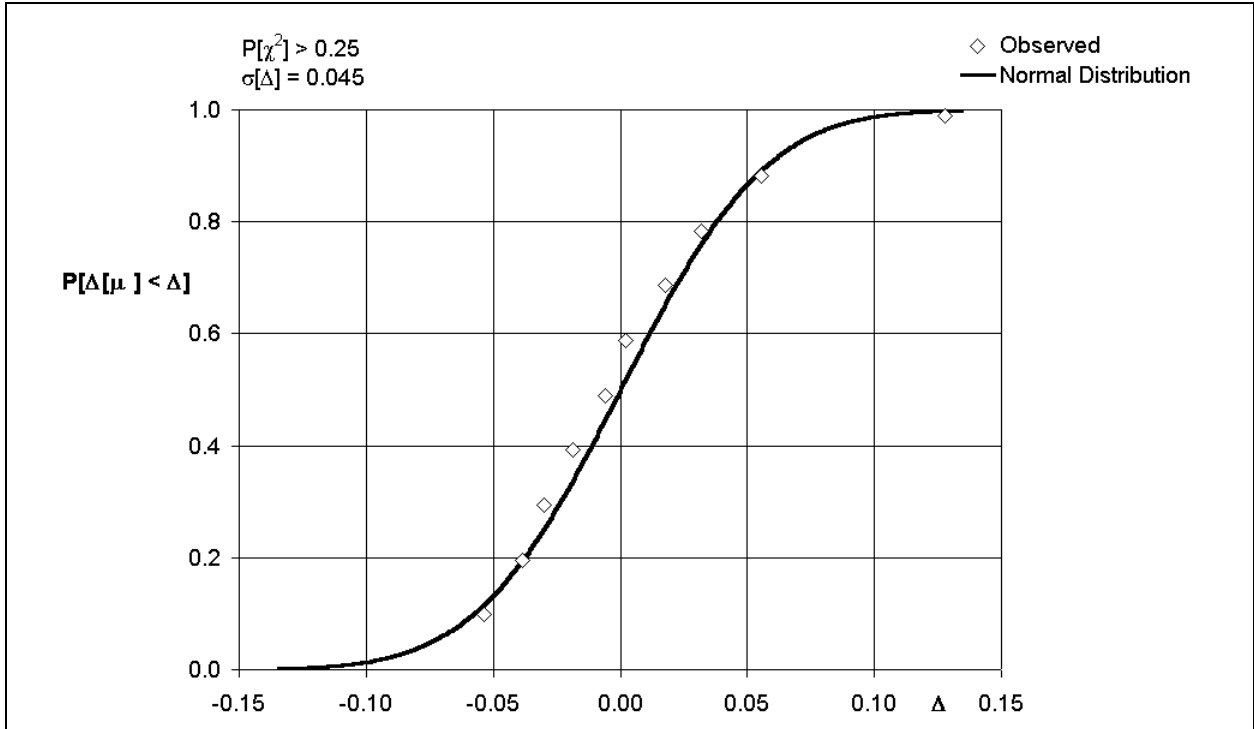
Figure 6.3: Distribution of measured data about correlation for aircraft tyres
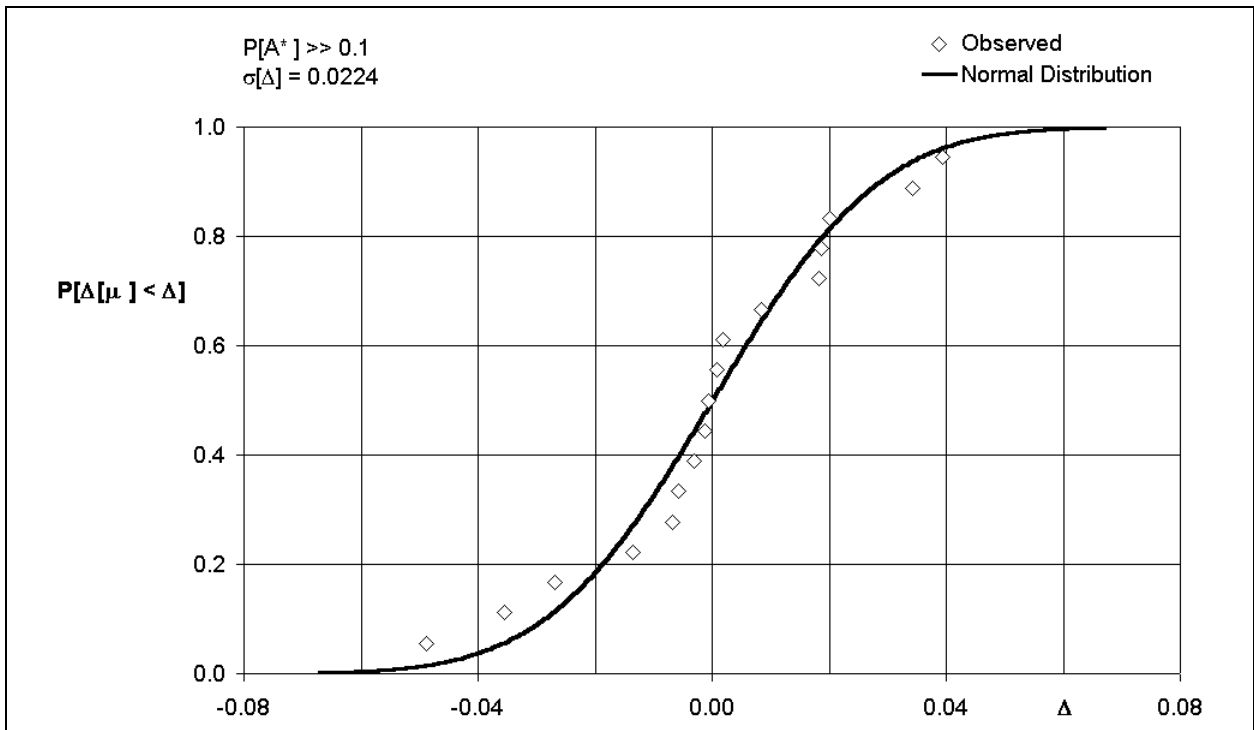
Figure 6.4: Distribution of measured data about correlation for ASTM type tyres

7. COEFFICIENT OF BRAKING FRICTION – SKIDDING ON DRY RUNWAY

All attempts to formulate schemes to represent the friction coefficient for a tyre *skidding* on any pavement have been empirical. By common consent, such an approach is an unavoidable consequence of the complex interactions between the tyre compound, the tread pattern and the topography of the ground. Because of this complexity, the present study has not sought a general formulation. A model has been constructed for a specific class of tyre slipping and sliding over a particular type of surface. Thus, although the mathematical formulation given could well be adaptable to a general case, the numerical values in the formulation apply only to aviation tyres in contact with surfaces typically found on runways. It is possible that this restriction could be couched in terms of the visco-elastic properties of rubber compounds, the physics of tread pattern design and the civil engineering definitions of surfacing aggregates. Such an approach has not been attempted, which leaves the matter of range of applicability of the modelling open to question. This aspect of the study is briefly considered in Section 10 in the context of experiments conducted on wet runways.

In Section 6, a correlation is given for the case of aviation tyres under static conditions on dry runways. Even this fundamental case is addressed empirically. However, the relationship:

$$\mu_{SKID\ STATIC} = \frac{\mu_{REF}}{1+\eta_0 \dfrac{p/p_a}{Z^{1/3}}} \qquad\qquad 7.1$$

is based on observations and comments gathered from the writings of workers in the field of rubber technology. The constants μ_{REF} and η_0 are obtained from study of experimental data and are dependent on the nature of the tyre design and the compound from which the tyre is made.

Now, the constant η_0 can be interpreted to be associated with the absorption of strain energy in the footprint – no energy is absorbed in the brake pads because the brakes are locked in the experimental process from which the data are obtained. If this interpretation is valid, then it may also be thought that, in a full skid at speed, the footprint also absorbs kinetic energy. This leads to

$$\mu_{SKID\ DRY} = \frac{\mu_{REF}}{1+\left(\eta_0 + \eta_1 \dfrac{V^2}{2g}\right)\dfrac{p/p_a}{Z^{1/3}}} \qquad\qquad 7.2$$

as a possible model for coefficient of friction when skidding in dry conditions. This formulation is valid for all speeds *on dry runways* if and only if the topography of the runway surface has no influence on interactions between the tread compound and the ground.

It is generally accepted that the balance between micro-texture and macro-texture has little effect on the magnitude of friction coefficient in the dry for those types of surface used for aerodrome

runways. However, there is little evidence to test this assumption. Nor, for that matter, is there more than a small body of data in the public domain to check the applicability of the model. The information readily to hand has been taken from Reference 7 and is shown in Figures 7.1, 7.2 and 7.3. The correlation of the measured data within the framework afforded by Equation 7.2 is discussed in sub-section 7.1.

7.1   Discussion

The set of data under conditions of full skid from Reference 7 covers a limited, yet representative, range of speed, load and inflation pressure. In order to augment the set, some information from slipping tests has been used. This implies an additional assumption – that slip ratio has negligible effect on skidding friction for relatively high values of slip ratio. This assumption anticipates the results of the modelling reported in Section 8. Thus, in this case, Equation 7.2 is re-written

$$\mu_{SKID\ DRY} = \frac{\mu_{REF}}{1 + \left(\eta_0 + \eta_1 \dfrac{v^2}{2g} \right) \dfrac{p/p_a}{Z^{1/3}}} \qquad\qquad 7.3$$

where $v = sV$.

A feature of the data from Reference 7 is the uncertainty associated with the measurements. No assessment of uncertainty is given in the reference. However, the extent of the scatter in Figure 7.1 would suggest that the design of the experiment was in some way compromised. First, the testing was conducted with a braking system that cycled from free rolling to full skid in less than a second. Thus, slip ratio and all the measured forces varied rapidly with time. There is no doubt that the frequency responses of the instrumentation would have had a substantial effect on both the values recorded and on the time correlation of the measured variables. Second, the tyre used in the experiment was subject to extremely harsh treatment. There was no obvious evidence of the effect of wear, presumably because any such effect was masked by the deficiencies in instrumentation noted above. However, it would not be surprising if tyre wear made a significant contribution to uncertainty in the experimental data.

The model described by Equations 7.2 and 7.3 represents the accumulated data very well – see Figures 7.1, 7.2 and 7.3. The value $\eta_1 = 0.019$ implied by the correlation procedure results in a standard error $\sigma\left[\Delta\left[\mu_{SKID\ DRY} \right] \right] = 0.077$ for the distribution of measurements about the model. The data (see Figure 7.4) are Normally distributed – $P\left[\chi^2 \right] > 0.15$ – thus, the uncertainty associated with the scatter about the correlation may be calculated using the properties of the Normal distribution: $U\left[\Delta\left[\mu_{SKID\ DRY} \right] \right]_{0.95} = \pm 0.15$. This is somewhat larger than the uncertainties found in many experiments. On the other hand, the attempt to conduct a series of skidding tests in the dry on full-scale aircraft tyres is unprecedented. If it were not for these data, the task of modelling operations on *contaminated* surfaces would have been almost impossible.

It is unfortunate that the set of data is so sparse at the higher of the tested values of load. Using the statistical *t*-test, the data presented in Figures 7.2 and 7.3 can be shown to be consistent with the model. However, an uncritical examination of the data could have led to the unwarranted conclusion that there was no effect of speed on the coefficient of friction in full skid. Furthermore, the data could also have led to the inference that the effect of inflation pressure at constant load is the reverse of that expected from static tests.

Finally, the correlation is based on 155 measurements; the uncertainty of an independent calculation of coefficient of friction in a full skid on a dry runway is, therefore,

$$U\left[\mu_{SKID\ DRY}\right]_{0.95} = \frac{\pm 0.15}{\sqrt{155}} = \pm 0.012 \qquad 7.4$$

This figure is applicable at the 95% level of probability and may be used in the assessment of the contribution of coefficient of friction in a full skid to uncertainty in performance calculations using the correlation presented here.

Figure 7.1: Effect of footprint translation speed on $\mu_{SKID\ DRY}$
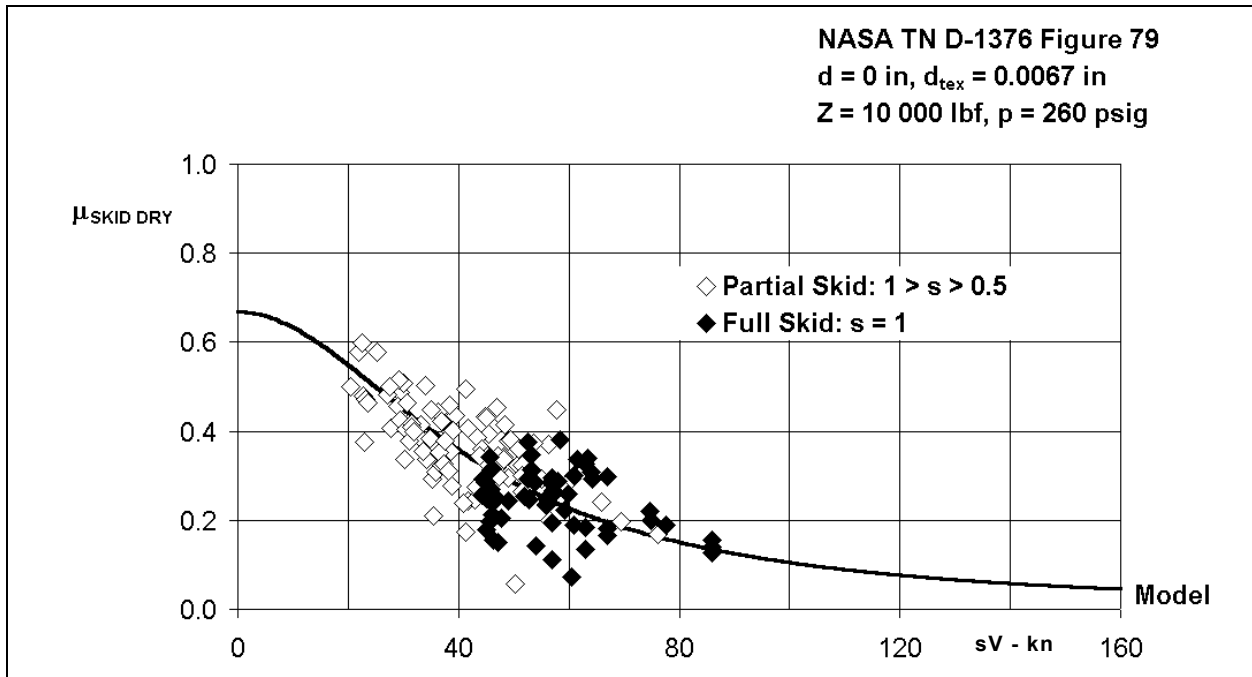**(Z = 10000 lbf, p = 260 psig)**
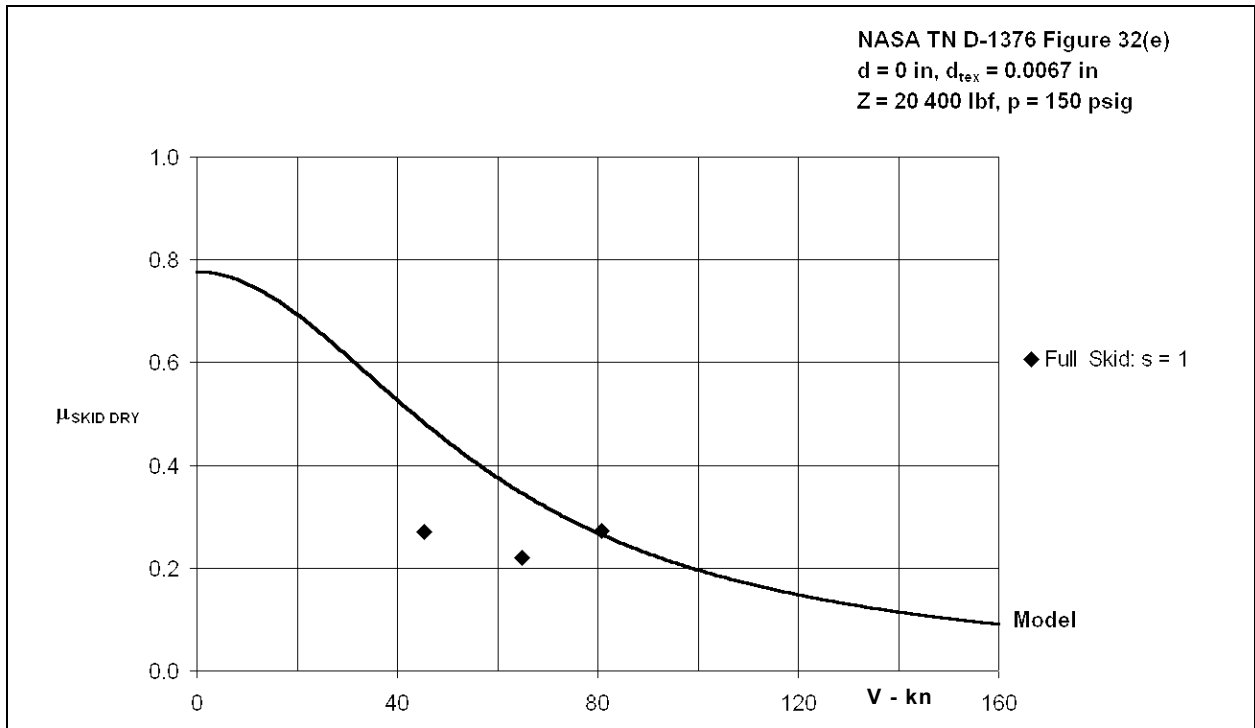
Figure 7.2: Effect of footprint translation speed on $\mu_{SKID\ DRY}$
(Z = 20400 lbf, p = 150 psig)
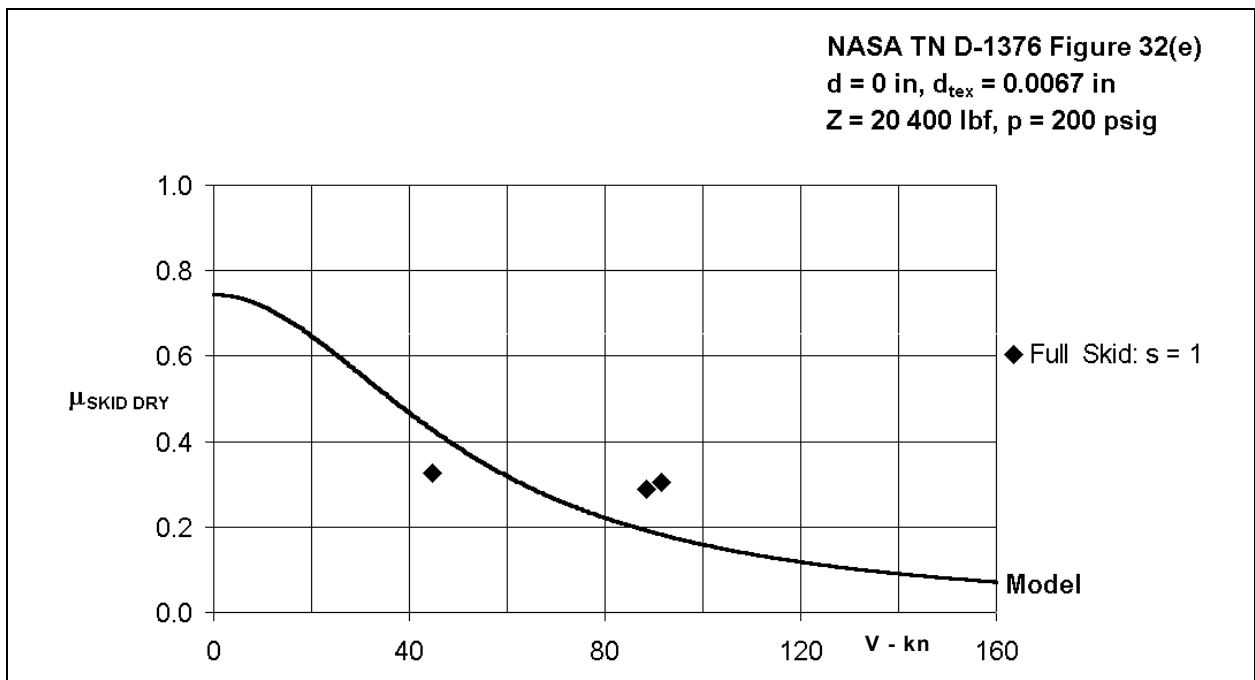
Figure 7.3: Effect of footprint translation speed on $\mu_{SKID\ DRY}$
(Z = 20400 lbf, p = 200 psig)
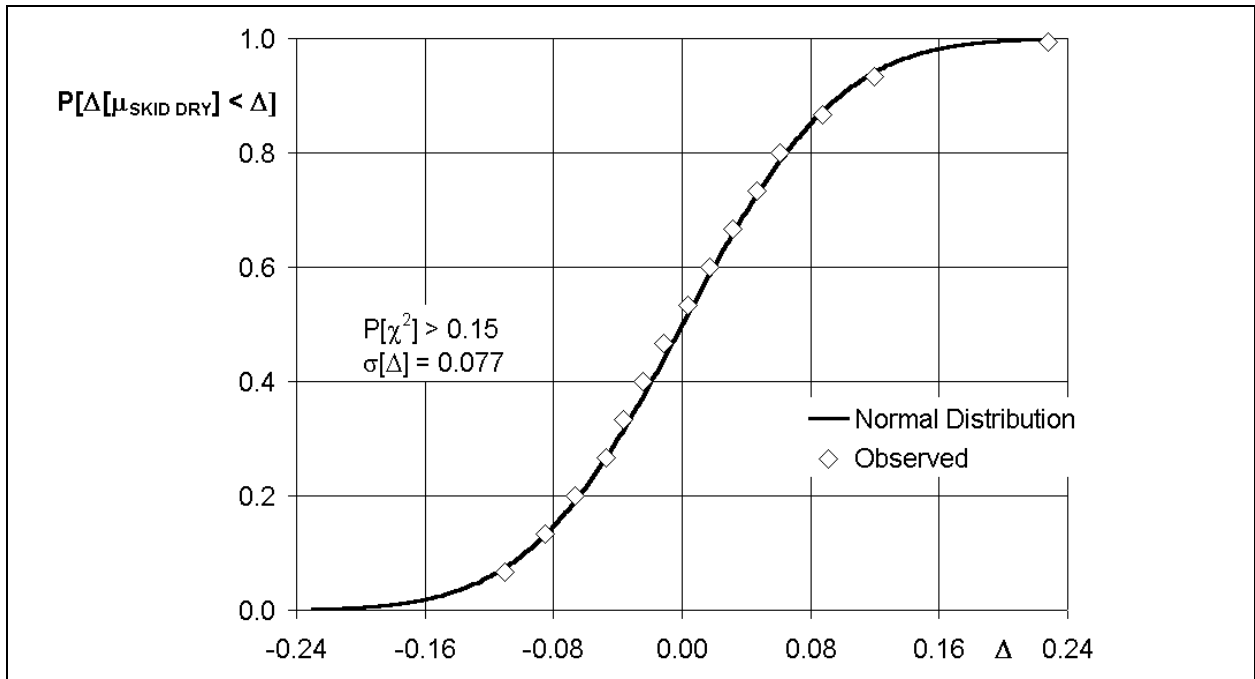
Figure 7.4: Distribution of measurements of $\mu_{SKID\ DRY}$ **about correlation**

8. COEFFICIENT OF BRAKING FRICTION – SLIPPING ON DRY RUNWAY

The general shape of the variation of braking friction coefficient with slip ratio has been understood and described in detail in many publications. Figure 8.1 shows the effect of varying slip ratio and translation speed on the coefficient of braking friction. Experimental work in both laboratory and the field has confirmed that the initial rise in coefficient is determined by properties of the tyre.[18] Furthermore, it has been claimed that the initial slope is substantially independent of translation speed and is, therefore, wholly dependent on slip ratio.
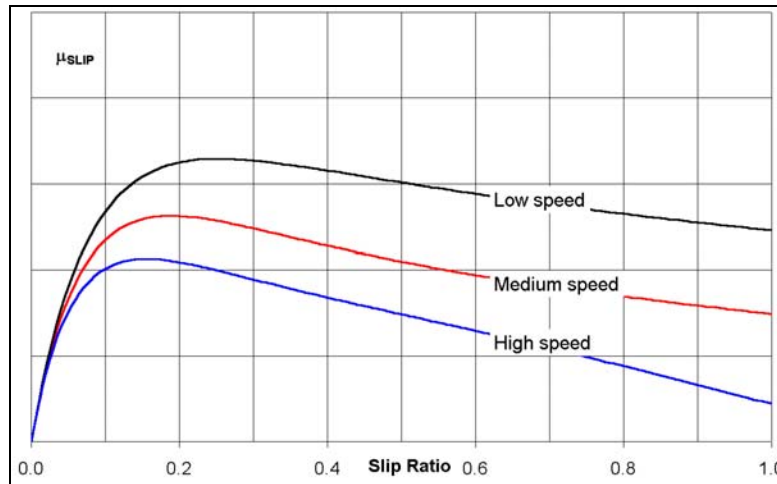
Figure 8.1: Effect of speed and slip ratio on coefficient of braking friction

At the other end of the slip curve, to quote Reference 34, "the same piece of tyre tread is sliding bodily over the road". This is a case of steady state sliding. For fixed conditions of tyre tread, temperature and contamination the friction value is dependent only on speed. The model described in Section 7 is a realistic, yet empirical, formulation for this *sliding* or *skidding* friction in the dry.

In this part, a plausible mathematical description of the *slipping* curve is sought that will default to the skidding value when slip ratio becomes unity. Similarly, at low slip, the function chosen must reflect the observations described above. In addition, at intermediate values of slip – beyond the value for maximum braking friction – the representation of friction coefficient is required to be such that slip ratio has minimal effect in this (dynamically unstable) region of the slip curve.

In the absence of a simple unifying theory, treatments in the literature are mainly descriptive.[19] Such descriptions almost invariably divide the slip range into at least two portions and formulate a separate mathematical description for each. In this section, a simple mathematical relation is used to describe all the features outlined. Furthermore, experimental data are used to show that the relationship is an adequate empirical model.

---

[18] See, for instance, Reference 34.
[19] See, for example, Reference 35.

8.1 Model

When a braking torque is applied to a rolling wheel,[20] the mean circumferential speed of the wheel is less than the forward speed of the axle. This speed differential arises from deformation and sliding of the tread material in the tyre-ground contact area. The overall effect is referred to as *braking slip*. In principle, the angular velocity of the braked tyre is a function of the inflated radius of the tyre modified for the effects of distortion induced by rolling and braking. In practice, there is little to be gained from over-complicating the estimation process. Consequentially, slip ratio is defined here as

$$s = 1 - \frac{\omega R}{V} \qquad 8.1$$

where R is a geometric value and is *not* adjusted for the effects outlined above.

Equation 8.1 can be re-arranged

$$sV = V - \omega R \quad (= v) \qquad 8.2$$

Thus, the effective translation speed, v, of the footprint is the difference between the translation speed of the vehicle and the peripheral speed of the wheel, assuming no deflection due to normal load or distortion due to stresses generated in rolling and braking. In a full skid, the angular velocity of the wheel is zero so, $s = 1$ and the translation speeds of the wheel and footprint are identical.

In Section 7 it was shown that a plausible representation of coefficient of friction – at high values of slip ratio so that $0.5 < s \leq 1$ – could be obtained by a modification of the relation developed in Section 8 for static coefficient of braking friction. Thus[21]

$$\mu_{SKID\ DRY} = \frac{\mu_{REF}}{\left\{ 1 + \left(\eta_0 + \eta_1 \frac{v^2}{2g} \right) \frac{p/p_a}{Z^{1/3}} \right\}} \qquad 8.3$$

In order to accommodate the requirements of the slipping model outlined at the beginning of this section, a function of slip ratio is sought that tends to zero with slip ratio and to unity as slip ratio tends to unity. A simple function that fulfils these requirements is the exponential $\left(1 - e^{\eta_2 s} \right)$ so that $\eta_2 < 0$. The function is zero at $s = 0$ for all η_2 and its value is sufficiently close to unity when $\eta_2 s < -5$. Taking[22] $\eta_2 = -12$, coefficient of friction in slip may be calculated using

---

[20] See Reference 33 for a fuller description of slipping phenomena.
[21] Note that speed dependent terms are calculated at the translation speed of the footprint.
[22] See Section 11 where the value of this exponent is explored for slipping on wet runways. The dry value is a default that follows from the variation in the wet when fluid density tends to zero.

$$\mu_{SLIP\ DRY} = \left(1 - e^{\eta_2 s}\right)\mu_{SKID\ DRY} \qquad\qquad 8.4$$

8.2   Data

The applicability of this relationship has been tested by comparing calculations using the function given in Equation 8.4 with measurements from Figure 79 of Reference 7. These data were collected from experiments conducted in the test rig at NASA Langley on a circumferentially ribbed aircraft tyre. Inflation pressure was 260 psig and the vertical load was 10 000 lbf. Several braked runs were carried out yielding 25 cycles of the system, until the tyre was virtually destroyed.

An "on-off" braking system had been installed which cycled from the free-rolling condition to full skid and back to freely rolling in less than F second. Because of the oscillatory inputs, there is some doubt concerning instrumentation responses and the effects of the concomitant over-swing on time correlation of the measured quantities.

Measured data are shown in Figures 8.2 to 8.26 together with appropriate calculations. The distribution of the differences between measurements and calculations is shown in Figure 8.27. In addition, because the maximum coefficient of braking friction is often used as a starting point for calculating system efficiencies, Figure 8.28 has been prepared. This figure shows the relation between the maxima as calculated from the model and those observed during the testing reported in Reference 7.

8.3   Coefficient of Braking Friction in Slip

A favourable feature of the model described by Equation 8.4 is that only one additional freedom is introduced over and above those used to describe the skidding case. Thus, the mathematical description of the coefficient of braking friction for aircraft tyres slipping on a dry runway is fully described by a relationship that contains just four empirical constants $\left(\mu_{REF}, \eta_0, \eta_1, \eta_2\right)$. In addition, to use the method, it is necessary to know four independent variables:

1. slip ratio
2. speed
3. inflation pressure (in absolute measure), and
4. the normal load on the tyre.

The initial slope of friction coefficient with respect to slip ratio has been observed[23] to be independent of speed. Referring back to Figure 8.1, this requirement of the modelling is satisfied. It is unfortunate that detailed experiments for aircraft style tyres braking on dry runways are rare. However, the cycles of the NASA braking system plotted in Figures 8.2 to 8.26 serve to illustrate the predictive capabilities of the model under quite demanding conditions. Data in Figures 8.2 and 8.25 are not wholly consistent with the model – these two examples are to some extent, perverse in appearance. With these exceptions, the comparison between prediction and

---

[23]   Reference 34 is one amongst many sources for this observation.

experiment is remarkably consistent. This close agreement is even more encouraging when the circumstances of the data collection are considered. Each plot represents approximately a second of recording. All the measured variables are subject to oscillatory excitation. Thus, limitations in time correlation and differential over-swings contribute to scatter of measurements about the predictions. Despite this, the standard error of the deviations between model and measurement is $\sigma[\Delta] = \pm 0.097$. There are 382 measurements in the comparison and the distribution of the deviations is approximately Normal – see Figure 8.27. It follows that the uncertainty at the 95% level of significance in an estimate of coefficient of braking friction from this evidence is $U\left[\mathrm{E}\left[\mu_{SLIP\ DRY}\right]\right]_{0.95} = \pm 0.01$.

8.4 Maximum Coefficient of Braking Friction

Maximum coefficient of friction developed when a system cycles at constant speed is a variable central to the treatment of braking system efficiency. In each cycle of the experiment considered here, the maximum value of instantaneous friction coefficient observed has been plotted in Figure 8.28 as a function of the mean speed in the cycle. The variation of $\mu_{MAX\ DRY}$ obtained from the model is also shown in the figure.

A t-test shows that the mean deviation of the "measured" values from those estimated is not significantly different from zero at the 15% level of probability. Further, the standard error of the deviations is $\sigma[\Delta] = \pm 0.04$ and the distribution of the deviations, as shown in Figure 8.29, is not significantly different from Normal. There are 25 measured values, so the uncertainty in an estimate of $\mu_{MAX\ DRY}$ from the modelling is $U\left[\mu_{MAX\ DRY}\right] = \pm 0.016$ at the 95% level of significance, on the evidence of this experiment.

Figure 8.2: Effect of slip ratio on coefficient of braking friction (Cycle 1, *V* = 89 kn)

Figure 8.3: Effect of slip ratio on coefficient of braking friction (Cycle 2, *V* = 86 kn)

Figure 8.4: Effect of slip ratio on coefficient of braking friction (Cycle 1, V = 67 kn)

Figure 8.5: Effect of slip ratio on coefficient of braking friction (Cycle 3, V = 64 kn)

Figure 8.6: Effect of slip ratio on coefficient of braking friction (Cycle 7, *V* = 57 kn)
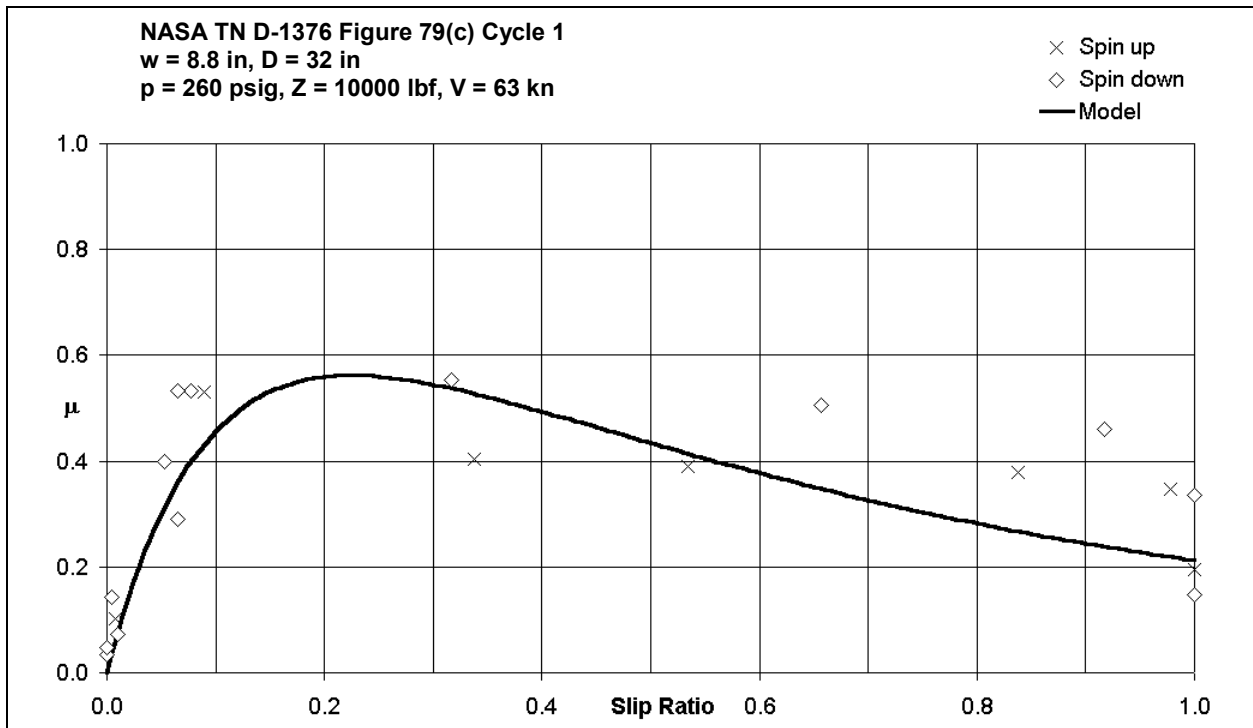
Figure 8.7: Effect of slip ratio on coefficient of braking friction (Cycle 1, *V* = 63 kn)
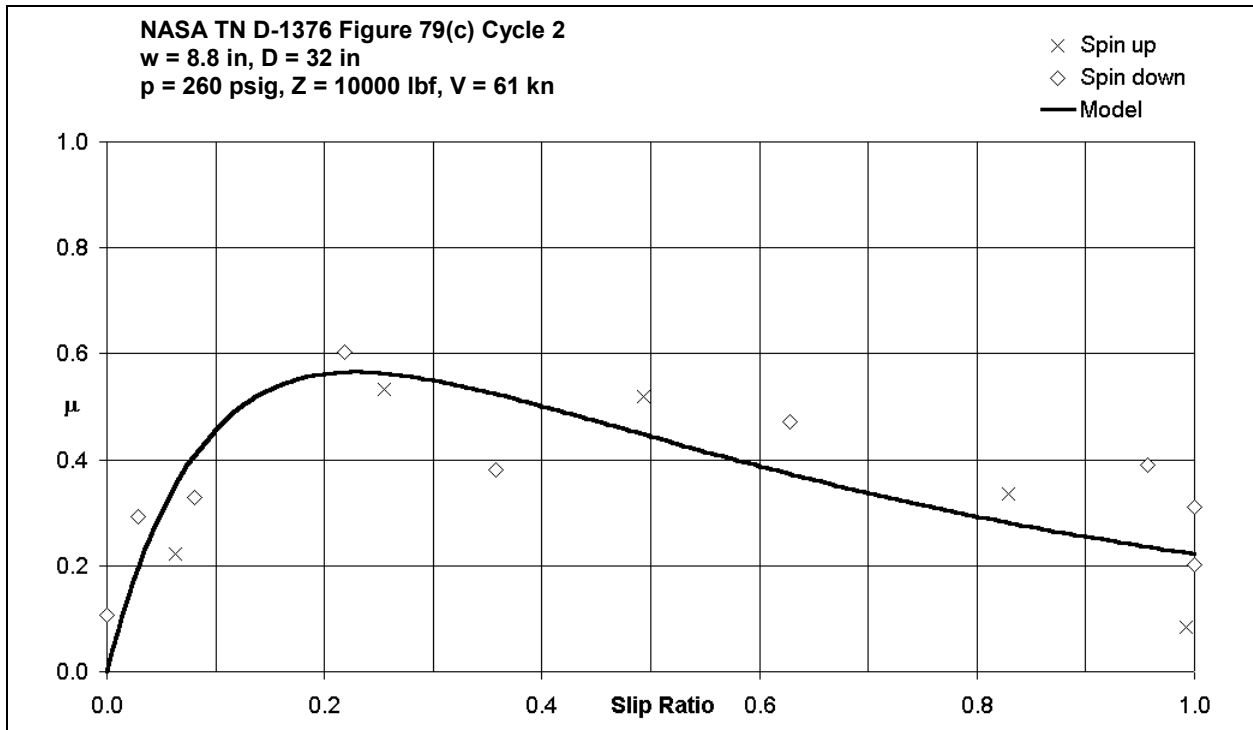
Figure 8.8: Effect of slip ratio on coefficient of braking friction (Cycle 2, *V* = 61 kn)
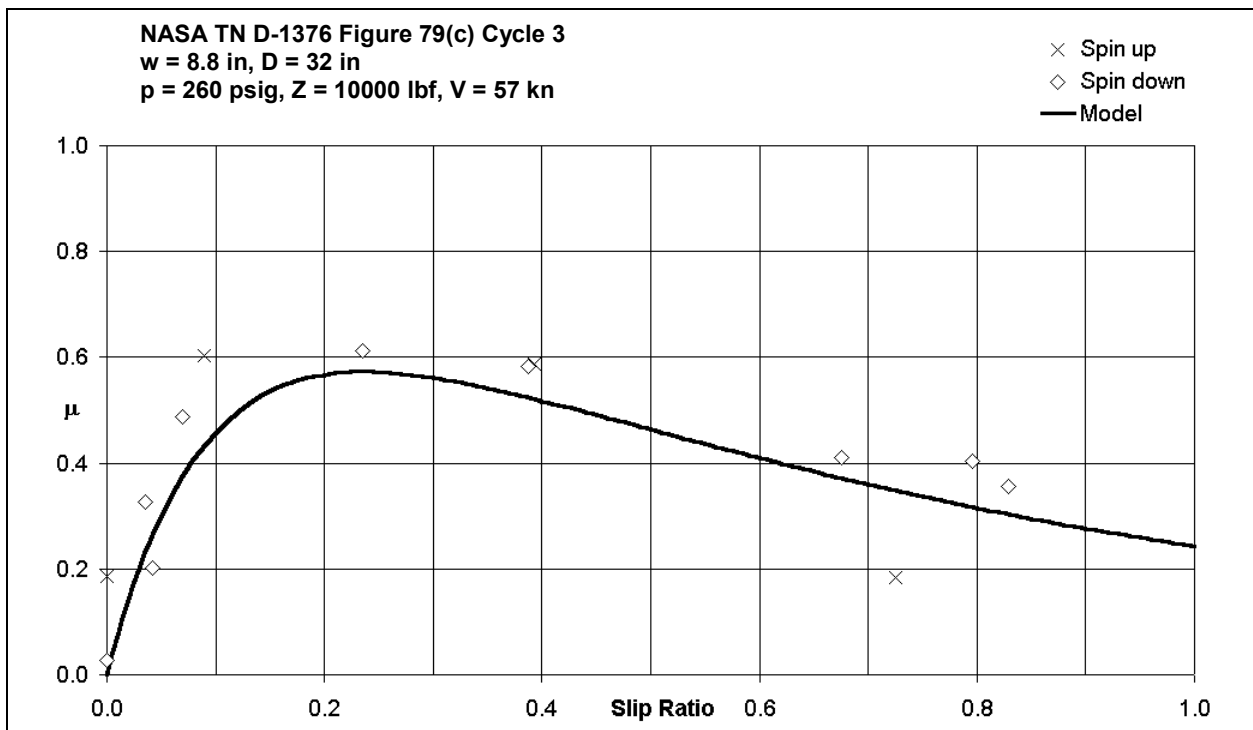
Figure 8.9: Effect of slip ratio on coefficient of braking friction (Cycle 3, *V* = 57 kn)
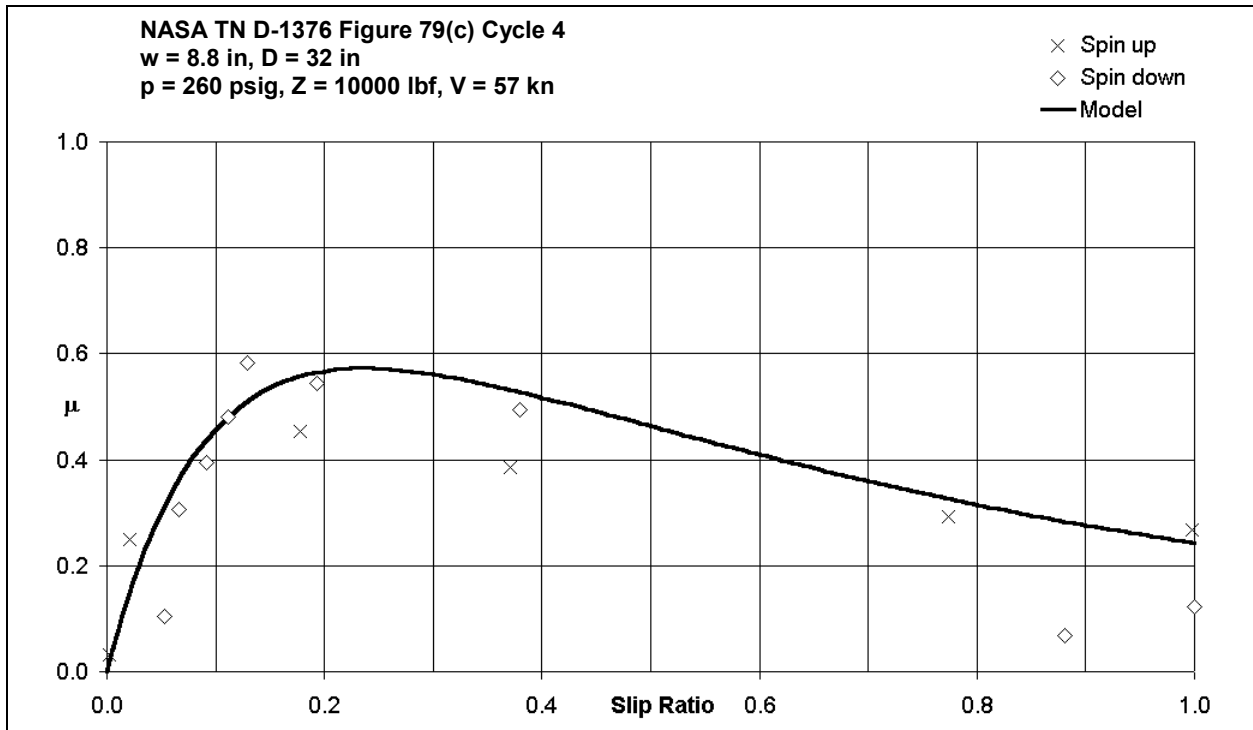
Figure 8.10: Effect of slip ratio on coefficient of braking friction (Cycle 4, V = 57 kn)
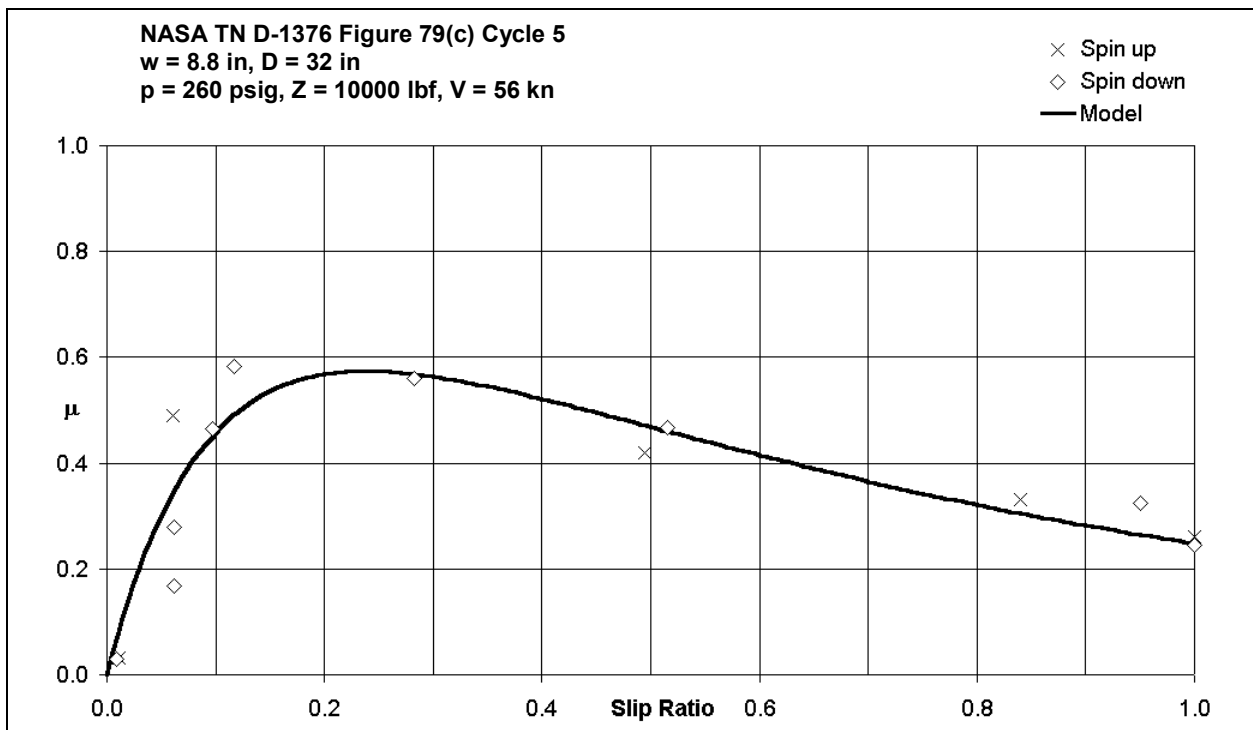
Figure 8.11: Effect of slip ratio on coefficient of braking friction (Cycle 5, V = 56 kn)
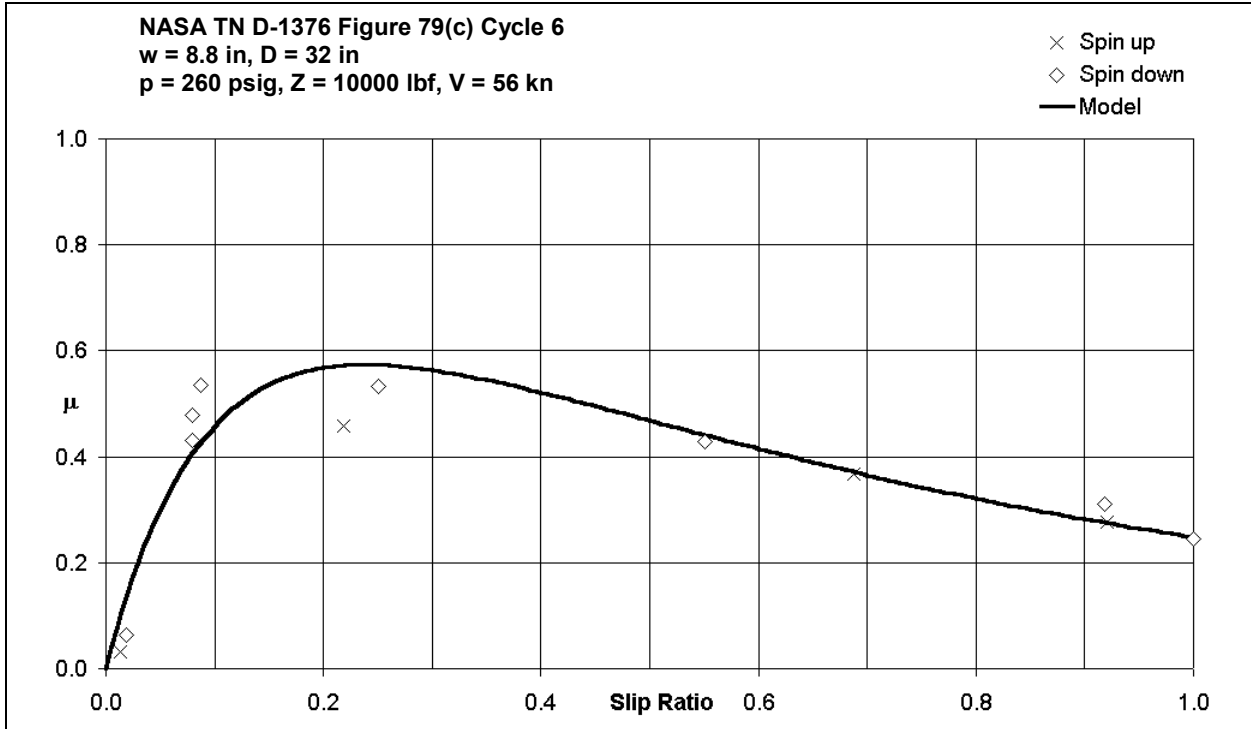
Figure 8.12: Effect of slip ratio on coefficient of braking friction (Cycle 6, *V* = 56 kn)
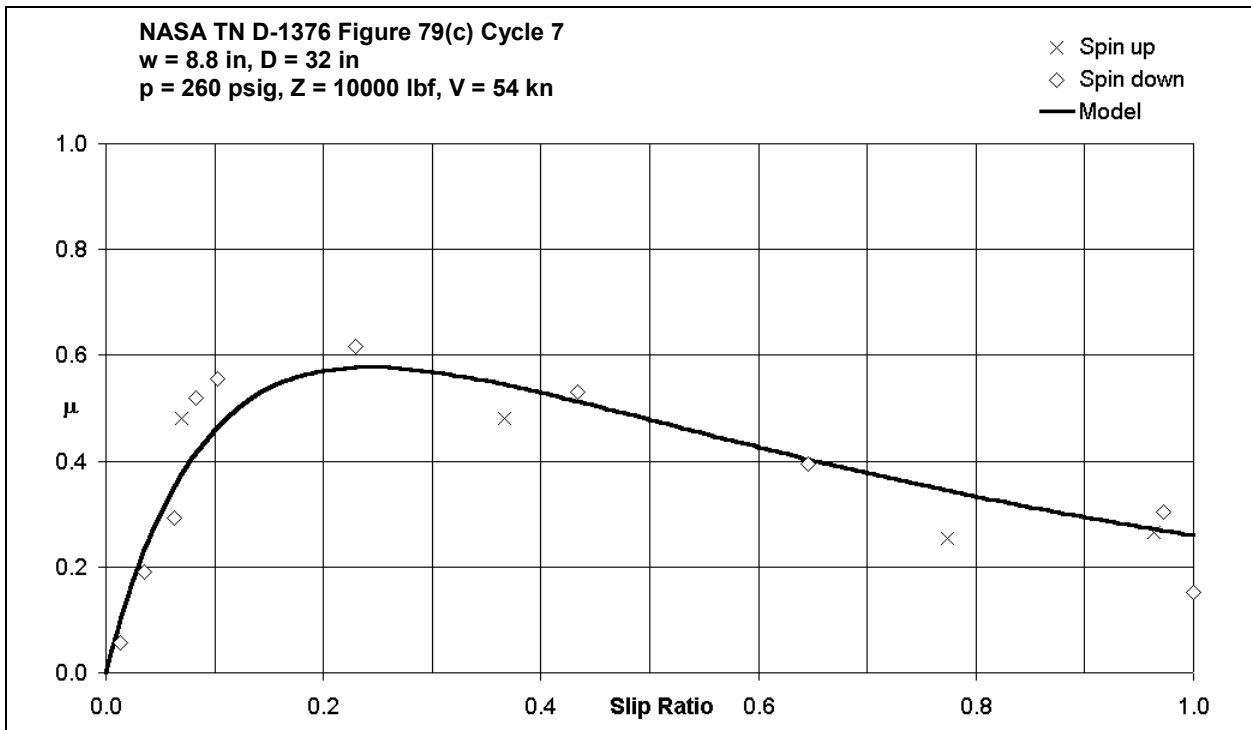
Figure 8.13: Effect of slip ratio on coefficient of braking friction (Cycle 7, *V* = 54 kn)
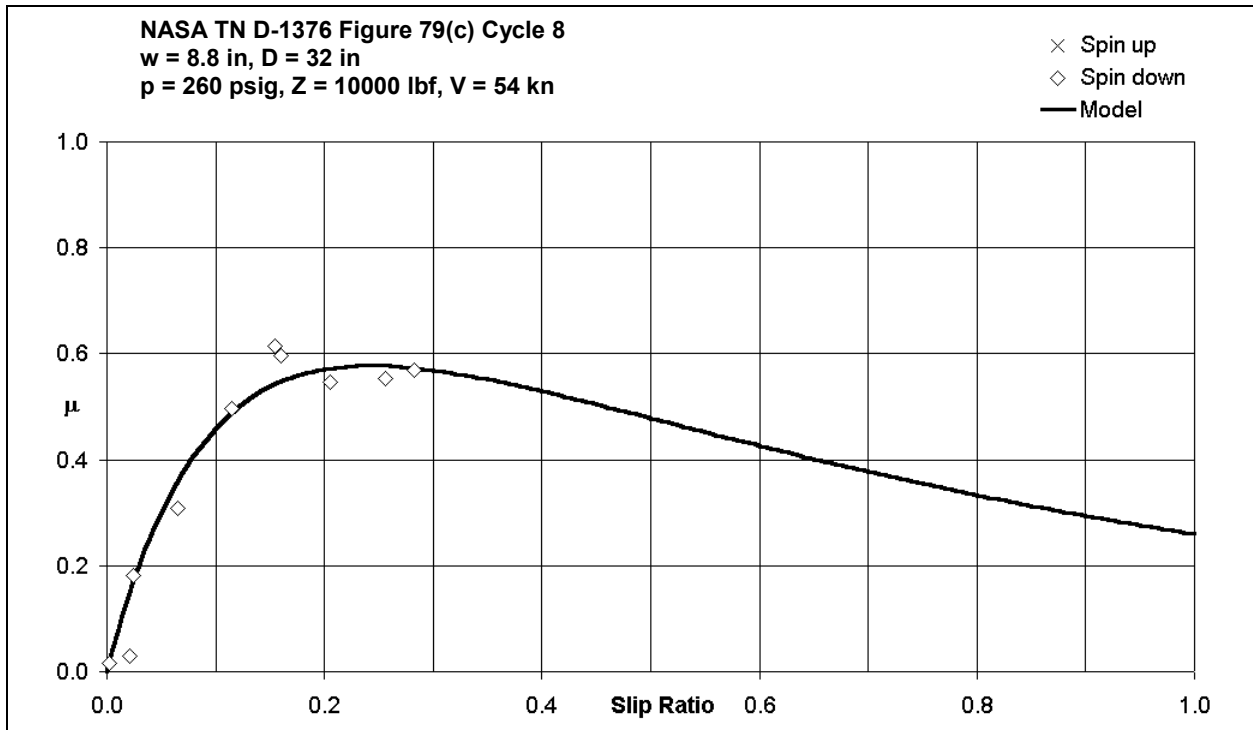
Figure 8.14: Effect of slip ratio on coefficient of braking friction (Cycle 8, V = 54 kn)
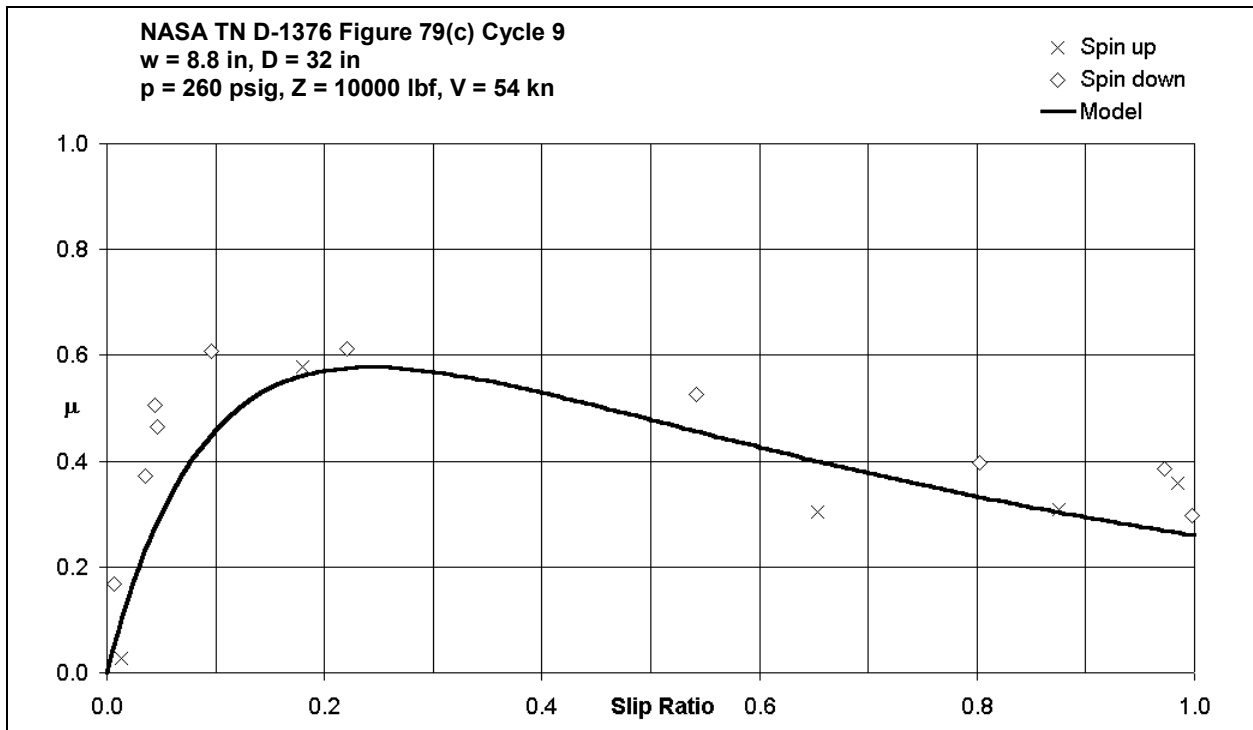
Figure 8.15: Effect of slip ratio on coefficient of braking friction (Cycle 9, V = 54 kn)

85
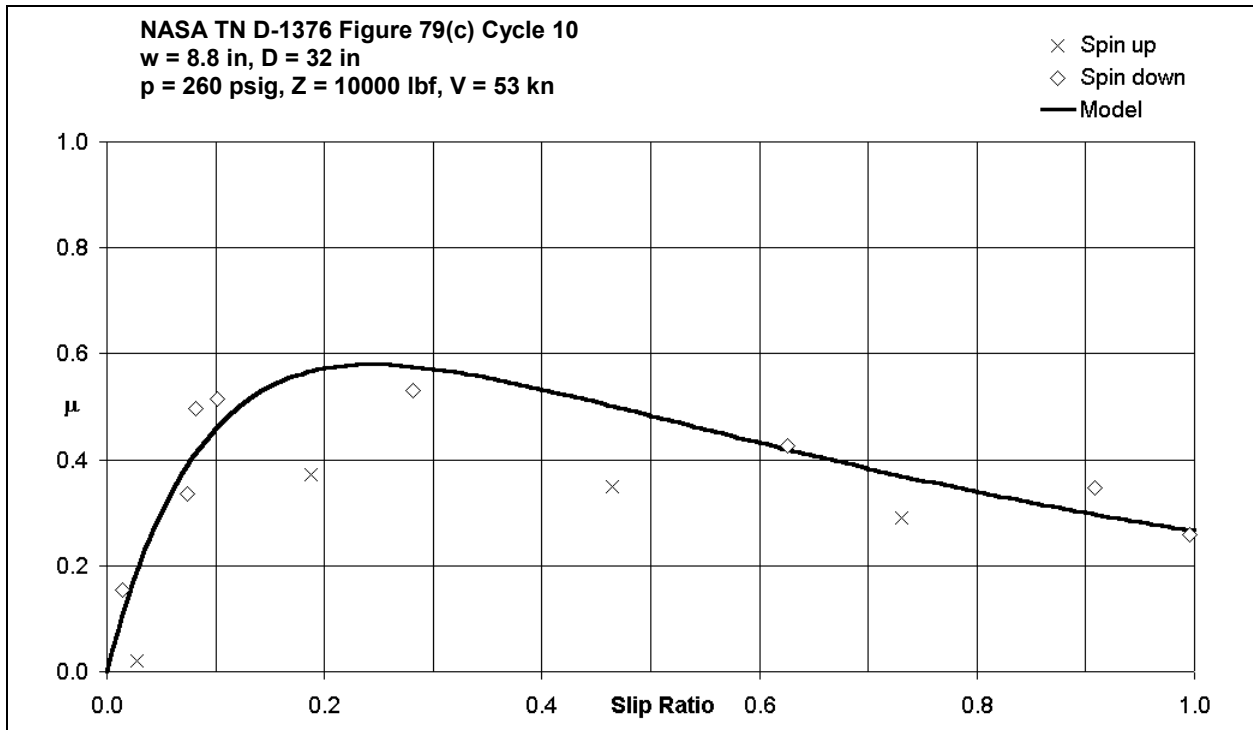
Figure 8.16: Effect of slip ratio on coefficient of braking friction (Cycle 10, V = 53 kn)
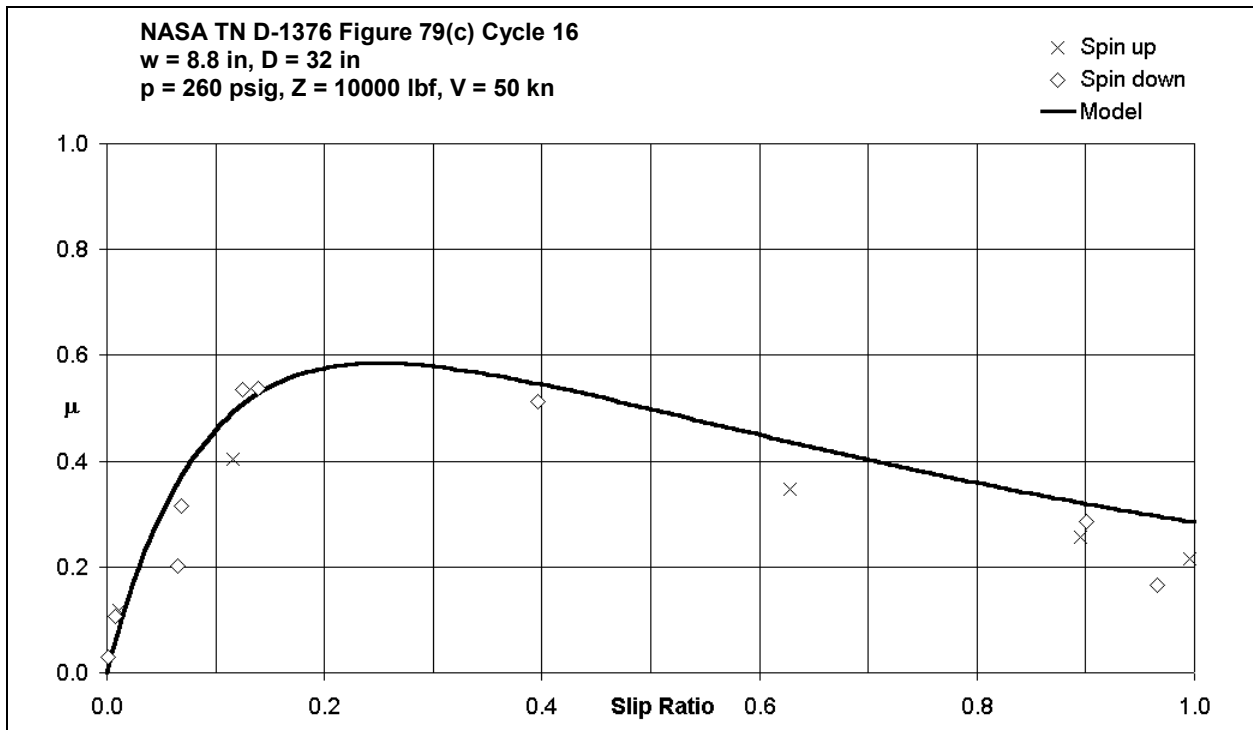
Figure 8.17: Effect of slip ratio on coefficient of braking friction (Cycle 16, V = 50 kn)
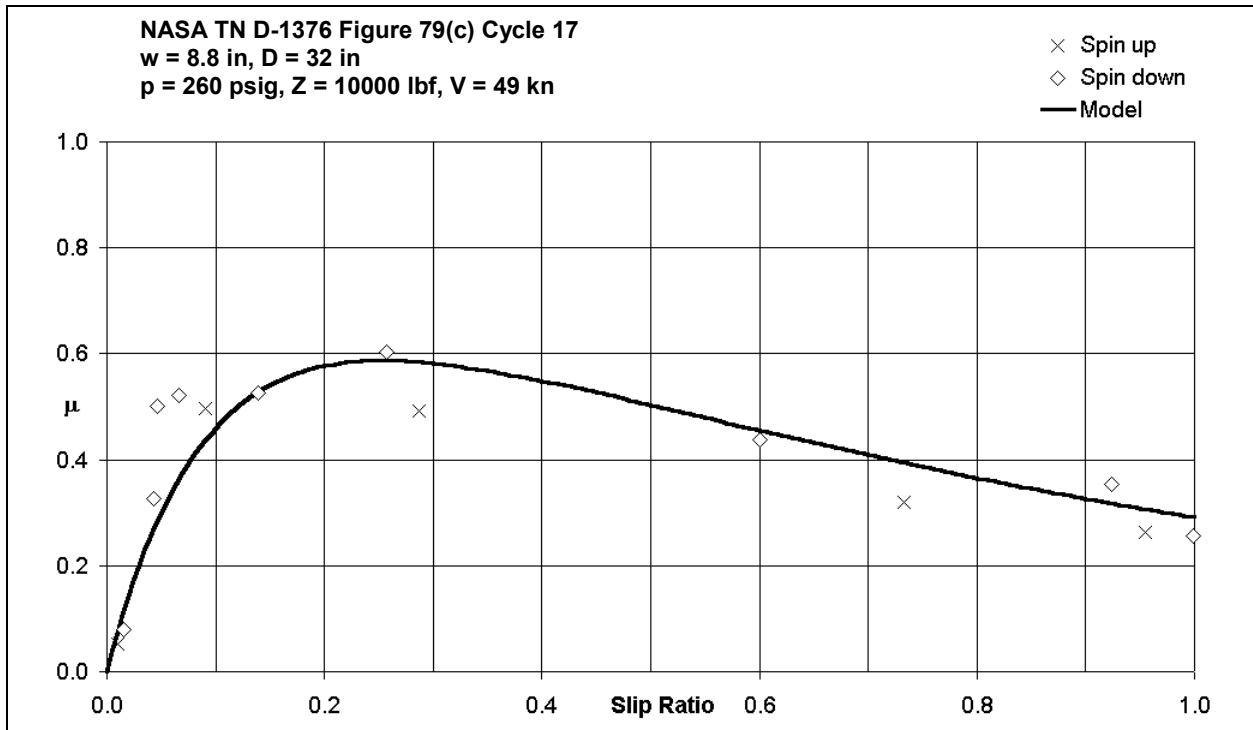
Figure 8.18: Effect of slip ratio on coefficient of braking friction (Cycle 17, V = 49 kn)
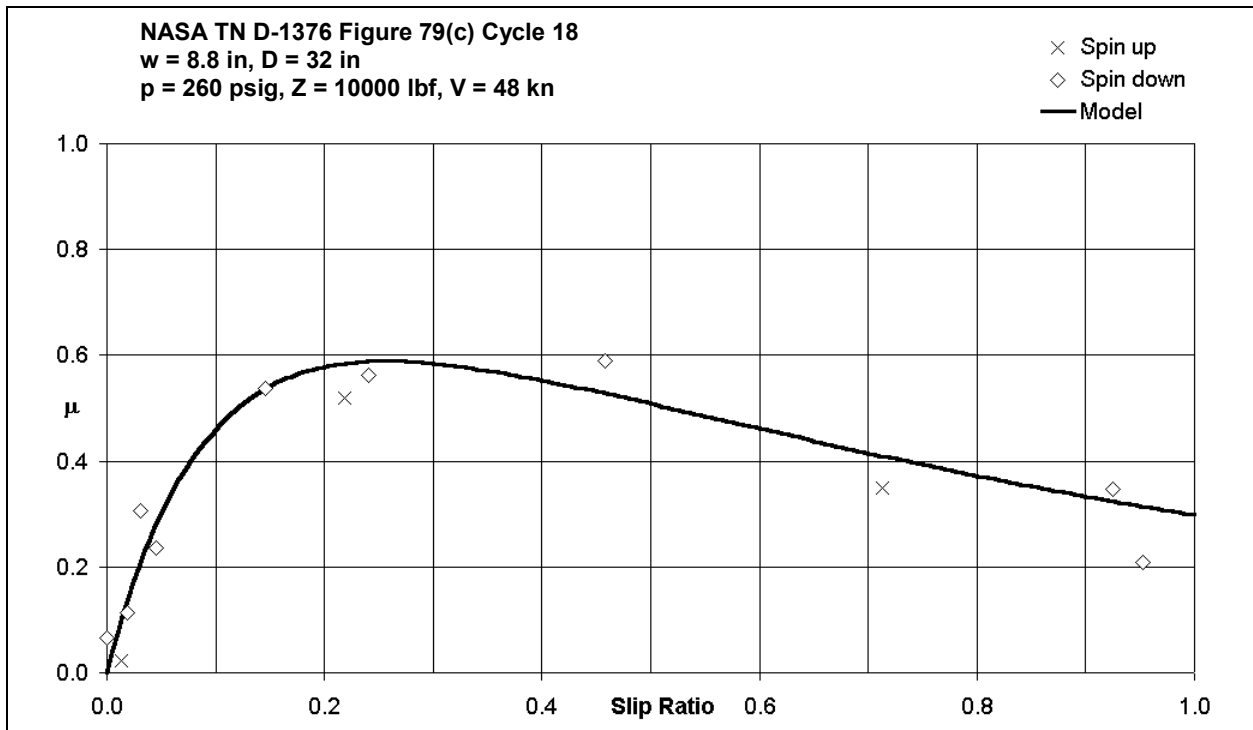
Figure 8.19: Effect of slip ratio on coefficient of braking friction (Cycle 18, V = 48 kn)
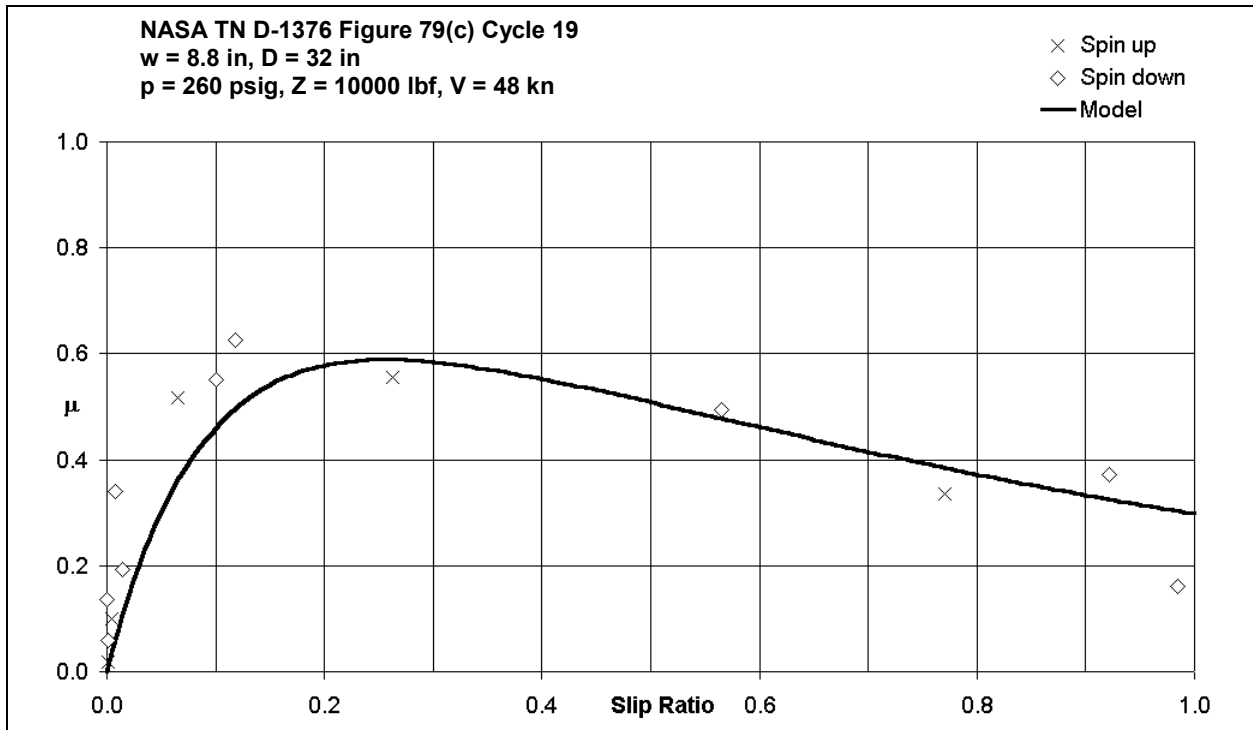
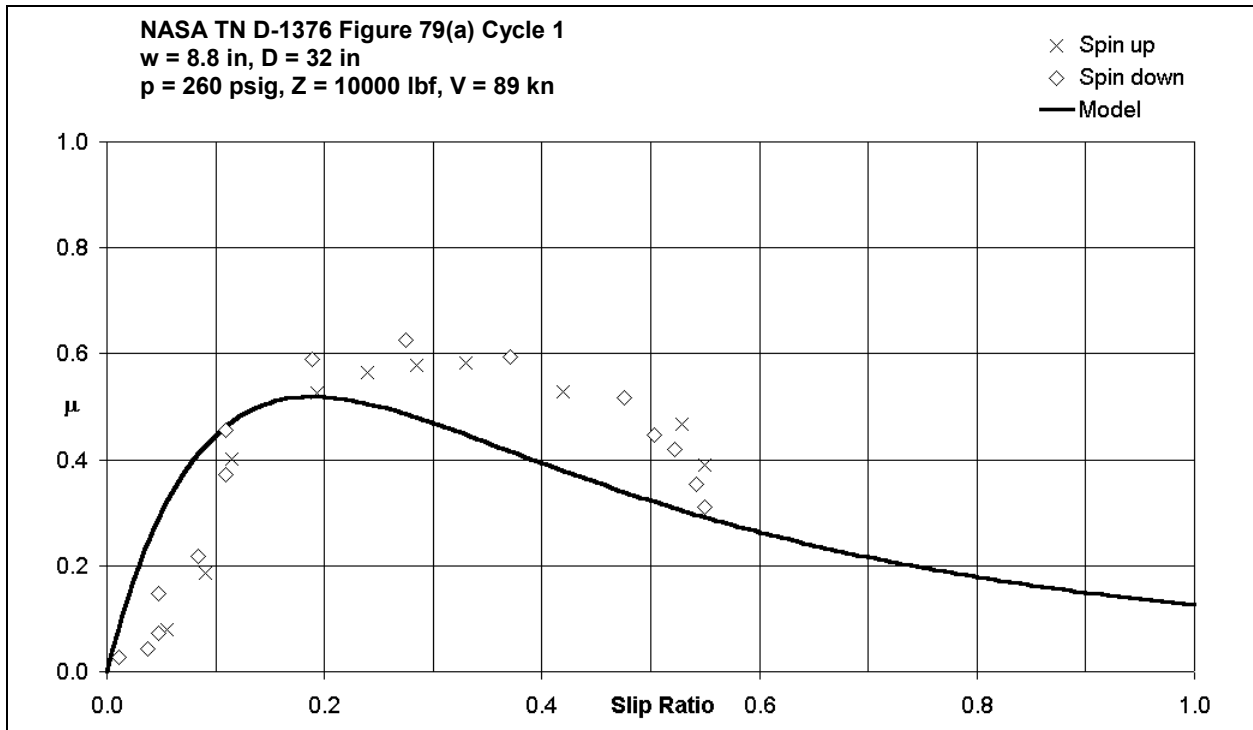**Figure 8.20: Effect of slip ratio on coefficient of braking friction (Cycle 19, V = 48 kn)**
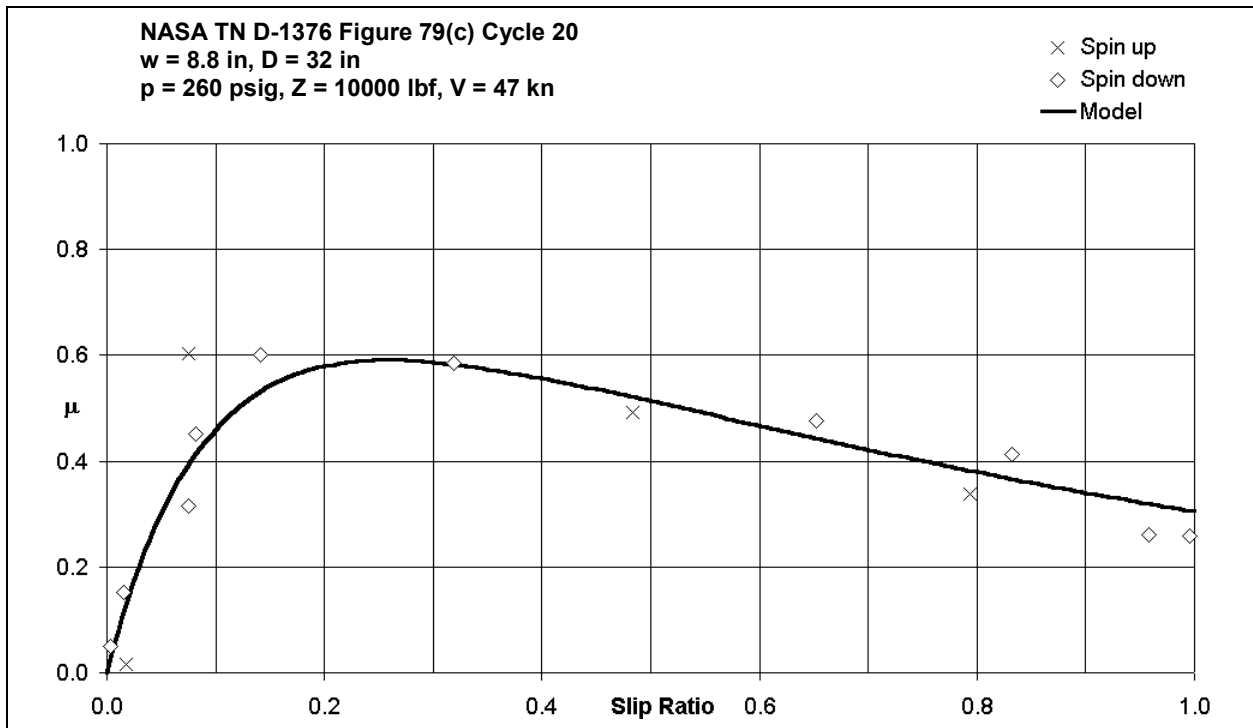
Figure 8.21: Effect of slip ratio on coefficient of braking friction (Cycle 20, V = 47 kn)
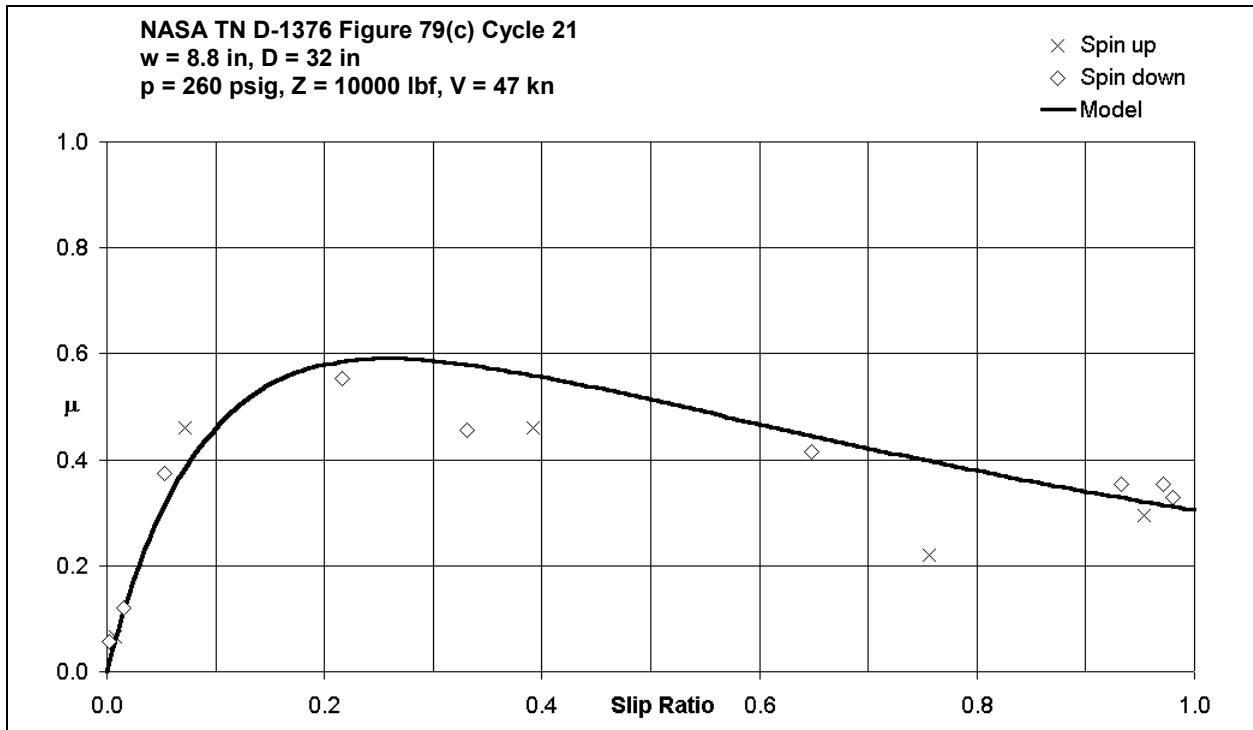
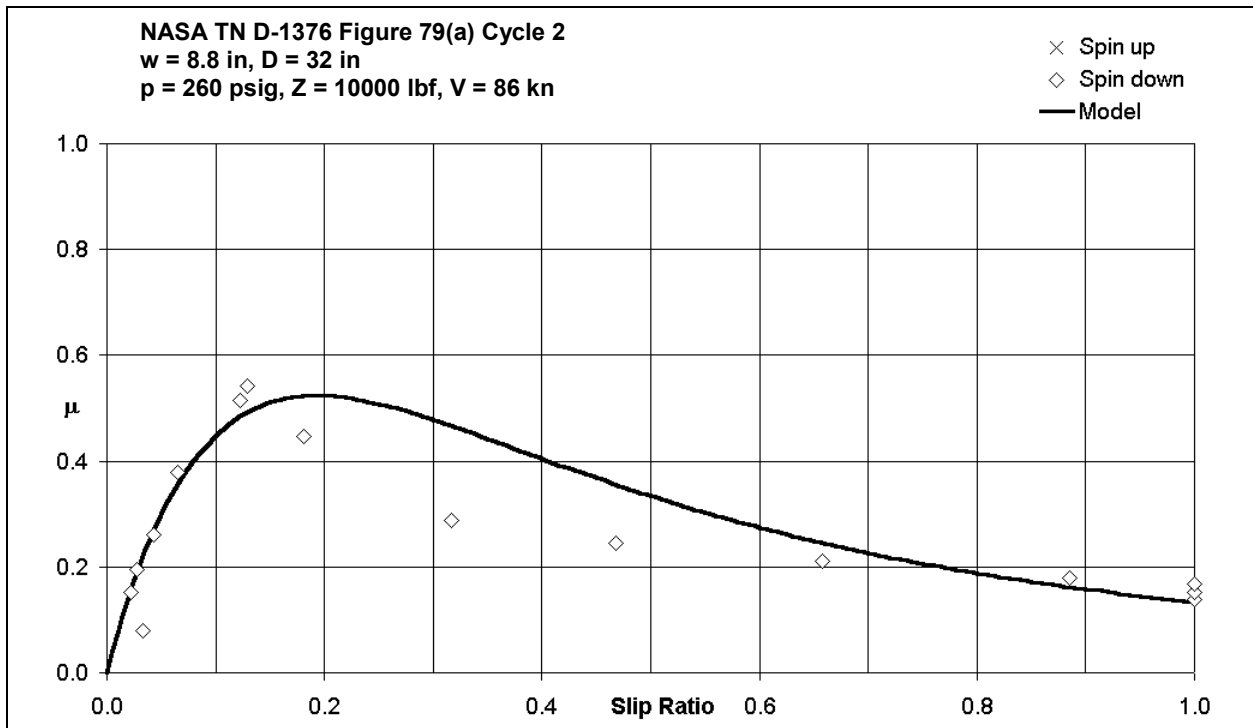**Figure 8.22: Effect of slip ratio on coefficient of braking friction (Cycle 21, $V = 47$ kn)**
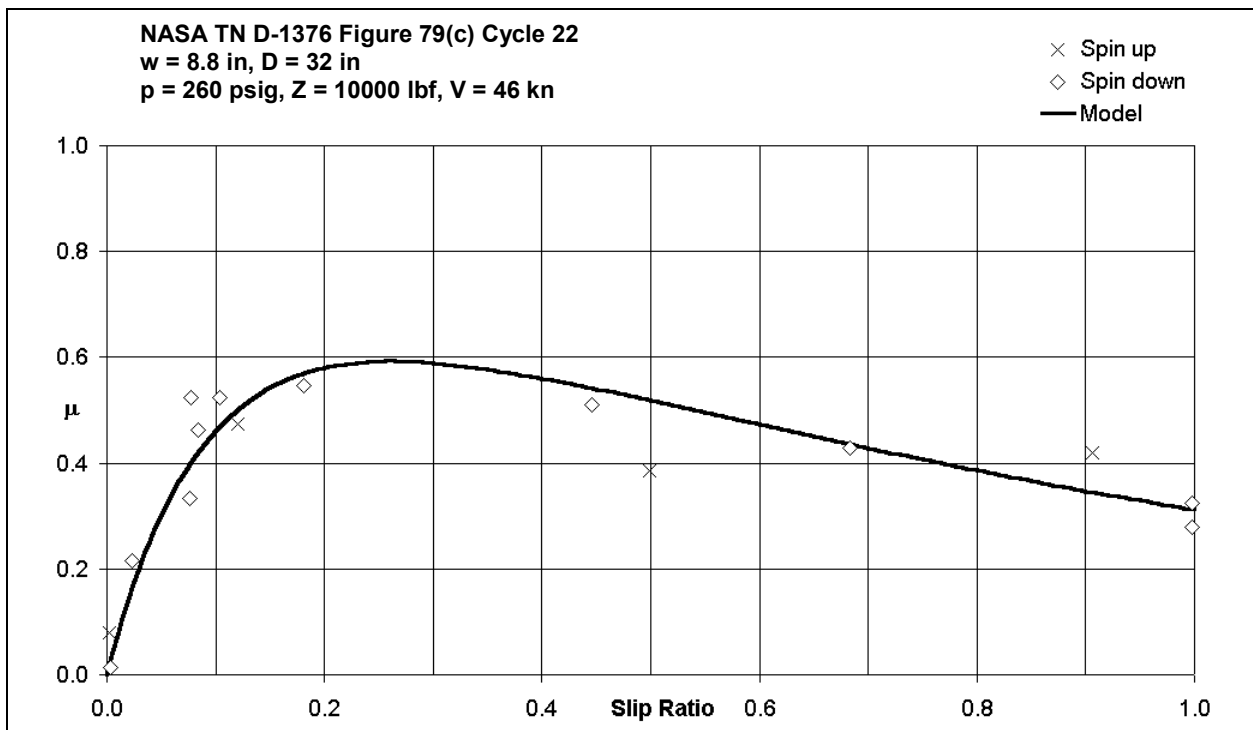
Figure 8.23: Effect of slip ratio on coefficient of braking friction (Cycle 22, $V = 46$ kn)
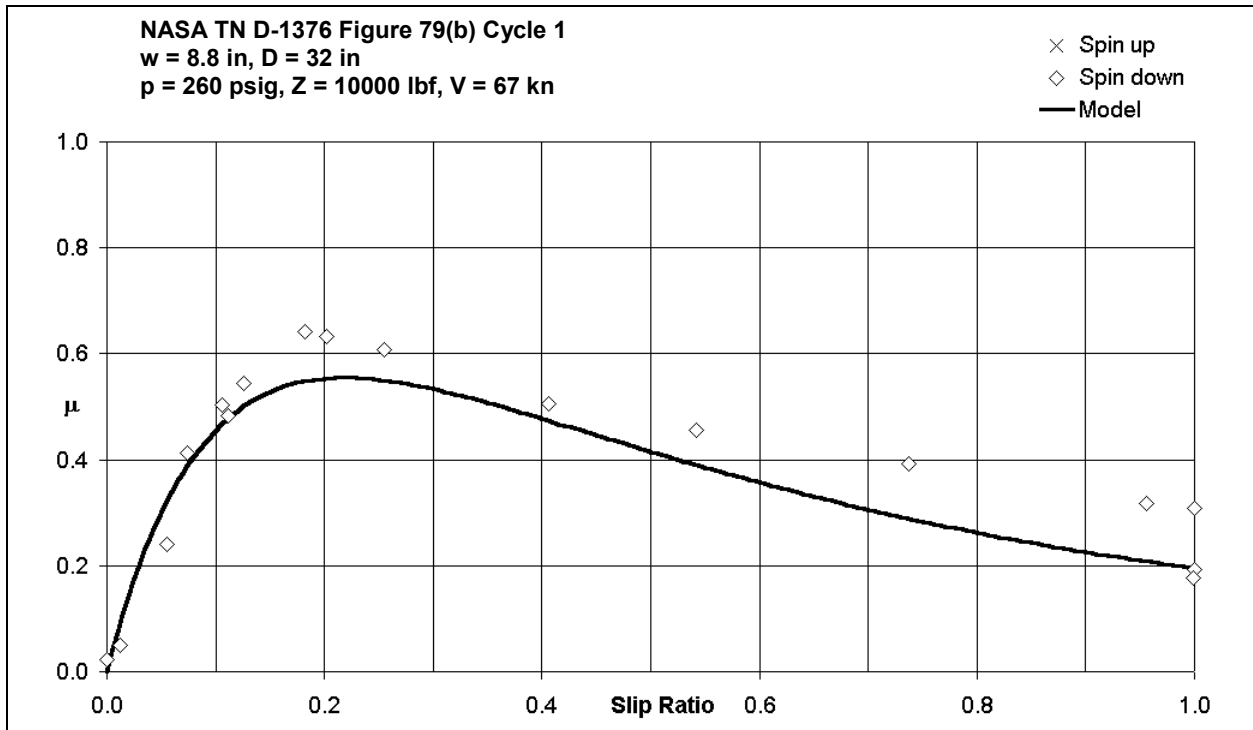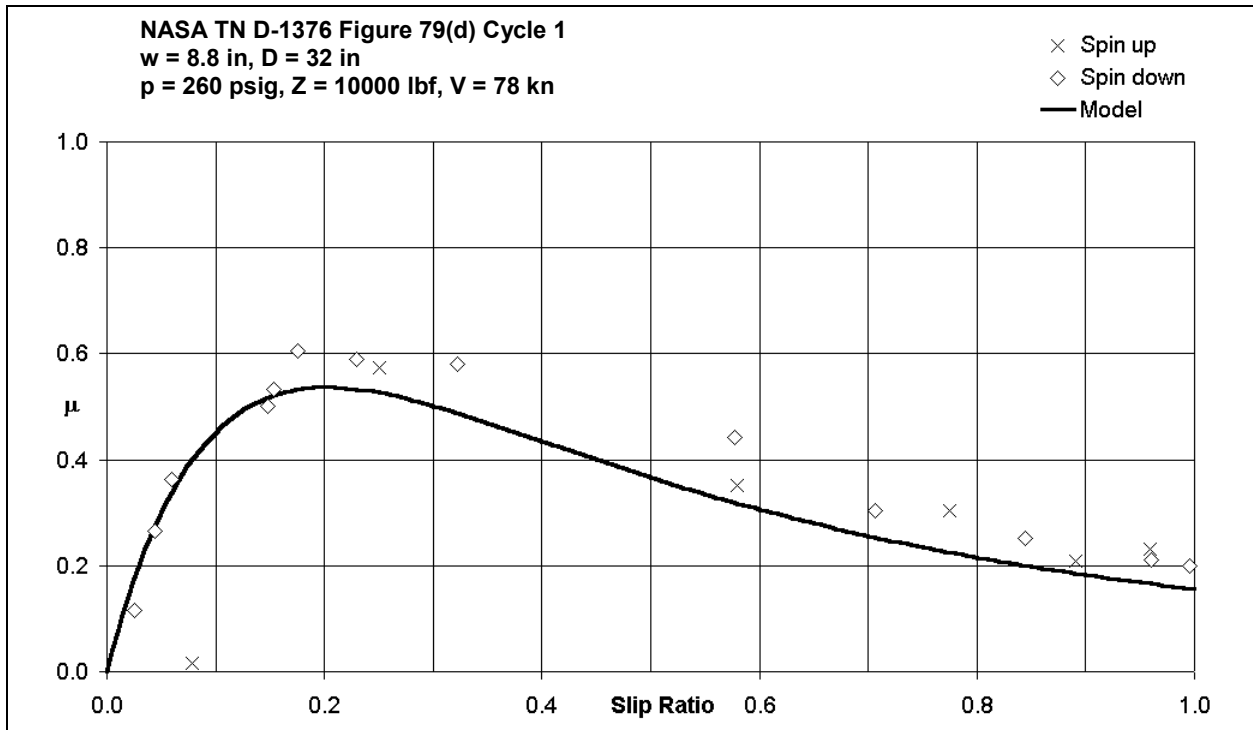
Figure 8.24: Effect of slip ratio on coefficient of braking friction (Cycle 1, *V* = 78 kn)
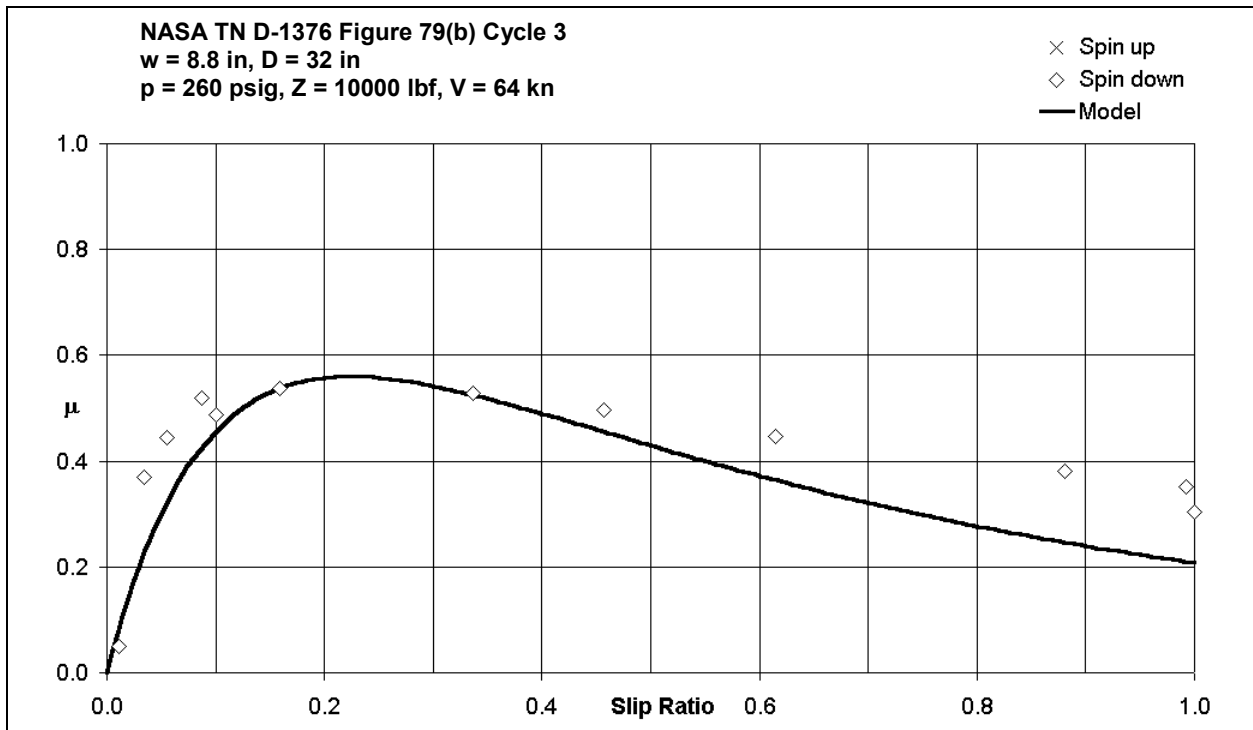

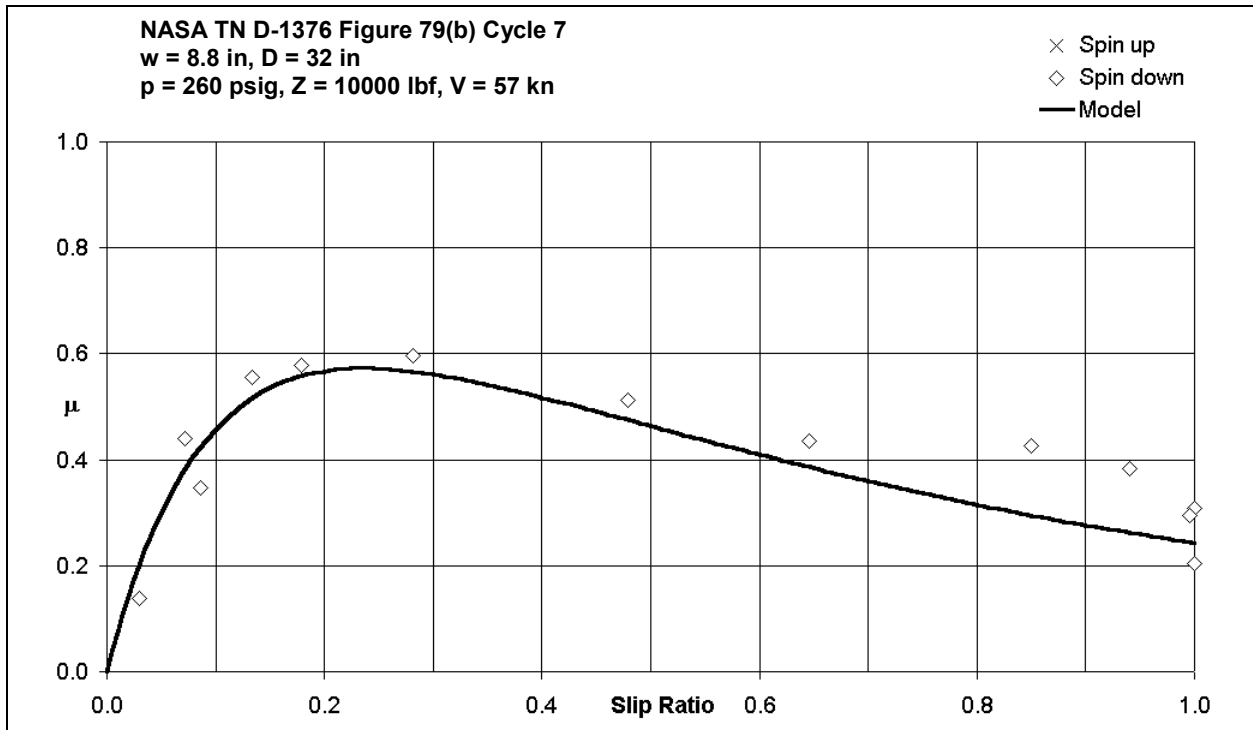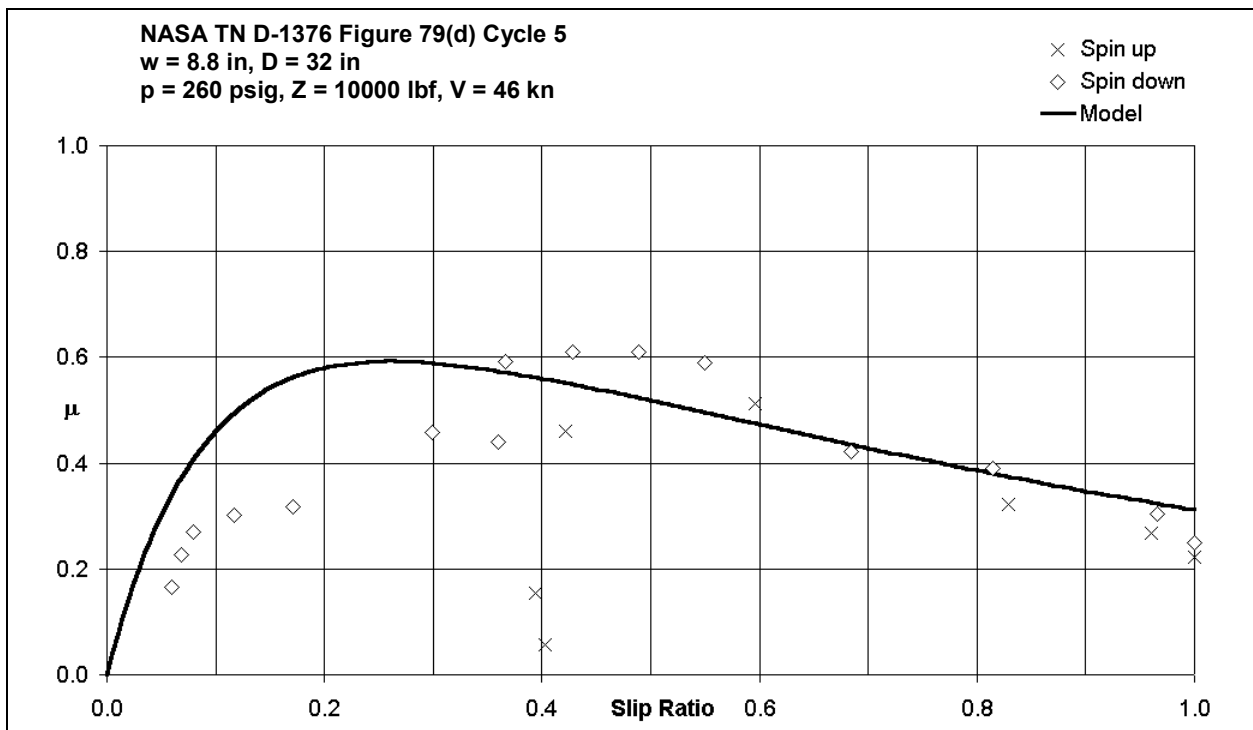**Figure 8.25: Effect of slip ratio on coefficient of braking friction (Cycle 5, *V* = 46 kn)**
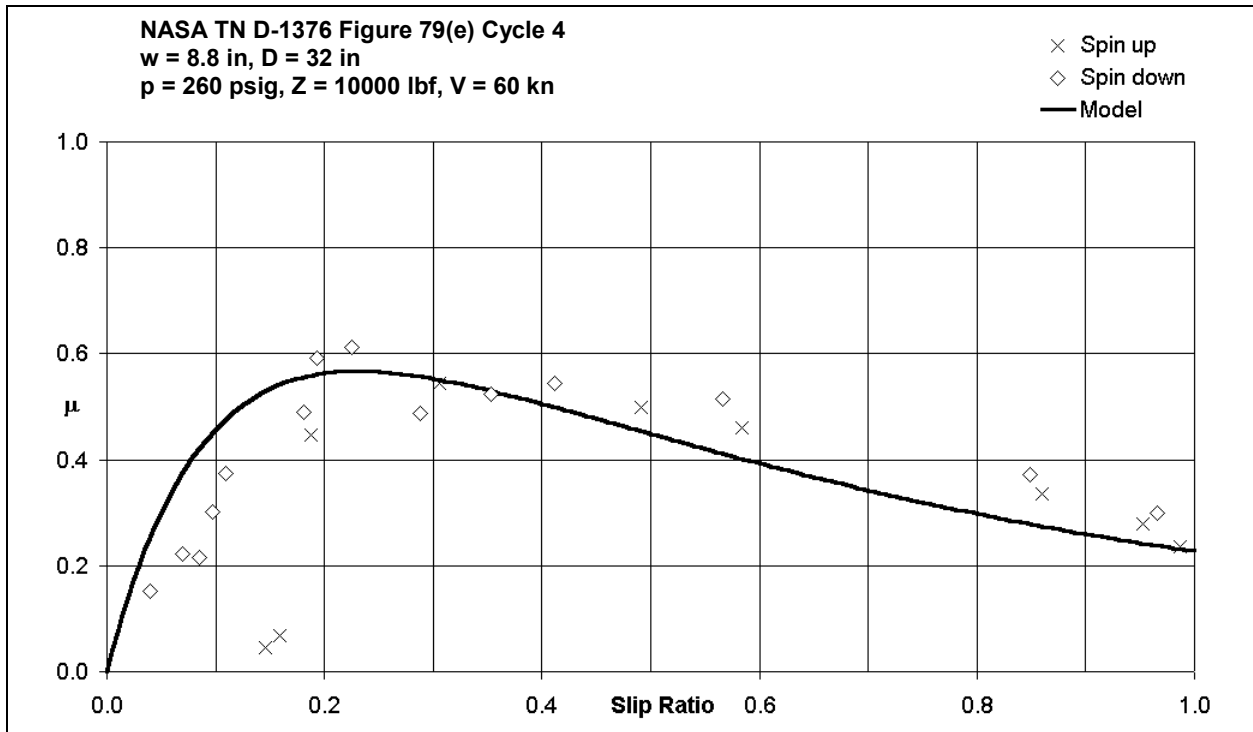
Figure 8.26: Effect of slip ratio on coefficient of braking friction (Cycle 4, *V* = 60 kn)
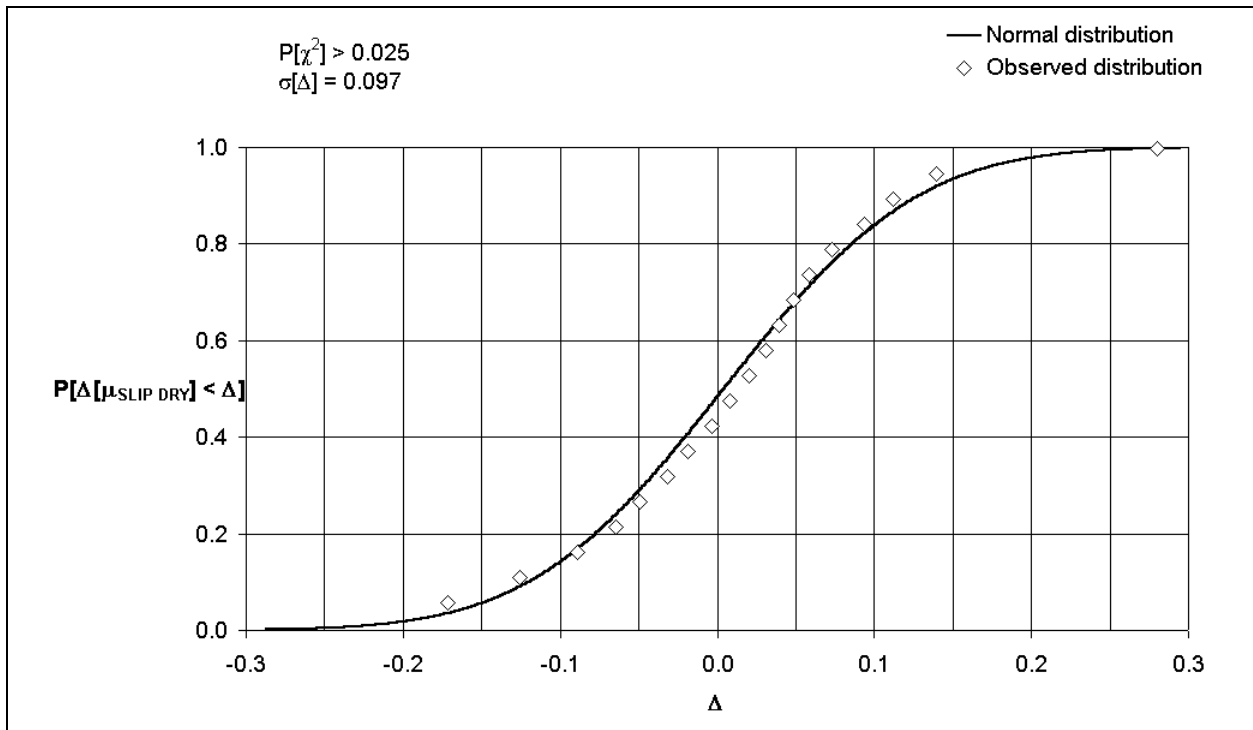
Figure 8.27: Distribution of measured friction coefficients about mathematical model

91
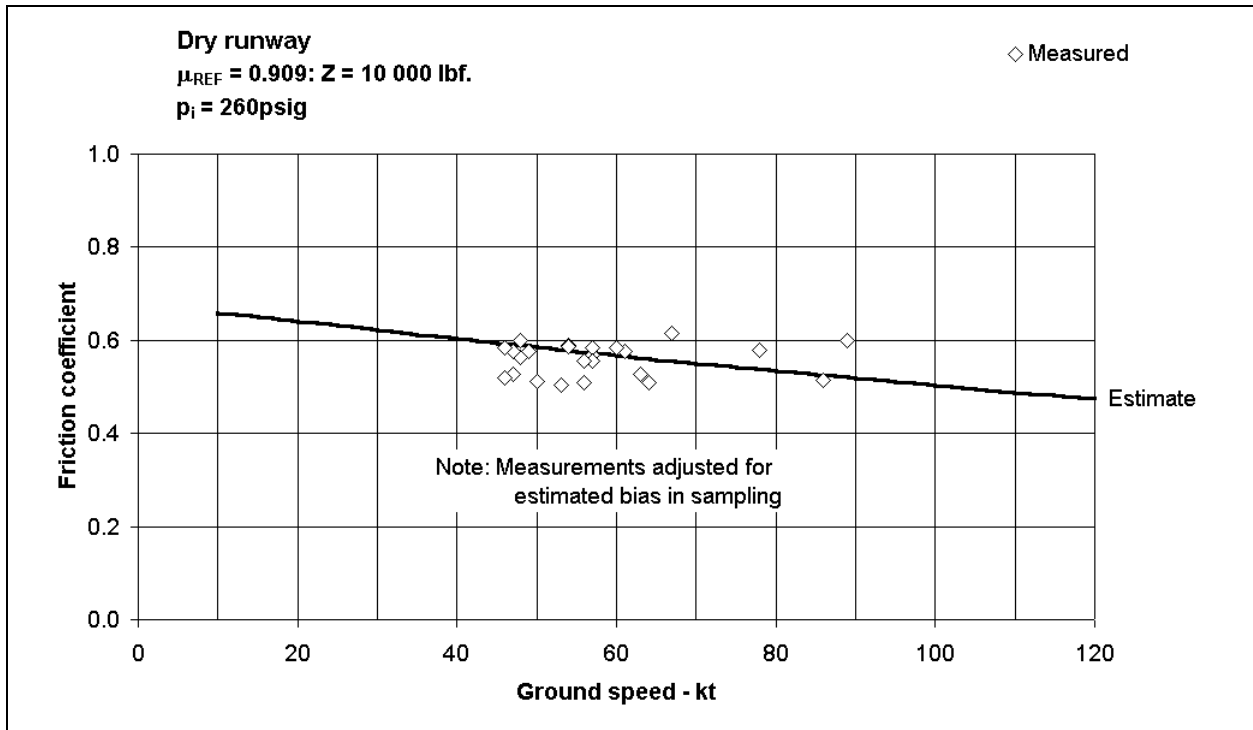
Figure 8.28: Effect of ground speed on maximum coefficient of braking friction
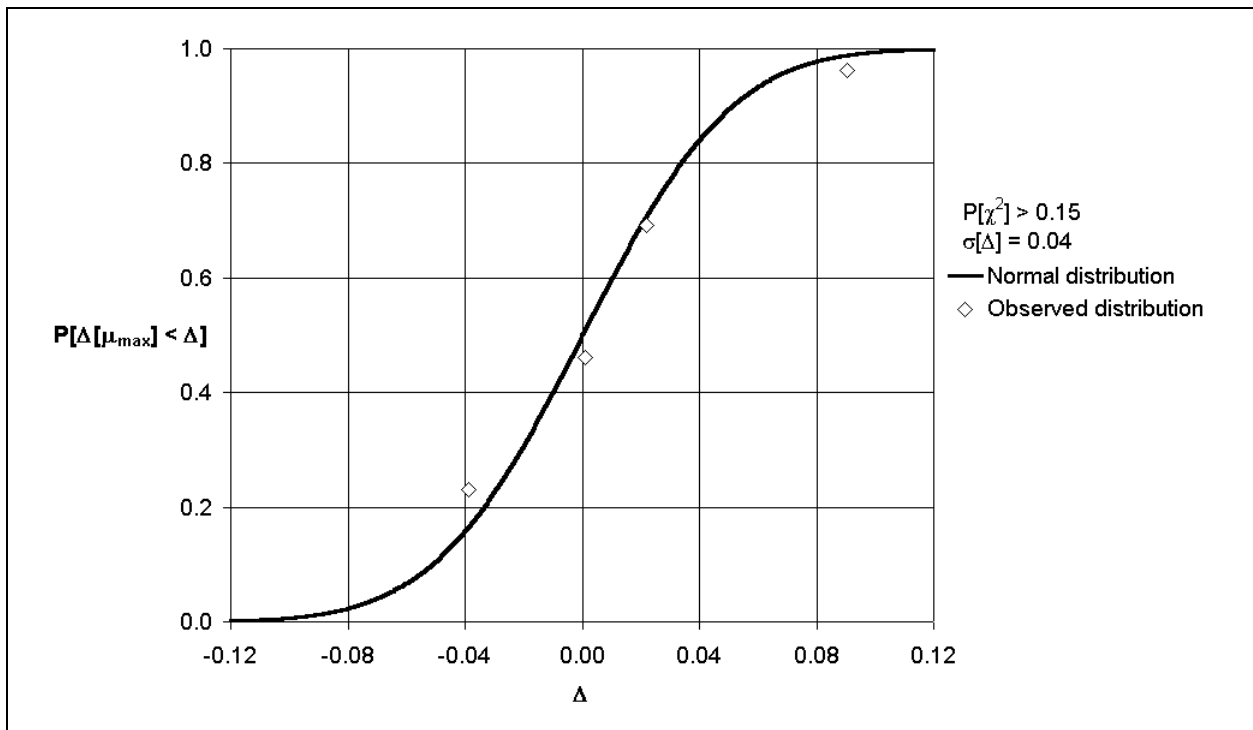
Figure 8.29: Distribution of deviation of measured from calculated values of maximum coefficient of braking friction

9. PRESSURES UNDER FOOTPRINT OF TYRE ON WET RUNWAY

In general, the presence of a fluid on a runway decreases the available braking force that can be generated when skidding at constant total vertical load. This is perceived to arise because part of the load on the tyre is supported by the contaminating fluid. The area of the footprint within which a frictional force can be generated is therefore smaller than on a dry runway. As an aid to modelling, the contact area between the tyre and ground in wet conditions has been conceived to divide into three zones.[24] Figure 9.1 illustrates this conception.

Zone 1 is the region where impact of the tyre with the surface fluid generates sufficient pressure to overcome the inertia of the fluid. Much of the fluid is either ejected as spray or forced beneath the tyre into the tread grooves (if present) or into the drainage paths provided by the surface texture. Throughout Zone 1 a continuous, relatively thick layer of fluid is present between the tyre and the runway surface; the only retarding force developed is that due to fluid drag. In addition, fluid pressure generated in this zone is the principal cause of two phenomena:

1. There is an inwards deformation of the tyre surface in the contact area, the extent of which depends on the tyre vertical deflection, forward speed and inflation pressure.

2. During rolling, there is a forward shift of the centre of pressure in the tyre-ground contact area. The displacement of the centre of pressure from its static position (beneath the wheel axle) increases with increase in forward speed, fluid depth and density. During braking, a further redistribution of bearing pressure occurs in the contact area so that the centre of pressure moves rearward. Thus, in wet conditions the centre of pressure in the contact area of a braked tyre may be in front of or behind the axle.

Zone 2 is a transition region. After the bulk of the fluid is displaced, a thin film remains between the tyre and the runway surface. At the rear of Zone 1, and in Zone 2, viscous effects prevent a rapid outflow of fluid. These viscous effects also serve to maintain fluid pressures. The thin film first breaks down at points where the local bearing pressure is high – for example, at sharp surface asperities. In the presence of such a lubricant as water, the coefficient of friction of rubber on hard surfaces is greatly reduced from the dry surface value. Thus, in general, very little frictional force is generated wherever a thin film of fluid persists. In the model developed in sub-section 9.1, it is assumed that no friction is generated in this zone.

Zone 3 is the region of predominantly dry contact; it is here that most of the braking force is generated. The tendency for tread elements towards the rear of the contact area to slide may be increased by the presence of fluid at the edges of the contact area.

In wet conditions, the coefficient of friction between tyre and ground depends on the relative sizes of Zones 1, 2 and 3. These are determined by:

- surface texture,
- depth of fluid,

---

[24] See Reference 33.

- density of fluid,
- viscosity of fluid,
- tread pattern of the tyre,
- inflation pressure of the tyre, and
- time for a tread element to pass through the contact area.

Figure 9.1 also shows the effect of forward speed on the relative sizes of Zones 1, 2 and 3. In Figure 9.1b, the tyre forward speed is higher than in Figure 9.1a so that Zone 1 extends farther back into the contact area and Zones 2 and 3 occupy a horseshoe-shaped region at the rear. In Figure 9.1c, at a still higher speed, contact with the ground is all but lost. In this condition, the tyre develops very little braking force. Finally, in Figure 9.1d, the tyre is moving at such a speed that Zone 1 extends throughout the contact area. In this case, dry contact with the ground is no longer maintained and the tyre is said to be ***planing***.

In sub-section 9.1, appropriate values for the mean pressures acting in the three zones are proposed, and the implications of those proposals are discussed in terms of the statistical properties of the deviations of the measured pressures from the correlations presented.

9.1　Pressures in Area of Dry Contact (Zone 3)

Typical measurements of the mean bearing pressure are shown in Figure 9.2 for an aircraft tyre at rest under load on a dry runway for a range of inflation pressures. These data are taken from Reference 36.

Bearing pressure is defined by

$$p_b = \frac{Z}{A_F}$$

9.1

where Z is vertical load and A_F is the area of the footprint.[25]

In the original analysis of Reference 36, a linear least squares fit was made to the bearing pressure as a function of the inflation pressure in relative measure. For some reason, a correlation with inflation pressure in absolute measure was not attempted. Such a correlation is investigated here. A paired t-test, comparing the values of p_b/p_a with those of $p/p_a (=1+p_i/p_a)$ shows that the probability exceeds 0.2 that the distribution of each set is representative of the other.[26] This implies that the footprint area, under static conditions, is given by

$$A_F = \frac{Z}{p}\left(=\frac{Z}{p_i+p_a}\right)$$

9.2

This relationship is used throughout the project as a convenient reference area.

---

[25]　It is not clear in Reference 36 how the area of the footprint was measured.
[26]　Under most circumstances, a probability in excess of 0.05 is acceptable as a criterion.

Furthermore, an Anderson-Darling test for Normality on the distribution of residuals about the 1:1 correlation shows the probability that the distribution conforms to the Normal distribution is well in excess of 10%. In addition, there are thirteen measurements and the standard error (deviation) of the residuals about the correlation is approximately ± 8 lbf/in^2; the standard error of an estimate of a mean value of bearing pressure from the correlation is, therefore, ± 2.2 lbf/in^2. This is approximately 1% of the largest inflation pressure at which tests were done.

When a loaded tyre slides on a rough surface, the way in which friction forces are generated in the footprint varies with both speed and the roughness of the surface. Changes occur in the pressure distribution in the footprint, which depend on the size of the asperities in the surface. However, the tyre is in vertical equilibrium, so that the mean pressure in the area of dry contact remains the same as when the tyre is at rest. Thus, it is assumed that the pressure under the dry part of the tyre footprint is represented by the inflation pressure – in ***absolute measure***.

9.1.2   Pressure in Zone 1

In the three-zone model (see sub-section 9.1.3), it is assumed that the pressure in Zone 1 is sufficient to overcome the inertia of the fluid. Thus, it may be expected that the pressure is equal to the kinetic pressure. In practice, measurements published, in Reference 37, for the observed pressure in the groove of a ribbed aircraft tyre, can be shown to be represented by the kinetic pressure. These measurements are shown in Figure 9.3 for two inflation pressures – 90 psig and 150 psig – over a speed range so that $20 \leq V \approx 100$ kn. Kinetic pressure is also shown in the figure.

A two-tailed paired t-test, comparing the values of $\mathrm{M}[q]$ with $\mathrm{E}[q]\left(= \rho V^2/2\right)$ shows that there is a probability in excess of 0.25 that the distribution of each set is representative of the other.[27] It is therefore assumed that the pressure in Zone 1 is identical to the kinetic pressure.

9.1.3   Pressure in Zone 2

No simple theory has been advanced to suggest a formulation for the pressure in this zone. In Reference 37, measurements are presented for the pressure under the rib of a tyre rolling in water on a smooth surface. These measurements are plotted in Figure 9.4 for two inflation pressures over a range of speed so that $5 \leq V \approx 100$ kn. Kinetic pressure is shown on the figure together with an empirical correlation for the pressure under the rib.

The trends within the measurements suggest that a correlation should reflect the tendency for the pressure under the rib to tend to the kinetic pressure as speed reaches a limiting value for each inflation pressure.

Let $q/p = \theta$ and defining[28]

---

[27]   Under most circumstances, a probability in excess of 0.05 is acceptable as a criterion.
[28]   Note that inflation pressure is defined in absolute measure in this context.

$$\varphi = \frac{\sin[\theta]}{\sin[\theta] + \cos[\theta]} \qquad\qquad 9.3$$

the function

$$\delta\left[\frac{q_v}{p}\right] = \frac{q_v - q}{p} = a_0 \varphi^{m_1} (1-\varphi)^{m_2} : \varphi \le 1$$

$$\delta\left[\frac{q_v}{p}\right] = 0 : \varphi > 1, \qquad\qquad 9.4$$

where $(a_0, m_1, m_2) = (3.138,\ 0.4,\ 2.4)$, is an adequate description of the data.

Using a two-tailed, paired t-test to compare the values of $\mathrm{M}[q_v]$ with $\mathrm{E}[q_v]$, it can be shown that there is a probability in excess of 0.2 that the distribution of each set is representative of the other.

In the absence of other experimental evidence, it is assumed that the **_mean_** pressure in Zone 2 is identical to the pressure under the rib of a tyre rolling on a smooth surface.

9.2   Statistics of Model

The experiment reported in Reference 37 used the same pressure system to measure both the pressure in the groove and that under the rib. It is therefore legitimate to study the deviations of the measured pressures from the separate correlations in combination. As a prudent check, it can be shown, using an F-test, that the variances of the deviations about each correlation are not significantly different even at the 15% level of significance. The standard error of the pooled deviations is ± 14.5 lbf/in^2. This value is based on 37 measurements: the standard error of an estimate of the pressure in Zone 1 or 2 is, therefore approximately ± 2.4 lbf/in^2. This is approximately 1.3% of the largest pressure measured in the experiment. Also, an Anderson-Darling test for Normality shows that $P[A^*] \gg 0.1$.

Using these correlations as a model to predict mean pressures in the three zones of the footprint of an aircraft tyre implies a standard error for prediction in the order of ± 2.5 lbf/in^2. Since the distributions are probably Normal, the uncertainty associated with a value calculated using these assumptions is in the order of ± 5 lbf/in^2 at the 95% level of significance.
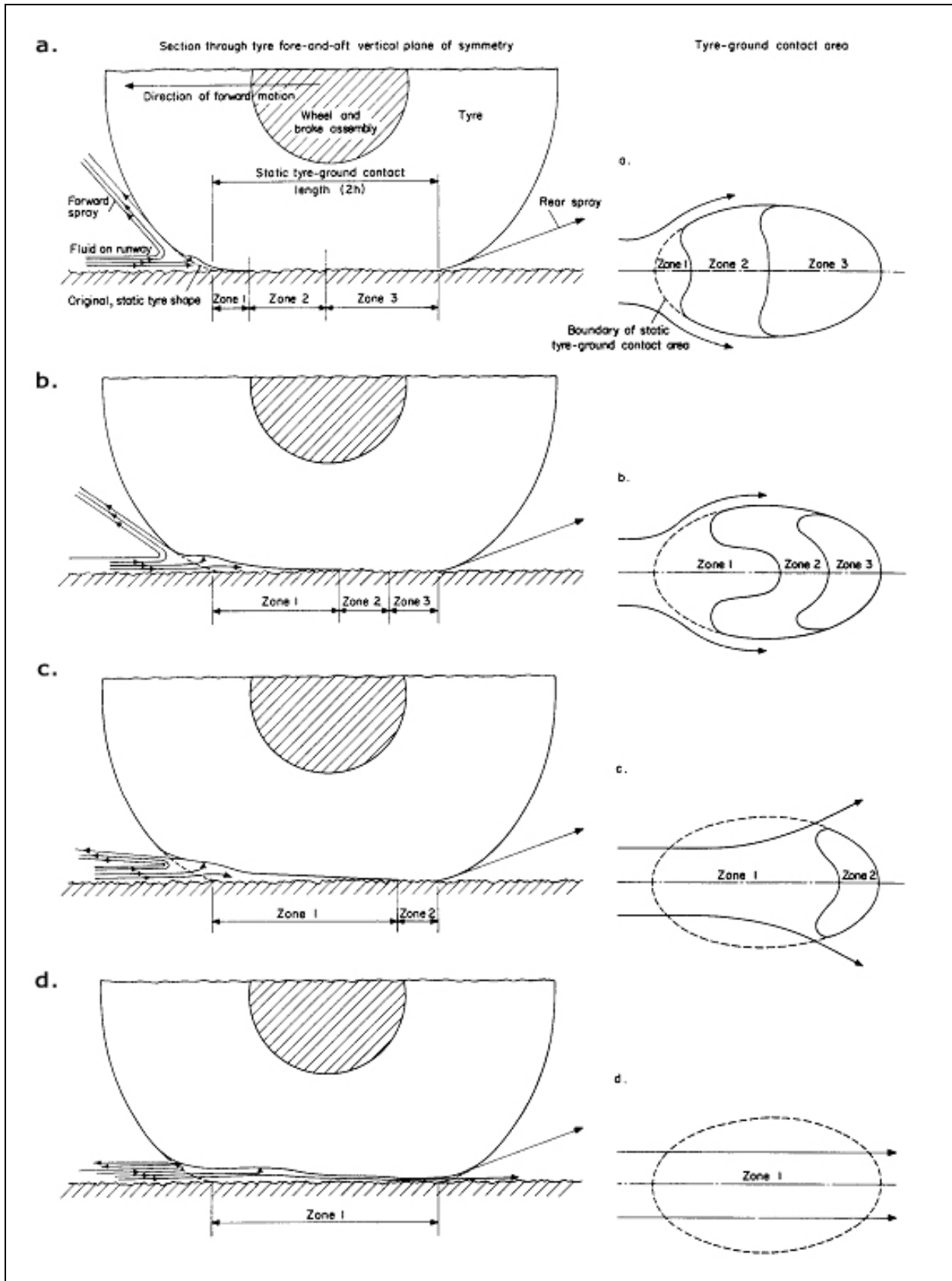
Figure 9.1: Conceptual model of contact area between tyre and ground in wet conditions
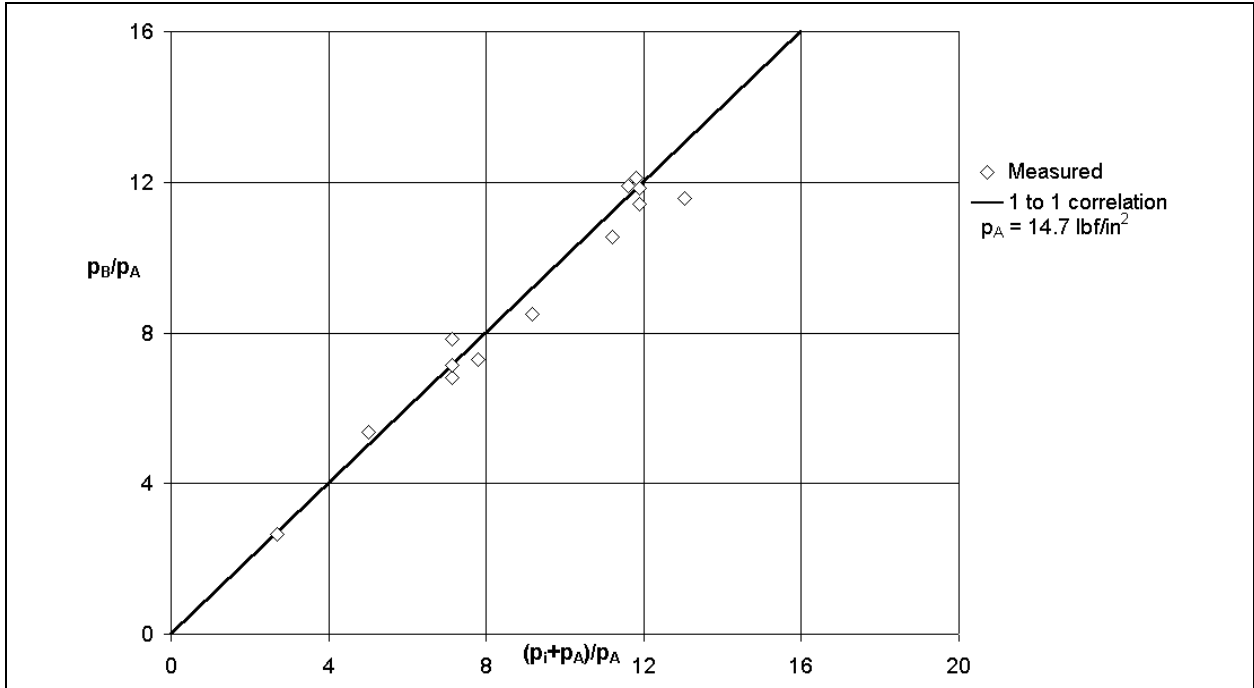
Figure 9.2: Effect of inflation pressure on mean bearing pressure – static aircraft tyre
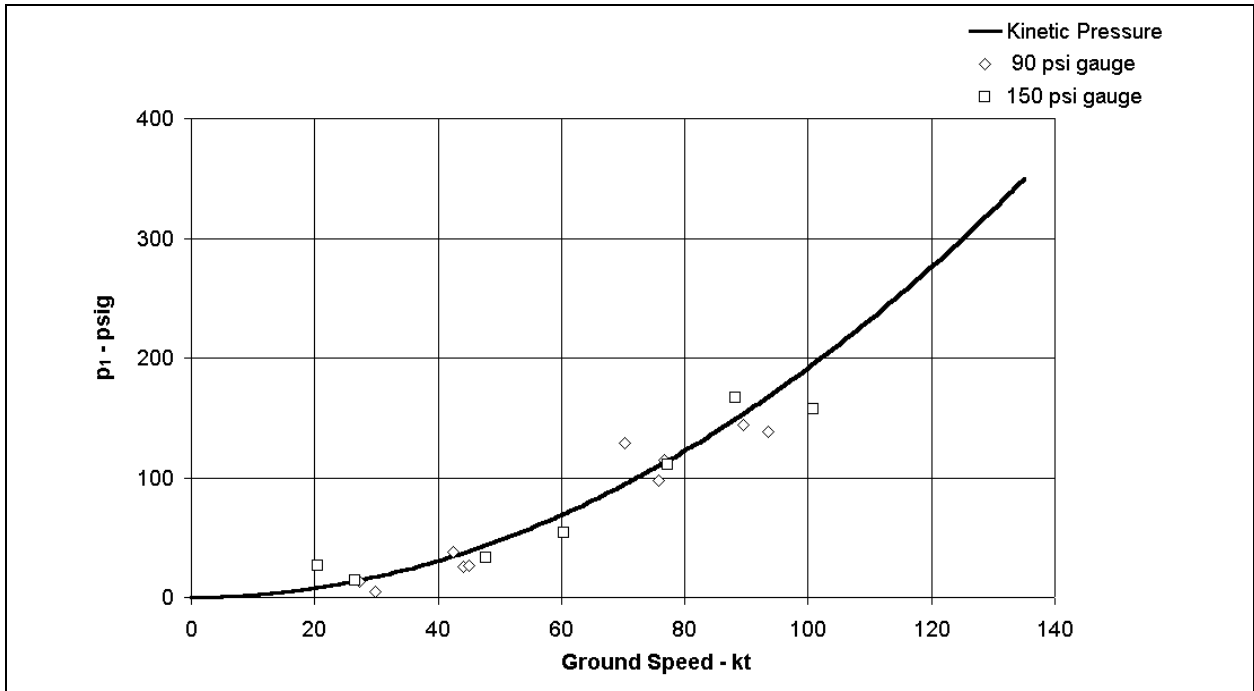
Figure 9.3: Effect of ground speed on pressure in Zone 1

98
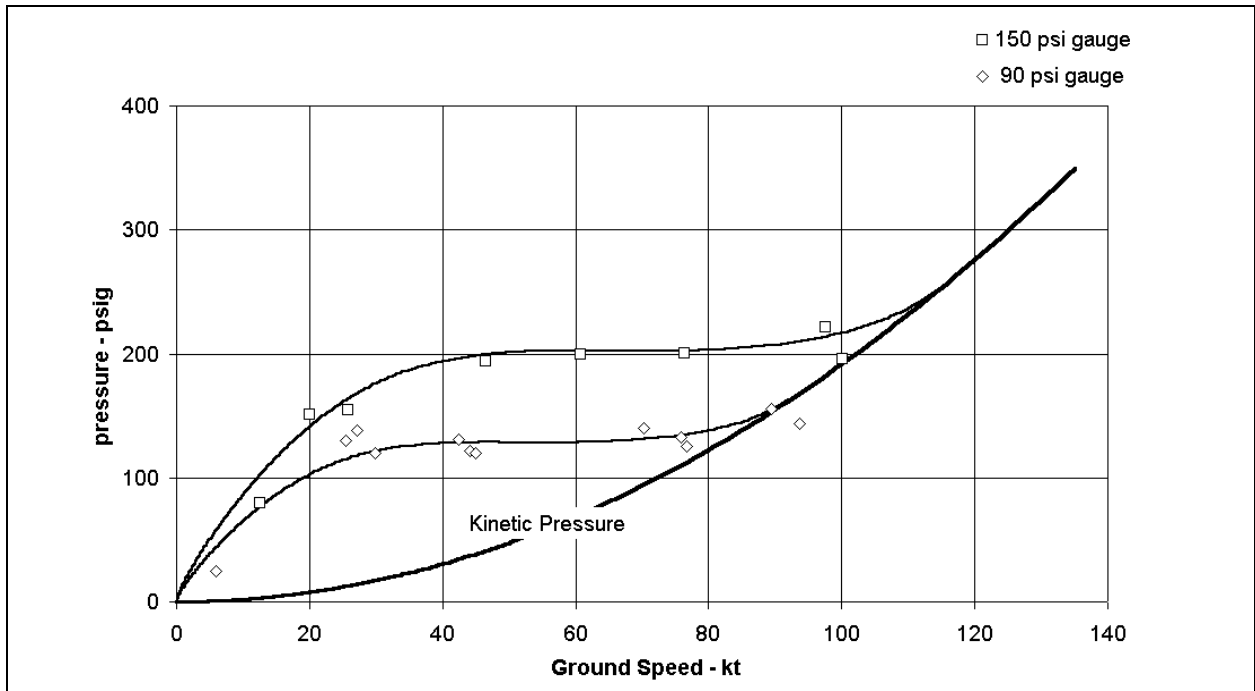
Figure 9.4: Effect of ground speed and inflation pressure on pressure in Zone 2

10. COEFFICIENT OF BRAKING FRICTION – SKIDDING ON WET RUNWAY

The simple empirical model presented in Sections 6 and 7 for coefficient of braking friction when skidding on dry surfaces is a suitable starting point from which to develop a mathematical description of coefficient of braking friction when skidding on wet surfaces. The concept of the three-zone model of pressures in the footprint of the tyre is used[29] as an aid to extending the dry model to incorporate the effects of a wetted runway.

In the process of formulation, some care has been exercised to ensure that the wet model defaults to dry when water depth tends to zero. This concern has led to the introduction of a characteristic water depth and macro-texture depth. Furthermore, the wet model has been constructed in such a way as to ensure that coefficient of friction in a skid may vanish under appropriate conditions of speed, texture depth and water depth. No specific data for such conditions have been studied. However, during the process of modelling and correlation, plausible conditions have been identified at which friction coefficient becomes zero.

For a specific design of tyre, coefficient of braking friction when skidding on wet surfaces depends on five variables:

1. Inflation pressure
2. Vertical load
3. Ground speed
4. Depth of the surface macro-texture and
5. Water depth

References 36 and 38 present sets of data that are the results of systematic studies of the effects of the first four of these variables. During the reported experiments, attempts were made to control the depth of water to a consistent value so that $d = 0.02$ in. However, these attempts were only partially successful, particularly in the cases where texture depth was largest and surface drainage was most effective. The perceived variability between tests may well be, in part, a consequence of inconsistency in water depth.

Data from Reference 7 are also used in the construction of the model. These data were collected from experiments conducted using the facility at NASA Langley. The specific experiments used here are for tyres that are judged to be close to production models and were conducted in a degree of wetness that simulated "...conditions measured on an actual runway during a heavy rain shower." The average depth of water used was 0.15 inch. However, the trough through which the tyre moved had an undulating surface. The depth varied so that $0 < d < 0.3$ in.

In this section, the mathematical basis of the extension of the dry model is explained and the process of identifying the new modelling components is summarised. The relationship between the mathematical (empirical) model and experimental data is explored in practical, statistical

---

[29] A mathematical model of the pressures under the footprint is given in Section 9.

terms. Finally, the model is used to show that there is significant "within-test" and "between-test" variability for both experimental facilities from which test data were used.

10.1 Model

Modelling equations are based upon the model that was shown, in Section 7, to represent an aviation tyre in full skid on a dry runway. That model is extended using a factor that has been derived from the concept of the ***three-zone*** model of the area under the footprint of a moving tyre. Pressures in the three zones are calculated using the mathematical model given in Section 9.

Consider the three-zone model of tyre footprint as described in Section 9. Now, the total load normal to the runway is supported by the sum of the products of the pressures and areas in the three zones.

$$Z = qS_1 + q_v S_2 + pS_3 \qquad\qquad 10.1$$

It may be assumed that all braking force is developed only in Zone 3 – the area of dry contact. By definition, braking force in the wet is the product of total vertical load and coefficient of braking friction in the wet. This can be equated to the product of vertical load in Zone 3 and coefficient of braking friction in the dry.

$$Z\mu_{SKID\ WET} = pS_3\mu_{SKID\ DRY} \qquad\qquad 10.2$$

Combining Equations 10.1 and 10.2 and re-arranging,

$$\mu_{SKID\ WET} = \frac{\mu_{SKID\ DRY}}{\left(1 + \dfrac{S_1}{S_3}\dfrac{q}{p} + \dfrac{S_2}{S_3}\dfrac{q_v}{p}\right)} \qquad\qquad 10.3$$

When dry contact with the runway is lost, planing is said to occur and coefficient of friction becomes either negligible or not significantly different from zero. Equation 10.3 reflects that phenomenon in that $\mu_{SKID\ WET} \rightarrow 0$ as $S_3 \rightarrow 0$.

However, in its current form the equation is not particularly helpful as a means of correlation. A simple adaptation of the modelling may be done by letting

$$\frac{S_1}{S_3} = \frac{\varphi_0}{1 - \varphi_0\,q/p} \quad \text{and} \quad \frac{S_2}{S_3} = \frac{\varphi_1'}{1 - \varphi_0\,q/p} \qquad\qquad 10.4$$

Substituting Equation 10.4 into Equation 10.3

$$\mu_{SKID\ WET} = \frac{\mu_{SKID\ DRY}}{\left\{1 + \left(\dfrac{\varphi_0}{1 - \varphi_0\, q/p}\right)\dfrac{q}{p} + \left(\dfrac{\varphi_1'}{1 - \varphi_0\, q/p}\right)\dfrac{q_v}{p}\right\}} \qquad 10.5$$

Multiplying both numerator and denominator of the right hand side of Equation 10.5 by $\left(1 - \varphi_0\, q/p\right)$, substituting $\varphi_1' = \varphi_1\, p/p_a$ and collecting terms,

$$\mu_{SKID\ WET} = \mu_{SKID\ DRY}\left(\frac{1 - \varphi_0\, q/p}{1 + \varphi_1\, q_v/p_a}\right) \qquad 10.6$$

In this special form, the three-zone model can be used as a vehicle for correlating the data given in References 7, 36 and 38. The process of correlation is described in sub-section 10.2.

10.2   Correlation of Data

The quantities in Equation 10.6, with the exception of φ_0 and φ_1, either are measured in the experimental process or can be calculated. Thus, $\mu_{SKID\ WET}$ and inflation pressure are more or less direct measurements, whilst q and q_v can be calculated using the relationships given in Section 9. Furthermore, $\mu_{SKID\ DRY}$ can be calculated using the relationships given in Section 7.

Now, re-arrange Equation 10.6 so that

$$\left(1 - \frac{\mu_{SKID\ WET}}{\mu_{SKID\ DRY}}\right) = \varphi_0\left(\frac{q}{p}\right) + \varphi_1\left(\frac{q_v}{p_a}\frac{\mu_{SKID\ WET}}{\mu_{SKID\ DRY}}\right) \qquad 10.7$$

The terms in brackets may be treated as variables in a correlation process. For every set of tests in the database, Equation 10.7 can be solved by the method of least squares or some equivalent technique for φ_0 and φ_1. These values can then be correlated appropriately with independent variables in the database.

In particular, values of φ_0 from the tests of References 36 and 38 were observed to vary inversely with depth of the macro-texture. Assuming the mean water depth was 0.02 in, the relation $\varphi_0 = 0.65\left\{d\,/\left(d + d_{tex}\right)\right\}$ was found to be a reasonable fit to the data.

However, reflecting on the relations given in Section 9 at Equations 9.3 and 9.4, pressures in Zone 1 and Zone 2 are equal for both $\varphi = 0$ and $\varphi = 1$; that is, when $q/p = 0$ and $q/p = \pi/2$. As macro-texture depth tends to zero, it may be assumed that the pressures in Zone 1 and Zone 2 are equalised when planing occurs. In other words $\varphi_0 = 2/\pi = 0.6366$, for a smooth runway. Thus, it is assumed that

$$\varphi_0 = \frac{2}{\pi}\left(\frac{d}{d+d_{tex}}\right) \qquad\qquad 10.8$$

In order to continue the process, Equation 10.7 can be further re-arranged so that

$$\left\{\left(1-\varphi_0\frac{q}{p}\right)\frac{\mu_{SKID\ DRY}}{\mu_{SKID\ WET}}-1\right\}=\varphi_1\frac{q_v}{p_a} \qquad\qquad 10.9$$

where φ_0 is calculated from Equation 10.8.

For all the tests in the database, Equation 10.9 is solved for φ_1. These values were found to correlate so that

$$\ln\left[\frac{\left(1-e^{(-d/d_0)}\right)}{E[\varphi_1]}\right]=\varphi_{12}\left(1-e^{(-d_{tex}/d_{tex0})}\right)\left(\ln\left[\frac{1}{1-Z/pwD}\right]\right)^n \qquad\qquad 10.10$$

where

$n=\varphi_{10}\left(1+\varphi_{11}\ln\left[d_{tex}/d_{tex_0}\right]\right)$, $\varphi_{10}=-0.0282$, $\varphi_{11}=3.9$, $\varphi_{12}=1.9$, $d_0=0.004\text{in}$ and $d_{tex_0}=0.00234\text{in}$

Values of $E[\varphi_1]$ calculated from Equation 10.10 are plotted in Figure 10.1 against the values of $M[\varphi_1]$ obtained from "best" fits to the measured friction data.

Define

$$\Delta[\varphi_1]=E[\varphi_1]-M[\varphi_1] \qquad\qquad 10.11$$

The distribution of these differences between the measured and expected values from the modelling Equation 10.10 is shown in Figure 10.2. The calculation is sufficiently representative of the values obtained from fitting the measured friction data to justify the use of the relation in Equation 10.10 as part of a mathematical model. The quality of the fit that the model provides to the measured friction data is considered in sub-sections 10.3 and 10.4.

10.3   Data

As is shown in Table 10.1, data from References 7, 36 and 38 cover wide ranges of vertical load and inflation pressure, together with a substantial range of runway texture depth. Speed coverage is adequate.

Measurements of coefficients of braking friction in full skid are shown in Figures 10.3 to 10.29 for the tests reported in References 36 and 38. Similarly, the measurements from Reference 7 are shown in Figures 10.31 to 10.35. In all cases, calculations from the model as described in Equations 10.6, 10.8 and 10.10 are included on the plots. In addition, the calculated value for coefficient of friction when skidding on a dry runway is shown for reference in each case. A table in the top right hand corner of each plot gives the relevant values of the independent variables for the test.

The distribution of the total deviations of measurements from the model is shown in Figure 10.30 for the data from References 36 and 38. A similar distribution of total deviations of measurements from the model for the data from Reference 7 is shown in Figure 10.36.

There are also sufficient different test series to enable a study of the variability that occurs between tests in the context of the mathematical model. Thus, the distribution of mean deviations from the model of each test series is presented in Figure 10.37 and is discussed in sub-section 10.4.

Table 10.1: Test conditions covered for skidding on wet runways

Description	d_{tex} - in	d - in	p_i - psig	V - kn	Z - lbf
Polished concrete	0.0039	0.02	$25 < p < 180$	$8 < V < 50$	$2240 < V < 10080$
Concrete	0.01	0.15	$120 < p < 260$	$23 < V < 100$	$10000 < V < 20000$
Fine texture asphalt	0.0157	0.02	$25 < p < 180$	$8 < V < 50$	$2240 < V < 10080$
Quartzite macadam	0.0669	0.02	$60 < p < 180$	$8 < V < 50$	$6270 < V < 7840$

10.4 Discussion

The mathematical model set out in Equation 10.6 is a complete description of coefficient of braking friction for skidding on a wet paved runway. Although Equation 10.6 is superficially simple, the composition of the factor φ_1 is not. Now, the factor $(1 - \varphi_0 q/p)$ is adequate to ensure that coefficient of friction becomes zero in an appropriate way. Nevertheless, the shape of the curve of friction coefficient against speed is determined mainly by the value of φ_1. It is from the requirement to match data over a wide range of all the variables that the complexity in Equation 10.10 arises. Figures 10.1 and 10.2 show the match between the calculation of Equation 10.10 and the individual, "best-fit" values of the factor. In general, the match is very close; it is only for the smoothest – and therefore least representative – case that there is a slight deterioration in the quality of the fit. Consequently, the relationship between the model and measurements for the smoothest runway does show some minor deficiencies. For instance, the model is not a particularly good fit to the data for Figure 10.12. However, a plausible combination of variability in water depth, inflation pressure and vertical load could be used to find an "exact" fit to the data using the model. This is true for every case investigated.

In spite of the clear differences between the model and measurements in a minority of cases, the standard error of the total deviations between the two for the data from References 36 and 38 is only $\sigma[\Delta] = \pm 0.04$. The distribution – see Figure 10.30 – is not significantly different from Normal.

Data from Reference 7 are not so comprehensive in terms of a systematic coverage of the variables. These data do have the merit of extending coverage of normal load to 20,000 lbf, inflation pressure to 260 psig and water depth to 0.15 in. Again, the standard error of the total deviations between the model and the measurements is $\sigma[\Delta] = \pm 0.041$, which is not significantly different from the value calculated for data from References 36 and 38. Furthermore, the distribution of the deviations between mathematical model and experiment is shown to be Normal in Figure 10.36.

By combining these two distributions, it can be shown that the standard error of the deviations of the whole database from the model is $\sigma[\Delta] = \pm 0.0402$ based on 681 individual measurements. It follows that the uncertainty associated with a calculation of $\mu_{SKID\ WET}$ from the model is $U[\mu_{SKID\ WET}]_{0.95} = \pm 0.003$. This value can be used in standard uncertainty calculations when assessing estimates of aircraft braking performance.

The mathematical model can be used to assess the performance of the two testing facilities from which experimental data have been acquired. If the model has empirical merit, the mean deviations from the model of measurements from specific tests may be taken to represent "between-test" variability. Because there are 32 separate tests in the database, the distribution of "between-test" variability can be studied using a χ^2-test. It can be shown, using an F-test, that the variance of the mean deviations for the tests from References 36 and 38 is not significantly different from the variance of the mean deviations for the tests from Reference 7. By combining the sets, it can be shown, using a χ^2-test, that the distribution of the "between-test" variability is not significantly different from the Normal distribution – see Figure 10.37. It was shown above that the total variability of the experimental data from the model was also Normal. Thus, since the sum (or difference) of two Normal distributions is also Normal, it may be asserted that the "within-test" variability of the test facilities is Normal.

Now, the standard error of the total variability is $\sigma[\Delta] = \pm 0.0402$ and the standard error of the "between-test" variability is $\sigma[\Delta]_1 = \pm 0.0222$. The standard error of the "within-test" variability is therefore $\sigma[\Delta]_2 = \pm 0.0335$ for both facilities. These statistics are of profound interest when comparing experimental data from these or any other facilities with the mathematical model.
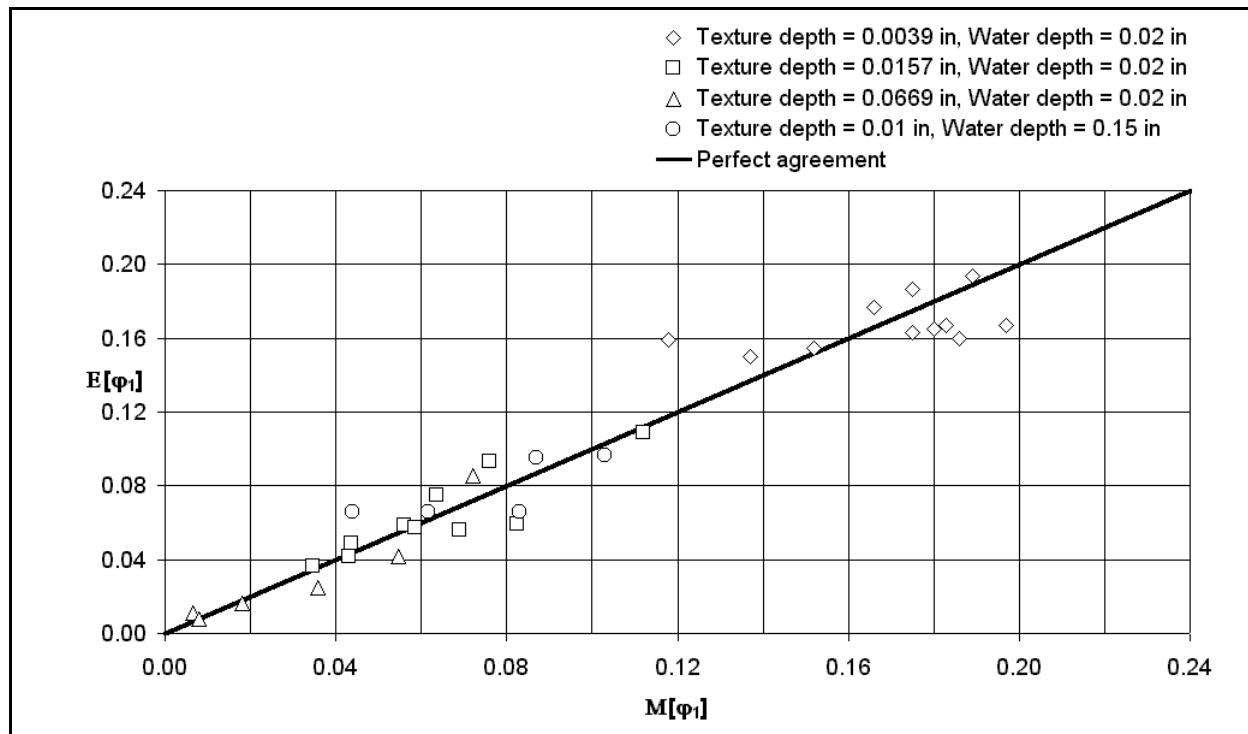
Figure 10.1: Observed and calculated values of φ_1 compared
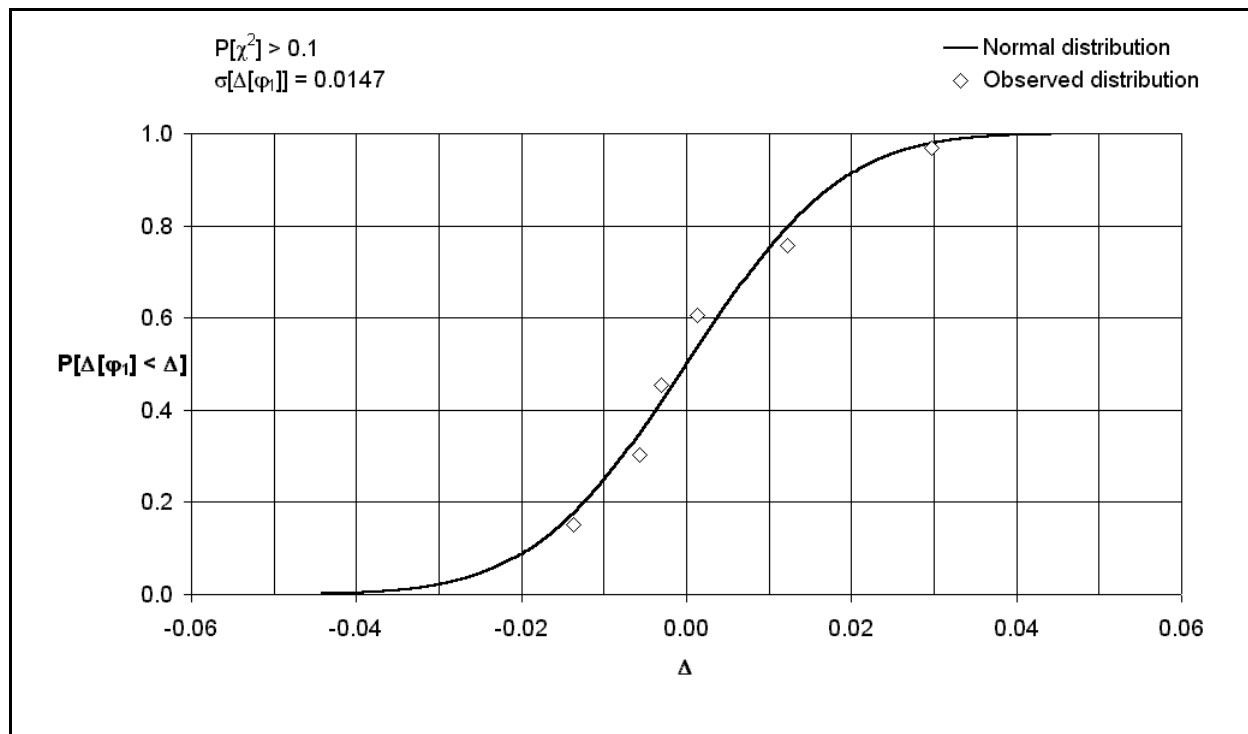
Figure 10.2: Distribution of deviations of observed values of φ_1 from calculated values
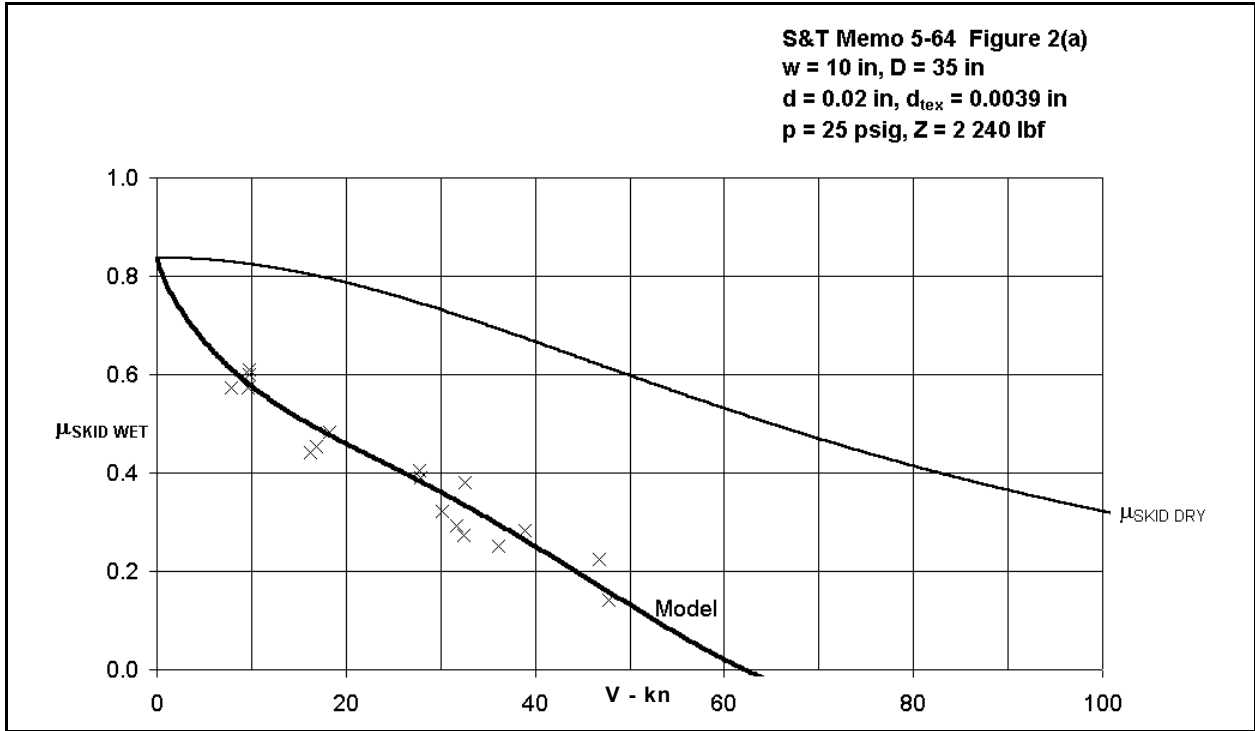
Figure 10.3: Effect of ground speed on coefficient of friction in full skid (Data points from Reference 36, Figure 2(a))
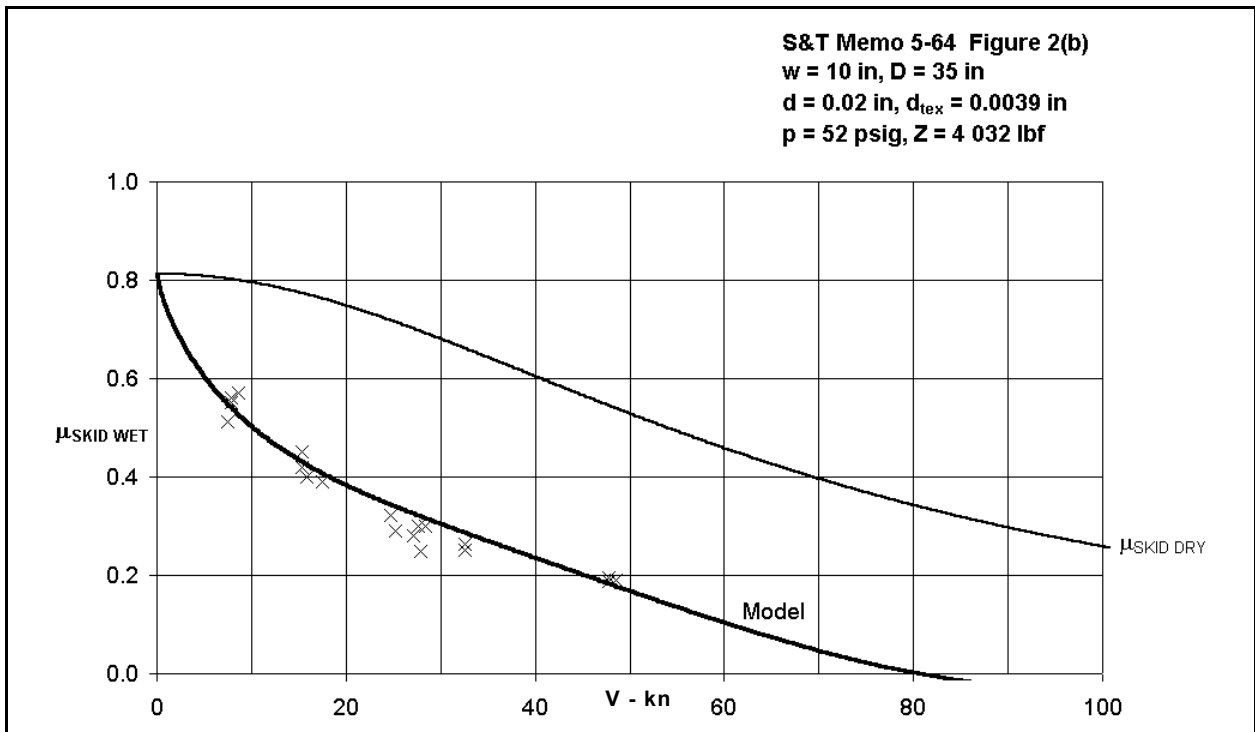
Figure 10.4: Effect of ground speed on coefficient of friction in full skid (Data points from Reference 36, Figure 2(b))
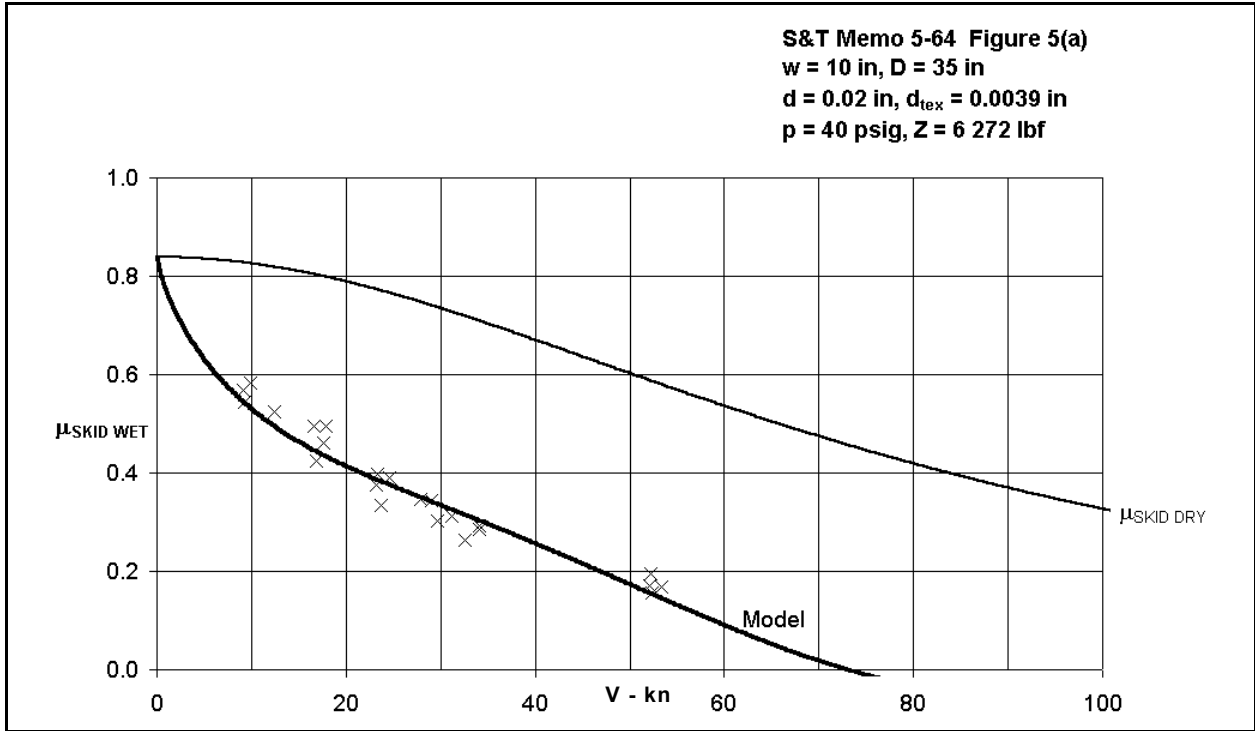
**Figure 10.5: Effect of ground speed on coefficient of friction in full skid
(Data points from Reference 36, Figure 5(a))**

**Figure 10.6: Effect of ground speed on coefficient of friction in full skid
(Data points from Reference 36, Figure 5(b))**

**Figure 10.7: Effect of ground speed on coefficient of friction in full skid
(Data points from Reference 36, Figure 5(c))**

**Figure 10.8: Effect of ground speed on coefficient of friction in full skid
(Data points from Reference 36, Figure 5(d))**

Figure 10.9: Effect of ground speed on coefficient of friction in full skid (Data points from Reference 36, Figure 5(e))

Figure 10.10: Effect of ground speed on coefficient of friction in full skid (Data points from Reference 36, Figure 5(f))

**Figure 10.11: Effect of ground speed on coefficient of friction in full skid
(Data points from Reference 38, Figure 1)**

**Figure 10.12: Effect of ground speed on coefficient of friction in full skid
(Data points from Reference 38, Figure 2)**

**Figure 10.13: Effect of ground speed on coefficient of friction in full skid
(Data points from Reference 36, Figure 2(d))**

**Figure 10.14: Effect of ground speed on coefficient of friction in full skid
(Data points from Reference 36, Figure 3(a))**

113

S&T Memo 5-64 Figure 3(b)
w = 10 in, D = 35 in
d = 0.02 in, d_{tex} = 0.0157 in
p = 52 psig, Z = 4 032 lbf

Figure 10.15: Effect of ground speed on coefficient of friction in full skid
(Data points from Reference 36, Figure 3(b))

S&T Memo 5-64 Figure 6(a)
w = 10 in, D = 35 in
d = 0.02 in, d_{tex} = 0.0157 in
p = 40 psig, Z = 6 272 lbf

Figure 10.16: Effect of ground speed on coefficient of friction in full skid
(Data points from Reference 36, Figure 6(a))

114
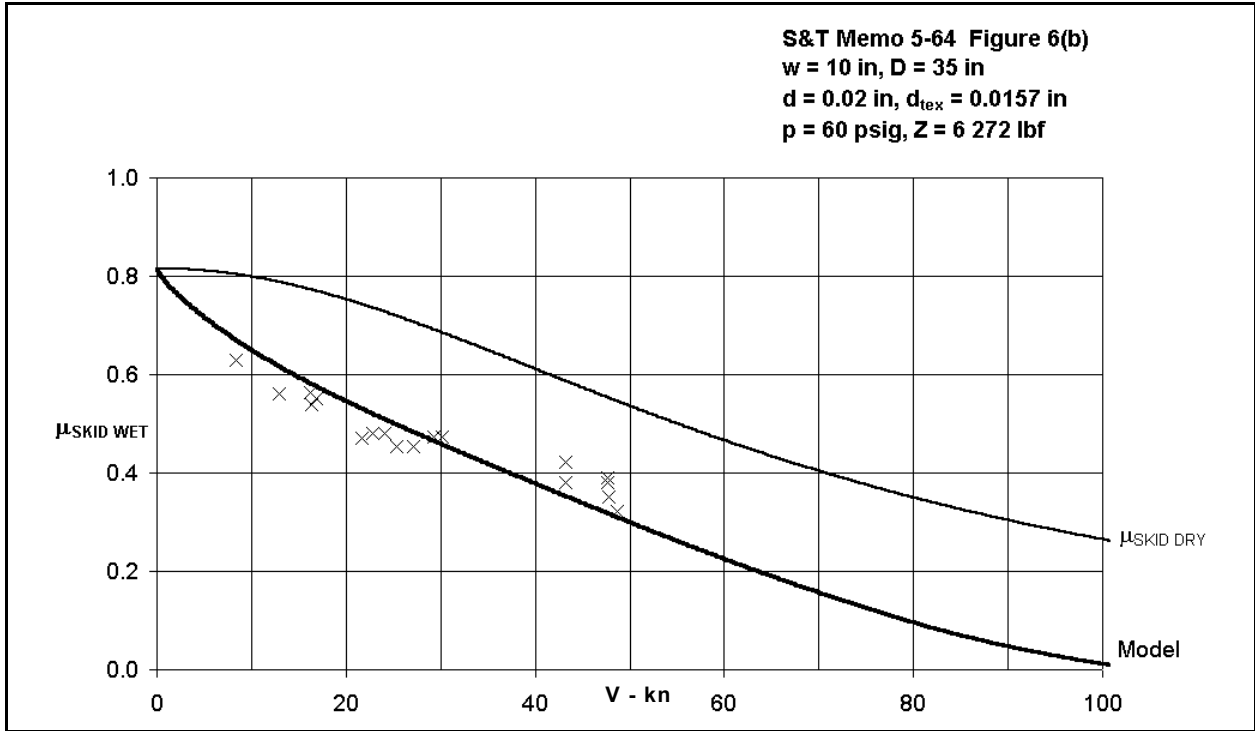
**Figure 10.17: Effect of ground speed on coefficient of friction in full skid
(Data points from Reference 36, Figure 6(b))**
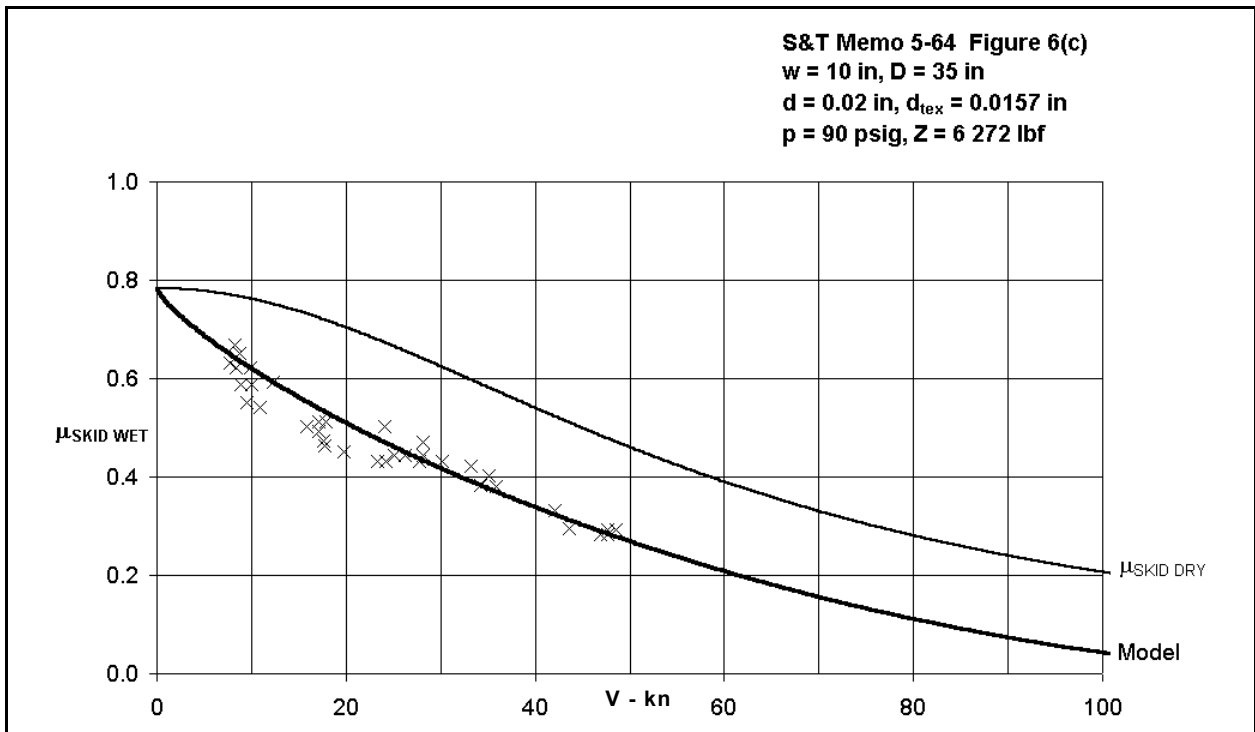
**Figure 10.18: Effect of ground speed on coefficient of friction in full skid
(Data points from Reference 36, Figure 6(c))**
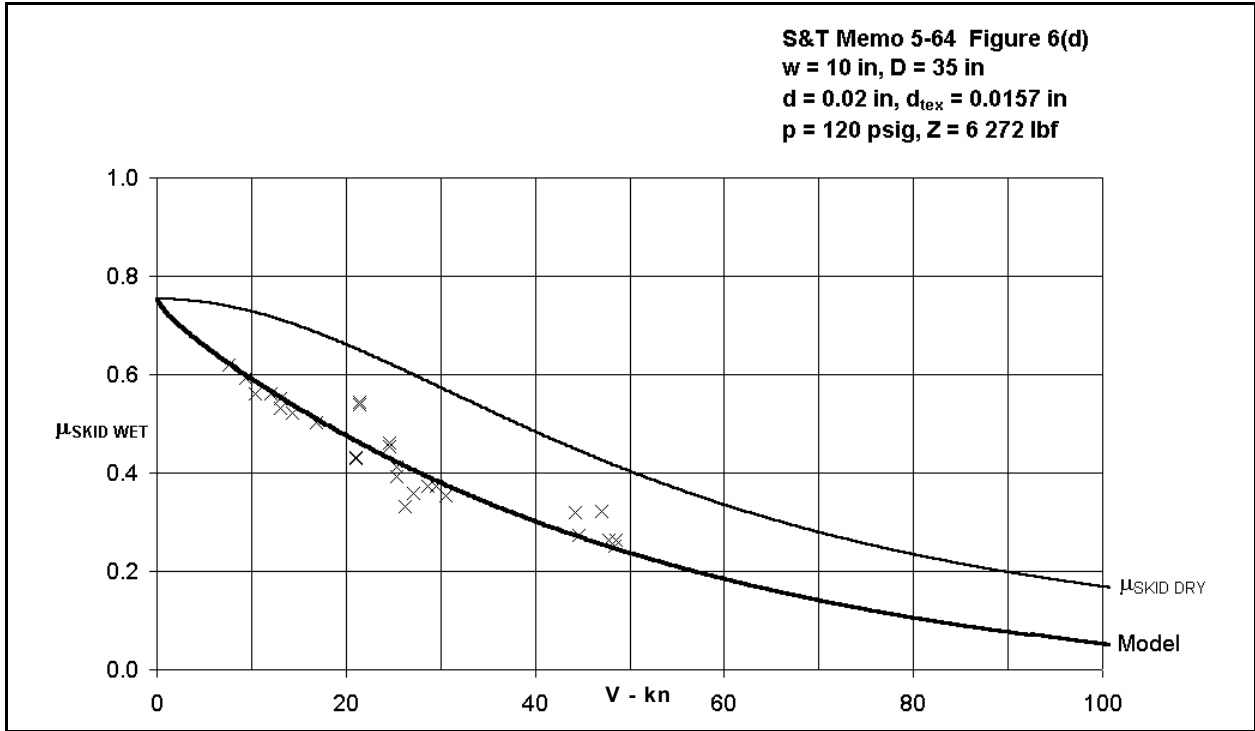
**Figure 10.19: Effect of ground speed on coefficient of friction in full skid
(Data points from Reference 36, Figure 6(d))**
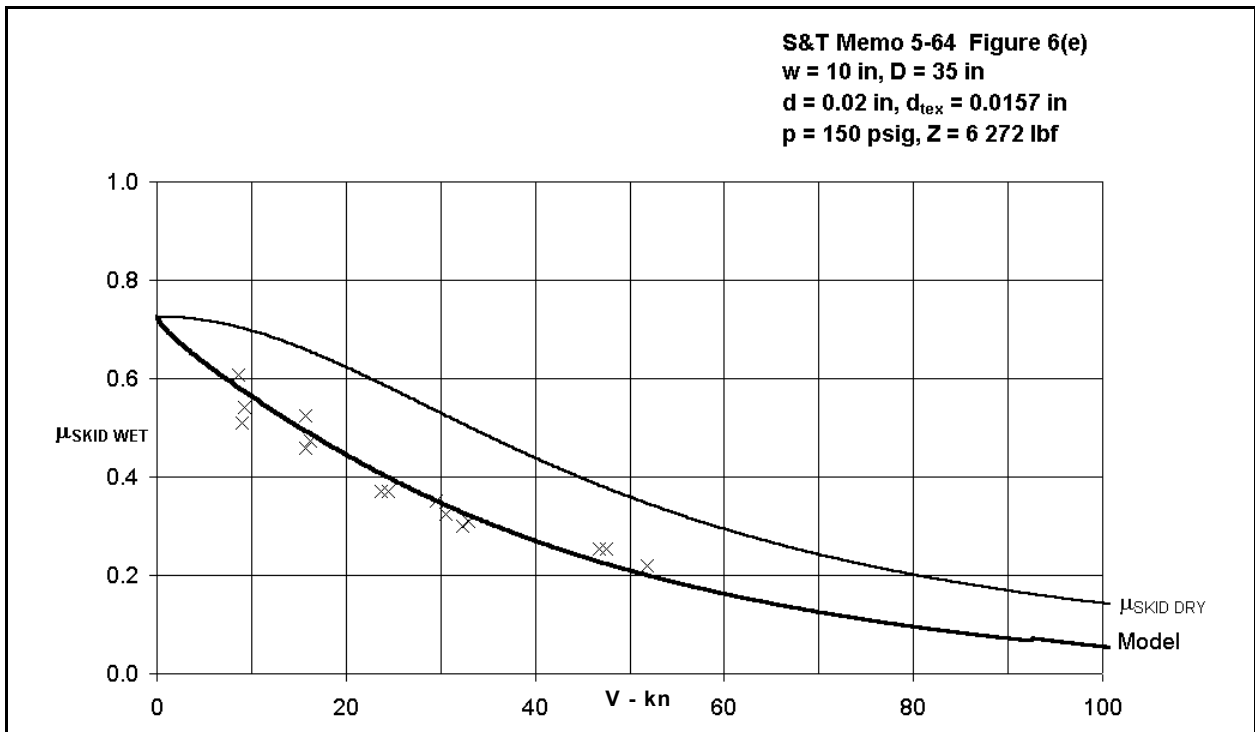
**Figure 10.20: Effect of ground speed on coefficient of friction in full skid
(Data points from Reference 36, Figure 6(e))**
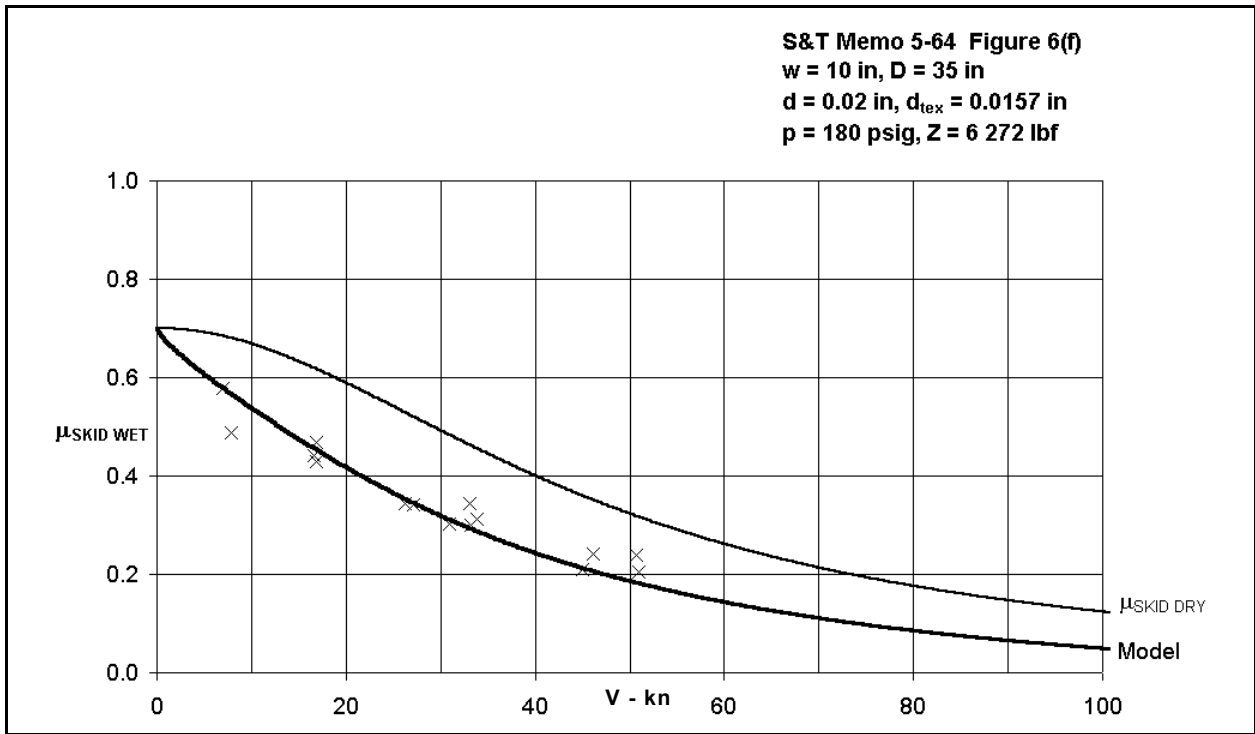
Figure 10.21: Effect of ground speed on coefficient of friction in full skid (Data points from Reference 36, Figure 6(f))
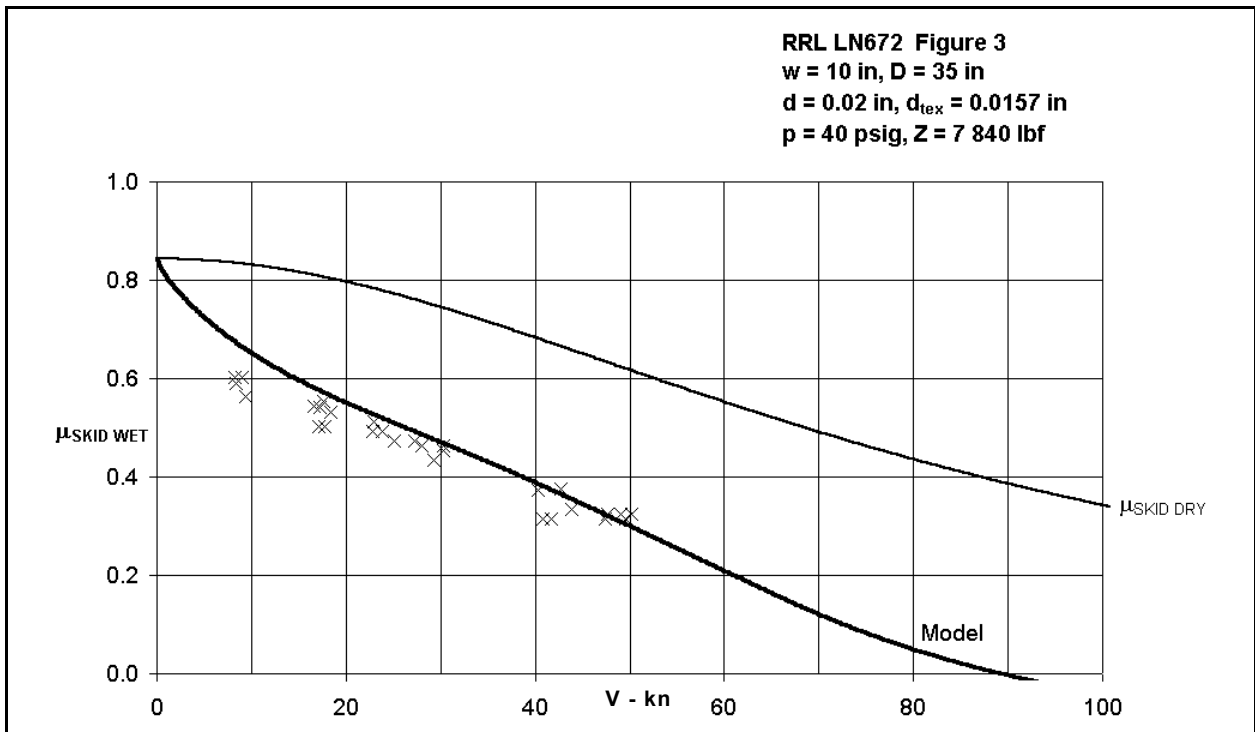
Figure 10.22: Effect of ground speed on coefficient of friction in full skid (Data points from Reference 38, Figure 3)
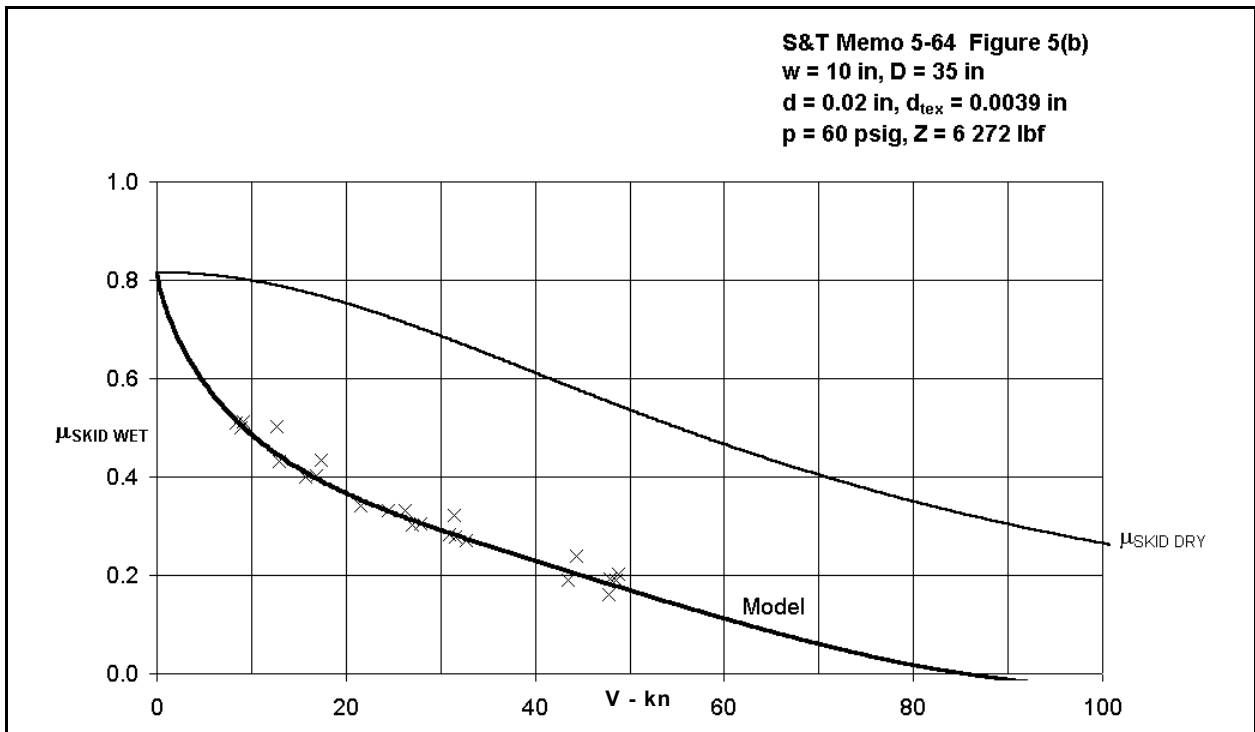
117
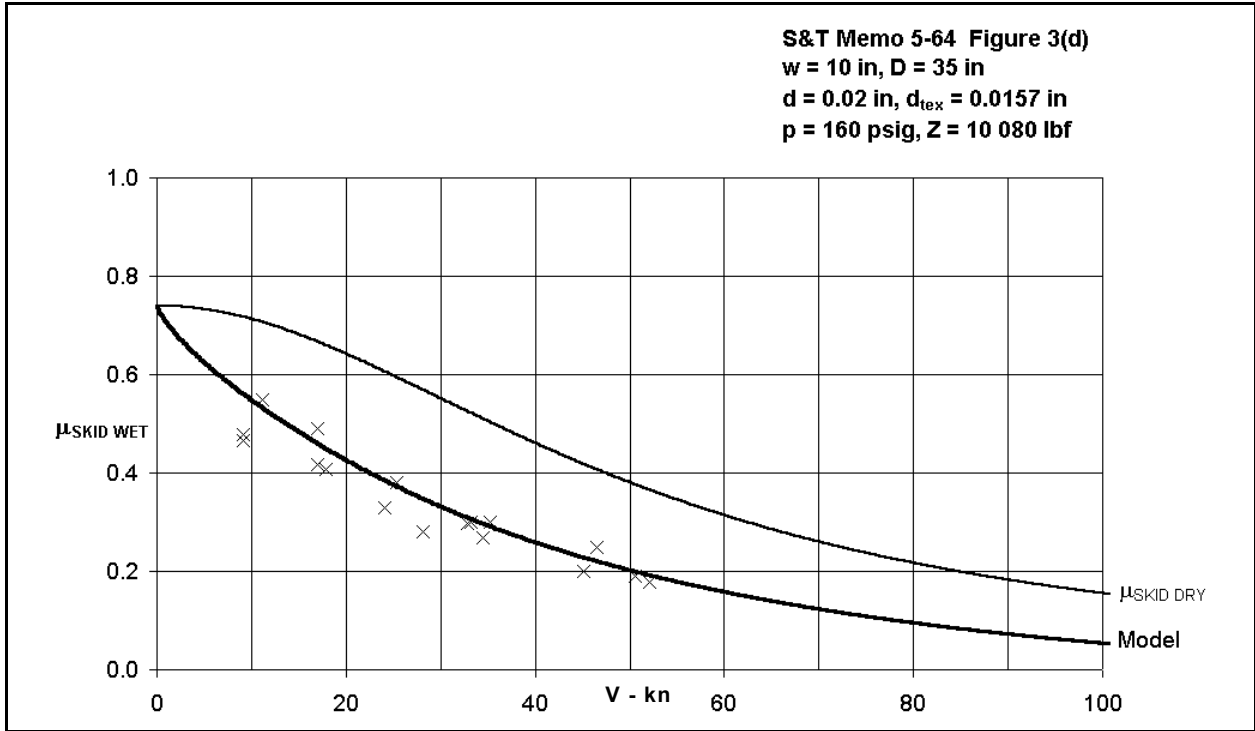
Figure 10.23: Effect of ground speed on coefficient of friction in full skid (Data points from Reference 36, Figure 3(d))
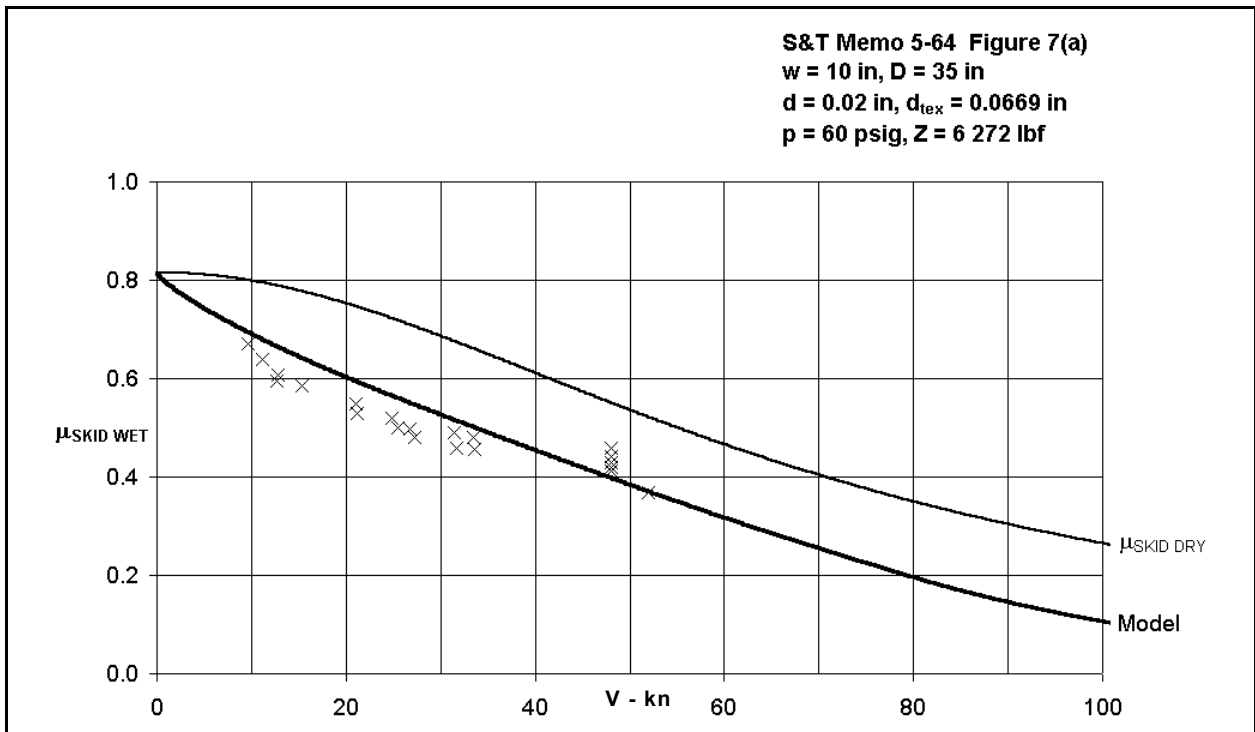
Figure 10.24: Effect of ground speed on coefficient of friction in full skid (Data points from Reference 36, Figure 7(a))
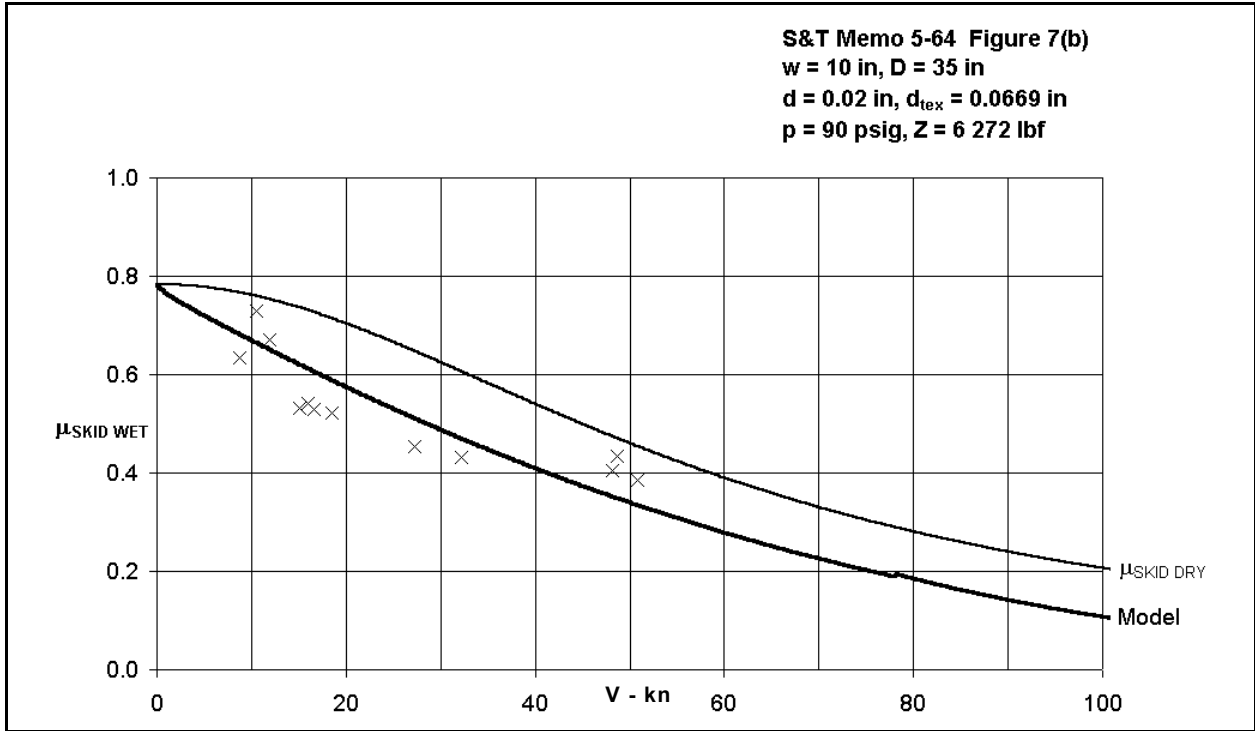
Figure 10.25: Effect of ground speed on coefficient of friction in full skid (Data points from Reference 36, Figure 7(b))
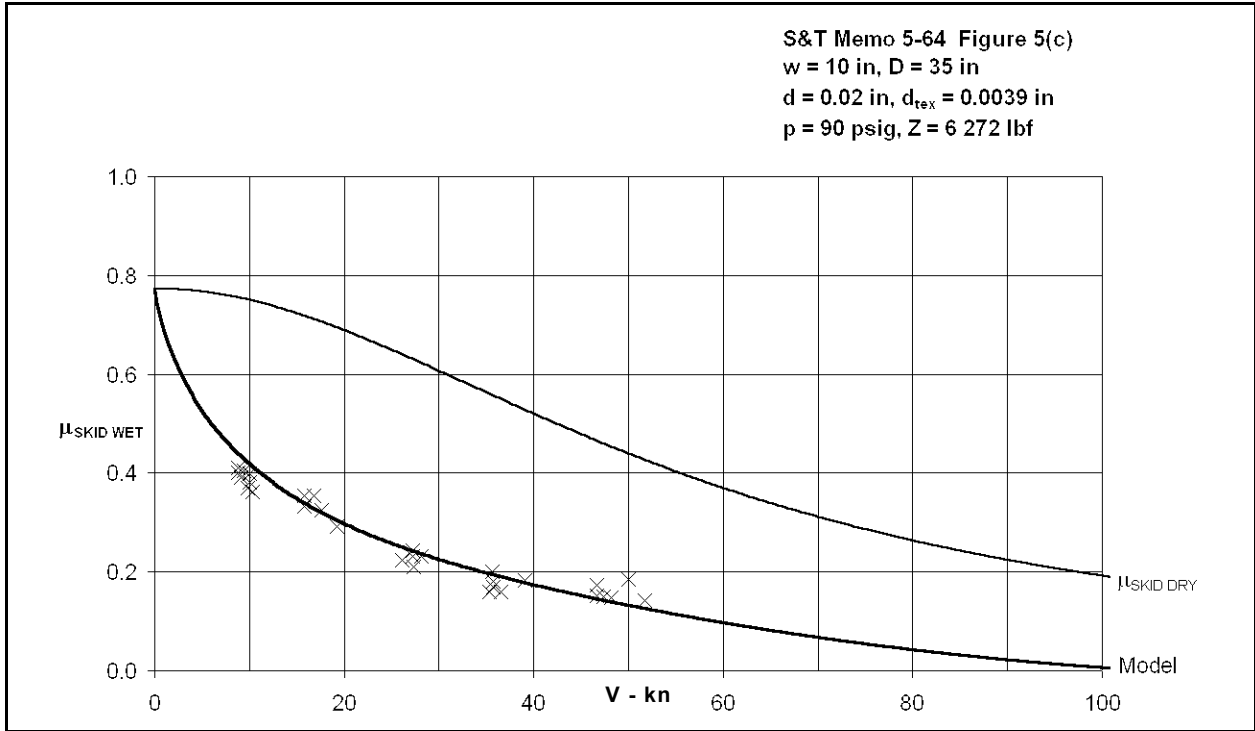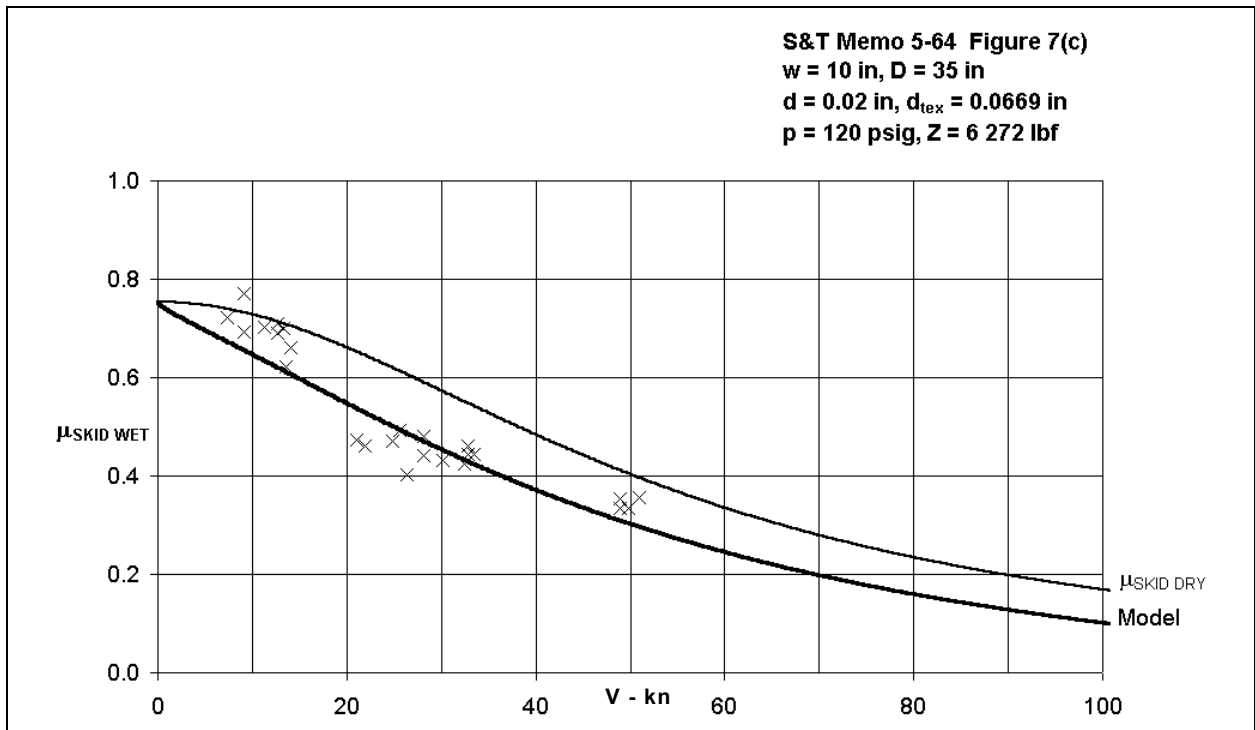

Figure 10.26: Effect of ground speed on coefficient of friction in full skid (Data points from Reference 36, Figure 7(c))
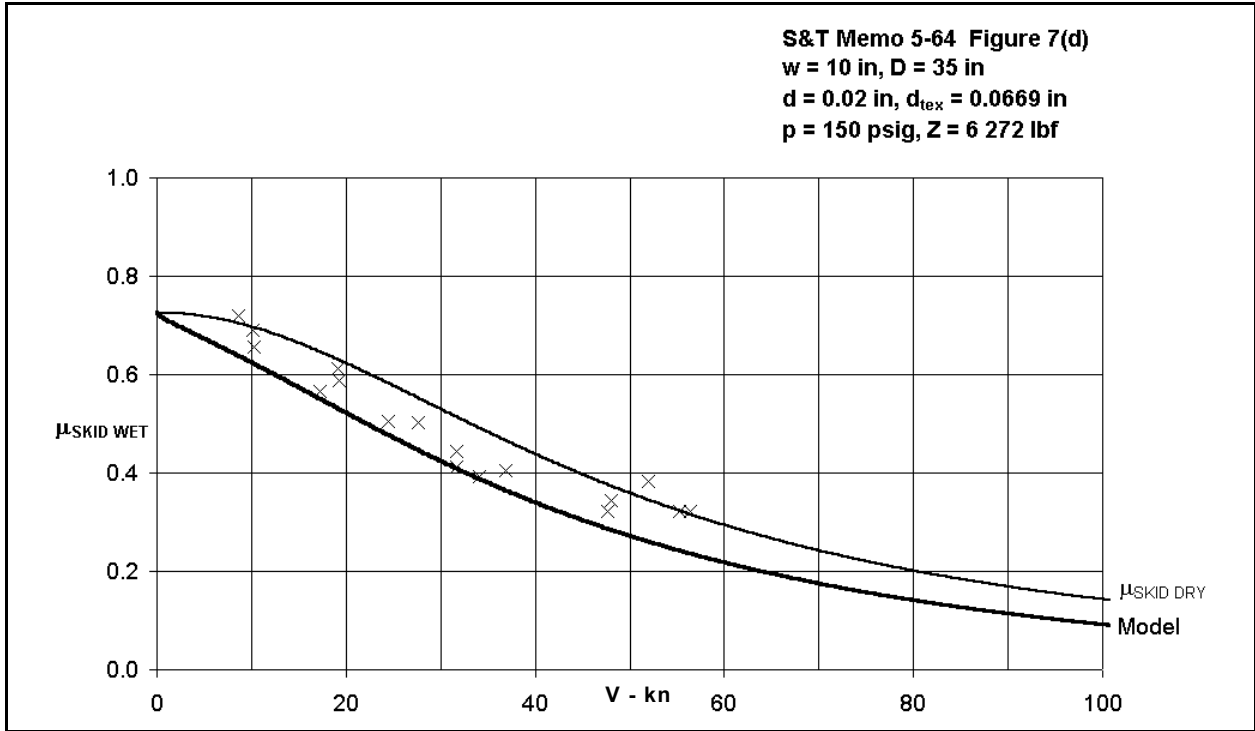
Figure 10.27: Effect of ground speed on coefficient of friction in full skid (Data points from Reference 36, Figure 7(d))
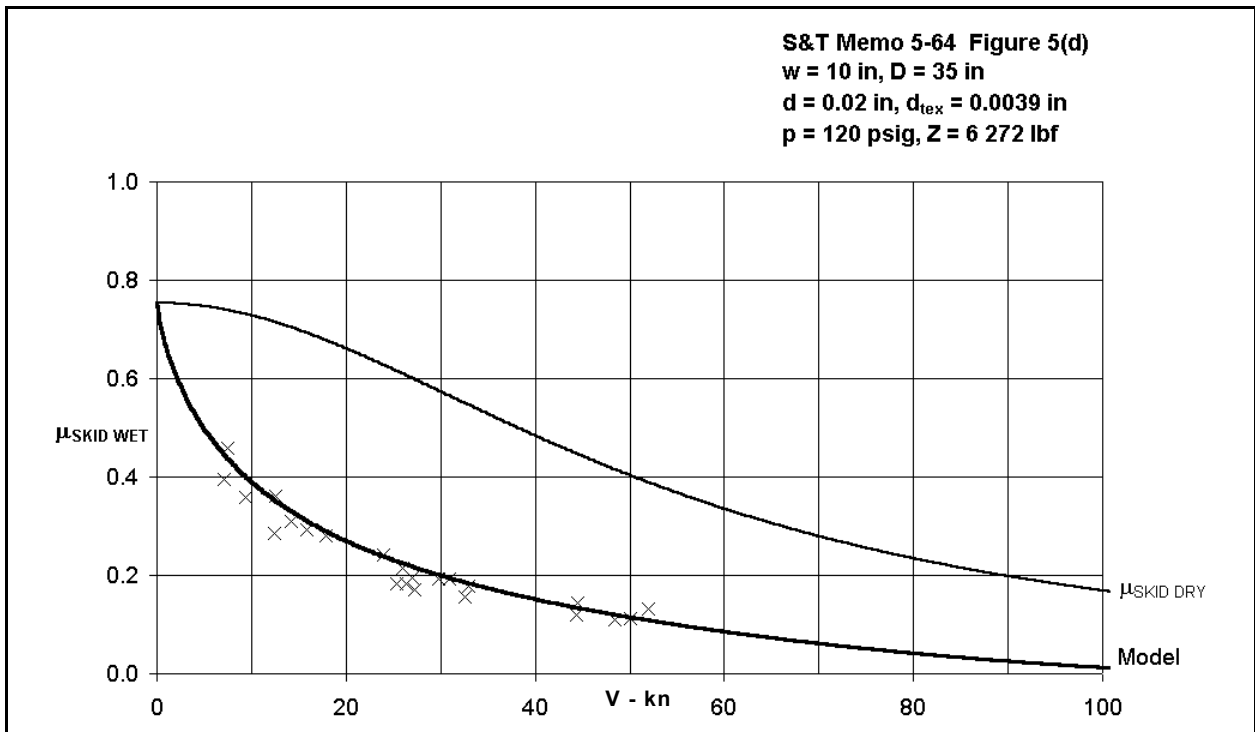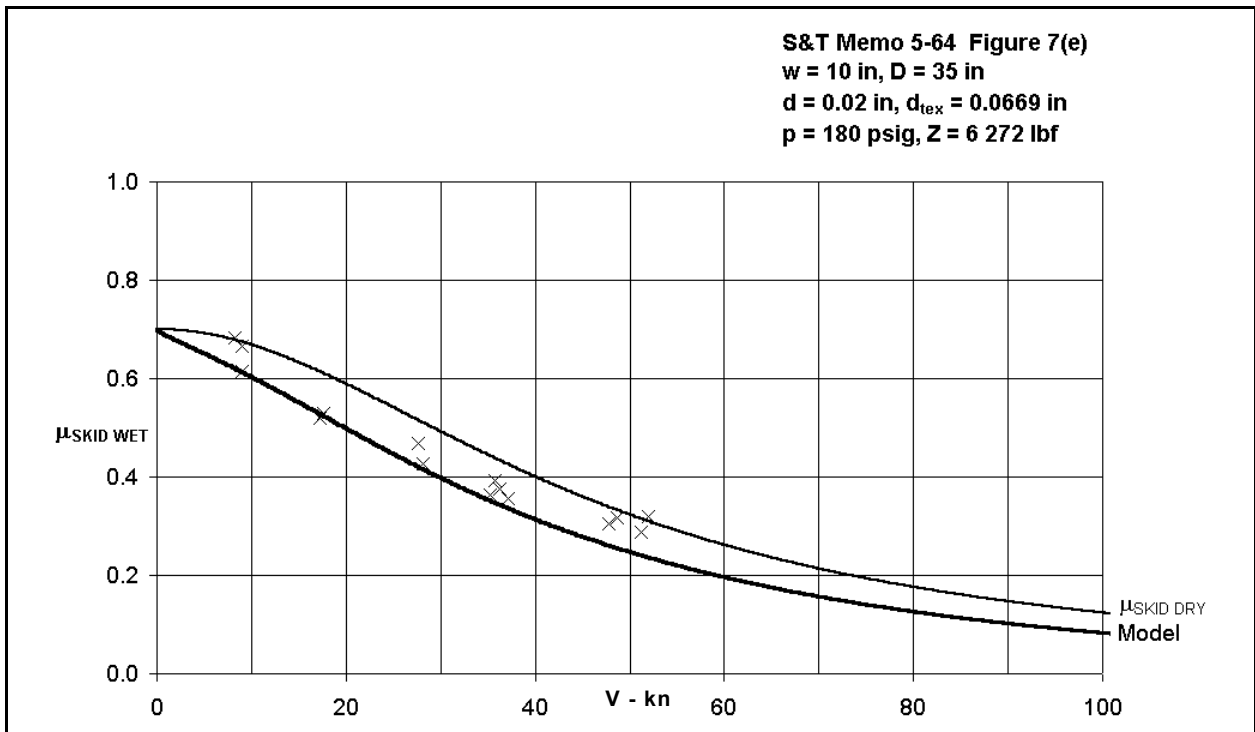

Figure 10.28: Effect of ground speed on coefficient of friction in full skid (Data points from Reference 36, Figure 5(a))
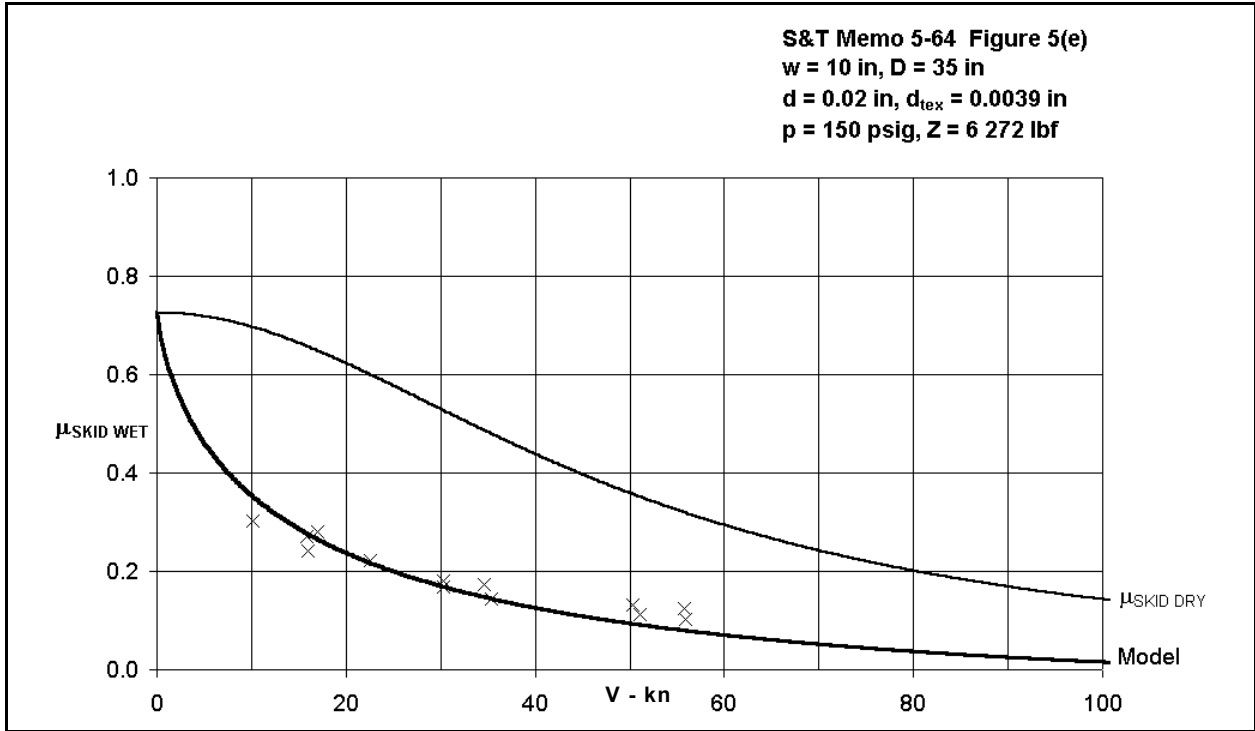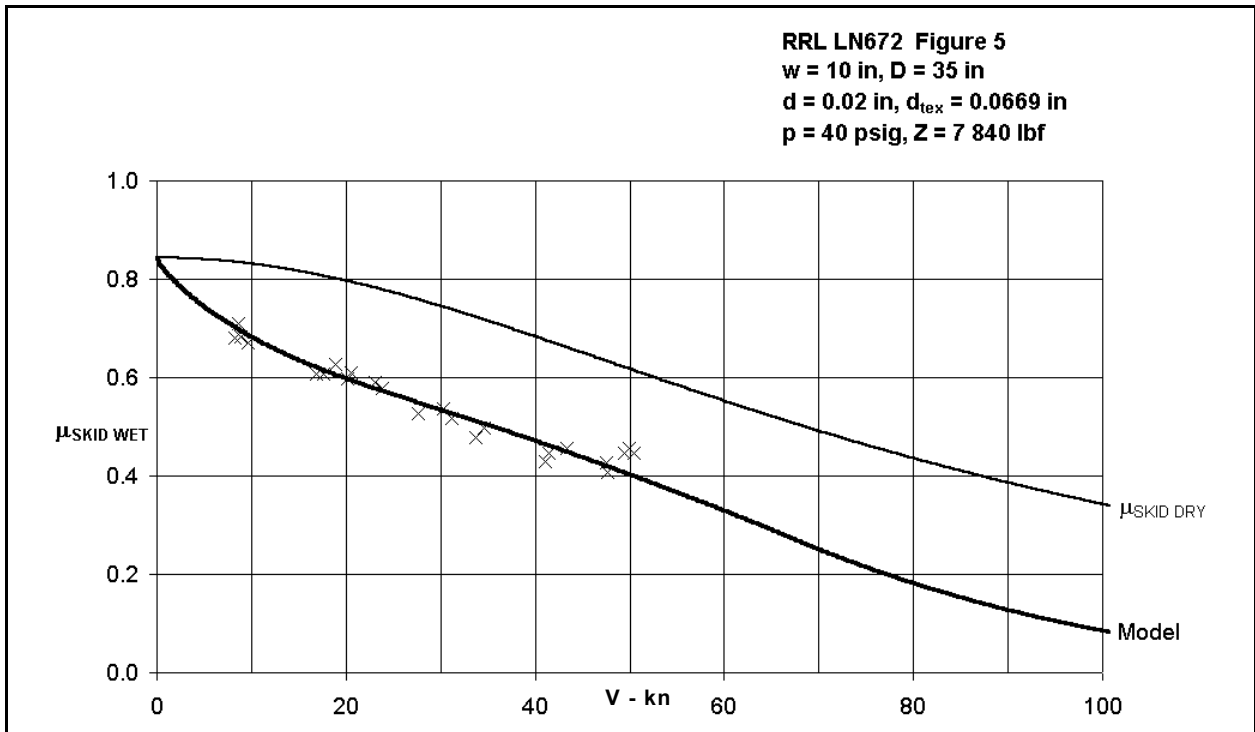
**Figure 10.29: Effect of ground speed on coefficient of friction in full skid
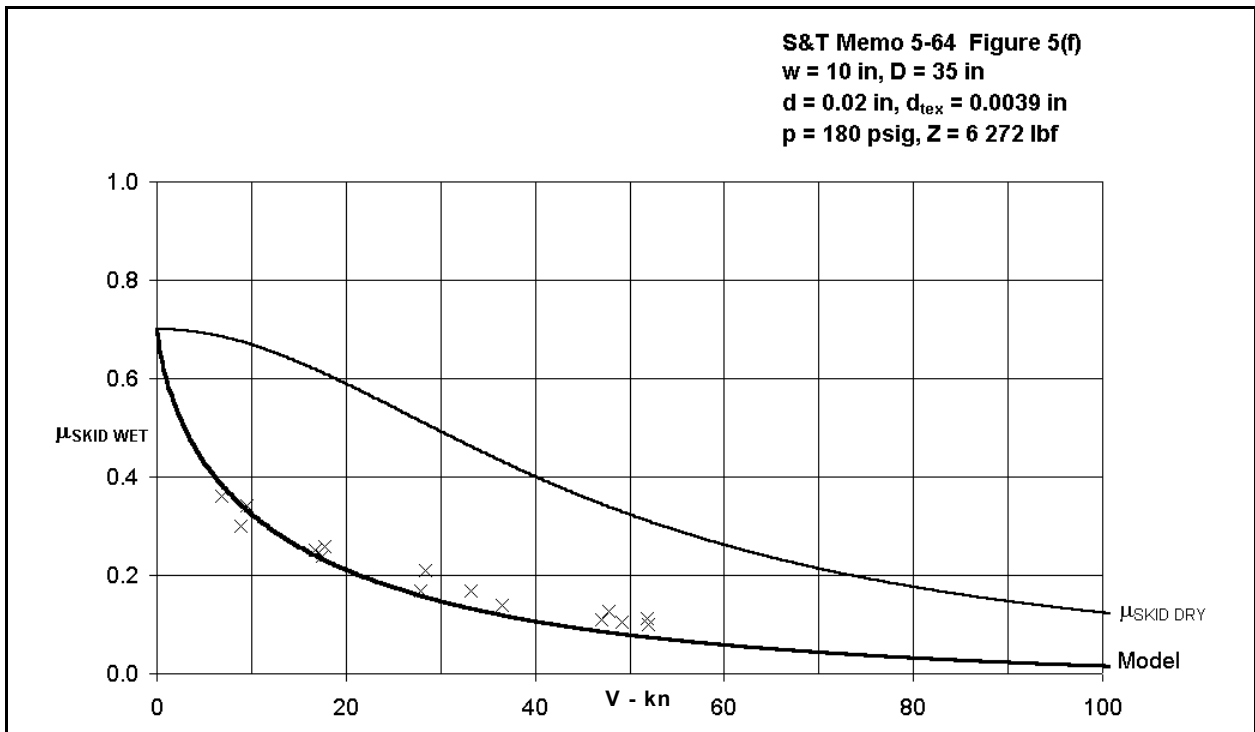(Data points from Reference 38, Figure 5)**
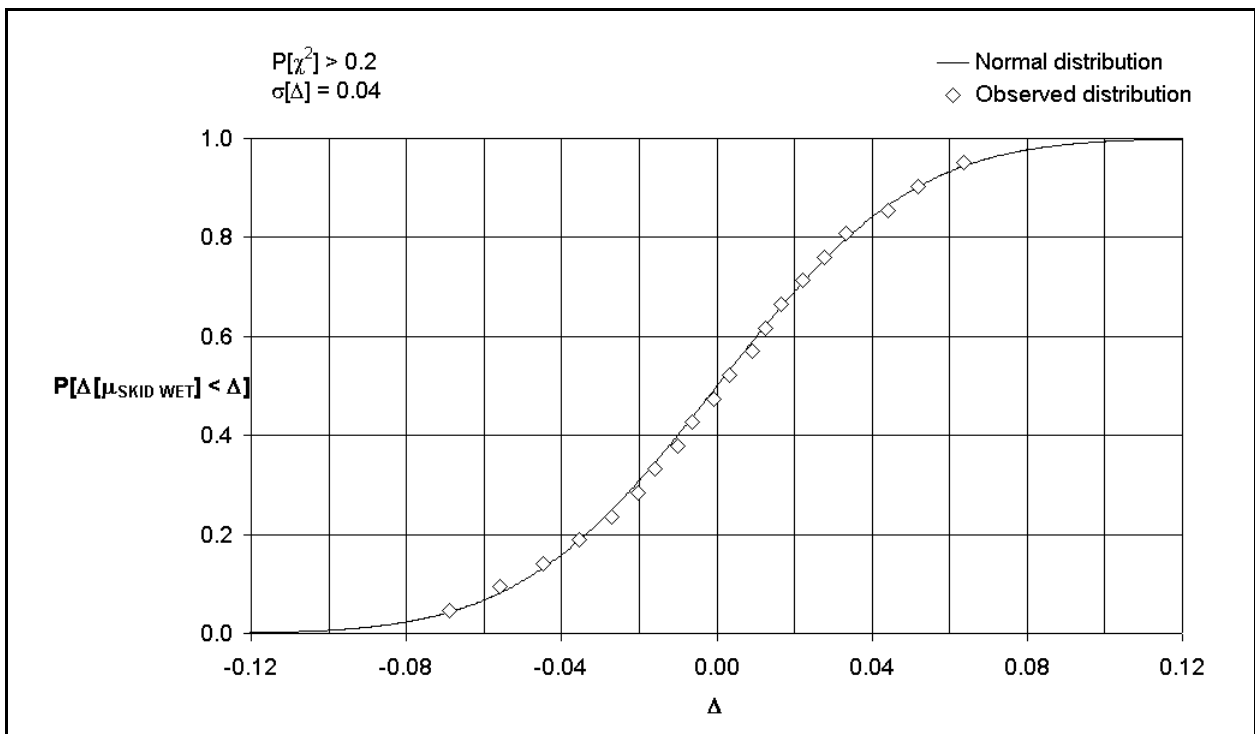
**Figure 10.30: Distribution of measurements of coefficient of braking friction about model –
Road Research Laboratory**
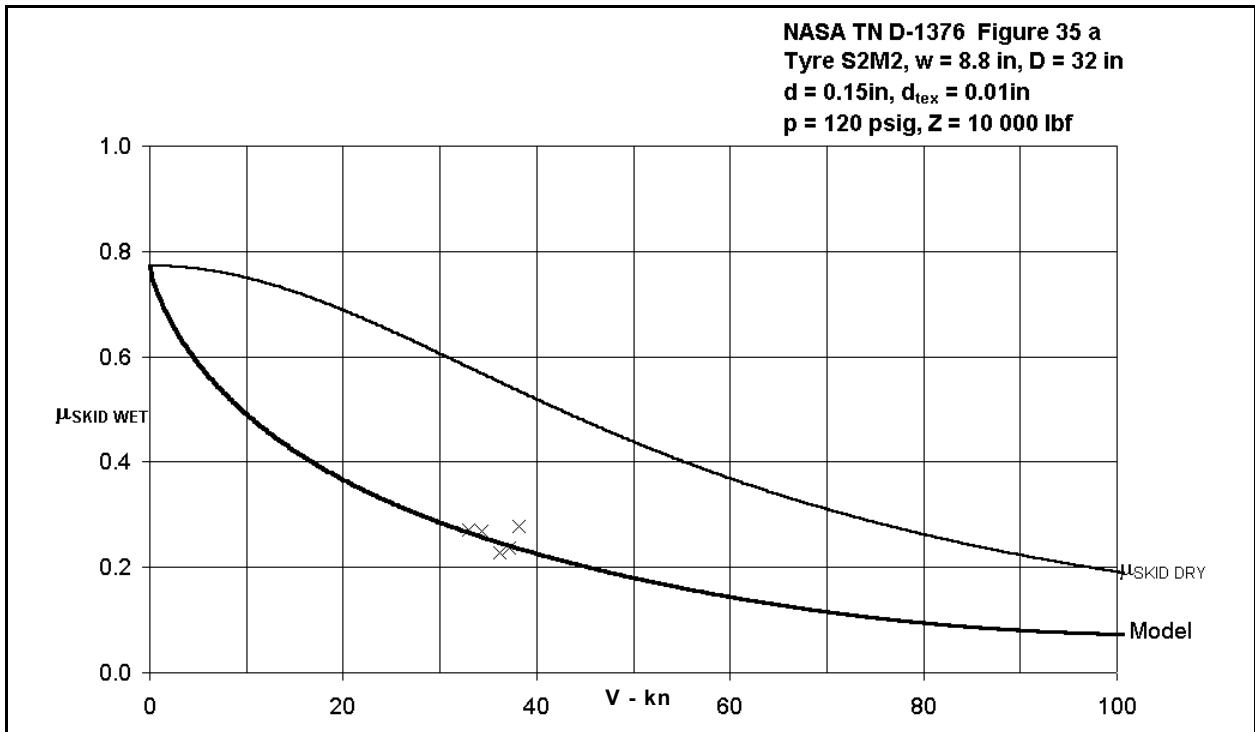
**Figure 10.31: Effect of ground speed on coefficient of friction in full skid
(Data points from Reference 7, Figure 35 a ($p = 120$ psig))**
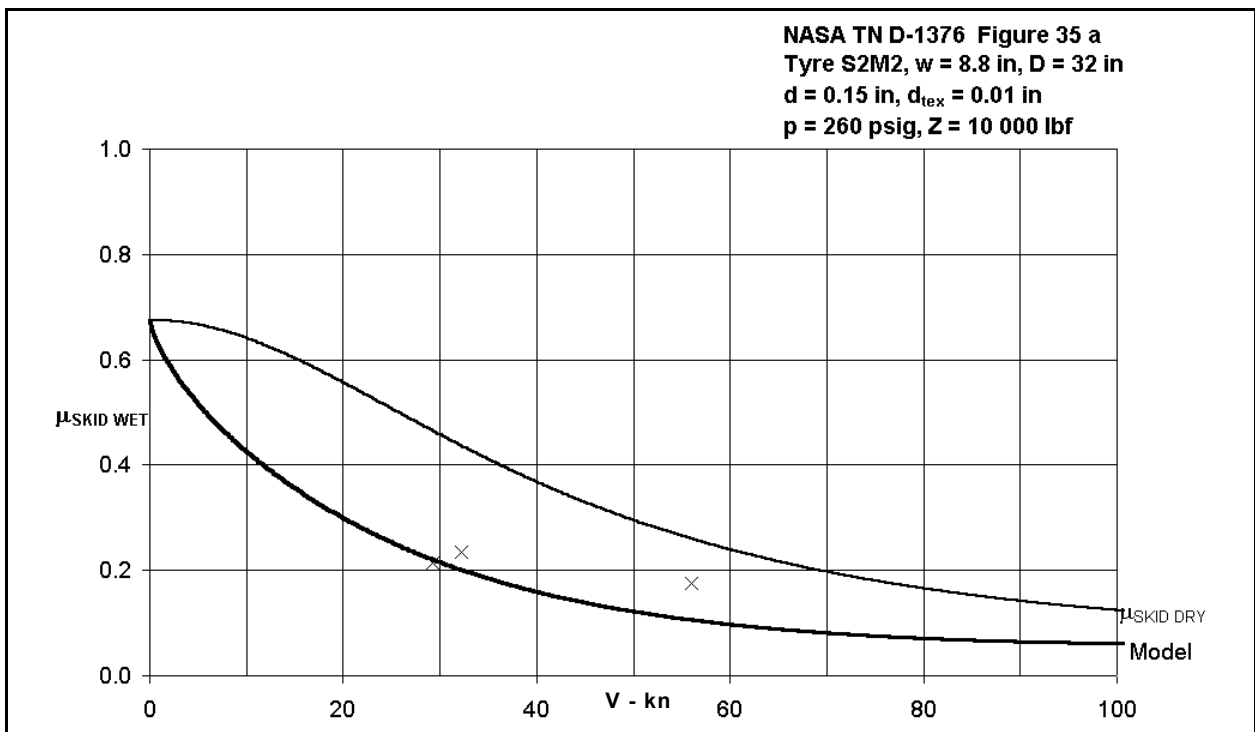
**Figure 10.32: Effect of ground speed on coefficient of friction in full skid
(Data points from Reference 7, Figure 35 a ($p = 260$ psig, $z = 10000$ lbf))**
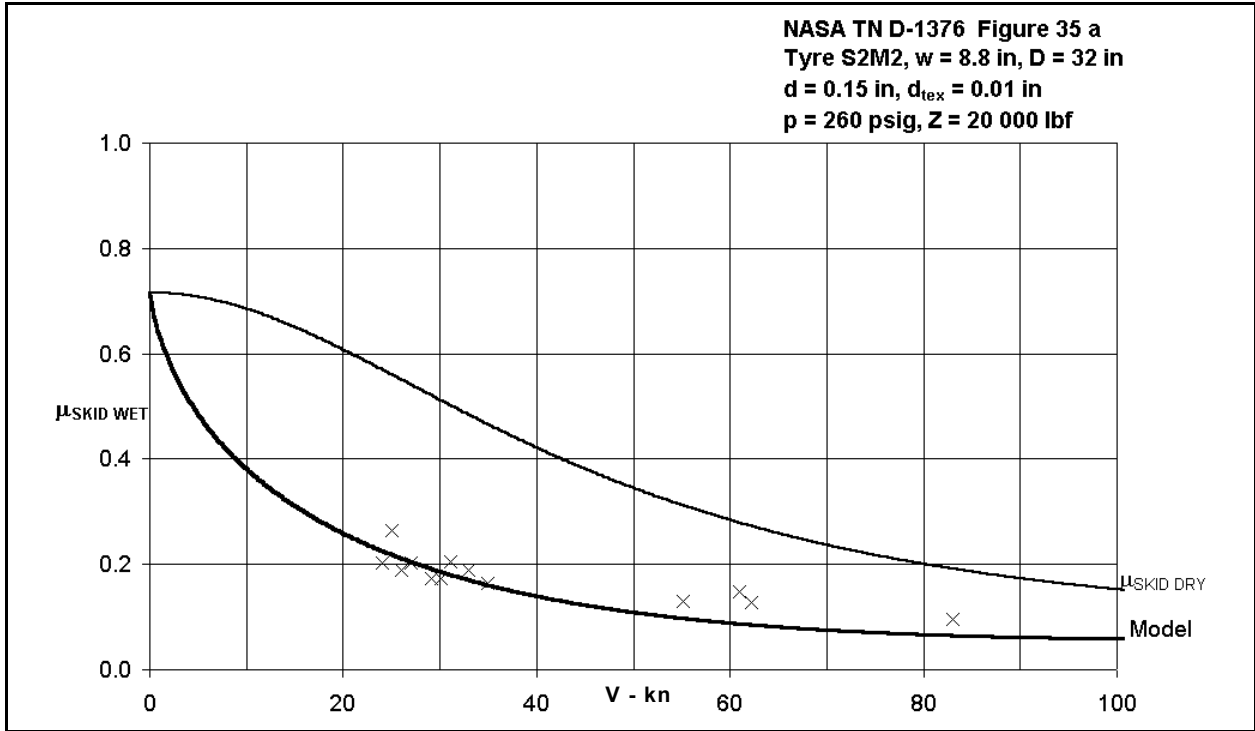
Figure 10.33: Effect of ground speed on coefficient of friction in full skid (Data points from Reference 7, Figure 35 a ($p = 260$ psig, $z = 20000$ lbf))
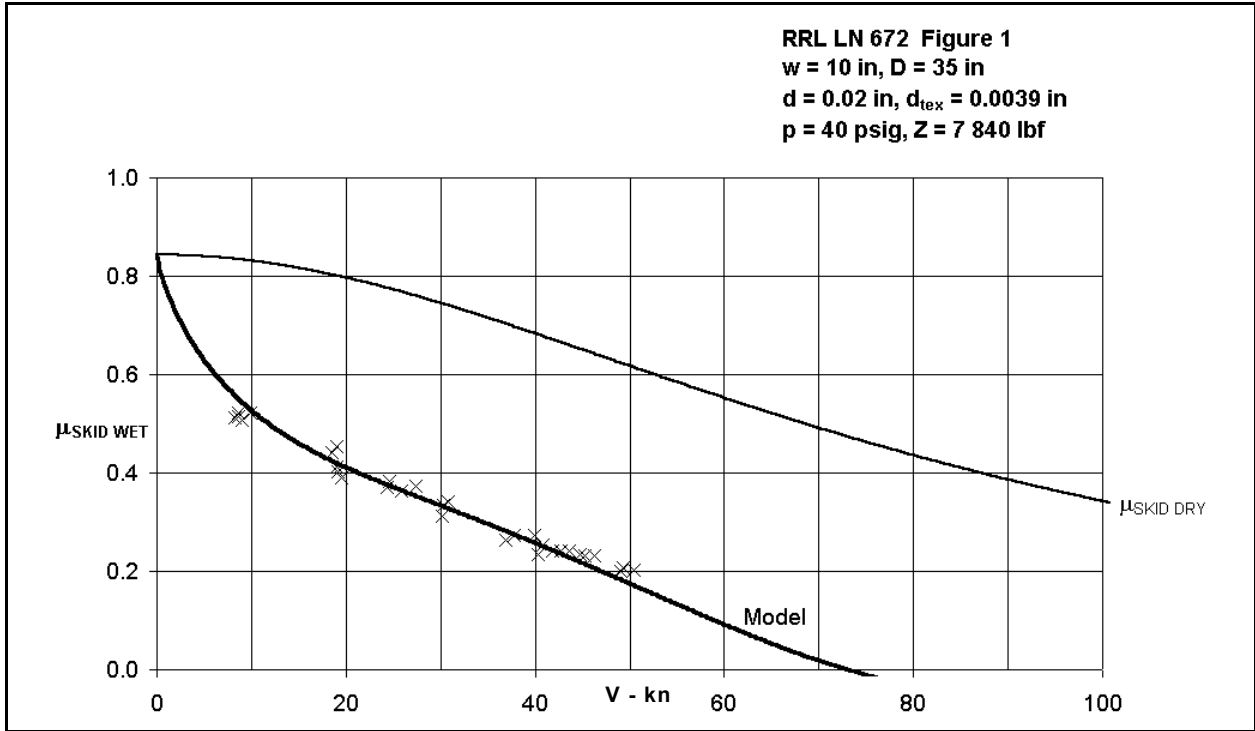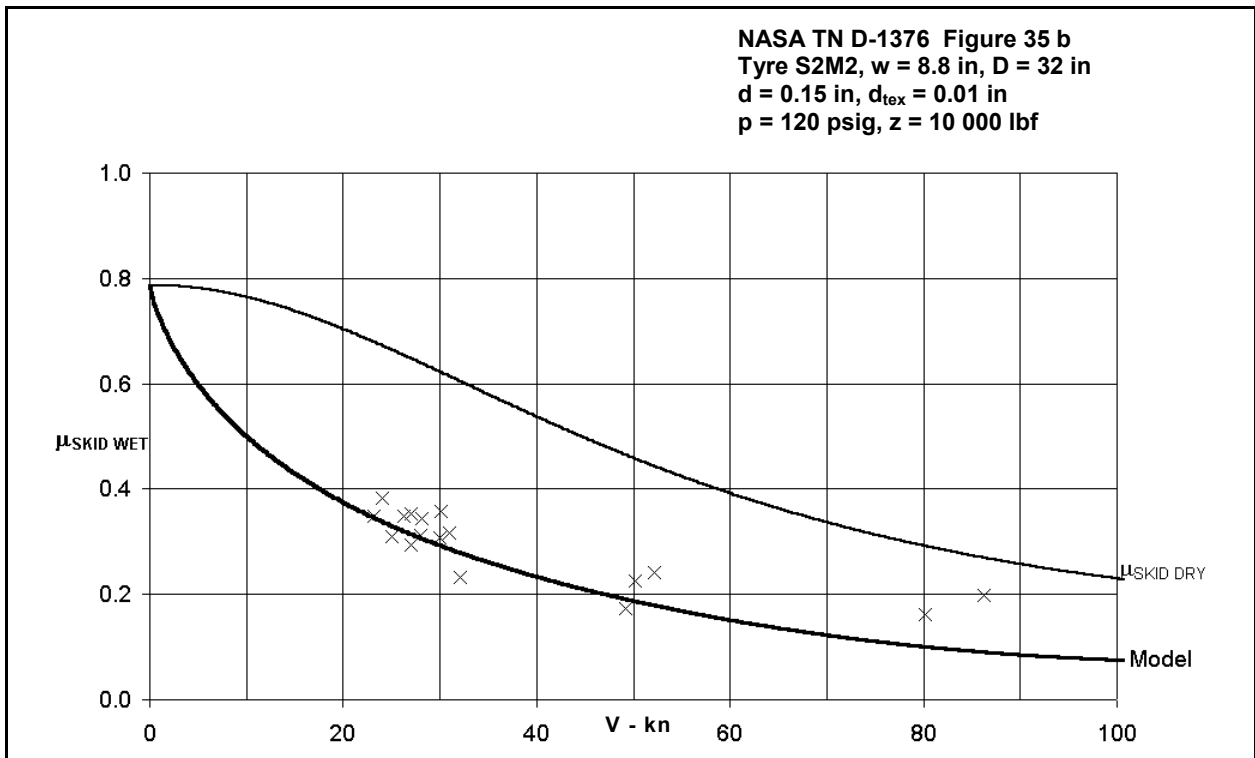

Figure 10.34: Effect of ground speed on coefficient of friction in full skid (Data points from Reference 7, Figure 35 b ($p = 120$ psig))
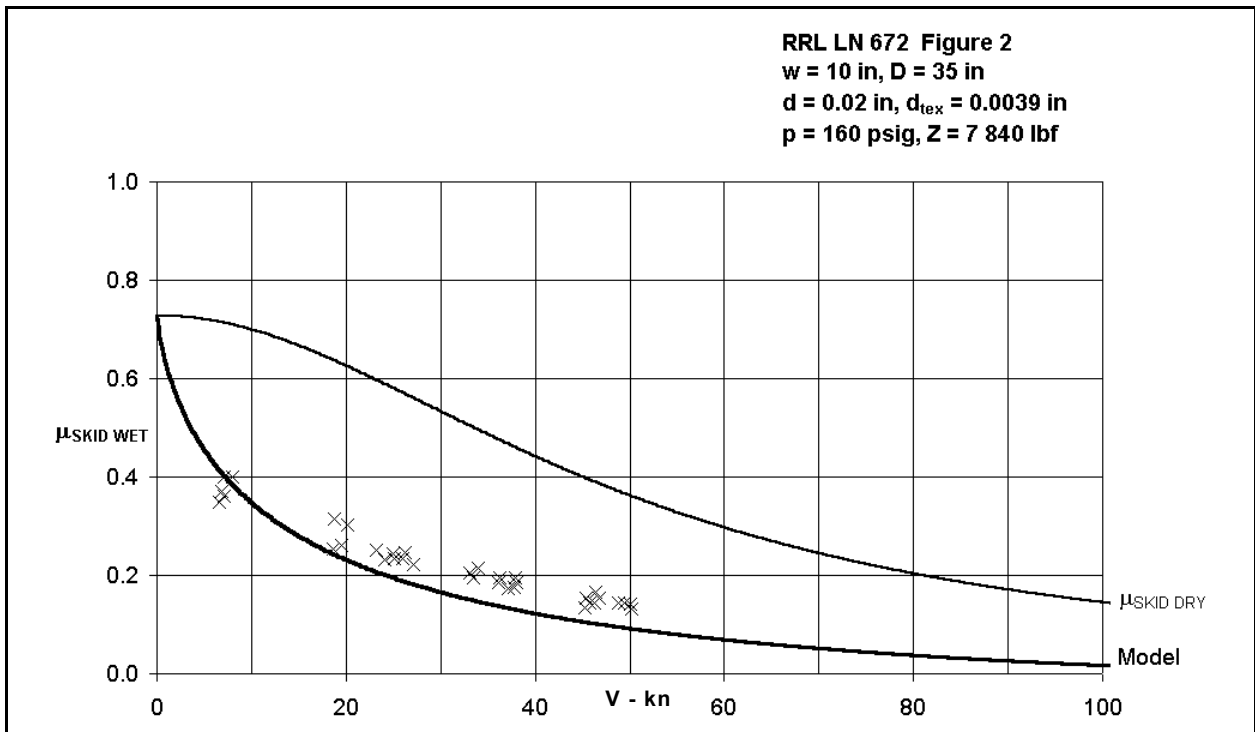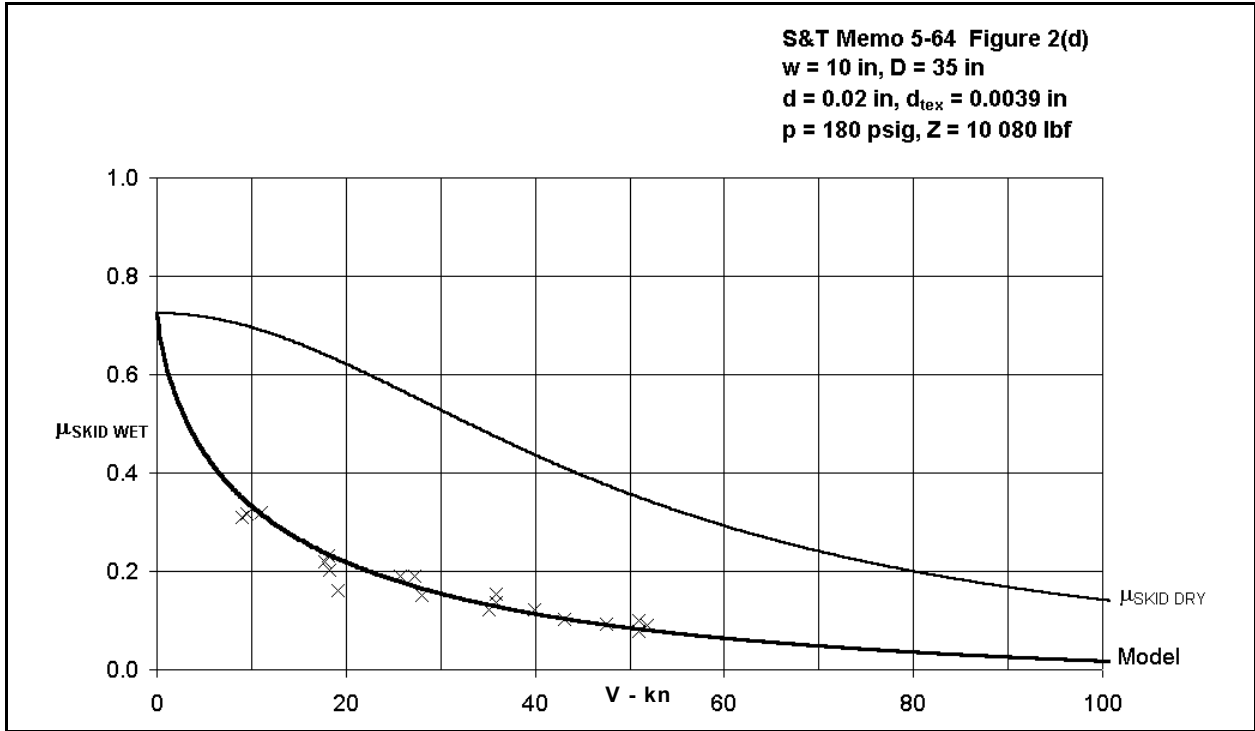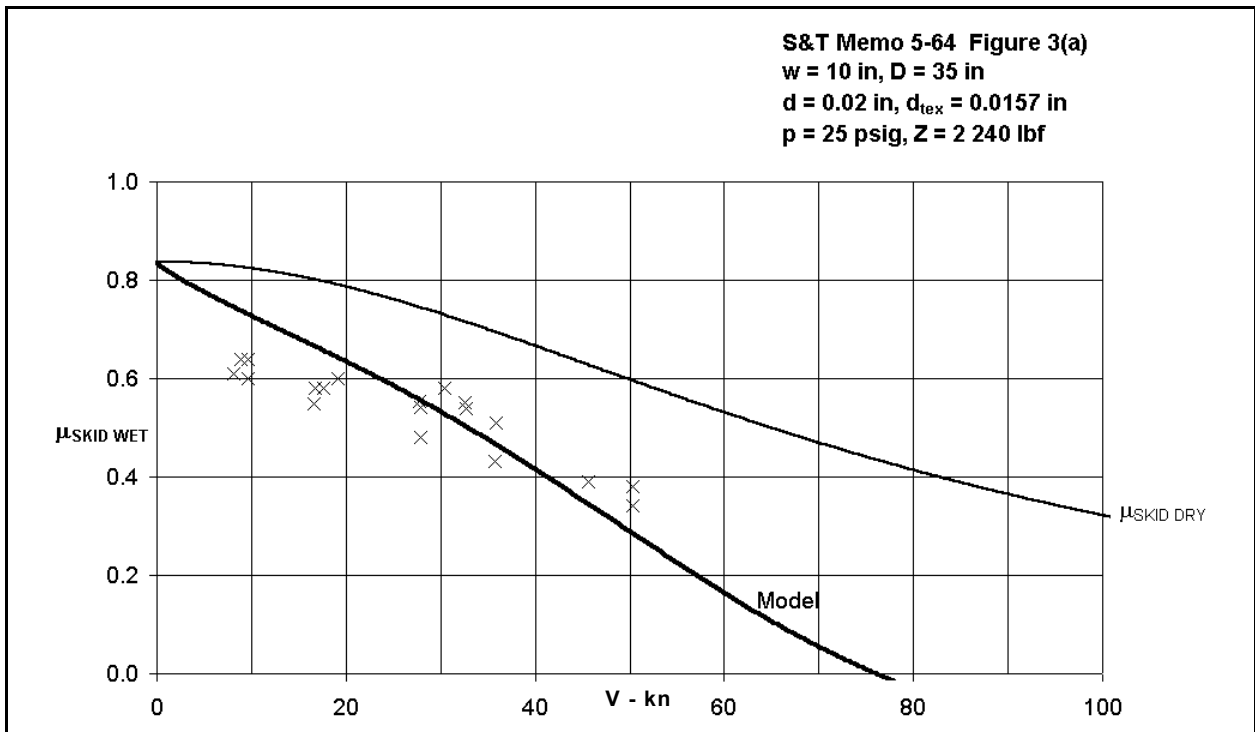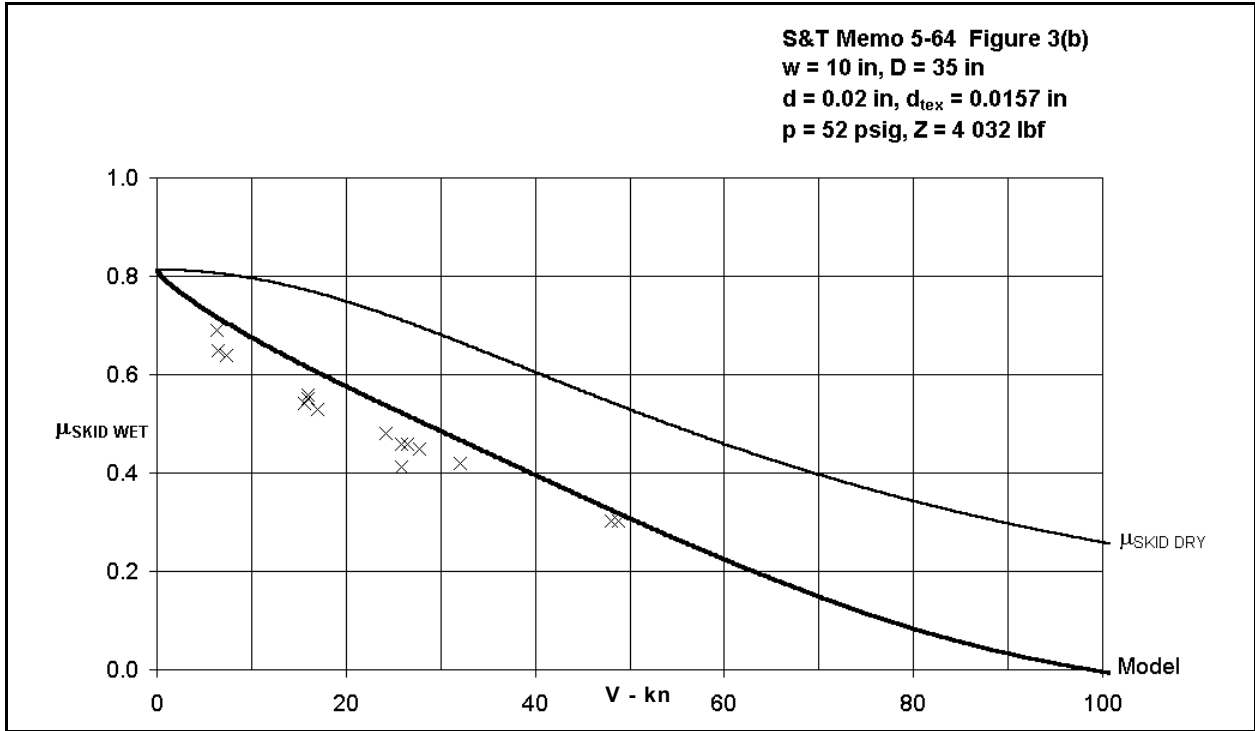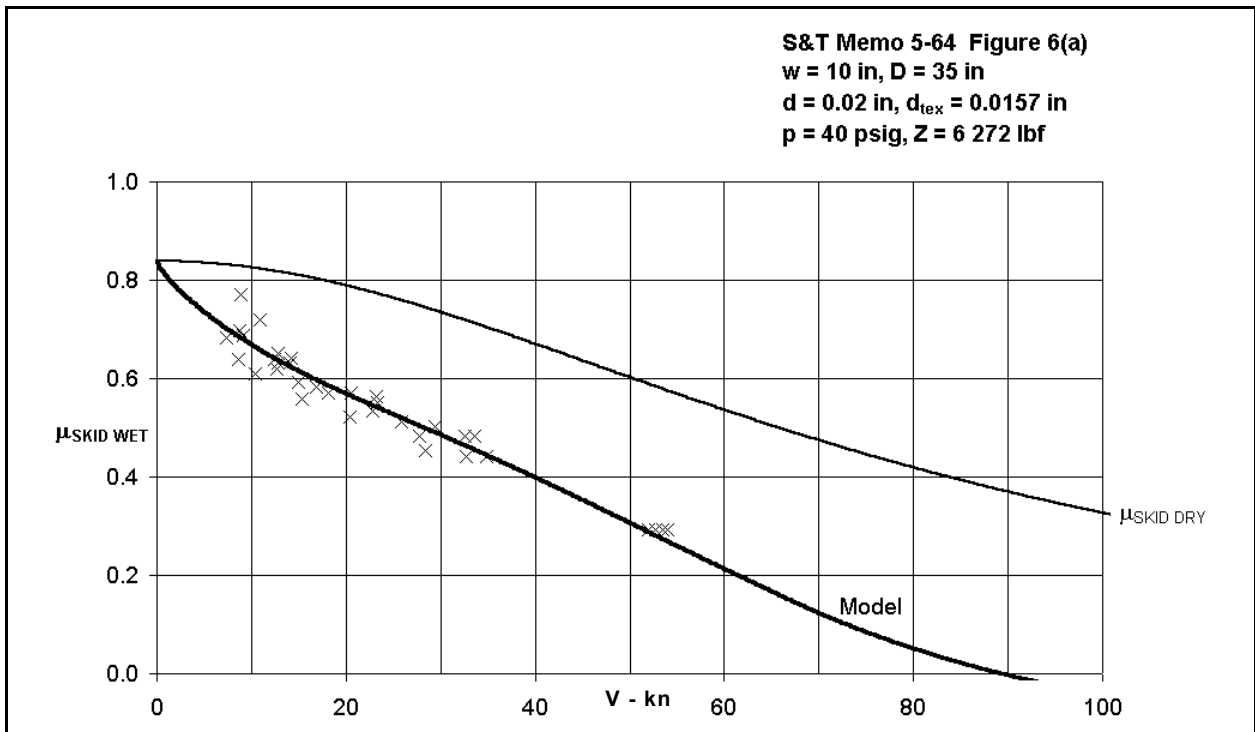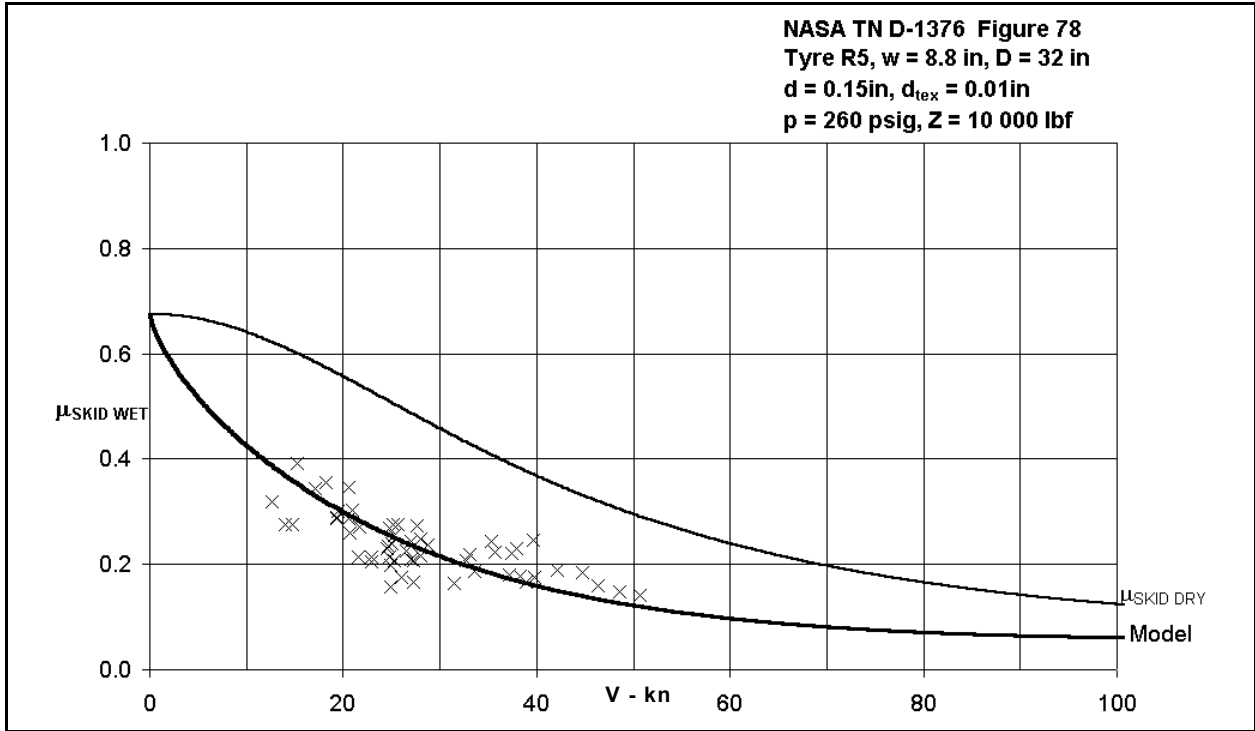
**Figure 10.35: Effect of ground speed on coefficient of friction in full skid
(Data points from Reference 7, Figure 78)**
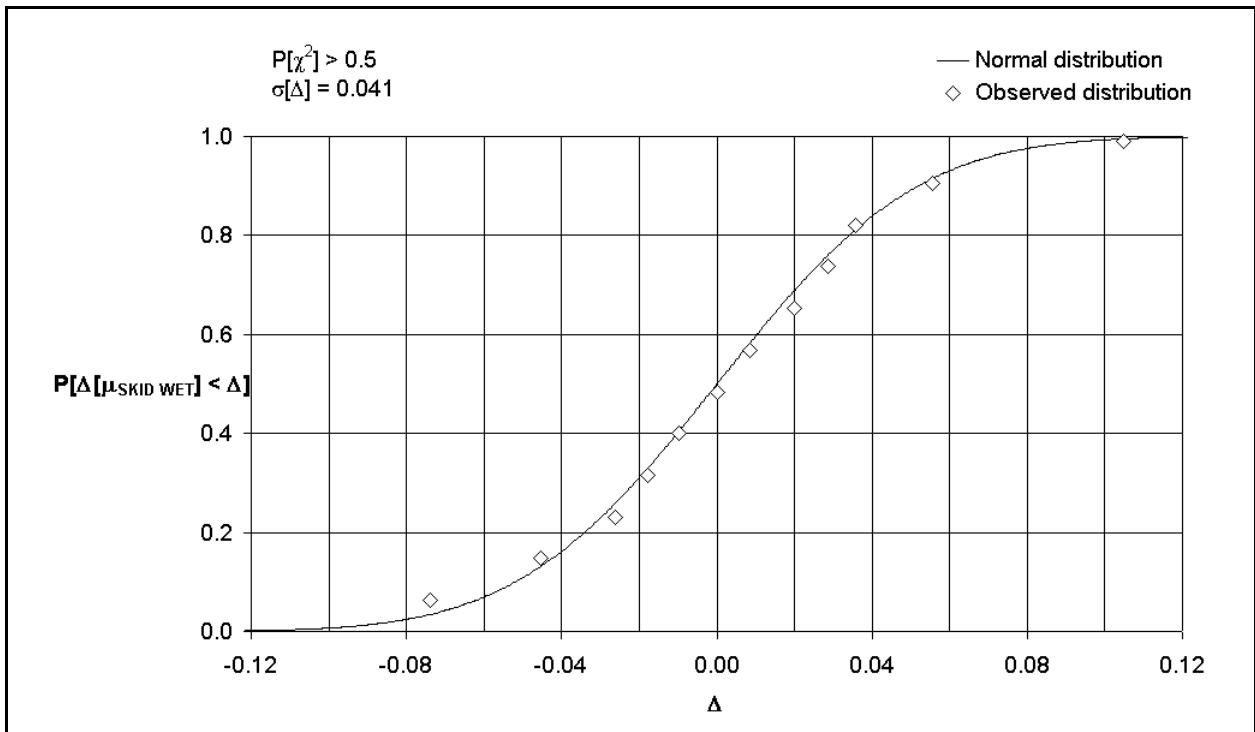
**Figure 10.36: Distribution of deviation of friction measurements from model –
NASA test rig**
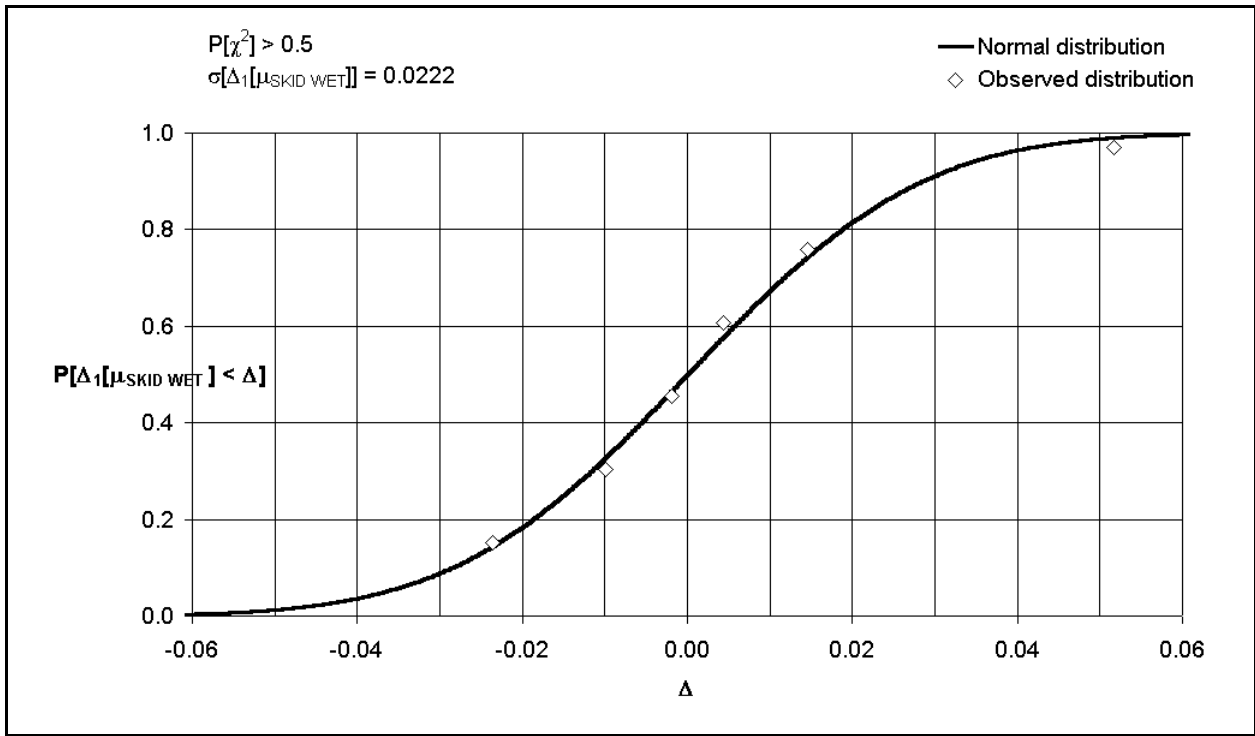
Figure 10.37: Distribution of variation of $\mu_{SKID\ WET}$ between tests – both test facilities

11. COEFFICIENT OF BRAKING FRICTION – SLIPPING ON WET RUNWAY

The mathematical modelling of the effects of a variety of contaminants on decelerating forces during operations on paved runways is intended to be as simple as possible within the constraints imposed by the complexity of the physical and statistical processes that are involved. Slipping on wet runways is considered here to be similar to slipping on a dry runway. That case is considered in Section 8; the mathematical model is built up from the static case through a simple additional term to describe the effect of a skid. An exponential factor is then used to modify the skidding case to represent the effects of slip ratio.

Furthermore, the effect of skidding in the wet is treated in Section 10. Again, the treatment is essentially straightforward in that the transition from dry to wet is made using the ratio of two simple functions as a factor. In this section, the same factor is applied to coefficient of braking friction in the dry slipping case. In this way, a consistent progression from static friction coefficient in the dry right through to slipping in the wet is accomplished. Because each successive complication is described by means of a simple modification in mathematical description, the most complex case defaults to the simplest quite naturally.

In common with the approach used in Sections 3 to 10, comparisons are made with appropriate experimental data. Data from References 3 and 39 are used to show that the modelling is empirically robust and statistically consistent. In addition, maximum coefficient of braking friction has been obtained for each braking cycle and is compared with a value calculated from the model.

11.1 Model

When a braking torque is applied to a rolling wheel,[30] the mean circumferential speed of the wheel is less than the forward speed of the axle. This speed differential arises from deformation and sliding of the tread material in the tyre-ground contact area. The overall effect is referred to as *braking slip*. In principal, the angular velocity of the braked tyre is a function of the inflated radius of the tyre modified for the effects of distortion induced by rolling and braking. In practice, there is little to be gained from over-complicating the estimation process. Consequentially, slip ratio is defined here as

$$s = 1 - \frac{\omega R}{V} \qquad\qquad 11.1$$

Equation 11.1 can be re-arranged so that

$$sV = V - \omega R \quad (= v) \qquad\qquad 11.2$$

---

[30] See Reference 33 for a fuller description of slipping phenomena.

Thus, the effective translation speed, v, of the footprint is the difference between the translation speed of the vehicle and the peripheral speed of the wheel, assuming no deflection due to normal load or distortion due to stresses generated in braking. In a full skid, the angular velocity of the wheel is zero, so $s = 1$ and the translation speeds of the wheel and footprint are identical.

In Section 10 it was shown that a good representation of coefficient of friction in a skid on a wet runway could be obtained by a modification of the relation developed in Section 7 for coefficient of braking friction when skidding on a dry runway. Thus[31]

$$\mu_{SKID\ WET} = \frac{\mu_{REF}}{\left\{ 1 + \left(\eta_0 + \eta_1 \frac{v^2}{2g} \right) \frac{p/p_a}{Z^{1/3}} \right\}} \frac{\left(1 - \varphi_0 q/p \right)}{\left(1 + \varphi_1 q_v/p_a \right)} \qquad 11.3$$

In order to accommodate the requirements of the slipping model, a function of slip ratio is sought that tends to zero with slip ratio and to unity as slip ratio tends to unity. A simple function that fulfils these requirements is the exponential $\left(1 - e^{\eta_2 s} \right)$ so that $\eta_2 < 0$. The function is zero at $s = 0$ for all η_2 and its value is sufficiently close to unity when $\eta_2 s < -5$. In the case of a dry runway it is shown in Section 8 that a value of $\eta_2 = -12$ was sufficient to enable calculation of coefficient of braking friction in slip over the whole operational speed range. However, in the case of a wet runway, this simple modification to the model was found not to be effective. However, the mathematical relationship adopted to describe the link between skidding and slipping coefficients of braking friction in the dry is still used for the wet case. Thus,

$$\mu_{SLIP\ WET} = \left(1 - e^{\eta_2 s} \right) \mu_{SKID\ WET} \qquad 11.4$$

11.2   Data Sources

It is noted in Reference 3 that, in wet conditions, the effect of slip ratio on coefficient of braking friction changes as speed increases. At high speed, there is a tendency for the maximum coefficient of braking friction and the skidding value to converge. In the context of the modelling strategy adopted for describing the effect of slip ratio, Equation 11.4, this implies that the exponent, $-\eta_2$, reduces as speed increases. The variation of the exponent with speed is shown in Figure 11.1 together with a correlating function.

Two separate sources of experimental data have been used to establish a correlation that can be adopted as a model for the wet, slipping case. First, an investigation was carried out at the Road Research Laboratory in co-operation with the British Ministry of Aviation to study braking performance of aircraft tyres on wet surfaces using the Heavy Load Test Vehicle. Results from the slip study were reported in Reference 39. Two inflation pressures were used – 40 psig and 160 psig. A vertical load of 7840 lbf was applied and speeds up to 60 mph were used.

---

[31]   Note that speed dependent terms are calculated at the translation speed of the footprint.

In order to enable the exercise of more control over the braking process and the extent of over swings, the system for applying the brake on the test wheel had been modified to slow down the application rate. After the modification, in general, the braked wheel spun down to the slip ratio for peak braking force in about two seconds. There is no discussion of the instrumentation design in the reference, so it is not clear how well the measurements of slip and braking force are correlated in time.

Texture depth of the surfaces was such that $0.0039 < d_{tex} < 0.0669$ in. Water depth was assessed during testing and was maintained so that $0.005 < d < 0.045$ in. An average value of 0.02 inch was quoted. Consequently, calculations have been done at $d = 0.02$ in. Eighteen runs are considered and the data are plotted in Figures 11.2 to 11.19.

In Reference 7, an extended investigation is reported of the effect of varying tread pattern and runway contamination on rolling, skidding and slipping coefficients of friction. Many of the treads were not representative of production tyres; so the present study has considered only a limited selection of the data presented in the reference. In total, 24 cycles of the braking system have been studied covering a speed range so that $20 < V \leq 100$ kn. The tyre was inflated to $p_i = 260$ psig and a vertical load, $Z = 10000$ lbf, was applied. Depth of the macro-texture of the concrete runway was $d_{tex} \approx 0.01$ in and water depth on the undulating runway was so that $0 < d \leq 0.3$ in. All calculations for this series of tests assume that $d = 0.15$ in. Data are shown plotted against slip ratio in Figures 11.20 to 11.43. Variation of friction coefficient in slip, as calculated from the model of Equation 11.4 is shown for each test. In addition, the deviations between model and experiment have been calculated and the distribution of those deviations is shown in Figure 11.44.

Maximum coefficient of braking friction is often used as a datum from which to assess the efficiency of a braking system. The modelling equations can be used to calculate this quantity $E[\mu_{MAX\ WET}]$. In addition, the experimental variations of friction coefficient with slip ratio were used to find a "best-fit" value $M[\mu_{MAX\ WET}]$. These values are shown in Figure 11.45 and the distribution of the differences between the two values,

$$\Delta[\mu_{MAX\ WET}] = M[\mu_{MAX\ WET}] - E[\mu_{MAX\ WET}] \qquad 11.5$$

is plotted in Figure 11.46 and is compared there with the Normal distribution.

11.3 Discussion

11.3.1 Effect of Ground Speed on Exponent

It has been a matter of observation from experimental studies carried out at NASA[32] that for a wet runway, the effect of slip on coefficient of braking friction is different from that on a dry runway. In order to ensure that the overall modelling strategy could be kept as simple as

---

[32] Reference 3 is a typical example.

possible, the exponential factor $\left(1-e^{\eta_2}\right)$ is used for the case of a wet runway in the same way as in the case of a dry runway. To accommodate the requirement to modify the effect of slip ratio as speed increases it is possible to allow the absolute value of the exponent to decrease.

Referring to Figure 11.1, the values of the exponent needed to ensure a "best" fit to the experimental data are clearly lower at high speed than at low speed. There is no theory on which to base a relation. In order to achieve both a simple default to the dry value and to account for speed variation only in the wet, a correlating parameter related to kinetic pressure, $q = \rho V^2/2$ is chosen. In the dry, there is no fluid so the fluid density can be set to zero; hence, kinetic pressure is zero for all speeds. Although it has been found convenient in other parts of this study to use the ratio of kinetic pressure to inflation pressure as a variable, the device is not satisfactory in this case. Thus, since it is desirable, if possible, to use variables with no dimensions, the ratio q/p_a is used as the base for correlation.

Now, this ratio varies so that $0 \le q/p_a < \infty$, so it is convenient to form the variable $1/\left(1+q/p_a\right)$ which always lies between zero and unity for positive values of q/p_a. Using this transformation it is possible to correlate the values of the exponent so that

$$\eta_2 = \eta_{20}\left(\frac{1}{1+q/p_a}\right)\left(1+\eta_{21}\left(\frac{q/p_a}{1+q/p_a}\right)\right) \qquad 11.6$$

where $\eta_{20} = -12$ and $\eta_{21} = 2.5$.

Equation 11.6 is one among many possible ways of relating the exponent and speed. It is, however, one of the simplest that enables the appropriate defaults to be maintained.

11.3.2 Comparison Between Model and Experiment

Applying the correlation of Equation 11.6 in the modelling Equation 11.4, the effect of slip ratio on coefficient of braking friction can be calculated for appropriate values of the independent variables. Results from calculations are compared with experiment in Figures 11.2 to 11.43. **It is emphasised that the curves shown in the figures have been calculated from the model – the curves are in no sense a "best" fit to the experimental data to which they are compared.** Without exception, the model and the experiment are in broad agreement. Trends with the independent variables that are evident in the experimental data are reflected in the model. In particular, the effect of speed is simulated very closely both in relation to the skidding value and at slip ratios close to those for maximum coefficient of friction.

Furthermore, the evidence of Figures 11.2 to 11.19 supports the contention that the effect of texture depth is successfully accounted for in the model.

However, as the wheel spins down from rolling freely, there is a rapid initial increase of coefficient of braking friction with slip ratio. The model and the experiment do not match well in

this phase of the operation of the braking systems used. Consider the scatter that is evident in the distribution of deviations of the model from the experiment – see Figure 11.44. Much of this scatter stems from the measurements taken in the region of the slip curve between zero and the value for maximum friction coefficient. It has been noted that there are possible mismatches in the frequency response of the instrumentation systems. If that were the case, then those mismatches would have maximum impact in this region of the slip curve.

The standard error of deviations between model and experiment is $\sigma\left[\Delta\left[\mu_{SLIP\ WET}\right]\right] = 0.071$ a value that is larger than would be expected from a quasi-static set of tests. The distribution shown in Figure 11.44 is symmetrical about the origin but is not Normally distributed. On the other hand, there is an experimental database of some 580 measurements; even though the deviations from the model are not normally distributed, there is no safety critical consequence in assuming that, the partition values for a 95% confidence interval are those for a normal distribution. Thus, the uncertainty – at the 95% level of probability – associated with an estimate $E\left[\mu_{SLIP\ WET}\right]$ may be estimated to be $U\left[\mu_{SLIP\ WET}\right]_{0.95} = \pm0.006$. Of course, if the model is to be used to explore safety critical criteria in the extreme tails of the distribution, then a more detailed study of the distribution is needed.

11.3.3 Maximum Coefficient of Braking Friction

This quantity is often used as the basis for a measure of the efficiency of a braking system. Figure 10.45 shows the maximum value, $E\left[\mu_{MAX\ WET}\right]$ calculated from the model for a given set of values of the independent variables as it is related to a "measured" value $M\left[\mu_{MAX\ WET}\right]$. This measured value has been obtained by using an arbitrary "best" fit to the slip curve paying close attention to achieving a close fit near to the maximum value. It is believed that is the technique that has been adopted by other investigators in the field.

A one-to-one relation relates the two derivations very closely. Using a *t*-test, there is a probability in excess of 0.2 that the estimate represents the measurement. In addition, the distribution of the deviations between measurements and model – as shown in Figure 11.46 – is not significantly different from a Normal distribution. It is noted that $\chi^2 > 0.3$. Because the standard error of the deviations is $\sigma[\Delta] = 0.037$, and there are 42 measurements, then the uncertainty – at the 95% level of probability – associated with an estimate of $E\left[\mu_{MAX\ WET}\right]$ can be calculated to be $U\left[\mu_{MAX\ WET}\right]_{0.95} = \pm0.011$. This value can be used in assessing the implications of maximum coefficient of braking friction in system performance studies.
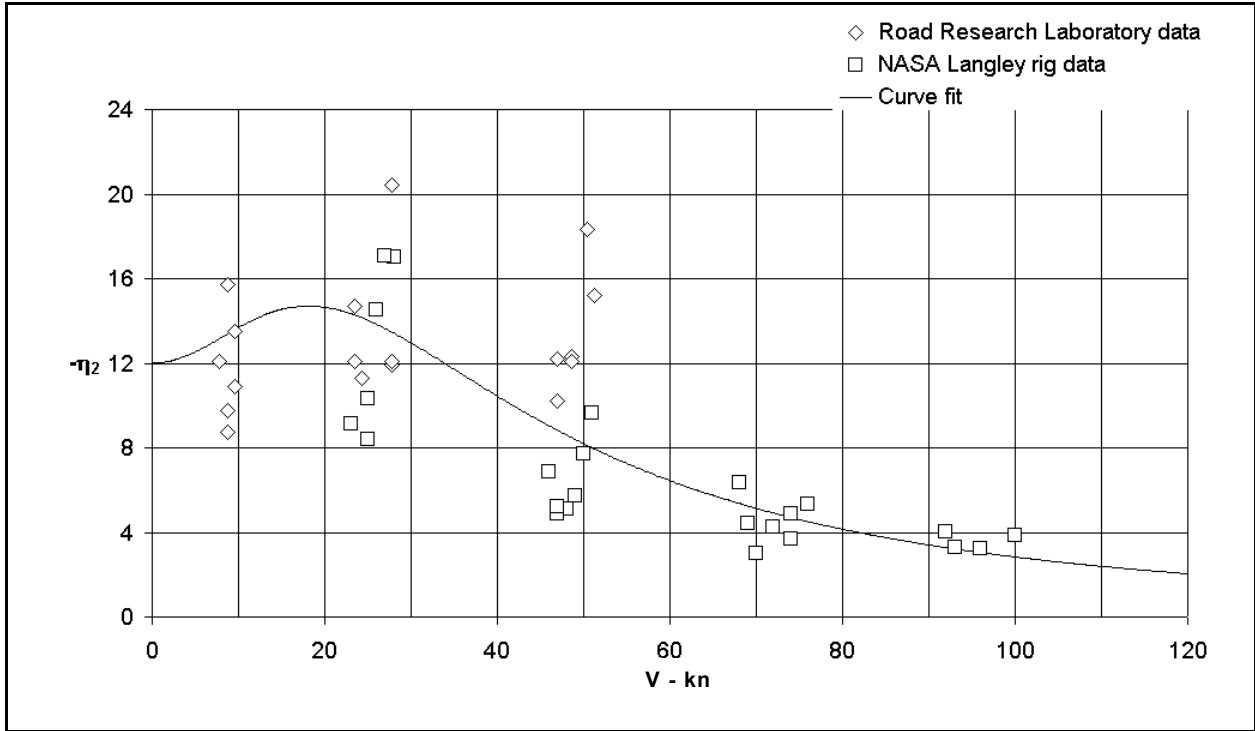
Figure 11.1: Effect of ground speed on exponent η_2
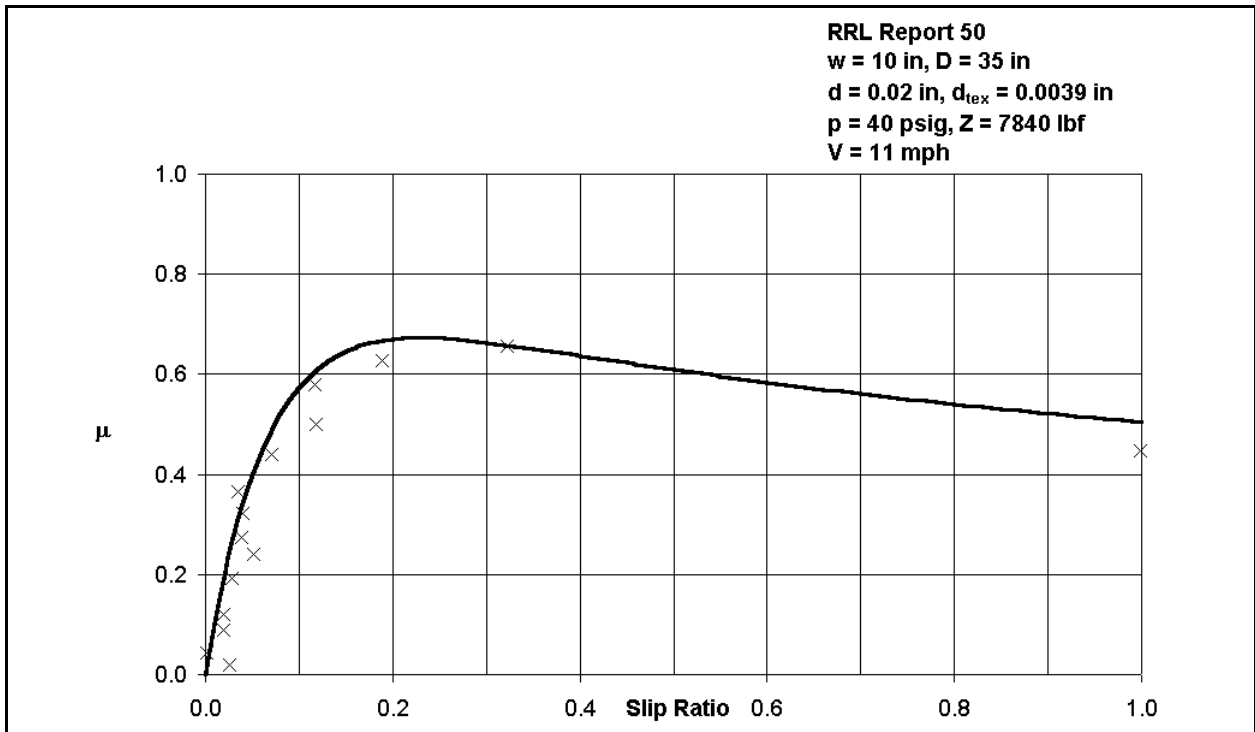
Figure 11.2: Effect of slip ratio on coefficient of braking friction on wet runway
($V = 11$ mph, $p = 40$ psig)

132
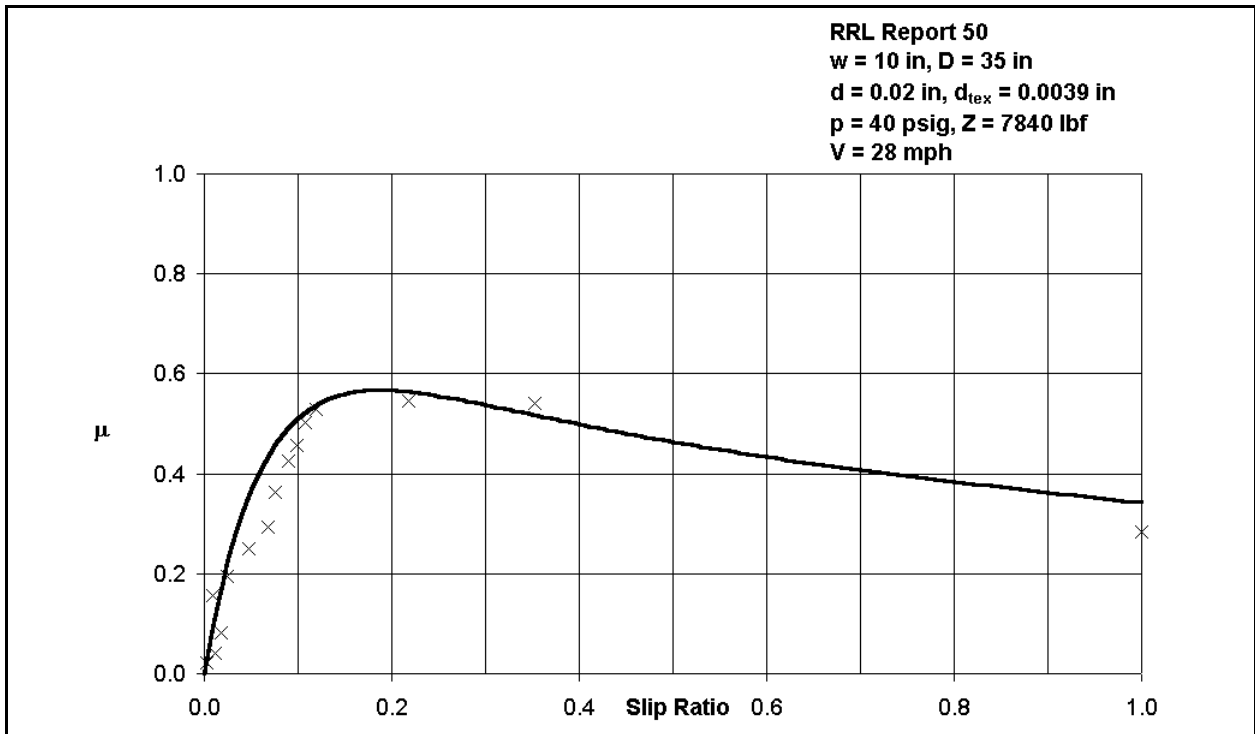
Figure 11.3: Effect of slip ratio on coefficient of braking friction on wet runway
($V = 28$ mph)
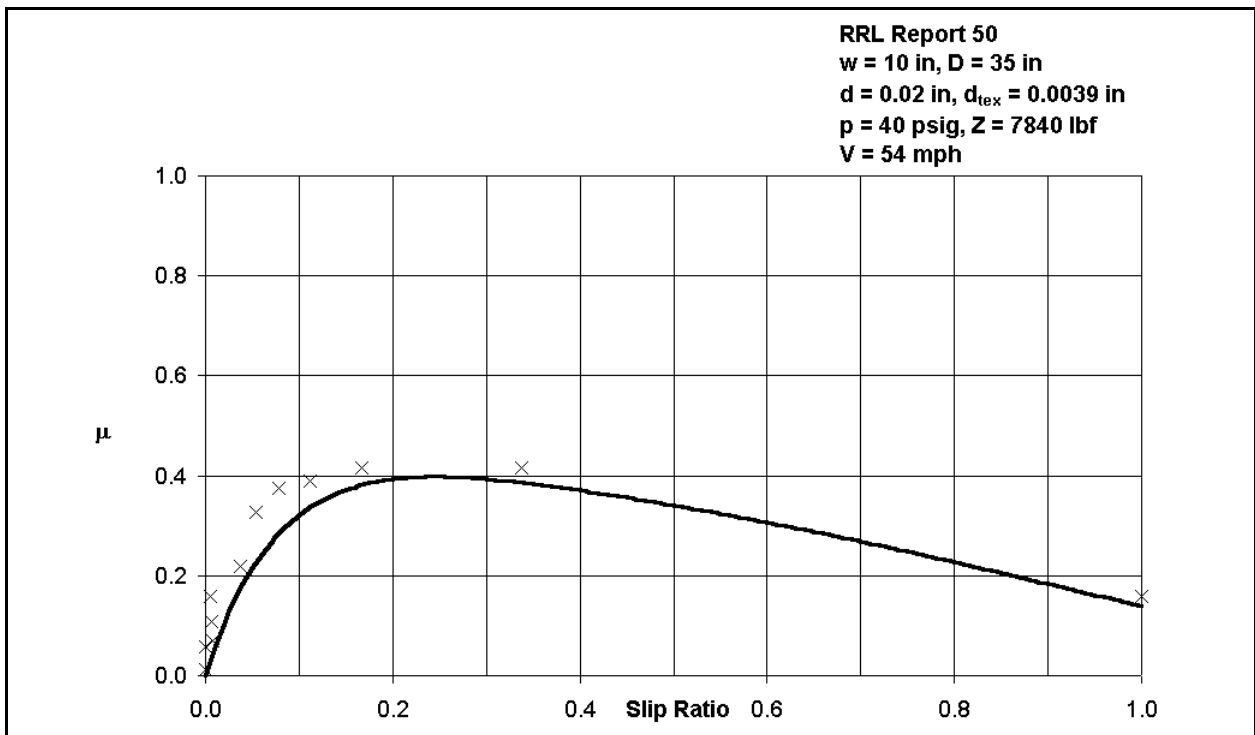
Figure 11.4: Effect of slip ratio on coefficient of braking friction on wet runway
($V = 54$ mph, $p = 40$ psig)
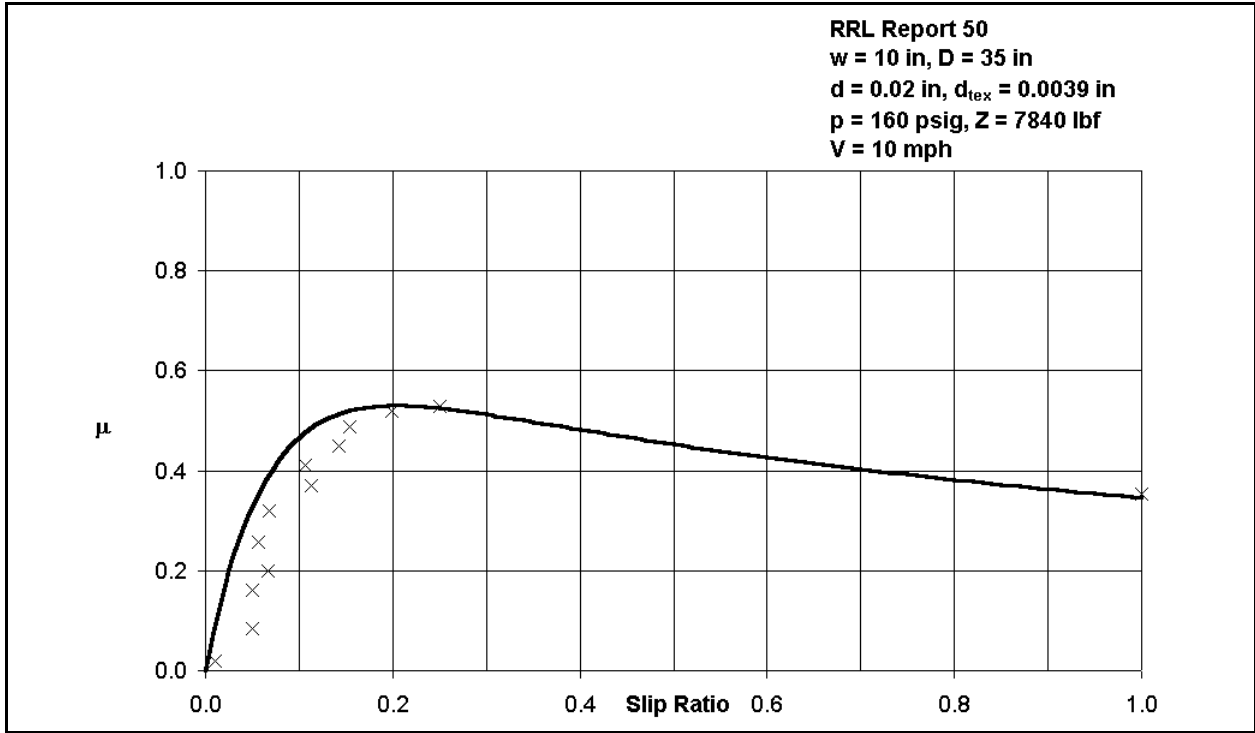
Figure 11.5: Effect of slip ratio on coefficient of braking friction on wet runway
($V = 10$ mph, $p = 160$ psig, $d_{tex} = 0.0039$ in)
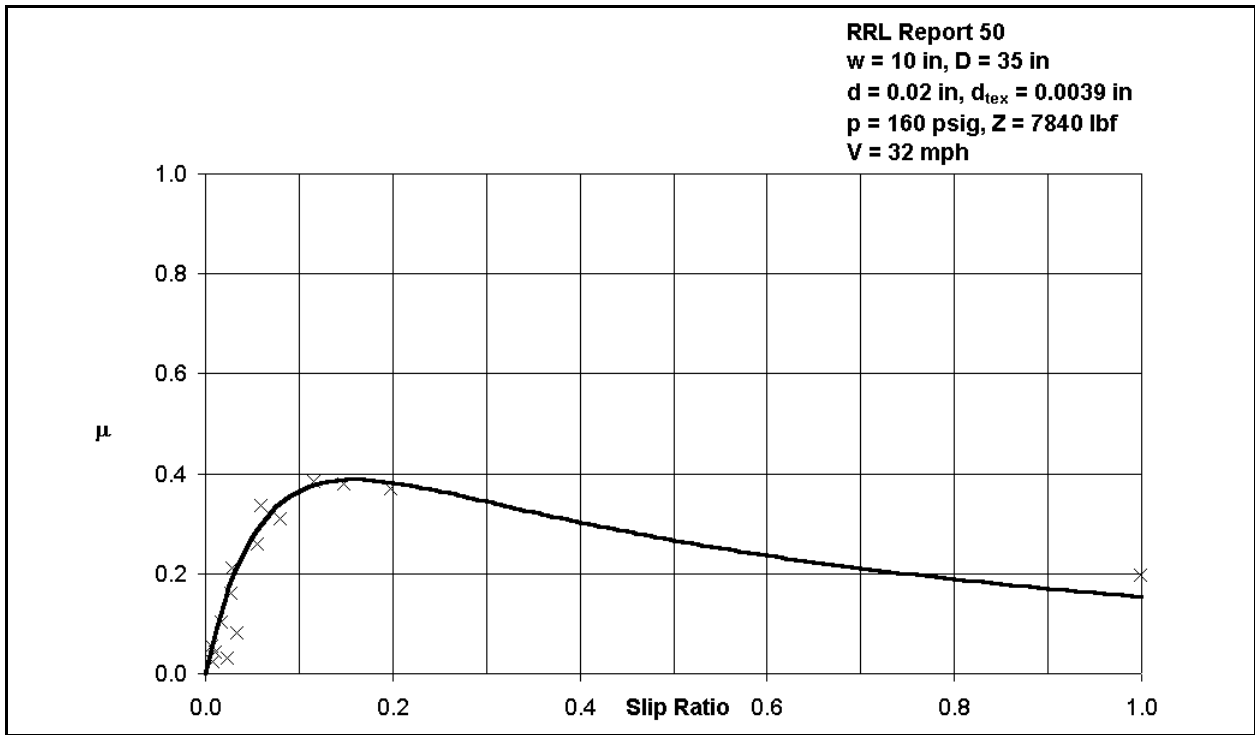
Figure 11.6: Effect of slip ratio on coefficient of braking friction on wet runway
($V = 32$ mph, $p = 160$ psig, $d_{tex} = 0.0039$ in)

134
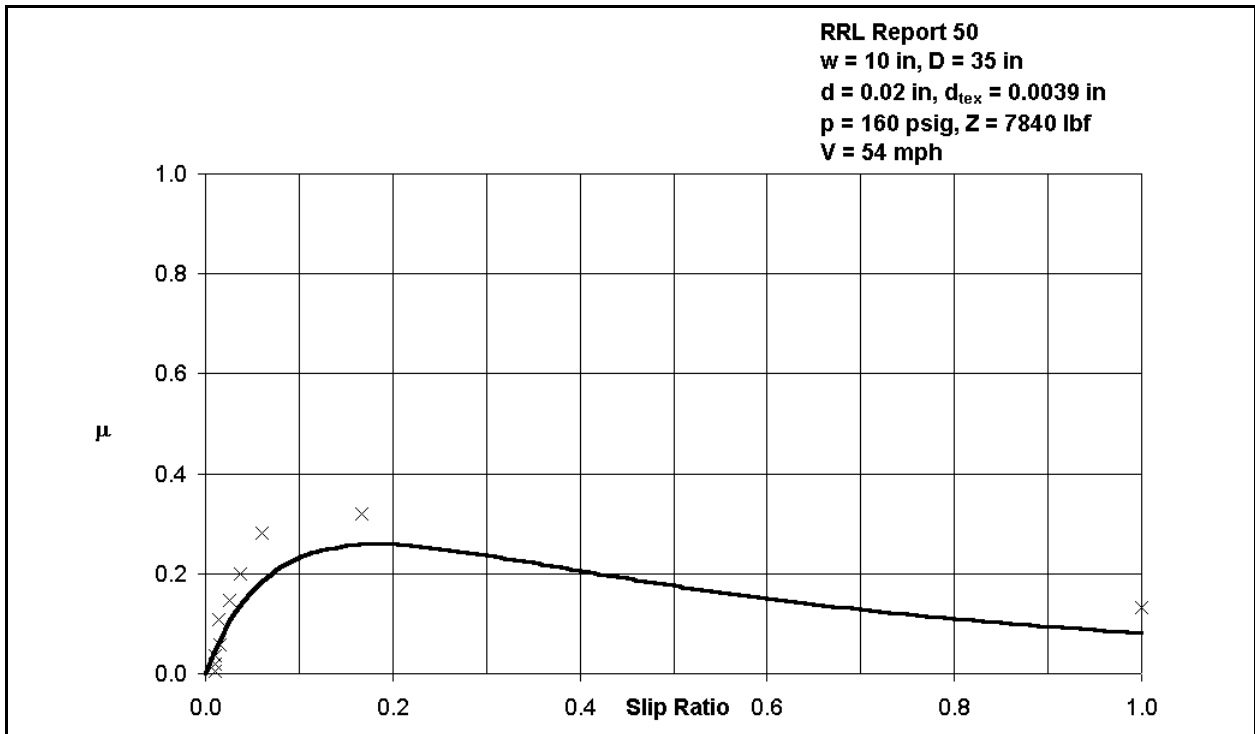
Figure 11.7: Effect of slip ratio on coefficient of braking friction on wet runway
(V = 54 mph, p = 160 psig)

Figure 11.8: Effect of slip ratio on coefficient of braking friction on wet runway
(V = 10 mph, p = 40 psig, d_{tex} = 0.0157 in)

135
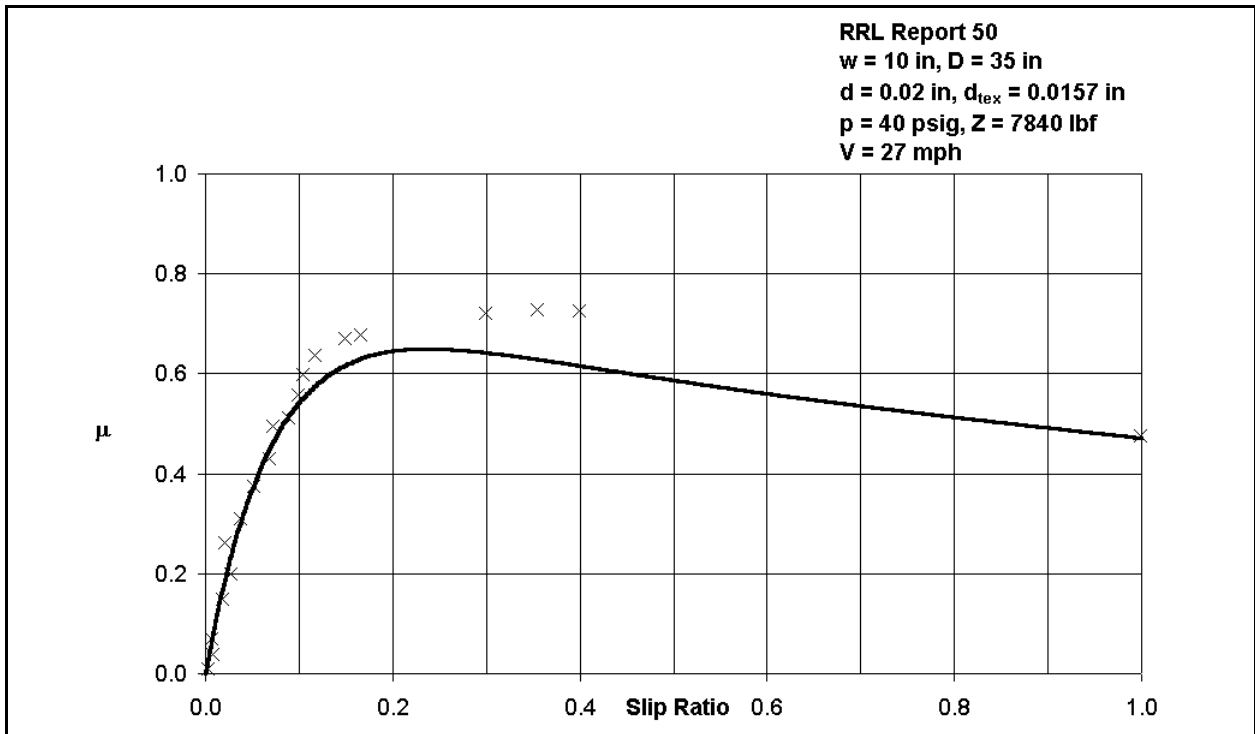
Figure 11.9: Effect of slip ratio on coefficient of braking friction on wet runway
(V = 27 mph, p = 40 psig, d_{tex} = 0.0157 in)
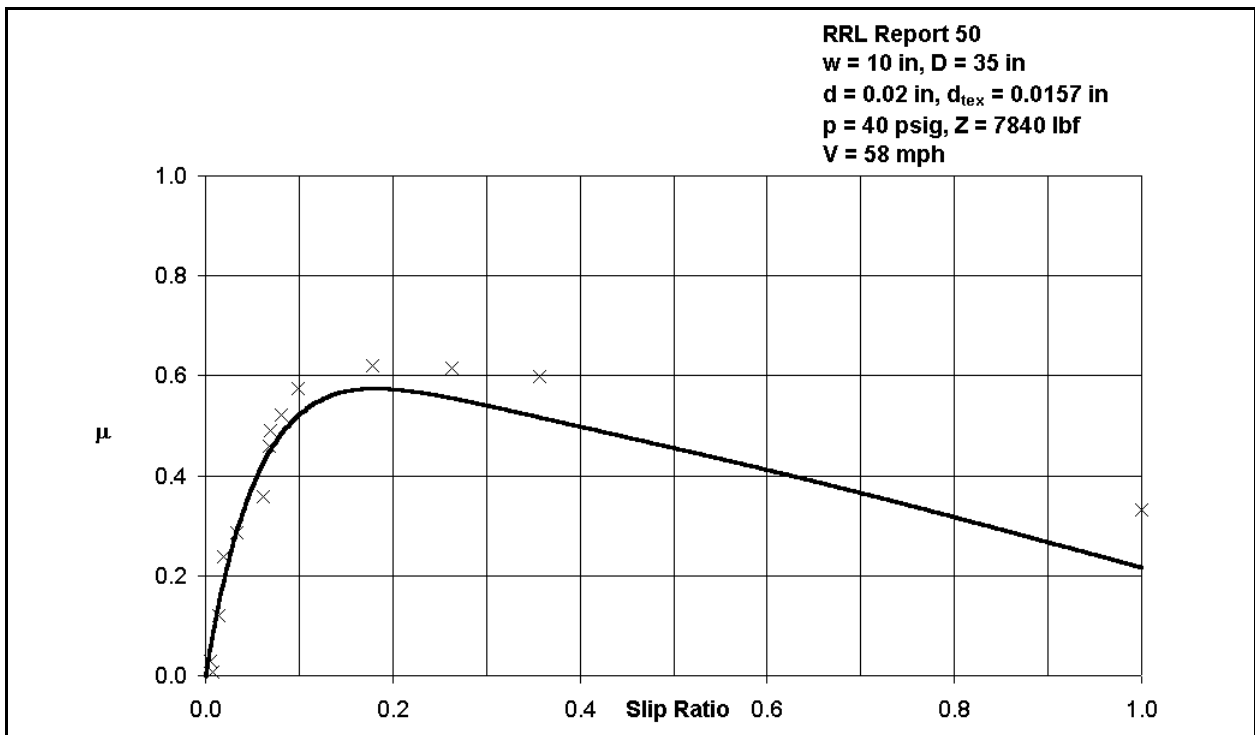
Figure 11.10: Effect of slip ratio on coefficient of braking friction on wet runway
(V = 58 mph)
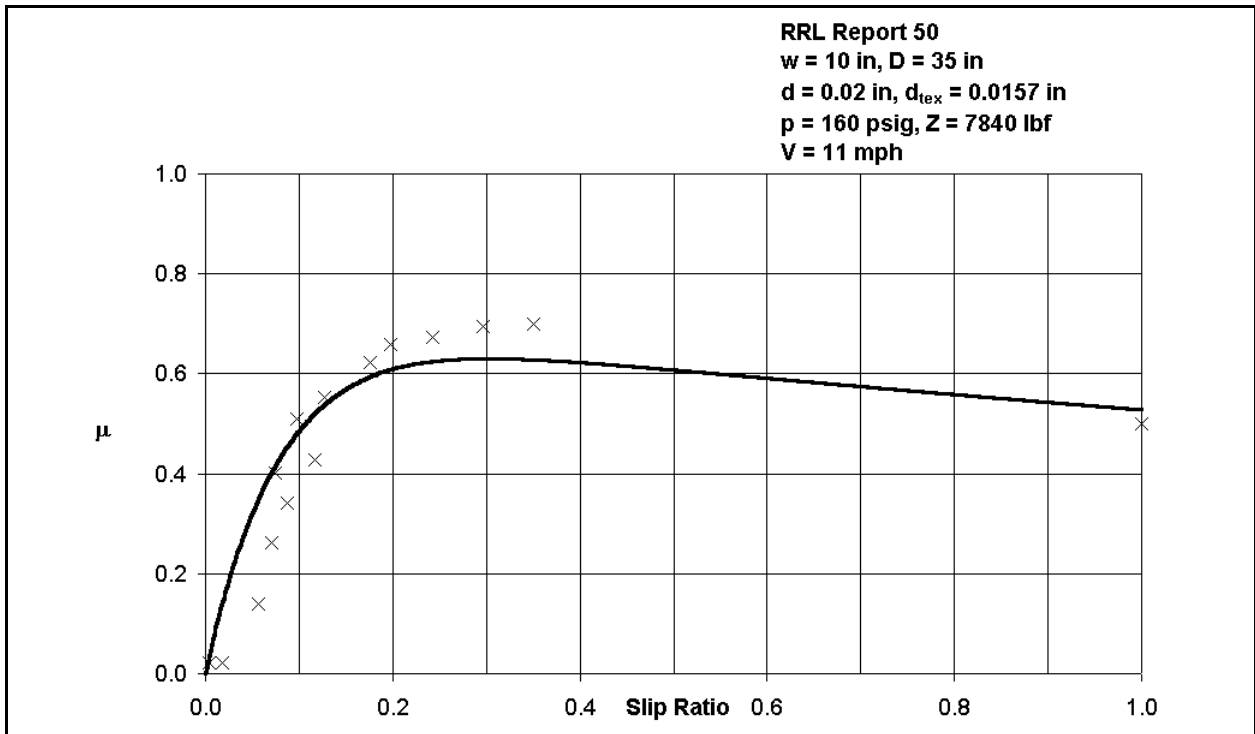
Figure 11.11: Effect of slip ratio on coefficient of braking friction on wet runway
($V = 11$ mph, $p = 160$ psig)
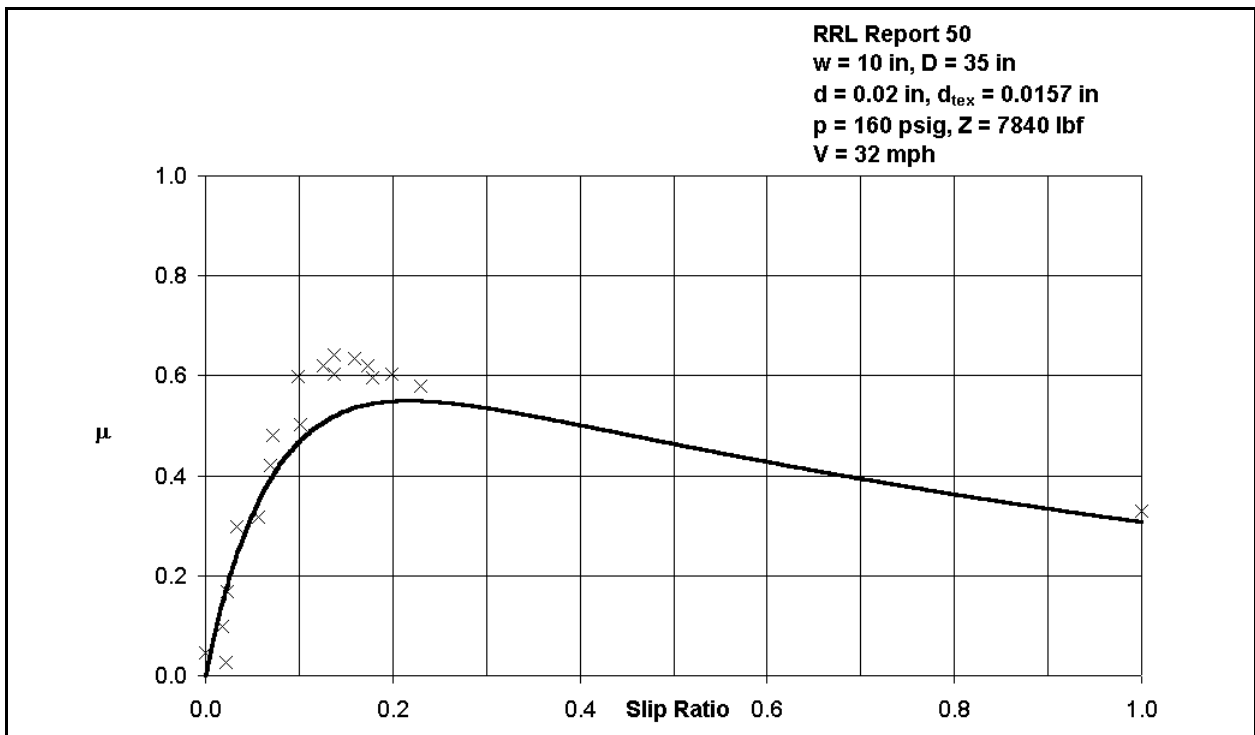
Figure 11.12: Effect of slip ratio on coefficient of braking friction on wet runway
($V = 32$ mph, $p = 160$ psig, $d_{tex} = 0.0157$ in)
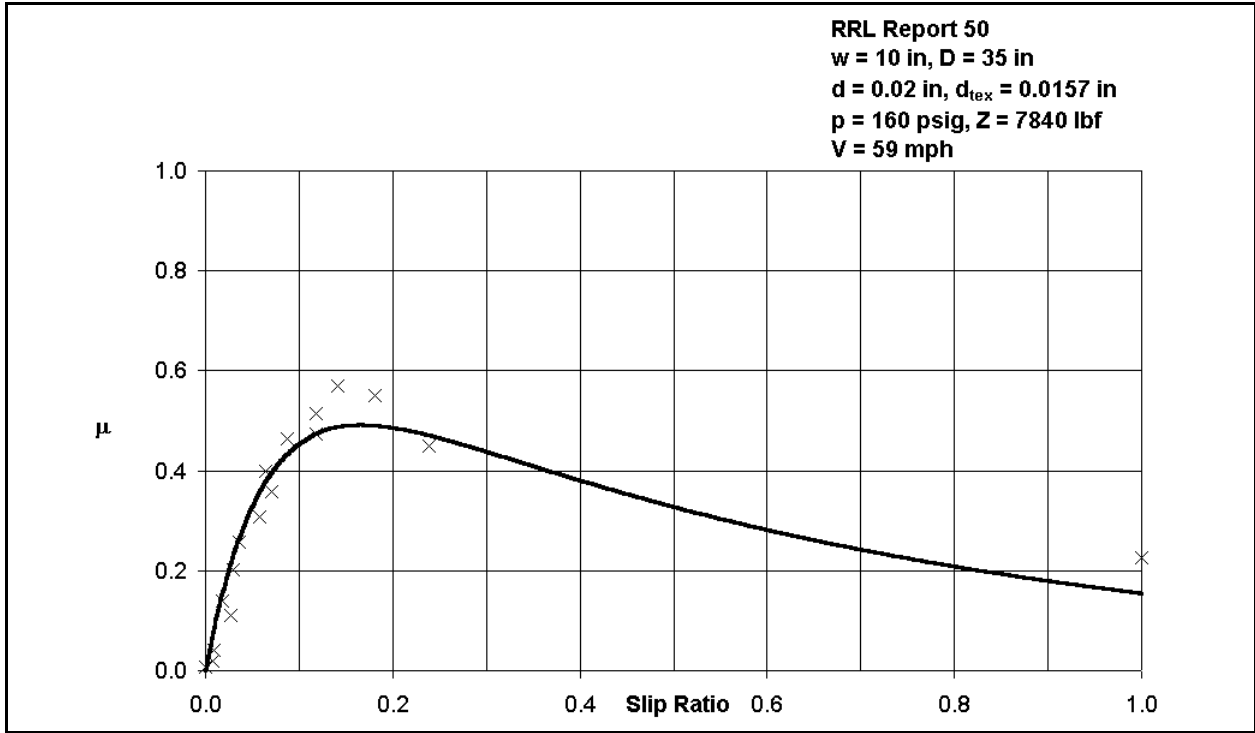
Figure 11.13: Effect of slip ratio on coefficient of braking friction on wet runway
(V = 59 mph)
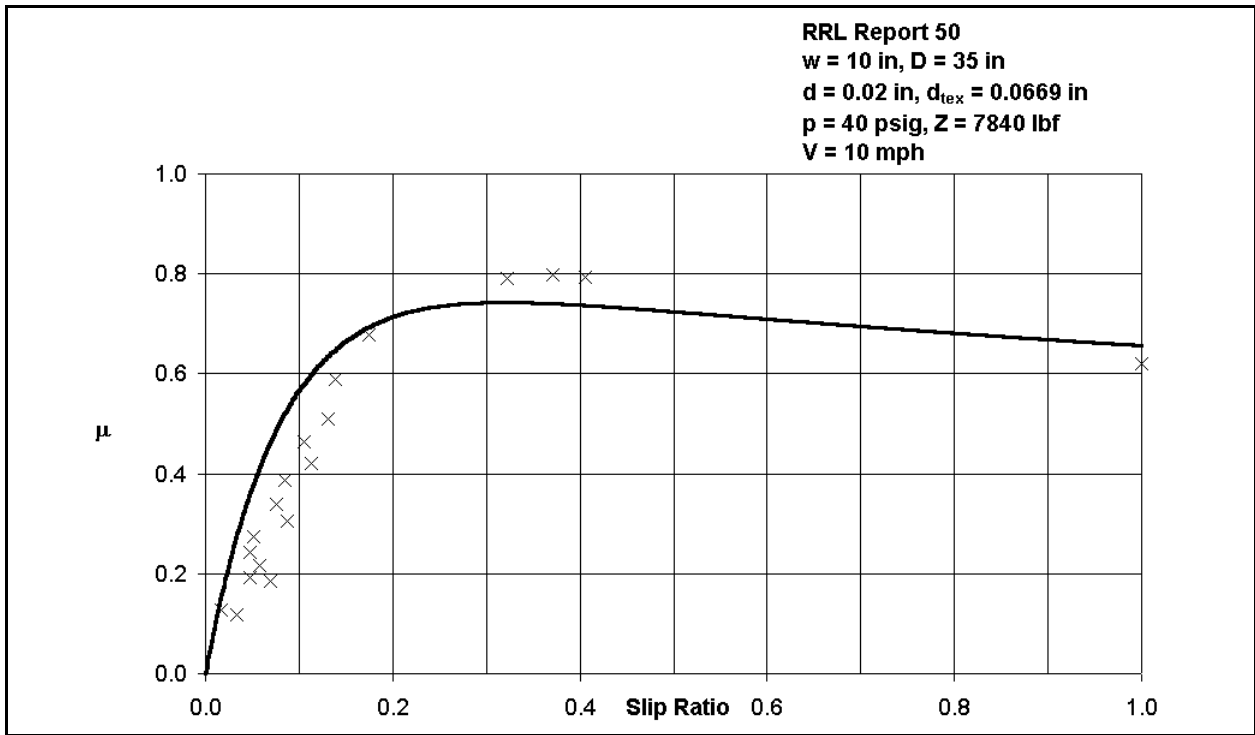
Figure 11.14: Effect of slip ratio on coefficient of braking friction on wet runway
(V = 10 mph, p = 40 psig, d_{tex} = 0.0669 in)
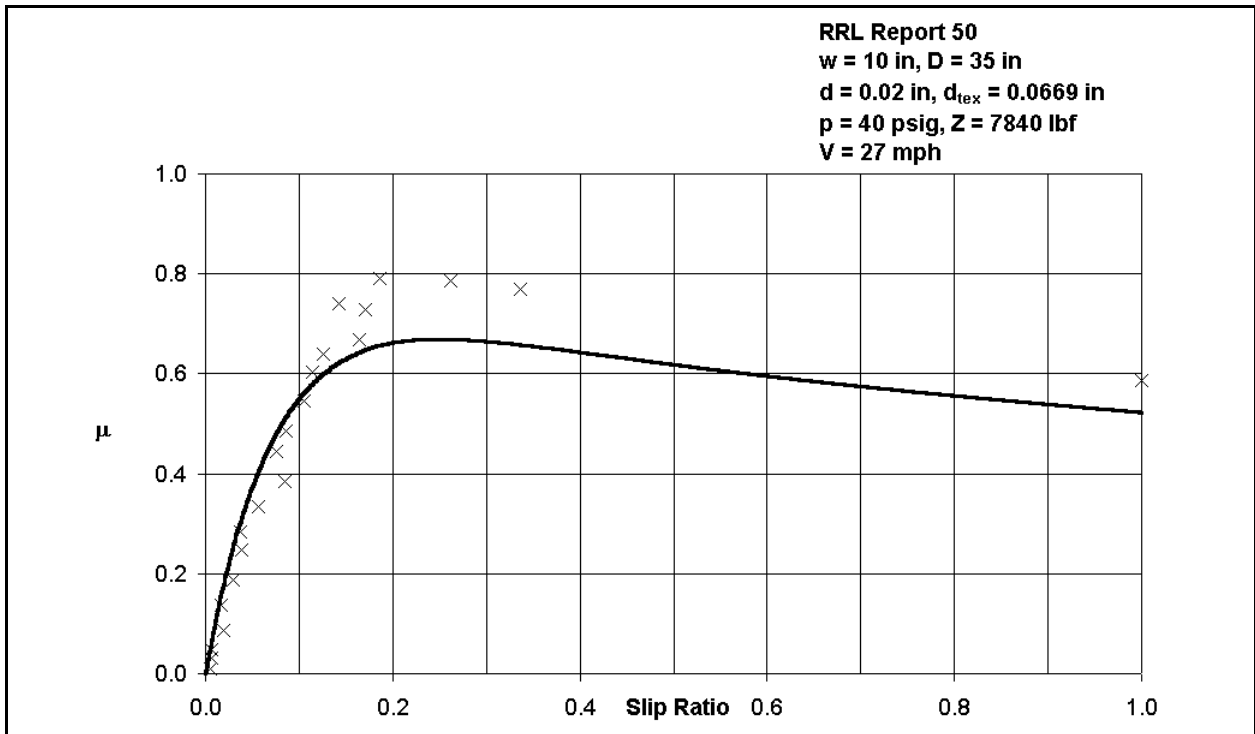
Figure 11.15: Effect of slip ratio on coefficient of braking friction on wet runway
(V = 27 mph, p = 40 psig, d_{tex} = 0.0669 in)
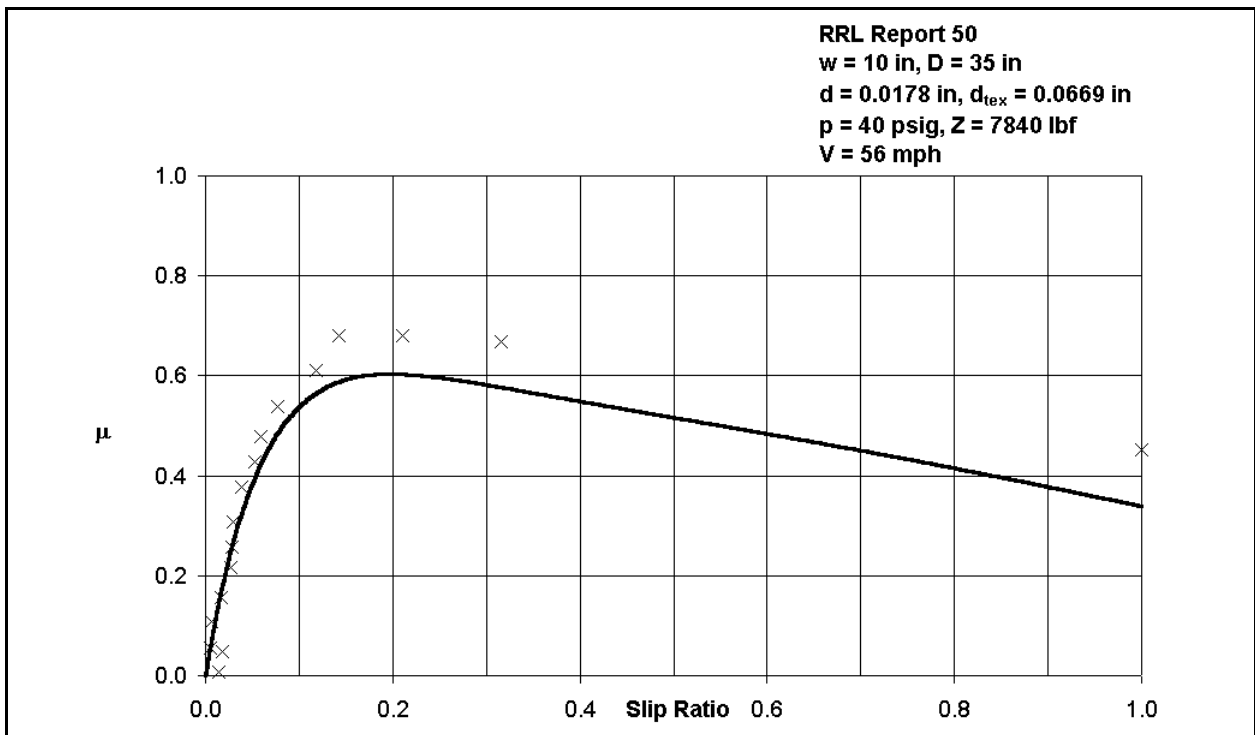
Figure 11.16: Effect of slip ratio on coefficient of braking friction on wet runway
(V = 56 mph)
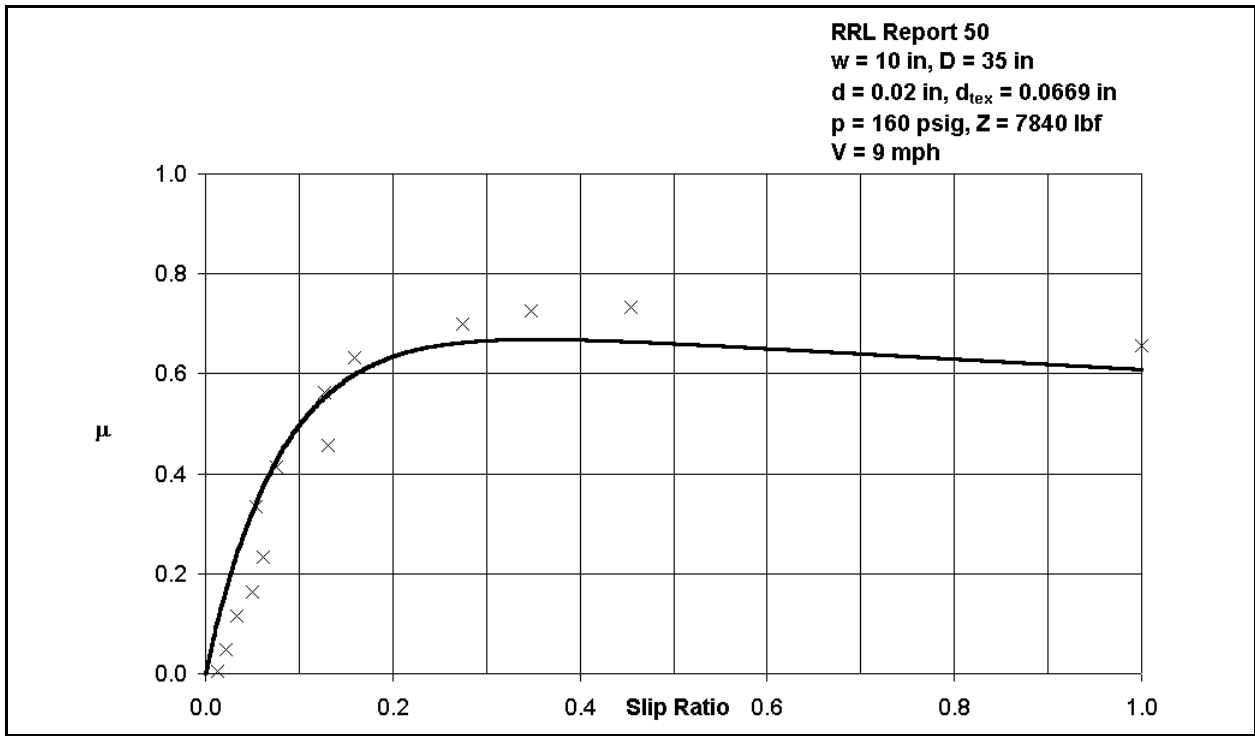
Figure 11.17: Effect of slip ratio on coefficient of braking friction on wet runway
($V = 9$ mph)
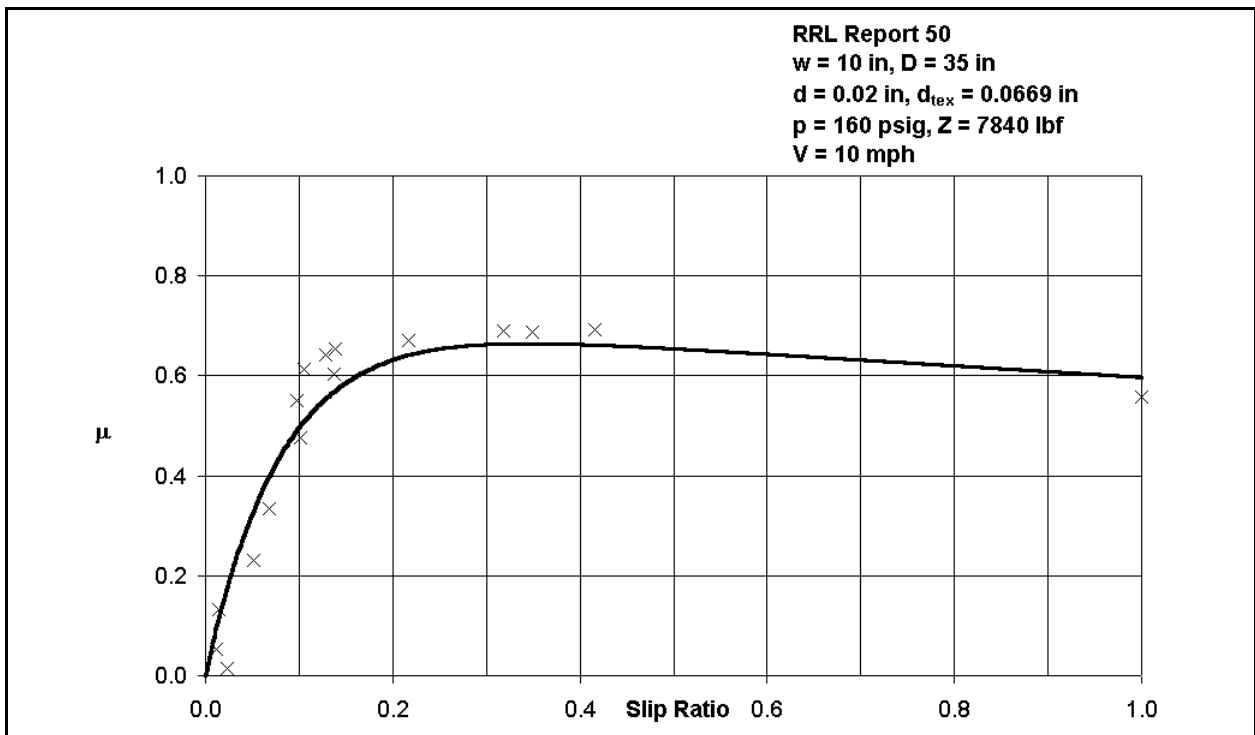
Figure 11.18: Effect of slip ratio on coefficient of braking friction on wet runway
($V = 10$ mph, $p = 160$ psig, $d_{tex} = 0.0669$ in)
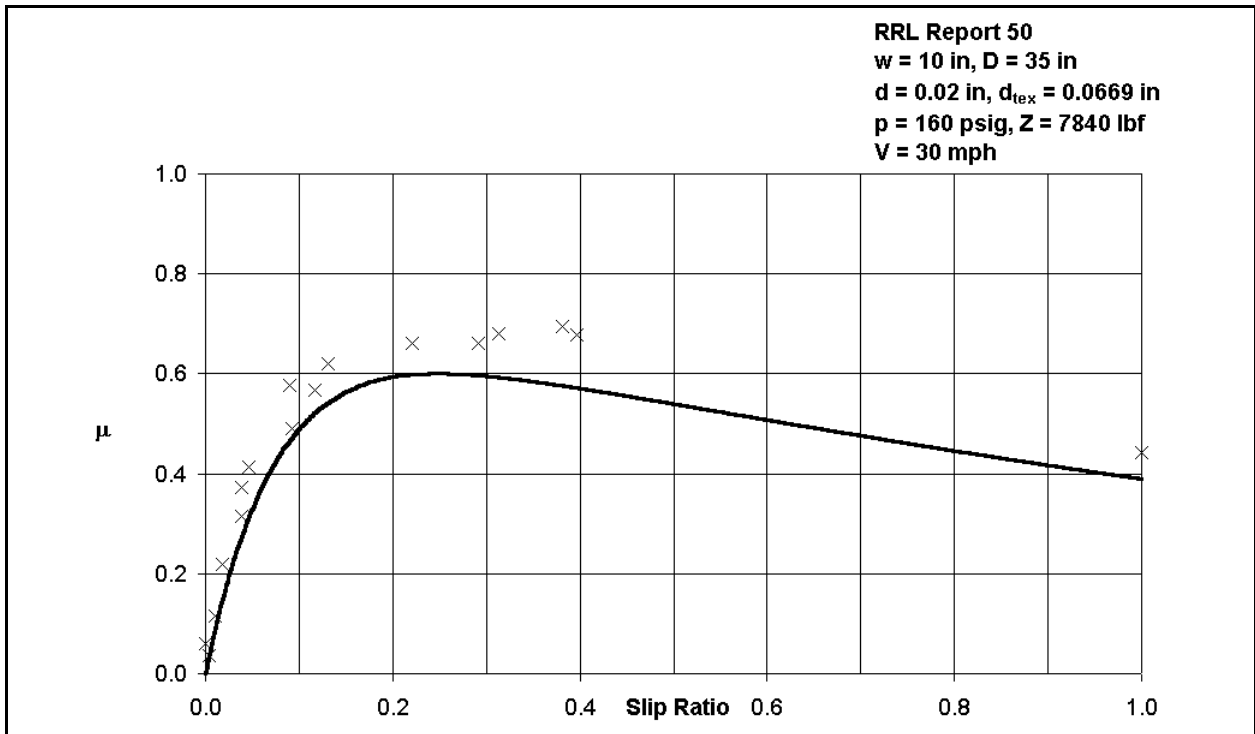
Figure 11.19: Effect of slip ratio on coefficient of braking friction on wet runway
($V = 30$ mph)
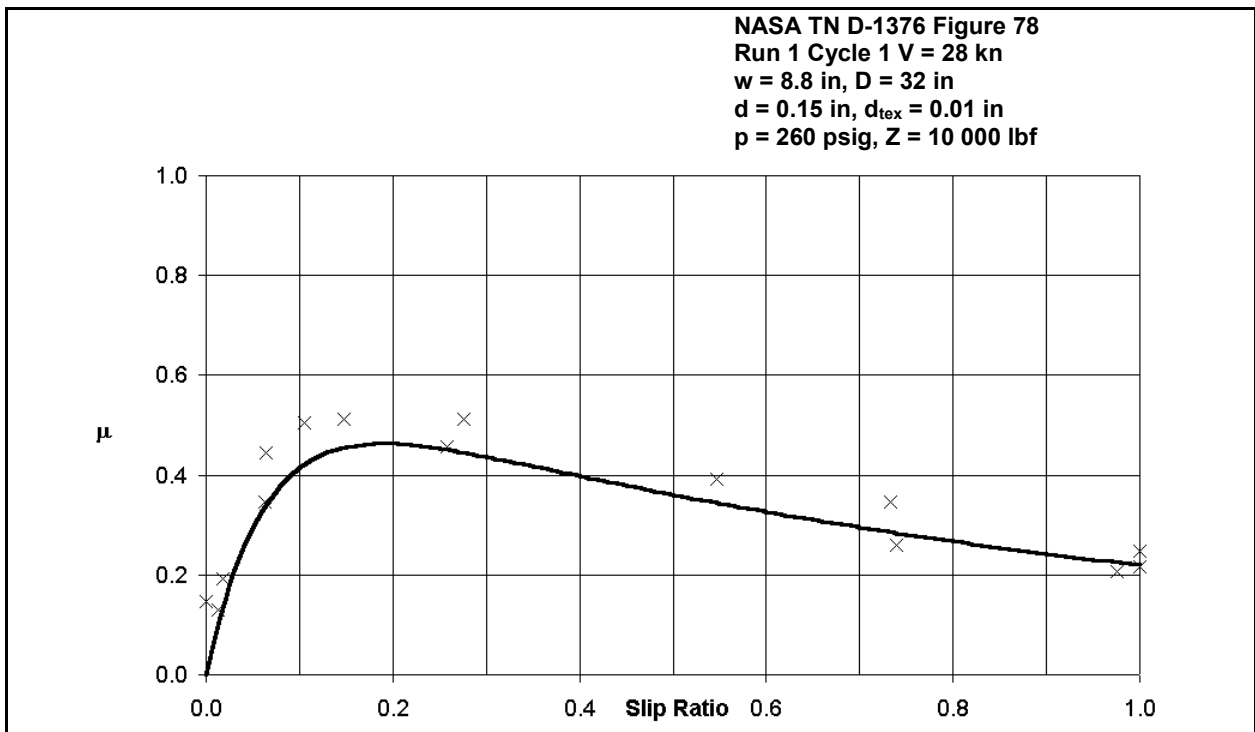
Figure 11.20: Effect of slip ratio on coefficient of braking friction on wet runway
(Reference 7, Figure 78 – Run 1, Cycle 1)

141
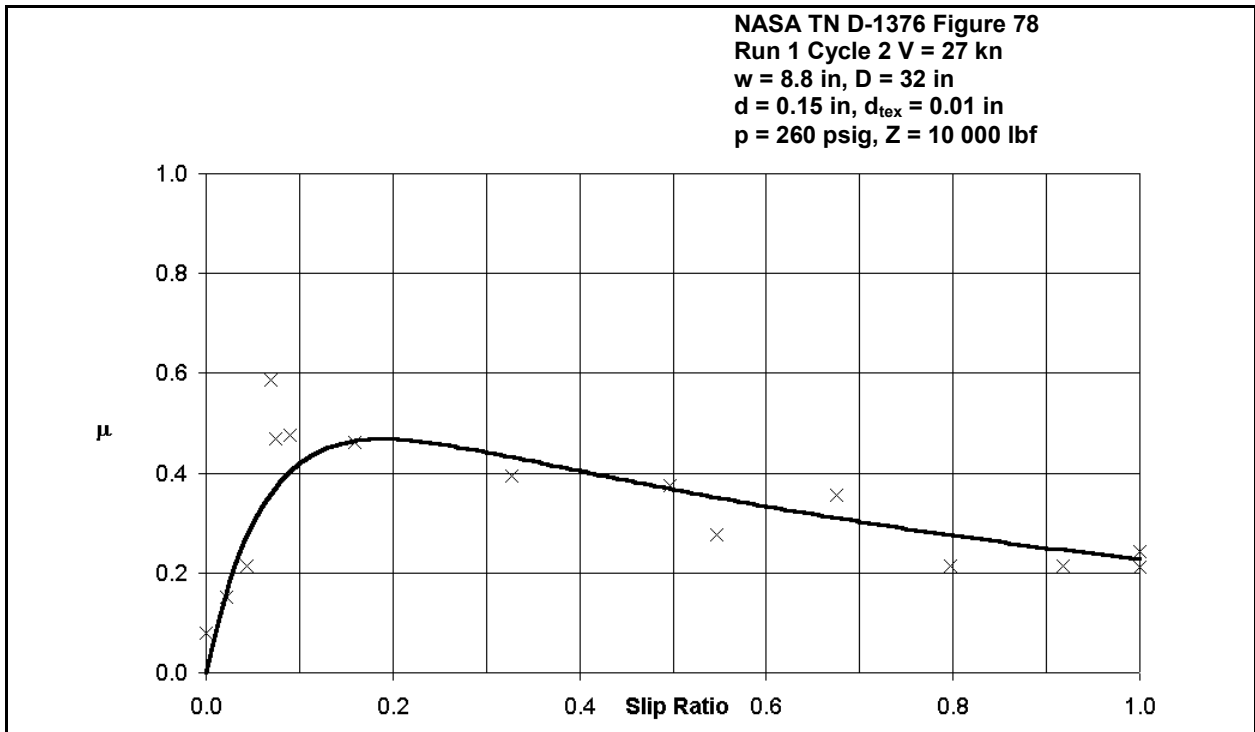
Figure 11.21: Effect of slip ratio on coefficient of braking friction on wet runway (Reference 7, Figure 78 − Run 1, Cycle 2)
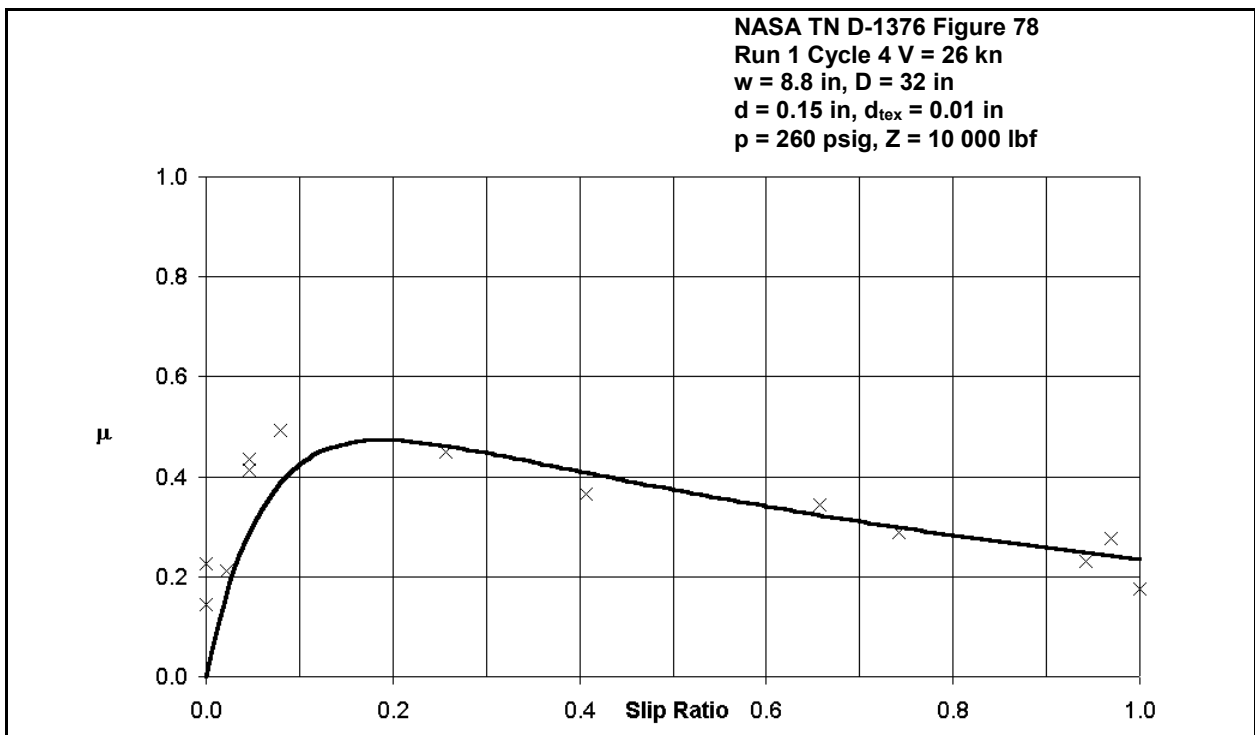
Figure 11.22: Effect of slip ratio on coefficient of braking friction on wet runway (Reference 7, Figure 78 − Run 1, Cycle 4)
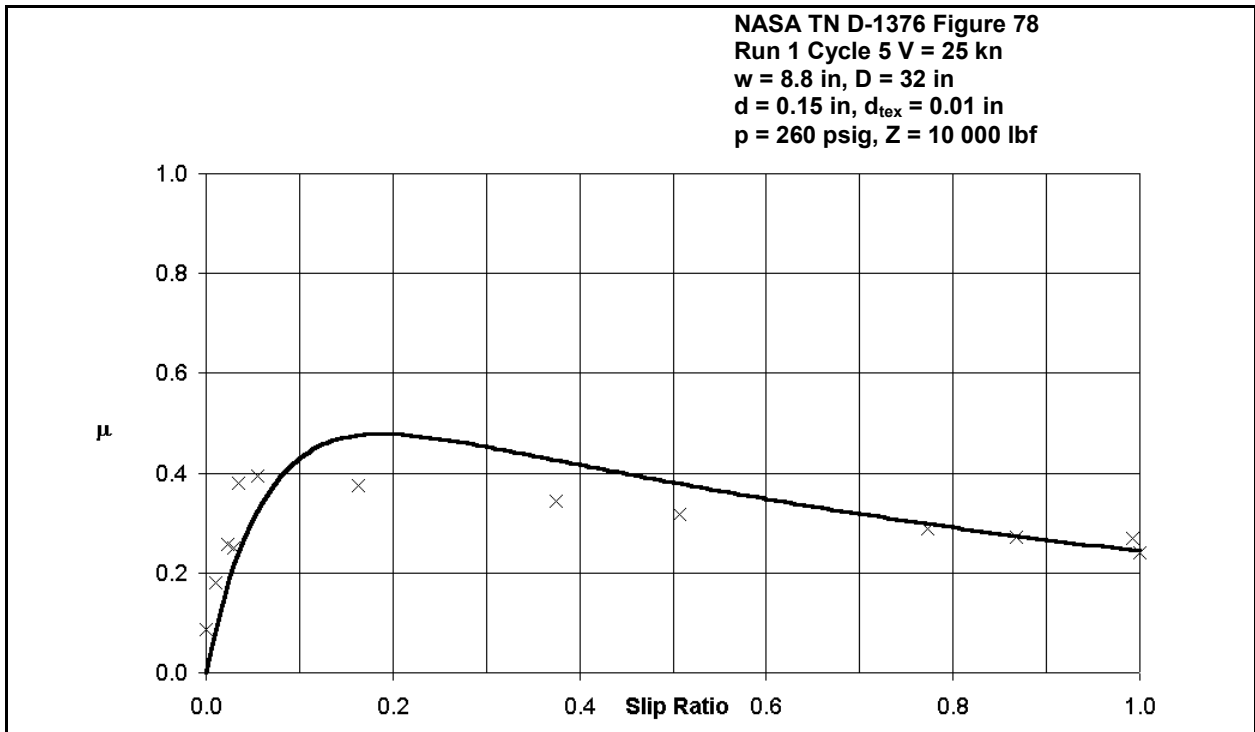
Figure 11.23: Effect of slip ratio on coefficient of braking friction on wet runway (Reference 7, Figure 78 – Run 1, Cycle 5)
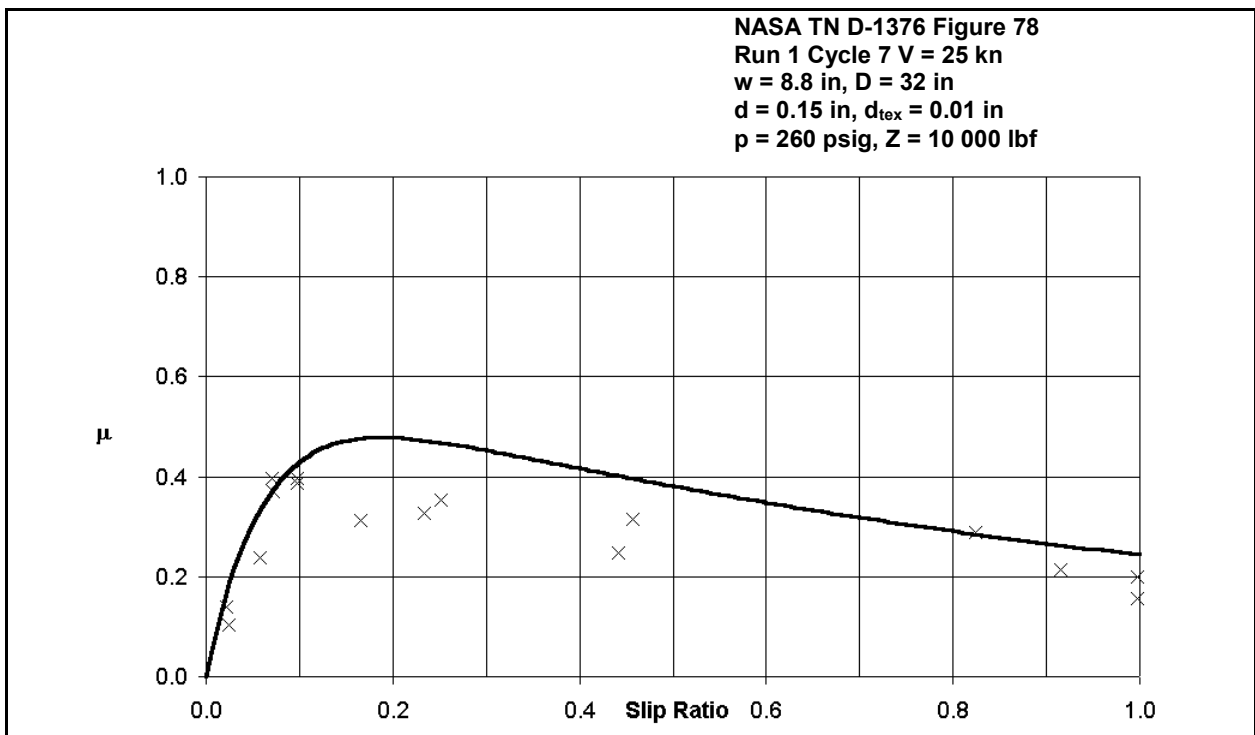
Figure 11.24: Effect of slip ratio on coefficient of braking friction on wet runway (Reference 7, Figure 78 – Run 1, Cycle 7)
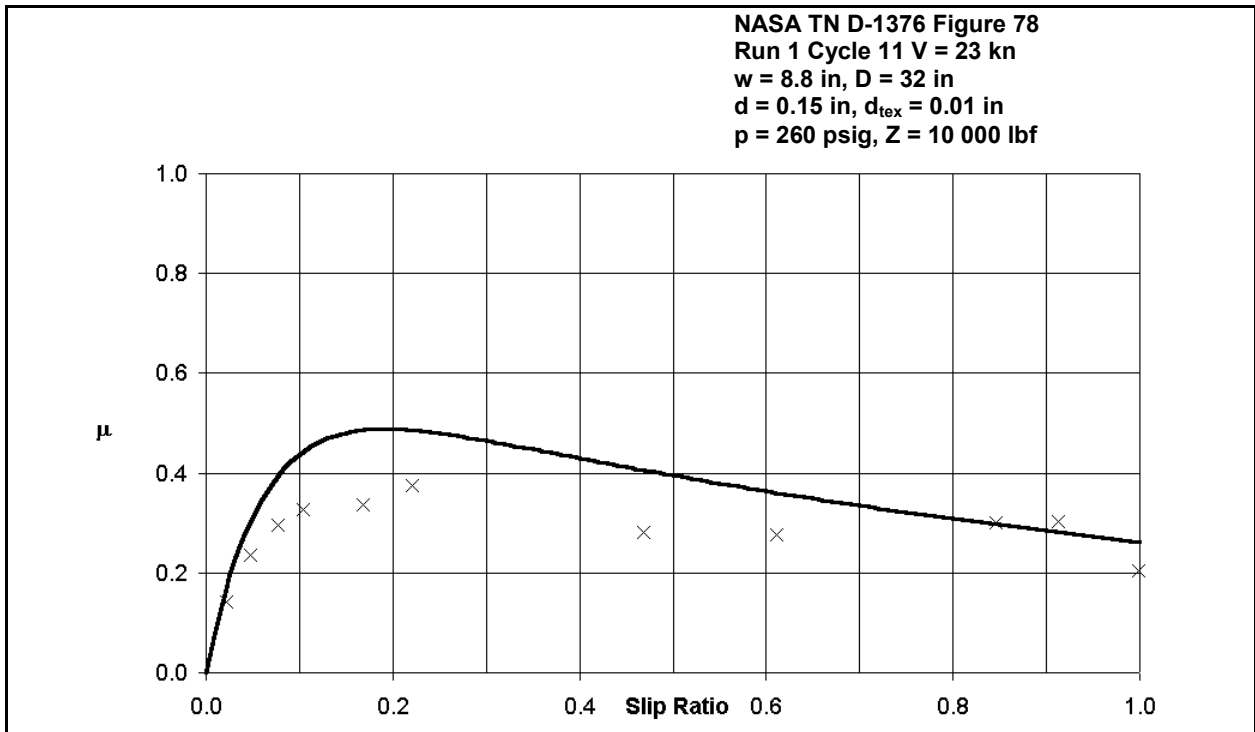
Figure 11.25: Effect of slip ratio on coefficient of braking friction on wet runway (Reference 7, Figure 78 – Run 1, Cycle 11)
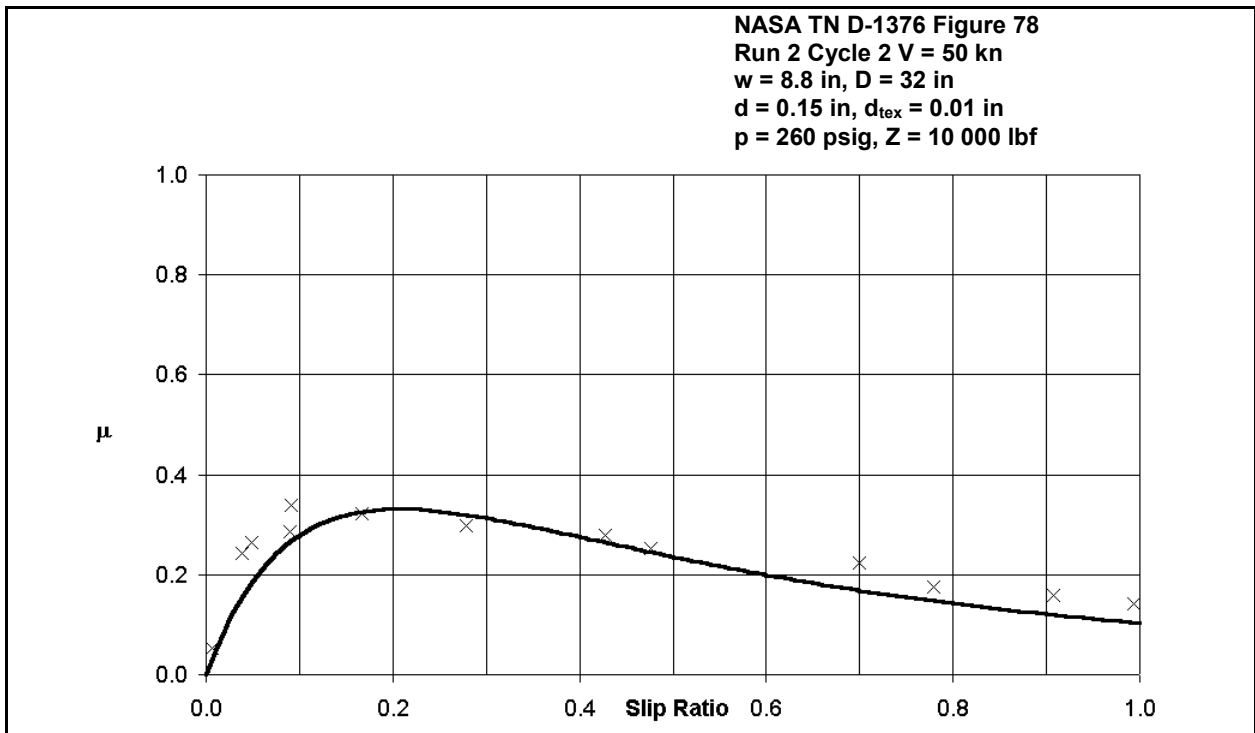
Figure 11.26: Effect of slip ratio on coefficient of braking friction on wet runway (Reference 7, Figure 78 – Run 2, Cycle 1)
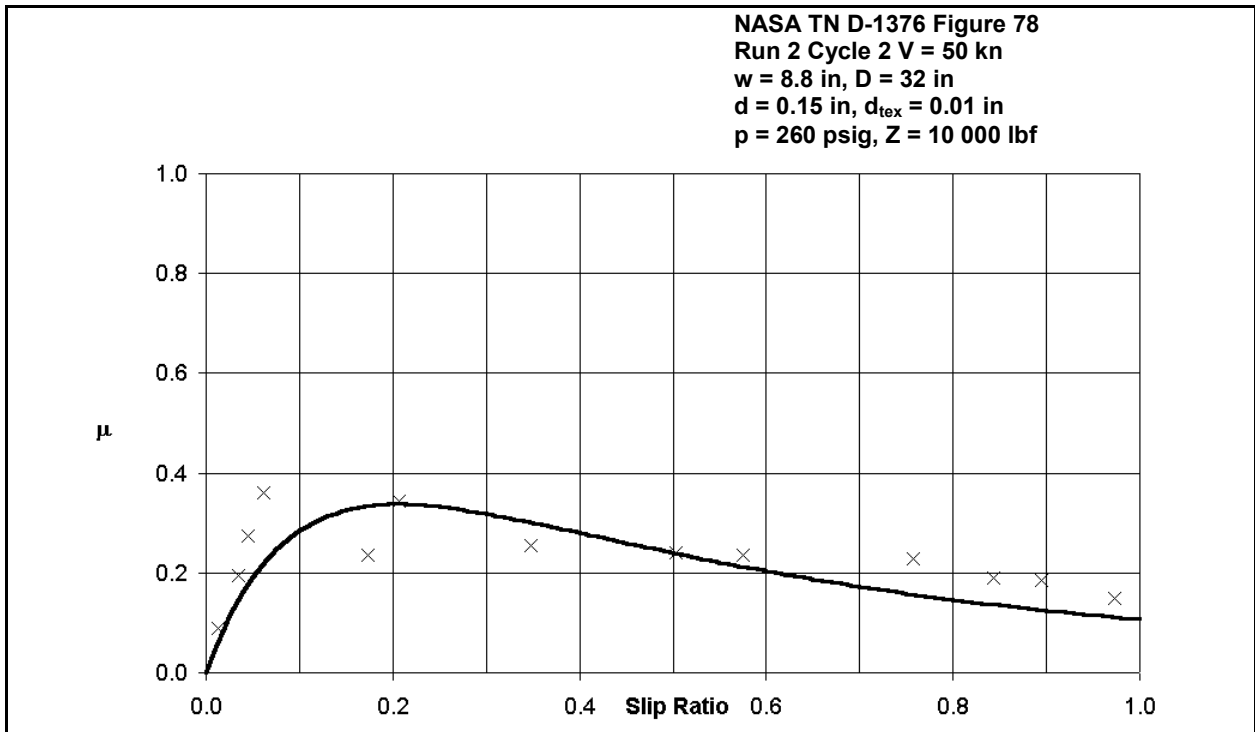
**Figure 11.27: Effect of slip ratio on coefficient of braking friction on wet runway
(Reference 7, Figure 78 – Run 2, Cycle 2)**
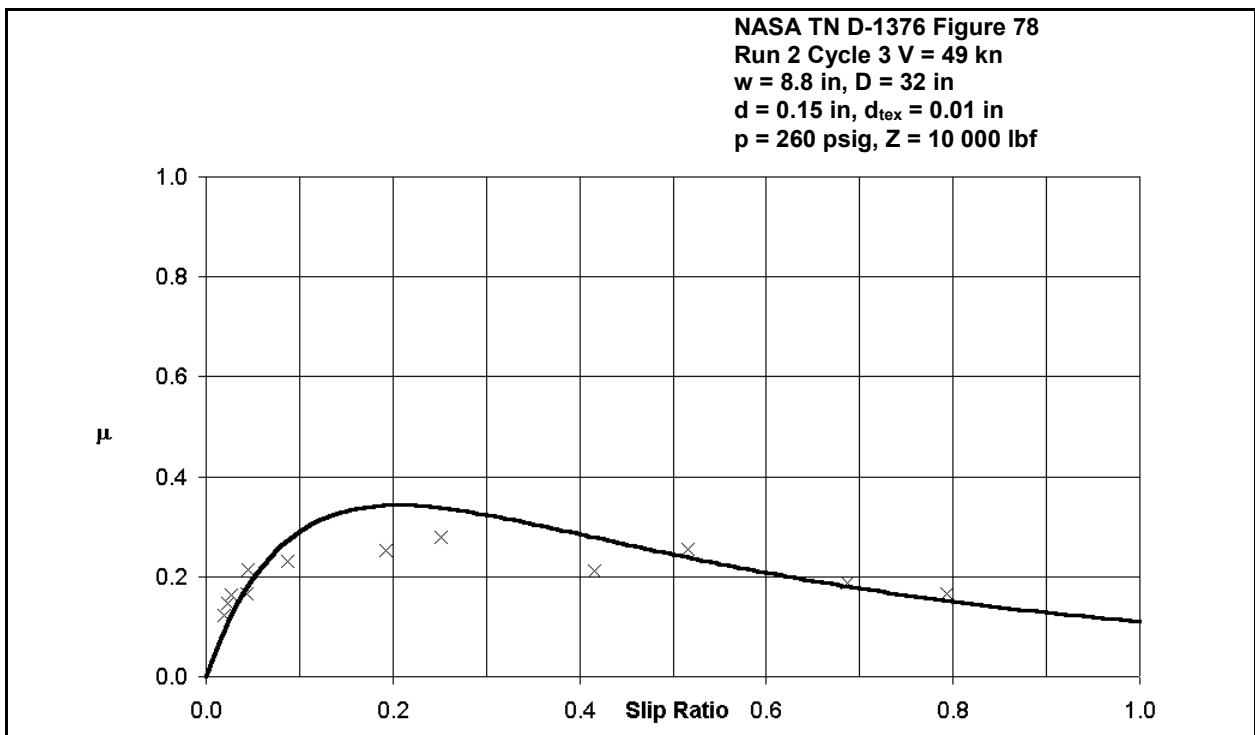
**Figure 11.28: Effect of slip ratio on coefficient of braking friction on wet runway
(Reference 7, Figure 78 – Run 2, Cycle 3)**
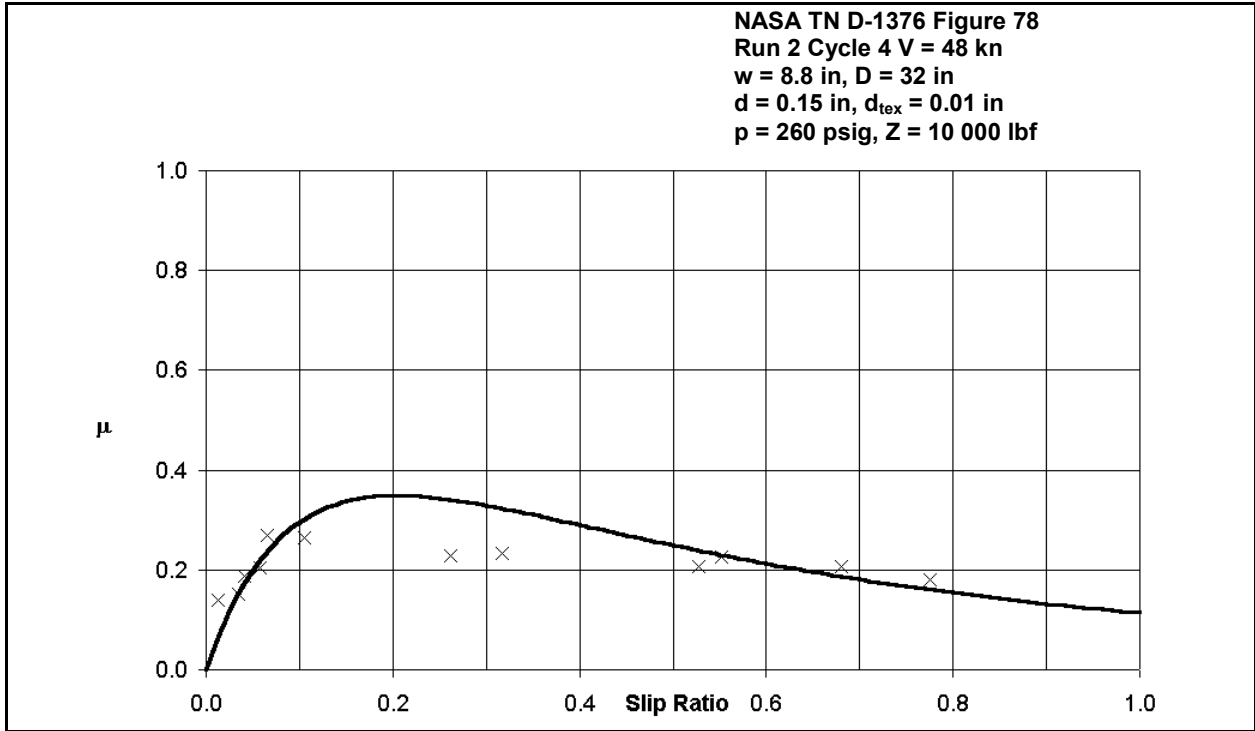
**Figure 11.29: Effect of slip ratio on coefficient of braking friction on wet runway
(Reference 7, Figure 78 − Run 2, Cycle 4)**
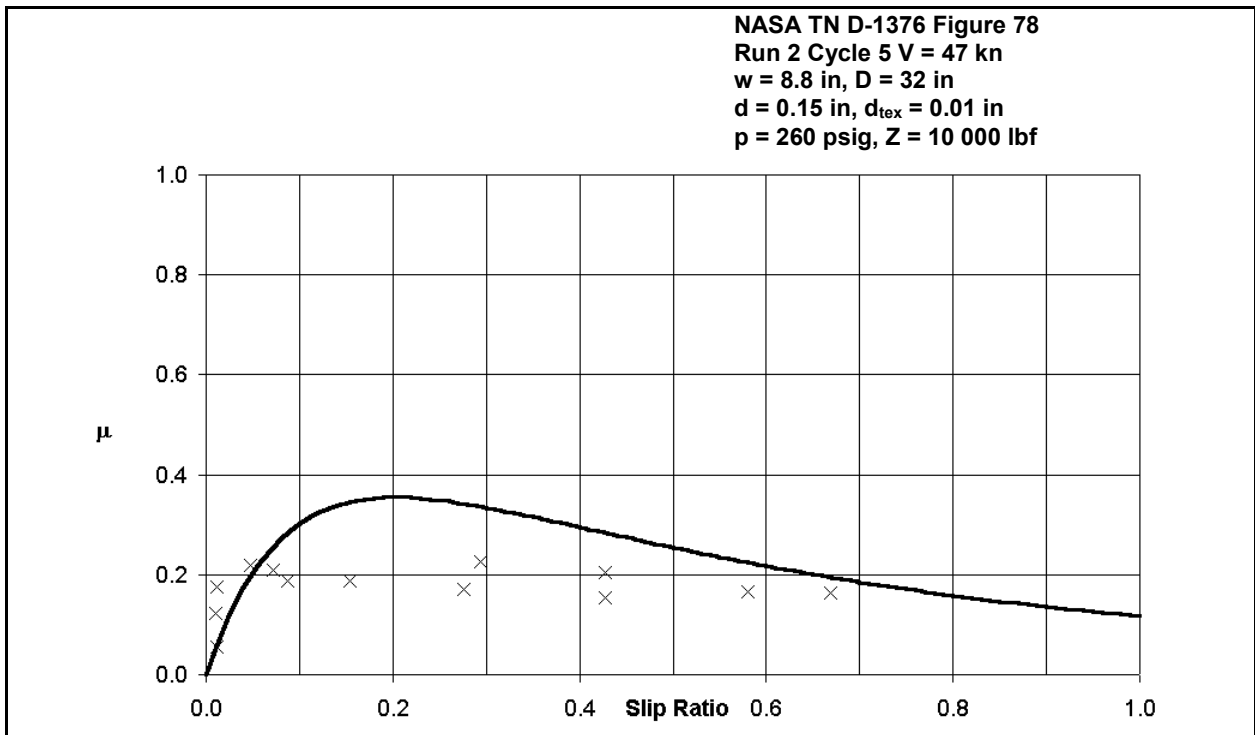
**Figure 11.30: Effect of slip ratio on coefficient of braking friction on wet runway
(Reference 7, Figure 78 − Run 2, Cycle 5)**

146
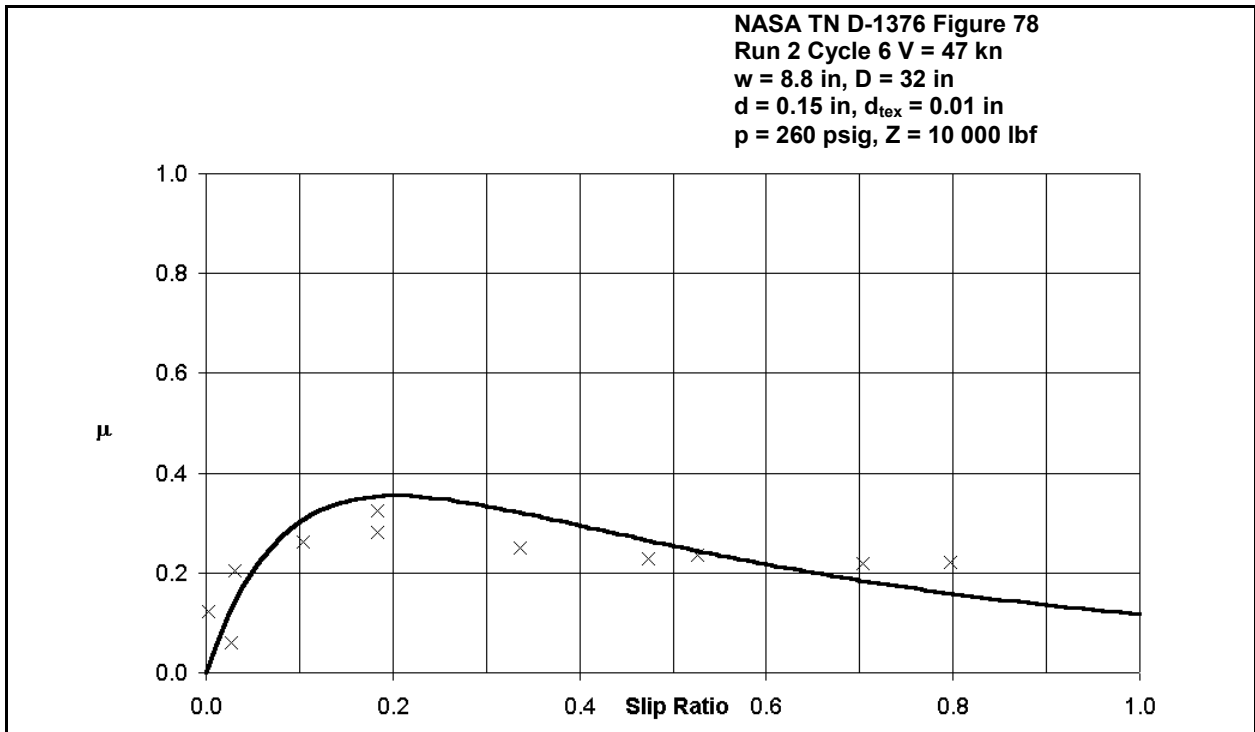
Figure 11.31: Effect of slip ratio on coefficient of braking friction on wet runway
(Reference 7, Figure 78 – Run 2, Cycle 6)
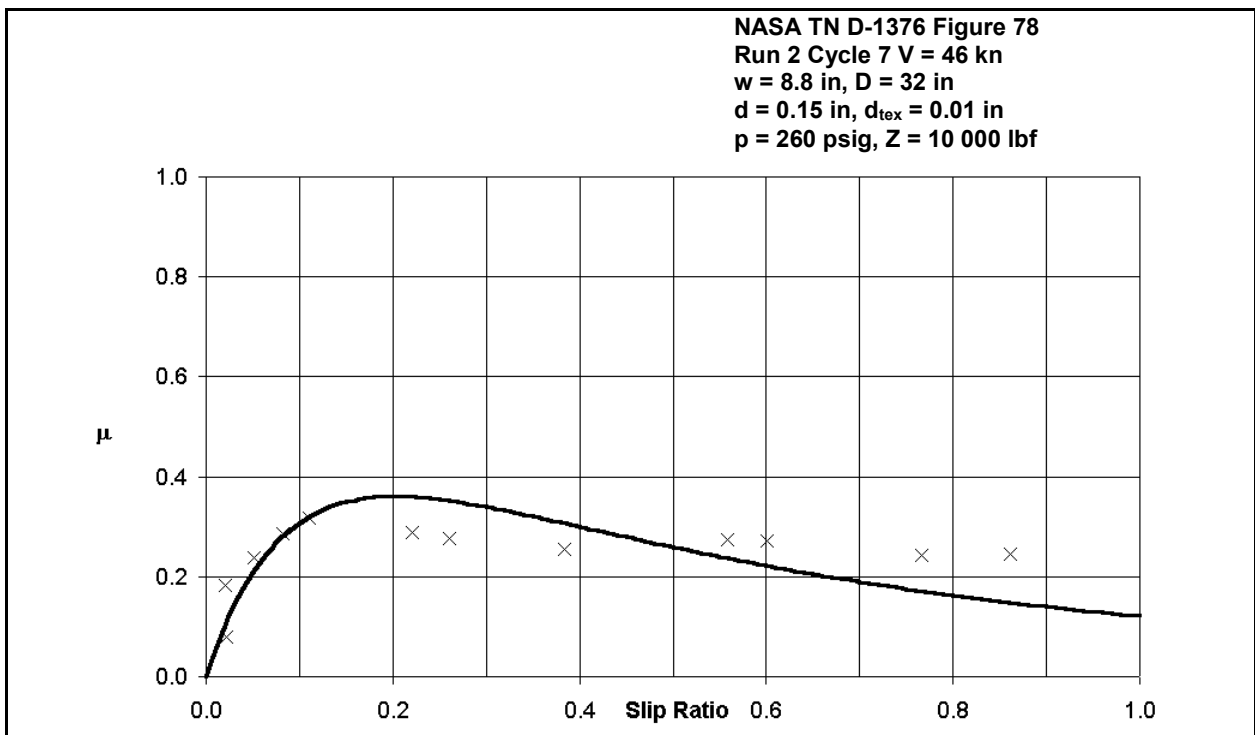
Figure 11.32: Effect of slip ratio on coefficient of braking friction on wet runway
(Reference 7, Figure 78 – Run 2, Cycle 7)
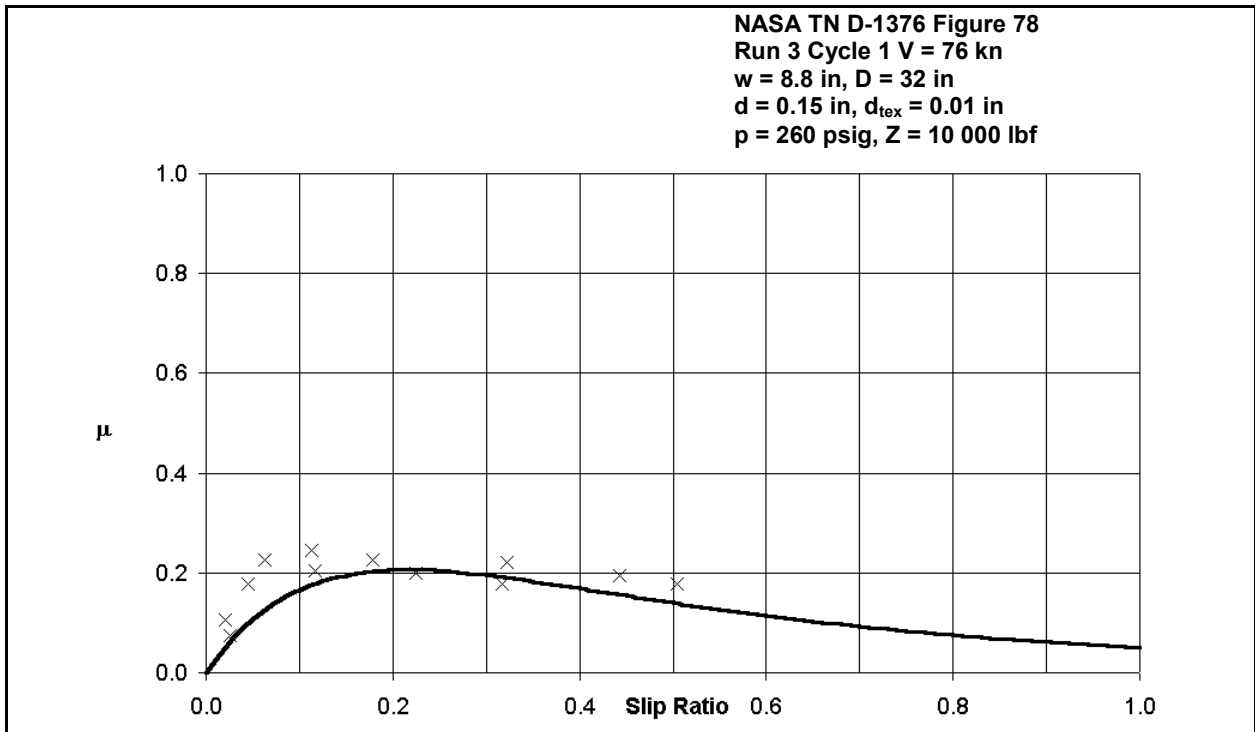
Figure 11.33: Effect of slip ratio on coefficient of braking friction on wet runway (Reference 7, Figure 78 – Run 3, Cycle 1)
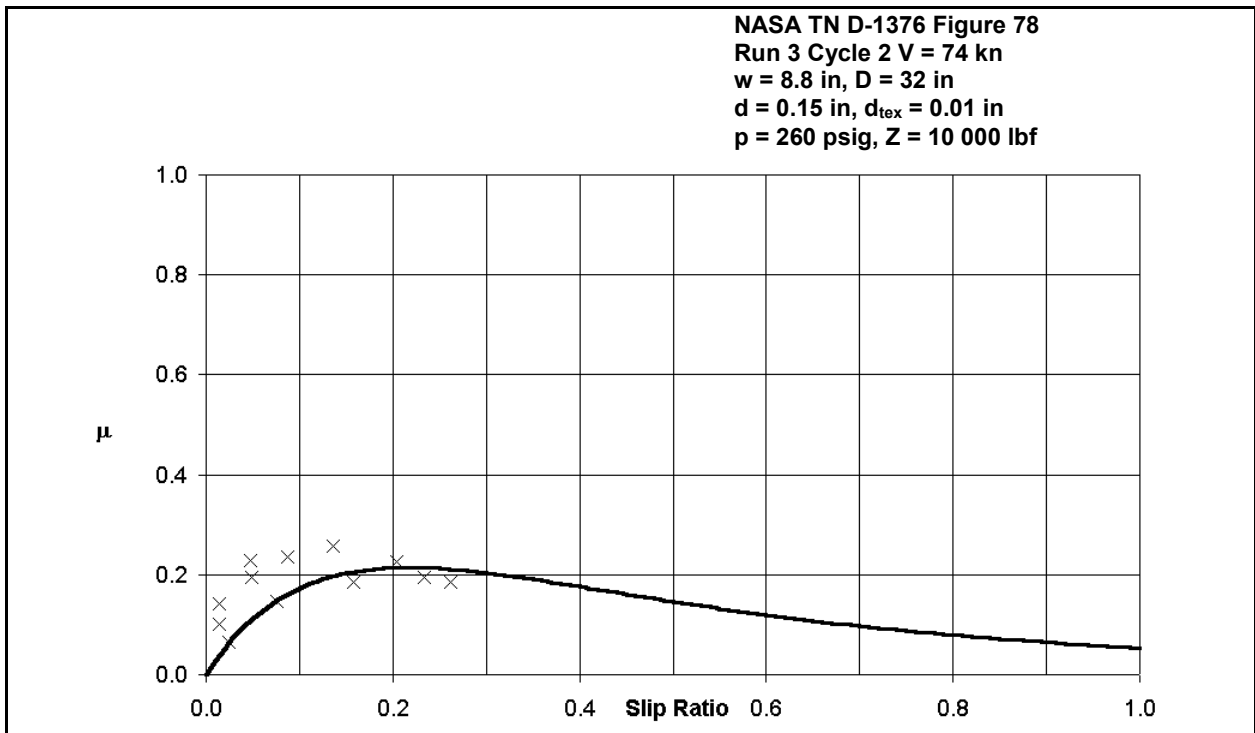
Figure 11.34: Effect of slip ratio on coefficient of braking friction on wet runway (Reference 7, Figure 78 – Run 3, Cycle 2)
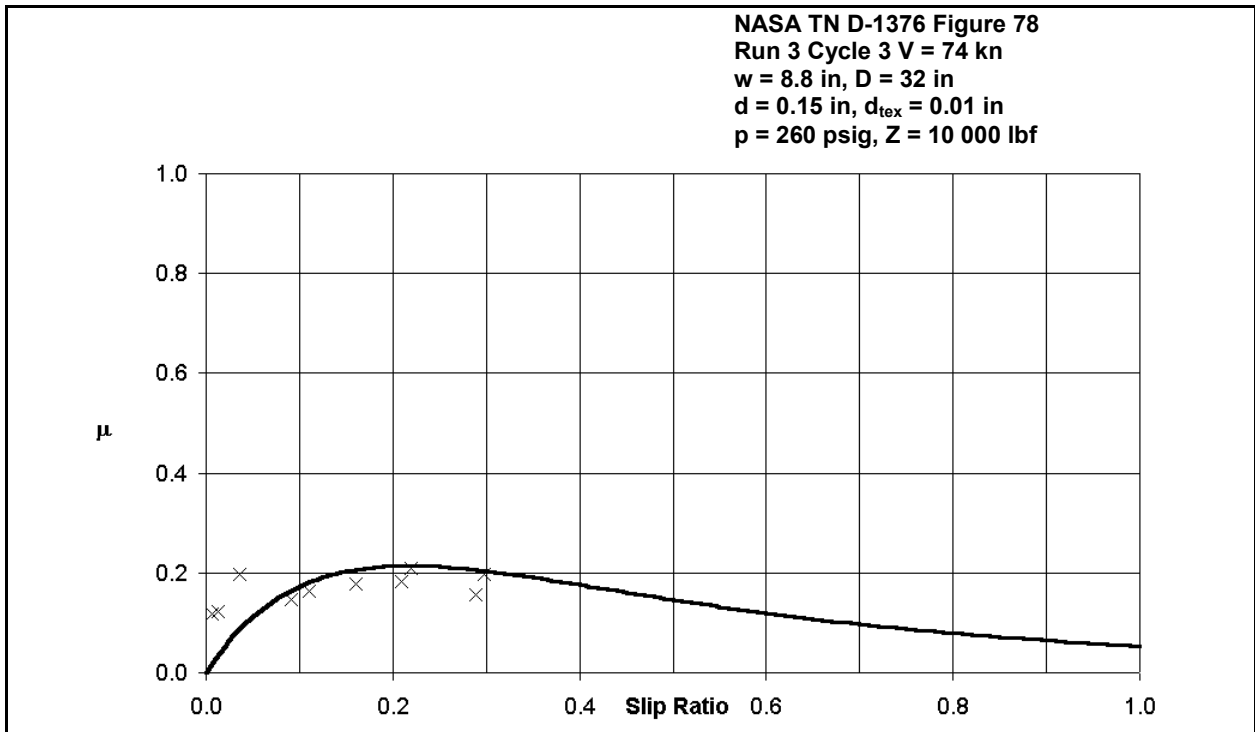
Figure 11.35: Effect of slip ratio on coefficient of braking friction on wet runway (Reference 7, Figure 78 − Run 3, Cycle 3)
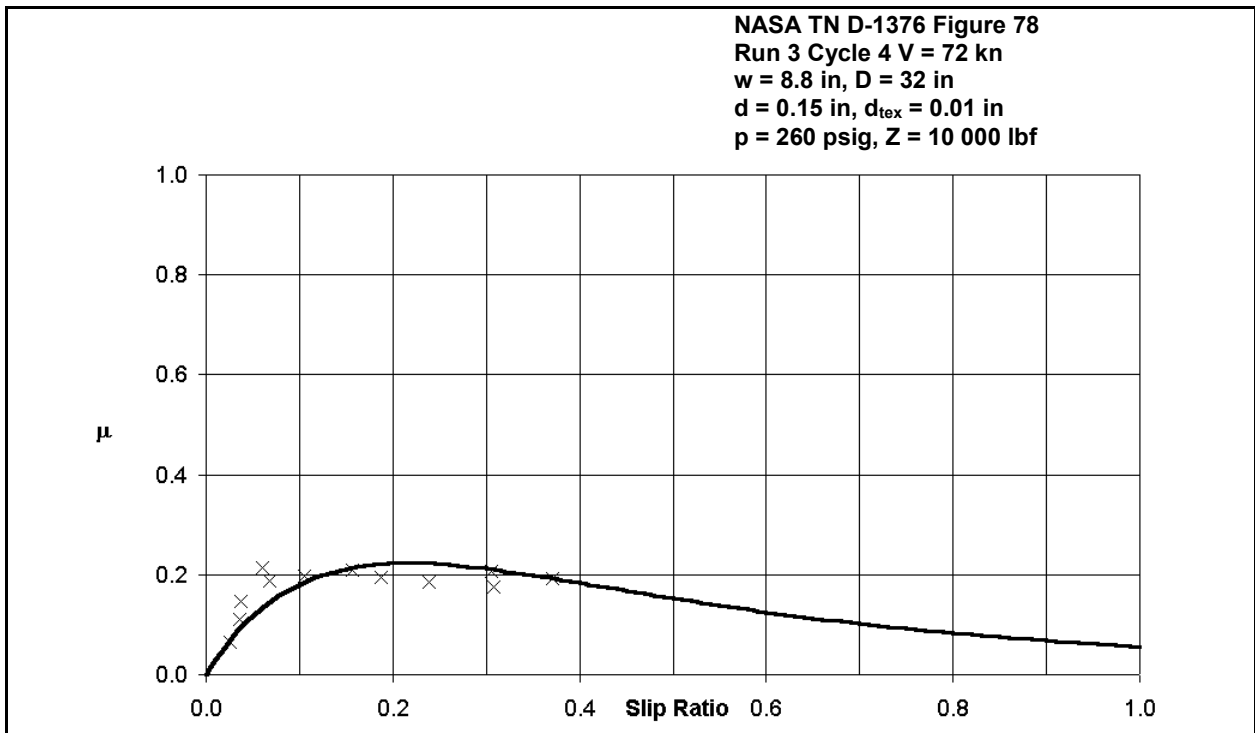
Figure 11.36: Effect of slip ratio on coefficient of braking friction on wet runway (Reference 7, Figure 78 − Run 3, Cycle 4)

149

NASA TN D-1376 Figure 78
Run 3 Cycle 5 V = 70 kn
w = 8.8 in, D = 32 in
d = 0.15 in, d_{tex} = 0.01 in
p = 260 psig, Z = 10 000 lbf
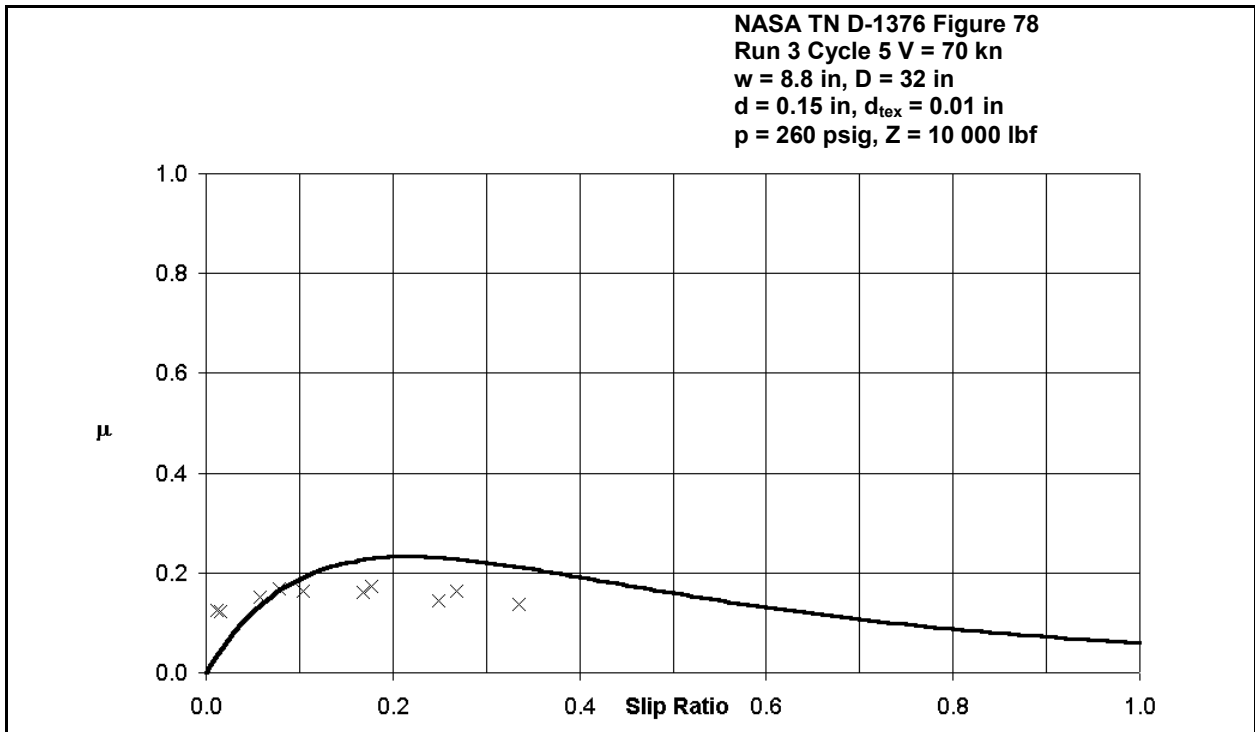
Figure 11.37: Effect of slip ratio on coefficient of braking friction on wet runway
(Reference 7, Figure 78 – Run 3, Cycle 5)

NASA TN D-1376 Figure 78
Run 3 Cycle 6 V = 69 kn
w = 8.8 in, D = 32 in
d = 0.15 in, d_{tex} = 0.01 in
p = 260 psig, Z = 10 000 lbf
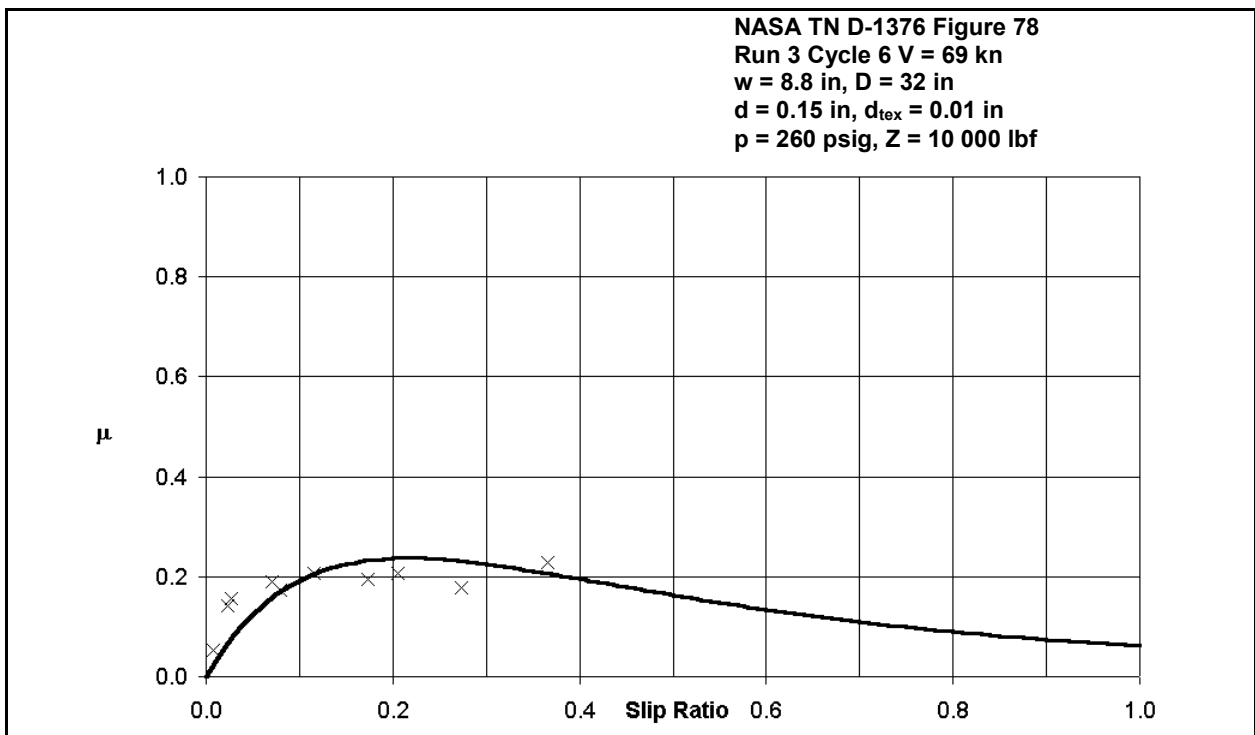
Figure 11.38: Effect of slip ratio on coefficient of braking friction on wet runway
(Reference 7, Figure 78 – Run 3, Cycle 6)

150
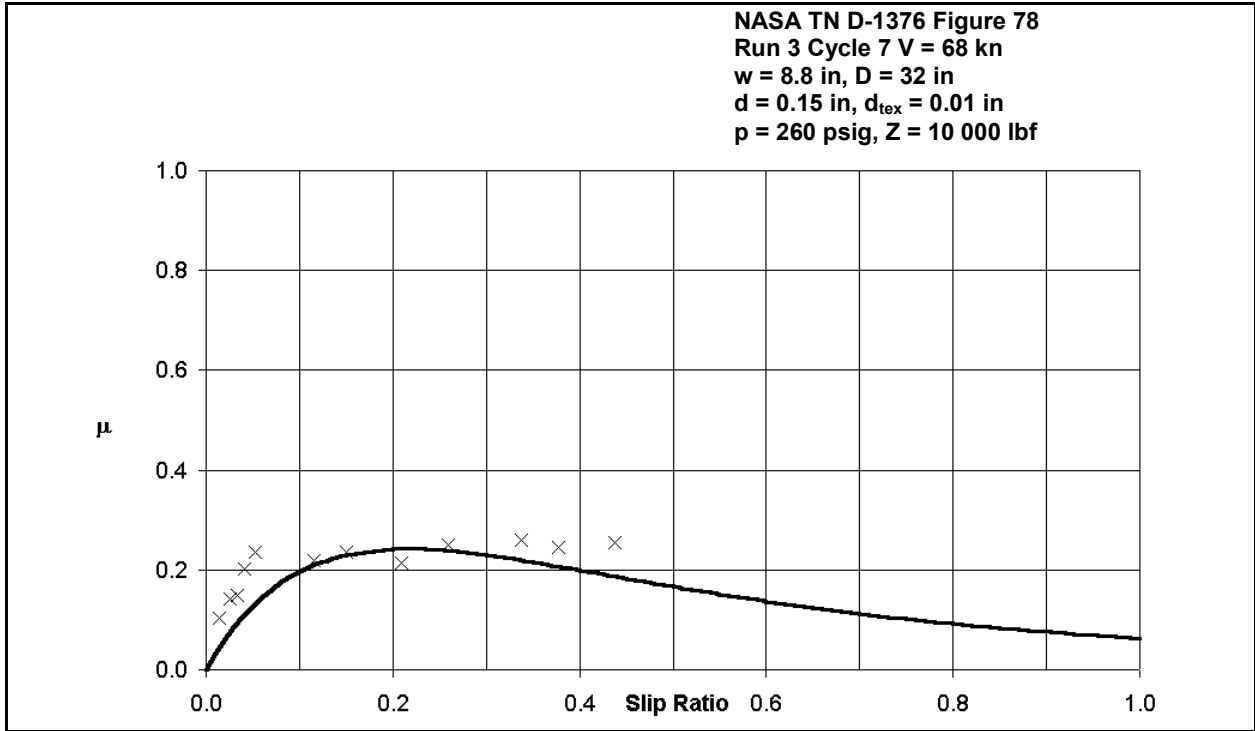
Figure 11.39: Effect of slip ratio on coefficient of braking friction on wet runway
(Reference 7, Figure 78 − Run 3, Cycle 7)
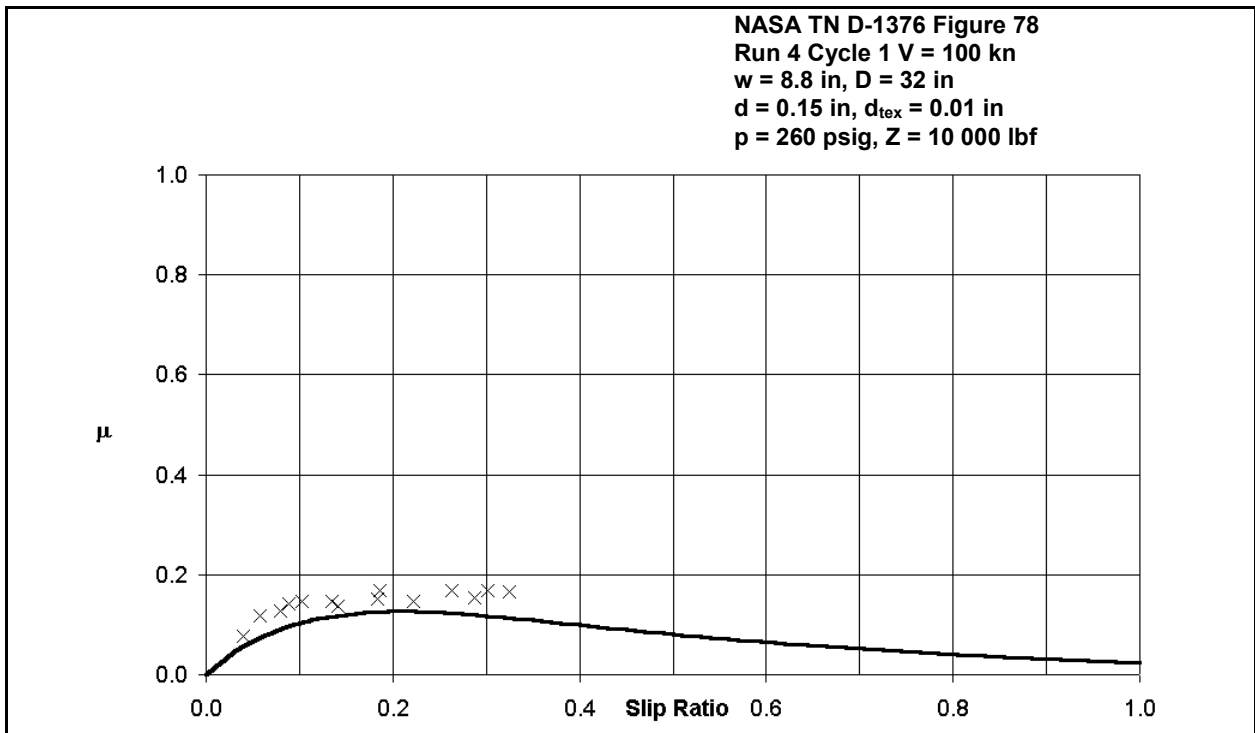
Figure 11.40: Effect of slip ratio on coefficient of braking friction on wet runway
(Reference 7, Figure 78 − Run 4, Cycle 1)

151
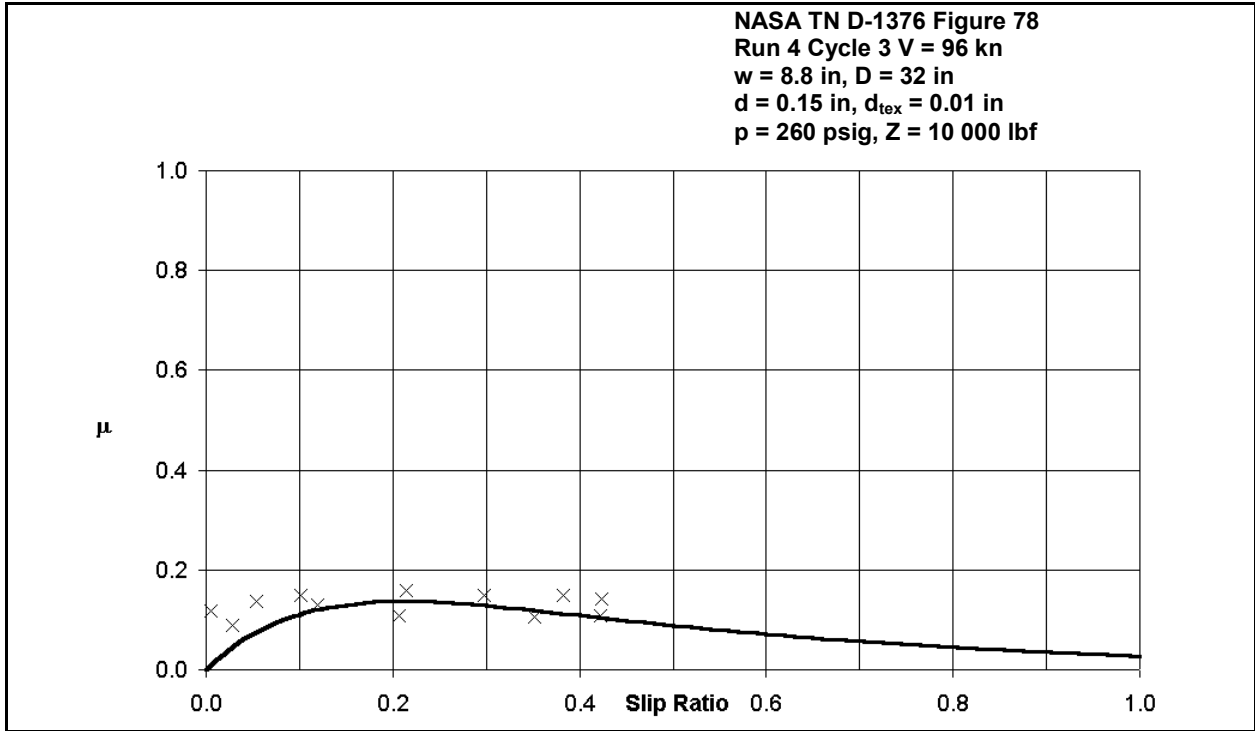
**Figure 11.41: Effect of slip ratio on coefficient of braking friction on wet runway
(Reference 7, Figure 78 − Run 4, Cycle 3)**
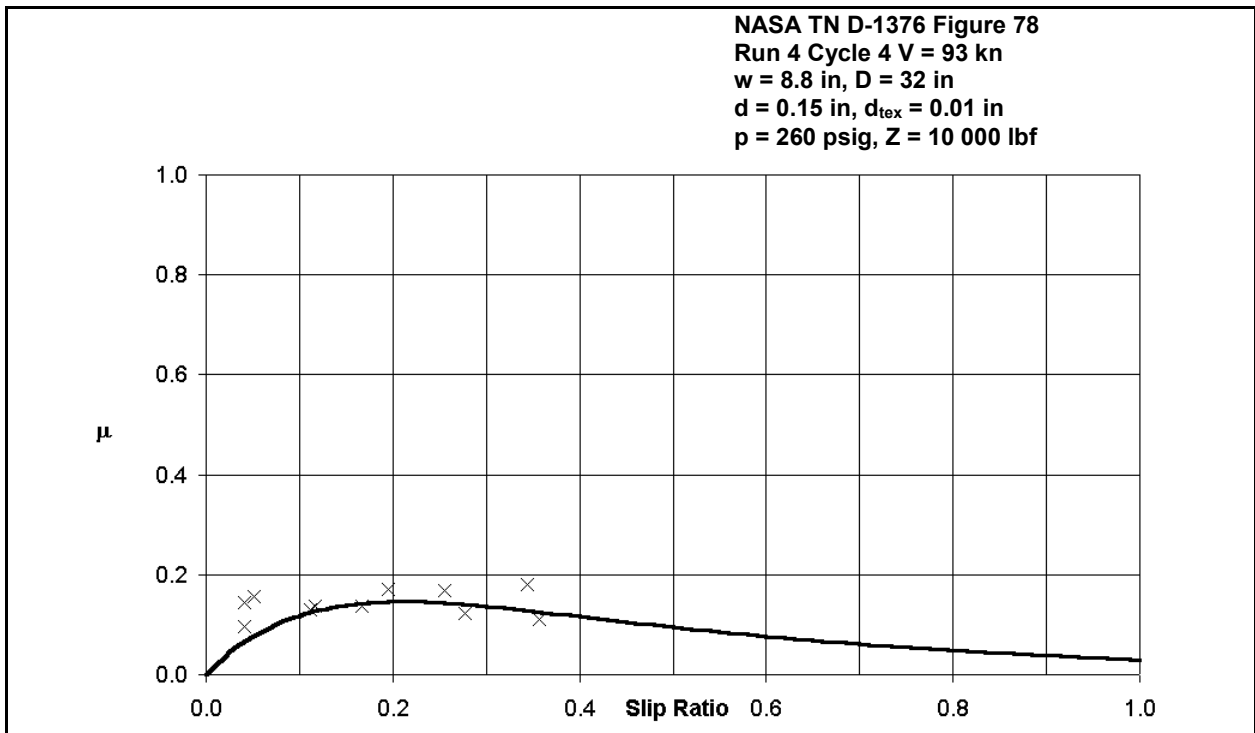
**Figure 11.42: Effect of slip ratio on coefficient of braking friction on wet runway
(Reference 7, Figure 78 − Run 4, Cycle 4)**
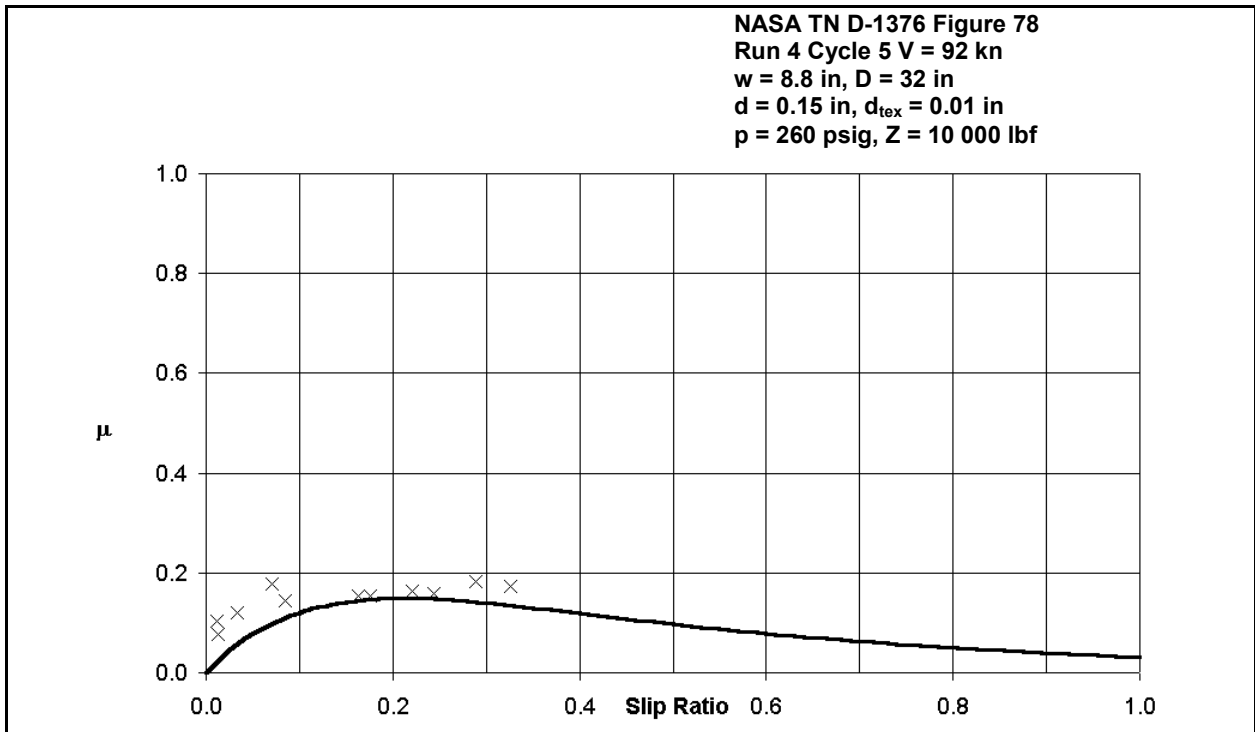
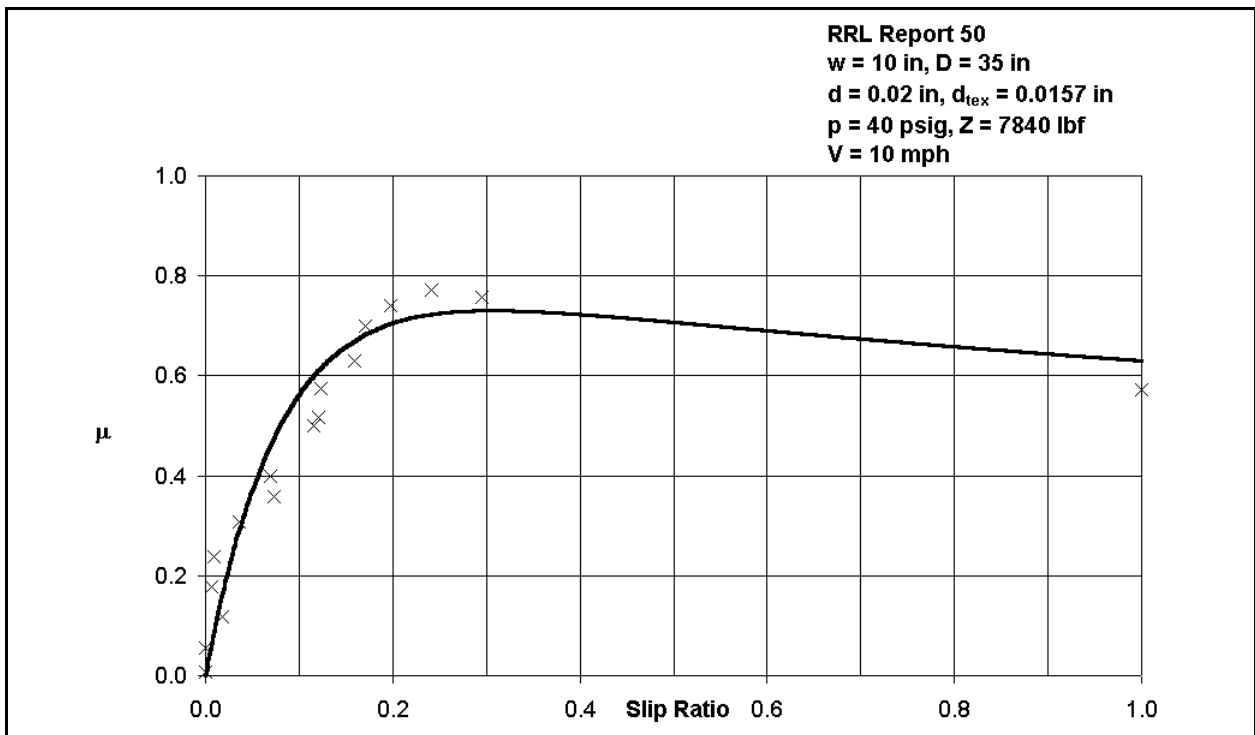**Figure 11.43: Effect of slip ratio on coefficient of braking friction on wet runway
(Reference 7, Figure 78 – Run 4, Cycle 5)**
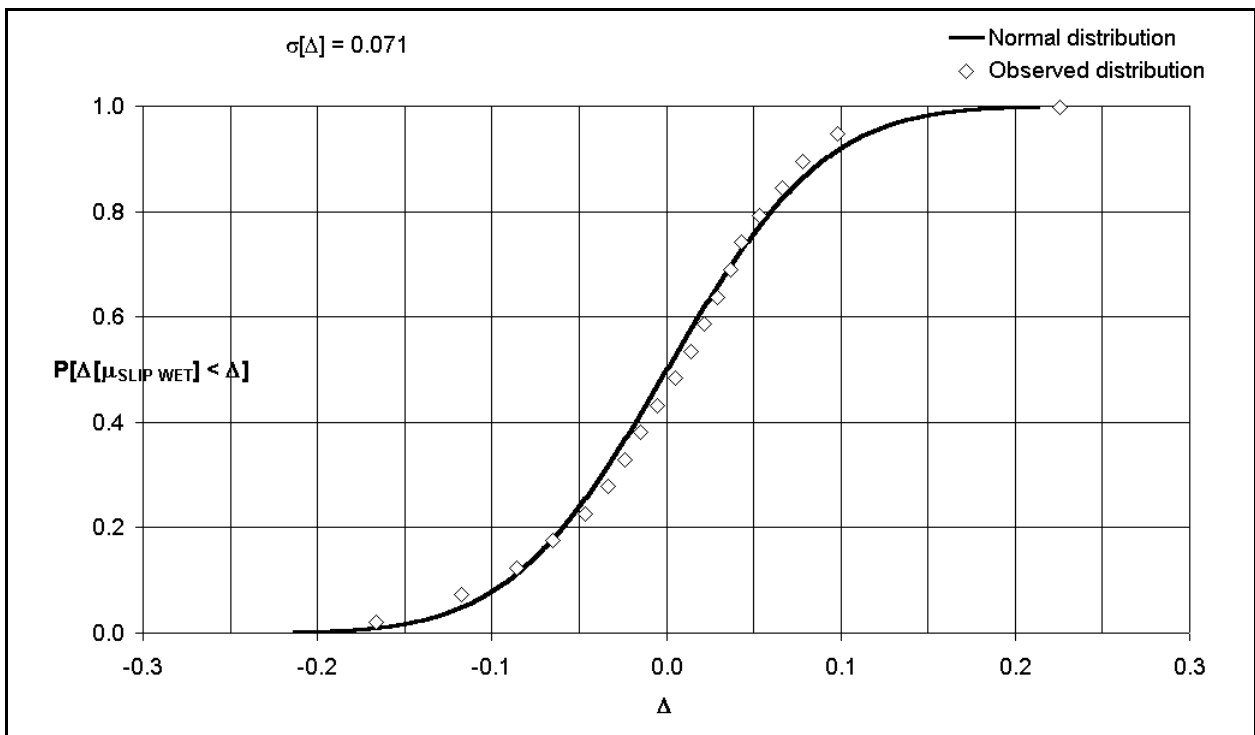

Figure 11.44: Distribution of deviations of experimental data from model
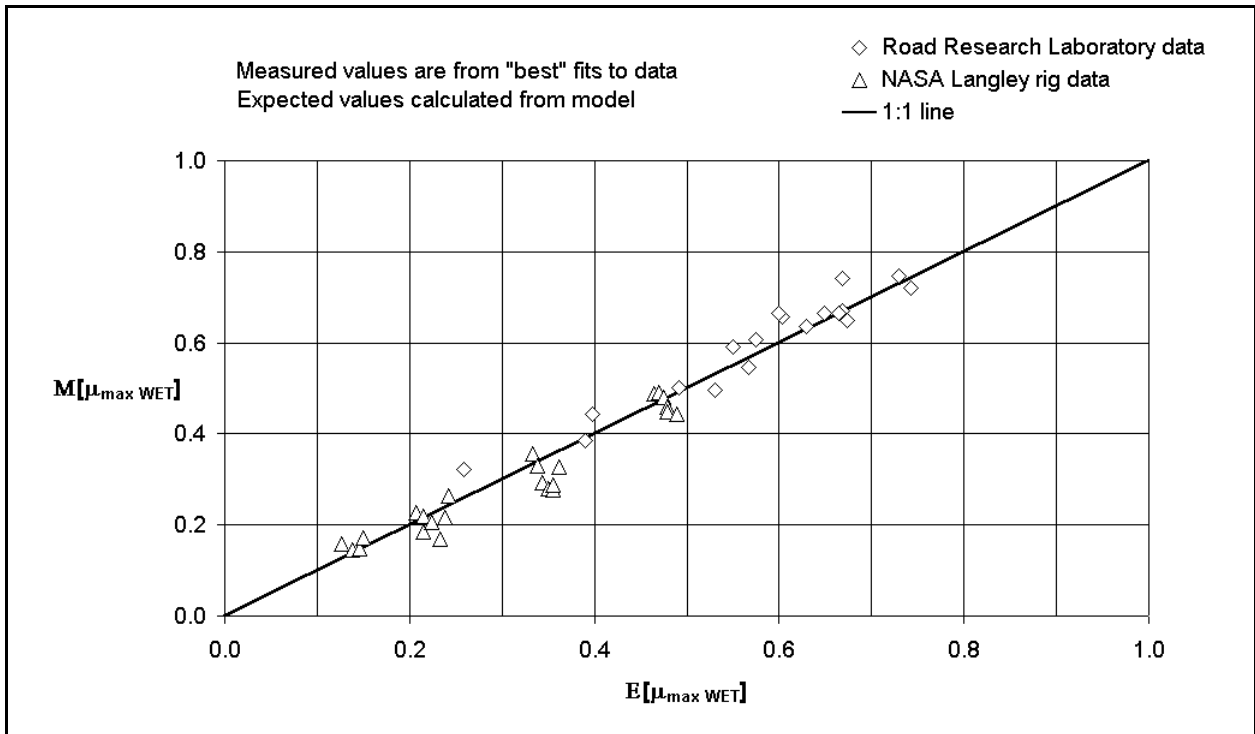
Figure 11.45: Comparison of estimates and experimental values of $\mu_{MAX\ WET}$
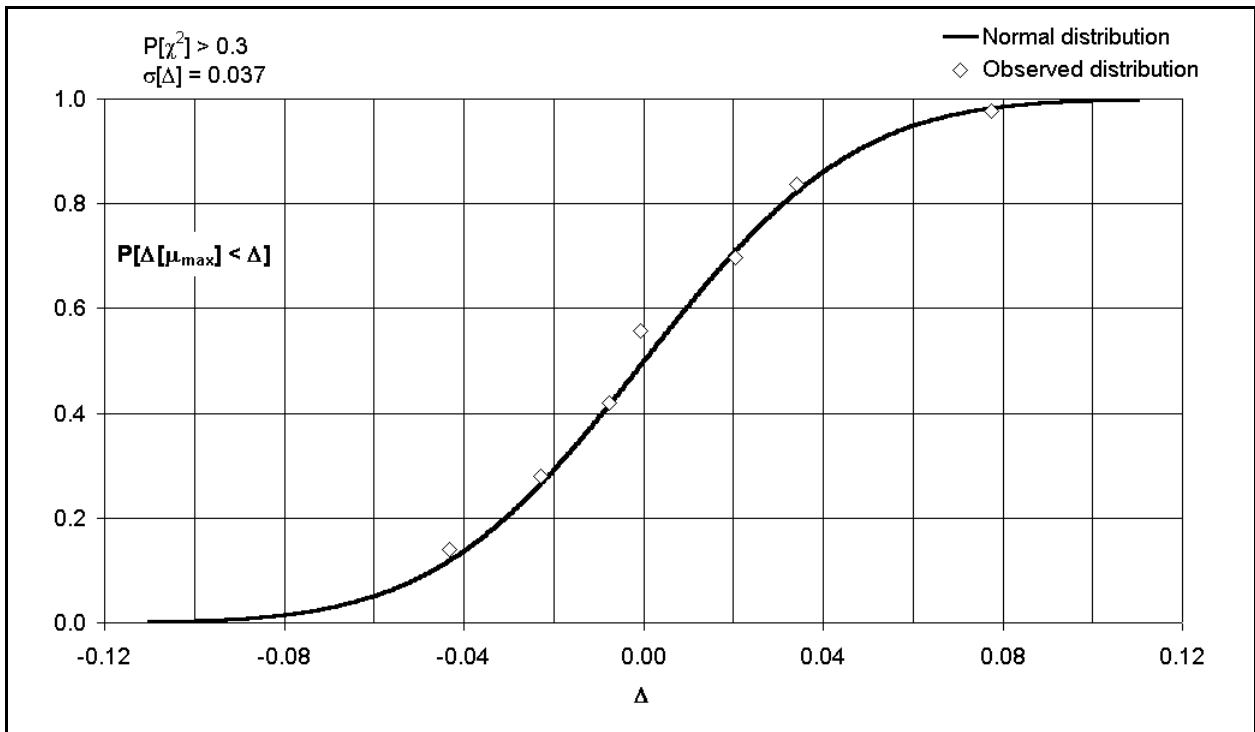
Figure 11.46: Distribution of difference between estimates and experimental values of $\mu_{MAX\ WET}$

154

12.   ROLLING AND BRAKING ON ICE AND SNOW

For the construction of an empirical, mathematical model, it is assumed that the frictional interaction between rubber and ice is no different, in principle, from the interaction of rubber and dry runways. Fundamental to this process is the assumption that there exists a reference coefficient of friction between rubber (or tyre compound) and ice. Effects of inflation pressure, vertical loading, speed and slip ratio are assumed exactly analogous to those that are used in the case of dry and wet runways.

However, both experimental data and anecdotal evidence show that there is a difference between the friction *coefficients* on ice and those on the surface of a standard runway. The difference arises from the physical properties of ice: a brief description of these is quoted. Furthermore, these physical properties also give rise to a weak, but identifiable, dependence of friction coefficient on the temperature of the iced surface. Information from laboratory experiments using rubber blocks sliding over ice has been used to create an empirical framework that describes this variation. However, ground temperature was not monitored for much of the experimental data considered here. It is therefore not feasible to do other than describe, statistically, the inferred values of reference coefficient of friction.

Experimental evidence suggests that there are at least three classes of winter-contaminated runway to be allowed for when considering coefficients of braking friction. By far the smaller of these bodies of data collected to enable the building of a model is for operation on *glazed* ice. Only three values of reference coefficient of friction have been calculated. However, sets of data have been assembled from experiments on various surfaces described as "loose snow" and "compressed snow and ice". These two groupings are sufficiently large to enable a simple statistical treatment.

The mathematical model developed here has the effect of unifying results from experiments that have been conducted over several decades on aircraft fitted with braking systems of varied sophistication. Two types of aircraft were fitted with on/off systems, whilst the other three types that were studied were fitted with adaptive systems. Whilst the systems *per se* were not modelled, the effect of each system has been accounted by way of the slip ratio. In the earliest case, maximum coefficient of friction was monitored as a function of speed. Given that the model can be interrogated for μ_{MAX}, it is a simple task to iterate for μ_{REF}. In all other cases, the braking system was accounted by introducing the concept of an *average* coefficient[33] of braking friction or by inferring an operative slip ratio from braking tests on a dry runway.

Within the body of data collected to establish the empirical model, two sets contained sufficient information to enable a comparison to be made between accelerometer readings taken from tests on an automobile in a full skid and the reference coefficient of friction obtained from modelling aircraft behaviour. Although this study is presented in Appendix C, the results are sufficiently promising to merit an investigation in greater depth should appropriate data be forthcoming from other ground vehicles.

---

[33] A similar concept was used by NASA in various publications; however, the limits of slip ratio used by NASA were applicable only to the rig at Langley where slip ratio was closely monitored.

12.1 Physical Structure of Ice

The following description relates to *glazed* ice and is quoted almost *verbatim* from Reference 40.

"Ice can be described as having an open prismatic structure, being composed of an agglomerate of interlocking crystals. These crystals characteristically are coated with a thin film of liquid water at temperatures even below their melting point. The layer provides a transition from the rigid structure of the bulk of the crystal to that of water and has a thickness of several hundred molecules.

The existence of a thin liquid film on ice gives rise to the well-known phenomenon of **regelation**.[34] Since the volume of ice is greater than that of the water from which it is made, the application of the smallest pressure to an ice crystal produces melting. Thus, load support for a tyre or ski sliding at low speed on ice is provided across a thin liquid-film, so that the resulting friction is remarkably low. When the sliding body passes on, the film freezes because of the minute expansion accompanying the release of pressure. Experience shows that the friction of both snow and ice increases as the ambient temperature drops, and this is well explained by the increased difficulty in melting at the lower temperatures. At higher sliding speeds, frictional melting assists the pressure melting mechanism in establishing the liquid layer.

Care must be exercised in distinguishing between liquid layers existing between individual ice crystals and those existing at an ice-solid boundary. Thus, regelation at a solid boundary has been described in the previous paragraph in association with pressure melting. Regelation between individual ice crystals is brought about by a crystallization of surface films under the action of compressive loading. It is a remarkable fact that while melting of ice crystals occurs at an external boundary when load is applied, the reverse process of regelation takes place simultaneously between individual internal crystals. Thus, melting and freezing occur simultaneously at different interfaces. Furthermore, internal regelation accompanies the loading phase and external regelation the subsequent unloading phase. A satisfactory explanation of these apparently contradictory phenomena has not yet evolved, but the explanation must lie in the nature of the liquid films on individual ice crystals and at solid boundaries.

Thus, in the latter case there is a gradual transition across the film between two extreme molecular structures corresponding to pure ice and pure water respectively. It is certain that between individual ice crystals the variation in film properties is substantially less. In both cases, the structure of the liquid film cannot be described in terms of self-repeating elementary cells. Consequently, there is no sharply defined melting point, and in the case of ice-solid boundaries, the film thickness decreases gradually with decreasing temperature rather than making an abrupt disappearance.

Apart from wide variations in the properties of surface films on ice, investigators have from time to time claimed different forms of crystallographic symmetry within the ice itself. Thus, octahedra, tetrahedra and triangular prisms have been proposed as typical molecular geometry within the lattice structure of an ice crystal. Exact reproducibility of results from friction

---

[34] Process by which ice melts when subjected to pressure and freezes again when the pressure is removed.

experiments is extremely difficult to obtain because of the complex structure of ice itself and the wide variation in shear strength across the surface film."

From the sets of data in sub-sections 12.3.3 to 12.3.7, three classes of ice have been identified that may be encountered when operating on contaminated runways at low temperatures. Because the study presented is empirical, it is not necessary to accept any of the physical interpretations. It is convenient, however, to believe that the phenomenon of regelation occurs in all cases involving ice or the compression of snow. Thus, a similar empirical model can be used to describe coefficients of braking friction on all winter-contaminated runways. It may be, of course, that the presence of snow inhibits regelation; such an effect would explain the variations between and within the identified classes.

12.2 Modelling

Modelling equations are based on the concepts introduced in Sections 6, 7 and 8 for dry runways.

$$\mu_{SLIP\ ICE} = \frac{\mu_{REF\ ICE_i}\left(1-e^{\eta_2 s}\right)}{\left(1+\left(\eta_0+\eta_1\dfrac{v^2}{2g}\right)\dfrac{p/p_a}{Z^{1/3}}\right)} \qquad\qquad 12.1$$

where

$$\mu_{REF\ ICE_i} = \mathrm{E}\left[\mu_{REF\ ICE_i}\right] + z\sigma\left[\mu_{REF\ ICE_i}\right] : i = 1,2 \qquad\qquad 12.2$$

and

$$\mu_{REF\ ICE_i} = 0.25\hat{T}^{1/2}\left(1-0.8\hat{T}\right) : i = 3 \qquad\qquad 12.3$$

and $i = 1$ is loose snow; $i = 2$ is ice and compressed snow; $i = 3$ is glazed ice. The parameter z is the percentage point in the normal distribution at the chosen level of probability. Transformed temperature is given by:

$$\hat{T} = 1 + \frac{T}{50} \qquad\qquad 12.4$$

where T is measured on the Celsius scale.

In some of the cases where measurements were made in operations on compacted snow, temperature was recorded. In that case, a correlation with temperature has been identified as

$$\mu_{REF\ ICE_i} = 0.8\hat{T}^{1/2}\left(1-0.8\hat{T}\right) : i = 2 \qquad\qquad 12.5$$

It is not possible to identify a correlation with temperature in the case of loose snow.

12.3 Discussion

12.3.1 Friction Coefficient for Rubber Sliding on Ice

Data for the master curve of a natural rubber gum sliding on ice are shown in Figure 12.1. These data were given in Reference 41. The curve fitted to the data is quite arbitrary. It has been devised solely to enable a similar curve to be fitted to data from tyre tests. However, the form of the curve is

$$\mu_{REF\ ICE} = 8.2\hat{T}^{1/2}\left(1 - 0.8\hat{T}\right) \qquad\qquad 12.6$$

The curve fit of Equation 12.6 was found so that the distribution of data about the fitted curve was normal. This distribution is shown in Figure 12.2. Furthermore, the standard error of that distribution was found to be $\sigma[\Delta[\mu]] = 0.315$. This value is not significantly different from that calculated for the measurements at $T = -35°C$. It is assumed that the format imposed on the data is transportable to other rubber compounds on ice.

12.3.2 Reference Friction Coefficient for Aircraft Tyres Sliding on Ice

Fourteen values of μ_{REF} have been obtained from tests reported in References 22, 42 and 43. The data are plotted in Figure 12.3. In the absence of evidence to the contrary, it has been assumed that μ_{REF} correlates with temperature in the same way as for the rubber compound considered in Reference 42. In these cases, Equations 12.3 and 12.5 apply.

A *t*-test has been used to show that the three cases for glazed ice are probably not from the same distribution as the eleven cases from tests on compressed snow. This is an obvious conclusion that can be drawn from inspection of the plots in Figure 12.3.

However, the temperature of the ground cover has not been consistently published in the tests considered here. In order to make as much use as is possible of the data, the reference coefficient of friction on loose snow and on compacted snow with ice have been studied statistically. There are twelve measurements of $\mu_{REF\ ICE_1}$ and twenty-one measurements of $\mu_{REF\ ICE_2}$. The distributions of both these quantities are shown on Figure 12.4. The distributions share a common standard deviation so that $\sigma\left[\mu_{REF\ ICE_1}\right] = \sigma\left[\mu_{REF\ ICE_2}\right] = 0.084$. Mean (or expected) values are $E\left[\mu_{REF\ ICE_1}\right] = 0.36$ and $E\left[\mu_{REF\ ICE_2}\right] = 0.25$. An Anderson-Darling test implies that the distributions are probably normal. It may be expected that conditions that are identifiable in these two categories will be represented by the expected (mean) values given with an uncertainty at the 95% level of significance so that $U\left[\mu_{REF\ ICE_1}\right]_{0.95} = U\left[\mu_{REF\ ICE_2}\right]_{0.95} = \pm0.165$.

12.3.3 Data from Reference 42 – NASA TR R-20

Data published in this reference were collected from tests on an instrumented C-123B aircraft. Braking runs were made with the application of ***maximum*** braking. Main wheel tyres were

158

inflated to 65 psig. All data were analysed to eliminate the effects of aerodynamic forces and moments. However, for the test runs of interest here, the maximum coefficient of friction during system cycling was recorded and plotted as a function of ground speed. These data are reproduced in Figures 12.5 and 12.6.

It is possible, using Equation 12.1 iteratively, to find a value for $\mu_{REF\ ICE}$ that enables the calculation of satisfactory values of μ_{max}. Results of the calculations are superimposed on the data in Figures 12.5 and 12.6. Speed histories of μ_{SKID} are also included for reference, although there are no measured data to confirm the calculations under these conditions.

12.3.4 Data from Reference 43 – NASA TN D-6098

Data published in this reference were collected using an instrumented C-141A aircraft. Braking runs were made with the application of **maximum** braking. All data were analysed to eliminate the effects of aerodynamic lift and drag. Tyre inflation pressure on the eight wheels of the main undercarriage was maintained at 110 psig throughout the whole of the testing. Presentation of friction data is in the form of line plots of friction coefficient against speed. Although it is not explicitly stated, it appears that the friction coefficient quoted is an instantaneous value. Thus, the effect of brake-system cycling is presumably masked by drawing a "mean" line through the speed history of friction coefficient. In these circumstances, it has been assumed that the antiskid system has been functioning normally as an on/off system. In that case, the value of friction coefficient at any speed is likely to be an *average* value. This is described as $\mu_{av(0,1)}$ and is defined as the slip-weighted average coefficient for $0 \leq s \leq 1$. That is:

$$\mu_{av(0,1)} = \frac{\int_0^1 \mu ds}{\int_0^1 ds} \qquad\qquad 12.7$$

The seven runs are plotted in Figures 12.7 to 12.13. Given that the model of Equation 12.1 has been used to deduce values of the reference coefficient of friction, the prediction of the effect of speed on braking coefficient for every case is encouraging evidence that the modelling philosophy is physically robust. Furthermore, the values presented are for a variable of considerable complexity. This leads to the conclusion that, even for a braking system of the on/off type, the concept of a reference coefficient of friction is of great utility. The relationship between reference coefficient of friction and Runway Condition Reading is considered in Appendix C.

12.3.5 Data from Reference 22 – NASA TP 2917

Information published in this reference was collected from tests on a Boeing 727 and a Boeing 737. Both aircraft were instrumented so that analysis could eliminate the effects of aerodynamic force and moments. Braking runs were made with the application of maximum braking. The tabulated data are reproduced as plots in Figures 12.14 to 12.26.

Figure 12.14 shows data from a maximum braking run for the Boeing 727. The dry runway modelling of Section 8 has been used to deduce that the adaptive braking system on this aircraft cycles between values of slip ratio so that $0.035 \le s \le 0.09$. It is therefore assumed that the registered coefficient of friction is an average so that

$$\mu_{av(0.035,0.09)} = \frac{\int_{0.035}^{0.09} \mu \, ds}{\int_{0.035}^{0.09} ds} \qquad 12.8$$

This value has been used in Equation 12.1 for each case to iterate for the reference coefficient of friction. As in the case of the C141A, there is sufficient evidence to suggest that the modelling philosophy is physically robust.

For the Boeing 737, the variation of slip ratio with speed has been deduced from a braked run on a dry runway as shown in Figure 12.22. It has been assumed that the braking system behaves on all types of contamination in the same way. Thus, the characteristic has been used in conjunction with Equation 12.1 to deduce values for the reference coefficient of friction. The four available runs are shown in Figures 12.23 to 12.26. Again, the model reflects the data in a convincing manner.

12.3.6 Data from References 14, 15 and 16 – Falcon 20

The data have been extracted from time histories of acceleration and speed from the references. In all cases, ground speed was compared to integrated accelerometer data, where necessary small adjustments – never greater than ± 0.01 – were made to the accelerometer readings to ensure a match between measured speed and that from the integrated accelerometer readings. In addition, after the integration check had been done, accelerometer data were smoothed using a simple exponential smoothing algorithm with a damping factor of 0.7. Although the speed traces were quite smooth, the same exponential smoothing was used for speed in order to account for the small phase shift that is introduced in the smoothing process.

Appropriate adjustments have been made to account for rolling friction, idling thrust, aerodynamic drag and aerodynamic lift. In particular, the methods of Section 5 have been used to account for the decelerating effect of loose snow. Measurements were also made of slip ratio and a mean variation with speed has been deduced. This mean variation has been used for all seventy runs on the eighteen flights that have been analysed. Data for each flight are shown in Figures 12.27 to 12.44.

Conditions for the first five flights considered are described as "loose snow". The modelling implies that the reference coefficient of friction varies so that $0.4 \le \mu_{REF\ ICE} \le 0.45$. There is some suggestion in the data either that the reference coefficient of friction varies from run to run within a flight or that the mean variation of slip ratio is not wholly appropriate for every case. However, the model is sufficiently representative of the measurements.

Flight 14 of the series conducted in 1996 is shown on Figures 12.32 and 12.33. The first plot is for four runs over compacted snow covered by thin ice. A reference coefficient of friction so that $\mu_{REF\ ICE} = 0.3$ provides a good estimate of the mean coefficient of braking friction for all four runs. Application of "double sand" results in the data of Figure 12.33. A value of reference coefficient of friction so that $\mu_{REF\ ICE} = 0.4$ provides a reasonable estimate of the measured mean coefficient of braking friction. The remainder of the flights in the 1996 series (Figures 12.34 to 12.36) are again for loose snow of varying depths. The range of values for reference coefficient of friction to provide a good estimate of braking friction is so that $0.35 \leq \mu_{REF\ ICE} \leq 0.48$.

The first flight considered in the 1997 series – bare and dry with occasional ice patches – is shown in Figure 12.37. A calculation is shown treating the runway as if it were bare and dry. This modelling is a good prediction of the measurements except for the sporadic excursion when, presumably, the aircraft encounters a patch of ice. This is another indication that the modelling is a good representation. Figures 12.38 and 12.39 show data for loose snow and are similar to the previous year's testing.

Flight 1 of the 1998 series was conducted on the runway covered with "some loose snow and ice patches"; the data are shown in Figure 12.40. In order to make a good estimate of the mean value of the coefficient of braking friction, a value of reference coefficient of friction so that $\mu_{REF\ ICE} = 0.75$ has been used.[35] This value is clearly related to the extent of the surface contamination, which was not recorded. The balance of the tests considered for this year was carried out on loose snow and are shown in Figures 12.41 to 12.44.

12.3.7 Data from Reference 44 – NASA TN D-4323

Two runs using the test rig at NASA Langley are shown in Figures 12.45 and 12.46. Ice temperature was not published in the reference. However, a value for $\mu_{REF\ ICE} = 0.11$ enables the prediction of the average braking coefficient from the model. It is not clear how these data fit in with other inferences concerning reference coefficient of friction. This is because the icy track was sprinkled with water prior to the passage of the tyre. Given the value of reference coefficient of friction, the effects of speed, inflation pressure and normal load are well predicted by the model. This is further confirmation that the modelling strategy is reliable.

12.4   Conclusions

Associating icy surface contaminants with a reference coefficient of friction enables the prediction of coefficient of braking friction throughout the speed range of all aircraft considered. This conclusion can be extended with confidence to all aircraft, whether the braking systems are of the modern, adaptive type or older, on/off systems.

Three ice-like contaminants have been identified. These are, in ascending order of skid resistance,

---

[35]   See Appendix C for discussion of the relation between James Braking Index and reference coefficient of friction. It is shown there that this value of reference coefficient of friction is predicted by the James Braking Index.

1. Glazed ice,
2. Compacted snow, and
3. Loose snow.

It is shown in Appendix C that the reference coefficient of friction between a runway contaminated with ice or snow can be predicted from the James Braking Index. The reference coefficient of friction can therefore be made the basis of a robust prediction system.
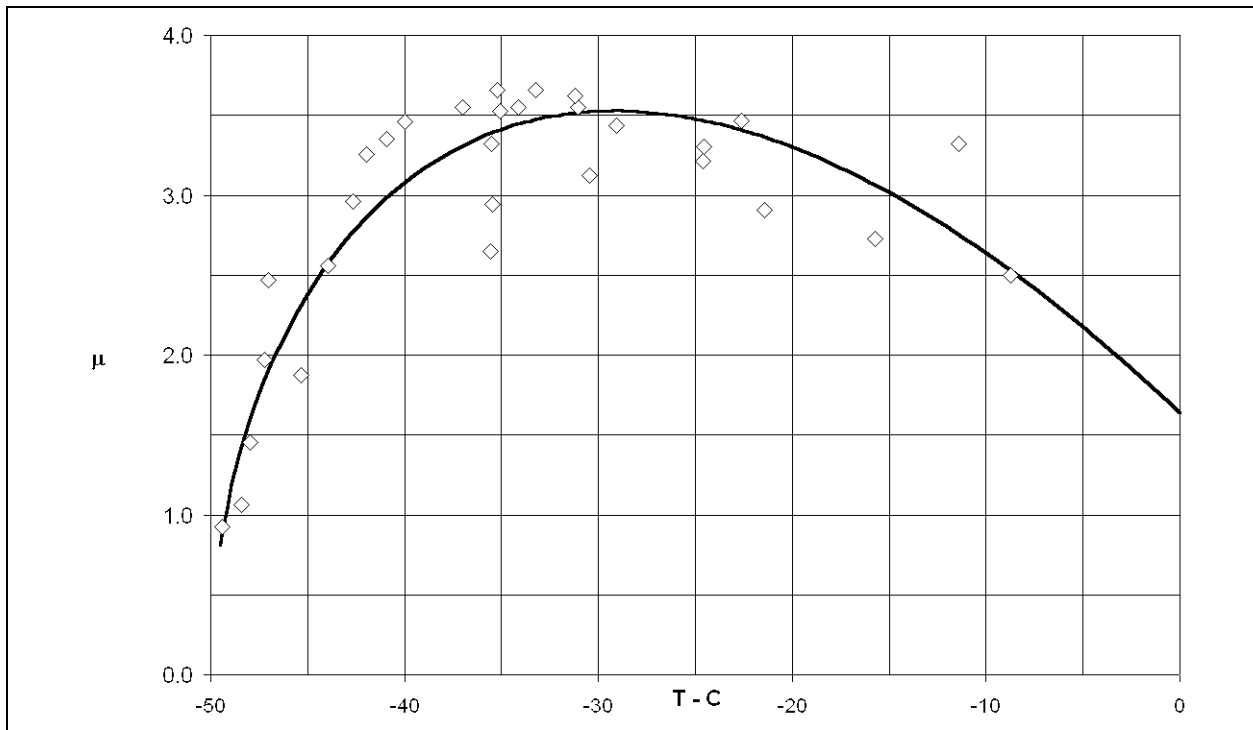
Figure 12.1: Effect of ground temperature on friction coefficient between natural rubber and ice
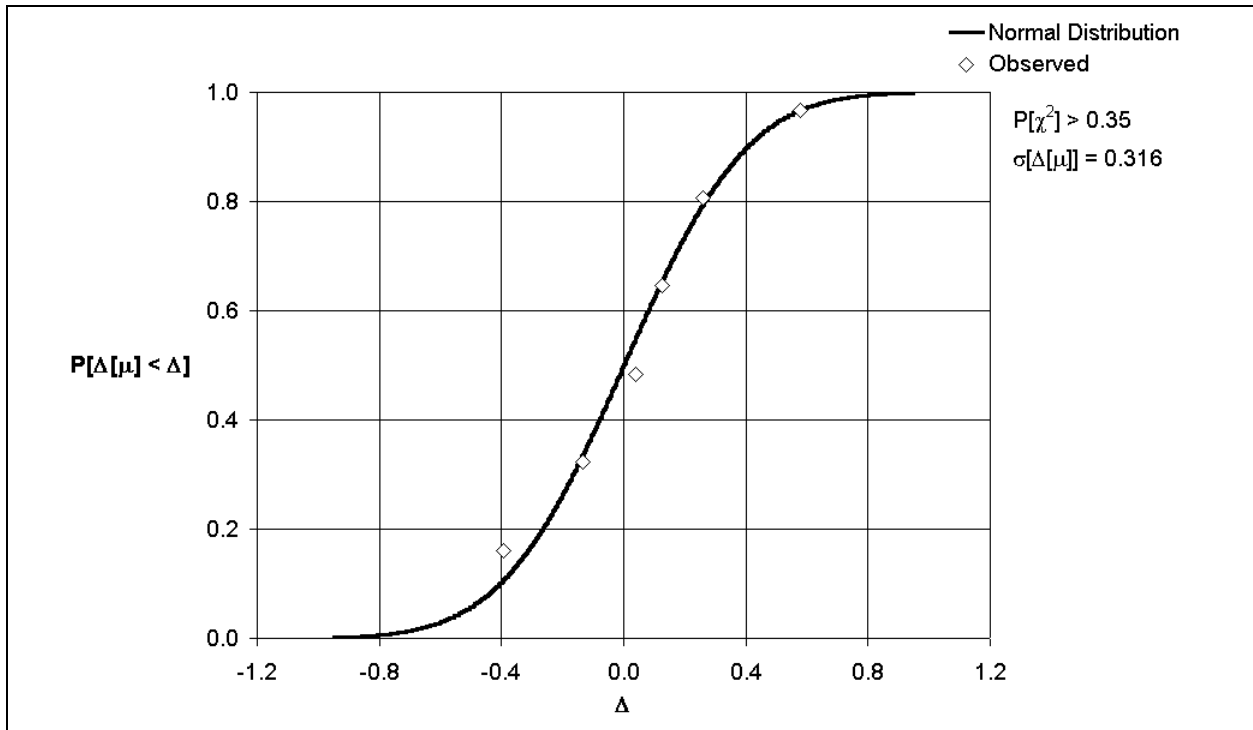
Figure 12.2: Distribution of measurements about correlation for natural rubber
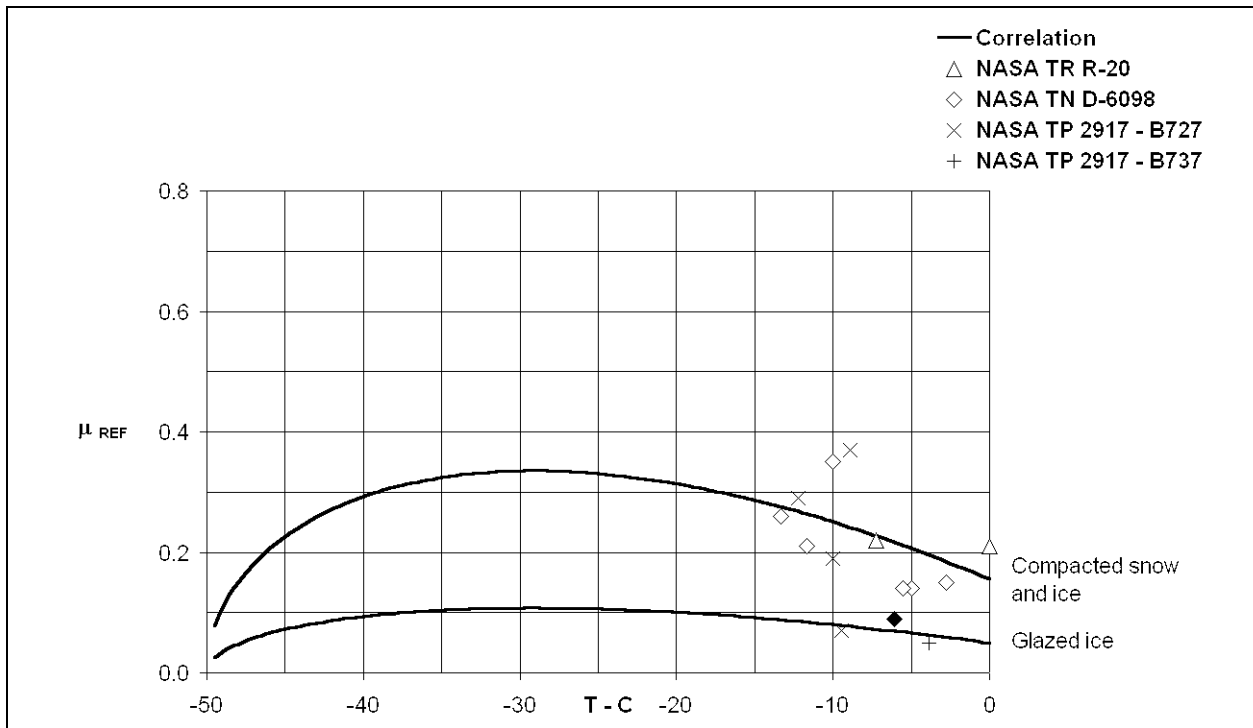
Figure 12.3: Effect of ground temperature on μ_{REF} for aircraft tyres on ice
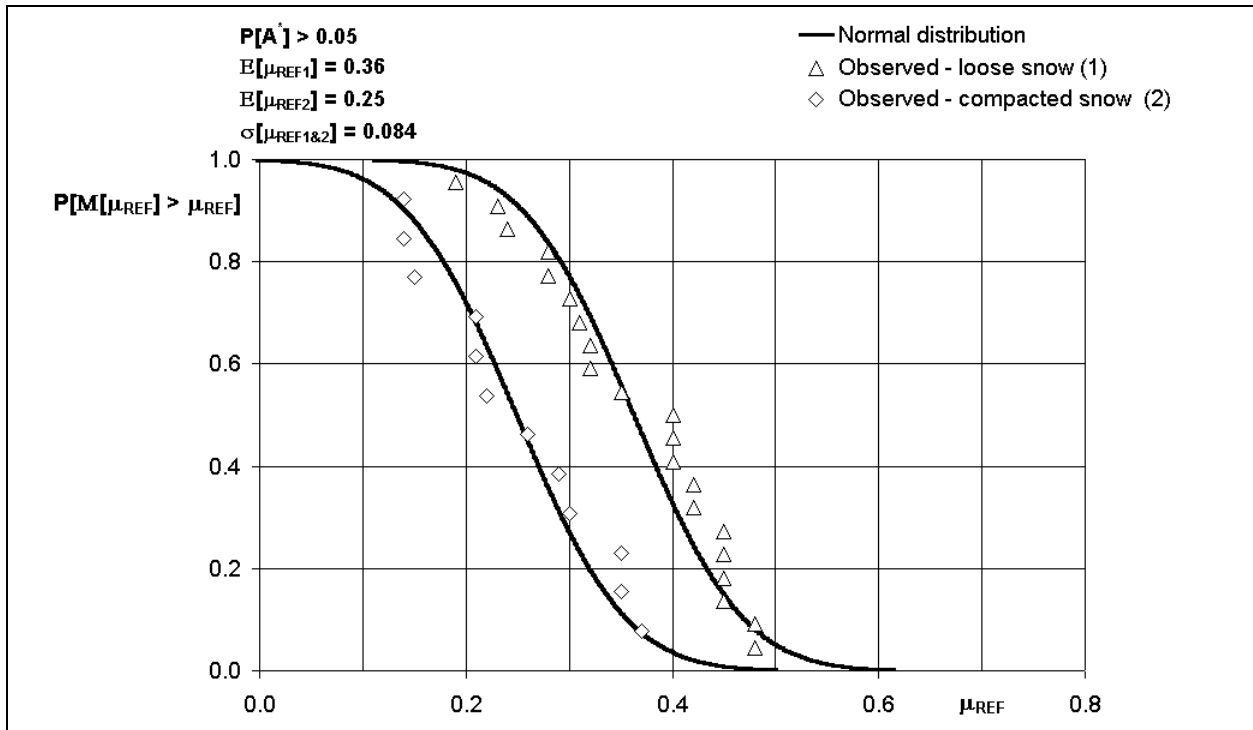
Figure 12.4: Distribution of observed values of μ_{REF} **for aircraft tyres on ice and snow**
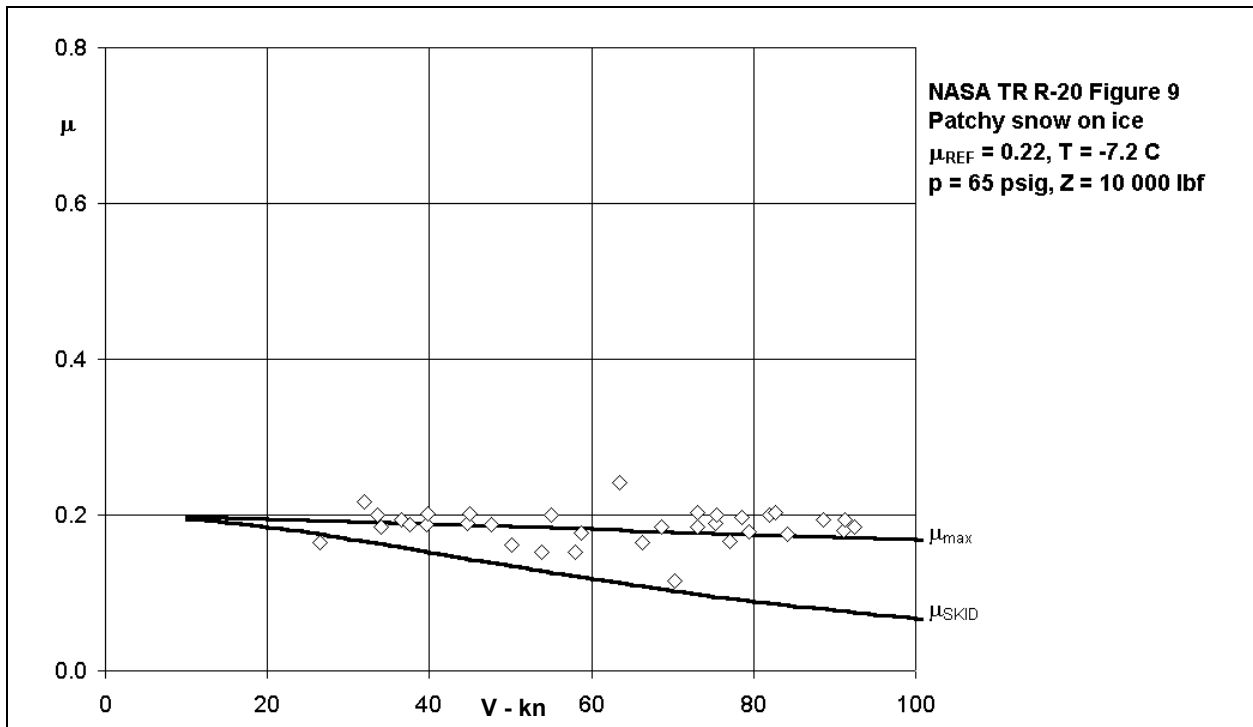
Figure 12.5: Effect of ground speed on μ_{max} **for C123B on ice and snow**

(μ_{REF} **= 0.22,** $T = -7.2$**°C)**
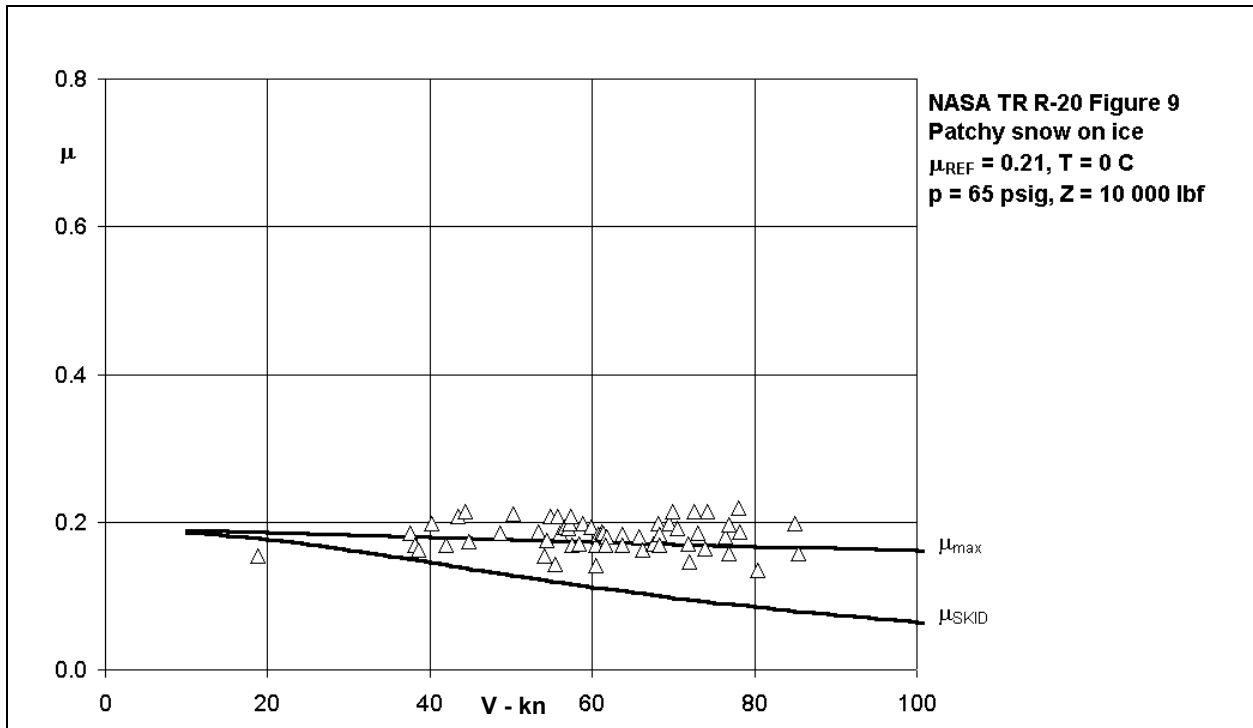
Figure 12.6: Effect of ground speed on μ_{max} for C123B on ice and snow

(μ_{REF} = 0.21, T = 0°C)
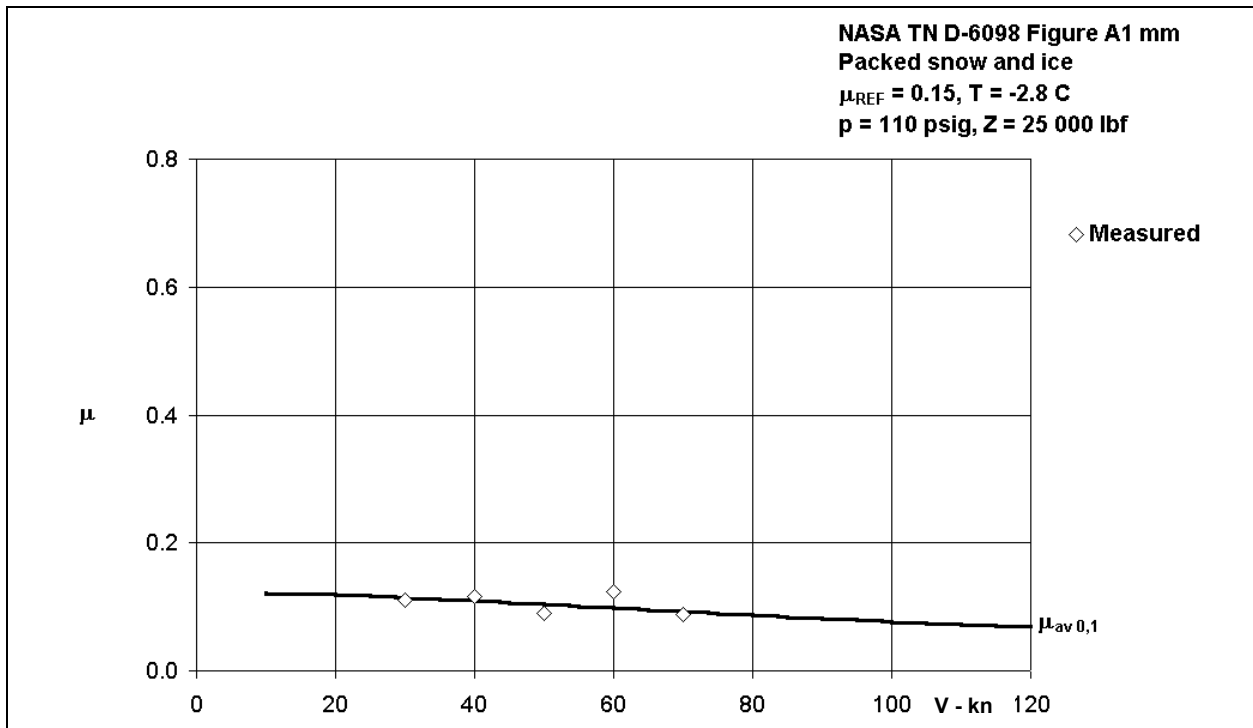
Figure 12.7: Effect of ground speed on μ_{max} for C141A on ice and snow – on/off system

(μ_{REF} = 0.15, T = –2.8°C)
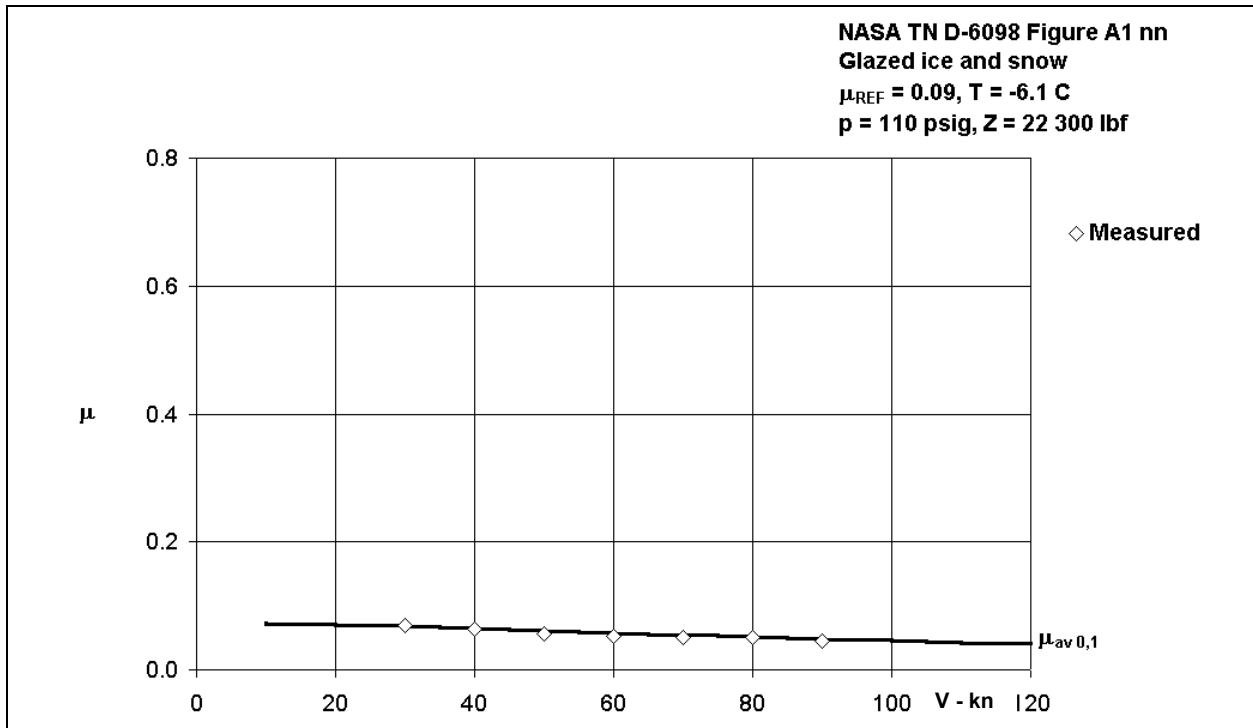
Figure 12.8: Effect of ground speed on μ_{max} for C141A on ice and snow – on/off system (μ_{REF} = 0.09, T = −6.1°C)
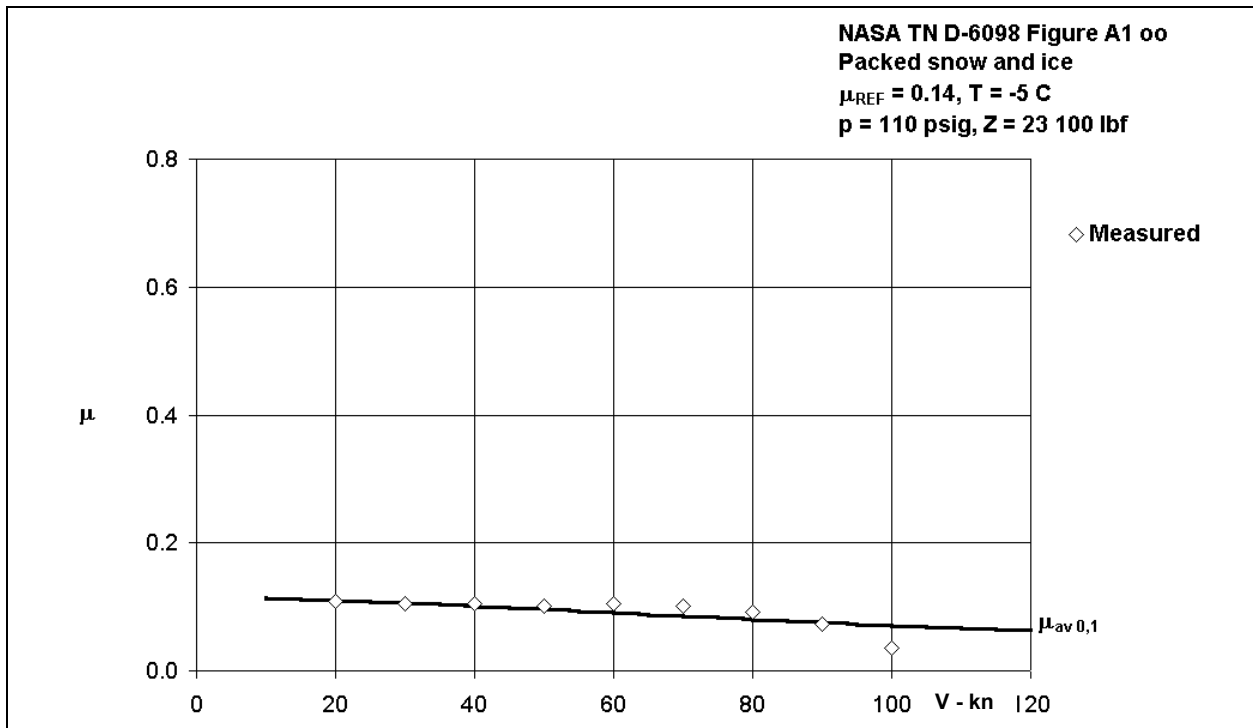
Figure 12.9: Braking friction coefficient for C141A on ice and snow – on/off system (Reference 43 Figure A1–oo)
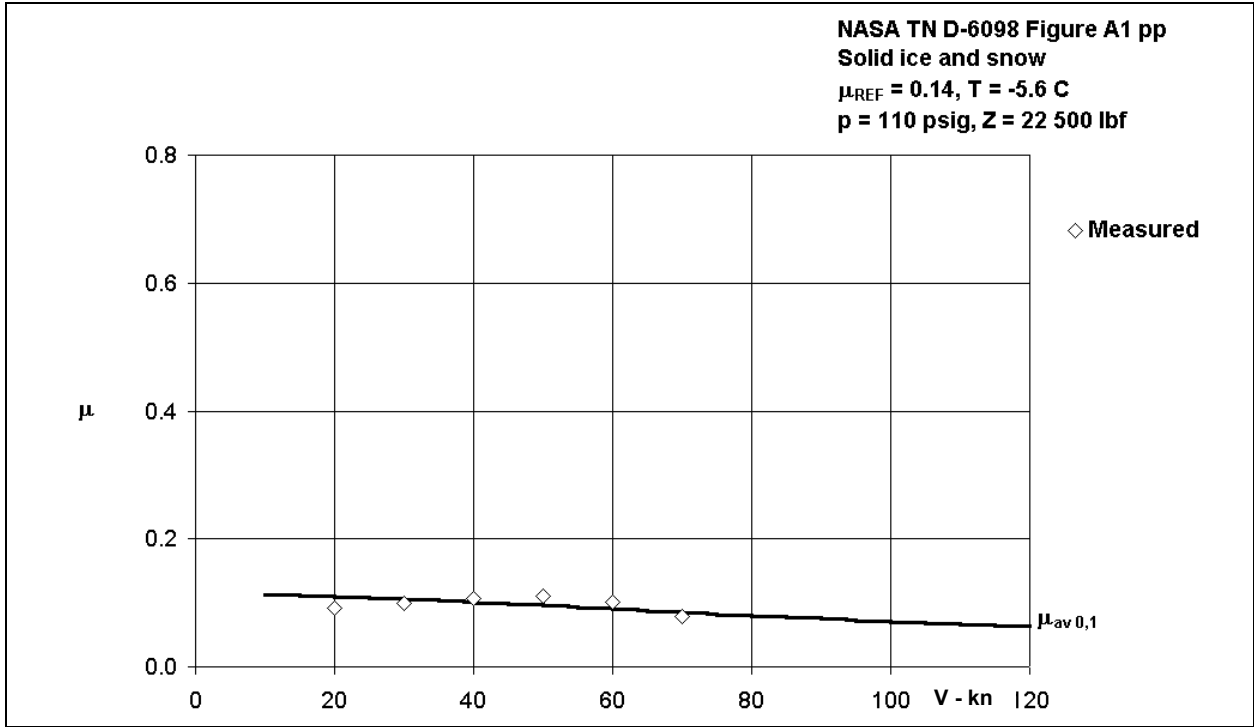
Figure 12.10: Braking friction coefficient for C141A on ice and snow – on/off system (Reference 43, Figure A1–pp)
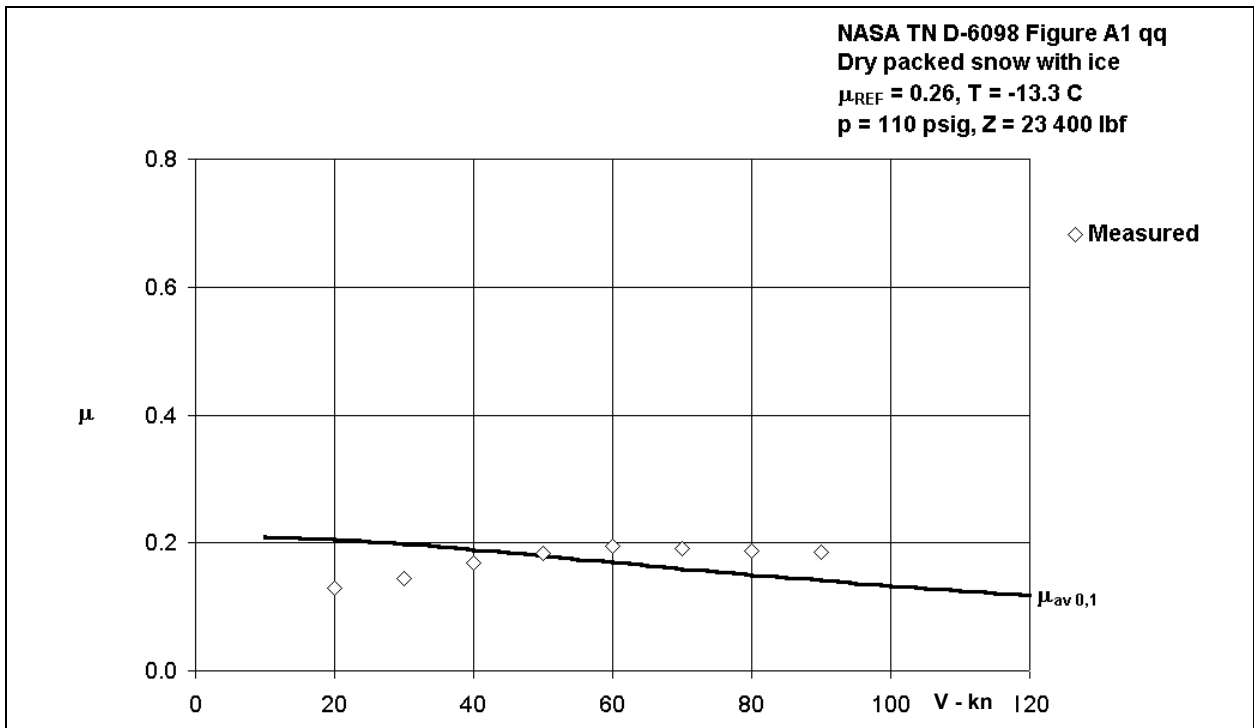
Figure 12.11: Braking friction coefficient for C141A on ice and snow – on/off system (Reference 43, Figure A1–qq)
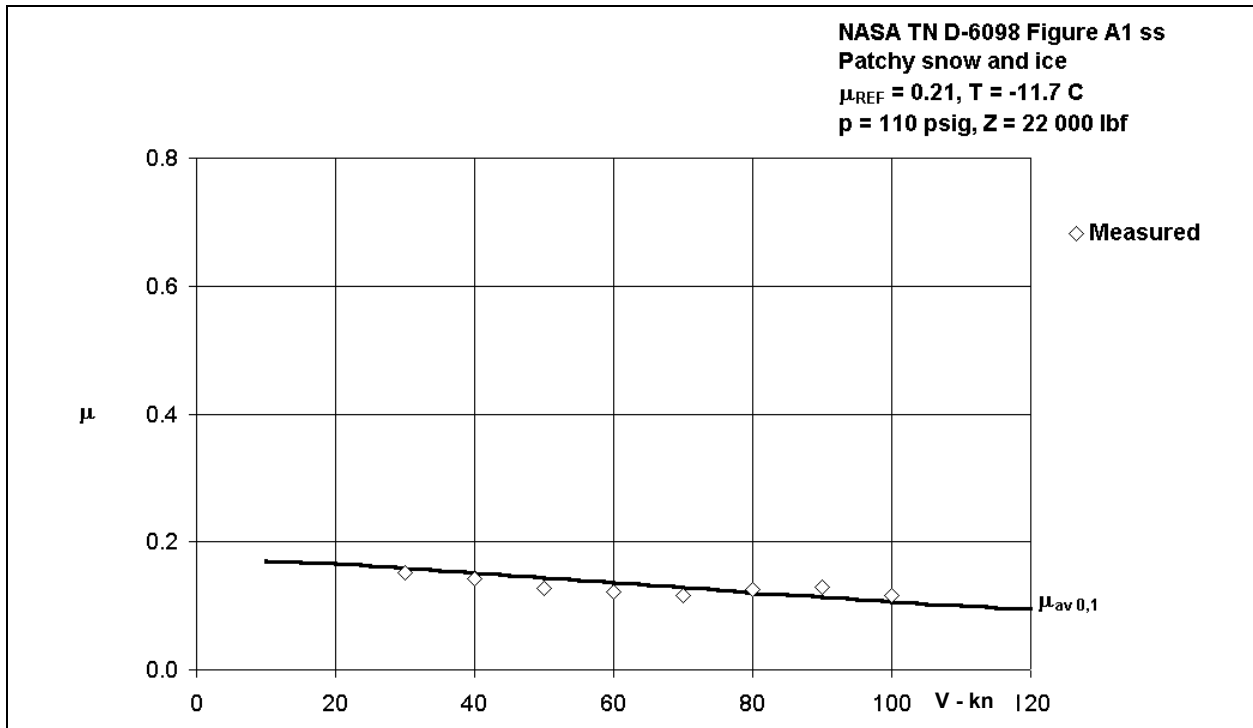
Figure 12.12: Braking friction coefficient for C141A on ice and snow – on/off system (Reference 43, Figure A1–ss)
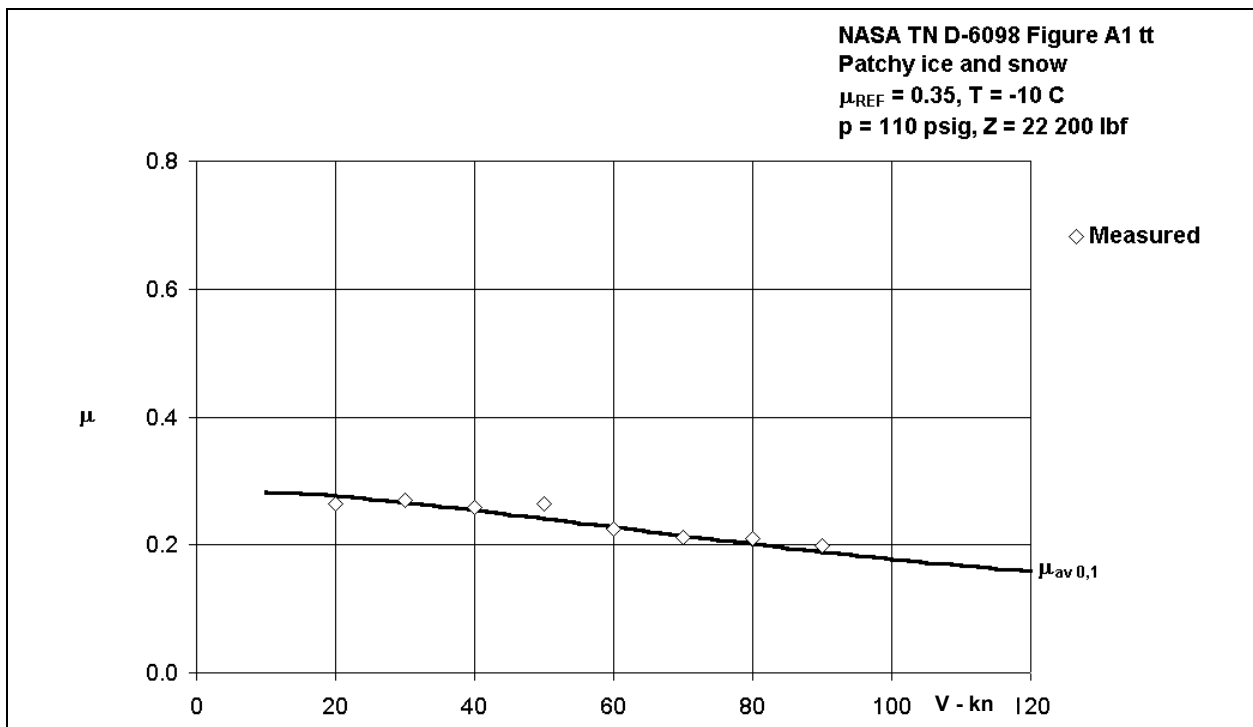
Figure 12.13: Braking friction coefficient for C141A on ice and snow – on/off system (Reference 43, Figure A1–tt)
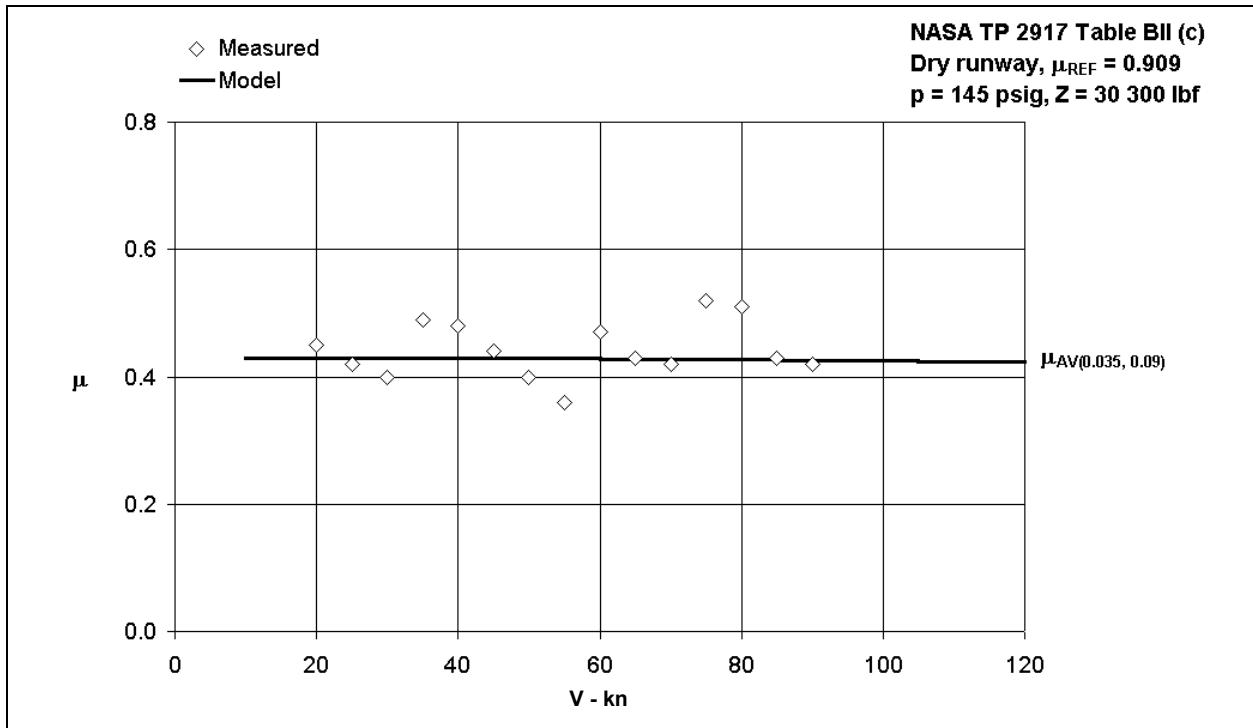
Figure 12.14: Braking friction coefficient Boeing 727 on dry runway – adaptive system
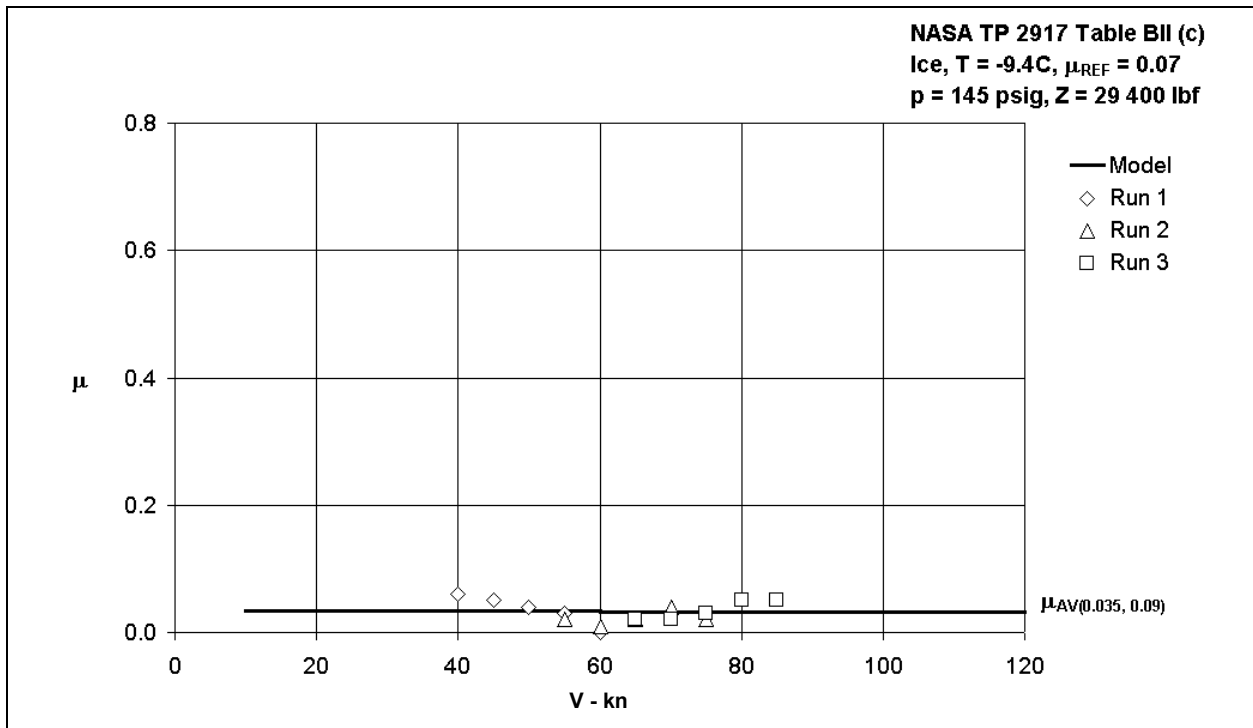
Figure 12.15: Braking friction coefficient for Boeing 727 on ice – adaptive system (Ice)
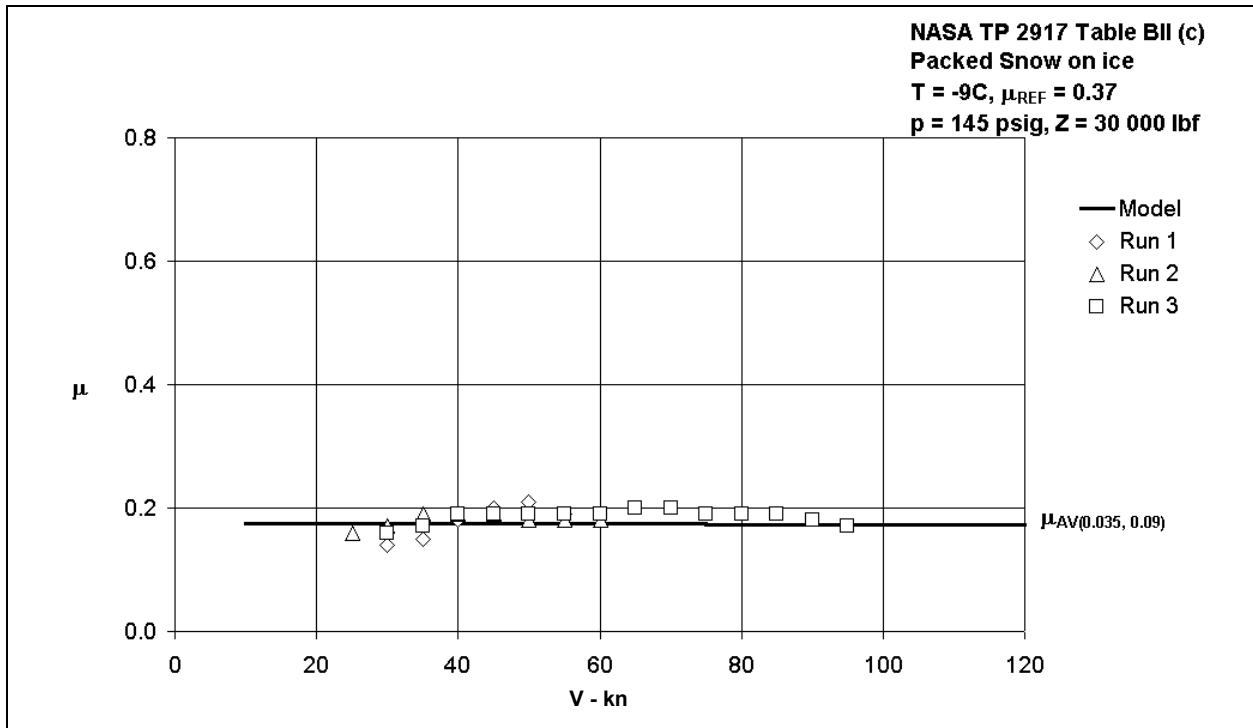
Figure 12.16: Braking friction coefficient for Boeing 727 on ice – adaptive system (Packed snow on ice)
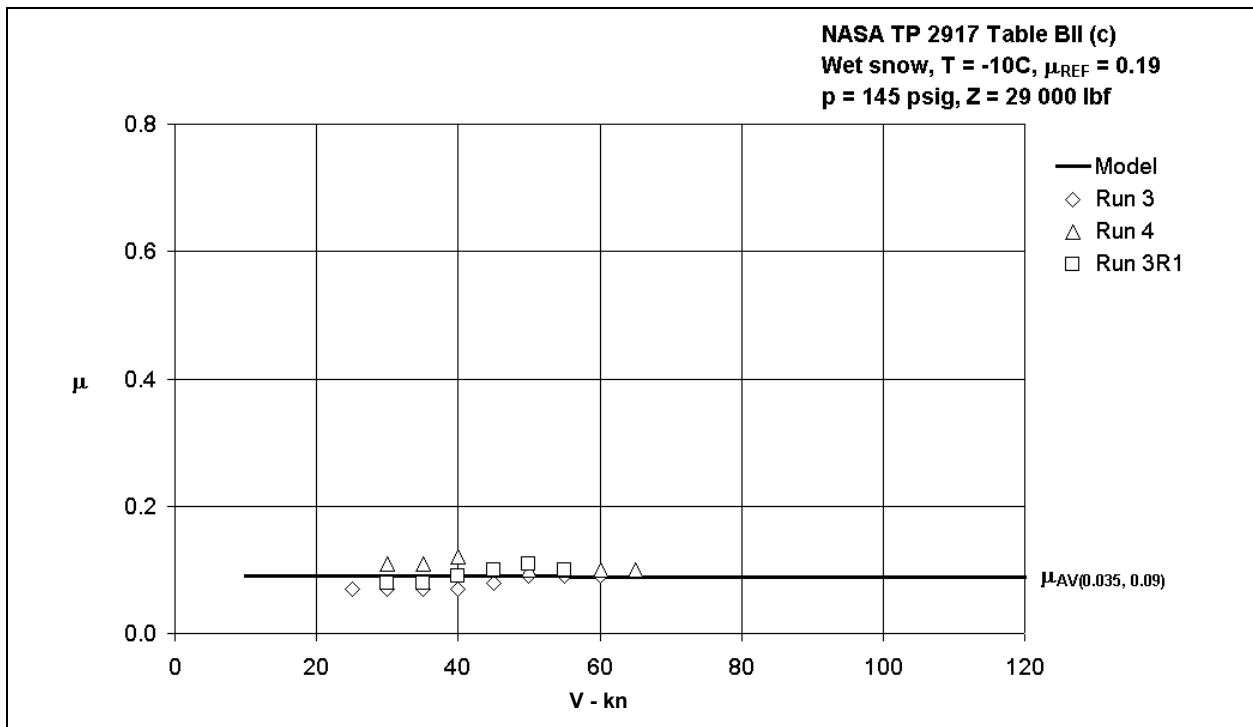
Figure 12.17: Braking friction coefficient for Boeing 727 on ice – adaptive system (Wet snow)
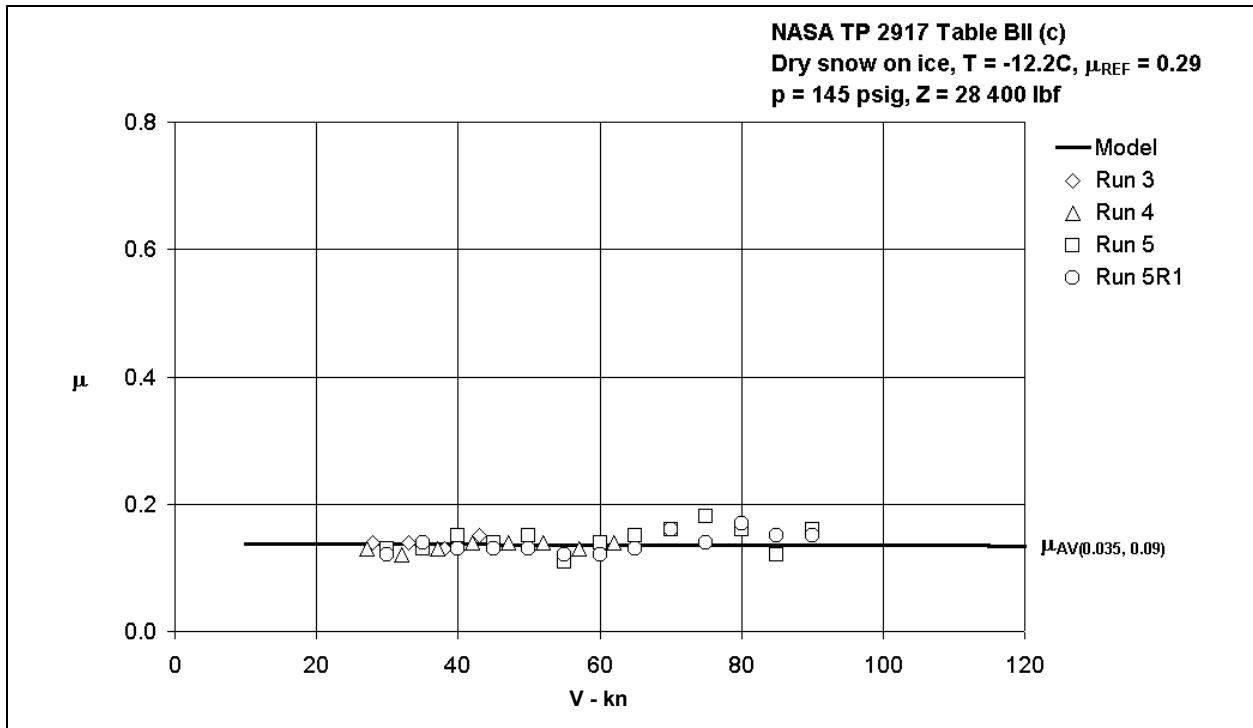
Figure 12.18: Braking friction coefficient for Boeing 727 on ice – adaptive system (Dry snow on ice)
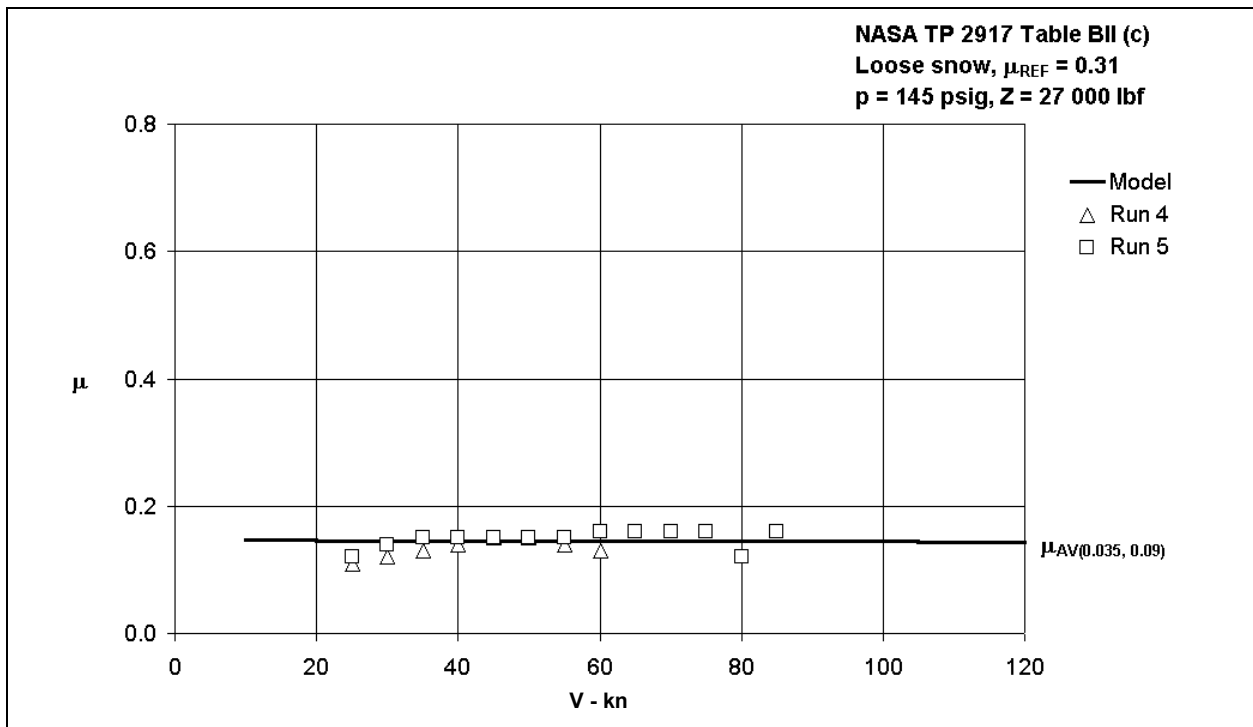
Figure 12.19: Braking friction coefficient for Boeing 727 on ice – adaptive system (Loose snow, μ_{REF} = 0.31)
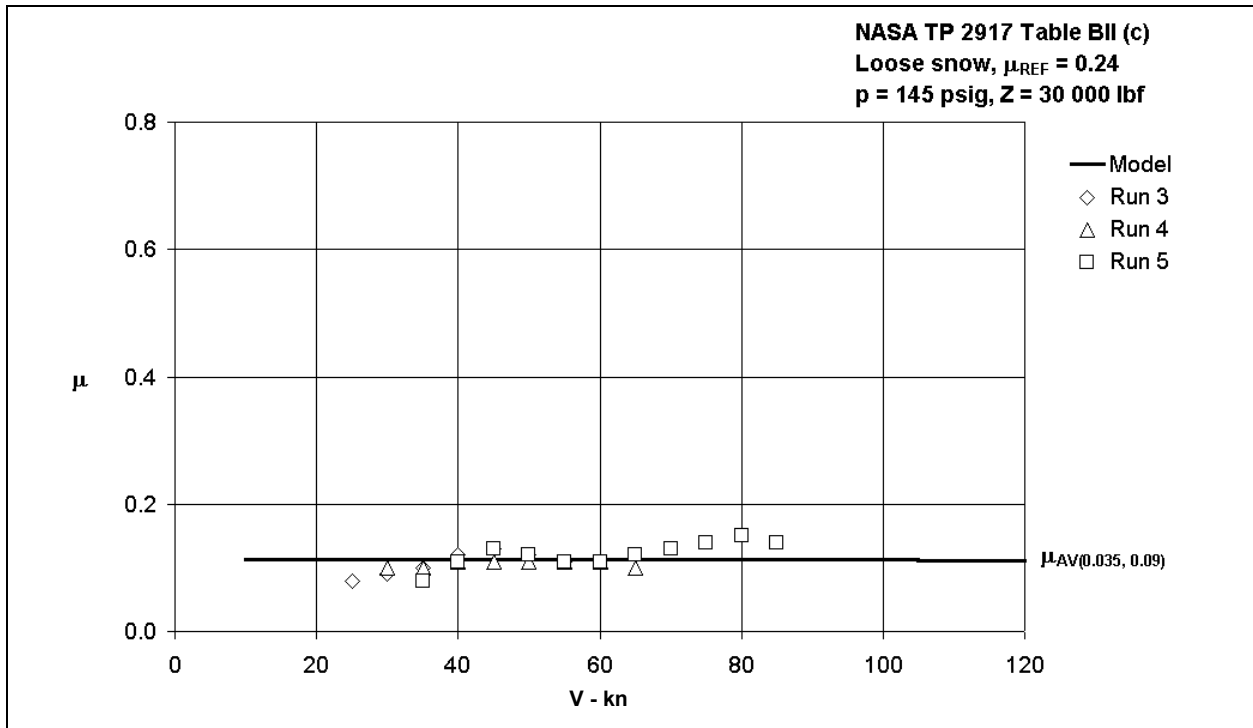
Figure 12.20: Braking friction coefficient for Boeing 727 on ice – adaptive system (Loose snow, μ_{REF} = 0.24)
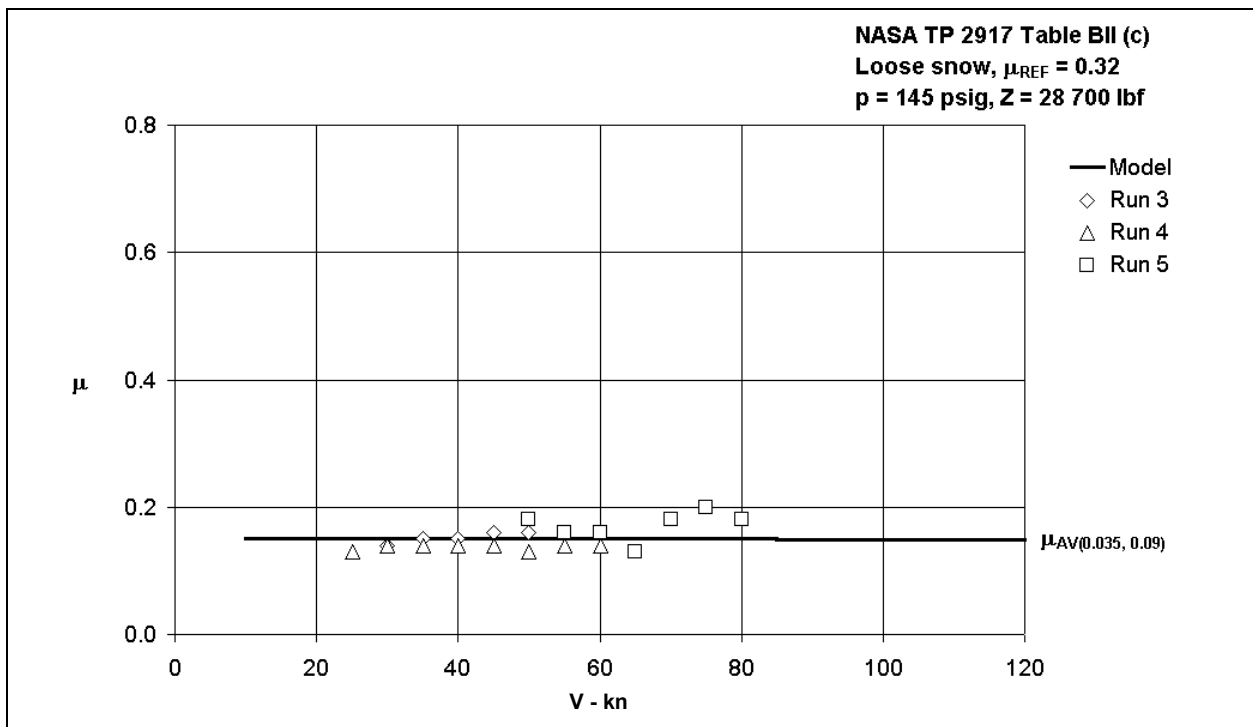
Figure 12.21: Braking friction coefficient for Boeing 727 on ice – adaptive system (Loose snow, μ_{REF} = 0.32)
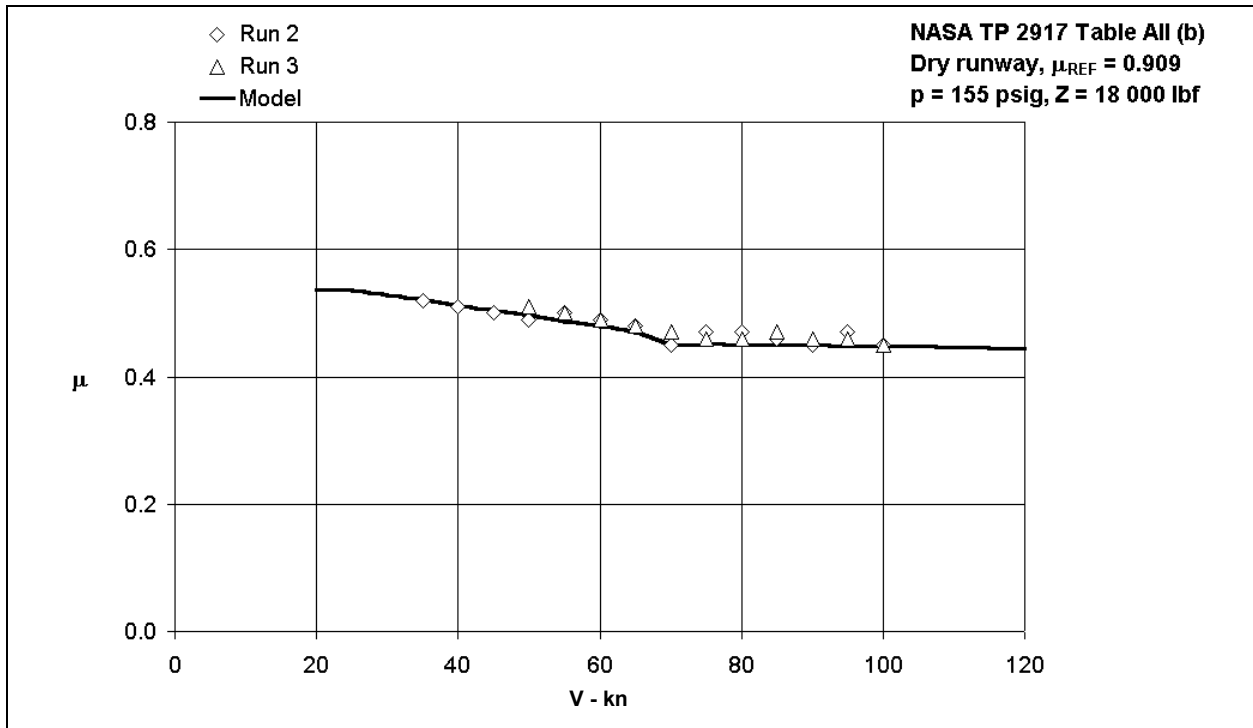
Figure 12.22: Braking friction coefficient Boeing 737 on dry runway – adaptive system
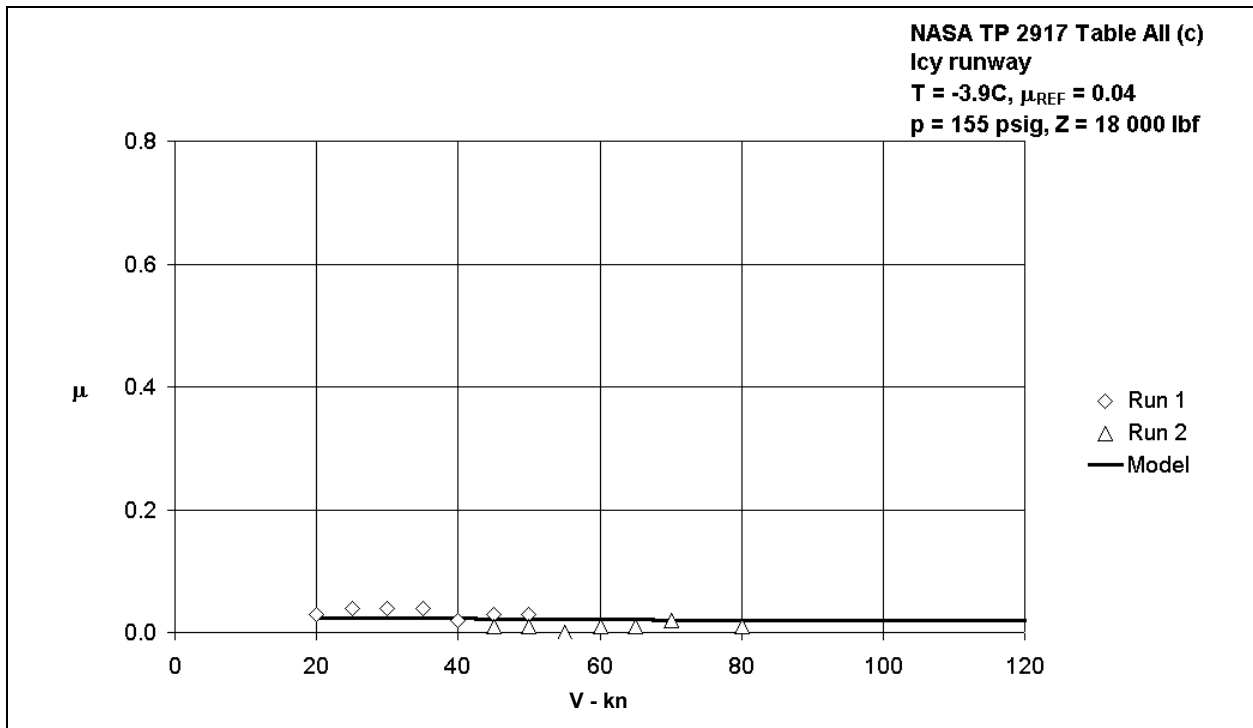
Figure 12.23: Braking friction coefficient for Boeing 737 on ice – adaptive system (Icy runway)

173
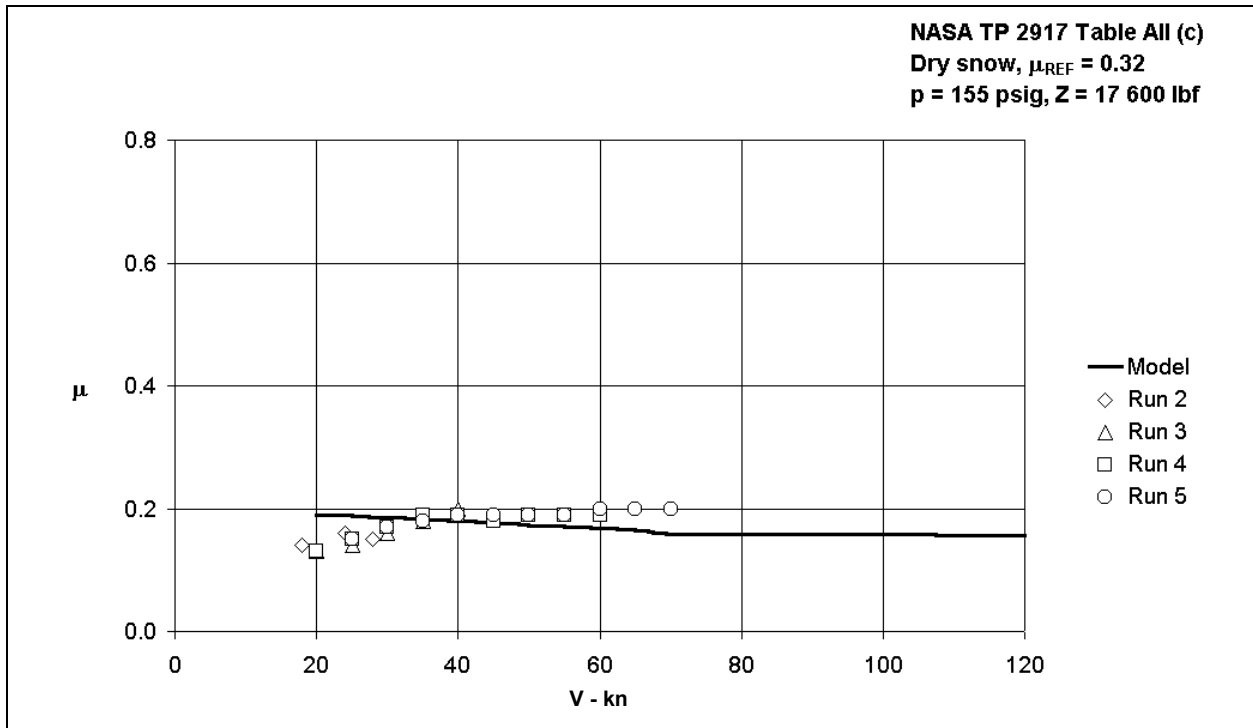
Figure 12.24: Braking friction coefficient for Boeing 737 on ice – adaptive system (Dry snow, μ_{REF} = 0.32)
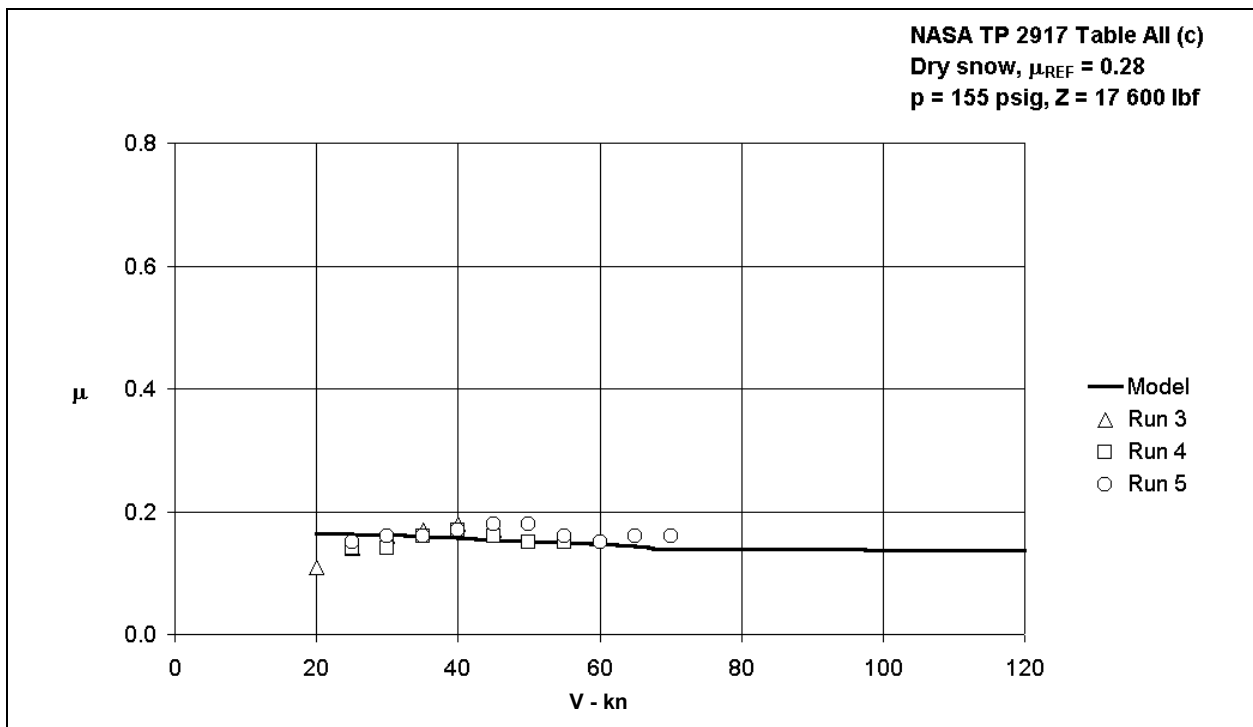
Figure 12.25: Braking friction coefficient for Boeing 737 on ice – adaptive system (Dry snow, μ_{REF} = 0. 28)
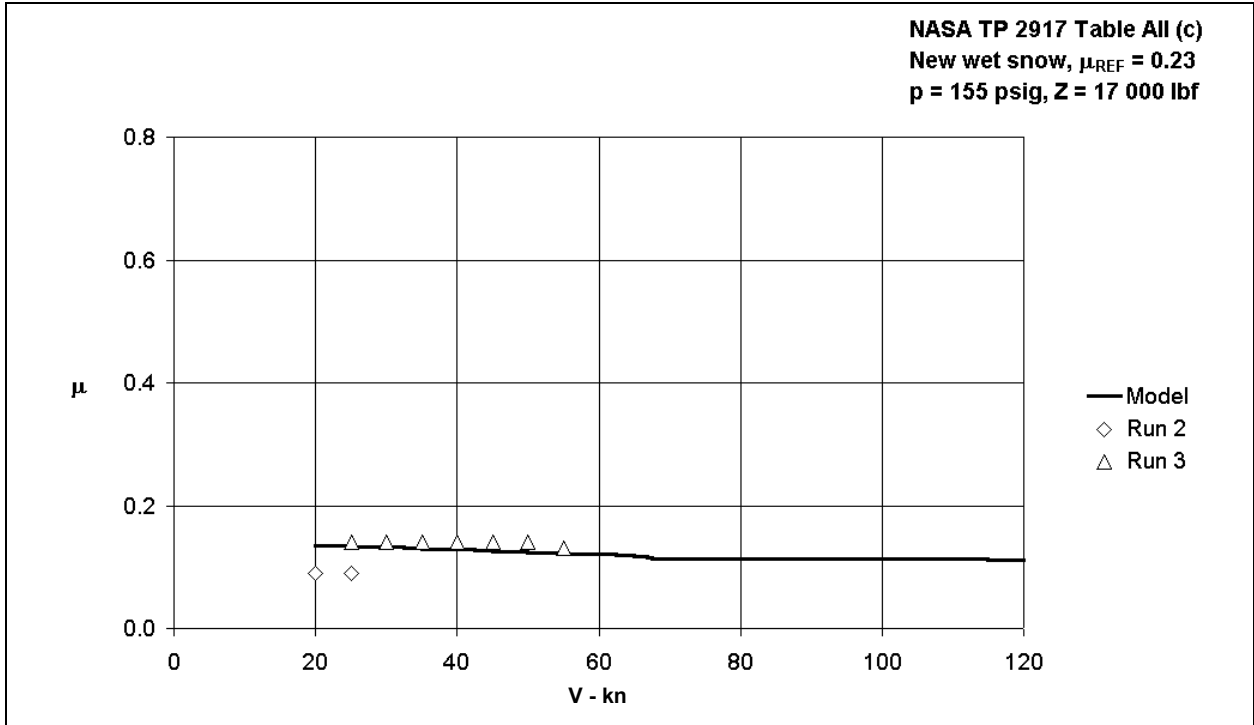
Figure 12.26: Braking friction coefficient for Boeing 737 on ice – adaptive system (New wet snow)
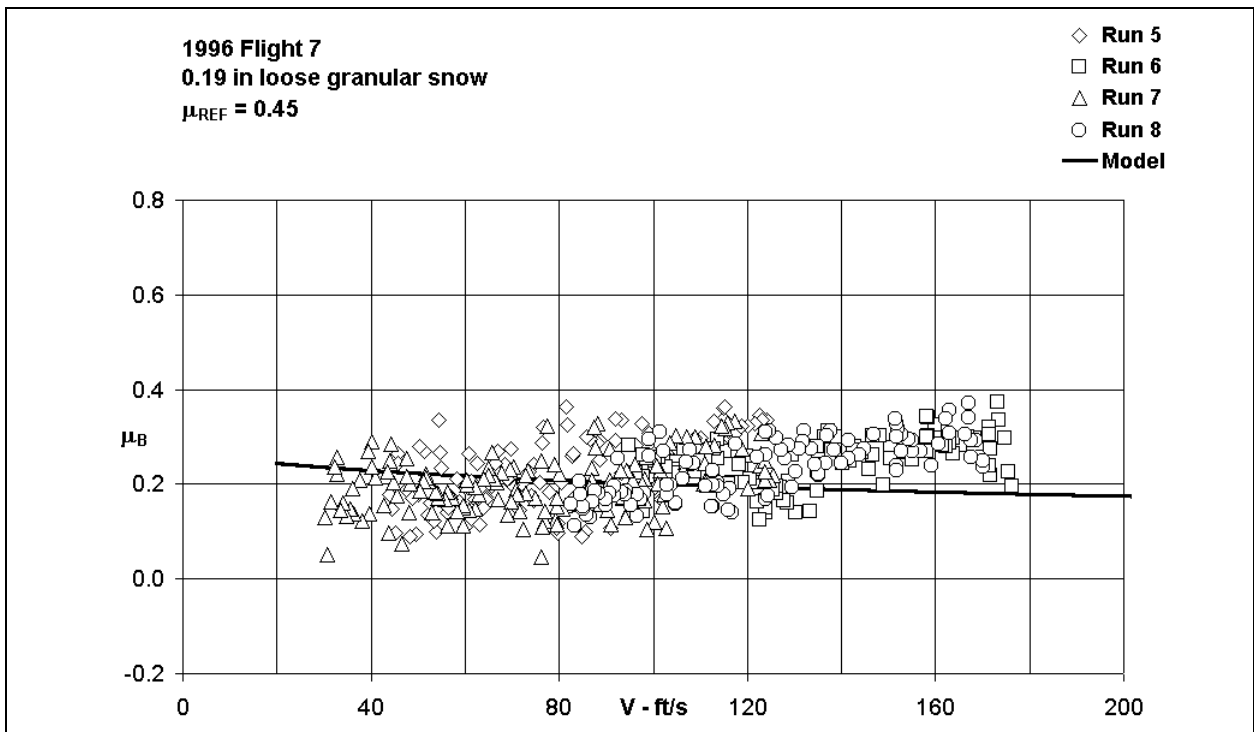
Figure 12.27: Braking friction coefficient for Falcon 20 on ice – adaptive system (Reference 14, Flight 7)
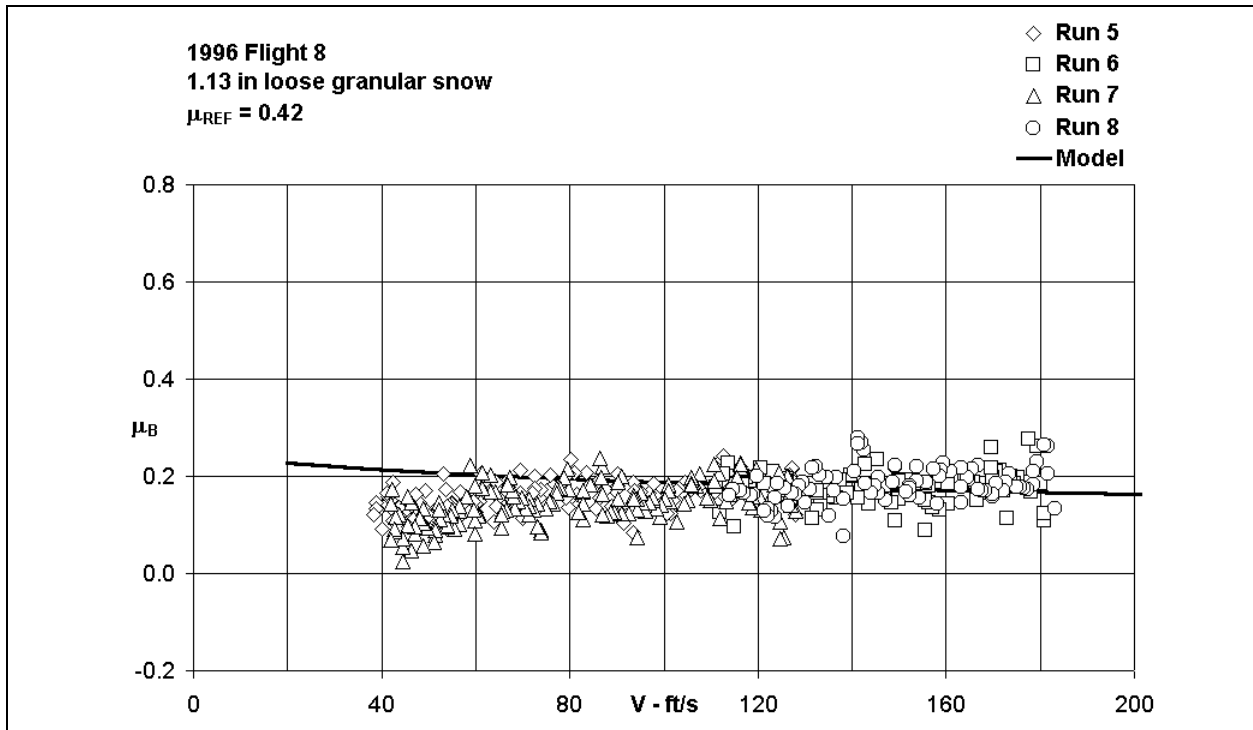
Figure 12.28: Braking friction coefficient for Falcon 20 on ice – adaptive system (Reference 14, Flight 8)
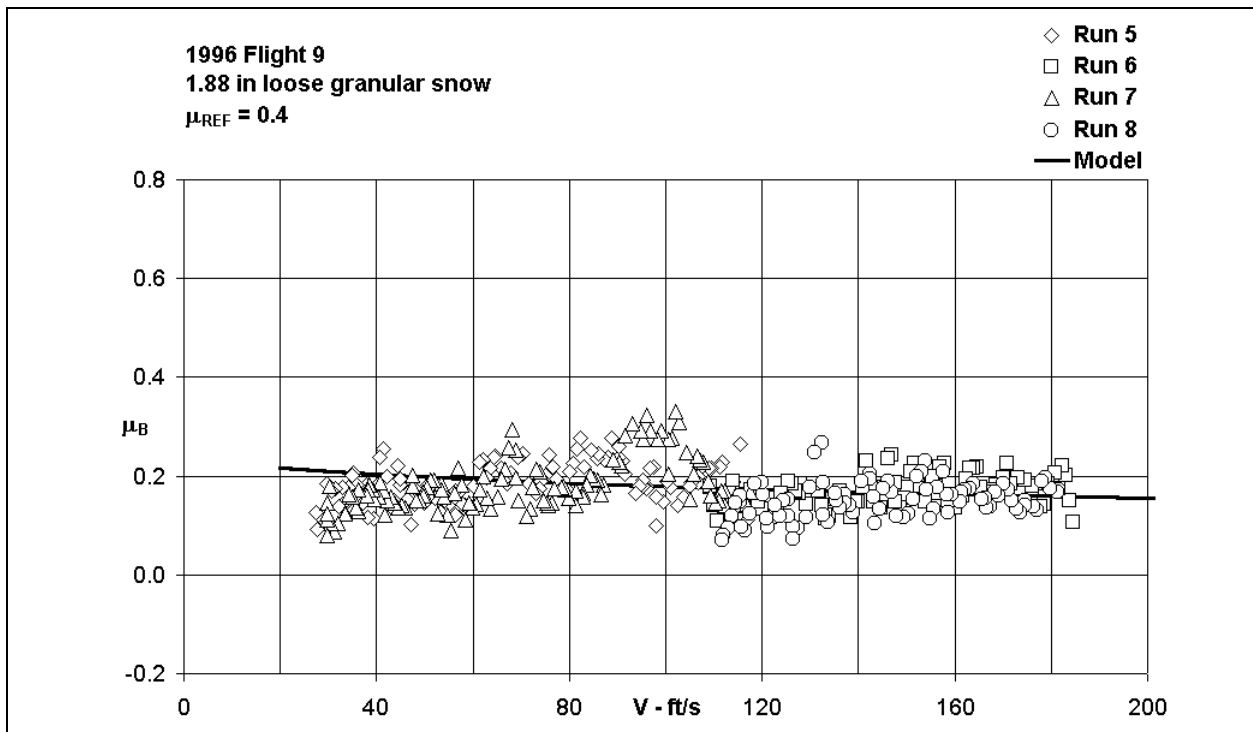
Figure 12.29: Braking friction coefficient for Falcon 20 on ice – adaptive system (Reference 14, Flight 9)
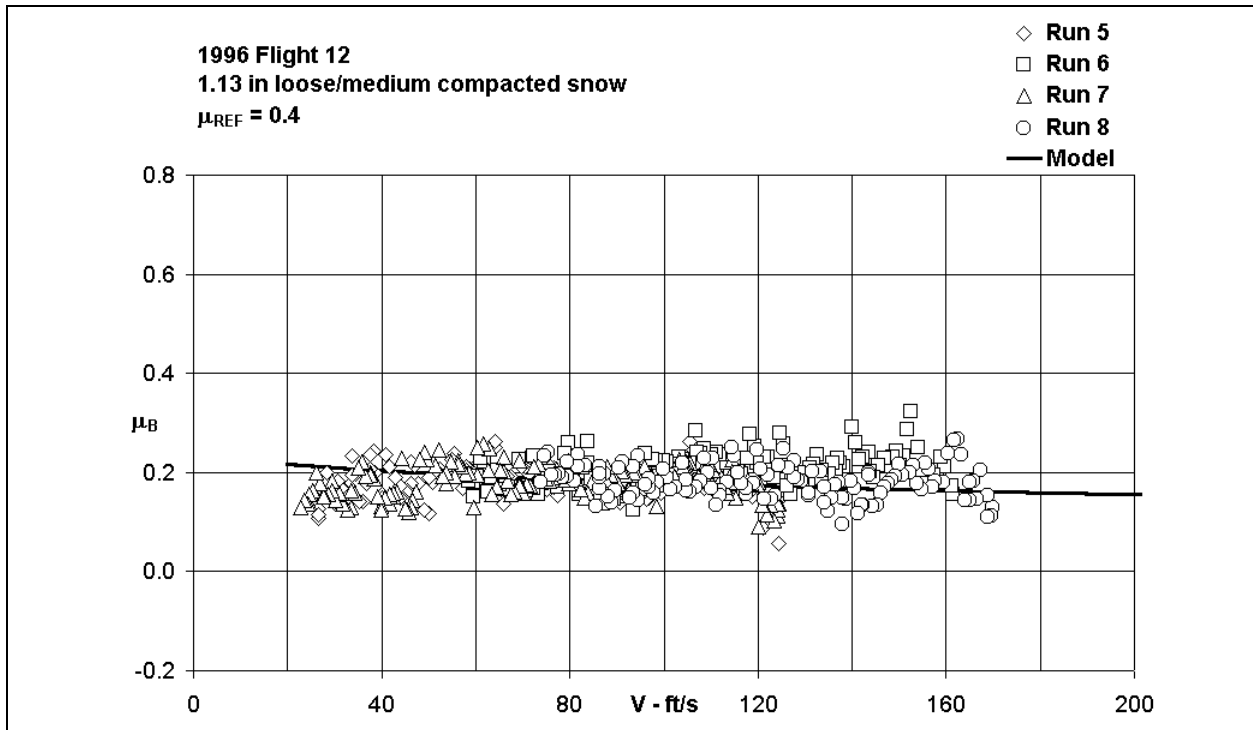
Figure 12.30: Braking friction coefficient for Falcon 20 on ice – adaptive system (Reference 14, Flight 12)
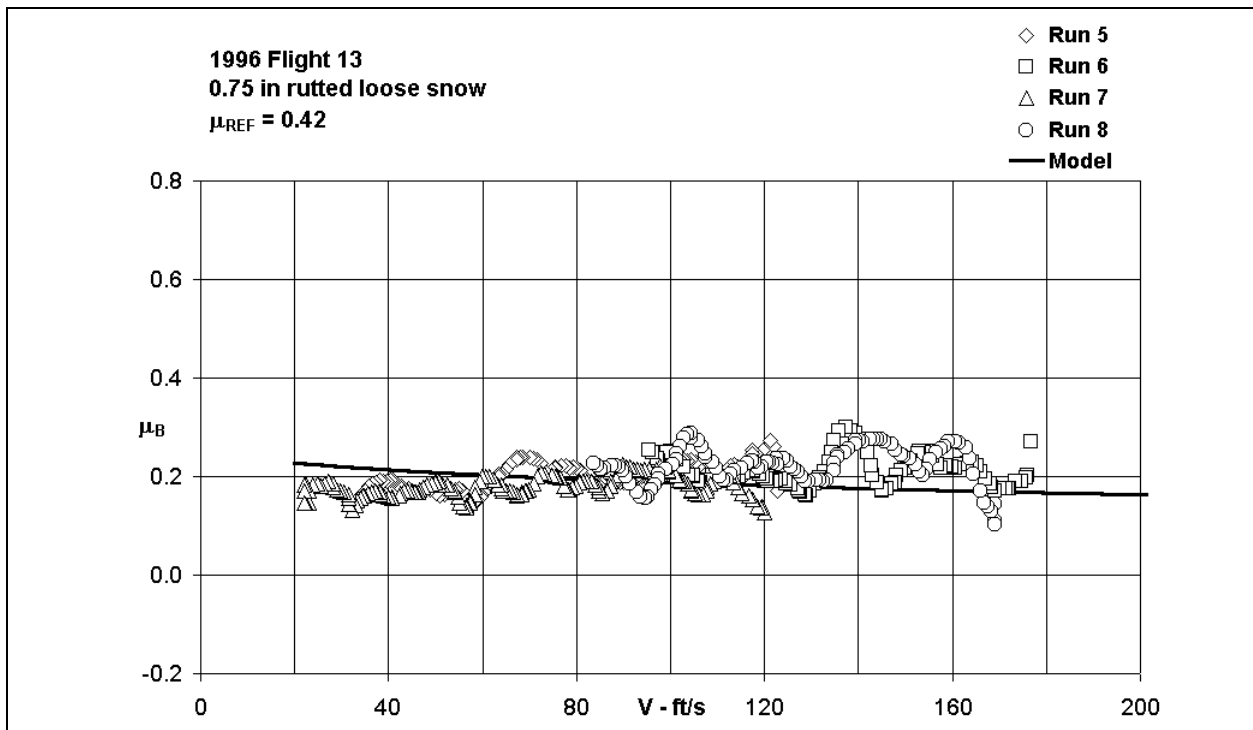
Figure 12.31: Braking friction coefficient for Falcon 20 on ice – adaptive system (Reference 14, Flight 13)
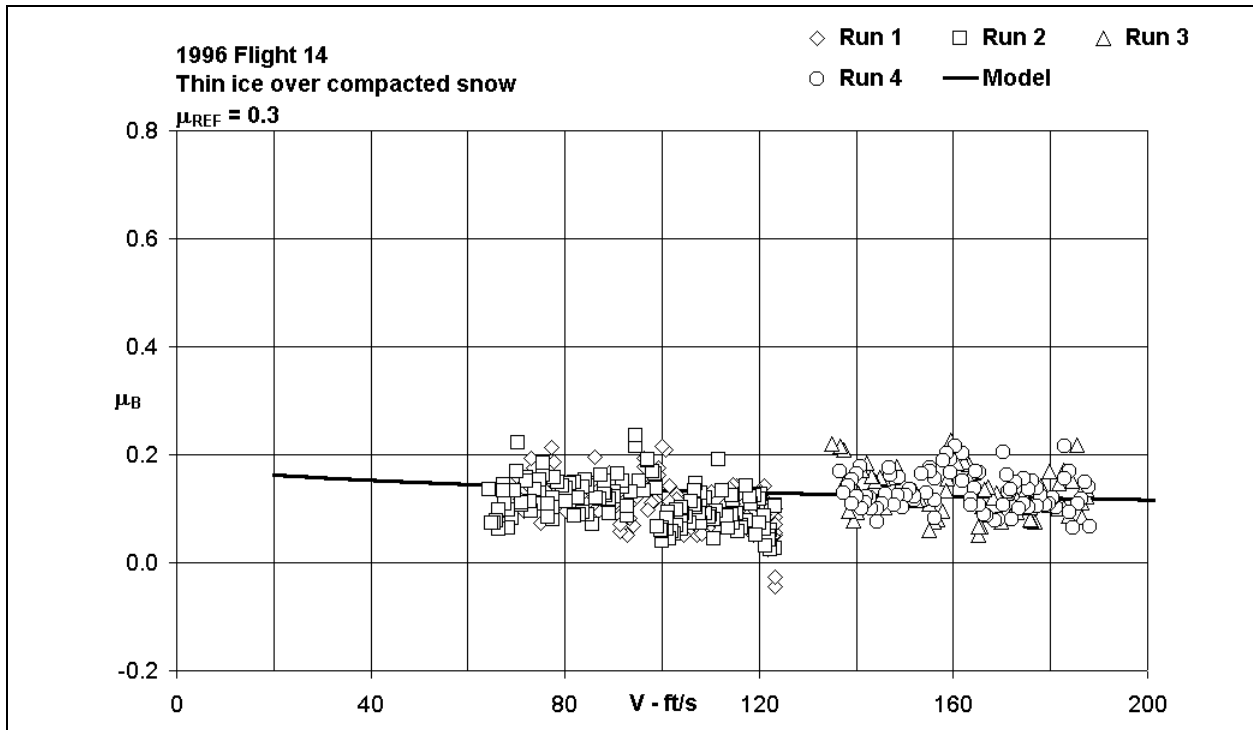
Figure 12.32: Braking friction coefficient for Falcon 20 on ice – adaptive system (Reference 14, Flight 14)
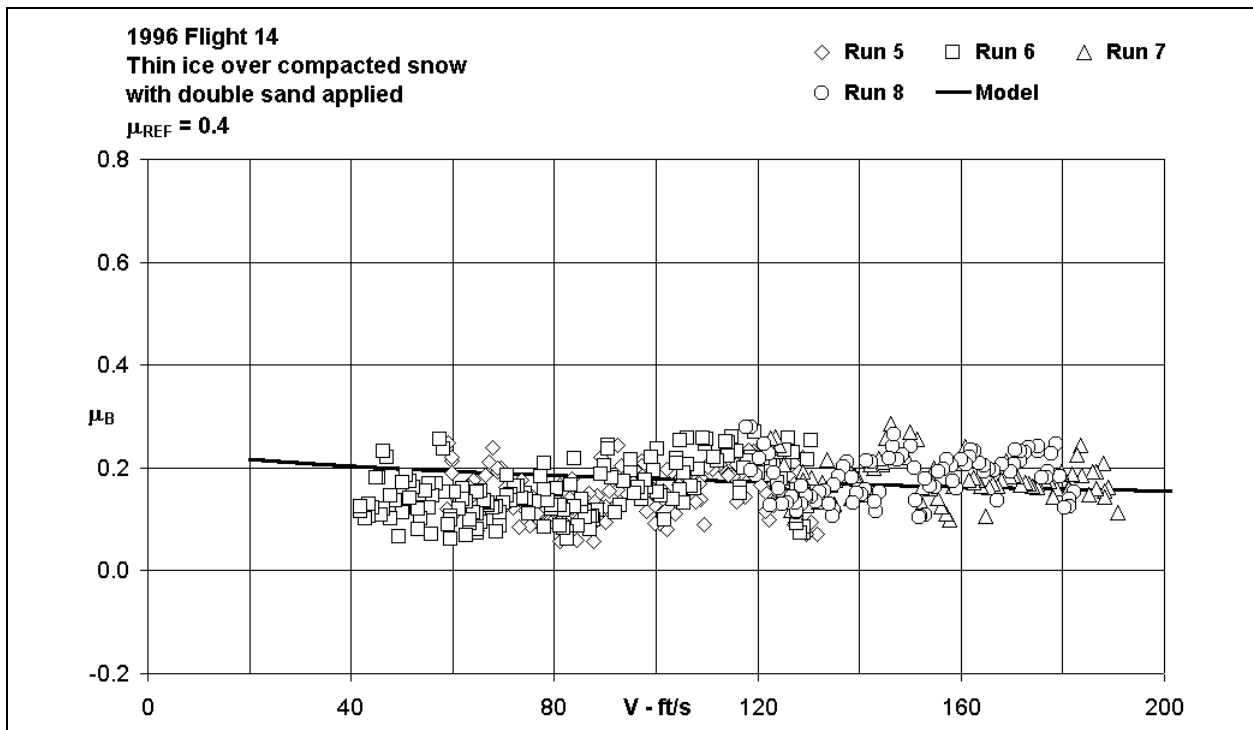
Figure 12.33: Braking friction coefficient for Falcon 20 on treated ice – adaptive system
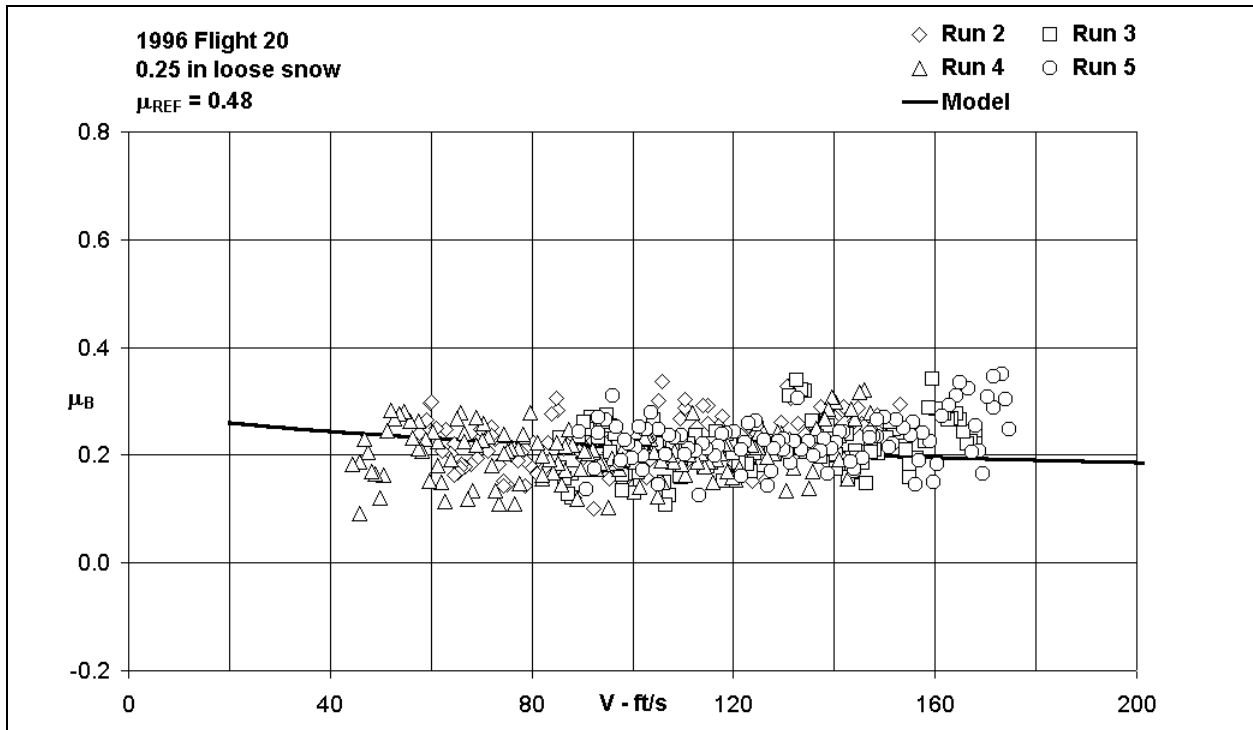
Figure 12.34: Braking friction coefficient for Falcon 20 on ice – adaptive system (Reference 14, Flight 20)
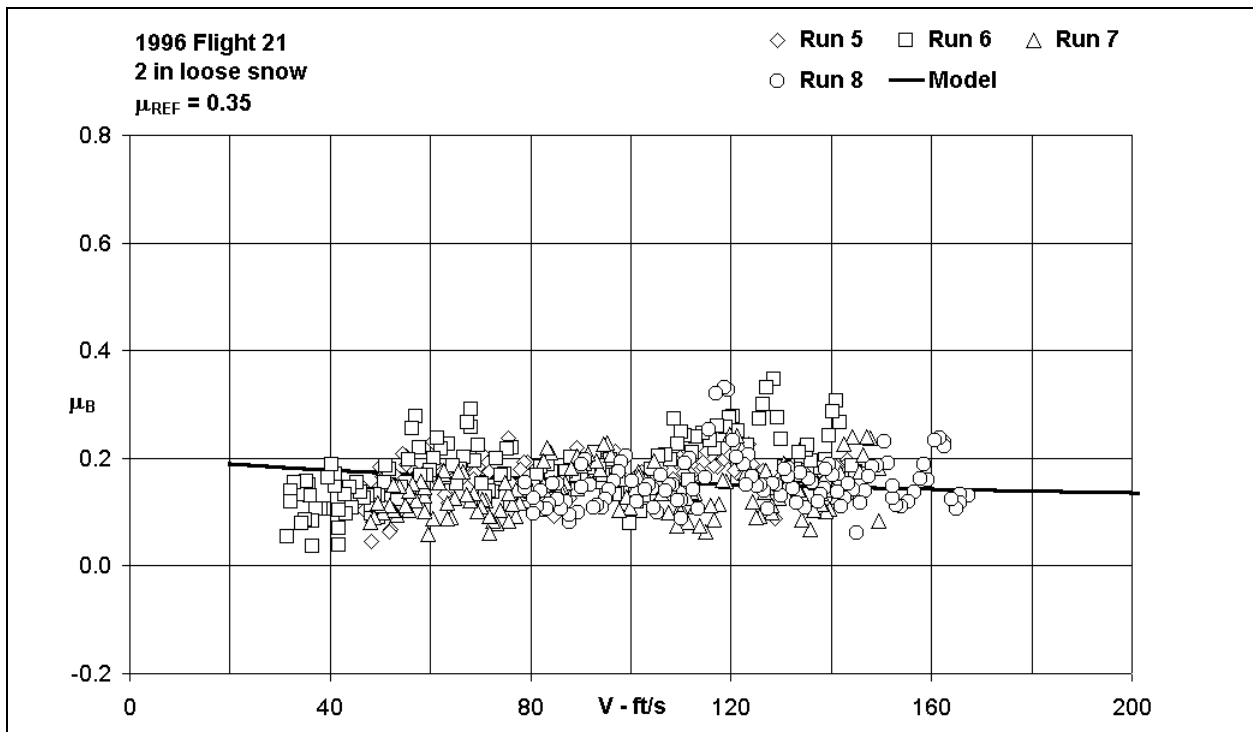
Figure 12.35: Braking friction coefficient for Falcon 20 on ice – adaptive system (Reference 14, Flight 21)
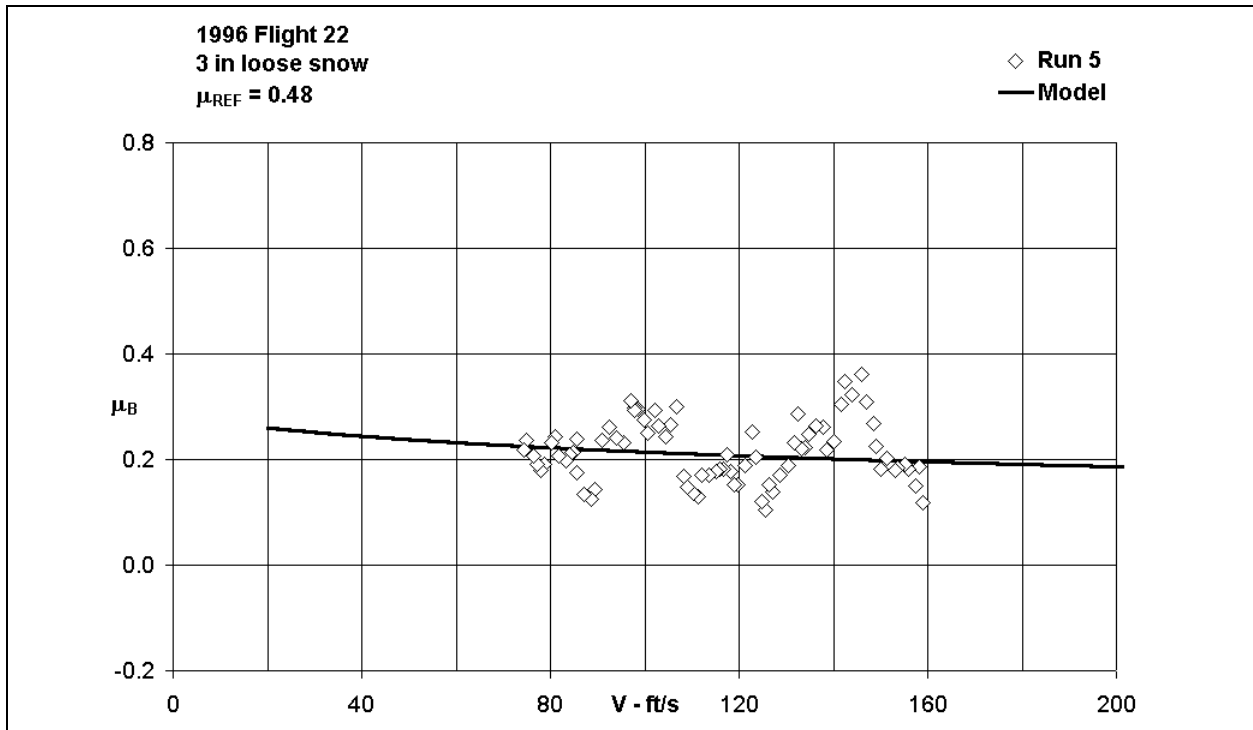
Figure 12.36: Braking friction coefficient for Falcon 20 on ice – adaptive system (Reference 14, Flight 22)
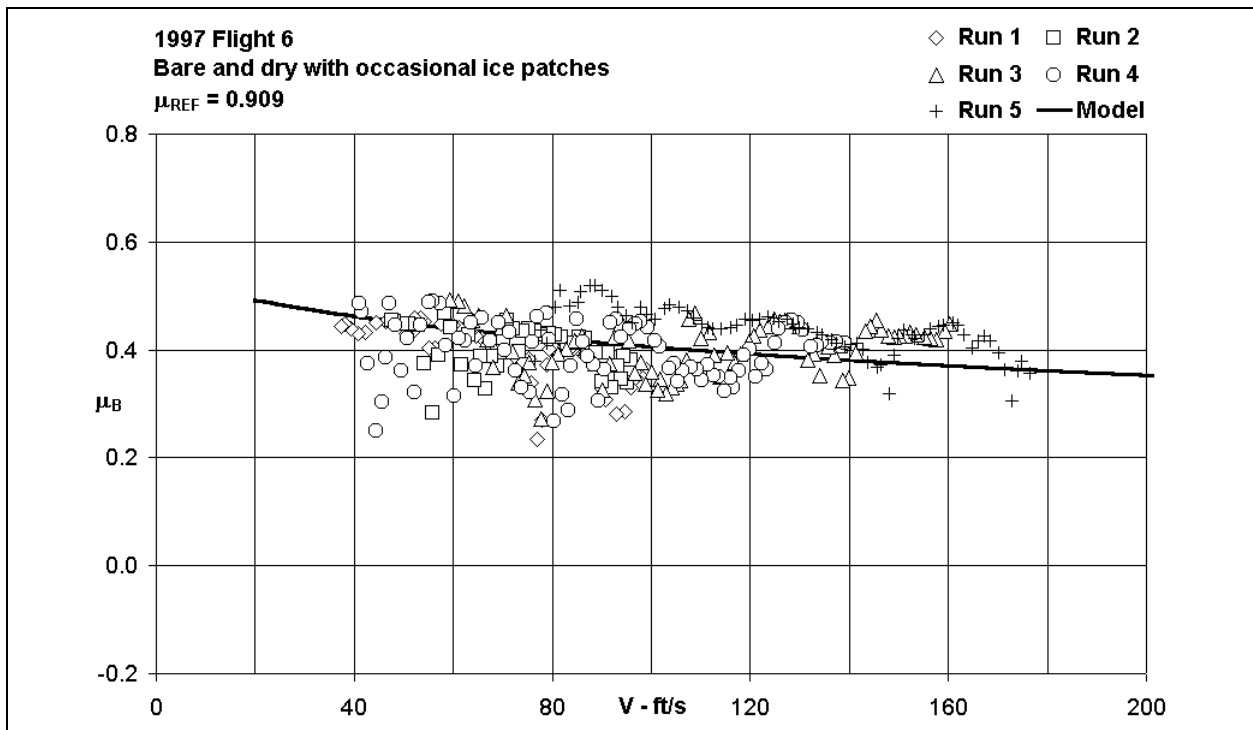
Figure 12.37: Braking friction coefficient for Falcon 20 on mainly dry runway – adaptive system
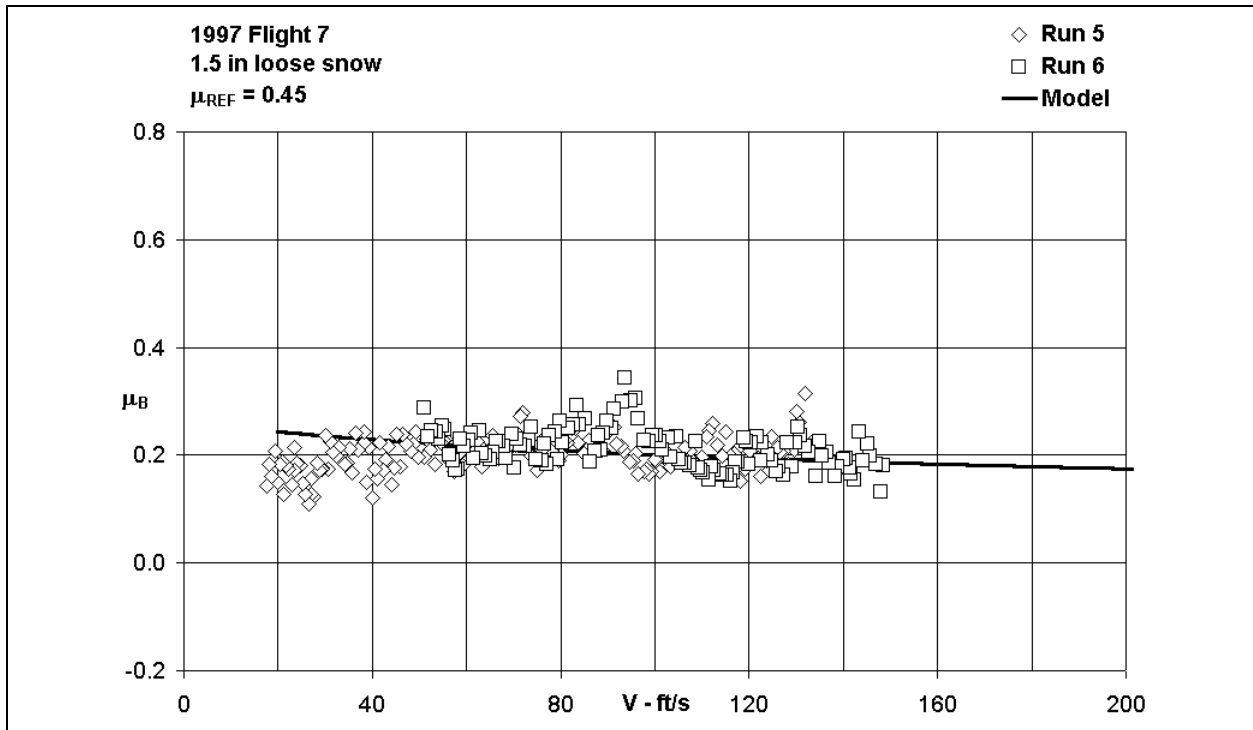
Figure 12.38: Braking friction coefficient for Falcon 20 on ice – adaptive system (Reference 15, Flight 7)
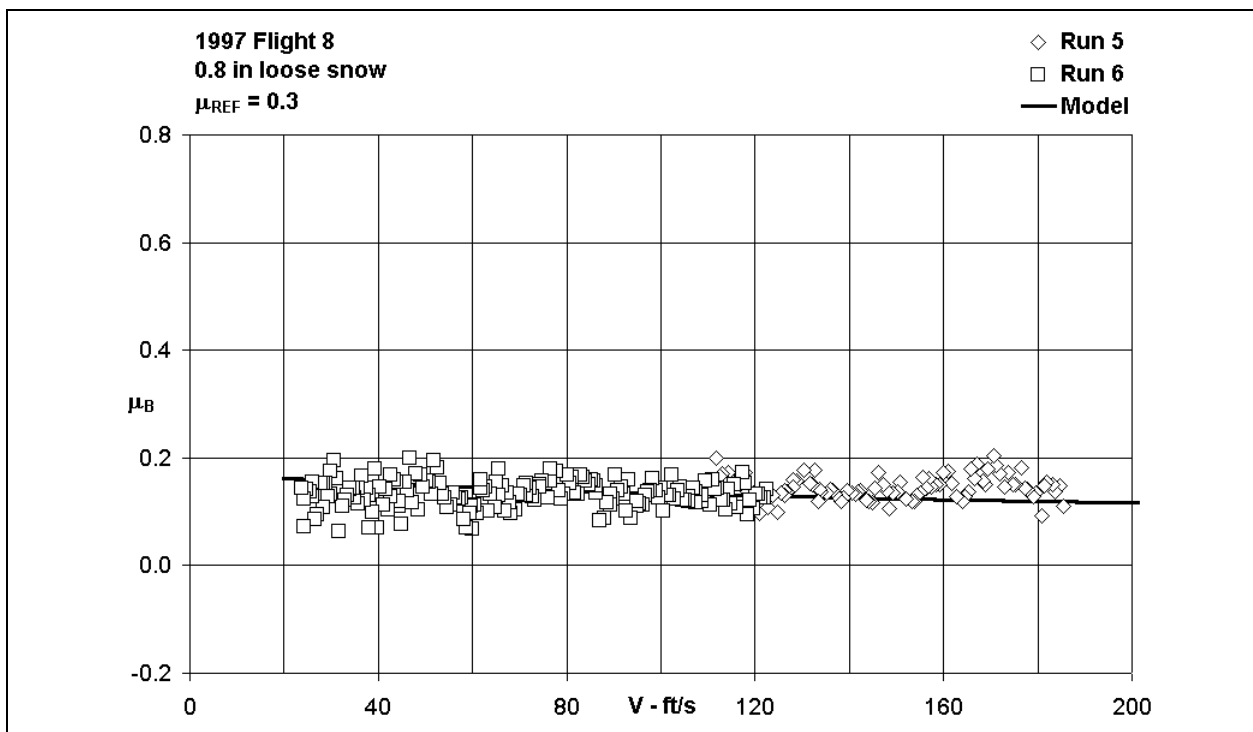
Figure 12.39: Braking friction coefficient for Falcon 20 on ice – adaptive system (Reference 15, Flight 8)
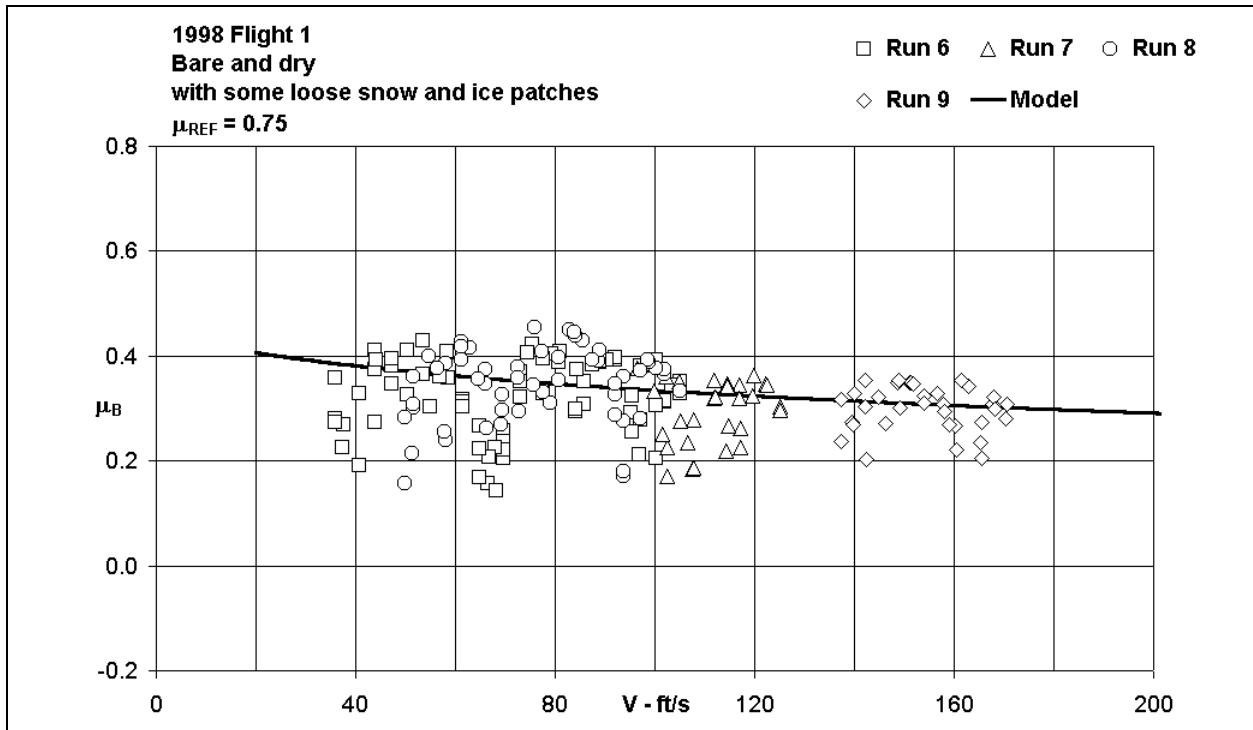
Figure 12.40: Falcon 20 on non-uniformly contaminated runway – adaptive system
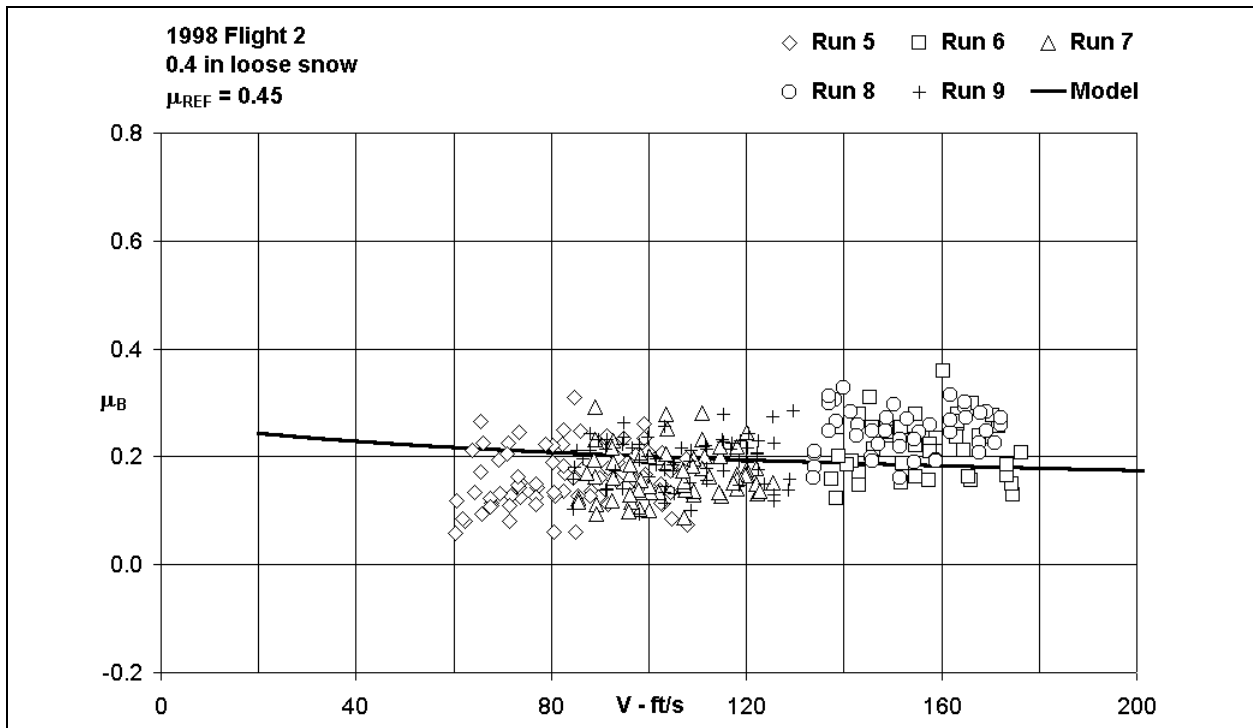
Figure 12.41: Braking friction coefficient for Falcon 20 on ice – adaptive system (Reference 16, Flight 2)
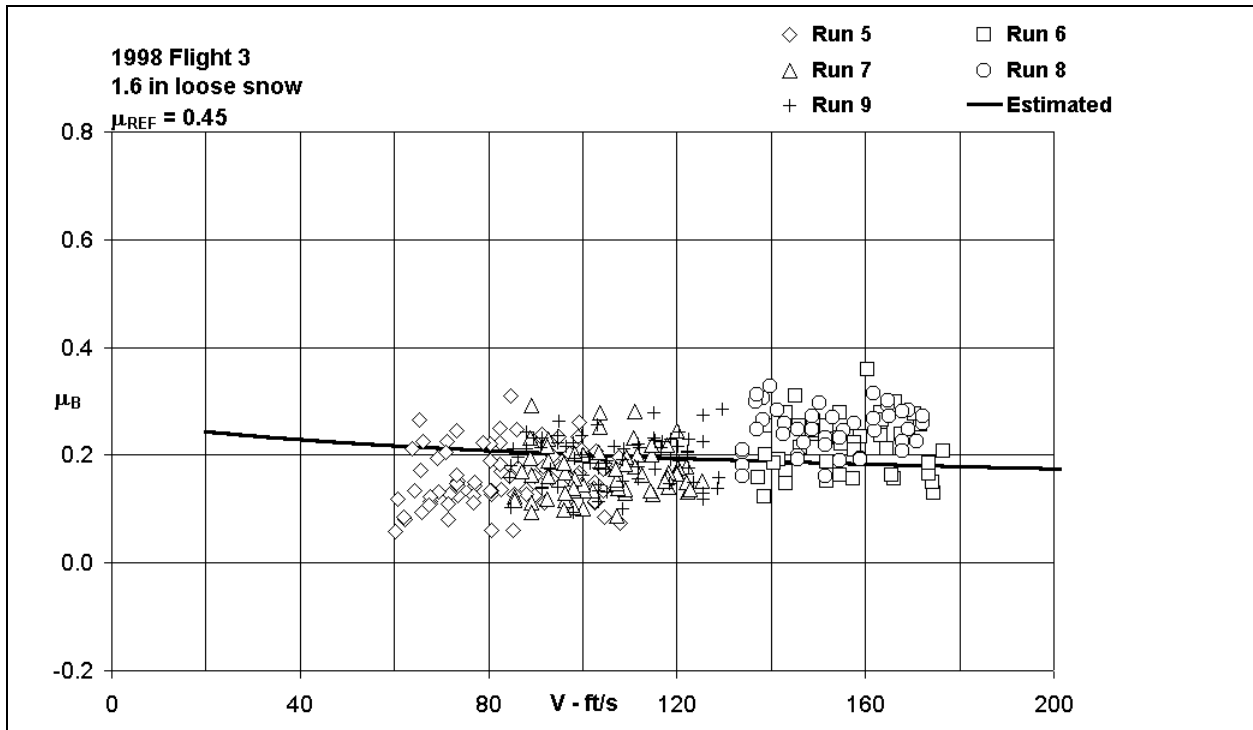
Figure 12.42: Braking friction coefficient for Falcon 20 on ice – adaptive system (Reference 16, Flight 3)
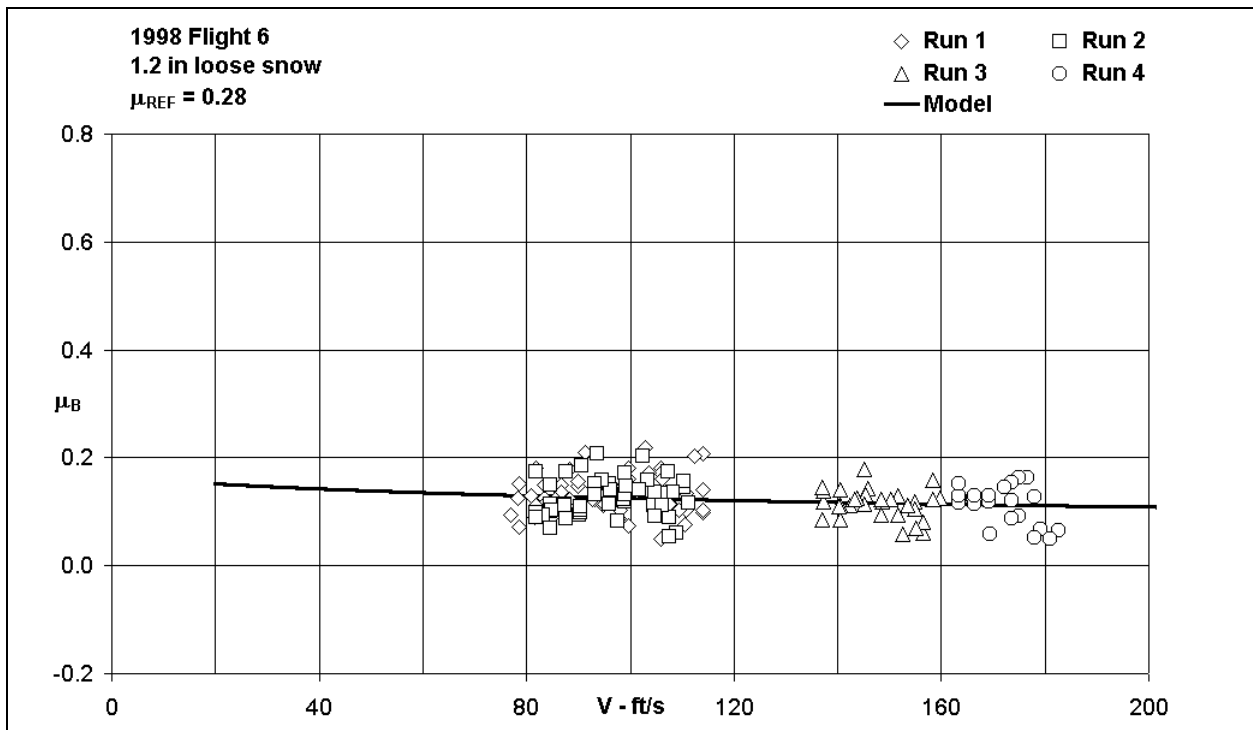
Figure 12.43: Braking friction coefficient for Falcon 20 on ice – adaptive system (Reference 16, Flight 6)
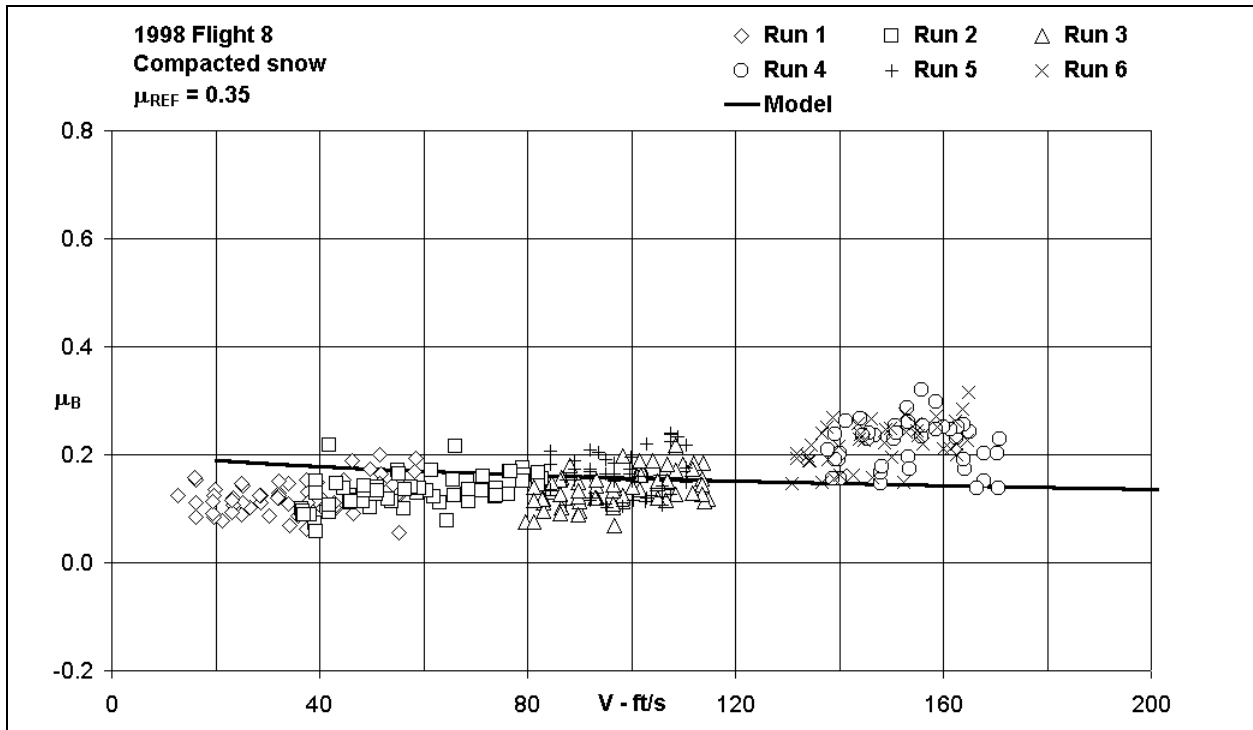
Figure 12.44: Braking friction coefficient for Falcon 20 on ice – adaptive system (Reference 16, Flight 8)
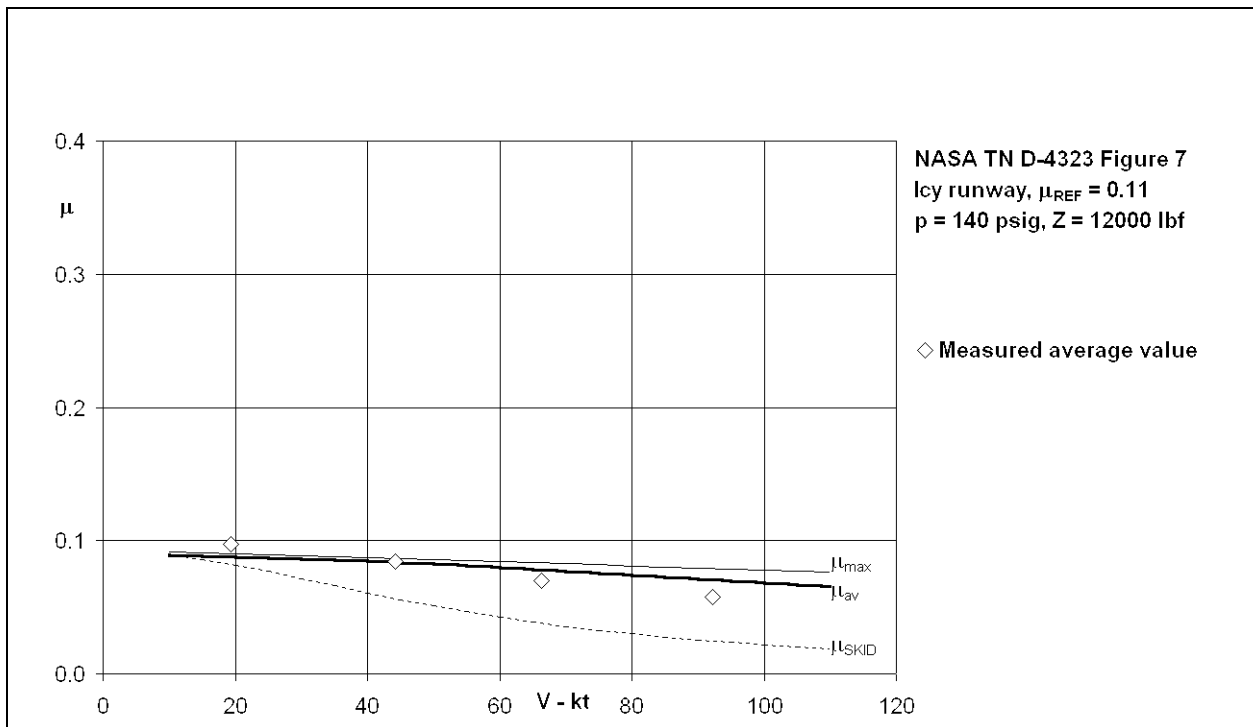
Figure 12.45: Effect of speed on average braking coefficient for single wheel ($p = 140$ psig, $Z = 12000$ lbf)
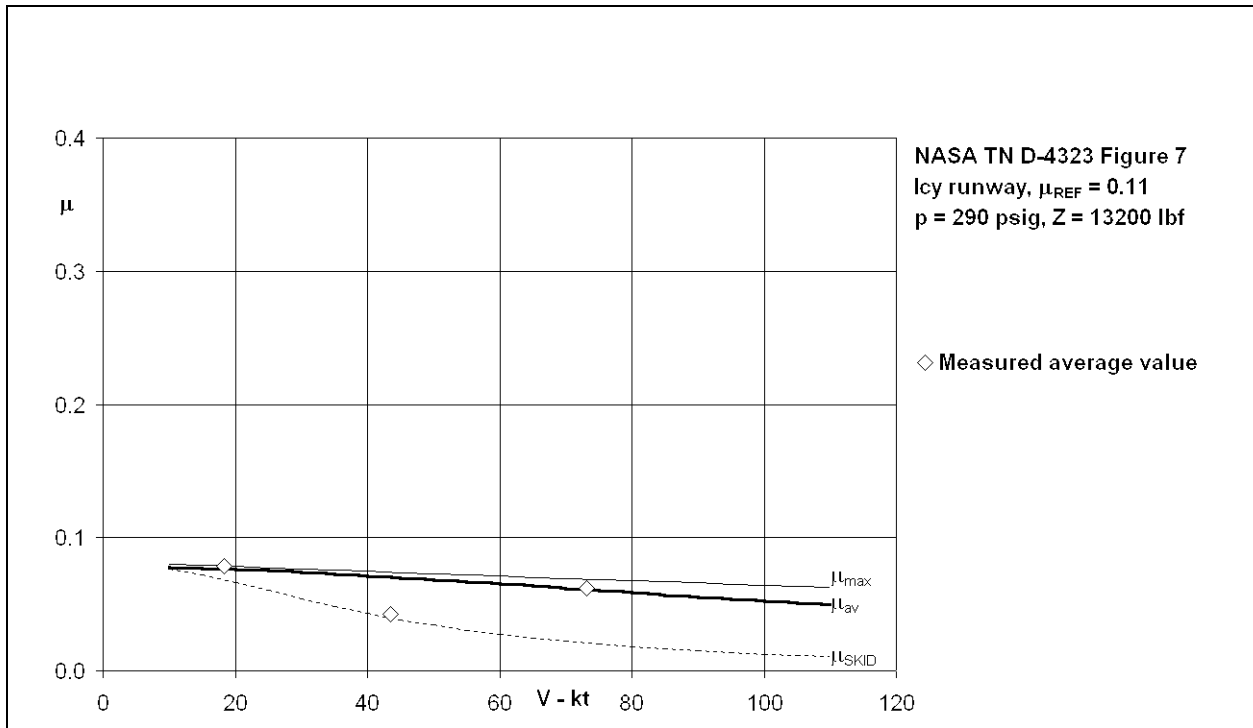
Figure 12.46: Effect of speed on average braking coefficient for single wheel
(p = 290 psig, Z = 13200 lbf)

REFERENCES

1.   ESDU. *Statistical analysis of wet runway friction for aircraft and ground test machines*. ESDU Data Item 99015 with Amendment A. October 2000.

2.   Hadekel, R. *The mechanical characteristics of pneumatic tyres*. S&T Memo 10/52. November 1952.

3.   Leland, T.J.W. and Taylor, G.R. *An investigation of the influence of aircraft tire-tread wear on wet runway braking*. NASA TN D-2770. April 1965.

4.   Key, E.J. and Minter, E.M. *Aircraft braking friction trials on a coarse open-graded macadam surface*. RAE TR 69123. June 1969.

5.   ESDU. *Statistical methods applicable to analysis of aircraft performance data*. Data Item 91017 with Amendments A to D. September 1997.

6.   Horne, W.B., Joyner, U.T. and Leland, T.J.W. *Studies of the retardation force developed on an aircraft tire rolling in slush or water*. NASA TN D-0552. September 1960.

7.   Horne, W.B. and Leland, T.J.W. *Influence of tire tread pattern and runway surface condition on braking friction and rolling resistance of a modern aircraft tire*. NASA TN D-1376. September 1962.

8.   Barrett, R.V. *Drag and spray measurements from a small pneumatic tyre travelling through a water layer*. (Interim report of work carried out at Bristol University for Ministry of Aviation.) S&T Memo 11-63. December 1963.

9.   Sugg, R.W. *Drag of a large and small pneumatic tyre travelling through water, slush and snow*. S&T Memo 9-66. 1966.

10.   Williams, J.R. and Beatty, I. *An investigation into the drag due to slush using a Canberra aircraft*. Cranfield Institute of Technology Report CIT-FI-71-010. 1971.

11.   *Yearbook of the Tire and Rim Association Inc*. Akron, Ohio. 1968.

12.   Browne, A.L. *The physics of tire traction: theory and experiment – tire traction on snow-covered pavements*. Plenum Press, New York and London. 1974.

13.   van Es, G.W.H. *Rolling resistance of aircraft tires in dry snow*. NLR TR 98165. December 1998.

14.   Martin, J.C.T., Croll, J.B. and Bastian, M. *Braking friction coefficient and contamination drag obtained for a Falcon 20 aircraft on winter contaminated runway surfaces*. National Research Council Canada LTR-FR-132. September 1996.

15.   Croll, J.B., Martin, J.C.T. and Bastian, M. *Falcon 20 aircraft performance testing on contaminated runway surfaces during the winter of 1996/1997*. National Research Council Canada LTR-FR-137. August 1997.

16.   Croll, J.B., Martin, J.C.T. and Bastian, M. *Falcon 20 aircraft performance testing on contaminated runway surfaces during the winter of 1997/1998*. National Research Council Canada LTR-FR-151. Transport Canada TP 13338E. December 1998.

17.   Richmond, P.W. *Motion resistance of wheeled vehicles in snow*. CRREL report 95-7. March 1995.

18.   Shanks, D.H. and Barrett, R.V. *Performance of aircraft pneumatic tyres in soft soil*. Aeronautical Journal (pp. 20-28). January 1981.

19.   Shapiro, L.H. et al. *Snow mechanics. Review of the state of knowledge and applications*. CRREL Report 97-3. 1997.

20.   Dorsey, N.E. *Properties of ordinary water substance*. Reinhold Publishing Corporation, New York. 1940.

21.   Browning, A.C. and Kervell, B.C. *High-speed taxiing and braking trials of a Beverley aircraft on a runway covered in wet snow, crisp snow and shallow slush*. RAE Technical report 67193. August 1967.

22.   Yager, T.J., Vogler, W.A. and Baldasare, P. *Evaluation of two transport aircraft and several ground test vehicle friction measurements obtained on various runway surface types and conditions. A summary of test results from joint FAA/NASA runway friction program*. NASA Technical Paper 2917. February 1990.

23   Lidström, M. *Aircraft rolling resistance in loose dry snow. A theoretical analysis*. A special issue of VTI report 173A. Linköping. 1979.

24.   LaChapelle, E.R. and Perla, R.I. *Mechanical properties of the soft slab*. Alta avalanche study – Project B, Report 2. June 1967.

25.   Foehn, P. and Camponovo, C. *Improvements by measuring shear strength of weak layers*. ISSW Proceedings 6.5 Paper 3. 1996.

26.   Schallamach, A. *Load Dependence of Rubber Friction*. Proceedings Physical Society – Volume 65. 1952.

27.   Thirion, P. *Revue Générale Caoutchouc*, 23,101 – 1946

28.   Horne, W.B., Smiley, R.F. and Stephenson, B.H. *Low-speed yawed rolling and some other elastic characteristics of two 56-inch diameter, 24 ply rating aircraft tyres*. NACA TN 3235. 1954.

29.   Horne, W.B., Smiley, R.F. and Stephenson, B.H. *Low-speed yawed rolling and some other elastic characteristics of two 26-inch diameter, 12 ply rating aircraft tyres*. NACA TN 3604. 1956.

30.   Horne, W.B. and Smiley, R.F. *Low-speed yawed rolling and some other elastic characteristics of two 40-inch diameter, 14 ply rating aircraft tyres*. NACA TN 4109. 1958.

31.   Smiley, R.F. and Horne, W.B. *Mechanical properties of pneumatic tyres with special reference to modern aircraft tyres*. NACA TN 4110. 1958. (NASA TR R-64. 1960.)

32.   Horne, W.B. and Merritt, L.R. Private Communication.

33.   ESDU. *Frictional and retarding forces on aircraft tyres. Part 1 – Introduction*. ESDU Data Item 71025 with amendments A to D. April 1995.

34.   Gough, V.E. *Physics of tire traction – Theory and experiment* (pp 281 – 297). Plenum Press. 1974.

35.   Andresen, A. *Is friction tire dependent*? Proceedings of IMAPCR '96. Transportation Development Centre of Transport Canada. TP 12943. October 1996.

36.   Anon. *Tests with a heavy load skidding machine to determine the friction coefficient between an aircraft tyre and various wet surfaces. Part 2, locked-wheel trials on the Road Research Laboratory track at Crowthorne*. Ministry of Aviation S&T Memo 5-64. June 1964.

37.   Horne, W.B. and Joyner, U.T. *Traction of pneumatic tyres on wet runways* (pp 9-17). Conference on aircraft operation problems, NASA Langley Research Center. NASA SP 83. May 10-12, 1965.

38.   Williams, T. *Measurements of locked wheel braking force coefficients on a variety of wet surfaces using smooth and patterned aircraft tyres*. RRL LN-672-TW. September 1964.

39.   Williams, T. *The relation between braking force coefficient and slip for an aircraft tyre braked on four wet surfaces*. Road Research Laboratory RRL Report N° 50. 1966.

40.   Moore, D.F. *The friction of pneumatic tyres* (pp129-130). Elsevier Scientific Publishing Company, Oxford. 1975.

41.   Grosch, K.A. *The physics of tire traction – theory and experiment* (pp 143 – 163). Hays and Browne (Eds). Plenum Press, New York and London. 1974.

42.   Sawyer, R.H. and Kolnick, J.J. *Tyre-to-surface friction-coefficient measurements with a C-123B airplane on various runway surfaces*. NASA TR R-20. November 1959.

43.   Yager, T.J., Phillips, W.P., Horne. W.B. and Sparks, H.C. *A comparison of aircraft and ground vehicle stopping performance on dry, wet, flooded, slush, snow and ice-covered runways*. Final report on project combat traction, a joint USAF-NASA program. NASA TN D-6098. November 1970.

44.   Leland, T.J.W., Yager, T.J. and Joyner, U.T. *Effects of pavement texture on wet-runway braking performance*. NASA TN D-4323. January 1968.

BIBLIOGRAPHY

The documents that have been studied in the course of constructing and confirming the mathematical model described in this report are listed in date order. Many of these documents contain data that have been omitted from both the construction of the model and from the justification. The major reason for not considering much of the data is that many of the sources have not recorded sufficient information to allow analysis in the format of this modelling. For example, many sources do not quote the depth of the macro-texture of the runways for which test data in wet conditions were collected. In the context of the modelling, this renders the information useful only in a qualitative way. In addition, contaminant depth is frequently not recorded. So, although references often contain valuable insights to the problem of friction loss due to contamination, data recording deficiencies render much of the research unusable as an aid to *quantifying* the extent of the problem.

1	A Schallamach	*The load dependence of rubber friction*. The British Rubber Producers Association. Publication Number 166: 1952
2	R Hadekel	The mechanical characteristics of pneumatic tyres. S&T Memo 10/52: November 1952
3	A Schallamach	*Frictional temperature rises on rubber*. The British Rubber Producers Association. Publication Number 250: 1955
4	CG Giles FTW Lander	*The skid-resisting properties of wet surfaces at high speeds – exploratory measurements with a small braking force trailer*. Road Research Laboratory RN/2431/CGG.FTWL. April 1955
5	Esiaslav N Harrin	*Low tire friction and cornering forces on a wet surface.* NASA TN 4406. September 1958
6	A Schallamach	*Friction and abrasion of rubber*. Rubber chemistry and technology, Vol. XXXI No. 5, December 1958
7	Richard H Sawyer Joseph J Kolnick	*Tire-to-surface friction-coefficient measurements with a C-123B airplane on various runway surfaces.* NASA TR R-20. 1959.
8	Richard H Sawyer Sidney A Batterson Esiaslav N Harrin	*Tire-to-surface friction under wet conditions*. NASA Memo 2-23-59L. March 1959.
9	A Schallamach DN Turner	*The wear of slipping wheels.* The British Rubber Producers Association. Publication Number 338: 1960.
10	Robert F Smiley Walter B Horne	*Mechanical properties of pneumatic tires with special reference to modern aircraft tires*. NASA TR R-64. 1960.
11	Walter B Horne Upshur T Joyner Trafford JW Leland	*Studies of the retardation force developed on an aircraft tire rolling in slush or water*. NASA TN D-552. September 1960.

12	D Bulgin GD Hubbard MH Walters	*Road and laboratory studies of friction of elastomers.* Presented at the fourth Rubber Technology Conference, London, 1962.
13	Jack J Shrager	*Vehicular measurements of effective runway friction.* Final Report Project 308-3X. Federal Aviation Agency, May 1962.
14	Walter B Horne Trafford JW Leland	*Influence of tire tread pattern and runway surface condition on braking friction and rolling resistance of a modern aircraft tire.* NASA TN D-1376. September 1962.
15	KA Grosch	*The relation between the friction and visco-elastic properties of rubber.* The Natural Rubber Producers' Association, Publication No. 468, 1963.
16	FTW Lander T Williams	*Tests on the effect of wheel load and inflation pressure on the locked wheel braking performance of an aircraft tyre braking under wet conditions on typical surfaces.* Road Research Laboratory LN/455/FTWL.TW, October 1963.
17	RV Barrett	*Drag and spray measurements from a small pneumatic tyre travelling through a water layer.* S&T Memo 11/63. December 1963.
18	-	*Tests with a heavy load skidding machine to determine the friction coefficient between an aircraft tyre and various wet surfaces.* Part 2. S&T Memo 5/64, June 1964.
19	T Williams	*Measurements of the locked wheel braking force coefficients on a variety of wet surfaces using smooth and patterned aircraft tyres.* Road Research Laboratory LN/672/TW, September 1964.
20	-	*Tests with a heavy load skidding test vehicle incorporating a Mark 1 maxaret anti-locking brake system to determine braking force coefficients between an aircraft tyre and various wet surfaces.* S&T Memo 10/64, January 1965
21	T Williams	*Tests to determine the effect of tyre wear on the skidding resistance of an aircraft tyre under wet conditions.* Road Research Laboratory LN/817/TW, April 1965.
22	Trafford W Leland Glenn R Taylor	*An investigation of the influence of aircraft tire-tread wear on wet runway braking.* NASA TN D-2770. April 1965.
23	ES Lawrence	Measurements of the skidding resistance of truck tyres in wet conditions to determine the effects of tread pattern, tread material and tyre construction. Road Research Laboratory LN/859/ESL, May 1965.
24	Walter B Horne Upshur T Joyner	*Traction of pneumatic tires on wet runways.* Proceedings of Conference on Aircraft Operating Problems, NASA SP-83, pp9 17. May 1965.

192

25	Sidney A Batterson	*A study of the dynamics of airplane braking systems as affected by tire elasticity and brake response.* NASA TN D-3081. October 1965.
26	RW Sugg	*The drag of a large and small pneumatic tyre travelling through water, slush and snow.* S&T Memo 9/66. 1966.
27	Barbara E Sabey	*Road surface texture and the change in skidding resistance with speed.* Road Research Laboratory RRL Report No. 20, 1966.
28	T Williams	*The relation between braking force coefficient and slip for an aircraft tyre braked on four wet surfaces.* Road Research Laboratory RRL Report No. 50, 1966.
29	FTW Lander	*Measurements of the skidding resistance on the main North/South runways at RAE Farnborough.* Road Research Laboratory RRL Technical Note No. 115, 1966.
30	KE Holmes	*A comparison of sideway force and braking force coefficients at 30mph using a smooth tyre on six wet surfaces of different textures.* Road Research Laboratory RRL Technical Note No. 53, March 1966.
31	H Ordman	*A grease patch method for measuring the depth of texture of road surfaces.* Road Research Laboratory RRL Technical Note No. 122, October 1966.
32	HW Kummer WE Meyer	*Tentative skid-resistance requirements for main rural highways.* National Cooperative Highway Research Program Report 37, 1967.
33	FTW Lander	*A vehicle for measuring the skidding resistance of roads and runways under heavy loading conditions.* Road Research Laboratory RRL Report No. LR 56, 1967.
34	Barbara E Sabey GN Lupton	*Measurement of road surface texture using photogrammetry.* Road Research Laboratory RRL Report No. LR 57, 1967.
35	JK Meades	*Braking force coefficients obtained with a sample of currently available radial ply and crossed ply car tyres.* Road Research Laboratory RRL Report No. LR 73, 1967.
36	G Maycock	*Experiments on tyre tread patterns.* Road Research Laboratory RRL Report No. LR 122, 1967.
37	Edward R LaChapelle Ronald I Perla	*Mechanical properties of the soft slab.* US Department of Agriculture, Forest Service. Alta Avalanche Study, Report No. 2, June 1967.
38	AC Browning BC Kerwell	*High-speed taxying and braking trials of a Beverley aircraft on a runway covered in wet snow, crisp snow and shallow slush.* RAE Technical Report TR 67193, August 1967.

39	Barbara E Sabey	*Wet road skidding resistance at high speeds on a variety of surfaces on A1*. Road Research Laboratory RRL Report No. LR 131, 1968.
40	FTW Lander T Williams	*The skidding resistance of wet runway surfaces with reference to surface texture and tyre conditions.* Road Research Laboratory RRL Report No. LR 184, 1968.
41	JK Meades	*The effect of tyre construction on braking force coefficients.* Road Research Laboratory RRL Report No. LR 224, 1968.
42	NF Ross K Russam	*The depth of rainwater on road surfaces*. Road Research Laboratory RRL Report No. LR 236, 1968.
43	Trafford JW Leland Thomas J Yager Upshur T Joyner	*Effects of pavement texture on wet-runway braking performanc*e. NASA TN 4323. January 1968.
44	BJ Allbert	*Tyres and hydroplaning.* Society of Automotive Engineers, Automotive Engineering Congress, 680140, January 1968
45	A Schallamach	*Recent advances in knowledge of rubber friction and tire wear.* Rubber Chemistry and Technology, Vol. 41, No. 1, February 1968.
46	George W Brooks (Chairman)	*Pavement grooving and traction studies.* Proceedings of Conference held at Langley Research Center, NASA SP-5073, November 1968.
47	KB Wallace DH Trollope	*Water pressure beneath a skidding tyre.* Wear, 13 (1969) pp109 118.
48	GC Staughton	*Some measurements of braking force coefficient on six airfield test surfaces.* Road Research Laboratory RRL Report No. LR 225, 1969.
49	DE Weller DP Maynard	*Treatments to retexture a worn concrete surface of a high-speed road.* Road Research Laboratory RRL Report No. LR 250, 1969.
50	KE Holmes RD Stone	*Tyre forces as a function of cornering and braking slip on wet road surfaces.* Road Research Laboratory RRL Report No. LR 254, 1969.
51	EJ Key EM Minter	*Aircraft braking friction trials on a coarse open graded macadam runway surface.* RAE Technical Report TR 69123, June 1969.
52	KE Holmes	*Braking force/braking slip. Measurements over a range of conditions between 0 and 100 percent slip*. Road Research Laboratory RRL Report No. LR 292, 1970.
53	GC Staughton	*The effects of tread pattern depth on skidding resistance.* Road Research Laboratory RRL Report No. LR 323, 1970.

54	Walter B Horne Howard C Sparks	*New methods for rating, predicting and alleviating the slipperiness of airport runways.* Society of Automotive Engineers, National Air Transportation Meeting, 700265, April 1970.
55	Walter B Horne Upshur T Joyner	*Determining causation of aircraft skidding accidents or incidents.* Presentation at 23rd Annual International Safety Seminar, Flight Safety Foundation Inc., October 1970.
56	Thomas J Yager W Pelham Phillips Walter B Horne	*A comparison of aircraft and ground vehicle stopping performance on dry, wet, flooded, slush-, snow-, and ice-covered runways.* Final Report of Project Combat Traction, a Joint USAF-NASA Program. NASA TN D-6098. November 1970.
57	JR Williams I Beaty	*An investigation into the drag due to slush using a Canberra aircraft.* Cranfield Institute of Technology. CIT-FI-71-010, 1971
58	Thomas J Yager W Pelham Phillips Perry L Deal	*Evaluation of braking performance of a light, twin-engine airplane on grooved and ungrooved pavements.* NASA TN D-6444, October 1971.
59	Walter B Horne Thomas J Yager Robert K Sleeper Leslie R Merritt	*Preliminary test results of the joint FAA-USAF-NASA runway research program. PartI – Traction measurements of several runways under wet and dry conditions with a Boeing 727, a diagonal braked vehicle and a Mu-meter.* NASA Langley Working Paper, LWP – 1016, December 1971.
60	-	*Measurement of runway friction – Airplane/DBV/Mu-meter correlation tests.* Federal Aviation Administration, Report No. FS-160-65-68-4, January 1972.
61	John A Tanner	*Performance of an aircraft tire under cyclic braking and of a currently operational antiskid braking system.* NASA TN D-6755, May 1972.
62	Walter B Horne Thomas J Yager Robert K Sleeper Eunice G Smith Leslie R Merritt	*Preliminary test results of the Joint FAA-USAF- NASA runway research program. Part II – Traction measurements of several runways under wet, snow-covered and dry conditions with a Douglas DC-9, a diagonal-braked vehicle and a Mu-meter.* NASA Langley Working Paper, LWP 1051, September 1972.
63	Robert C Dreher Robert K Sleeper John R Nayadley, Sr	*Experimental investigation of an accelerometer controlled automatic braking system.* NASA TN D-6953, October 1972.
64	GF Salt WS Szatkowski	*A guide to levels of skidding resistance for roads.* Transport and Road Research Laboratory TRRL Report No. LR 510, 1973.

65	T Williams JK Meades BS Riley	*The wet road grip of lorry tyres: a comparison of three types*. Transport and Road Research Laboratory TRRL Report No. LR 544, 1973.
66	GN Lupton T Williams	*Study of the skid resistance of different tyre tread polymers on wet pavements with a range of surface textures*. American Society for Testing and Materials. Special Technical Publication 530, 1973.
67	Donald F Hays Alan L Browne (Editors)	*The physics of tyre traction: theory and experiment*. Plenum Press, New York – London, 1974.
68	DRC Cooper	*Measurement of road surface texture by a contactless sensor*. Transport and Road Research Laboratory TRRL Report No. LR 639, 1974
69	GN Lupton T Williams	*Wet road skidding resistance*. Transport and Road Research Laboratory TRRL Supplementary Report 86UC, 1974
70	Walter B Horne	*Elements affecting runway traction*. Society of Automotive Engineers, Air Transportation Meeting, 740496, April 1974.
71	EJ Key EM Minter	*Aircraft trials to assess the Dunlop Mk.2 and Mk.5 anti-skid systems*. RAE Technical Report TR 74049, August 1974.
72	-	*Studies concerning snow, ice and slush on runways*. The Aeronautical Research Institute of Sweden. Report FFA MU-792/3. 1974.
73	Leslie R Merritt	*Concorde landing requirement evaluation tests*. Federal Aviation Administration. Report No. FAA-FS-160-74-2, August 1974.
74	Bo Norrbom Knut Fristedt	*Studies concerning snow, ice and slush on runways*. The Aeronautical Research Institute of Sweden. FFA Memo 106, 1975.
75	Desmond F Moore	*The friction of pneumatic tyres*. Elsevier Scientific Publishing Company, Amsterdam-Oxford-New York, 1975.
76	T Williams JK Meades	*Effects of tread pattern depth and tyre grooving on lorry tyre skidding resistance*. Transport and Road Research Laboratory TRRL Report No. LR 687, 1975
77	WV Levitsky	*Report on the coefficient of friction evaluation of new Portland cement concrete broomed finish runway 11/29 Mirabel International Airport*. Transport Canada, AK-71-09-004, January 1975.
78	JW Blanchard	*An analysis of the B727 and DC9 trials on wet runways with the Mu-meter and diagonal braked vehicle (DBV)*. Civil Aviation Authority Paper 75015. January 1975.

79	JH Williams	*Analysis of standard USAF runway skid resistance tests*. Airforce Civil Engineering Centre Technical Report AFCEC TR 75-3.
80	LR Merritt	*Analysis of tests conducted by the French Ministry of Armed Forces Flight Test Center for the Service Technique Aeronautique utilizing a Caravelle 116 aircraft and a diagonal braked vehicle*. Federal Aviation Administration Report No. FS-160-75-2, October 1975.
81	Thomas J Yager Robert C Dreher	*Traction characteristics of a 30x11.5-14.5, Type VIII, aircraft tire on dry, wet and flooded surfaces*. NASA TM X-72805, February 1976.
82	Walter B Horne John L McCarty John A Tanner	*Some effects of adverse weather conditions on performance of airplane antiskid braking systems*. NASA TN D-8202, July 1976.
83	-	*Correlation investigation of runway surface friction measurement equipment under winter conditions*. Transport Canada Report AK-71-09-19. September 1976.
84	Kenneth E Hodge (General Chairman)	*Aircraft safety and operating problems*. Proceedings of Conference at Langley Research Center. NASA SP-416, October 1976.
85	Sandy M Stubbs John A Tanner	*Behaviour of aircraft antiskid systems on dry and wet runway surfaces. A velocity-rate-controlled pressure-bias-modulated system*. NASA TN D-8332, December 1976.
86	John A Tanner Sandy M Stubbs	*Behaviour of aircraft antiskid systems on dry and wet runway surfaces. A slip-ratio-controlled system with ground speed reference from unbraked nose wheel*. NASA TN D-8455, October 1977.
87	RW Sugg	*A means of specifying a standard reference wet surface for a military aircraft*. S&T Memo 1-79. 1979.
88	I Beaty RW Sugg	*Trials to compare the stopping performance of three antiskid systems and to demonstrate methods to determine aircraft stop distances on the standard military reference wet surface*. S&T Memo 3-79. 1979.
89	RW Sugg I Beaty RJ Nicholls	*The friction classification of runways*. S&T Memo 6-79. 1979.
90	Mats Lidström	*Aircraft rolling resistance in loose dry snow. A theoretical analysis*. The National Road and Traffic Research Institute, Linköping, Sweden. A special issue of VTI Report 173A. 1979.
91	Mahinder K Wahi	*A tyre runway interface friction prediction model concept*. J. Aircraft, (Article No. 79-4086) Vol. 16, No. 6, June 1979.

92	Sandy M Stubbs John A Tanner Eunice G Smith	*Behaviour of aircraft antiskid systems on dry and wet runway surfaces. A slip-velocity-controlled pressure-bias-modulated system.* NASA Technical paper 1051. December 1979.
93	K Fristedt B Norrbom	*Studies of contaminated runways.* The Aeronautical Research Institute of Sweden. FFA Memo 121. Stockholm 1980.
94	Thomas J Yager Ellis J White	*Recent progress towards predicting aircraft ground handling performance.* NASA Technical Memorandum 81952. 1981.
95	WJG Pinsker	*Tyre drag below and above aquaplaning speed on surfaces covered with slush and water.* RAE Technical Report, TRE 81068. May 1981.
96	HA Wilkins BS Riley	*The road grip of commercial vehicle tyres.* Transport and Road Research Laboratory TRRL Supplementary Report No. 768, 1982.
97	WB Horne F Buhlmann	A *method for rating the skid resistance and micro-/macro-texture characteristics of wet pavements. Frictional interaction of tyre and pavement*, ASTM STP 793. WE Meyer and JD Walter, Eds., American Society for testing and Materials, 1983.
98	Satish K Agrawal	*Braking of an aircraft tire on grooved and porous asphaltic concrete.* Final Report DOT/FAA/CT-82/147, DOT/FAA/RD-82/77. January 1983.
99	Thomas H Morrow	R*eport on the performance reliability and correlation of the Mu-meter and SAAB friction tester under self-wetting and simulated rainfall conditions*. Federal Aviation Administration, Report No. FAA-AAS-82-VI, March 1983.
100	DJ Mitchell	*Current views on use of runway friction measuring machines.* Engineering Sciences Data Unit. Paper P270.
101	Thomas J Yager William A Vogler Paul Baldasare	*Summary report on aircraft and ground vehicle friction correlation test results obtained under winter runway conditions during joint FAA/NASA runway friction program.* NASA Technical Memorandum 100506. March 1988.
102	S Colbeck (Chairman)	*The international classification for seasonal snow on the ground. Working group on snow classification.* Issued by The International Commission on Snow and Ice and the International Glaciological Society. 1990.
103	Thomas J Yager William A Vogler Paul Baldasare	*Evaluation of two transport aircraft and several ground test vehicle friction measurements obtained for various runway surface types and conditions. A summary of test results from joint FAA/NASA runway friction program.* NASA Technical Paper 2917. February 1990.

104   W Wagner
      A Saul
      A Pruβ

International equations for the pressure along the melting and along the sublimation curve of ordinary water substance. J. Phys. Chem. Ref. Data, Vol. 23, No. 3, 1994.

105   Ahmed K Noor
      John A Tanner

Computational modelling of tires. NASA Conference Publication 3306.

106   Paul W Richmond

Motion resistance of wheeled vehicles in snow. CRREL Report 95-7, March 1995.

107   -

Frictional and retarding forces on aircraft tyres. Part 1: Introduction. ESDU Data Item 71025 with Amendments A to D, April 1995.

108   Paul Föhn
      Christian Camponovo

Improvements by measuring shear strength of weak layers. ISSW Proceedings 6.5 Paper 3, 1996.

109   JB Croll
      JCT Martin
      M Bastian

Determination of Falcon 20 landing distances on winter contaminated runways as a function of the James Brake Index. National Research Council Canada. NRC No. 32173, Transport Canada Publication TP 12891E, August 1996.

110   James C Wambold

Evaluation of ground test friction measuring equipment on runways and taxiways under winter conditions. Transport Canada Publication TP 12866E, September 1996.

111   JCT Martin
      John B Croll
      Matthew Bastian

Braking friction coefficient and contamination drag obtained for a Falcon 20 on winter contaminated runway surfaces. National Research Council Canada. LTR-FR-132, September 1996.

112   G Argue
      A Krol

Runway winter friction measurement trials at North Bay airport. Aerodrome Safety, Civil Aviation, Transport Canada Publication TP 12887E. October 1996.

113   Art Jordan

Proceedings of the international meeting on aircraft performance on contaminated runways. Transportation Development Centre of Transport Canada. TP 12943, October 1996.

114   Robert H Daugherty
      Thomas J Yager

Texture modification of the shuttle landing facility runway at Kennedy Space Center. NASA Technical Paper 3626, May 1997.

115   JB Croll
      JCT Martin
      M Bastian

Falcon 20 aircraft performance testing on contaminated runway surfaces during the winter of 1996/1997. National Research Council Canada. LTR-FR-137. August 1997.

116   Lewis H Shapiro *et al*

Snow mechanics. Review of the state of knowledge and applications. CRREL Report 97-3, August 1997.

117   Mark Doogan
      Eric Herrmann
      Phil Lamont

Braking Friction Coefficient and Contamination Drag for the Dash 8 on winter contaminated runways. de Havilland Inc. DHC-D4547-97-09, September 1997.

118	Angelo Boccanfuso	*Proceedings of the technical advisory group steering committee meeting on aircraft performance on contaminated runways.* Transport Canada. TP 13257, October 1997.
119	Gerard WH van Es Alfred LC Roelen Eric AC Kruijsen Maijn KH Giesberts	*Safety aspects of aircraft performance on wet and contaminated runways.* Flight Testing and Safety Department National Aerospace Laboratory, NLR. Presented at the 10th annual European Aviation Safety Seminar, Amsterdam, March 1998.
120	GWH van Es	*Rolling resistance of aircraft tires in dry snow.* National Aerospace Laboratory NLR. NLR-TR-98165, July 1998.
121	JB Croll JCT Martin M Bastian	*Falcon 20 aircraft performance testing on contaminated runway surfaces during the winter of 1997/1998.* National Research Council Canada. LTR-FR-151, Transport Canada Publication TP 13338E, December 1998.
122	GWH van Es	*Method for predicting the rolling resistance of aircraft tires in dry snow.* Journal of Aircraft, Volume 36, Number 5, pp 762-768.
123	Gerard WH van Es	*Hydroplaning of modern aircraft tires.* National Aerospace Laboratory NLR. Technical Paper 1999.
124	Gerard WH van Es	*Method for predicting the rolling resistance of aircraft tires in dry snow.* National Aerospace Laboratory NLR. Technical paper TP-99240. 1999.
125	Armann Norheim Nirmal K Sinha Thomas J Yager	*Effects of the structure and properties of ice and snow on the friction of aircraft tyres on movement area surfaces.* Tribology International, Volume 34, Number 9, September 2001.
126	-	*Statistical analysis of wet runway friction for aircraft and ground test machines.* ESDU Data Item 99015 with Amendments A and B September 2003.

APPENDIX A

AIRCRAFT TYRE MODEL ROLLING IN SATURATED CLAY

Introduction

The scheme for correlating and analysing data from tests in fresh, unworked snow has been based on the presumption that there is a similarity between the resistance to motion generated on a wheel rolling in snow and that for a wheel rolling on soft ground. For thin layers of snow on paved runways, the similarity between that case and soft ground of semi-infinite depth is marginal and it would be imprudent to pursue the analogy too far. However, the guidance to correlation that can be found from studying a systematic series of tests is often invaluable.

Now, the study reported in Reference A1 was based on a dimensional analysis and the data contained in the report were the result of a systematic series of experiments that, uniquely, covered a wide speed range. Two inflatable tyres were used: these tyres were model scale replicas of tyres fitted to the Blackburn Beverley and the Gloster Meteor. In this appendix, the data for the Beverley model are considered solely to show the development of a correlation scheme for soft ground testing and the factors that the scheme has in common with that adopted for aircraft and other vehicles when rolling over snow-covered runways. Relevant data are summarised in Table A1. The statistics of the measurements and correlating functions are also briefly studied.

Correlation

The experiments reported in Reference A1 were based on a dimensional analysis. However, the subsequent analysis of the data did not attempt to define a mathematical model of the results. Three groupings of the two force coefficients and non-dimensional rut depth have been found, all of which correlate with speed number N $\left(\text{where } N^2 = \rho V^2 / C_u \right)$. These groupings are:

$$\Phi_1 = \frac{C_G}{\left(s_{RUT}/D \right)^{1/3} C_Z^2} = \frac{0.8}{\left(1+N^2 \right)^{1/2}} \left\{ 1+16.25 \left(1 - 1 / \left(1+N^2 \right)^{1/2} \right)^4 \right\} \qquad \text{A1}$$

Where $C_G = G / D^2 C_u$ and $C_Z = Z / D^2 C_u$.

$$\Phi_2 = \frac{s_{RUT}/D}{C_Z^2} = \frac{0.075}{\left(1+N^2 \right)^{1/2}} \left\{ 1+6.67 \left(1 - 1 / \left(1+N^2 \right)^{1/2} \right)^4 \right\} \qquad \text{A2}$$

and, dividing Equation A1 by Equation A2,

$$\Phi_3 = \frac{C_G}{\left(s_{RUT}/D\right)^{4/3}} = 10.67 \left\{ \frac{\left[\left(1+16.25\left(1-1\Big/\left(1+N^2\right)^{1/2}\right)^4\right)\right]}{\left[\left(1+6.67\left(1-1\Big/\left(1+N^2\right)^{1/2}\right)^4\right)\right]} \right\} \qquad \text{A3}$$

The grouping described in Equation A3, but not the correlating function, has been used as a guide to the correlation scheme for aircraft rolling in snow. Figures A1 to A3 show the effects of speed number on the non-dimensional groupings.

The modelling equations have been deliberately limited in the freedoms allowed for fitting. Thus, only two freedoms have been allowed for both Equations A1 and A2. The fit to the data is very encouraging in spite of the constraints imposed in the curve-fitting process. There is some evidence to suggest that the values of speed number at which the maximum and minimum values of the two functions occur are missed by the function described. However, the statistics (see below) of the scatter about the correlating functions can be interpreted to imply that further refinements and complications in the curve-fitting process are not justifiable. The derivation of the fit to the third group maintains the same constraints as those imposed in the process of fitting the first and second groups.

Results from the other inflatable tyre studied in the experiment conform to the same model. However, further study is necessary because tyre diameter does not seem to be the most effective basis on which to define a reference area for force coefficients.

It is concluded that there is considerable merit in using the data from Reference A1 as a good guide to the analysis of speed effects on the forces generated on tyres rolling in soft ground. Furthermore, there appears to be considerable promise that modelling of operations on soft ground can be unified with modelling of operations on snow-covered runways.

Statistics

Using standard methods, it can be shown that

$$C_V^2\left[\Phi_1\right] = C_V^2\left[C_G\right] + \frac{1}{9}C_V^2\left[s_{RUT}/D\right] + 4C_V^2\left[C_Z\right] \qquad \text{A4}$$

$$C_V^2\left[\Phi_2\right] = C_V^2\left[s_{RUT}/D\right] + 4C_V^2\left[C_Z\right] \qquad \text{A5}$$

$$C_V^2\left[\Phi_3\right] = C_V^2\left[C_G\right] + \frac{16}{9}C_V^2\left[s_{RUT}/D\right] \qquad \text{A6}$$

Where the coefficient of variation C_V, of a quantity $[x]$ is defined by $C_V[x] = \sigma[x]/\mathrm{E}[x]$.

Given estimates of the coefficients of variation of the measured variables on the right hand side of Equations A4 to A6, the coefficients of variation of the correlating functions can be calculated. Conversely, given estimates of the coefficients of variation of the scatter about the

correlations described by Equations A1 to A3, Equations A4 to A6 can be solved simultaneously for the coefficients of variation of the measured variables. The results of both these sets of calculations are contained in Table A2. Clearly, from inspecting the correlations as shown in Figures A1 to A3, the correlating functions provide an adequate collapse of the data. Furthermore, the relationships described by Equations A1 to A3 are a satisfactory representation of the variations of the functions with speed number N. The coefficients of variation, as indicated by the scatter about the correlations seem to be reasonable with no evidence of unacceptable over-fitting.[1] Thus, it seems from the evidence in Table A2 that the estimates given in Reference A1 for coefficients of variation for the measured variables are quite conservative. This is illustrated in Figure A4, which is a plot of coefficient of resistive force for a range of rut depths. None of the measurements differs from the correlation by more than approximately 10% of the correlated value. On this evidence and on that of the correlations, it may be inferred that a less conservative estimate for the precision of the variables obtained in this particular test series should be based on coefficients of variation of the order 0.05 (5%).

Table A1: Soft ground data from Reference A2

Wheel	Series	D in	p psig	C_u psi	N	s/D	C_Z	C_G	$\dfrac{C_G}{(s/D)^{1/3} C_Z^2}$	$\dfrac{s/D}{C_Z^2}$	$\dfrac{C_G}{(s/D)^{4/3}}$
B	214	8	25	3.3	0.111	0.026	0.57	0.083	0.859	0.080	10.73
B	214	8	25	3.3	0.691	0.024	0.57	0.076	0.815	0.074	11.03
B	214	8	25	3.3	1.357	0.020	0.57	0.069	0.782	0.062	12.70
B	214	8	25	3.3	2.228	0.018	0.57	0.079	0.924	0.055	16.67
B	214	8	25	3.3	3.113	0.018	0.57	0.088	1.038	0.055	18.73
B	214	8	25	3.3	3.977	0.019	0.57	0.103	1.183	0.058	20.24
B	214	8	25	3.3	4.841	0.018	0.57	0.112	1.312	0.055	23.68
B	214	8	25	3.3	5.696	0.018	0.57	0.113	1.325	0.055	23.92
B	312	8	15	1.93	0.102	0.034	0.65	0.107	0.779	0.080	9.68
B	312	8	15	1.93	1.159	0.025	0.65	0.091	0.737	0.059	12.45
B	312	8	15	1.93	1.748	0.021	0.65	0.090	0.770	0.050	15.48
B	312	8	15	1.93	2.883	0.020	0.65	0.118	1.032	0.047	21.79
B	312	8	15	1.93	4.009	0.024	0.65	0.142	1.163	0.057	20.47
B	312	8	15	1.93	5.121	0.026	0.65	0.159	1.267	0.062	20.59
B	312	8	15	1.93	6.215	0.025	0.65	0.163	1.321	0.059	22.32
B	312	8	20	1.93	7.382	0.021	0.65	0.153	1.310	0.050	26.36
B	313	8	20	1.93	0.094	0.048	0.82	0.180	0.735	0.071	10.29
B	313	8	20	1.93	1.156	0.036	0.82	0.156	0.702	0.054	13.11
B	313	8	20	1.93	1.736	0.033	0.82	0.163	0.757	0.049	15.42
B	313	8	20	1.93	2.874	0.034	0.82	0.215	0.986	0.051	19.50
B	313	8	20	1.93	3.967	0.034	0.82	0.270	1.238	0.051	24.49
B	313	8	20	1.93	5.118	0.041	0.82	0.296	1.277	0.061	20.94
B	313	8	20	1.93	6.248	0.037	0.82	0.260	1.160	0.055	21.08
B	313	8	20	1.93	7.398	0.031	0.82	0.226	1.068	0.046	23.16
B	314	8	25	1.93	0.088	0.075	0.98	0.305	0.753	0.078	9.64
B	314	8	25	1.93	1.458	0.051	0.98	0.245	0.688	0.053	12.95
B	314	8	25	1.93	2.002	0.049	0.98	0.281	0.800	0.051	15.69
B	314	8	25	1.93	2.842	0.046	0.98	0.326	0.948	0.048	19.80
B	314	8	25	1.93	3.980	0.054	0.98	0.451	1.242	0.056	22.09

---

[1]   All the distributions satisfy tests for normality.

Wheel	Series	D in	p psig	C_u psi	N	s/D	C_Z	C_G	$\dfrac{C_G}{(s/D)^{1/3} C_Z^2}$	$\dfrac{s/D}{C_Z^2}$	$\dfrac{C_G}{(s/D)^{4/3}}$
B	314	8	25	1.93	5.119	0.066	0.98	0.539	1.389	0.069	20.21
B	314	8	25	1.93	6.261	0.055	0.98	0.398	1.089	0.057	19.02
B	314	8	25	1.93	7.400	0.044	0.98	0.324	0.957	0.046	20.88

Table A2: Coefficients of variation for measured variables and correlating functions

Variable or function	Coefficient of variation	
	From data in Reference A2	Correlations of Equations A1 - A3
C_G	**0.075**	0.05
C_Z	**0.1**	0.05
s/D	**0.05**	0.05
Φ_1	0.2	**0.1**
Φ_2	0.2	**0.1**
Φ_3	0.1	**0.075**

Numbers printed in bold type have been used to calculate the numbers (in the same column) printed in standard type.
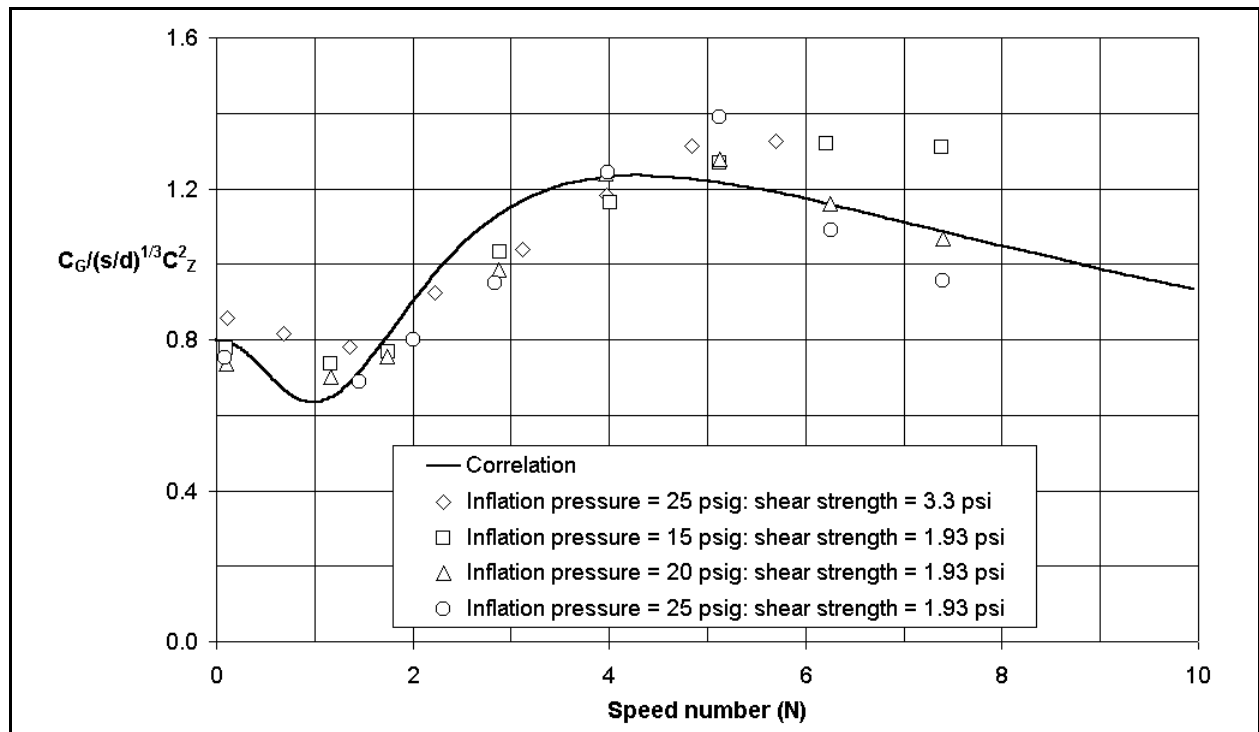
Figure A1: Effect of speed number on first correlating function
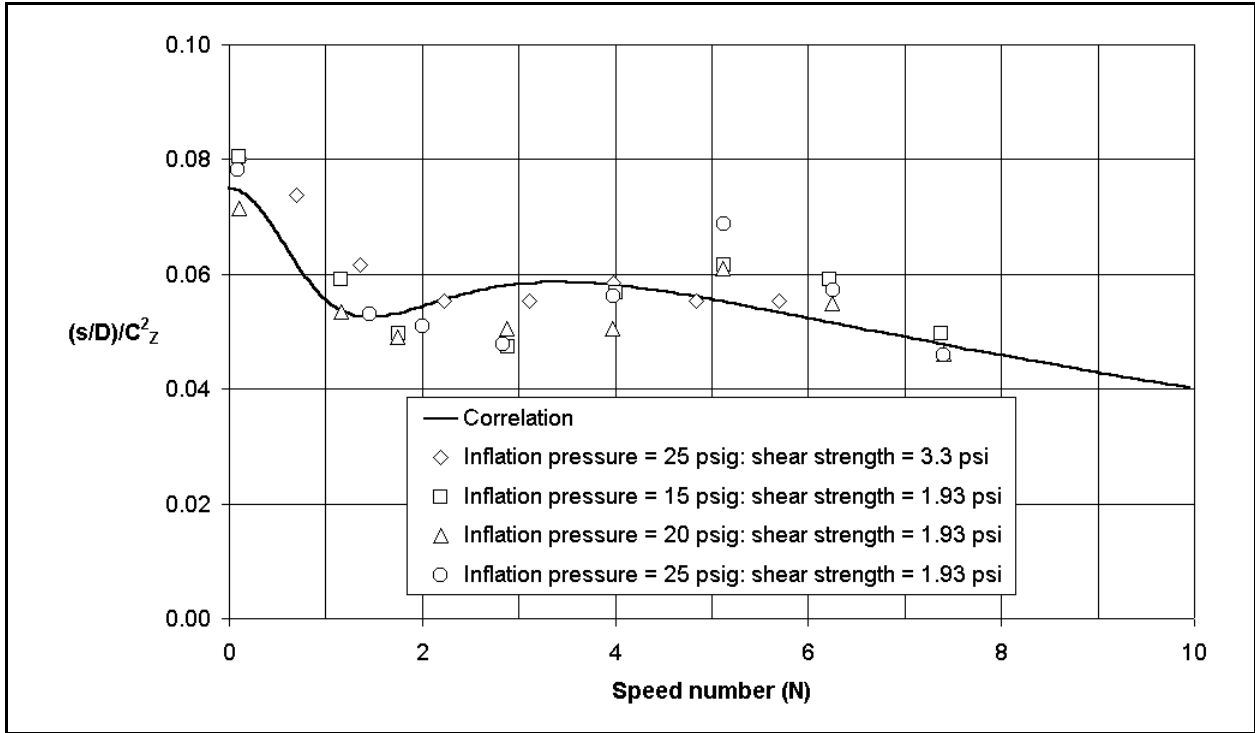
Figure A2: Effect of speed number on second correlating function
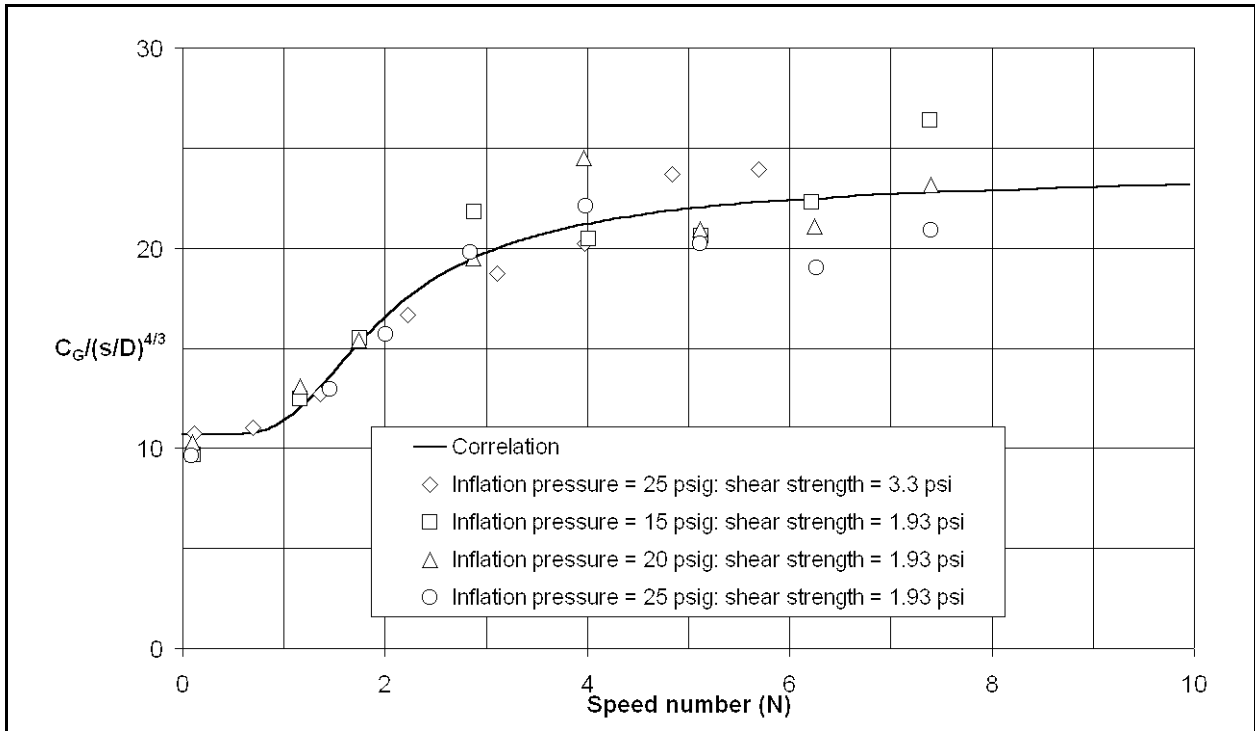
Figure A3: Effect of speed number on third correlating function
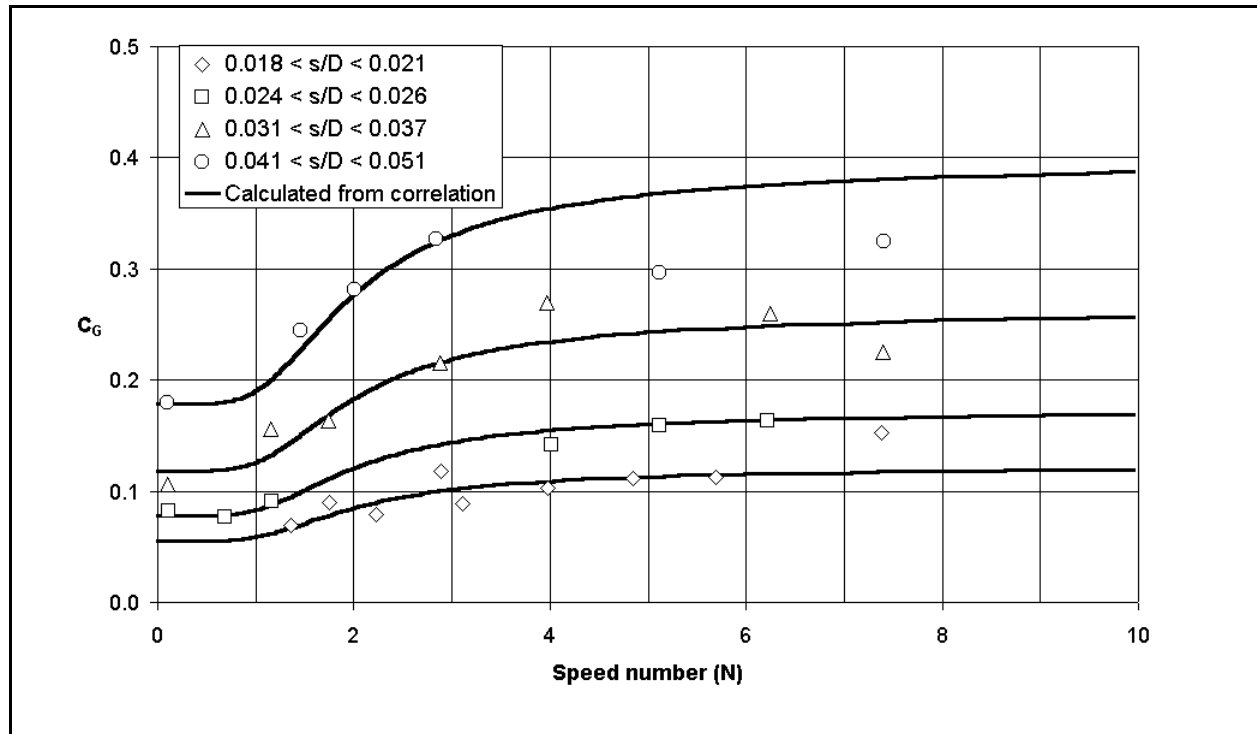
Figure A4: Effect of speed number and rut depth on coefficient of resistive force

References

A1.   Shanks, D.H. and Barrett, R.V. *Performance of aircraft pneumatic tyres in soft soil.* Aeronautical Journal (pp. 20-28). January 1981.

A2.   Shapiro, L.H. et al. *Snow mechanics. Review of the state of knowledge and applications.* CRREL Report 97-3. 1997.

APPENDIX B

SHEAR STRENGTH AND CHARACTERISTIC SPEED FOR FRESH, LOW-DENSITY SNOW

Shear strength data, from Reference B1 for bonded snow over a temperature range so that $-3 > T - C > -10$ are collected from many sources; but there is no indication of how well the curve fitted to the median value

$$C_u = 5.6 \times 10^4 e^{-12.8 R_{VOID}^2}$$

B1

describes any individual source of data. References B2 and B3 contain shear strength information for snows of low density that is more or less in the range of density for the aircraft testing. None of these data were included in the compendium. Because the snow with which aircraft operators are concerned is likely to be new and of low specific gravity, the information for these low density snows are studied in this appendix in an attempt to assess the statistical implications of using the correlation.

Figures B1 and B2 show the effect of void ratio on, respectively, shear strength and characteristic speed $b \left(= \sqrt{C_u / \rho} \right)$ for low-density snow. It is clear that a significant range of void ratio has been covered in the testing reported in the main text. In particular, the testing on the Beverley and the Citation II was conducted at each end of the range indicated in the figures.

The data from Reference B2 were collected as part of a set of experiments to determine shear strength in the context of avalanche initiation. Data from this document had been collected using a penetrometer[1] developed especially for the purpose. In principle, it is a brass-tipped wooden cone and is dropped from several heights into the snow surface. A mean value of "resistive" pressure C_s is calculated. This has been related[2] to mean shear stress in the layer by

$$C_u = 0.0674 C_s$$

B2

The depth of the layer over which the mean value was calculated was 0.5 ft. Fourteen measurements were taken in the concluding months of one (1967) avalanche season at Alta in Utah. The experiment was not designed to obtain the characteristic speed b: other parameters were sought. The value of resistive pressure was collected purely incidentally. Table B1 is a summary of the data.

In general, at these low densities, it appears from Table B1 that weathering affects both density and shear strength in equal measure so that characteristic speed remains sensibly constant over time. The prediction for characteristic speed is lower than the mean value for the measurements.

---

[1]   From comments in other literature, it appears that this piece of equipment has been used extensively in experimental work since this first use.

[2]   See Reference B4.

This has little significance for the analyses undertaken so far. However, the prediction does reflect the tendency in the measurements to exhibit a minimum, nearly constant value at these densities. It is also encouraging that the data fall well within the limits recommended in the compendium.

The fitted curve has little physical significance as void ratio tends to unity. It may be expected that when void ratio is unity (that is, density is zero), both shear strength and characteristic speed will be zero. However, the mathematical form of the simple fitted curve precludes the prediction of this tendency. In order to satisfy such a criterion, a more complicated function would have to be deduced.

The data for shear strength from Reference B3 were collected from an experiment that was designed to demonstrate various phenomena. In particular, under the specific conditions of the experiment, the tested snow failed in brittle mode. No record was published of specific gravity for any of the 120 records plotted in Figure 5 of the reference. In order to make some use of the information it is initially assumed that the correlation of Equation B1 applies. Thus, an estimate of void ratio and therefore density and characteristic speed can be made. From these data the mean (expected) values for shear strength $\mathrm{E}[C_u]$, void ratio $\mathrm{E}[R_{VOID}]$ and characteristic speed $\mathrm{E}[b]$ are calculated. In order to define a probability ellipse at the 95% level of significance, it is necessary to estimate the standard error in shear strength due to random errors in void ratio and all other sources.

Let the variance of the measured values of shear strength be the sum of the variance due to snow density (or void ratio), the variance due to random errors in the measuring equipment and the random error due to shear strength *per se*. Thus,

$$\mathrm{var}\big[\mathrm{M}[C_u]\big] = \mathrm{var}[C_u] + \left(\frac{\partial C_u}{\partial R_{VOID}}\right)^2 \mathrm{var}\big[[R_{VOID}]\big] \qquad \text{B3}$$

where $\mathrm{var}[C_u]$ is the sum of the variance due to measurement error and that due to the distribution of C_u.

Now, the relation given in Equation B1 can be differentiated with respect to R_{VOID} so that

$$\frac{\partial C_u}{\partial R_{VOID}} = 2 \times (-12.8) \times R_{VOID} C_u \qquad \text{B4}$$

Thus, at the expected values, $\mathrm{E}[C_u] = 35.5 \ \mathrm{lbf/ft^2}$ and $\mathrm{E}[R_{VOID}] = 0.758$,

$$\left(\frac{\partial C_u}{\partial R_{VOID}}\right)^2 \approx 474,500 \left(\mathrm{lbf/ft^2}\right)^2 \qquad \text{B5}$$

From the measured data, $\text{var}\big[\text{M}[C_u]\big] = 15.2^2$. Let half the variance in these measured values be due to variability in void ratio.

Then, $\sigma[C_u]\big(=15.2/\sqrt{2}\big) = 10.75$ and $\sigma[R_{VOID}]\big(\approx 15.2/\sqrt{474500 \times 2}\big) \approx 0.0156$. The approximate envelope of data is, therefore, the ellipse:

$$\left\{ \frac{\text{E}[R_{VOID}]}{1.96\sigma[R_{VOID}]} \pm 1 \right\}^2 + \left\{ \frac{\text{E}[C_u]}{1.96\sigma[C_u]} \pm 1 \right\}^2 = 1 \qquad\qquad \text{B6}$$

shown in Figure B1.

A similar argument can be used to obtain an approximate envelope for derivations of characteristic speed from the information in Reference B3. It can be shown that $\text{E}[b] = 8.84$ and that $\sigma[b] = 1.97$. The ellipse based on these data is shown in Figure B2.

Inspection of Figures B1 and B2 is sufficient to show that the data from Reference B3 may be interpreted so that there is no contradiction between the limits as defined in the compendium and those data.

Table B1: Summary of results from Reference B2

Date - 1967	Time	ρ - slug/ft^3	C_u - lbf/ft^2	b - ft/s	Crystal type and slab structure
26 February	1300	0.052	0.73	3.75	Heavily rimed dendrites
14 March	1500	0.062	1.12	4.25	Rimed stellar crystals and graupel
15 March	1100	0.093	1.39	3.87	Slab of 14 March
16 March	1500	0.160	3.17	4.45	Slab of 14 March
19 March	0800	0.062	0.60	3.11	Heavily rimed assortment and graupel
19 March	1500	0.057	0.86	3.88	New snow and light winds since 0800
29 March	1500	0.088	1.32	3.87	Alternate layers: stellar, graupel and stellar
30 March	1100	0.052	0.53	3.19	Rimed assortment
30 March	1700	0.108	2.58	4.89	Same snow as at 1100 but with sun and wind crust 1 in thick
1 April	1500	0.036	0.66	4.28	Clusters of needles and stellars with light rime
13 April	1100	0.108	2.91	5.19	Damp snow – 1 day old
6 May	1700	0.201	3.44	4.14	Wet snow
11 May	1500	0.057	0.60	3.24	Partially melted dendrites
13 May	1700	0.052	0.46	2.97	Moderately rimed stellars
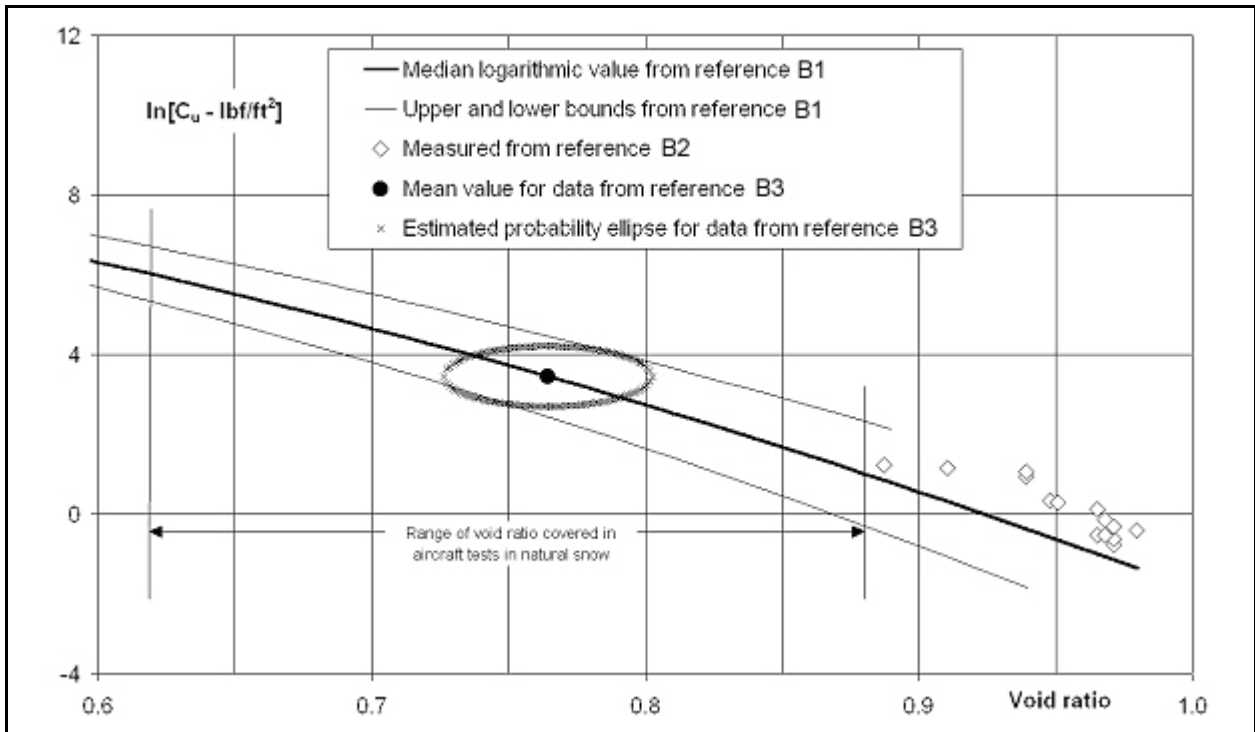
Figure B1: Effect of void ratio on shear strength for low-density snow
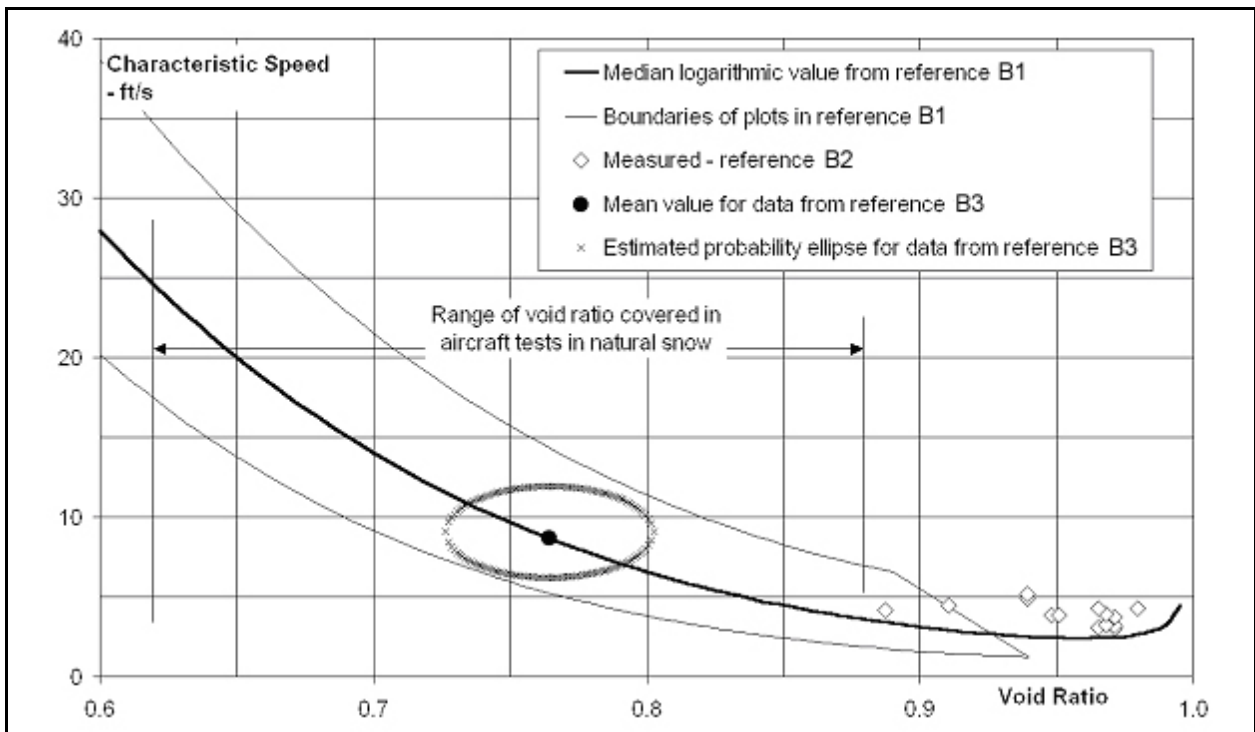
Figure B2: Effect of void ratio on characteristic speed for low-density snow

References

B1.   Shapiro, L.H. et al. *Snow mechanics. Review of the state of knowledge and applications*. CRREL Report 97-3. 1997.

B2.   LaChapelle, E.R. and Perla, R.I. *Mechanical properties of the soft slab*. Alta avalanche study – Project B, Report 2. June 1967.

B3.   Foehn, P. and Camponovo, C. *Improvements by measuring shear strength of weak layers*. ISSW Proceedings 6.5 Paper 3. 1996.

B4.   Shanks, D.H. and Barrett, R.V. *Performance of aircraft pneumatic tyres in soft soil*. Aeronautical Journal (pp. 20-28). January 1981.

APPENDIX C

ESTIMATION OF REFERENCE COEFFICIENT OF FRICTION FROM JAMES BRAKING INDEX

Introduction

A method is developed that substantiates the use of the James braking decelerometer[1] as a means to predict the reference coefficient of friction for tyres braked on runways subject to winter contamination. The method is justified using data collected from two sources.

1. Data from NASA using a C141A as a test aircraft – see Reference C1
2. Measurements made by Transport Canada during the course of the Joint Winter Runway Friction Measurement Program and published in References C2, C3 and C4 are also used.

Although nearly three decades separate the test programmes, there is no perceptible difference between the results.

Modelling

The James Braking Index (JBI) is the reading of an accelerometer calibrated in "*g*" units. The accelerometer is firmly fixed in a vehicle, which is driven at constant speed (usually 30 mph) along a runway. Locked wheel braking is applied and the mean value of the accelerometer readings is defined as the JBI. Similarly, the Runway Condition Reading (RCR) is collected using an accelerometer calibrated in units of feet per second.

For this study, it has been assumed that the vehicle used for the testing weighed 4000 lbf. The load on each wheel is, therefore, 1000 lbf and the inflation pressure is 30 psig. Furthermore, it has been assumed that, at the temperatures appropriate for the persistence of a cover of winter contamination, the reference coefficient of friction between automobile tyres and the contaminated runway is the same as that for aircraft.

Consider the relation for skidding coefficient of friction, which can be obtained from Equation 12.1 of the main text by setting slip ratio to unity.

$$\mu_{SKID\ ICE} = \frac{\mu_{REF\ ICE}}{\left(1+\left(\eta_0 + \eta_1 \frac{V^2}{2g}\right)\frac{p/p_a}{Z^{1/3}}\right)} \qquad \text{C1}$$

Given that the JBI or RCR is a measure of $\mu_{SKID\ ICE}$, Equation C1 can be rearranged so that

---

[1] In this context, the Runway Condition Reading – RCR – when suitably factored is equivalent to the James Braking Index.

$$\mu_{REF\ ICE} = \mu_{SKID\ ICE}\left(1+\left(\eta_0+\eta_1\frac{V^2}{2g}\right)\frac{p/p_a}{Z^{1/3}}\right)$$
C2

Thus, reference coefficient of friction and skidding coefficient of friction are connected by a linear relation. Data for skidding coefficient of friction from the references are plotted in Figure C1 against the reference coefficient of friction that gives the best fit for the aircraft data. The relation implied by Equation C2 is also shown on the plot.

Discussion

Consider Figure C1: the friction model calculation is almost exactly equivalent to a least squares fit to the two sets of data. In addition, the two sets of data conform to the same (skewed) distribution as demonstrated in Figure C2. Thus, if necessary, coefficients at the same levels of probability can be transferred from one set of data to the other.

In Figure C3, the distribution of $\mu_{SKID\ ICE}$ about the model is shown to be normal with a standard error so that $\sigma\left[\mu_{SKID\ ICE}\right]=0.052$. The uncertainty associated with the relation between reference coefficient of friction and the JBI is so that $U\left[\mu_{SKID\ ICE}\right]_{0.95}=0.1$. Furthermore, because the relation is based on 26 measurements, the uncertainty in an estimate of reference coefficient of friction from the correlation is $U\left[\mu_{REF\ ICE}\right]_{0.95}=0.1/\sqrt{26}=0.02$.
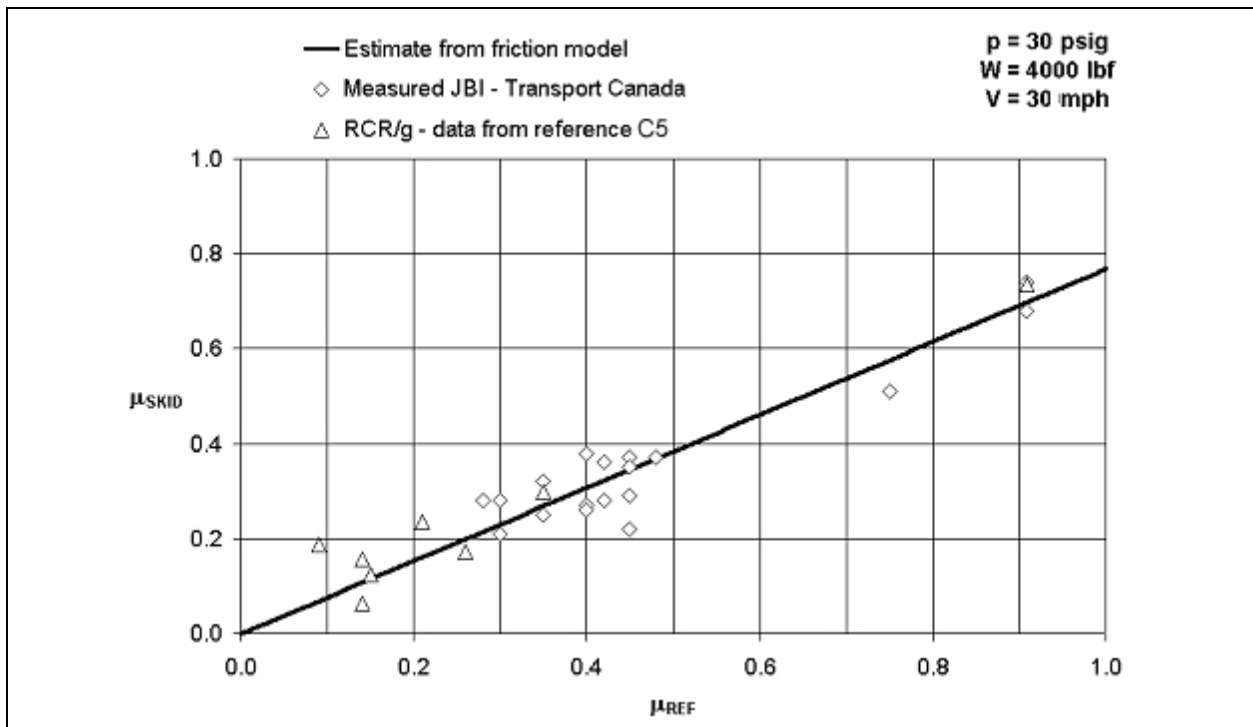
Figure C1: Relation between JBI and reference coefficient of friction
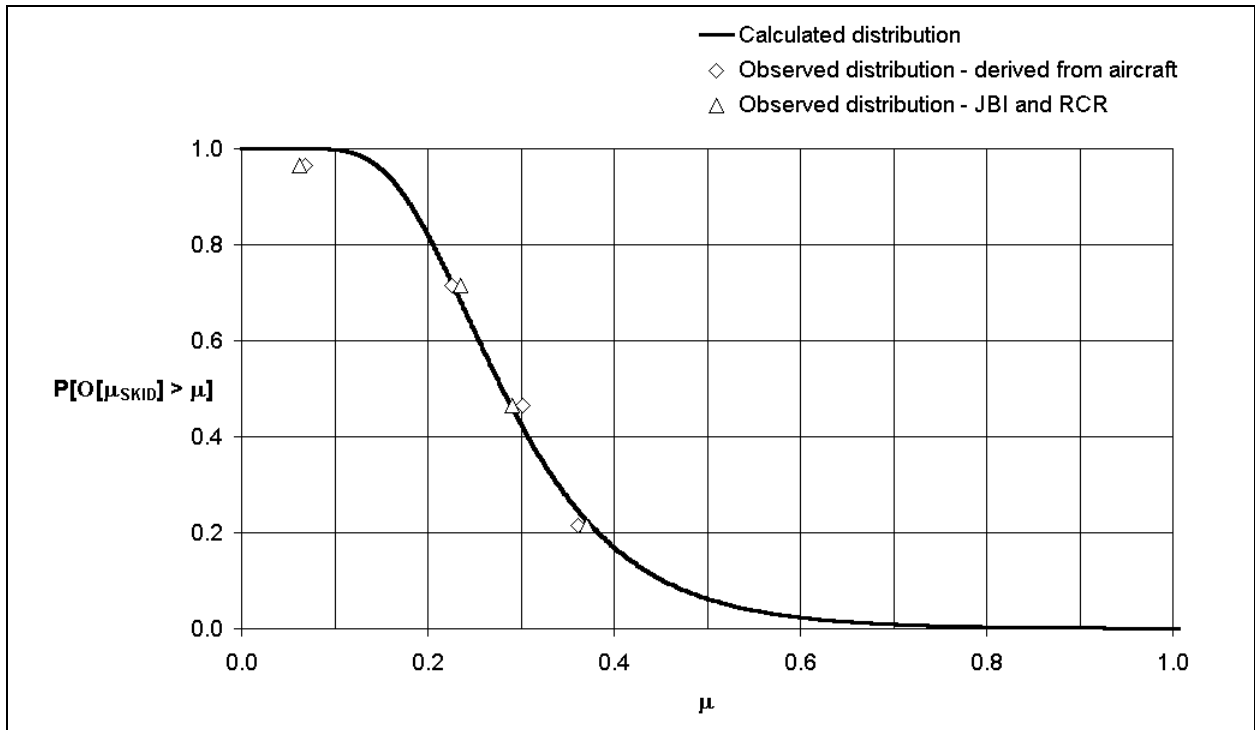
Figure C2: Distribution of measurements of two sources of $\mu_{SKID\ ICE}$
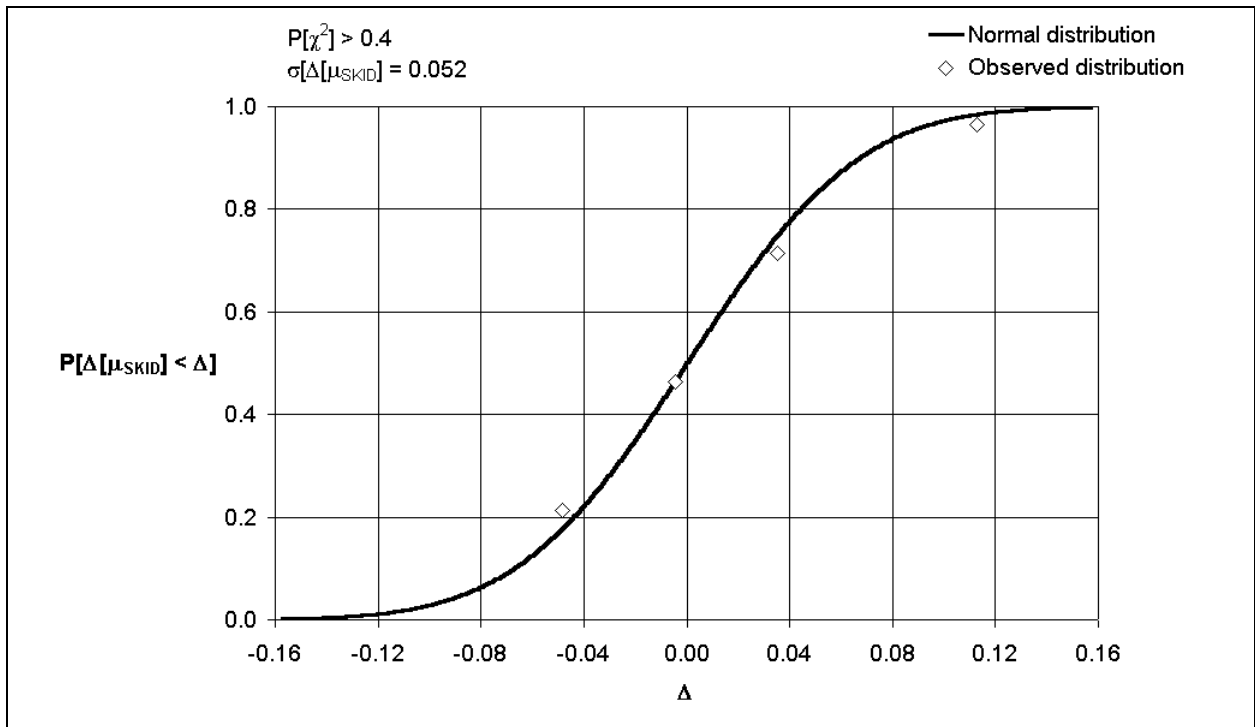
Figure C3: Distribution of JBI about model

References

C1.   Yager, T.J., Phillips, W.P., Horne. W.B. and Sparks, H.C. *A comparison of aircraft and ground vehicle stopping performance on dry, wet, flooded, slush, snow and ice-covered runways*. Final report on project combat traction, a joint USAF-NASA program. NASA TN D-6098. November 1970.

C2.   Martin, J.C.T., Croll, J.B. and Bastian, M. *Braking friction coefficient and contamination drag obtained for a Falcon 20 aircraft on winter contaminated runway surfaces*. National Research Council Canada LTR-FR-132. September 1996.

C3.   Croll, J.B., Martin, J.C.T. and Bastian, M. *Falcon 20 aircraft performance testing on contaminated runway surfaces during the winter of 1996/1997*. National Research Council Canada LTR-FR-137. August 1997.

C4.   Croll, J.B., Martin, J.C.T. and Bastian, M. *Falcon 20 aircraft performance testing on contaminated runway surfaces during the winter of 1997/1998*. National Research Council Canada LTR-FR-151. Transport Canada TP 13338E. December 1998.

C5.   Moore, D.F. *The friction of pneumatic tyres* (pp129-130). Elsevier Scientific Publishing Company, Oxford. 1975.

APPENDIX D

FALCON 20 – BALANCE OF LONGITUDINAL FORCES

Introduction

At the beginning of the joint research programme conducted by Transport Canada and other agencies, two flights of the Falcon 20 were devoted to the determination of the balance of longitudinal forces on an uncontaminated runway with engines at idle. In the analysis of Reference D1, it was assumed that brochure thrust and aerodynamic drag were known and the balance of forces was achieved by solving for rolling friction. A linear variation of the coefficient of rolling friction with speed was identified. This strategy was adopted in the absence of a method for estimating the coefficient of rolling friction.

As part of the modelling developed in the main report, Section 3 defines a straightforward method to estimate this coefficient. Given this method and assuming that lift coefficient is known, it is therefore possible to analyse the tests of Reference D1 in such a way as to determine aerodynamic drag coefficient and forces due to the power units.

Analogue plots of speed and acceleration against time were presented in Reference D1. These data have been digitised and have been used to establish a model of the Falcon 20 within a plausible framework. The framework is set out in this Appendix together with a justification of the format used.

Forces Normal To Runway

The total normal load on the undercarriage is the total weight less the aerodynamic lift.[1]

$$Z = W - 0.5\rho SV^2 C_L \qquad\qquad \text{D1}$$

This vertical load is distributed between the four wheels on the main undercarriage and the two wheels on the nose undercarriage. It has been assumed that the nose undercarriage carries a proportion $\lambda (= 0.1)$ of the total load. Hence, the load carried by one wheel on the nose undercarriage is

$$Z_N = \lambda Z / n_N \qquad\qquad \text{D2}$$

In addition, the load carried by one wheel on the main undercarriage is

$$Z_M = (1 - \lambda) Z / n_M \qquad\qquad \text{D3}$$

---

[1]   This assumes that the runway is horizontal. However, the error in normal force is unlikely to exceed 10 lbf when operating on normal runways at the weight of the Falcon 20.

Furthermore, for each configuration of flap and airbrake tested, the lift coefficient at the ground angle of attack has its own value taken from Reference D1. These are listed in Table D1.

Although the vertical loads assumed for each tyre are approximations, the effects of quite large errors are not serious. This is because the vertical force balance is used only to estimate the coefficient of rolling friction. In the correlation of Section 3 of the main report, only the cube root of the normal force appears.

Table D1: Conditions covered in rolling friction tests in 1996

Flight	Flap	Airbrake	C_L	Power	Runway condition	Speed range
96/4	15	In	0.2	Idle	Wet	$10 < V$ - kn < 100
96/4	15	Out	0.1	Idle	Wet	$50 < V$ - kn < 90
96/4	40	Out	0.3	Idle	Wet	$45 < V$ - kn < 90
96/10	15	In	0.2	Idle	Dry	$60 < V$ - kn < 120
96/10	15	Out	0.1	Idle	Dry	$45 < V$ - kn < 115
96/10	40	Out	0.3	Idle	Dry	$40 < V$ - kn < 95

Forces Parallel to Runway

It is assumed that the axes of the final propelling nozzles are parallel to the runway when the aircraft is in its ground attitude. Then, the balance of forces parallel to the runway can be represented by

$$-W(\dot{V} + \sin[\varepsilon]) + X_{G_0} - D_{POWER} - D_{AIRFRAME} - G_{ROLL} = 0 \qquad \text{D4}$$

where the drag force arising from operation of the power units is given by

$$D_{POWER} = D_{MOMENTUM} + D_{SPILL} + D_{AFTERBODY} \qquad \text{D5}$$

the airframe drag comprises

$$D_{AIRFRAME} = D_{DATUM} + D_{FLAP} + D_{AIRBRAKE} \qquad \text{D6}$$

and the rolling resistance is

$$G_{ROLL} = n_N Z_N \{\mu_{ROLL}\}_N + n_M Z_M \{\mu_{ROLL}\}_M \qquad \text{D7}$$

Coefficients of rolling friction are, from the correlation in Section 3 of the main report,

$$\frac{p_i/p_a}{Z_i^{1/3}} \{\mu_{ROLL}\}_i = 0.0062 + 2.31 \times 10^{-5} \frac{V^2}{2g}: \qquad i = M \text{ or } N \qquad \text{D8}$$

The quantities that are known are

- Aircraft weight
- Ambient conditions
- Airspeed and thus kinetic pressure
- Time rate of change of airspeed
- Runway slope
- Rolling resistance
- Airframe reference geometry

These are sufficient to enable the solution of Equation D4 for the drag components specified in Equations D5 and D6, if a suitable modelling strategy can be found.

Consider first, the inlet momentum component $D_{MOMENTUM}$. This is given by

$$D_{MOMENTUM} = \dot{m}_0 V \qquad \qquad \text{D9}$$

For the incompressible speeds encountered on ground roll to stop for the Falcon 20, it may be assumed that the inlet mass flow rate, $\dot{m}_0$, is constant. For ground idling, $D_{MOMENTUM}$ is, therefore, a linear function of true airspeed.

Consider now D_{SPILL}. For pitôt intakes, spillage drag coefficient can be approximated by an empirical function of inlet mass flow ratio. That is

$$C_{D_{SPILL}} = k\left(1 - \frac{\dot{m}_0}{\dot{m}_{CAPTURE}}\right)^2 \qquad \qquad \text{D10}$$

Now,

$$\frac{\dot{m}_o}{\dot{m}_{CAPTURE}} = \frac{\rho_0 A_0 V}{\rho_0 A_1 V} \qquad \qquad \text{D11}$$

D_{SPILL} can therefore be written

$$D_{SPILL} = qSC_{D_{SPILL}} = kqS - \frac{kS\dot{m}_0}{\rho_0 A_1}V_0 + \frac{kS\dot{m}_0^2}{2\rho_0 A_1^2} \qquad \qquad \text{D12}$$

The first term on the right hand side of Equation D12 can be considered a part of D_{DATUM}: the coefficient of V_0 in the second term is constant. That term can therefore be included in the momentum drag. The third term, because all the components are constant, can be included in X_{G_0}. Clearly, such a strategy violates prudent thrust-drag accounting practice. However, the strategy is constructed solely to enable a statistical analysis: no recommendations are made that a thrust-drag accounting scheme should be based upon this approach.

In addition, the last power term in Equation D5, $D_{AFTERBODY}$, is given by

$$D_{AFTERBODY} = qSC_{D_{AFTERBODY}}$$ D13

In general, afterbody drag coefficient is related directly to engine pressure ratio. Because the speed range considered is low, it is assumed that engine pressure ratio, and hence afterbody drag coefficient is constant.[2] $D_{AFTERBODY}$ is therefore treated as part of D_{DATUM}.

The components of airframe drag in Equation D6 are conventional and may be written

$$D_{AIRFRAME} = qSC_{D_{AIRFRAME}} = qS\left(C_{D_{DATUM}} + C_{D_{FLAP}} + C_{D_{AIRBRAKE}}\right)$$ D14

Now, for conventional plain, split or slotted flaps, the incompressible increment in drag coefficient due to flap deflection correlates approximately with $\sin^2[\beta_F]$. Furthermore, it may be assumed that there is no cross coupling between the increase in drag due to airbrake and that due to flap deflection. Equation D14 may be written:

$$D_{AIRFRAME} = qS\left(C_{D_{DATUM}} + \varphi_\beta \sin^2[\beta_F] + \varphi_\delta \delta_{AIRBRAKE}\right)$$ D15

Where the two values for $\delta_{AIRBRAKE}$ are unity for airbrake open and zero for airbrake closed.

To summarize, Equation D4 can be re-arranged and re-written to include these assumptions so that

$$-W\left(\dot{V} + \sin[\varepsilon]\right) - G_{ROLL} = X_{G_0} + \dot{m}_0 V + qS\left(C_{D_{DATUM}} + \varphi_\beta \sin^2[\beta_F] + \varphi_\delta \delta_{AIRBRAKE}\right)$$ D16

Using the method of least squares to solve the multiple linear regression[3] represented by Equation D16, $\left(X_{G_0}, \dot{m}_0, C_{D_{DATUM}}, \varphi_\beta \text{ and } \varphi_\delta\right)$ can be found because they are the coefficients of known quantities on the right hand side of Equation D16.

Results

In this section, the results of solving Equation D16 for 1300 measurements of speed and acceleration are presented and discussed. The data were obtained by digitising the analogue measurements presented in Reference D1 from trials conducted at North Bay airport in 1996. As a check on the accuracy of the digitisation, the acceleration data were integrated with respect to time and compared with the measured speeds. A typical example for one test run is shown in Figure D1. There is no doubt that the digitising process has faithfully reproduced the analogue data.

---

[2] This assumption is consistent with the assertion that gross thrust is constant.
[3] See Reference D3 for the method of solution and Reference D4 for an example of the application of the method.

In Figure D2, the aerodynamic forces and those relating to the power units are plotted. They are shown as positive forces in the direction of the drag axis. In this case, the drag axis is parallel to the runway. Also shown in Figure D2 is the correlation that results from solving Equation D16. This correlation is:

$$D = -399.5 + 0.99V + qS\left(0.0389 + 0.1375\sin^2[\beta_F] + 0.0384\delta_{AIRBRAKE}\right)$$ D17

For a single engine, the correlation implies that the idling static gross thrust under the conditions encountered at North Bay is approximately 200 lbf. The (constant) value of inlet **mass** flow rate is approximately 0.5 slug per second. For an engine of this design, operating at its design point, the specific thrust may be expected to be in the region of 1400 lbf/slug/s. Because the idling condition is far removed from the design point, it is not surprising that the specific idling thrust is less than a third of the design value.

For the three aircraft configurations tested on the ground, the values of drag coefficient can be calculated from Equation D17. These values are given in Table D2 and are compared there with the values quoted in Reference D1. The differences are not serious. However, the values obtained from Equation D17 are consistent with a set of power forces that match the measured performance of the aircraft as represented by the time histories given in Reference D1. The values of drag coefficient quoted in Reference D1 are nearly consistent with those from Equation D17. It was not possible to reconcile the thrust information quoted in Reference D1 with that obtained from the correlation exercise conducted here.[4]

Table D2: Airframe drag coefficient for ground operations – Falcon 20

Flap	Airbrake	Drag Coefficient	
		Equation D17	Reference D1
15	In	0.0481	0.05
15	Out	0.0865	0.076
40	Out	0.1341	0.132

The deviations of the measured forces about the correlation given in Equation D17 are approximately normally distributed with a standard error so that $\sigma[\Delta[D]] = \pm126\,\text{lbf}$. The distribution is shown in Figure D3 where it is compared with a normal distribution. A χ^2 *"goodness of fit"* test for normality of the distribution of measurements about the correlation was used. The value found was such that $P[\chi^2] > 0.5$. This implies that the distribution of measurements is highly likely to be normal and appropriate conclusions concerning confidence intervals and limits for the measuring system can be drawn safely.

It may be expected that, for the instrumentation, flap configurations and engine settings used for the testing on the Falcon 20 in 1996, forces will be precise to $\pm250\,\text{lbf}$ at the 95% confidence level. For testing on runways contaminated with snow, slush or ice, any significant change in precision may be attributed to uncertainties in defining the depth and mechanical properties of the contaminants.

---

4   A typographical error was discovered after Reference D1 was published.

Conclusions

Digitised values of the analogue data for speed and acceleration from Reference D1 are mutually consistent. In addition, these digitised values have been used in conjunction with runway slope, weight and estimates of rolling friction to produce a coherent model of idling power and aerodynamic drag coefficient for ground operations with the Falcon 20.

If contaminant properties and depths can be adequately defined, analysis of decelerating force due to contamination may be expected to be precise to within $\pm\,250\,\text{lbf}$ at the 95% level of confidence.
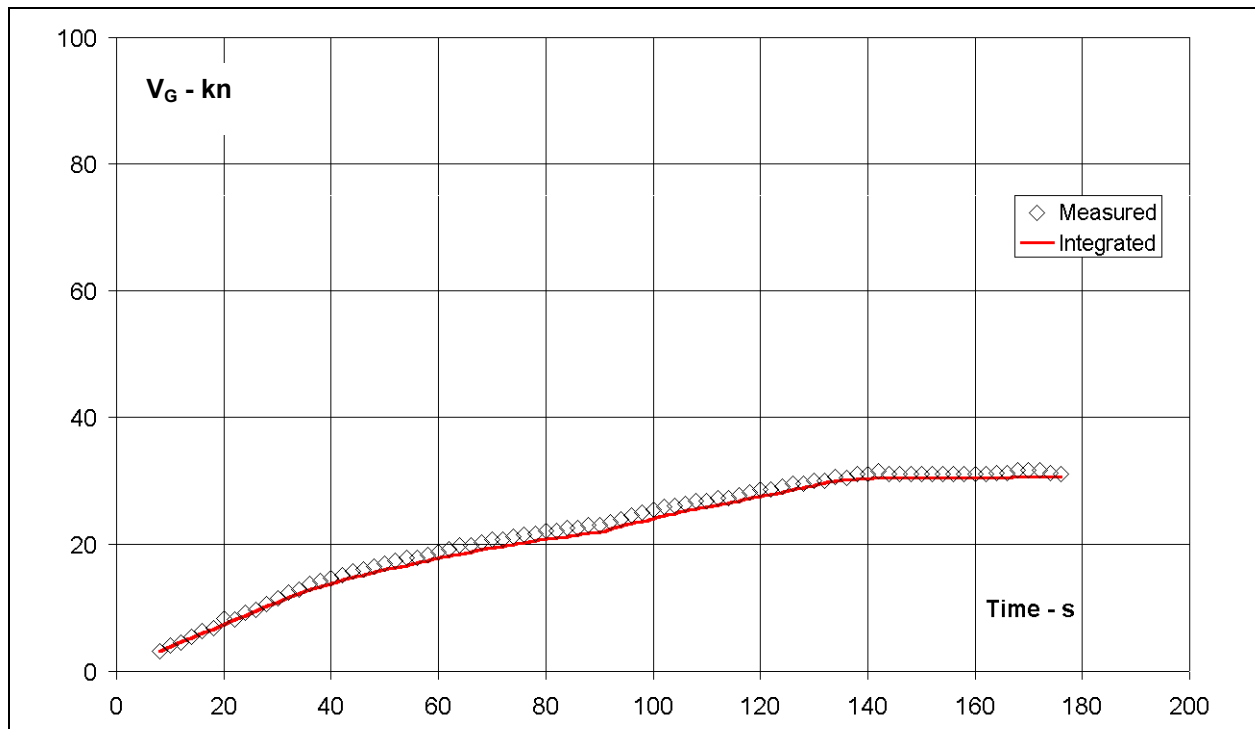
**Figure D1: Example of measured and integrated speeds - Falcon 20
at North Bay in 1996**
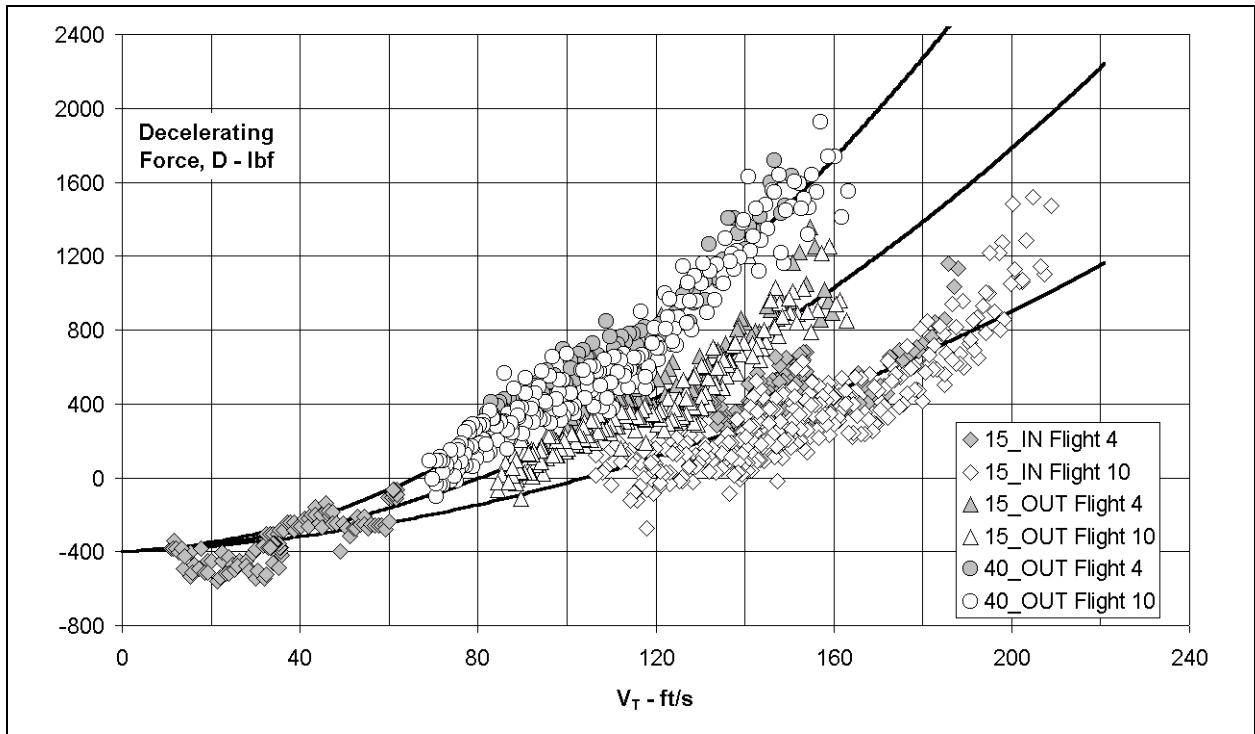
Figure D2: Measured decelerating force and correlation compared
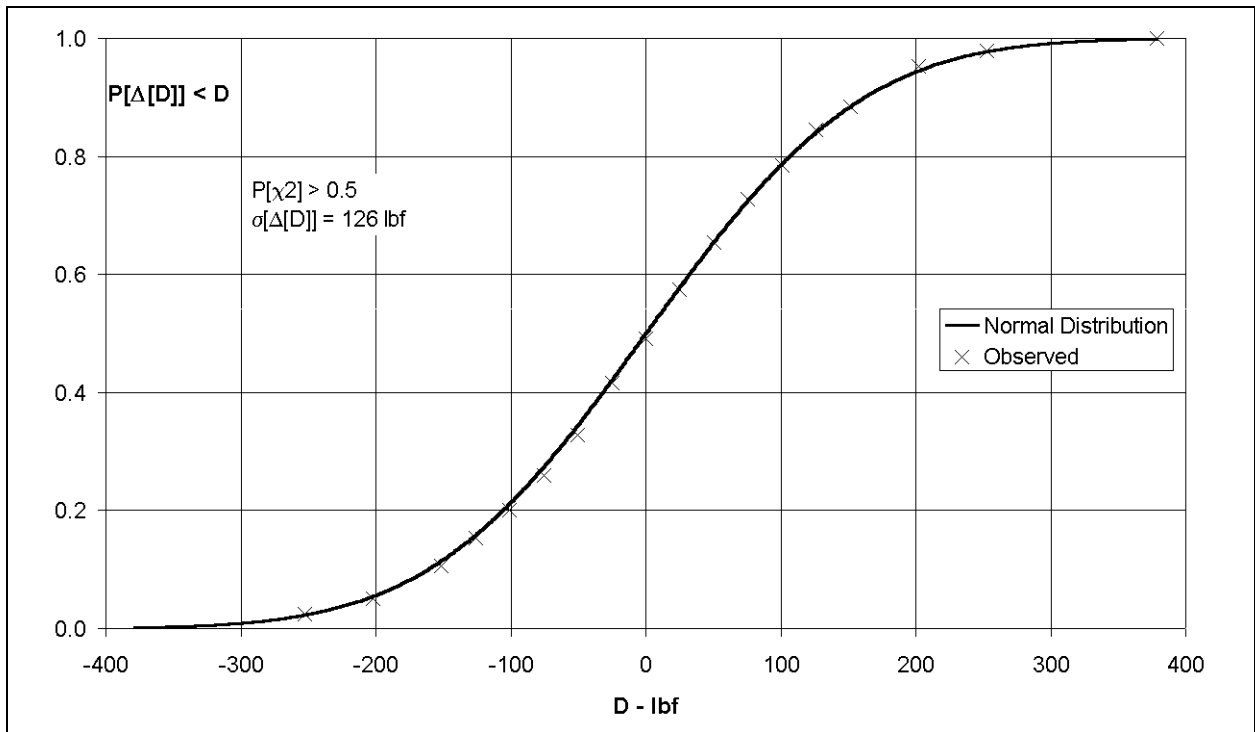
Figure D3: Distribution of measured forces about correlation

References

D1.   Martin, J.C.T., Croll, J.B. and Bastian, M. *Braking friction coefficient and contamination drag obtained for a Falcon 20 aircraft on winter contaminated runway surfaces*. National Research Council Canada. LTR-FR-132. September 1996.

D2.   Croll, J.B., Martin, J.C.T. and Bastian, M. *Falcon 20 aircraft performance testing on contaminated runway surfaces during the winter of 1996/1997*. National Research Council Canada. LTR-FR-137. August 1997.

D3.   ESDU. *Statistical methods applicable to analysis of aircraft performance data*. ESDU Data Item 91017 with amendments A to D. September 1997.

D4.   ESDU. *Example of statistical techniques applied to analysis of measurements of the landing airborne manœuvre*. ESDU Data Item 92022. October 1992.

APPENDIX E

FALCON 20 – OPERATIONAL SLIP RATIO

Introduction

Mathematical models have been developed in the main report that describe coefficient of braking friction for the type of tyre used for aircraft. The modelling is principally empirical but has some basis in the physics of interactions between rubber compounds and hard surfaces. In particular, coefficient of friction in a partial skid is calculated using the equations[1]

$$\mu_{SLIP\_DRY} = \frac{\mu_{REF}\left(1 - e^{\eta_2 s}\right)}{1 + \left(\eta_0 + \eta_1 \dfrac{v^2}{2g}\right)\dfrac{p/p_a}{Z^{1/3}}} \qquad \text{E1}$$

and

$$\mu_{SLIP\_WET} = \mu_{SLIP\_DRY}\left(\frac{1 - \varphi_0\, q/p}{1 + \varphi_1\, q_v/p_a}\right) \qquad \text{E2}$$

In both Equations E1 and E2, all speed dependent terms are calculated at v - the footprint translation speed. This is given by

$$v = sV \qquad \text{E3}$$

In Section 12 of the main report, the format of Equations E1 and E2 has been shown to apply to partial skids on runways contaminated by ice.[2] Now, one objective of the current studies is to attempt the statistical description of contamination due to ice and similar substances. This is likely to take the form of a distribution of the reference coefficient of friction, which is fundamental to the application of the method outlined in Sections 8 and 11 of the main report and summarised in Equations E1, E2 and E3.

In order to collect a substantial body of information that can be used to establish such a distribution, it is clear that as many as possible of the braked ground runs on the Falcon 20 need to be studied to obtain values of the reference coefficient of friction. Thus, it is necessary to know at least the mean values of slip ratio as a function of speed and (if necessary) type of contaminant.

---

[1]   See Sections 8 and 11 of the main report of terms in Equations E1, E2 and E3.
[2]   The case of compacted snow is currently under study and will probably be treatable as an extension of the iced case.

Reference E1 contains sufficient slip ratio information for the Falcon 20 used by Transport Canada to enable a correlation with speed and to suggest that the type of contaminant does not substantially affect the mean slip ratio expected for a given speed. A correlating function is developed here that may be applicable, at least in form, to braking systems that are similar in design to that on the Falcon 20.

Correlation

At speeds less than approximately 30 ft/s, the anti-skid system on the Falcon 20 is not active. This suggests that the speed dependence of slip ratio, which is illustrated by the data plotted in Figure E1, may be described in terms of multiples of this minimum operational speed $V_0 = 30$ ft/s. Such a device may then enable a more general application of the correlation developed here. Inspection of the variation of the measured values of slip ratio with speed in Figure E1, suggests that there is an inverse relation between speed and slip ratio. Combining these two observations leads to a correlating format so that

$$s = \frac{s'}{\left(1 + V/V_0\right)}$$ E4

Note that the denominator of the right hand side of Equation E4 is such that, when speed reduces to zero, the calculated slip ratio remains bounded.

Equation E4 can be re-arranged so that

$$s' = s\left(1 + V/V_0\right)$$ E5

The statistic s' may be studied to determine the properties of its distribution.

Physically, slip ratio for a braked wheel is bounded. In particular, slip ratio cannot be negative and as speed increases, the data in Figure E1 imply that slip ratio tends to zero. Thus, because speed is finite, the statistic s' has a lower bound of zero. Similarly, the upper bound of the statistic s' can be inferred. When speed is zero and slip ratio reaches its maximum value of unity then $s' = 1$. This condition is purely hypothetical because this type of system is inoperative below $V = V_0$.

Now, a Beta distribution of the first kind $\beta_1\left[s', m, n\right]$ is a simple distribution whose range is such that $0 \le s' \le 1$ with parameters m and n. These parameters may be calculated from a set of measurements so that

$$m = \frac{\left(1 - \mathrm{E}\left[s'\right]\right)\mathrm{E}^2\left[s'\right]}{\mathrm{var}\left[s'\right]} - \mathrm{E}\left[s'\right]$$ E6

and

$$n = \frac{m\left(1 - \mathrm{E}\left[s'\right]\right)}{\mathrm{E}\left[s'\right]} \qquad \text{E7}$$

For the set of measurements considered, $\mathrm{E}\left[s'\right] \approx 0.362$ and $\mathrm{var}\left[s'\right] \approx 0.0135$. It has been argued that the range of s' is such that $0 \le s' \le 1$: thus s' may conform to a Beta distribution of the first kind with parameters $m = 6$ and $n = 10.3$.

The probability density function for the distribution is, then

$$dP = \frac{s'^{5}\left(1 - s'\right)^{9.3} ds'}{\mathrm{B}\left[6,\ 10.3\right]} \qquad \text{E8}$$

The accumulated probability of this distribution is plotted in Figure E2. The probability associated with a χ^2-test for goodness of fit for the distribution is such that $P\left[\chi^2\right] > 0.5$. Thus, the variation of mean slip ratio with speed for the Falcon 20 is defined by a relatively simple statistic.

Discussion

In all, data from 32 runs are included in the compilation of the statistical distribution of the parameter s'. Because each of the four wheels was measured separately on each run, the distribution has been determined from 128 statistically independent measurements. Inspection of Table E1 reveals that a wide range of contaminants has been covered. No evidence has been found to suggest that contaminant has a significant effect on the mean slip at any speed in the range $30 \le V$ - ft/s<180. Furthermore, there is no significant difference between the performances of the four wheel-brakes as determined by the statistic s'. This is borne out by inspection of Figure E1 and by a t-test.

The distribution of the statistic s' can be used for at least two analytical purposes for the Falcon 20. On the one hand, its mean value $\mathrm{E}\left[s'\right] = 0.362$ can be used to determine a value of slip ratio for any given speed. Thus,

$$s = \frac{\mathrm{E}\left[s'\right]}{\left(1 + V/V_0\right)} = \frac{0.362}{\left(1 + V/30\right)} \qquad \text{E9}$$

in order to calculate an effective value of an average reference friction coefficient by iteration in Equation E1 for all available sets of measurements. The resulting values of reference coefficient of friction may then be studied to determine distributions and other relevant statistical attributes.

On the other hand, the percentage points shown in Table E2 can also be used to predict slip ratio and hence, average braking performance for the aircraft on a runway whose characteristics are known, at any chosen level of probability. For example, the 5% point of the distribution of s' is $s'_{0.05} = 0.186$. This is the lower, 95% bound of the distribution of s' and defines the boundary so that the probability of slip ratio exceeding the value calculated from

$$s = \frac{s'_{0.05}}{\left(1 + V/V_0\right)} = \frac{0.186}{\left(1 + V/30\right)} \tag{E10}$$

is 0.95 for all speeds greater than 30 ft/s. These values of s could be used for any surface for which the reference value for friction coefficient is known, to predict the lower bound of average braking performance – if, of course, the 95% level is to be used as a boundary value. Other relevant values for the percentage points of s' are given in Table E2.

Examples

Dry Runway

In the series of tests conducted during the winter of 1995-96, three braked ground runs were measured on a dry runway. The data, adjusted for aerodynamic lift and drag, power unit forces and rolling resistance are plotted in Figure E3. Using the methods implicit in Equations E1, E2, E3 and E4 together with appropriate values of the percentage points of the distribution of s' from Table E2, an effect of ground speed on mean braking coefficient of friction can be estimated. These calculations are also shown in Figure E3.

At speeds so that $V > 120$ ft/s, the estimate of **mean** braking coefficient of friction and the measured values of coefficient of friction due to braking are in close agreement. For speeds so that $V < 120$ ft/s, the estimate of **mean** braking coefficient of friction is somewhat greater than the measurements. In fact, the measured values of friction coefficient due to braking drift towards the lower bounds of the distribution of **mean** values as implied by the statistic s'. This implies that the system as a whole under-performs at these lower speeds in relation to the system performance as defined by the measurements of s' in the winter of 1997-98.

Wet Runway

In the series of tests conducted during the winter of 1995-96, two braked ground runs were measured on a wet runway; no measurement of the depth of water was given. Braking friction data, adjusted for aerodynamic lift and drag, power unit forces and rolling resistance are plotted in Figure E4. Using the methods implicit in Equations E1, E2, E3 and E4 together with appropriate values of the percentage points of the distribution of s' from Table E2, an effect of ground speed on mean braking coefficient of friction can be estimated. It has been assumed that the depth of water present on the runway was 0.04 inches (1 millimetre). These calculations are also shown in Figure E4.

There is more scatter in the measured data in the wet than on the dry runway, particularly at higher speeds. This additional scatter is due in the main to a more active cycling of the anti-skid system. As in the case of the dry runway, there is a tendency for the system to deliver lower friction coefficients at low speed than those calculated using the mean slip ratio determined from the distribution of s'.

However, overall, the reduction in the average measured friction coefficient that occurs from dry runway to wet runway is reproduced in the calculations. This is further confirmation that the modelling for complete aircraft, developed as it has been from a variety of single wheel tests, is a realistic tool for calculating braking friction coefficients.

Iced Runway

In the series of tests conducted during the winter of 1995-96, two braked ground runs measured on an icy runway have been considered to illustrate the use of the methods developed. Braking friction data, adjusted for aerodynamic lift and drag, power unit forces and rolling resistance are plotted in Figure E5. Using the methods implicit in Equations E1, E2, E3 and E4 together with appropriate values of the percentage points of the distribution of s' from Table E2 and assuming a reference value for coefficient of friction, an effect of ground speed on mean braking coefficient of friction can be estimated. The calculated values are also shown on Figure E5.

The reference value $\left(\mu_{REF} = 0.25\right)$ has been chosen so that the speed variation of slip ratio given by Equation E9 is such that the calculated values of braking friction coefficient reflect the mean measured values throughout the speed range. In so doing, a plausible variation with speed arises from the calculation. Again, this is confirmation that the modelling for complete aircraft, developed as it has been from a variety of single wheel tests, is a realistic tool for calculating braking friction coefficients over a wide range of contaminants.

Conclusions

Slip ratio data from braked ground runs on a wide range of contaminated runways have been shown to correlate with ground speed. The correlation is in the form of a simple statistic that conforms to a common type of skewed distribution.

Although the tests were conducted on runways for which contamination was varied from wet to ice and snow, there is no evidence that the slip ratio at any speed is affected by the degree or nature of the contaminant.

The expected value of the statistic will be used to analyse braking data from all the relevant runs on the Falcon 20. Thus, it is anticipated that a robust statistical description of friction coefficients will be created for winter-contaminated runways.

In addition, it is possible to use the correlation to produce estimates of the braking performance of the Falcon 20 at any level of probability for runways where the reference value of friction coefficient is known.

Table E1: Summary of surface condition data

Flight	Runs	Surface condition
98_01	6 – 9	60% bare and dry, 40% 0.125 in loose snow and ice patches.
98_02	5 – 9	100% 0.4 in loose snow on top of 60% asphalt and 40% ice.
98_03	5, 6	100% 1.6 in loose snow.
98_04	1 – 4	Changing conditions of chemically treated bare and wet/ ice.
98_06	1b – 4b	100% 1.2 in loose snow.
98_08	1 – 6	100% compacted snow with ice patches.
98_09	3, 4	Changing conditions: bare and wet, standing water, slush, snow.
08_10	1 – 5	Changing conditions: bare and wet, snow

Table E2: Falcon 20: percentage points of the distribution of s'

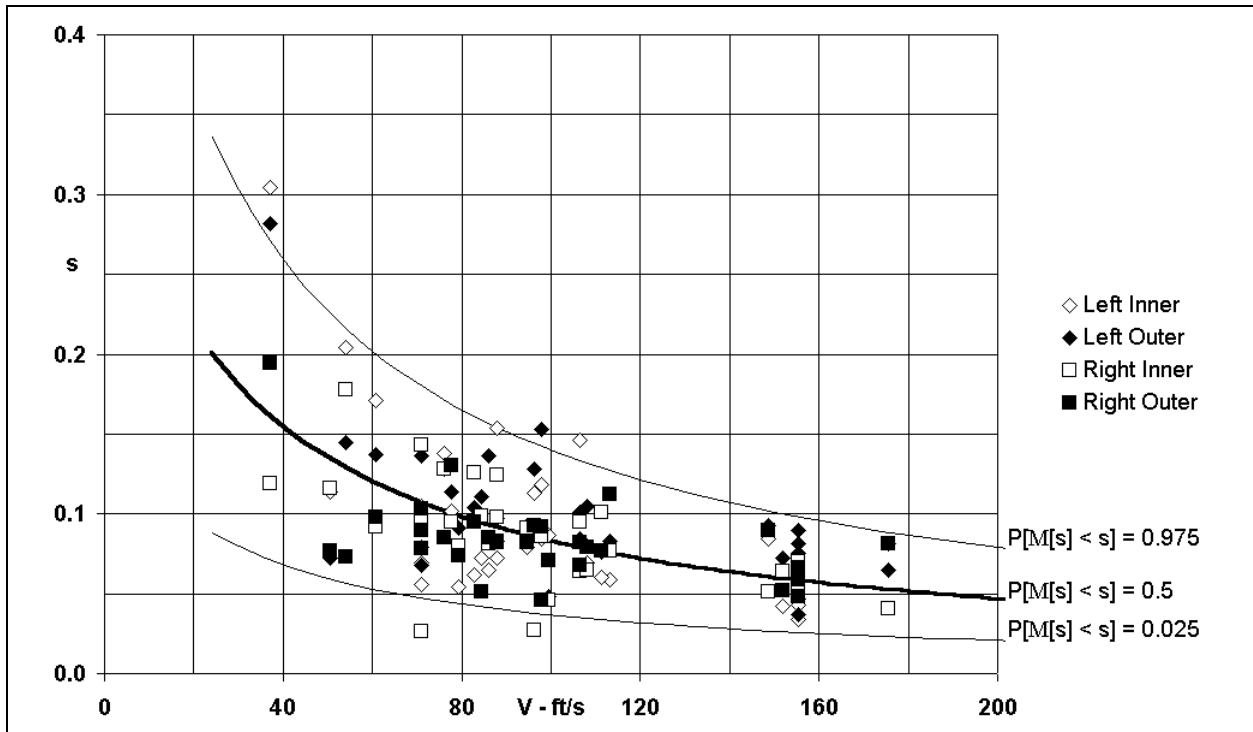| Percentage level $= 100 \times x$	Probability level x	s'
0.1%	0.001	0.083
1.0%	0.01	0.131
2.5%	0.025	0.159
5.0%	0.05	0.186
50.0%	0.5	0.362
95.0%	0.95	0.568
97.5%	0.975	0.606
99.0%	0.99	0.650
99.9%	0.999	0.734

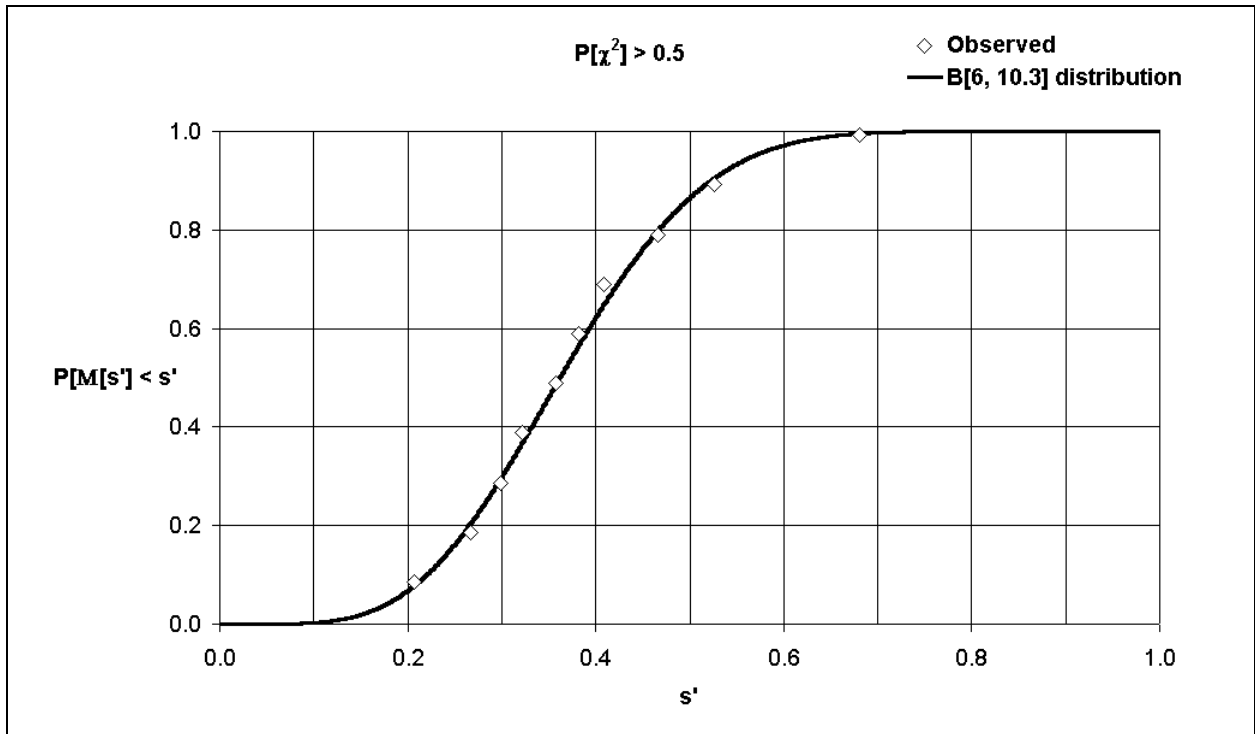**Figure E1: Effect of ground speed on slip ratio**

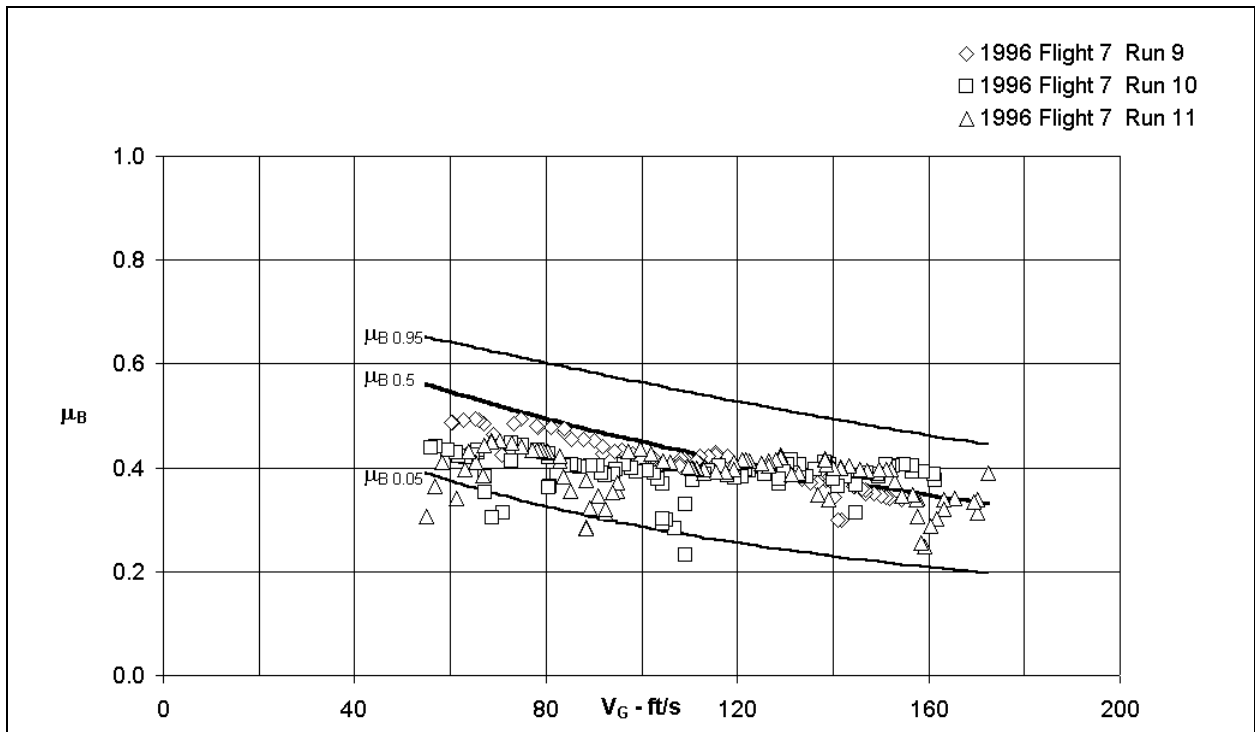**Figure E2: Accumulated probability for transformed slip ratio**

Figure E3: Effect of ground speed on braking coefficient of friction at various probability levels – dry runway
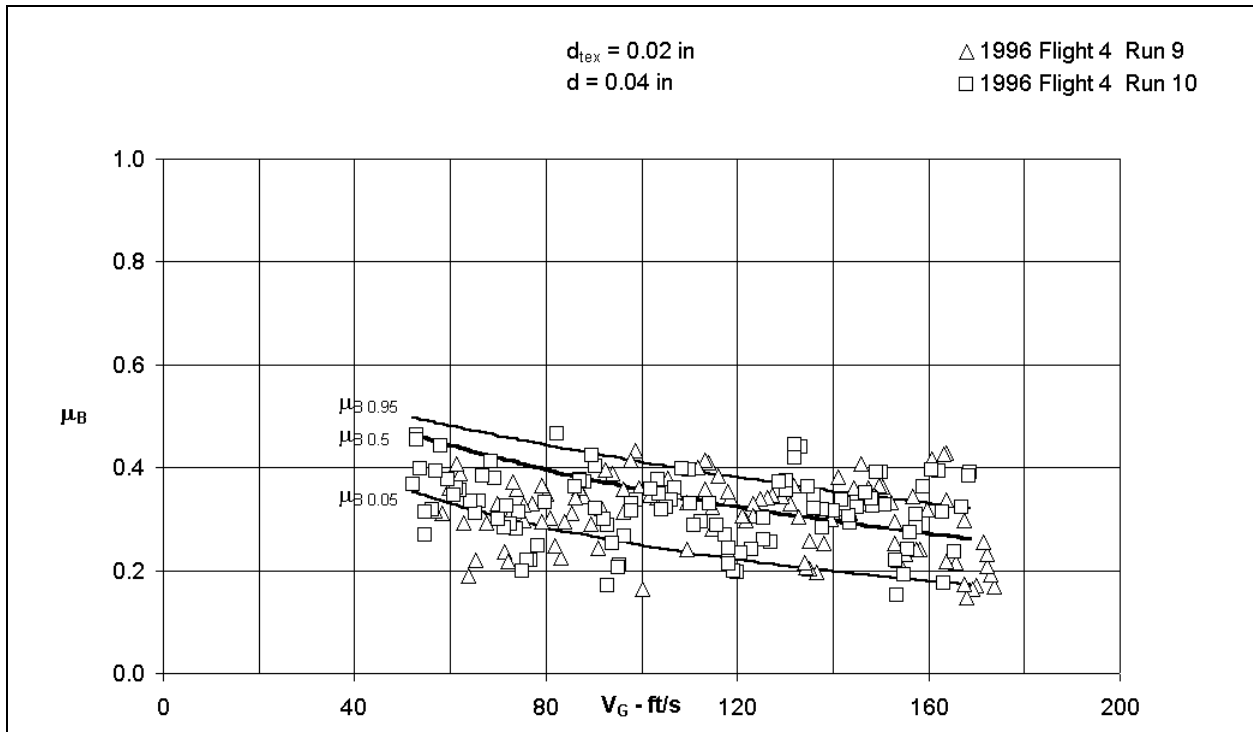
Figure E4: Effect of ground speed on braking coefficient of friction at various probability levels – wet runway
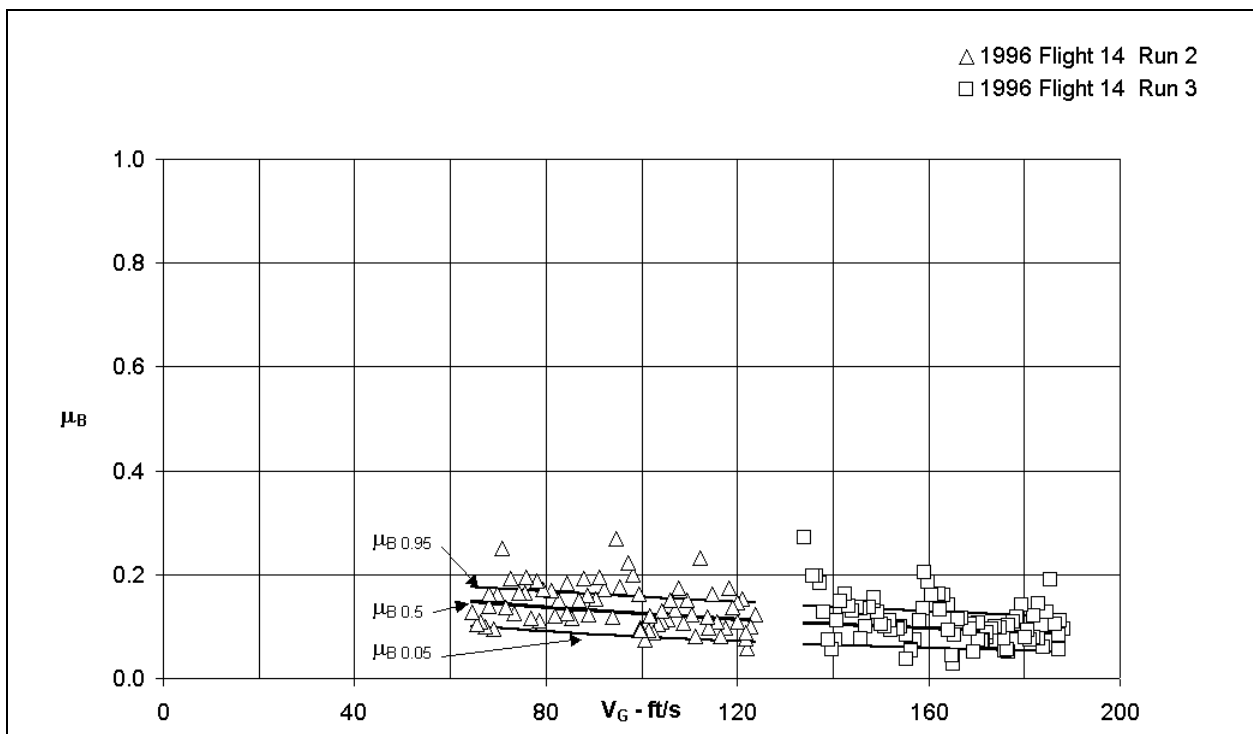

Figure 5: Effect of ground speed on braking coefficient of friction at various probability levels – icy runway: $\mu_{REF} = 0.25$

References

E1.   Croll, J.B., Martin, J.C.T. and Bastian, M. *Falcon 20 aircraft performance testing on contaminated runway surfaces during the winter of 1997/1998*. National Research Council Canada LTR-FR-151. Transport Canada TP 13338E. December 1998.

E2.   ESDU. *Statistical methods applicable to analysis of aircraft performance data*. ESDU Data item 91017 with amendments A to D. September 1997.